Ash Formation, Deposition and Corrosion When Utilizing Straw for Heat and Power Production

Frandsen, Flemming

Publication date:
2010

Document Version
Publisher's PDF, also known as Version of record

Ash Formation, Deposition and Corrosion When Utilizing Straw for Heat and Power Production

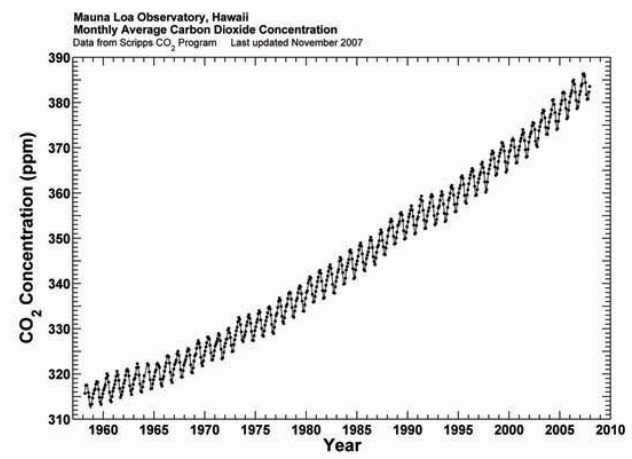

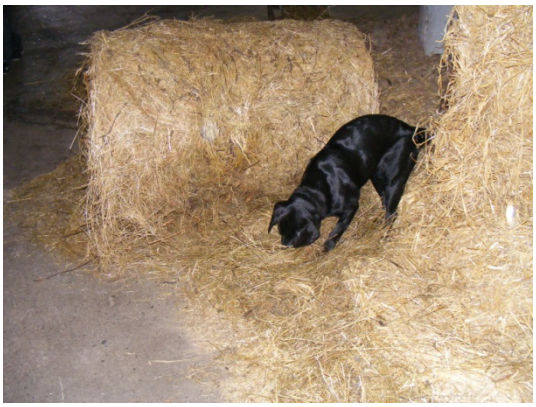

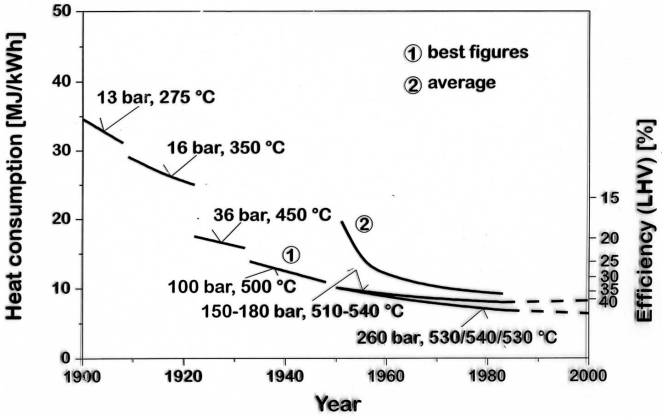

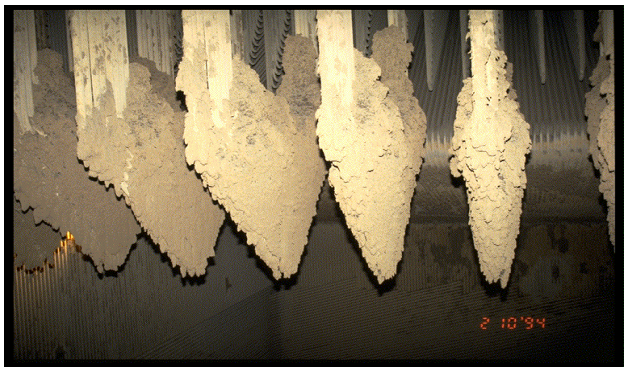

Publishable Doctoral Thesis, March 10, 2011

By Flemming J. Frandsen

Foreword:

This is a slightly modified version of my doctoral thesis, which was defended at DTU on January 28, 2011. The modifications, compared to the original doctoral thesis, is that I have split up the original chapter on release of critical elements (like K, S and Cl) and aerosol formation, into two chapters, dealing with release of critical elements and aerosol formation, respectively. The reason for this decision is a wish to give more credit to and provide a more complete outline of our work on release of critical elements during fixed-bed thermal conversion of biofuels. In the aerosol chapter, I have improved the graphics significantly and have added a section on the theory behind the Plug Flow Aerosol Condenser. The rest of the material presented in the thesis is virgin.

The thesis is the result of 18-24 months hard work, during which I have tried to condense the Danish experiences of ash and aerosol formation, deposition and corrosion during the thermal utilisation of straw for heat and power production. The thesis focuses on work carried out - mainly - within the CHEC Research Centre, DTU, on this subject, in the period 1991 to 2009. The thesis outlines several experimental investigations done within, or in close cooperation with, CHEC during the years.

First and foremost, I would like to thank Director of the Department of Chemical and Biochemical Engineering, DTU, Prof. Kim Dam-Johansen, for providing the economical framework that has made it possible to write this thesis. Secondly, my gratitude is extended to my DTU-colleague Asc. Prof. Peter A. Jensen, to Dr. Rainer Backman, as well as to my former colleague and life-long friend Dr. Bengt-Johan Skrifvars, for several inspiring discussions on this subject.

There is also a group of former Ph.D.-students at CHEC, including Karin H. Andersen, Hanne P. Nielsen, Lone A. Hansen, Jacob N. Knudsen and Simone van Lith, who have played each their own role in the inspiration leading to this thesis. I thank you all deeply for you inspiration.

In addition, my thanks go to the Danish Power Industry, formerly, Elsam, Elkraft, Energy E2, now jointly DONG Energy, Vattenfall, Vølund, BWE and formerly FLS Miljø. Several people from these companies acted as very valuable partners for the outline and interpretation of the data presented in this thesis during my years with CHEC.

I have played an active role in the Nordic as well as the European research community and would like to mention a few people of extraordinary importance in this field; Rob Korbee, Mikko Hupa, Peter Roberts, Leo Tognotti, Hartmut Spliethoff, Terry Wall, Stan Harding, Sven Unterberger and Ingwald Obernberger. Thanks to all of you for your inspiration and cooperation.

Thanks to Brian Brun Hansen, Anne Juul Pedersen and my mother, Karen, for very careful proofreading of this manuscript. In addition to Mille, Celina, Mathilde, Jose, Sophia, Tania, Katrine, Torben and Kim, thanks for providing an alternative to writing this thesis, especially when a break was needed in order to clear up my mind.

Also, a big and warm thanks to my two opponents during the doctoral thesis defense, Prof. Klaus R. G. Hein and Prof. Jost O. L. Wendt.

Finally, a deep thank you goes to my mother and my younger brother for family support and interest, as well as to my late father, to whom I dedicate this thesis.

Shortly after the Doctoral Defense:
My two opponents Prof. K.R.G. Hein (to the left) and Prof. J.O.L. Wendt on the right.

Havdrup, February 28, 2011
Flemming J. Frandsen

Table of content:

Chapter 1:

FIGHTING GLOBAL WARMING: BACKGROUND FOR THE THERMAL UTILIZATION OF STRAW

In November 2007, CO_2 concentration in the Earths atmosphere was about 384 parts per million per volume (ppmv), which is 100 ppmv (or 35 %) above the 1832 ice core levels of 284 ppmv. During the century running from 1905 to 2005, global surface temperature increased 0.74 ± 0.18 °C, causing the Intergovernmental Panel on Climate Change (IPCC) to conclude that 'most of the observed increase in globally averaged temperatures, since the mid-twentieth century very likely is due to the observed increase in anthropogenic greenhouse gas concentrations via an enhanced greenhouse effect [www.wikipedia.org, 'Global warming'].

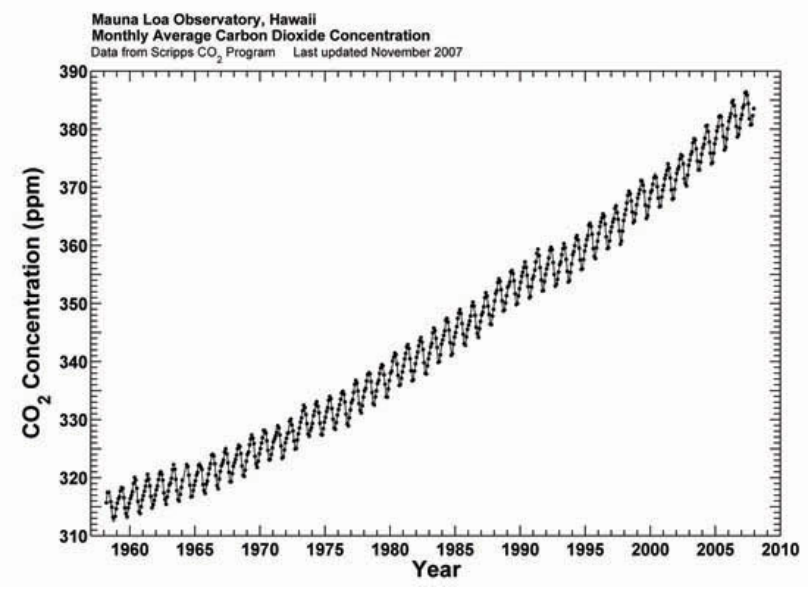

Figure 1-1: CO_2-level in the atmosphere from 1960 to 2007. It is evident that the level of CO_2 in the atmosphere has increased by ~ 20 % from 315 ppmv in 1960, to 385 ppmv in 2007. There is an annual fluctuation of about 3-9 ppmv in these measurements, roughly follo Northern Hemisphere growing season. The data originates from the Mauna Loa Observatory CO_2 Program.

Climate model projections indicate that average global surface temperature will most likely rise a further [1.1 – 6.4 °C] during the 21th century. Increasing global temperature is expected to cause sea levels to rise, increase the intensity of extreme weather events, bring significant changes to the amount and pattern of precipitation and most likely include an expansion of subtropical desert regions. Other expected effects include a decrease in agricultural yields, modifications of trade routes, glacier retreat, mass species extinctions, and an increase in the ranges of disease vectors [www.wikipedia.org, 'Global warming'].

1.1. The Greenhouse Effect

The greenhouse effect is the process by which the absorption and emission of infrared radiation by atmospheric gases, warm the lower atmosphere and surface of the Earth (see Figure 1-2).

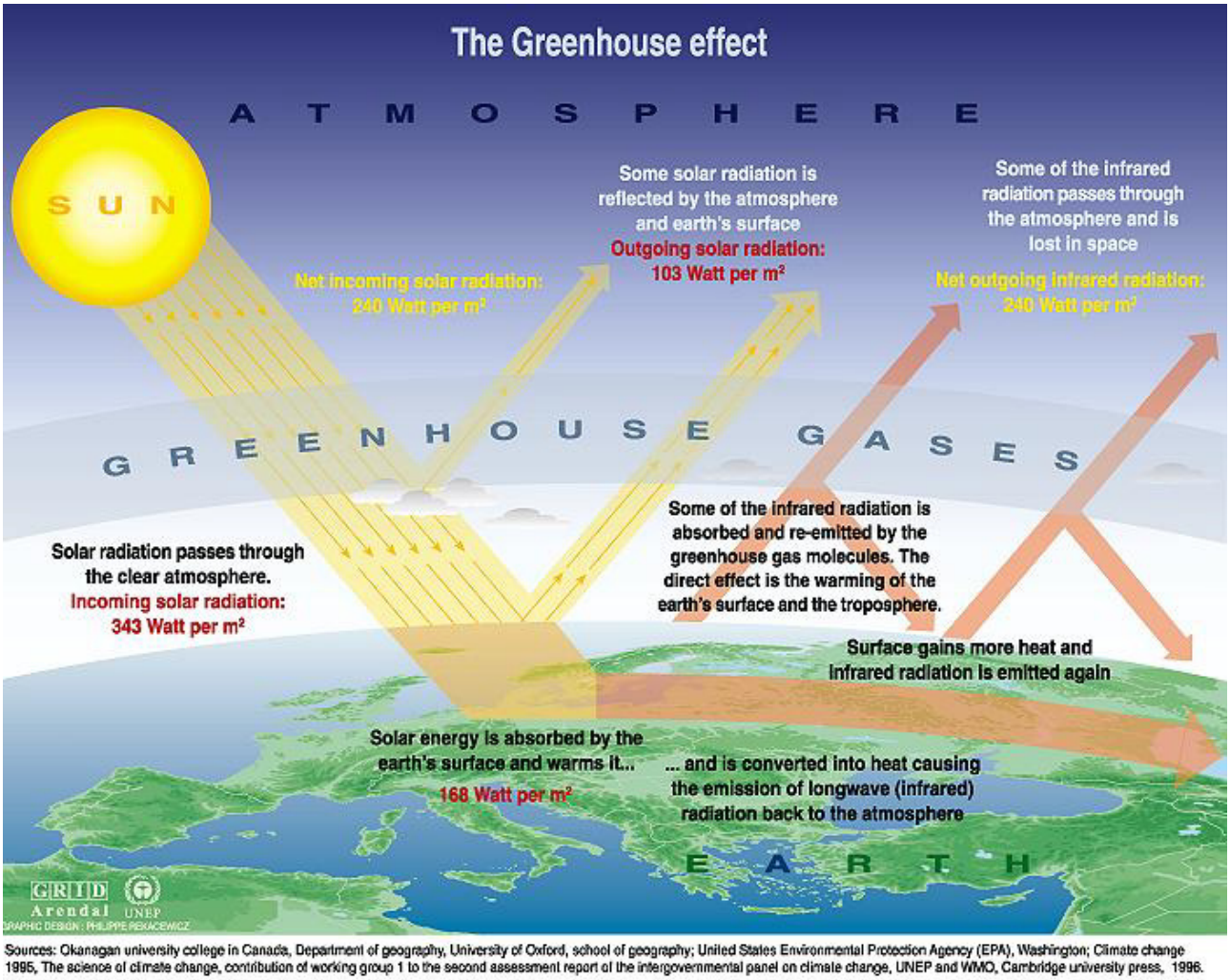

Figure 1-2: The principle of the green house gas effect.

The major greenhouse gases are H_2O, which causes about 36-70 % of the greenhouse effect (not including clouds), CO_2, which causes 9-26 %, CH_4, which causes 4-9 % and ozone (O_3), accounting for 3-7 % [www.wikipedia.org, 'Global warming']. Molecule for molecule, CH_4 is a more effective greenhouse gas than CO_2, but its concentration is much smaller meaning that its total radiative forcing is only about a quarter of that found with CO_2. Despite its relatively small concentration overall in the atmosphere, CO_2 is an important component of the Earth's atmosphere since it absorbs and emits infrared radiation, thereby playing a role in the greenhouse effect. Carbon dioxide is emitted into the atmosphere by a variety of natural sources, and over 95 % of the total CO_2-emissions would occur even if humans were not present on Earth. Fossil fuel burning has produced approximately 75 % of the increase in CO_2 from human activity, over the past 20 years (see Figure 1-1).

The level of CO_2 in the atmosphere and thereby the effect of global warming, is controlled by a delicate and sensitive balance between CO_2 produced for example by human beings and industrial activities, and CO_2 absorbed during photosynthesis or absorbed/released from seawater.

1.1.1. Formation and Emission of CO_2

Natural sources of atmospheric CO_2 include emissions from volcanic activity, combustion of organic matter and respiration processes of living aerobic organisms. In addition, it is also produced by various microorganisms through fermentation and cellular respiration. Man-made sources of CO_2 include the burning of fossil fuels for heating, power generation and transport, as well as some industrial processes such as cement production.

Combustion is a complex chemical reaction between a fuel and an oxidant. For a fuel – like oil, coal or biomass – composed of C, H, S, N, and perhaps some O, the net combustion reaction is:

$$C_\alpha H_\beta S_\gamma N_\delta O_\varphi . [H_2O]_\mu + \left(\alpha + \frac{\beta}{4} + \gamma + \frac{\delta}{2} + \frac{\varphi}{2}\right) O_2 \rightarrow \alpha CO_2 + \left(\frac{\beta}{2} + \mu\right) H_2O + \gamma SO_2 + \delta NO \quad (1\text{-}1)$$

Reaction (1-1) is an overall reaction, which may be divided into a number of sub-reactions as shown in Table 1-1.

Obviously, the first four reactions evolve heat, while the last reaction (evaporation of water) consumes some energy. This is the whole idea behind thermal fuel conversion, i.e. chemical

energy bound in the fuel is utilised for production of for example heat and power. In general, combustion of a solid fuel consists of three overlapping phases:

Reaction:	ΔH_R(25 °C) [kJ/mole]:
$C + O_2 \rightarrow CO_2$	-393.5
$C + ½O_2 \rightarrow CO$	-100.5
$CO + ½O_2 \rightarrow CO_2$	-283.0
$2\ H + ½O_2 \rightarrow H_2O(l)$	-241.8
$H_2O(l) \rightarrow H_2O(g)$	44.0

Table 1-1: Important sub-reactions in the thermal conversion of fuels.

- A heat-up/preheating phase, where the fuel is heated up, until combustible gases are released by thermal decomposition of the organic matrix of the fuel;
- Gas phase combustion of the gases released, and;
- Combustion of the residual solid fraction, i.e. char, by direct oxidation of the solid matrix by oxygen.

Direct combustion of fuels may in principle occur by fixed-bed firing on a grate, by fluidised bed combustion, or by (co-)firing in suspension. Each of these technologies poses different characteristics, and they are well-suited for fuels of quite different physical and chemical composition. In order to increase the total plant efficiency, most modern boilers produces both heat and power.

1.1.2. Absorption of CO_2 by Photosynthesis and the Earth's Oceans

Plants convert CO_2 to carbohydrates via photosynthesis, using energy from sun light and CO_2 to make triose phosphates (G3P), which are generally considered the first end-product of photosynthesis. It can be used as a source of metabolic energy, or combined and rearranged to form monosaccharide or disaccharide sugars, such as glucose or sucrose, respectively, which can then be transported to cells, stored as insoluble polysaccharides such as starch, or converted to structural carbohydrates, such as cellulose or glucans [www.wikipedia.org, 'Photosynthesis'].

A commonly used, slightly simplified equation, for photosynthesis is;

$$6CO_2 + 6H_2O + photons \rightarrow C_6H_{12}O_6 + 6O_2 \qquad (1\text{-}2)$$

Thus, photosynthesis may simply be defined as the conversion of light energy into chemical energy stored in plants. The rate of photosynthesis is affected by the concentration of CO_2 in the air, light intensity, and temperature [www.wikipedia.org, 'Photosynthesis'].

Another major player in controlling the delicate balance of CO_2 present in the atmosphere is the Earth's oceans, which contain CO_2 in the form of bicarbonate and carbonate ions. Bicarbonate is produced in reactions between cat ions from rock minerals, H_2O, and CO_2;

$$CaCO_3 + CO_2 + H_2O \rightarrow Ca^{2+} + 2HCO_3^- \qquad (1\text{-}3)$$

Reactions like eqn. (1-3) tend to buffer changes in atmospheric CO_2. However, since it produces an acidic compound, the pH of sea water decreases with an increase in CO_2-levels. The vast majority of CO_2 added to the atmosphere will eventually be absorbed by the oceans and become bicarbonate ion, but the process takes very long time ($\sim 10^2$ years) because most seawater rarely comes near the surface. As the oceans warm, CO_2 solubility in the surface waters decreases significantly.

1.2. Focus on Emissions from Heat and Power Producing Industries

As a result of the imbalance between released and consumed/absorbed CO_2, there has been a lot of focus on power production, as a major contributor of human produced CO_2 over the last couple of decades.

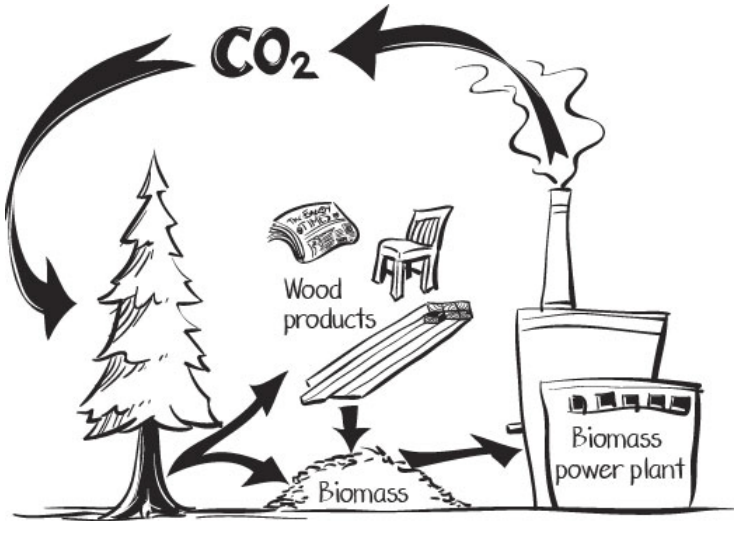

Figure 1-3: Part of the CO_2-cycle in the atmosphere. Carbon dioxide is emitted from combustion plants as a byproduct of power production, but could be consumed by biotic plants such as wood, straw or other biomasses, before being harvested and brought back to the biomass combustion plant, thereby closing the cycle.

The main question is whether it is possible to substitute some fossil fuels with fuels with a lower regeneration time, or whether we need new flue gas cleaning techniques in order to remove the CO_2 emission directly into the atmosphere. The principal role of power production is shown in Figure 1-3.

The basic idea of substituting fossil fuels by biomass is that biomasses have regeneration times in the order of [10^0-10^1 years], while the regeneration time of a bituminous coal seam may be in the order of [10^6 – 10^7 years]. Thus, CO_2 released by combustion of biomass will be re-consumed much more quickly by other plants via photosynthesis, compared to the time needed to regenerate a coal seam.

The history of fossil fuel based electricity generation shows that technology development, optimisation of the steam raising cycle, and fuel utilisation were major aspects of concern up to about the middle of the last century. These efforts led to a drastical reduction in specific fuel consumption from 3.5 tonnes coal equivalent (TCE)/MWh in 1885, down to less than 0.3 TCE/MWth today which – in turn – has resulted in a corresponding increase of total plant efficiency [Hein, 2008].

The rapid growth of the economies after World War II and the following increase in the demand for electricity led to new areas of concern, e.g. increasing unit size and capacity, plant up-scaling as well as availability improvements, in particular when utilising local fuels of variable quality. During 1960 to 1975, public electricity demand caused up-scaling of unit capacities and as a consequence, frequent unexpected outages of the boilers occurred and availabilities as low as < 70 % were experienced. Major causes for this were the formation of ash deposits on heat transfer surfaces in the radiative and convective sections of the combustion chamber and in the flue gas channel. Other problems frequently encountered were the erosion and corrosion of heat transfer equipment [Hein, 2008].

The US Clean Air Act of 1990 changed the way utilities burn coal. After 1990, utilities introduced scrubbers, low-NOx burners, fuel switching and fuel blending, just to name a few changes. The Clean Air Act Amendments also changed the way utilities did business, as they were now looking to buy and sell emission credits, which could be tied to fuel purchases and fuel contracts.

Fuel engineers were now not only concerned about how to burn the fuel, but also deeply concerned about slagging, fouling, corrosion and erosion in boilers. Utilities now looked not only for the heating value [MJ/kg] of a fuel but also on ash chemistry, grindability and proximate and ultimate analysis, especially the content of volatile N, S and Cl. Many utilities were not geared for this and did not have the people and expertise necessary for all the studies and evaluation that now had to be undertaken.

The behaviour of inorganic materials has always been recognised as one of the major factors affecting the design and operation of boilers that burn ash-producing fuels. The practical problems associated with ash behaviour may range from major slag falls damaging the bottom of a furnace to complete plugging of conventional passes. These issues result in loss of availability, over-designed systems, derating, or excessive maintenance. The ASME Research Committee on Corrosion and Deposits from Combustion Gases completed in the mid-1990s a status paper that estimated the total annual cost of ash-related problems in US-boilers at $ 1-3 billion/year. Clearly, ash-related problems in boilers represent an economic issue of national and international scope and importance.

In addition to changes in boiler operation caused by increasing demands, a liberalisation of the energy market was suggested in the mid-1990s. Utility operations up to 1995 placed major focus on the reliability of thermal fuel conversion systems. Government regulatory boards and utilities cooperated to establish practices that best served the public, and in many cases both bodies saw reliability as a more important consideration than economics. However, after 1995, many governments believed that electrical power rates could be lowered if the utility monopoly structure were replaced by a deregulated, free market structure of power generation. The United Kingdom demonstrated such price reductions, and the State of California was leading the US into similar practices. But, the economic benefits of deregulation cannot be achieved without changes in operation, including boiler operation, and fuel selection.

The environmental aspect of power production came into focus at the United Nations (UN) Climate Change Conference in Kyoto, Japan, in December 1997, were emission of greenhouse gases was the major issue. For the first time ever, legally binding emission reduction target levels for greenhouse gases were established worldwide. According to the Kyoto Agreement, total emissions must be reduced by 5.2 % by the year 2012.

The European Union, launched its RES-e directive in 2001, aiming at increasing the share of green electricity for the EU25, from 14 % to 21 % in 2010. Later, in 2005, the EU Biomass Action Plan was launched, aiming specifically at doubling biomass use by 2010.

In March 2007, a new EU Energy & Climate Change Package was launched, in which the Commission intended to maintain the EU's position as a world leader in renewable energy, by proposing a binding target of 20% of its overall energy mix to be sourced from renewable energy by 2020.

1.3. Danish Energy Policy and History

The Danish energy supply has been and still is covered mainly by utilization of fossil fuels such as coal and oil. Figure 1-4 shows that the proportion of natural gas and sustainable energy

sources utilized for energy production increased significantly on behalf of especially coal, but also oil, in the years 1980 – 2006.

Late in the 1960s, a public debate on the environmental consequences of energy production began in Denmark. The authorities were unprepared for this debate, due to the lack of a central base of know how on these issues.

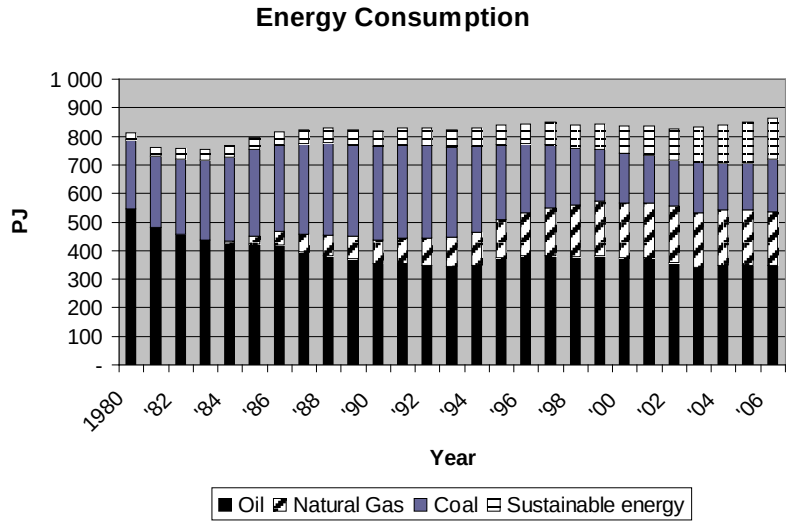

Figure 1-4: The Danish energy consumption in [PJ/year] during the period 1980 – 2006. Source: [ENS, 2008].

Therefore, in 1972, a new and independent government department on pollution control was founded. In 1974, this public organ turned into the Department of Environmental Protection [ENS, 2006].

The global oil crisis in 1973 emphasised that the energy supply was too uniform, and far too dependent on Middle Eastern-sourced oil. As a consequence, a critical evaluation of the energy supply was initiated, which led to the first Danish Energy Plan in 1976, designed to insure Denmark against fuel-supply crises similar to that experienced worldwide in 1973. The plan contained the suggestion of coal, natural gas and uranium, as the main energy sources for the country, and provided the first public funding of research and development of for example wind mills [CBT, 1998].

Later, in 1979, energy supply got its own government department, the Department of Energy [ENS, 2006]. In 1981 a second energy plan, Energi-plan 81, addressed the importance of socio-economic and environmental aspects, emphasising the need to reduce dependence on imported fossil fuels. Throughout the 1980s, oil and gas production in the North Sea was heavily extended, and a nation-wide natural gas distribution net was established (the effect of which is rather obvious in Figure 1-4, after 1986). In addition, the first subsidy schemes for the utilisation of straw and wood chips were implemented via increased taxes on fossil fuels (oil and coal), thereby making biomass competitive as a fuel [CBT, 1998].

A third energy plan, Energi 2000, was released in 1990 [CBT, 1998]. This plan was an ambitious attempt to increase the use of environmentally desirable fuels, defined at that time as natural gas, solar heat, wind, and biomass (straw, wood, liquid manure, and household waste). The ambitious objectives of Energy 2000 were, that based on 1988, in 2005, Denmark should achieve the following aims [CBT, 1998]:

- Reduce total energy consumption by 15 %;
- Increase the consumption of natural gas by 170 %;
- Increase the consumption of renewable energy by 100 %;
- Reduce the consumption of coal by 45 %;
- Reduce the consumption of oil by 40 %;
- Reduce CO_2-emission by not less than 20 %;
- Reduce SO_2-emission by 60 %, and;
- Reduce NO_X-emission by 50 %.

These objectives were attempted by means of energy saving, tax on CO_2-emissions, conversion to more environmentally friendly fuels by CHP generation, subsidised schemes for the construction and operation of district heating systems, and financial support for the establishing of biomass boilers in rural districts, to name just a few.

In order to ensure the achievement of the targets defined in Energy 2000, the government, the Conservative Party, the Liberal Party, and the Socialists Peoples Party, signed an agreement on June 14, 1993, on an increased use of biomass in the country's energy supply, stipulating that the power utilities must burn 1.4 Mtons of straw and wood chips per year, corresponding to approximately 20 PJ/year [CBT, 1998].

In 1993/94, the Department of Environmental Protection and the Department of Energy Supply were merged into the Department of Environment and Energy [ENS, 2006].

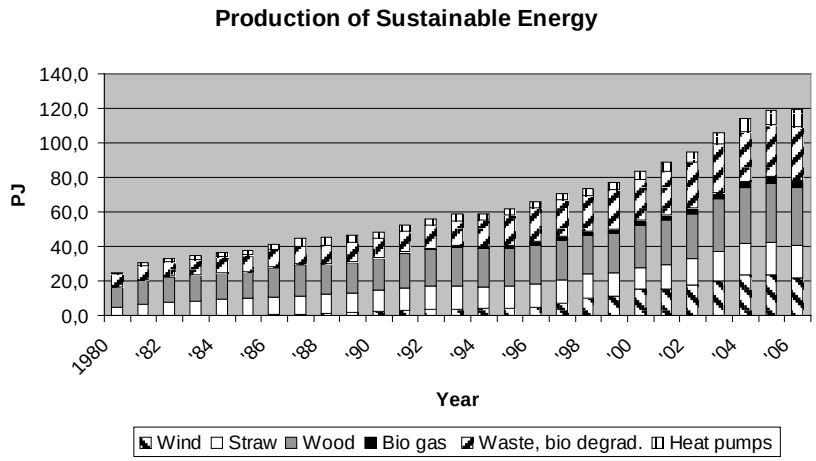

Figure 1-5: Production of energy in Denmark [in PJ/year], based on sustainable energy sources in the period 1980 – 2005. Source: [ENS, 2006].

The national energy plan, Energi 21, focussed from 1996 on the reduction of greenhouse gases. The important purpose of Energi 21 was to ensure that Denmark reduced its CO_2-emissions by 20 % by the end of 2005, compared to the 1988-level, and that emissions by the end of 2000 should be stabilised to under 1990-levels [CBT, 1998].

In Figure 1-5, the Danish production of energy in the period 1980 – 2005, based on sustainable energy sources is shown. It is evident that the share of wind, straw, wood, and biodegradable waste has increased over the actual period.

As a consequence of Danish and international energy policy during the last 30-35 years, several full-scale measuring campaigns have been conducted in order to investigate the thermal conversion and utilisation of straw for heat and power production - either in dedicated, straw-fired plants - or in conjunction with coal in PF boilers. Before we address the several different measuring campaigns on straw-fired plant, a brief introduction to the 'mother road' between incombustibles in a burning straw particle, and troublesome deposits on a heat transfer surface is outlined, below.

1.4. Operational Problems in the Thermal Conversion of Straw

The main route between a burning straw particle and troublesome deposits on a heat transfer surface can be divided into a number of consequetive steps:

- Release of critical ash forming elements (mainly K, S, and Cl) during heat-up, pyrolysis, and subsequent char burnout of the straw.
- Formation of aerosols by nucleation and coagulation of flame-volatilised elements, and formation and entrainment of residual ash (during char burnout).
- Transport of the different ash forming species, such as gases, liquids (droplets) and solids (particles), from the bulk gas to heat transfer surfaces, and adhesion of these ash species to the heat transfer surfaces.
- Build-up, sintering (consolidation) and shedding of deposits.

1.4.1. Release of Inorganics from Straw

In general, the inorganic fraction (incombustibles) in solid fuels can be present as either [1)] simple salts dissolved in pore water, [2)] organically bound, or, particularly in coal, [3)] as mineral inclusions (see Figure 1-6). In the organic phase, inorganic material is usually associated with oxygen-containing functional groups such as carboxylic acids. In the mineral phase, commonly

present in coal, inorganics are present mainly as Si-rich phases, clay minerals or Ca- or Fe-minerals/species.

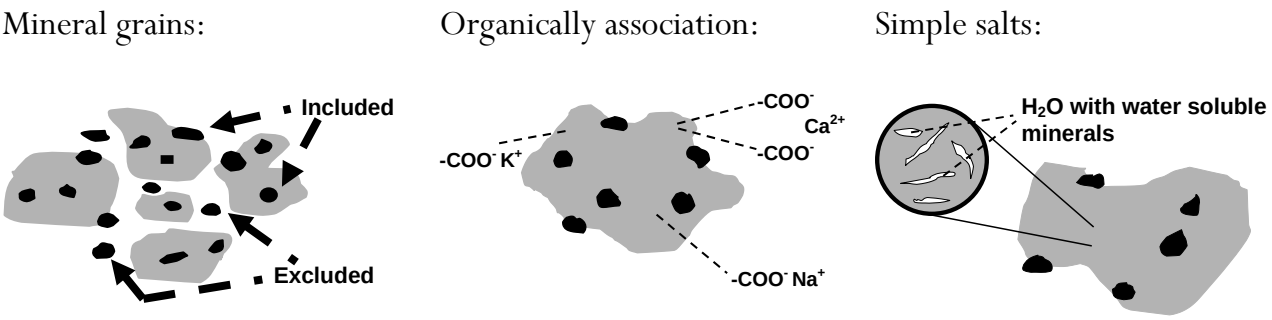

Figure 1-6: Types of inorganic metal association in solid fuels. Source: Reproduced after [Benson et al., 1993].

When introduced into a hot furnace, a fuel particle is heated, and undergoes a series of chemical and physical transformations. Initially, water evaporates, followed by devolatilisation and pyrolysis, where volatile compounds are released into the gas phase from the organic matrix of the fuel during its thermal degradation. Subsequently, the remaining char burns away (see Figure 1-7). A single fuel particle may generate more than one ash particle due to fragmentation processes going on.

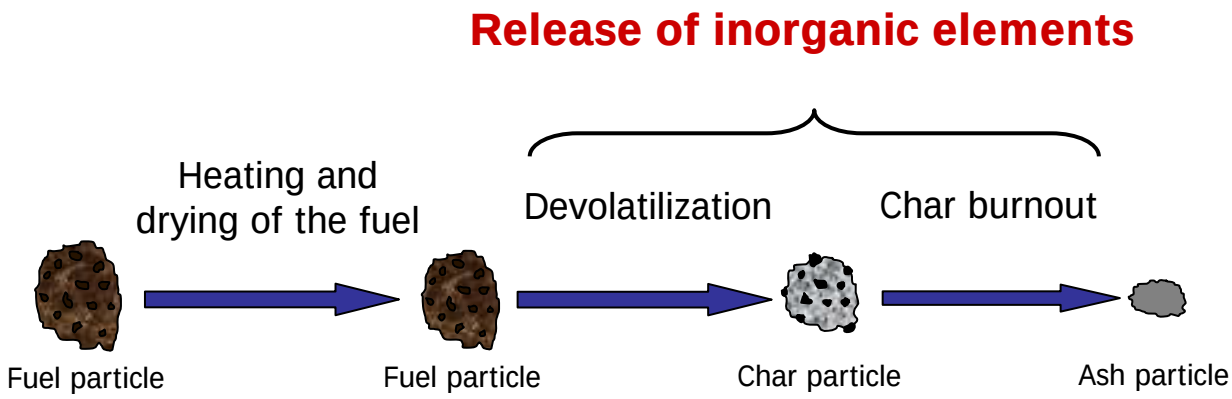

Figure 1-7: Principal sketch of the progress of the thermal conversion of a fuel particle.

Chlorine, Cl, and part of the S and K in straw are released into the gas phase in the combustion zone, where S will be present mainly as $SO_2(g)$, K as KCl(g) and KOH(g), and Cl as KCl(g) and/or HCl(g). The ratios of Si/K respectively (Cl+2S)/K controls the formation and stability of solid, non-volatile phases like K silicates and/or K_2SO_4. Gaseous K-species in the flame may react with fly ash particles or other components in the gas phase, thereby forming, for example K_2SO_4.

1.4.2. Formation of Fly Ash and Aerosols

The inorganic proportion of a fuel undergoes several complex chemical and physical transformations during devolatilisation/pyrolysis, and char burnout. Intermediate ash species including gases, liquids, and solids are formed, the size and composition of which, affect their subsequent behaviour. Residual ash formed may be divided into bottom ash and fly ash, in a ratio depending mainly on the furnace design, and the size and density of the residual ash particles. In grate-fired units, the major part of the residual ash ends up as bottom ash (approximately 70-95%) whereas in PF-fired boilers, fly ash constitutes the main part of the ash (80-95%). Fly ash is entrained down through the flue gas channel, where it may deposit on heat transfer surfaces. The flue gas is cooled as it passes through the boiler, i.e. it may become supersaturated, and e.g. K-species may condense, either heterogeneously on fly ash particles or heat transfer surfaces or, homogeneously, as submicron (aerosol) particles.

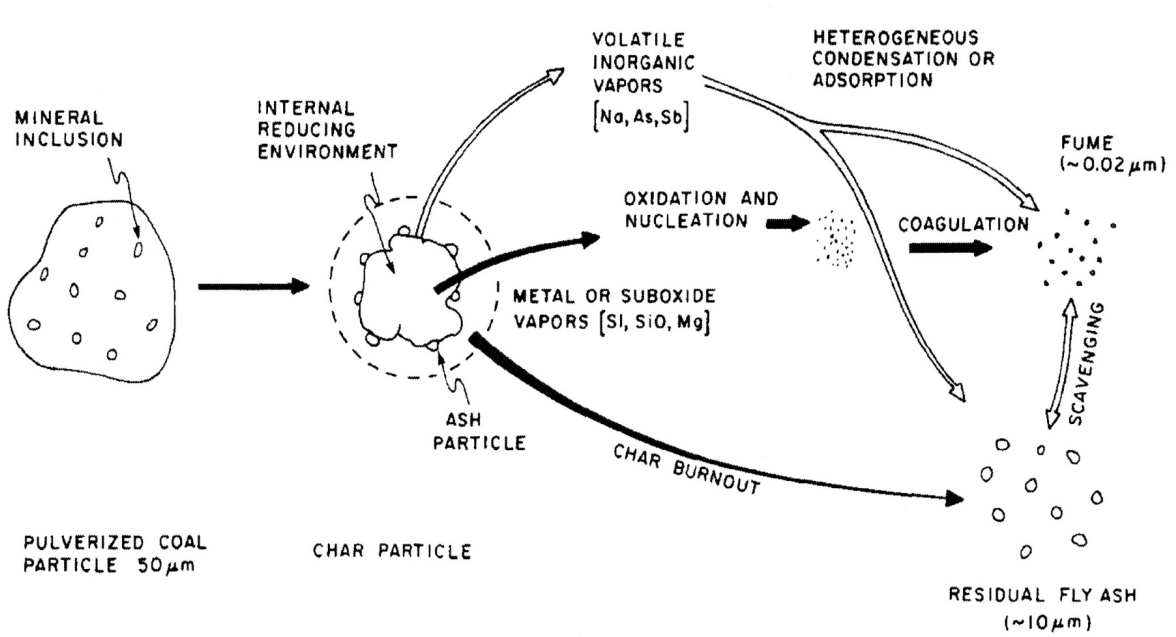

Figure 1-8: Major transformation routes from a burning solid fuel to a fly ash particle size distribution. Source: [Haynes et al., 1982].

Fly ash formation has through several decades been intensively studied for coal combustion, where it has at least a bimodal size distribution (see Figure 1-8). The larger particles originate from mineral grains in the coal, and their size distribution depends upon the characteristics of the actual coal and pretreatment of the coal as well as the actual combustion conditions [Benson et al., 1993; Bryers, 1996]. On the contraty, the submicron particles originate from homogeneous nucleation and the subsequent coagulation of flame-volatilised inorganic species (see Figure 1-8).

The behaviour of inorganics in straw can be compared to that in coal. Straw, however, contain large quantities of the flame-volatile elements, K, S and Cl, which means that the formation of submicron particles will be more pronounced in straw-fired boilers. [Christensen, 1995; Christensen et al., 1998] measured relatively high mass loadings (i.e. the mass of aerosols per unit gas volume) of submicron particles [75 - 2000 mg/Nm^3], consisting primarily of KCl and K_2SO_4, from grate-fired units burning different types of straw, while aerosol measurements at the Midtkraft-Studstrup PF boiler, showed aerosol mass loadings in the range [30 - 110 mg/Nm^3], during the co-firing of coal and straw.

How are these submicron aerosols formed ? In the furnace, K, S and Cl are released and a certain content of KCl is formed. When reaching the superheater section(s), the flue gas cools and KCl starts to react with SO_2 forming K_2SO_4. In case of rapid cooling or if there is not enough surface available for the heterogeneous condensation of all the KCl and K_2SO_4 formed, then there will be an excess of these molecules in the gas phase, forming clusters (i.e. groups of molecules), which, if they pass a certain critical size, form a new microscopic phase (i.e. extremely tiny particles) in the gas, by homogeneous nucleation.

Theoretical calculations by [Christensen, 1995; Christensen et al., 1998], showed that the formation of aerosols was initiated by the homogeneous nucleation of K_2SO_4, occuring in the temperature range 650 - 900 °C. The exact location of the nucleation temperature window depends on the elemental composition of the actual fuel. The particles grow subsequently by coagulation and heterogeneous condensation of K_2SO_4 and KCl. The recovery fractions of K, S and Cl, in the aerosols from straw firing on a grate, were found experimentally to be 4 – 32 % for K, 21 – 63 % for Cl, and 3 – 45 % for S [Christensen, 1995; Christensen et al., 1998]. The size distribution showed a distinct submicron peak with a mean diameter in the range of 0.15 - 0.36 μm.

This is how combustion aerosols are formed in straw-fired systems.

1.4.3. Transport of Ash Species, Adhesion and Build-Up of Deposits

Three main mechanisms by which ash species are transported to deposit surfaces are active in combustion systems; [1)] inertial impaction, [2)] thermophoresis and [3)] diffusion, followed by condensation of gaseous species. These mechanisms take place in combination, often starting with a thin, porous layer of condensed matter formed by diffusion and subsequent condensation, and then an accelerated growth caused by thermoforesis, and in particular by inertial impaction of the bigger fly ash particles.

Slagging deposit: Fouling deposit:

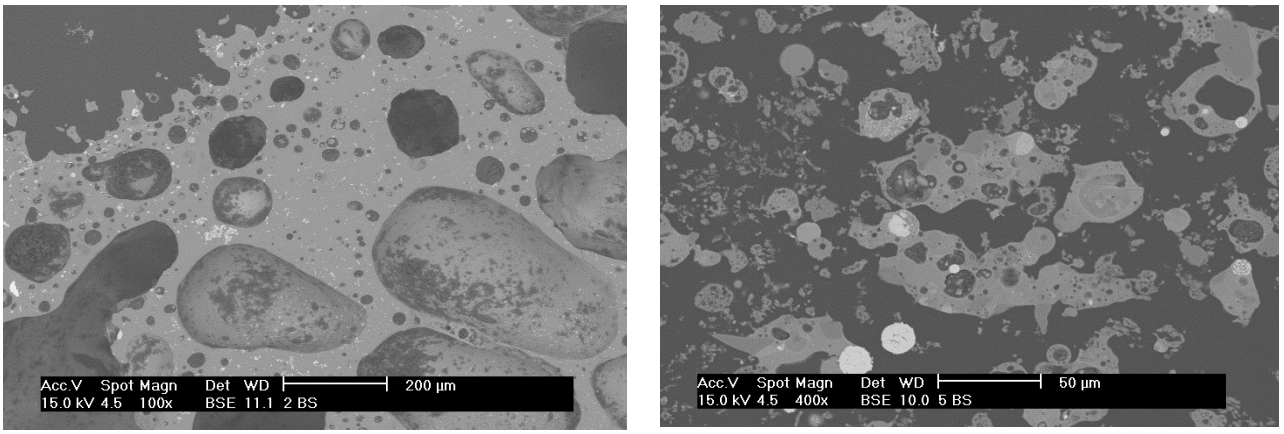

Figure 1-9: The internal texture of a slagging (left image) and a fouling deposit (right image) respectively. Notice that in the slag, the porosity shows up as rather big hollow gas pockets, while in the fouling deposit, the porosity constitute the gas in which sintered ash particles are present. No individual fly ash particles can be identified in the slagging deposit.

Deposits formed in utility boilers, may (roughly speaking) be divided into either slagging or fouling (see Figure 1-9):

- Slagging deposits occur in the combustion or furnace zone, where the flame is visible, the temperature is high, and radiant heat transfer is dominant. These deposits often consist of an inner powdery layer, covered by a molten or partly molten ash layer, chemically dominated by silicate and alkali species.
- Fouling deposits occur in the convective pass of boilers. They consist of sintered fly ash particles, and condensed flame-volatile species, and are usually loosely bonded. These deposits consist of an inner layer, rich in flame-volatilised species (often alkali salts) which provides a sticky surface for trapping inertially impacting, non-sticky particles.

Several studies on deposit formation and corrosion in straw-fired boilers are available either on the web or in the literature. In 1995, the first main contribution to the understanding of inorganics and deposition problems in straw-fired boilers was published [Miles et al., 1994, 1996; Baxter et al., 1996], and in the period 1993 - 2007, a number of full-scale investigations of ash and deposit formation, and corrosion, during straw utilisation for combined heat and power (CHP) production, has been carried out in Denmark.

[Jensen et al., 1997; Michelsen et al., 1998; Hansen et al., 2000] reported deposition probe and mature deposit studies from burning of cereal straws in four grate-fired CHP boilers; Haslev, Slagelse, Rudkøbing and Masnedø. The superheater deposits were shown to have a composition similar to fly ash, i.e. rich in K and Cl, whereas the furnace deposit was also rich

in Si and Ca. Furthermore, deposition fluxes in the superheater region were reported to correlate with aerosol concentration, which again correlated with the K-content in the fuel [Jensen et al., 1997]. An outline of this is provided in Chapter 4 of this thesis.

[Junker, 1997; Andersen, 1998] provided an outline of the consequences of co-firing of coal and straw in the full-scale Midtkraft-Studstrup PF-boiler from an ash and deposit formation point-of-view. Subsequently, large measuring campaigns have been conducted at the Studstrup Power Station, Unit 4, and at the Funen Power Station, Unit 3. An outline of two pioneering studies [Junker, 1997; Andersen, 1998] as well as data from other coal-straw co-firing campaigns [Sander and Wieck-Hansen, 2005; Overgaard et al., 2004], is provided in Chapter 5 of this thesis.

[Robinson et al., 1998; Junker et al., 1997], [Nielsen, 1998; Nielsen et al., 2000a; Theis et al., 2006a-c] and [Zheng et al., 2007] investigated deposit formation and alkali ash transformations and correlated the deposit Cl-content to the feedstock alkali-sulphur ratio, through experiments with a variety of coal and straw blends tested either in the Sandia Multifuel Combustor, the University of Toronto entrained flow reactor, or the CHEC entrained-flow reactor. Further details on these pilot-scale studies of co-firing are provided in Chapter 6.

1.4.4. Gas Phase K-S-Cl Chemistry

The sulphation of KCl is important in relation to aerosol formation, deposition and corrosion, as well as to the emission of acidic species, mainly SO_2 and HCl. During flue gas cooling, KCl may react with SO_2, and form K_2SO_4 according to the reaction:

$$2KCl + H_2O + SO_2 + ½O_2 \rightarrow K_2SO_4 + 2HCl \qquad (1\text{-}4)$$

The above *sulphation*-reaction may take place either by means of SO_2(g) and O_2(g), or by direct reaction with SO_3(g). If water is present in the system, HCl(g) will be the gaseous product of the sulphation reaction, otherwise it will be Cl_2(g).

There is still disagreement in the research community on whether K_2SO_4 will be formed in the gas phase, and subsequently condense on the heat transfer surfaces, or as aerosol particles, or whether KCl or KOH are deposited, followed by a subsequent sulphation of these within deposits.

Further details on and an outline of K-S-Cl chemistry and aerosol formation is provided in Chapter 7 of this thesis.

1.4.5. Corrosion in Straw-Fired Boilers

The nature of corrosive attacks observed on deposition probes exposed to flue gases from straw combustion, indicates that corrosion may be caused by gaseous chlorine, a mechanism quite well documented in the literature [Nielsen, 1998]. Chlorine may penetrate and destroy the oxide scale through cracks and pores, react with Cr and Fe at the metal-oxide scale interface, and thereby form volatile metal chlorides of Fe and Cr. Metal chlorides diffuse back through the oxide scale and form metal oxides in regions where the partial pressure of O_2 is higher, e.g. at the surface of the oxide scale. The result is the formation of a loose, non-protective oxide scale.

In order to keep corrosion rates at a reasonably low level, the final steam temperature in, say, dedicated straw-fired units are usually kept below 520 °C, which causes a relatively low electrical efficiency (24-26 %) when firing straw on a grate.

An outline of recent corrosion studies at plants (co-)fired with straw as well as research activities on this issue is outlined in Chapter 8 of this thesis.

1.4.6. Use of additives in Power Boilers

An often applied option to minimize deposition and/or corrosion is injection of an additive. Basically, two types of additives are available: [a)] one which will affect the gas phase alkali-S-Cl- and thereby the aerosol-chemistry in the system, or [b)] one that is depositing on the heat transfer surfaces together with fly ash particles, but posses chemical and physical characteristics inhibiting the sintering of the deposit. The first type of additive is particularly useful in systems fired with straw, where the initial deposit process is caused mainly by volatile alkali Cl- and S-species. The use of an additive in such systems may fix these volatile alkali species or affect the gas phase K-Cl-S chemistry and, thereby, the aerosol formation and ash deposition process significantly.

Several additive tests in full-scale, and in the CHEC entrained flow reactor have been conducted, and are outlined in Chapter 9 of this thesis.

1.4.7. Shedding of Deposits

Effective deposit removal is very important, in order to insure maximum boiler thermal efficiency and availability. Deposit shedding may be caused artificially as a part of the boiler operation, e.g. by soot blowing, or naturally, without any operational or mechanical influence. Mechanisms of natural shedding include [Zbogar et al., 2009]: [1)] erosion, [2)] gravity shedding,

and, [3] thermal shock. Erosion is the process of removing a sintered deposit by impacting SiO_2-rich fly ash particles. Gravity shedding occurs when the gravity force on a deposit is big enough to cause [1] a break inside the deposit, or, [2] flow of molten phases inside or along the surface of a deposit. A break inside a deposit will occur when the gravity force on the deposit piece is large compare to [1] the force holding the deposit together (deposit strength), or [2] the force adhering the deposit to the tube (adhesion) [Zbogar et al., 2009]. Melting can be considered as a type of gravity shedding, where by gravitational force acts on molten phases in a deposit, forcing it to flow down the heat transfer surfaces. Thermal shock-induced shedding is caused by temperature changes, due to the difference in the thermal expansion coefficients of tubes and deposits. A sudden temperature gradient (due to fluctuations of the flue gas- or steam temperature), may cause an uneven expansion of the [1] deposit and tube, or, [2] distinct, adjacent, deposit layers, leading to deposit fractures [Zbogar et al., 2009].

The dominating mechanism of shedding will depend on the deposit characteristics, as well as on the conditions inside the boiler. The deposit composition will directly influence deposit strength, the melting of the deposit, and thermal expansion, i.e. all the physical properties which will affect the shedding mechanisms. Flue gas temperature will influence the deposit surface temperature, and thereby the temperature-profile inside the deposit. This will again influence the above mentioned deposit properties as well as the physical state of the deposit [Zbogar et al., 2009].

Chapter 10 of this thesis outlines Danish activities on shedding of ash deposits in straw-fired boilers.

1.5. The Scope and Background of this Thesis

This thesis contains an outline of Danish experiences on utilisation of straw for heat and power production, seen mainly in relation to research activities within the CHEC Research Centre at the Department of Chemical and Biochemical Engineering at the Technical University of Denmark, 1991 to 2009. Focus is on ash and deposit formation and corrosion.

I have outlined the major findings on ash deposition and corrosion in grate-fired units, during co-firing in PF-fired suspension-boilers, and, finally, in pilot-scale facilities. Further details are available in Chapters 4-6. The main conclusion is that, in grate-fired units, utilisation of straw will cause problems if the steam temperature is kept too high. On the other hand, straw may be co-fired with coal, which is fully manageable from a deposition and corrosion point of view, provided that the coal co-fired is of high quality, i.e. contain a certain amount of alumino-silicates in its ash. Al-silicates from the coal ash will react with the K originating from the strawand release Cl as HCl, which are not nearly as harmful at high temperatures as when KCl(s) is deposited directly on the heat transfer surfaces. A change in the regulation on the

quality of the fly ash allowed for cement and concrete production has moved the main obstacle for coal-straw co-firing as a means of utilising straw for energy production in high-efficiency suspensions fired units. Now, only the potential problem of the poisoning of SCR-catalysts by K-species from the straw, remain to be solved.

I have also tried to connect the release of K, S, and Cl, gas phase chemical kinetics and physical transformations to aerosol formation. This is outlined in Chapter 7 of the thesis. In this context, Si/K and the Cl/K ratios play a major role in the release, although working in opposite directions. A high Si/K ratio indicates formation of non-volatile K silicates, while a high Cl/K ratio works in the opposite direction, indicating increased volatilization of K, through interactions with Cl. Also, the secondary capture of K, either by char or by active Ca-Si-rich ashes in the char structure, has been addressed. For the deposits, the Cl/S ratio in the fuel is very important, since the data presented in this thesis indicates that a high Cl/S in the fuel will cause a high Cl-level in the deposits, while an excess of S will cause the deposit chemistry to shift toward the less harmless K sulphate.

A detailed study of the link between fuel and aerosol chemistry in grate-fired units, indicated that fuel chemistry is controlling for aerosol mass loading and chemistry, at least when comparing different fuels in the same plant, see Chapter 8 for further details.

Concerning corrosion and material aspects in plants (co-)fired with straw, the data generated in Denmark during the last two decades are in line with deposition investigations, indicating potential severe corrosion in dedicated straw-fired plants (grates) but somewhat lower corrosion when co-firing straw with coal in suspension boilers. This is outlined in Chapter 9.

Chapter 10, deals with the application of additives for minimising aerosol formation and/or Cl-content in straw-fired boilers. A clear effect of additives on the aerosol mass loading and chemistry was shown at the straw-fired Avedøre Power Station, Unit 2, while test-firing in the CHEC-EFR (entrained flow reactor) indicated also that the deposit chemistry may be affected strongly by the choice of additive. The best choice for additive is and Al-Si – based material which will act in basically the same way as the coal ash in coal-straw co-fired systems.

Finally, Chapter 11 deals with deposit shedding, where we have been able to quantify the mass gain of deposit as well as heat-uptake in the probe via an intelligent new shedding probe design. The data from the shedding probe have been applied to take the modelling of deposit build-up and shedding to a whole new level of understanding and quantification.

Chapter 2:

COAL AND STRAW AS FUELS

As indicated in Chapter 1, straw may be fired either alone, in small-scale (< 100 MW_{th}) dedicated, grate-fired plants, or in conjunction with coal, in bigger suspension- or fluid bed-fired systems (> 100 MW_{th}). In order to understand the physical and chemical processes going on during the thermal conversion of coal and straw, this chapter outlines different fundamental and advanced fuel and ash characterisation methods, followed by an introduction to the chemical and physical characteristics of the fuels themselves.

2.1. Methods of Characterisation of Fuels and Ashes

It is common to report the composition of a fuel by two different standard analyses:

- A proximate analysis, including total moisture, volatile matter, ash and fixed carbon content in the fuel, and;
- An ultimate analysis, providing the elemental composition of the fuel, including the content of C, H, N, S, O (by difference), and (occassionally) Cl, in the fuel.

Concerning the parameters reported in the proximate analysis;

- Moisture (water) is usually present in cracks, fissures, crevices, and large pores of the fuel.
- Volatile matter consists of hydrocarbons, and other gases released during devolatilisation and thermal decomposition of the fuel. The main constituents of the volatile matter include H_2, O_2, CO, CH_4, H_2O, and C_XH_Y, but may vary greatly by fuel type.
- Fixed carbon is the combustible residue left after the release of volatile matter. It is not pure C, but usually contains small amounts of H, O, S and N. The fixed carbon in a proximate analysis is calculated by difference using the percentages of moisture, volatile matter, and ash from the proximate analysis.
- Ash is the non-combustible residue left after complete combustion of the fuel.

For each of the parameters in the proximate respectively the ultimate analyses, several different standard procedures are developed for its determination. For example (Australian) AS, (British) BS, (German) DIN, and (American) ASTM standards are available for the determination of the total moisture content in a fuel etc.

Usually, in addition to the proximate and ultimate analyses, the higher or lower heating value of the fuel is also determined. For coal, occassionally a speciation of sulphur on sulphatic, pyritic and organic forms is provided.

If the focus is on ash related issues such as fly ash quality, ash deposition or corrosion, usually a sample of the fuel is burned under controlled conditions, i.e. known atmosphere and temperature, and the resulting ash is then investigated for:

- Its chemical (bulk) composition, and;
- Its softening/melting behaviour (ash fusion) during heating in either an oxidising or a reducing atmosphere.

Standard analyses are usually supplied for a fuel. Nevertheless, in addition to these, a number of advanced analytical techniques may also be applied in order to investigate either a raw fuel or its ash behaviour, including:

- Scanning Electron Microscopic (SEM) analysis of the fuel and/or ash
- Simultaneous Thermal Analysis (STA) of the fuel and/or ash
- Investigation of viscosity vs. temperature of the ash
- Chemical fractionation analysis of the fuel

During the past 15 years, the CHEC Research Centre has contributed significantly to the development of STA and SEM-investigations of fuels and ashes. Below, is an outline of first how to produce reliable ash from a fuel sample, followed by a description of the development and application of SEM and STA for fuel and ash analyses. The investigation and measurement of ash viscosities will not be considered no further here, so the reader is referred to [Vargas et al., 2001; Vargas, 2001] for further details on this important ash analytical technique. Similarly, further details on chemical fractionation analyses can be found in [Zevenhoven, 2001].

2.1.1. Ashing of Fuels

In principle, the determination methods used for coal may also apply to biomass (including straw). However, due to the frequent organic association in straw via the bonding of inorganic species to O-containing functional groups, and the significant presence of simple inorganic salts,

it is necessary to prepare laboratory ash from straw, at a lower temperature than for coal, in order to prevent volatilisation, and chemical transformation of the inorganics in straw.

The most commonly applied method for characterising the inorganic matter of a fuel involves ashing of the fuel at high temperature, followed by elemental analysis. High-temperature ashing (HTA) is applied to produce ash from coal, following one of several available standard procedures (e.g. via ASTM D3172-89, DIN-51718, DIN-51719). The coal sample is crushed and dried in an oven at 105-110 °C, to a constant weight, in order to determine its residual moisture. The sample is then heated in a closed crucible (in order to prevent oxidation) at 815 °C to constant weight. Weight loss is caused by the release of volatile matter from the sample. The remaining sample is then placed in an oven at 750 °C with access to oxygen, causing the sample to burn. The weight loss during this treatment is equal to the amount of fixed carbon in the sample.

Nonetheless, the ashing procedure was adapted for biomass, since it was recognised that alkalis especially could be partly evaporated at the high standard ashing temperature, for straw, so the proximate analysis is now limited to 550 °C [Borman and Ragland, 1998].

[Llorente and García, 2006] conducted an investigation in order to study the effect of ashing temperature on the amount and concentration of elements in ashes from batches of four well-defined herbaceous biomasses: thistle (Cynara cardunculus), wheat straw, pine and poplar chips. Those four biomasses were combusted under controlled laboratory conditions at 400, 500, 550, 600 and 800 °C.

In Figure 2-1, the content of CO_2 respectively ash is plotted (on a dry base) as a function of the ashing temperature for the four biomasses investigated by [Llorente and García, 2006].

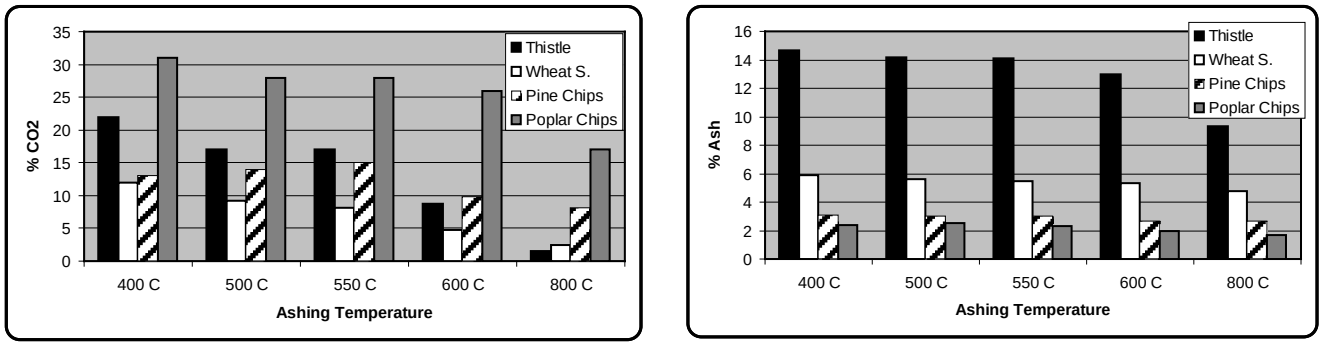

Figure 2-1: The content of CO_2 respectively ash in biomass on a dry base, as a function of the ashing temperature for four herbaceous biomasses. Source: [Llorente and García, 2006]

From Figure 2-1, it is evident that too high a temperature of ashing for a biomass sample may affect and modify the composition of the sample seriously. Thus, one will get a false image of the actual ash chemistry of a fuel if the ashifying is conducted at a two high temperature.

The results presented by [Llorente and García, 2006] indicate that the concentration of the elements K, Na, S and Cl is also affected seriously by the ashing temperature. The higher the ashing temperature, the lower the content of the crucial elements, due to evaporation from the sample. This correlates well with our studies of release of critical ash-forming elements from biomass fuels [Knudsen, 2004; van Lith, 2005].

In order to eliminate the risk of partial evaporation of inorganic constituents altogether, ICP-AES analysis is applied to the fuel more directly, without prior ashing. This procedure requires wet digestion of the biomass, for which optimised solvents and sequences have been defined. Typically, the results are expressed as mg/kg fuel.

As most of the elements are converted into their respective oxides, the resulting elemental composition is usually represented on an oxide basis, which is rather convenient, since the sum of an oxide analysis often approaches 100 %.

The standard bulk ash chemical analysis is traditional, but there are a number of major drawbacks of this type of approach. As illustrated in Chapter 1, elements may be associated either as mineral, organically or as simple salts in a fuel. By applying the standard ashifying technique all original elemental associations in the fuel are destroyed, see Figure 2-2.

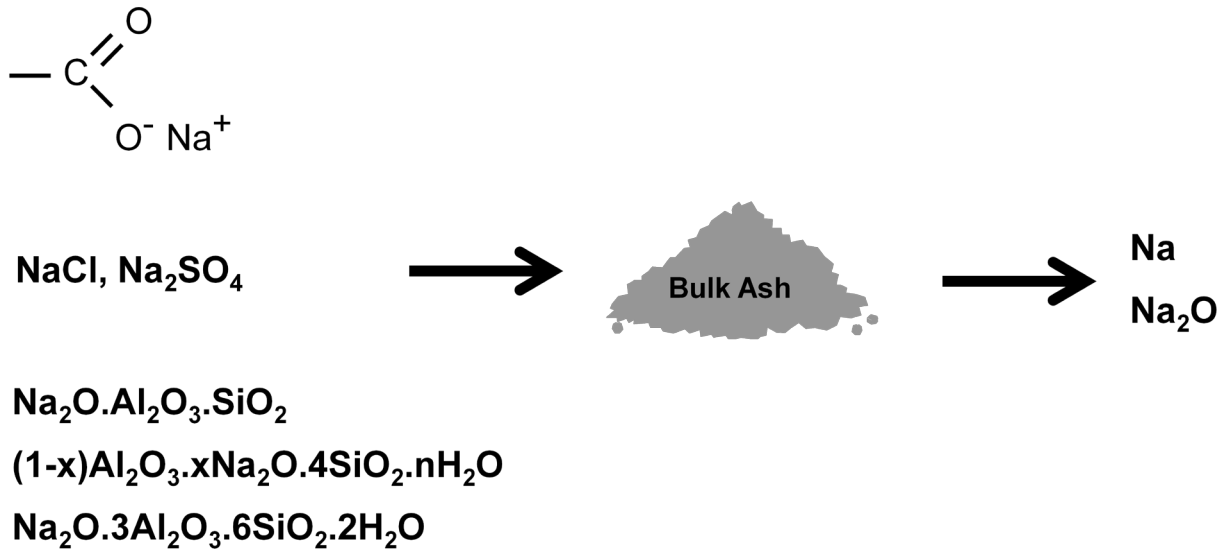

Figure 2-2: Associations of Na in a fuel, compared to the chemical presence in bulk ash. All major, original associations are transformed into an oxide, and very important information on the behaviour of each individual fraction of Na is lost.

During the ashifying procedure, all original associations of the inorganic elements are transformed into oxide form, i.e. Na originally present as organically associated Na or as a

simple salt, will now appear as Na_2O. Thus, very important information on the behaviour of the different associations of Na is lost. It may be convenient to express the content of Na in ash for a fuel on either an elemental base or as an oxide, but this does not provide any details on the original speciation of Na, and thereby the fate and behaviour of the original association of Na in that fuel. This problem is significant for fuels with a high content of organically associated elements or elements present as simple salts, such as low-rank coals or biomasses (including straw). For coals of a higher rank, most of the inorganics are actually presents as mineral inclusions, with a chemical nature close to the oxide basis applied in bulk ash chemical analysis. Nevertheless, even for coal, it could turn out to be problematic to base predictions of, say, ash behaviour on as bulk ash analysis, which is principally a rough mean/average chemistry of the coal ash. Thus, extreme care must be taken if basing predictions of ash behaviour solely on bulk ash chemistry. Other, more advanced, analytical techniques or – even better - real combustions tests in a set-up with a temperature-time history equal to full-scale thermal conversion of the straw, should supply the bulk ash chemistry.

Other, more advanced analytical techniques with the capability of distinguishing between the different types of elemental association in fuels are much needed. One such technique is Scanning Electron Microcopy (SEM).

2.1.2. Scanning Electron Microscopy

In an SEM, a powdery sample is mounted in an epoxy or a similar wax resin and is examined by an electron beam, see Figure 2-3. The analysis is carried out on a polished cross section of the embedded sample [Laursen, 1997]. Two signals are commonly applied for producing images of the sample: Secondary Electrons (SE) and Back Scattered Electrons (BSE). The origin of those is illustrated in Figure 2-4. Energy Dispersive X-ray (EDX) is commonly used in association with SEM, for semi-quantitatively chemical analysis of the sample.

Computer Controlled SEM (CCSEM) makes it possible to evaluate the size, shape (deviation from circularity), quantity, and composition of a huge number of mineral grains e.g. in a coal or individual particles in a fly ash sample, automatically.

Images based on SEs, reflect the surface structure/morphology of the sample, while for BSE-images, the signal intensity is a function of the atomic number of the sample in that particular point. In other words, the higher the atomic number of an element, the brighter that element appears on the image [Laursen, 1997]. Thus, BSE-imaging can be applied to distinguish phases in a sample, such as identifying mineral grains in a coal matrix.

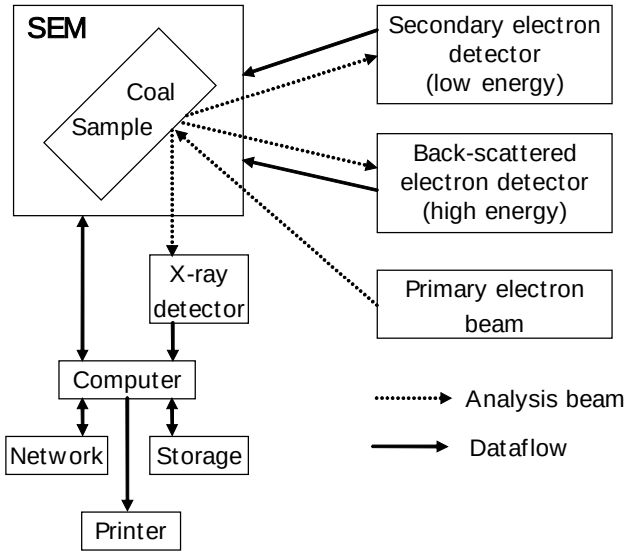

Figure 2-3: Typical configuration of CCSEM apparatus. Redrawn after [Skorupska , 1993]. Courtesy by [Laursen, 1997].

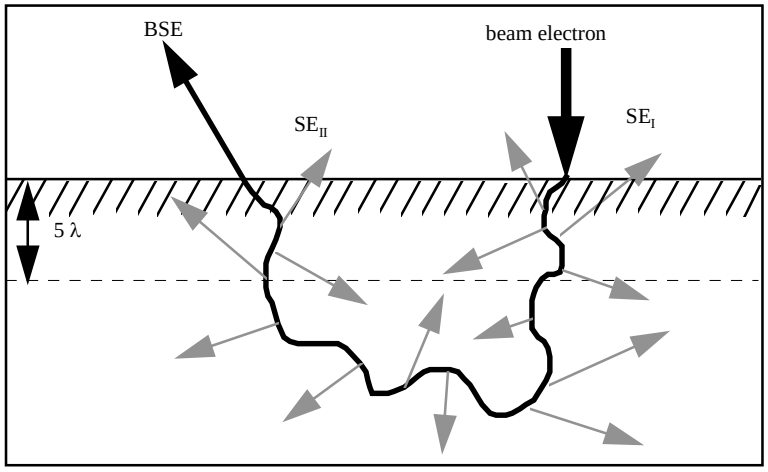

Figure 2-4: Origin of second-dary and back scattered electrons in a sample. Courtesy by [Laursen, 1997].

If an SEM is left overnight to analyse a sample in a certain predefined geometrical pattern, we call this Computer Controlled SEM (or simply CCSEM). CCSEM compositional data are based on EDX-spectra recorded in each point and analyzed in the pre-defined grid, i.e. each point is assigned to one of a series of compositional categories based on specific ratios between characteristic EDX-peaks. These categories are known as *mineral* categories even though the composition may also cover amorphous phases or salts.

In our original CCSEM-work, we adapted the CCSEM-chemistry classification for coal-derived fly ashes, developed at the Energy and Environmental Research Centre in Grand Forks, North Dakota (UND-EERC) throughout the 1980ties [Steadman et al., 1991]. A slightly modified algorithm for coal-derived fly ashes was presented in the Ph.D.-thesis of [Laursen, 1997].

Later CCSEM-analyses of ashes from wheat straw, revealed that their chemistry differs strongly from that of coal-derived ashes [Sørensen et al., 1997]. For example, mineral components

important in coal, such as clays and pyrite, do not constitute a significant proportion of the minerals present in ashes from wheat straw, where the most important mineral categories are quartz (including hydrated amorphous silica, $SiO_2.nH_2O$), various phosphor- and chloride-rich phases, and, arcanite (K_2SO_4).

Thus, as part of the national Danish Energy Research Program (EFP), and in close cooperation with GEUS (The Geological Survey of Denmark and Greenland) and DK-Teknik (The Danish Boiler Owners Association), an algorithm for analysing biomass (particularly wheat straw)-derived ashes, was developed and documented [Sørensen et al., 1997]. Initially, raw data were reduced by using the original coal-based algorithm [Laursen, 1997]. This caused a significant fraction of unclassified particles (~ 35-70 %), i.e. particles that did not fit the criteria for any of the existing coal-derived CCSEM-chemistry categories [Sørensen et al., 1997]. The compositions of the unclassified particles were subsequently studied in detail, and it was found that particles rich in Cl and S constituted a significant part of these, emphasising further the importance of mineral categories rich in Cl and S.

Thus, a much needed modification and improvement of the original coal-derived CCSEM-chemistry scheme, introduced a number of new categories:

- A composite chemistry category of KCl associated with silicates, named 'KCl+silicates'. These composite particles represent either Si-particles covered by condensed KCl, or close association between KCl and silicate, induced by settling of the sample in epoxy before it hardens.
- A category of particles rich in K, Ca, and Si, named 'K-Ca silicate'. This category had a very low Al content, in contrast to the clay-derived categories very often identified in coal or in fly ash from coal. The K-Ca silicates may form by reaction between silica from the straw and vaporised inorganic species in the flue gas.
- Additional chemistry categories for K_2SO_4 and KCl. These phases constitute significant part of especially the finer fly ash fractions from thermal conversion of biomass.
- A range of phosphates: 'K-phosphate', 'Ca-phosphate' and 'K-Mg phosphate' were included, in order to encompass ash particles formed during the thermal conversion of straw.
- The 'unclassified' group was subdivided into 'unclassified phosphates', -'sulphates', -'chlorides', and –'silicates' on the basis of their levels in P, S, Cl, and Si, respectively, based on the assumption that particles in these groups will behave differently, in terms of their response to high temperature.

In Table 2-1, a total listing of all the chemistry categories in the new, modified CCSEM chemistry classification scheme (developed for both coal- and biomass-derived fly ash particles) is presented.

The original COAL-BASED CCSEM Categories				The new BIOMASS-BASED CCSEM Cate-gories
[Laursen, 1997]				[Sørensen, 1999]
Quartz	Montmorill.	Ca aluminate	Apatite	K2SO4
Iron oxide	Illite	Pyrite	Ca-Al-P	K-Al silicate
Periclase	Fe-Al silicate	Pyrrhotite	KCl	K-Ca silicate
Rutile	Ca-Al silicate	Oxi. pyrrho.	Gypsum-rutile	KCl + silicate
Alumina	Na-Al silicate	Quartz-pyrite	Gypsum Al-Si	K-Phosphate
Calcite	Alum. Silicate	Clay-pyrite	Si-rich	K-Mg phos..
Dolomite	Mixed silicate	Fe-Cr oxide	Ca-rich	Uncl. Chloride
Ankerite	Fe silicate	Cr-Fe oxide	Ca-Si rich	Uncl. Sulfate
Kaolinite	Ca silicate	Gypsum	UNKNOWN	Uncl. Silicate

Table 2-1: Development of the CCSEM chemistry categories vs. time. The original classification scheme was developed for coal-derived fly ash particles and mineral grains, but was later extended with biomass-derived chemistry categories also.

Examples of CCSEM in action are provided in [Frandsen et al., 1997, 1998; Hansen, 1998; Hansen et al., 1999a,b; Hansen et al., 2000].

The major drawbacks of CCSEM are the sample preparation required and the fact that the SEM only analyses the outermost ~ 5-8 μm of the sample considered. Thus, significant deviations from bulk ash analyses may appear.

SEM-EDX and CCSEM have several limitations. A number of studies on the application and limitations of the SEM, have been reported in the literature. the main conclusions are;

- [Yang and Baxter, 1992] conducted a test in order to quantify the impact of instrumental settings, and sample preparations, on the measured size distribution obtained in a CCSEM analysis. The main system parameters investigated were: [1)] the acceleration voltage, [2)] the threshold level (between minerals and coal, and the mounting matrix in BSE images), [3)] the image type used (SE or BSE), [4)] the dispersion of mineral grains/ash particles in the sample, and the sample preparation technique. It was found that an increase in the acceleration voltage, a decrease in the threshold level, using SE instead of BSE, and dispersing the sample inadequately, affected the CCSEM results seriously, by enlarging the average particle size, artificially.

- [Galbreath et al., 1995] performed a collaborative, international study on quantitative coal mineral analysis by CCSEM. Six laboratories participated, and performed five analyses on three bituminous coal samples, forcusing on their content of calcite, kaolinite, pyrite and quartz. It was found that results from the same laboratory agreed within a repeatability relative standard deviation of 20%, whereas the results from different laboratories had reproducibility standard deviations between 21% and 83%. Especially, the precision of the kaolinite determinations was poor.
- [Mamane et al., 2001] examined several issues related to the quality and validity of CCSEM-data, including [1)] the stability of unattended CCSEM for multihour runs, [2)] the number of particles to be analysed in order to yield representative results, and [3)] the errors associated with CCSEM. A total of 2819 particles in 78 randomly selected fields of an ambient air sample, were analysed by CCSEM during an unattended 8 hour run. Particle diameter, aspect ratio, particle location, EDX-counts for 20 elements, and digital images of each particle were stored. The average number of particles per field [N/F], the average particle diameter [D_{ave}], the average mass loading per field [M_{ave}], and the average particle composition were calculated for subsets of the data, and then compared against results for the full data set in order to assess the stability of the CCSEM over time, and the number of particles needed to obtain representative results. These comparisons demonstrated excellent stability of CCSEM over an 8 hour run. Physical properties (represented by N/F, D_{ave}, and M_{ave}) of the sample were all characterized by analysing approximately 360 particles. Chemical properties of the sample (average elemental composition and major chemical class abundances) converged to within a few percent of their final values, after having analysed about 1000 particles.

Care must be taken when applying SEM to characterise fuels and ashes. Image quality and thereby the outcome of any analysis on a sample is dependent on the operator of the actual SEM-equipment. A certain knowhow about interpreting images is needed to ensure reliable conclusions from such analyses. Finally, a comparison of images from different sources is dangerous due to potential differences in the acceleration voltage and magnification. Often, in the literature, there is a serious lack of preciseness in the documentation of the system parameters applied in SEM. To conclude, the development of SEM-based analysis techniques, mainly CCSEM and SEMPC, have provided a new, and far more detailed, understanding of the association and interactions among mineral phases during combustion. Before the development of these techniques, one had to rely on bulk ash chemical analyses, which would give a rather precise, but very overall image of the chemistry of a given sample. However, there is a significant difference between the compositions and thereby the behaviour of a single fly ash particle, compared to the bulk ash chemical analysis of the sample, from which it originates. This is exactly what SEM-techniques contribute - detailed particle-to-particle chemistry. Not only from a fundamental understanding of ash and deposit formation as well as understanding deposit structure, but also from a modelling point of view, SEM has provided a big step toward

improved prediction of ash deposition [Frandsen, 2009]. Still, in 2009, SEM-analysis is a tool for experts only, which needs skilful operation and interpretation.

Another advanced analytical ash analysis that has developed during the last 10-15 years is quantification of fusion of an ash sample as a function of its temperature. One such technique is Simultaneous Thermal Analysis (STA).

2.1.3. Simultaneous Thermal Analysis of Ashes

Over several decades, laboratory tests have been carried out on fuel ashes in order to estimate their melting behaviour, and subsequently apply the results to estimate the ash deposition propensities of the ashes in full-scale combustion systems. Laboratory tests used to estimate the melting behaviour of ashes include an entire suite of methods [Hansen, 1998]. Commonly used are the conventional ash fusion tests; ISO-540, DIN-51730, ASTM-D1857-87, and AS-1038.15. All these methods imply controlled heat-up of an ash specimen of well-defined geometry, and the simultaneous determination of temperatures corresponding to specified geometrical shapes [Hansen, 1998] (see Figure 2-5).

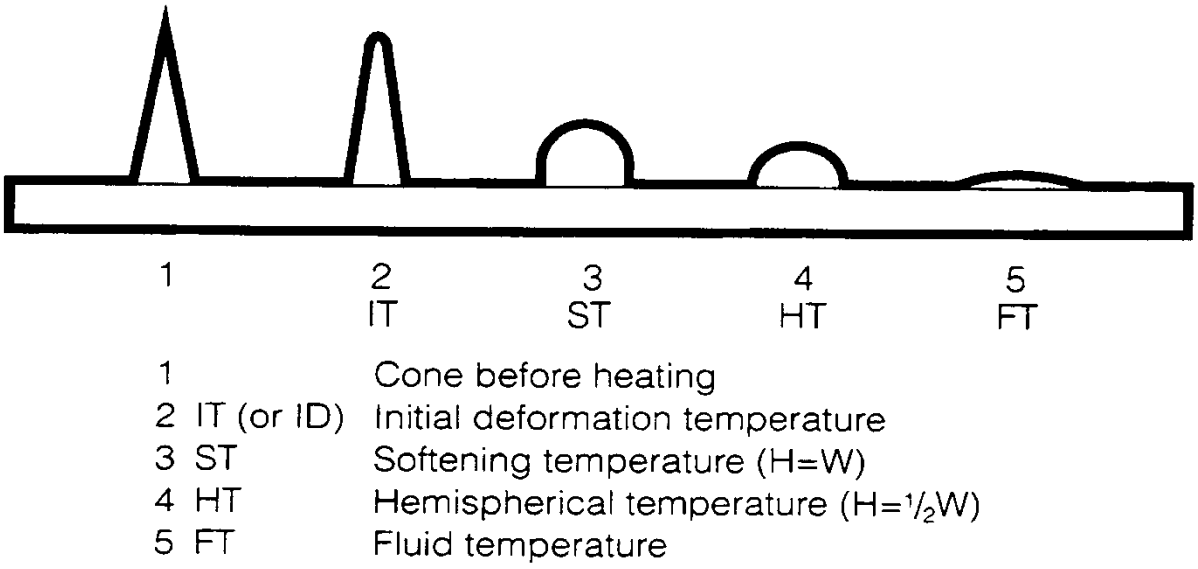

Figure 2-5: ASTM Standard Ash Fusion test. A number of characteristic geometrical shapes are defined, and the temperatures at which these shapes are observed during heat-up of the sample are applied to characterise the ash fusion of the sample.

Through these analyses, the progress in melting is described by three or four characteristic temperatures (corresponding to three or four specified geometrical shapes). The main criticism of the tests has been [Hansen et al., 1999a]:

- Their low reproducibility;
- Unreliability in the subsequent prediction of ash behaviour in real boilers, and;
- The relevance of the laboratory prepared ash applied in the analysis.

Alternatively, ash-melting behaviour has been determined based on electrical resistivity [Raask, 1979; Cumming and Sanyal, 1981; Gibson and Livingston, 1992; Sanyal and Metha, 1994] or conductance measurements of the ash [Conn and Austin, 1984; Cumming et al., 1985] during heat-up. Both methods detect the onset of fusion in the ash, as the temperature at which the electrical properties of the ash changes drastically [Hansen et al., 1999a]. Electrical conductance methods have higher repeatability than standard ash-fusion tests, and give better correlations of the field slagging experience. However, these methods include some practical difficulties, since a satisfactory contact between ash and an electrode is hard to achieve and maintain.

Thus, [Hansen, 1998; Hansen et al., 1999] developed a new method to quantify the melting behaviour of salt-rich, biomass-derived ashes, based on Simultaneous Thermal Analysis (STA), which implies continuous measurement of sample weight (thermogravimetric analysis, TGA), and temperature (differential scanning calorimetry, DSC), during sample heat-up. Weight measurement reveals any mass changes taking place in the sample, and by comparing the sample temperature to the temperature of an inert reference material, any heat-producing or -consuming (chemical or physical) process(es) occurring in the sample can be detected, and the involved energy subsequently quantified.

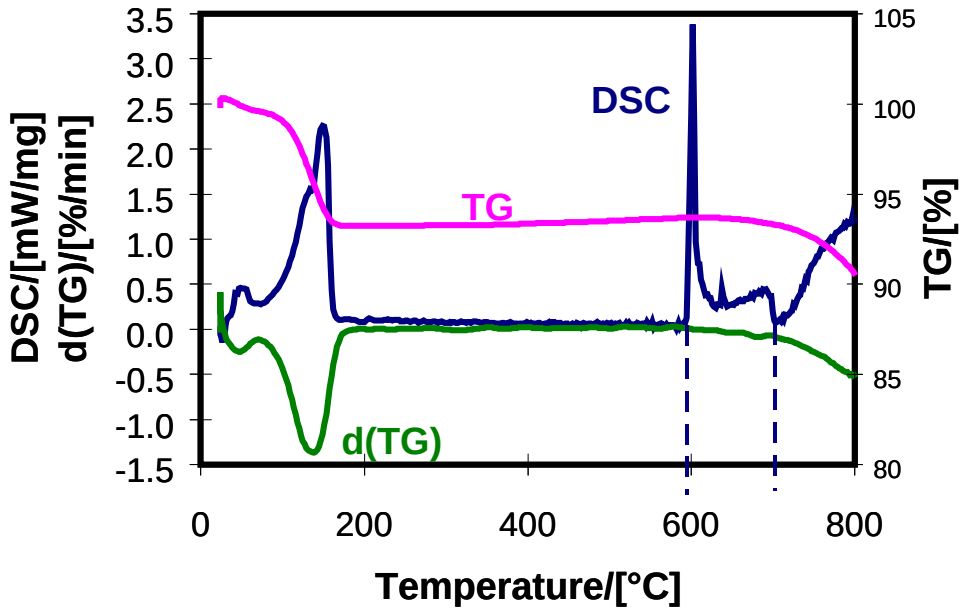

Figure 2-6: STA-curves for the binary mixture $CaCl_2$-KCl. Source: [Hansen et al., 1999a].

As an example of the STA-technique, in Figure 2-6, STA-curves for the binary mixture $CaCl_2$-KCl is shown. Three major peaks are observed in the DSC-signal. One below 200 °C, and two successive peaks above ~ 600 °C.

The two DSC-peaks below 200 °C, and above 700 °C, are both associated with a decrease in the TG-curve (i.e. a loss of mass); these interactions are most likely evaporation of material from the sample. The DSC-peak in-between 600 °C and 700 °C occurs at an almost constant mass of the sample. Thus, this peak corresponds most likely to melting occuring in the sample.

Conversion of the STA curves into a melting curve is outlined in details by [Hansen, 1998; Hansen et al, 1999a,b]. The basic principle is that the areas, under the DSC curve, are integrated. It is evident that the main melting on the DCS curve occurs in the temperature range of app. 600 °C to approximately 700 °C. When these data are integrated, they are seen to fit the theoretical curve based on the appropriate binary phase diagram, very well (see Figure 2-7).

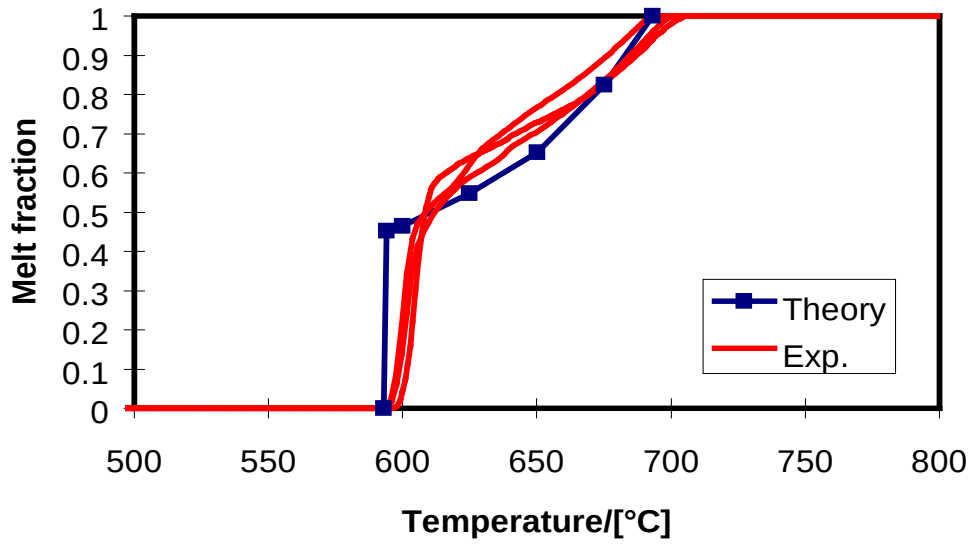

Figure 2-7: Theoretical and experimental melting curves for the system CaCl2-KCl. The theoretical curve is determined from the appropriate phase diagrams, while the experimental data originates from STA-measurements. Source: [Hansen et al., 1999a].

As an example of the application of the STA, melt curves for a suite of fly ash samples collected at the straw-fired Slagelse CHP boiler, are shown in Figure 2-8. For each ash, at a given temperature, the fraction of melt in that ash can be seen directly in the figure. This information may be applied to avoid depositional problems when designing furnaces [Hansen et al., 1999b].

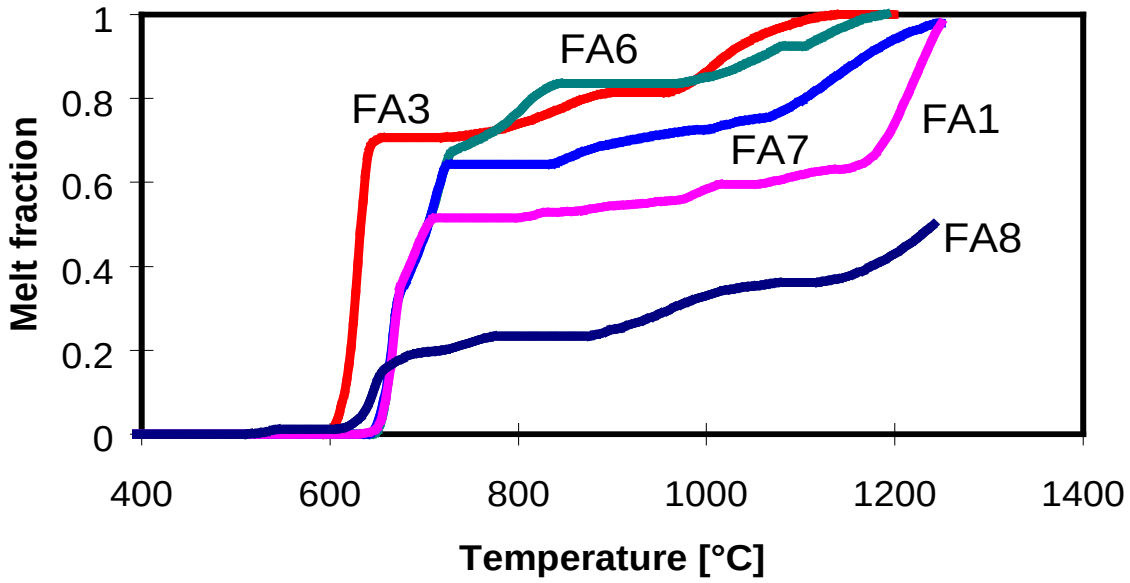

Figure 2-8: Melting curves for a suite of fly ash samples collected at the straw-fired Slagelse CHP grate-boiler. Source: [Hansen et al., 2000].

Another very important finding from the STA-work is illustrated in Figure 2-9, whereby the initial deformation temperature (IDT) is assumed to represent the temperature where the first tiny amount of molten phase is formed in the ash. Nevertheless, in reality, as can be seen on Figure 2-8, about 55 % of the sample is molten at that temperature, and, according to the STA the first droplet of molten phase is formed in the actual sample at a temperature almost 60 °C lower than the IDT. Thus, standard conus or cube ash fusion tests on salt-rich ashes from biomass (in particular straw) must be interpreted with extreme caution.

Similar data where derived for a number of fly and bottom ashes from straw and coal-straw co-fired plants. The result are shown in Figure 2-10, which illustrates that in some cases, the STA predicts melt formation at temperatures up to 300 °C lower than standard ash fusion tests. It is also apparent that this problem is most pronounced for salt-rich fly ashes from straw-firing, i.e. ashes with an ionic structure, while the difference between the predictions for fly and bottom ash is more similar for coal-straw co-firing.

At present, the described STA method work as an expert tool; STA-measurements are relatively easy to perform and the repeatability is good. Interpretation of the STA-signal, i.e. conversion from the STA curves to the melting curve is, on the other hand, far from simple, and cannot easily be standardised. Interpretation requires detailed knowledge of the chemical species in each ash sample, as well as the chemical interactions between these.

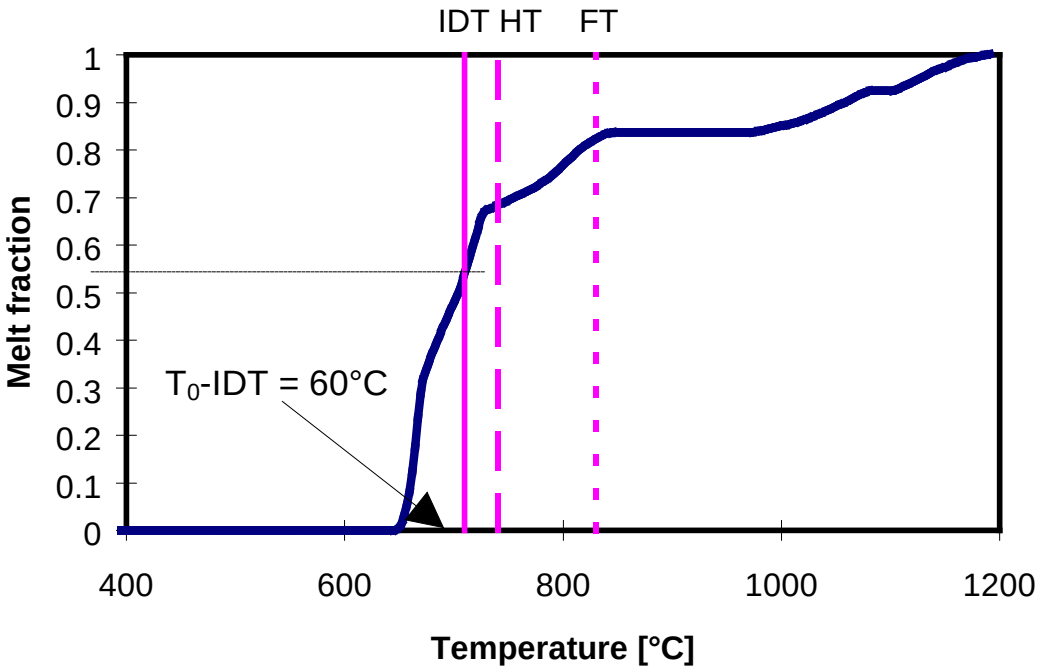

Figure 2-9: Connection between melting curve and ash fusion temperatures for fly ash FA6 from the Slagelse CHP straw-fired boiler. Source: [Hansen et al., 1999b].

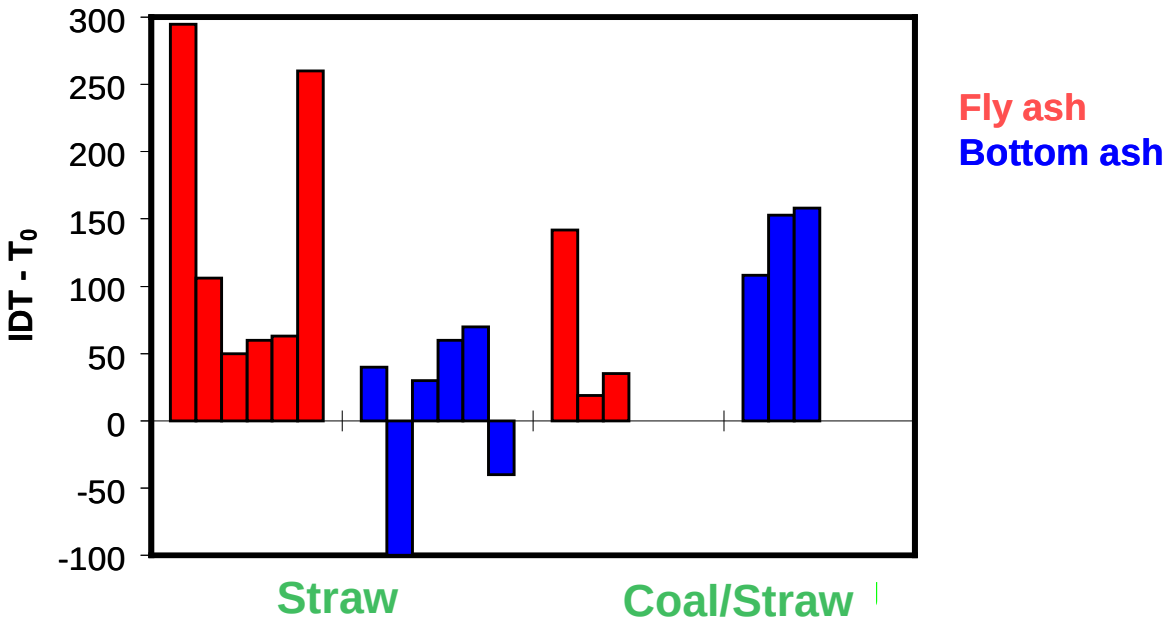

Figure 2-10: Difference between IDT (initial deformation temperature) and T_0, i.e. the temperatures of formation of the first droplet of molten phase, according to ash fusibility tests respectively STA. Source: [Hansen et al., 1999b].

Verification of the following conditions is important for the calculation of the melting curve of an ash sample:

- The occurrence of other processes accompanied by heat effects at zero weight change, i.e. chemical reactions and/or glass devitrification, can be excluded.
- Melting is complete at the end of the heat treatment. This may not be immediately evident. Even a *post mortem* SEM-analysis of the actual sample may have difficulties in confirming this.

Even, when these conditions are satisfied, the work of interpretation is complicated by ash characteristics, as it is a very complex and composite material, and several ash species may have similar evaporation temperatures. This makes the identification of evaporating species difficult and therefore makes it necessary in some cases to make use of an "average" evaporation enthalpy, in order to quantify melting [Hansen, 1998].

2.2. The Chemical Composition of Coal

Coal is a sedimentary, organic substance originating from vegetation and formed during millions of years in the crust of the earth. Elevated temperatures and pressures cause physical and chemical changes in the initial plant material transforming it first into peat, then lignite (brown coal), and, finally hard coals, see Figure 2-11:

$$Plant\ debris \rightarrow peat \rightarrow lignite \rightarrow anthracite \qquad (2\text{-}1)$$

The molecular structure of coal is very complex. It can be described as a mixture of amorphous organic material with interdispersed inorganic materials. Coal contains volatile combustible matter, moisture, intrinsic mineral matter (originating from dissolved salts in water), and extrinsic ash (due to mixing with soil). The chemical properties of coal depends upon [1)] the relative proportions of the chemical constituents present in the parent plant debris, [2)] the nature and extent of the changes which the constituents have undergone since deposition, and, [3)] the nature and quantity of the inorganic matter present [Sami et al., 2001].

Increasing coalification degree means lower oxygen, and hydrogen contents, and accordingly higher carbon levels, see Figure 2-12. Coal 'rank' is a measure of the degree of coalification, and increases with increasing maturity [Heikinnen, 2005].

Figure 2-12, shows that biomasses have highest O:C and H:C ratio, meaning a large quantity of hydroxylic-, carboxylic-, ether- and ketone-groups. These oxygen-containing groups act as bonding sites for inorganic species, which bond as chelates and/or cat-ions. Typically, these inorganic metals are released early in the thermal fuel conversion process, primarily during pyrolysis [Knudsen, 2004; van Lith, 2005].

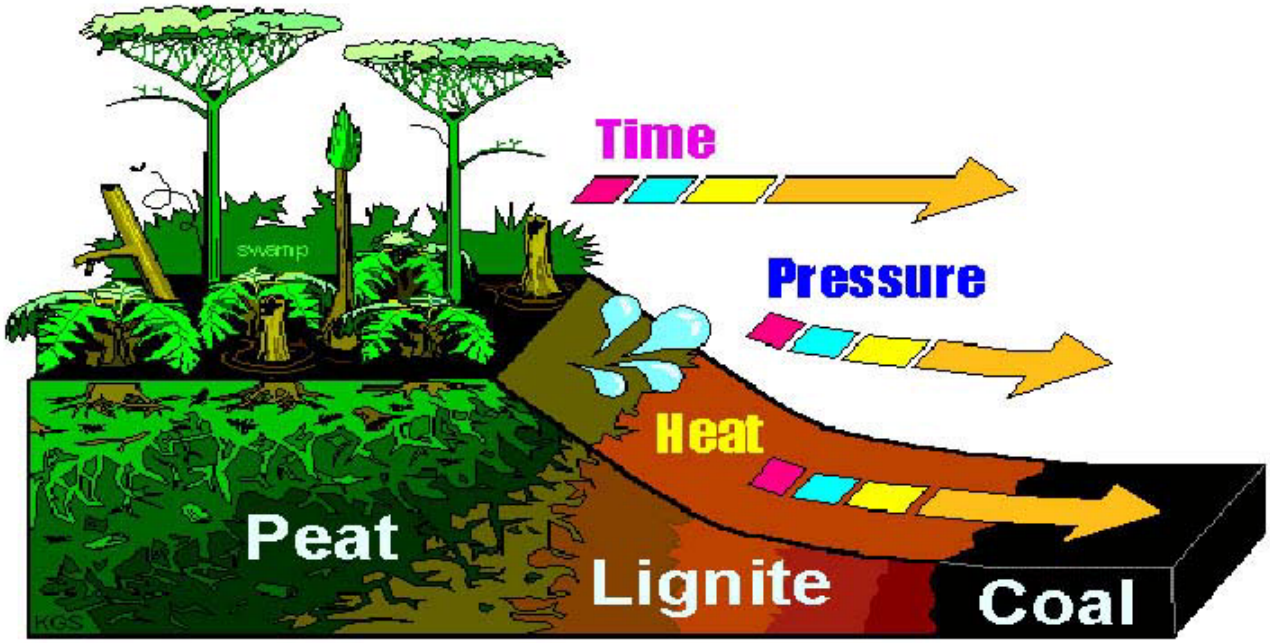

Figure 2-11: The process of coalification, i.e. formation of coal from degradation over time of plant tissue. Source: [Montana State University, 2006].

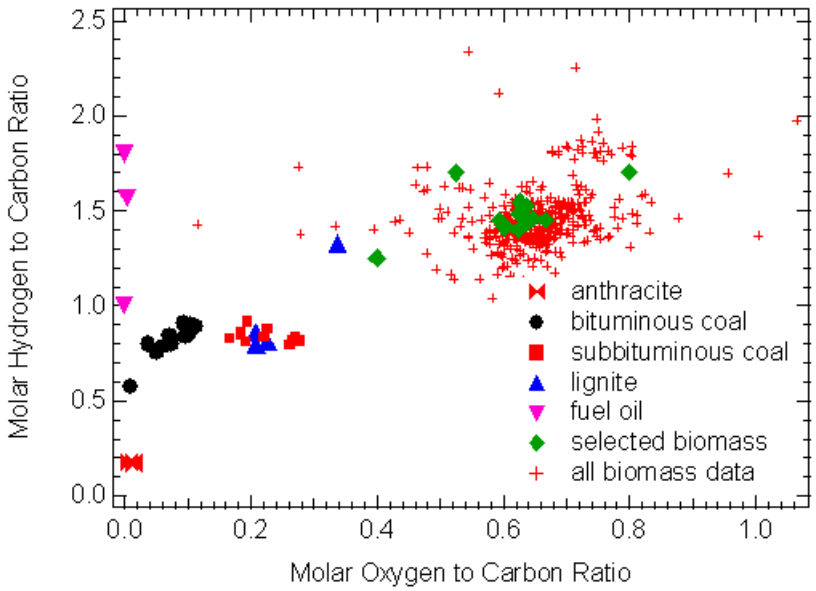

Figure 2-12: Molar H:C- and O:C-ratios for a suite of fuels covering the entire ranking range for coals, as well as biomass. Source: [Brigham Young University, 2010].

In Table 2-3, proximate, ultimate, and bulk ash analyses, for a suite of coals, covering all ranks from lignite to bituminous coal, are listed. Coals typically fired in Denmark, e.g. in conjunction with straw in PF-systems, would be high volatile bituminous coals such as Illinois #6 or Pittsburg #8, as seen in Table 2-3.

2.3. The Chemical Composition of Straw

Straw is in contradiction to coal created directly through the photosynthesis process, during which solar energy (light) is captured by pigments in the plant and then used to reduce atmospheric CO_2(g) into carbohydrate derivatives, such as cellulose, hemicellulose and lignin, through biological reactions with water.

Concerning the association of elements in straw, [Marschner, 2002] lists N, P, S, K, Mg and Ca as macronutrients (present in concentrations higher than 0.1 % dry basis) and Fe, Mn, Zn, Cu, B, Mo, Cl and Ni as micronutrients (present in concentrations lower than 0.1 % dry basis). The elements Na, Si and Co may be micronutrients or at least beneficial to the plant. Micronutrients have a predominantly enzymatic function, whereas macronutrients either are constituents of organic compounds or act as osmotica.

2.3.1. Macronutrients in Plants

After uptake in the plant mainly as $H_2PO_4^-$, P serves a very important function both in nucleic acids (DNA/RNA) and in energy transfer (ATP cycle). As a result of the latter role there is a fast exchange between inorganic and organic phosphate. High levels of phosphates may be stored as large polymers or as an organic ester, phytate (a hexaphosphate), especially in grains and seeds. The latter occurs mainly as Ca-Mg, K-Mg or K-Mg-Ca salts.

Sulfur is taken up predominantly as sulphate, but also as atmospheric SO_2. Sulphate is stored as a free divalent anion and occur bound to organic esterified structures as sulfolipids. It is also an important part of amino acids, proteins and coenzymes but is reduced before assimilation.

Potassium is taken up and occurs as a monovalent cation; plays a major catalytic (nonmetabolised) role in short and long-distance transportation, osmoregulation as well as photosynthetic and enzymatic processes. As counterions NO_3^- , Cl^- or organic acids (COO^-) are frequently mentioned.

Magnesium is associated predominantly as a divalent cation (Mg^{2+}) with phosphoryl groups, but firmly bound also to pectate in cell walls or precipitated as low-soluble phosphate salts. The best known occurrence of magnesium is covalent, in the chlorophyll molecule ($C_{55}H_{72}MgN_4O_5$), accounting for 6-25 % of the total magnesium.

Calcium plays a role in cation-anion balancing, osmoregulation, membrane and cell wall stabilisation. In the latter function, it is bound as a divalent cation to organic macromolecules with COO^- groups in a more or less exchangeable form. In addition, significant amounts of Ca may appear as water soluble or as phosphates. With the increase in Ca supply, in many plant

species the proportion of Ca-oxalate – $Ca(COO^-)_2$ – increases. The accumulation of Ca in crystallised Ca-oxalate is interpreted as an effective way deal with excessive (toxic) concentrations.

2.3.2. Micronutrients in Plants

Iron is taken up mostly as Fe(III) but also as Fe(II); occurs mostly in complexed organic form but also as organic sulphates. Especially in leaves iron can be stored in large amounts as phytoferrin, consisting of a protein shell with up to 5000 iron atoms (Fe(III)) in its interior.

Manganese is taken up mainly as Mn(II), and to a lesser extent Mn(III) and Mn(IV) it forms weak bonds with organic structures such as enzymes, proteins, carbohydrates and lipids. Like iron it plays an important role in redox processes.

Chlorine is taken up and appear in plants as monovalent ion chloride, although organic compounds also exist; plays a catalytic (nonmetabolised) role in photosynthetic and enzymatic processes as well as in osmoregulation.

2.3.3. Beneficial Elements in Plants

Sodium has a low uptake from soil as a salt, but occasionally replaces the osmotic function of potassium. Minor quantities are associated with organic structures.

Silicon is taken up from soil mostly as silicic acid, $Si(OH)_4$, and in grasses frequently deposited in cell walls as amorphous silica or crystalline phytoliths which play a role in plant rigidity and protection against pathogens.

2.3.4. Quantification of Elements

A quantification of the speciation is shown in Table 2-4, see [Korbee et al. 2001]. Three classes have been defined which express the type of association of inorganic elements in the plant tissue.

Table 2-2 gives a rough but quantitative overview of major inorganic elemental speciation. Although variations in a plant or between plants can be significant, it can be very useful to obtain a first estimate of the elements' distribution by combining the numbers from the table with the measured total amount of each element in the material of interest.

Element	Class 1 – Water-soluble (free ionic form)		
	Compound	Formula	Share of total element [%]
Na	Na-nitrate,chloride	$NaNO_3$, NaCl	>90 %
K	K-nitrate,chloride	KNO_3, KCl	>90 %
Ca	Ca-nitrate, chloride, phosphate	$Ca(NO_3)_2$, $CaCl_2$, $Ca_3(PO_4)_2$	20-60 %
Mg	Mg-nitrate, chloride, phosphate	$Mg(NO_3)_2$, $MgCl_2$, $Mg_3(PO_4)_2$	60-90 %
Si	Si-hydroxide	$Si(OH)_4$	< 5 %
S	Sulfate	SO_4^{2-}	> 90 % [1)]
P	Phosphate	PO_4^{3-}	> 80 % [1)]
Cl	Chloride	Cl^-	> 90 % [1)]
Element	**Class 2 - Organically associated (covalent or ionic bonding with tissue)**		
	Compound	Formula	Share of total element [%]
Ca	Ca-pectate	macro-molecule	0.8-2.6 %
Mg	chlorophyll, Mg-pectate	$C_{55}H_{72}MgN_4O_5$, macro-molec.	8-35 %
Mn	various organic structures	Mn^{2+}, Mn^{3+}, Mn^{4+}	> 90 % [1)]
Fe	org.complex, organic sulfates	Fe^{3+}, Fe^{2+}	> 80 % [1)]
S	sulfolipids, amino acids, protein	SO_4^{2-}, S	
P	nucleic acids	PO_4^{3-}	
Element	**Class 3 - Precipitated (pure compound, amorphous or crystalline)**		
	Compound	Formula	Share of total element [%]
Ca	Calciumoxalate	$CaC_2O_4.nH_20$	30-85%
Fe	phytoferritin	$(FeO{\cdot}OH)_8{\cdot}(FeO{\cdot}OPO_3H_2)$	up to 50 % in leave tissue
P	Phytates	Ca-Mg(-K)-salt of $C_6H_6[OPO(OH)_2]_6$	up to 50-86 % in seeds
Si	phytolite	$SiO_2{\cdot}\ nH_20$	70-90 %

[1)] For this specation no amounts have been found. The percentage given expresses that the speciation is the dominant one.

Table 2-4: Speciation of inorganic metarial in higher plants according to classes 'Water-soluble', 'Organically associated' and 'Precipitated'. Source: [Korbee et al., 2001].

Table 2-3 provides an overview of the chemical composition of Danish cereal straw. It is evident in Table 2-5 that K, Si, Ca, and Cl are the most abundant inorganic elements found in straw. Moreover, several different species of straw exists. In Table 2-4, the composition of five different species of straw are provided for comparison. Table 2-4 illustrates that Rape has a significantly higher Ca-content, while wheat straw is higher in Si than the others.

An investigation of the chemical composition of straw in relation to its quality in combustion and gasification processes, was carried out by [Sander, 1997]. A total of 89 samples of straw were collected from 38 farmers throughout Denmark, covering major types of soil and species of straw. A further 58 samples of straw and 12 samples of grain were collected at the Rønhave Experimental Station. The analysis programme included the content of ash, Cl, K, Na, and Ca in all samples, Si, Al, Fe, Mg, and P in most samples, and heating value, content of volatiles, S, Cd, C, N, H, cellulose, lignin and pentosan in selected samples [Sander, 1997]

The data show that cereal straw species are quite similar in composition. The only major difference was seen for Si, where there was a statistically significantly higher content in wheat straw compared to the other cereal species. Rape had a low content of Si, but a high content of Ca. The content of K and Cl was, however, similar to cereal straw [Sander, 1997].

The data collected were also used to investigate the influence of growing conditions on the chemical composition of straw, but showed no relation between soil type and the content of K and Cl in straw. On the other hand, there was a clear tendency for an increase in the content of Si and decreasing content of N with an increase in the content of clay in the soil. No relation between the chemical composition of straw, and the geographical location of the field was observed [Sander, 1997].

It was also tested whether there was any correlation between the fertiliser dose, and the chemical composition of the straw. No correlation between the supplied K, and the content of K in the straw, was found [Sander, 1997]

For all the straw species investigated, a positive correlation between the content of K and Cl in straw was observed. A surplus of K, compared with Cl, in the straw was observed, and there seemed to be a minimum level of 0.2 – 0.3 %(w/w) K in the straw [Sander, 1997]

A rain amount of 100 mm on a field will reduce Cl content to a very low level. The leaching of K by rain closely follows Cl, but keep a minimum level of approximately 0.2 %(w/w). The content of Ca, was not affected by rainfall [Sander, 1997]

Potassium fertilisers are normally supplied as KCl. Mass balances for the uptake of Cl show that fertilisers are the major sources of Cl. Thus, it was investigated whether the application of a Cl-free fertiliser will reduce the content of Cl in straw. In practice, this is done by applying K_2SO_4

instead of KCl as a fertilizer. The results show that the Cl-content in straw was significantly reduced when the Cl-dose from the fertiliser was reduced.

		Straw	
Water content and heating value	Unit	Typical	Variation
Water content	%(w/w)	14	8-23
Lower heating value (as received)	MJ/kg	14,9	12,3-16,9
Lower heating value (water and ash free)	MJ/kg	18,6	18,0-19,0
Chemical composition, Unit: %(w/w) on a dry basis			
Ash		4,5	2-7
Volatiles		78	75-81
Hydrogen, H		5,9	5,4-6,4
Carbon, C		47,5	47- 48
Nitrogen, N		0,7	0,3-1,5
Sulfur, S		0,15	0,1-0,2
Chlorine, Cl		0,4	0,1-1,1
Silicon, Si		0,8	0,1-1,5
Aluminum, Al		0,005	< 0,03
Iron, Fe		0,01	< 0,03
Calcium, Ca		0,4	0,2-0,5
Magnesium, Mg		0,07	0,04-0,13
Sodium, Na		0,05	< 0,3
Potassium, K		1,0	0,2-1,9
Phosphorous, P		0,08	0,03 – 0,2

Table 2-3: Fuel data for Danish cereal straw. Source: [Sander, 1997].

		Si		Ca		K		Cl	
Species	#	Mean	STD	Mean	STD	Mean	STD	Mean	STD
Winter Barley	10	0,29	0,20	0,40	0,06	0,90	0,34	0,41	0,32
Spring Barley	26	0,46	0,23	0,43	0,08	0,86	0,30	0,37	0,18
Wheat	33	0,90	0,40	0,33	0,09	1,00	0,44	0,41	0,29
Rye	10	0,35	0,21	0,27	0,05	0,97	0,15	0,24	0,15
Winter Rape	10	0,04	0,06	1,16	0,27	0,78	0,42	0,35	0,22

Table 2-4: Content of some inorganic elements in five straw species. #: Number of samples behind the statistics. Source: [Sander, 1997].

The content of K was not influenced by the applied amount of K-fertiliser. Similarly, the analysis of selected samples showed that an increased S-supply by the fertiliser does not increase the content of S in straw [Sander, 1997].

In Chapter 7, an outline of detailed investigations of the release of K, S and Cl from straw will be provided and linked to the gas phase K-S-Cl chemistry and aerosol formation in straw-fired boilers.

Chapter 3:

TECHNOLOGIES FOR THERMAL CONVERSION OF STRAW

The energy content in biomass (e.g. straw) may in principle be utilised for energy purposes, by a number of conversion processes, classified in accordance with the respective processing method, as follows;

- Biochemical routes; covering anaerobic digestion, microbial digestion, and acid hydrolysis, applied to convert wet biomass.
- Thermochemical routes; covering combustion, pyrolysis, gasification, and liquefaction, applied to convert dry biomass, using heat to decompose organic matter and thereby release internal (chemically) bonded energy, through various chemical and physical transformations.

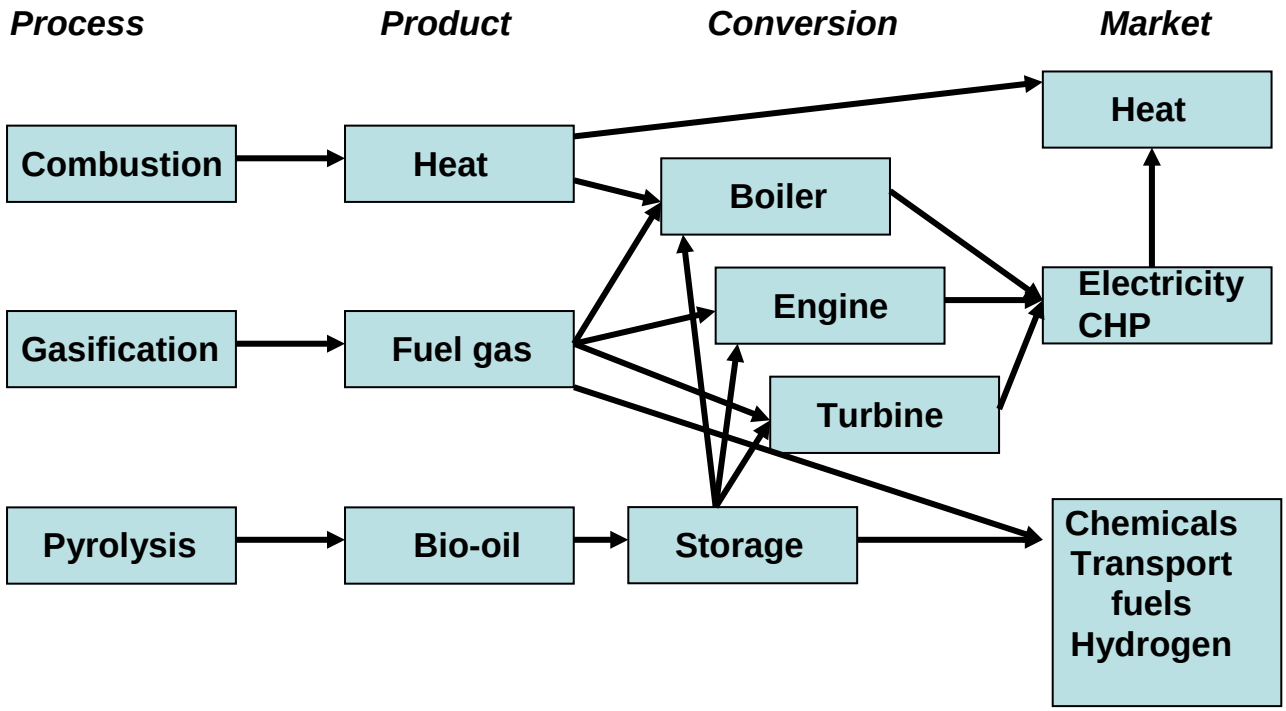

Figure 3-1: Thermal processes and products from biomass. Source: [Agarwal and Agarwal, 1999; Faaij, 2006].

In Figure 3-1, an overview of apparent routes for the thermo chemical conversion of biomass in general is shown. The figure illustrates the link between the process of thermal conversion (e.g. pyrolysis, gasification, combustion), the product (e.g. heat, fuel gas or bio-oil), the conversion medium (i.e. boiler, engine or turbine), and the market for the actual product.

Straw can be combusted alone, in dedicated straw-fired plants, but may also be co-fired with other fuels (e.g. coal or wood chips). Most dedicated straw combustion plants are based on either grate firing or fluidised bed boiler concepts. Technological alternatives to combustion are gasification and the pyrolysis of biomass (see Figure 3-1). Gasification produces an energy-rich gas, which can be used e.g. for co-firing in a large-scale boiler, or be utilised in district heating plants, industrial kilns, or other applications [Maciejewska et al., 2006].

In Denmark, the main options for thermal conversion of straw, are either grate-firing or different co-firing concepts. This chapter will provide a brief introduction to grate and pulverised fuel (PF)-firing (including methods of biomass pre-treatment).

3.1. Straw Pre-Treatment

Table 3-1 shows that the common forms of biomass are 7-9 times as voluminous as coal, and that straw has an even greater volume. By pressing the finely chopped or ground biomass into pellets or briquettes, its volume can be reduced to about twice that of coal for the same quantity of energy, which is reasonable for handling [Leckner, 2007].

Fuel:	**Ash [%]**	**Moisture [%]**	**Volume $[m^3/m^3\ coal]_{MJ}$**
Coal	10	10	1
Wood pellets	1	5	2
Wood powder	1	5	4
Wood chips	1	50	7
Saw dust	1	50	9
Bark	1	50	8
Straw briquettes	5	< 18	3
Straw bale	5	< 18	13
Straw natural	5	< 18	20

Table 3-1: Volume of typical biofuels compared to coal with the same energy content (calculated average data from various sources). Source: [Leckner, 2007].

Thus, pre-treatment of biomass is undertaken mainly in order to [Maciejewska et al., 2006]:

- Make it possible to utilise biomass in suspension-fired units, having e.g. a much higher efficiency, than in dedicated grate-based plants, and;
- Lower the costs of handling, storage and transportation, and thereby improve logistics by using a rather homogenous fuel, with a high energy-density and which is suitable for automatic continuous fuel feeding.

For a detailed, general outline of biomass pre-treatment techniques, please refer to [Maciejewska et al., 2006; NETBIOCOF, 2006].

3.1.1. Storage, Baling, Pelletizing and Briquetting of Straw

During storage, the moisture content, heating value, and dry matter content of straw will change due to degradation processes (microbiological activity) [Maciejewska et al., 2006]. In general, the higher the initial moisture content, the higher the dry matter loss. Thus, in order to keep material losses low, during long-term storage, the moisture content needs to be low (usually below 20 %(w/w)) [NETBIOCOF, 2006].

Several of the disadvantages of using raw straw, may be attributed to the low bulk density of the straw itself. Baling can be applied to improve the characteristics (moisture content and density) of agricultural residues for transportation and storage [Szomolanyiova et al., 2005]. The baled straw has low moisture content and can be stored for long periods without any significant dry matter loss or deterioration in quality [Maciejewska et al., 2006].

Another option for improving the low bulk density of straw is pelletising, which is a compacting process producing a homogenous fuel with a high energy density (8-11 GJ/m^3) [BioNorm, 2004]. Pellets may be considered as a dry, refined product that is easier to grind, making automatic handling and feeding possible, and having a relatively high energy density. The overall pelletising process consists of drying, milling, conditioning, pelletising, and cooling, followed by the separation of fines from the product, and, finally, packing. After drying, the particle size of the material is reduced, and homogenised, usually by hammer mills, as the material needs to be of uniform size before feeding into the pellet mill. Sizing is often followed by conditioning, for instance by steam addition, whereby the particles are covered with a thin liquid layer to improve their adhesion [BioNorm, 2004]. In order to improve the durability of the pellets and avoid dust emissions during transportation and storage, conditioning of raw material and/or addition of binding agents can be applied. Common binding agents include starch, molasses, natural paraffin, plant oil, lignin sulphate, and synthetic agents [Maciejewska et al., 2006].

The application of briquettes instead of pellets is another possible option, since the properties of briquettes allow the use of existing infrastructure based on coal-firing (transport, storage, feeding) without modifying the actual system.

The overall process of briquetting consists of the following steps [Maciejewska et al., 2006]:

- Delivery and blending of the biomass with a binding agent;
- Mixing and heating of the blend;
- Pressing of the blend to the actual physical shape of briquettes, and;
- Impregnation of the briquettes

The advantages of briquetting agricultural residues for boiler applications, are [BioNorm, 2004; Maciejewska et al., 2006]:

- The combustion rate of briquettes is comparable to that of coal;
- Uniform combustion can be achieved, and particulate emissions may be reduced;
- The storage properties are significantly improved, and;
- Transportation and feeding is more efficient.

Briquettes can be made from many types of biomass. The typical diameter of briquettes is 30 – 100 mm, with densities of 800 – 1200 kg/m^3 compared to 60 – 180 kg/m^3 for loose biomass [Szomolanyiova et al., 2005].

3.1.2. Drying of Straw

Drying is an endothermic process that removes moisture. When undertaken in a combustion chamber, drying uses energy released from the combustion process, thereby lowering the temperature in the combustion chamber, and affecting the thermal efficiency of the plant.

The reasons for drying straw actively, as a pre-treatment step, can be summarised as follows [Szomolanyiova et al., 2005; Maciejewska et al., 2006]:

- To improve the overall thermal efficiency of the plant, and reduce the biomass susceptibility;
- To reduce problems with storage such as fungi production (hygiene, health hazards) and self-ignition risks;
- To reduce the weight of the feedstock, which can be advantageous during transportation, and;
- To prepare the biomass for other, more advanced pre-treatment (e.g. the production of pellets or briquettes).

The drying of straw increases the total cost significantly, and drying to moisture contents lower than 10-15%, in a full-scale thermal conversion plant, is not advised, as it requires large installations and high energy consumption [BioNorm, 2004].

3.1.3. Washing/Leaching of Straw

A number of potential operational problems during combustion of straw, such as deposit formation (slagging, fouling), corrosion, sintering, and agglomeration (in fluidised beds), are related to the chemical composition of the straw (mainly the Cl, S, Na and K contents), see Chapters 1 and 2of this thesis.

Removal of the critical elements – mainly the alkalies, S and Cl – may, at least in principle, be performed by washing (leaching) straw with water. Through the pyrolysis of straw, at a moderate temperature, most of the K is retained in the char, while much of the heating value is present in the pyrolysis gas. Three possible pre-treatment processes, applying pyrolysis followed by different char treatment processes, are shown in Figure 3-2. In the first process, the biomass char is washed by water, whereby the K is extracted. In the second process, the pyrolysis is followed by gasification of the char, and in the third process, char is combusted at a low temperature, in order to retain K in the ash [Jensen et al., 2001a,b].

Another option, gasification of char with air and water, produces a gas with a reasonable calorific value. However, the reactivity of char when gasified with water, below 800 °C, is very low, while above this temperature, a significant fraction of K is released to the gas phase. Straw char may instead be burnt with oxygen at low temperatures (400-500 °C). However, a large flow of air is needed, in order to carry the energy from the char combustion reactor to the boiler.

The work of [Jensen et al., 2001a,b] focused on the process of pyrolysis and subsequent char wash in order to address some of the above mentioned problems. The key elements of the investigation were detailed laboratory investigations of K and Cl release from wheat straw, during pyrolysis, and the extraction of K and Cl, by water, from the resulting straw char.

The results concerning K and Cl release from wheat straw, can be summarised as follows [Jensen et al., 2001a,b]:

- Most of the Cl was released during the initial stages of pyrolysis in the temperature range [200 - 400 °C]. Increasing the heating rate, caused increased initial, Cl-release into the gas phase.

- K was released from the straw, and after the initial pyrolysis found as discrete particles or interchalated into the organic char matrix. At temperatures above 800 °C K silicates were found, indicating K-Si – interactions at higher temperatures (> 800 °C).
- The initial K-release into the gas phase at 700 °C, was explained by sublimaton of KCl. At higher temperatures K was released into the gas phase, either directly from the char matrix, or by the decomposition of K_2CO_3.

Based on these findings, it was recommended to apply a pyrolysis temperature of 500 to 600 °C for the pre-treatment process, since this implied a high degree of pyrolysis without a significant release of K into the pyrolysis gas. The release of a significant amount of Cl, however, was found to be almost impossible to avoid [Jensen et al., 2001a,b]. Later release studies performed on annual biomasses, under fixed-bed conditions, have confirmed this [Knudsen, 2004].

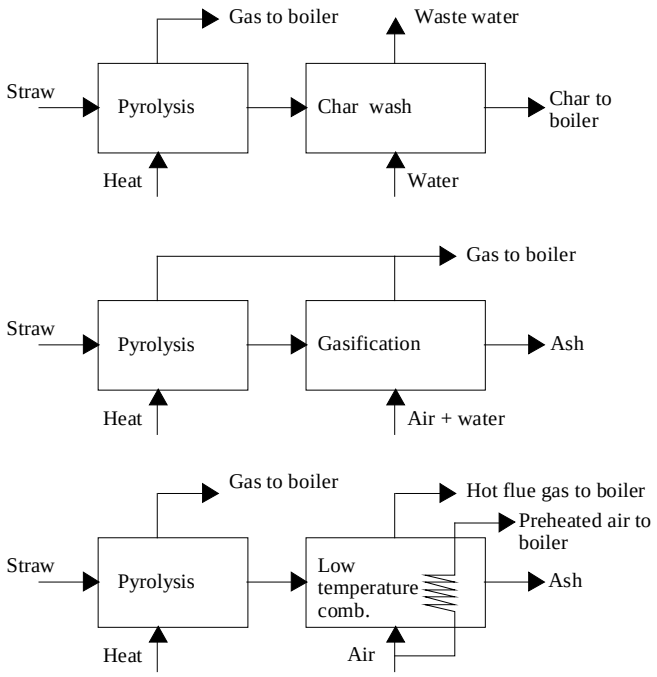

Figure 3-2: Three thermal pre-treatment concepts for the removal of K from straw, in order to minimize deposition and corrosion problems during subsequent combustion of the straw. Source: [Jensen et al., 2001a,b].

The results of the char extraction experiments can be summarised [Jensen et al., 2001a,b]:

- The extraction of K progress in a two-step mechanism. Approximately 40 to 60 % of the K is released within the first few minutes, followed by a much slower (secondary) release of most of the residual-K.
- Char from different straws showed very different secondary release rates.
- Increasing the water temperature from 25 to 80 °C, strongly increased the secondary release rate.
- Most Cl was released from the char, within a few minutes of an experiment.
- All char types pyrolysed at 500 °C had a residual amount of K of approximately 0.33 %(w/w), after a 24 hour extraction in clean water, corresponding to a relative residual amount of 5 to 10 %.

The economy of the pre-treatment process was compared with other concepts for large-scale utilization of straw for heat and power production. The alternatives were: [a)] co-combustion of raw straw in coal-fired boilers, [b)] co-combustion of leached straw in coal-fired boilers, and, [c)] a separate straw-fired boiler delivering steam to the turbine of a coal-fired boiler. The technical/ economical evaluation of char washing as a pre-treatment process, showed that [Jensen et al., 2001a,b]:

- The extraction of K from straw was much faster than the extraction of K from char.
- Fluid bed reactors were recommended for straw pyrolysis in power plant scale, although the international state of pyrolysis technology development did not (in 2001) give a sufficient basis for the establishment of straw pyrolysis in power plant scale.
- Utilisation as a raw-material for K in fertiliser production, was the most favourable method for waste water handling, at least from economic and environmental points of view.
- Electricity production cost was lower for co-combustion of pre-treated straw, than for dedicated straw-fired boilers.

Thus, pre-treatment concepts were found to be economically favourable compared to separate straw-fired boilers, but it was concluded that the target of 90 % K-removal could not be met by 2001 process technologies [Jensen et al., 2001a,b].

3.2. Thermal Conversion of Coal and Straw

When a fuel particle is placed in a hot furnace, it is heated up, dried, and pyrolysed, forming a char residue. During heat-up, the particle consumes energy, during pyrolysis there is an almost equal energy balance between the particle and its surroundings, while during char burnout, energy that can be utilised is released from the particle (see Figure 3-3).

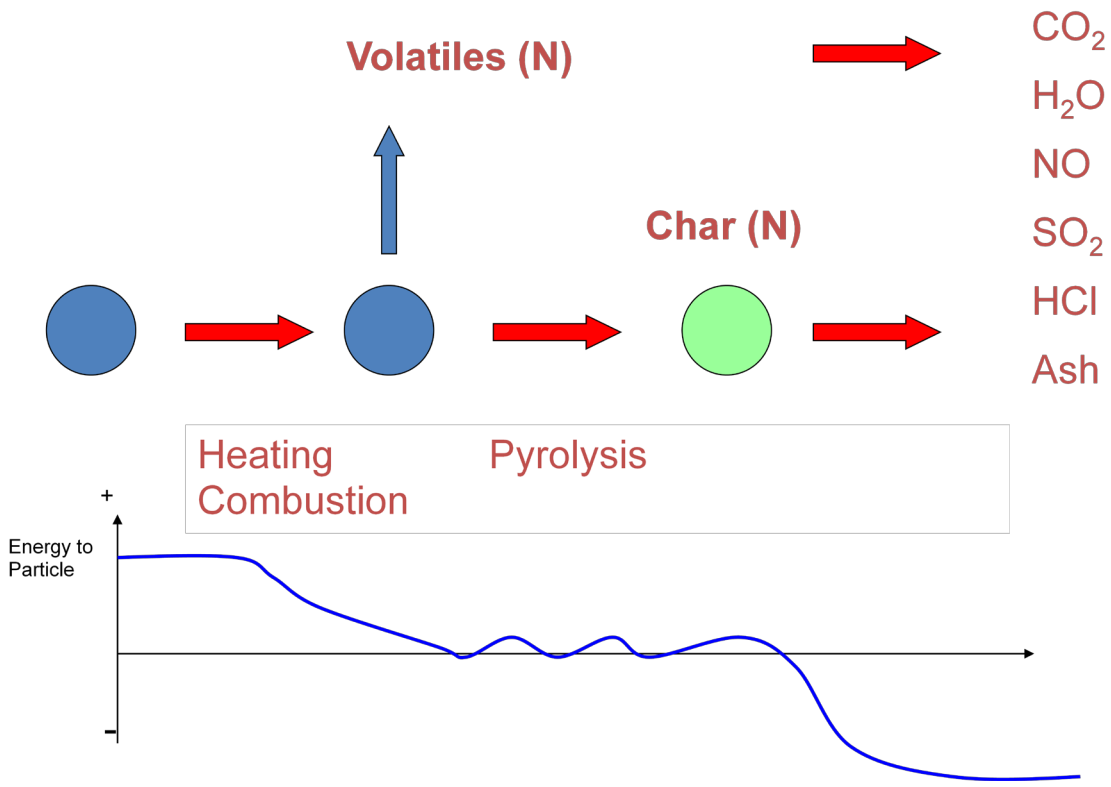

Figure 3-3: Link between heating, pyrolysis, char burn out of a fuel particle and energy exchange between the particle and its surroundings. During heat-up, the particle consumes energy, during pyrolysis there is an almost equal energy balance between the particle and its surroundings, while during char burnout, energy that can be utilised is released from the particle.

The volatiles from the fuel particle diffuse into the surrounding atmosphere where they mix with oxygen to form a flame. Pyrolysis products range from lighter volatiles (CH_4, C_2H_4, C_2H_6, CO, CO_2, H_2, NH_3, HCN, and SO_2 ao.) to heavier tars. Fully oxidised components such as CO_2, and H_2O, can be detected for oxygen-rich fuels such as biomass [Grønli, 1996; Stenseng, 2001; Heikkinen, 2005].

The composition and yield of volatiles, tars and char depend on several factors such as fuel type and composition, particle size, heating rate, final pyrolysis temperature, time at the final pyrolysis temperature, and pressure [Grønli, 1996; Stenseng, 2001; Heikkinen, 2005].

As with coal, the pyrolysis of biomass is a relatively slow chemical reaction, occurring at low temperatures. The reaction mechanisms are complex but can principally be defined in five stages [Sami et al., 2001]:

1. Moisture and volatile loss;
2. Breakdown of hemicelluloses: emission of CO and CO_2;
3. Exothermic reaction causing the biomass temperature to rise from 250 °C to app. 360 °C;
4. Emission of methane and ethane;
5. External energy is now required to continue the process;
6. Complete dissociation;

The solid carbonaceous residue (char) remaining after pyrolysis includes also inorganic components (ash). During the later stages of burnout, the char can be very porous, while inorganic ash inclusions may be seen on the char surface (see Figure 3-4).

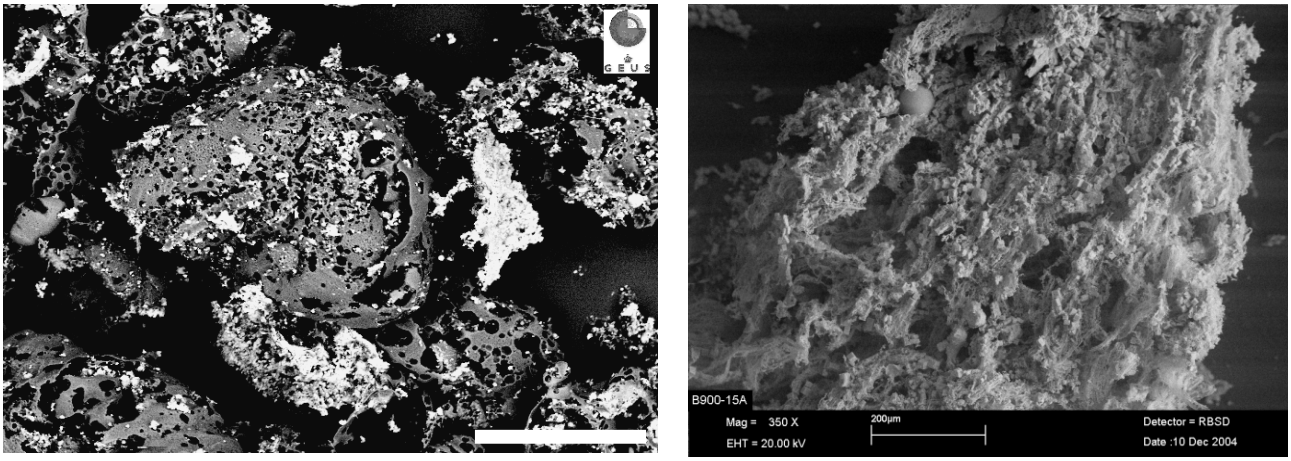

Figure 3-4: Examples of chars from a coal (left image) and a bark particle (right image), respectively. It is evident that the char has a rather open structure in both cases, and that ash inclusions becomes visible on the surface as a function of char burnout progression. Source: [Sørensen et al., 2000; Frandsen et al., 2006].

The carbon in the char undergoes heterogeneous reactions with gaseous species, generally governed by the following processes:

- Diffusion of gas phase oxidising reactant species to the particle surface. Oxygen transfer to the carbon/char surface can occur via O_2, CO_2, and/or H_2O;
- Adsorption of gas species;
- Chemical reaction of the adsorbed species;
- Desorption of the formed oxides;
- Diffusion of gas phase products through the boundary layer (gas film) surrounding the particle to the free stream.

The heterogeneous combustion of carbon/char occurs primarily via the following reactions [Sami et al., 2001]:

$$C + ½O_2 \rightarrow CO \quad (3\text{-}1)$$

$$C + O_2 \rightarrow CO_2 \quad (3\text{-}2)$$

$$C + CO_2 \rightarrow 2CO \quad (3\text{-}3)$$

$$C + H_2O \rightarrow CO + H_2 \quad (3\text{-}4)$$

The dominant reaction at high temperatures is reaction (3-2), while reaction (3-3) is significant at low temperatures (e.g. ignition conditions). Once CO and H_2 are released via heterogeneous reactions (3-3) and (3-4), they undergo oxidation in the gas phase [Sami et al., 2001].

Straw follows generally the same sequence of devolatilisation, pyrolysis, and char burnout, as seen for low-rank coals. However, there are some significant differences between coal and straw combustion. Coal densities typically range typically from 1100 kg/m^3 for low-rank coals, to 2330 kg/m^3, for high-density pyrolytic graphite, while the density of straw is around 100 kg/m^3 [Leckner, 2007]. In addition, straw usually consists of up to 70-80 % volatile matter, whereas coal only contains 10-50 % of volatile matter. When compared to coal, straw pyrolysis starts at lower temperatures and weight loss is higher in biomass, due to the higher content of volatile matter. Furthermore, the heating value of straw is significantly lower than that for coals.

3.3. General Considerations on Grate-Firing

Pile burners represent a historical, industrial method of wood combustion, and consist typically of a two-stage combustion chamber with a separate furnace, along with a boiler chamber located after the secondary combustion chamber [EERE, 2008]. Wood is introduced on a grate in the primary combustion chamber, and then combustion air is fed upwards through the grate and inwards from the walls. Combustion is completed in a secondary combustion zone using overfire air (see Figure 3-5). The wood fuel is introduced either on top of the pile or, through an underfeed arrangement by use of an auger. Ash is removed by isolating the combustion chamber from the furnace and manually dumping the ash from the grate after it has cooled down [EERE, 2008]. The big advantage of the pile burner is its simplicity and ability to handle wet, dirty fuels [EERE, 2008].

Stoker combustion improve on the operation of the pile burners, by providing a moving grate which permits continuous ash collection (see Figure 3-6) thereby eliminating the cyclic batch-like operation characteristics of traditional pile burners. In addition, the fuel is spread more evenly, usually by a pneumatic stoker, and in a thinner layer in the combustion zone, offering more efficient combustion.

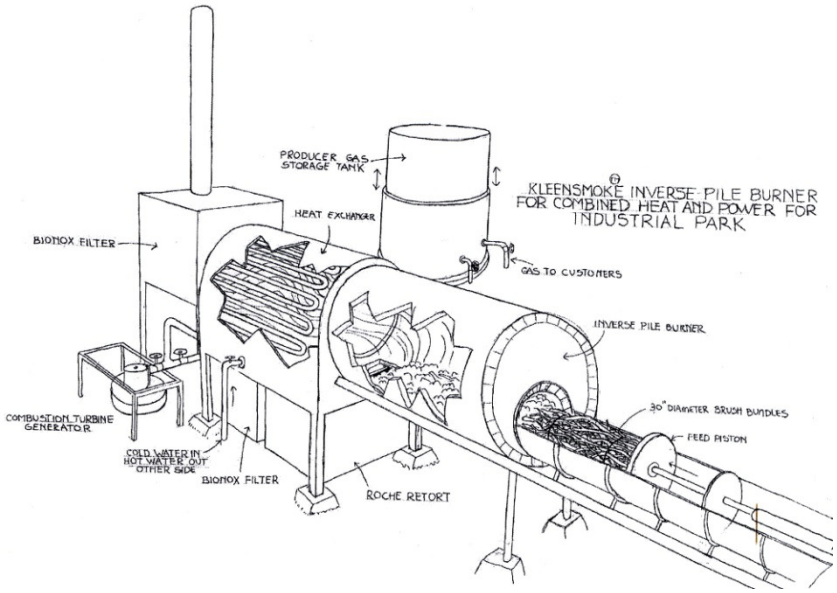

Figure 3-5:
Schematic drawing of the Inverse Pile Burner, Model 6032. Source: [EERE, 2008].

Stoker-fired boilers were first introduced in the 1920s for coal. In the late 1940s the Detroit Stoker Company installed the first traveling grate spreader stokers for wood. In the base stoker design, the bottom of the furnace is a moving grate cooled by underfire air. More modern designs include the sloping reciprocating water-cooled grate, which is attractive because of simplicity and low fly ash carry over. Combustion is completed by the injection of overfire air [EERE, 2008].

Thus, grate-firing is a proven technology, that has been used successfully for biomass fuels (mainly wood, but also straw) for many years. The thermal capacity range is broad - grate-fired boiler technology is available from 15 kW_{th} up to about 150 MW_{th}.

The key issues in grate firing are [a)] a homogeneous fuel particle size and quality, [b)] the proper sizing of the combustion chamber, and, [c)] an efficient mixing of the fuel and combustion air. The mechanical structure of the grate is defined according to the fuel properties. The most common types are [BioNorm, 2004]: [1)] the fixed flat grate, [2)] the fixed sloping grate, [3)] the vibrating grate, and [4)] the chain grate. There are also special grate types for special fuels, such as for waste incineration, or grates based on cigar-burners for straw-firing.

Grate-fired boilers are in general suitable for many types of fuels: coal, wood fuels, waste fuels, peat and even straw. Even fairly moist fuels can be burned on a grate. In comparison to

fluidised bed combustion, the thermal efficiency of a grate boiler is low, and the flue gas emissions are higher. It is also more sensitive to changes in fuel quality, particularly moisture content, and the automation of grate combustion may be quite difficult. However, the structure of the grate is simpler, meaning that the investment, operation, and, maintenance costs are in most cases low compared e.g. to suspension-fired systems [BioNorm, 2004].

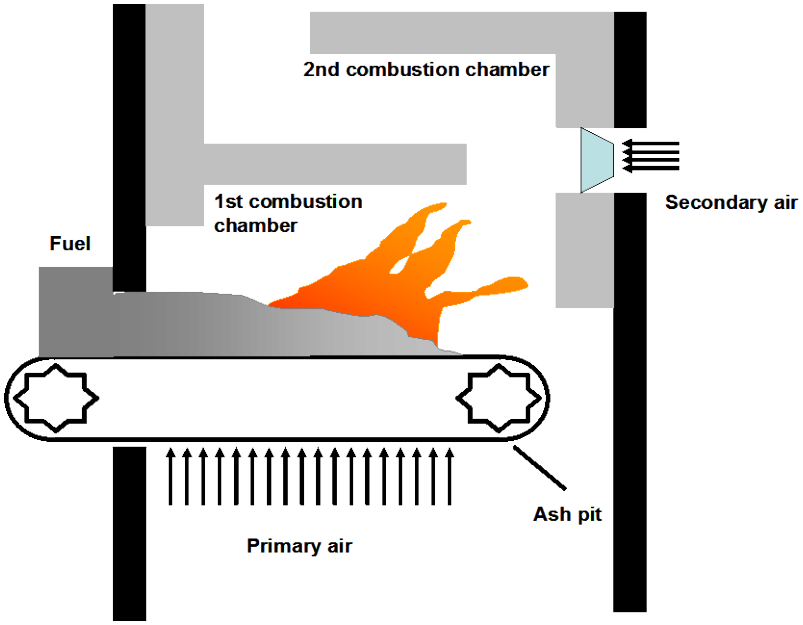

Figure 3-6: Travelling grate furnace. The vibrations of the grate cause the bed to move forward, and hence the reaction system can be considered a moving bed. On a travelling grate, the fuel burns in a fuel-bed on top of the grate.

A frequent problem in grate firing is the melting of ashes from the fuel fired, because temperatures in the combustion chamber may reach as high as 1300-1400°C. Ash melting problems may be reduced by using mechanical and water-cooled grates, and by avoiding the use of preheated combustion air, in the final burning area.

On mass-fired, reciprocating grates, a large volume of fuel is loaded onto the front of the grate and slowly burnt down to a small volume of ash at the back. The key is to maintain an even 20 – 25 cm bed of fuel and ash over the entire grate area. Grate problems are usually due to a shallow ash bed [Gittinger & Arvan, 1998].

Operators, when confronted with poor metering and/or fuel distribution tend to run the grate faster. While this may lower the bed height, it will shorten grate life due to higher wear rates, and, overheating of the grate bars. With the recommended fuel bed thickness, grate temperatures are lowered, wear is reduced and grate life increased. Achieving this optimum ash bed thickness requires controlled metering and proper distribution of the fuel to the grate [Gittinger & Arvan, 1998].

Concerning the lower furnace design of grate fired systems, this originally included modest overfire air (OFA) systems with multiple small diameter nozzles designed for 25 to 30 % of the total air supply and straight wall furnaces. The result was poor combustion performance due to inadequate turbulent mixing in the furnace. In order to increase air penetration and turbulent mixing, modern grate units, particularly for the incineration of RDF, are nowadays designed with fewer, larger diameter OFA nozzles capable of delivering a minimum of 50 % of the total air supply with nominal operation at 40 % of the total air supply (see Figure 3-7) [Gittinger & Arvan, 1998].

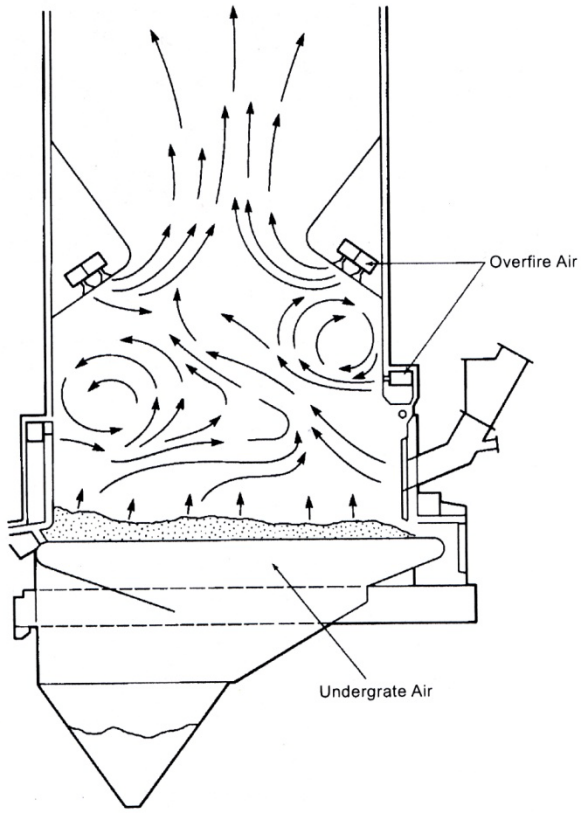

Figure 3-7:
The Controlled Combustion Zone (CCZ) lower furnace design developed by Babcock & Wilcox for refuse derived fuel (RDF)-firing on a grate. Source: [Gittinger & Arvan, 1998].

Superheater design is critical in straw-fired units because of the highly corrosive nature of the products. Superheater corrosion is a function of many variables including flue gas temperature, flue gas velocity, tube spacing, tube metal temperature, tube metallurgy and ash cleaning equipment (see Chapter 11 of this thesis for further details). Of these parameters, tube metal temperature, and tube material are the most critical.

In addition to corrosion concerns, the superheater must be designed to minimize fouling and the potential for erosion due to excessively high flue gas velocities.The usual maximum design gas velocity is ~ 9 m/s, but in practice the actual gas velocity is in the range [3 - 4.6 m/s], while the minimum superheater side spacing is 15 cm [Gittinger & Arvan, 1998].

The upper furnace must be sized to provide an adequate amount of furnace volume for complete burnout of the fuel in the furnace and to minimise CO-emissions. The furnace must also contain a sufficient heating surface to lower the flue gas temperatures in order to help reduce fouling in the superheater and boiler bank. As a general rule, the furnace size is set by volumetric requirements in smaller capacity boilers, and by maximum furnace exit gas temperature limits in larger capacity boilers [Gittinger & Arvan, 1998].

3.4. Straw-Firing on a Grate

A closer look at what is actually going on, physically and chemically, along the grate as a consequence of the proceeding straw combustion will show that the composition along the grate is a function of the position, meaning that two dimensions are needed to characterise the grate-fired system accurately (a height and length dimension). Since the bed is moving, different positions along the grate correspond to a certain residence time. In other words, the horizontal length dimension can be thought of as a time axis.

The grate may be divided into four zones (see Figure 3-8):

1. A heating and drying zone;
2. A pyrolysis and combustion zone;
3. A char combustion zone, and;
4. A char gasification zone.

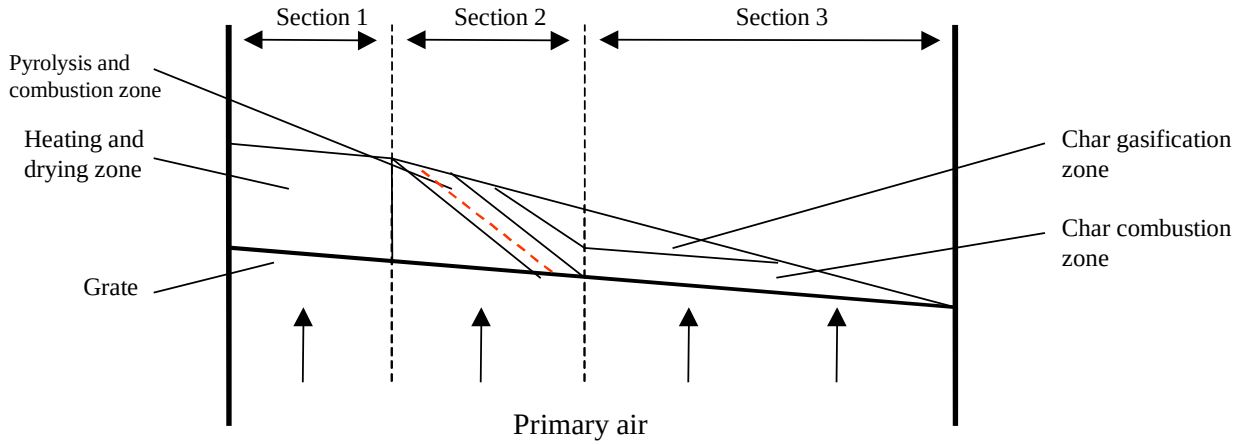

Figure 3-8: Illustration of the different combustion zones in the grate-firing of biomass.

The first zone encountered (see Figure 3-8) is the heating and drying zone, which is located at the beginning (high front end) of the grate, where the moist straw from the feeders is

introduced to the hot interior of the furnace. The length of this zone depends on several factors: [1)] the furnace temperature, [2)] the moisture content in the straw, [3)] the straw load, and, [4)] the flow pattern of the hot gases. Thus, the length of the heating and drying zone is not necessarily fixed, but may change instantaneously. The straw-bed dries from the top (upper surface) and downwards, against the direction of the primary air flow. This is because the top faces the hot furnace chamber, while the bottom of the straw-bed faces the relatively cold entrance of the primary air. If the primary air is dry and preheated, the straw might also be dried from beneath the grate.

The second zone is the pyrolysis/combustion zone. If the zone is described from the grate and upwards, in the direction of the primary air flow, the first phenomenon encountered is pyrolysis. At this point, the straw is completely dry, and has reached its decomposition temperature (200-300°C). Decomposition starts with the volatile matters being released, which consist mainly of hydrocarbons, and various N- and S-species, and will ignite, and burn rapidly, in the hot oxidising environment of the neighboring combustion zone.

There is no well-defined borderline between the pyrolysis and combustion zones, since pyrolysis gas will burn immediately after its release, if oxygen is available. This is illustrated in Figure 3-8 by a combined pyrolysis and combustion zone. The dashed line illustrates the propagating ignition front. Thus, the ignition front propagates opposite to the direction of the primary air flow, i.e. the ignition front moves towards the grate.

After the straw is drained for volatiles, the remaining char starts to burn. This is the third zone, the char combustion zone (see Figure 3-8). The oxygen content in wheat straw char is quite low hence a relatively large quantity of oxygen is needed for complete combustion, which causes oxygen in the combustion air to be consumed and the char combustion terminates. Thus, the char combustion zone is bounded by the depletion of oxygen in the primary air; and consequently, a very O_2-deficient zone will exist in continuation of the char combustion zone.

This fourth and last zone is the gasification zone, rich in unburned char and combustion products mainly CO_2 but also some H_2O. At the high temperature in the furnace, combustion products may react with the char, and cause gasification, producing more volatile compounds e.g. CO and H_2, which will burn when entering more O_2-rich levels in the furnace.

The fixed-bed type of combustion causes little contact between the flue gas and the bed, which seriously limits the possibility for interactions between flue gas components and the remaining char/ash. For instance, the volatile pyrolysis products will clear the bed in moments, leaving very little time for reactions with char and ashes. Furthermore, after devolatilisation the remaining char starts to burn without being in contact with the volatile components. This indicates that the initially formed pyrolysis products can only undergo homogenous reactions in the freeboard.

3.5. Co-Firing of Coal and Straw in PF Units

Another option for utilising straw for heat and power production, is to co-fire the straw with coal in PF-fired units, where the final superheater steam temperature, and thereby the electrical efficiency of the plant is usually much higher than in dedicated straw-fired plants, i.e. 580 – 630 °C compared to 480 – 520 °C in the straw plants. Thus, the electrical efficiency of co-firing in PF units is much higher (see Figure 3-9) and at the same time a certain amount of fossil fuel is substituted directly by CO_2-neutral straw.

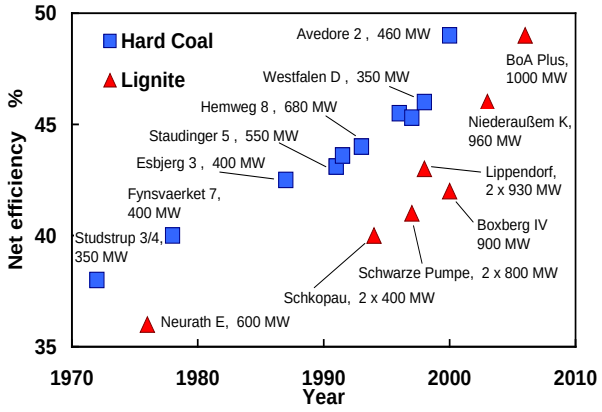

Figure 3-9: Development in net power plant efficiency in suspension-fired units, over the period 1970 – 2005. Notice that the efficiencies in these plants have increased from ~ 35 % to ~ 47 %, i.e. a much higher efficiency than what is actual in dedicated biomass-fired CHP-plants. Source: [Hein, 2008].

Most of the challenges in the co-firing of coal and straw, originate from the properties of the different fuels, which can be summarised as follows [Sami et al., 2001;BioNorm, 2004]:

- The volatile matter content is higher and the pyrolysis starts earlier for straw compared to coal (see Figure 3-3);
- The fractional heat contribution made by volatile substances in straw is approximately 70 %, compared to 30-40 % for coal, but the specific heating value of volatiles in MJ/kg is significantly lower for biomass fuels, i.e. 12-16 MJ/kg, compared to 25-30 MJ/kg for coal;
- Straw char has a higher oxygen content, compared to coal char, and is more porous and reactive;

Life Cycle Assessment studies, indicates that the use of straw, for electricity generation by co-firing with coal, causes environmental benefits in comparison with coal-based systems [Baxter and Koppejan, 2004; Baxter, 2004, 2005]. These environmental profits include reduction in the emissions of greenhouse gases (CO_2) and traditional pollutants (SO_2, NO_X) [Baxter and Koppejan, 2004];

- A certain amount of fossil fuel (coal) is substituted directly by CO_2-neutral straw so a certain decrease in CO_2-emission is expected.
- SO_X-emissions decrease, often proportionally to the straw share co-fired, since straw contain significantly less S than coal [Leckner, 2007].
- NO_X-emissions may either increase, decrease or remain at the same level, depending on the firing concept and operating conditions [BioNorm, 2004; Maciejewska, 2006].
- Straw has, generally, a lower ash content than most of the coals fired in Danish power stations. Thus, a certain decrease in the ash mass loading, and thereby in the rate of deposit build-up, is expected. Furthermore, the coal ash matrix acts as a chemical sink for most of the K present in, and released from straw, thereby releasing Cl as HCl, which decreases both Cl-induced corrosion (see Chapter 8, for further details), and the aerosol mass loading in co-fired systems compared to dedicated straw-fired plants [Sander et al., 2000].

In Denmark, most of the fly ash generated in PC and PF units is sold and reused for cement and/or concrete production. According to the European Coal Combustion Products Association, around 30% of the fly ash produced from coal in EU-25, is used for adding to concrete, replacing part of the cement in concrete. Thus, adding straw to coal – as done in co-fired PF units – raised a question concerning fly ash quality: Would fly ash retain a quality acceptable for cement and concrete production ?

European Standard EN 450 "Fly ash for concrete" is very important in this context, since the application of concrete provides the highest added value for fly ash [Maciejewska, 2006]. EN 450 originally referred only to fly ash of coal origin, but in 2004, CEN-members voted in favour of a revised version of the standard, namely EN 450-1. This revised version includes some fundamental amendments, one of which regards the acceptance of fly ash obtained from co-combustion, defined as "ash obtained from a mixture of pulverised coal and co-combustion materials, where the minimum percentage, by dry mass, of coal is greater than 80% and where the maximum proportion of ash derived from co-combustion material does not exceed 10%" [Maciejewska et al., 2006].

The impact of straw-derived ashes on concrete properties was studied by [Wang and Baxter, 2006a,b,c] for instance, who replaced 25% of the cement used in concrete with fly ash containing up to 40% straw. The general conclusion from the study was that straw-derived fly ashes behave similarly to coal-derived ashes, in terms of structural and performance properties when incorporated into concrete [Wang and Baxter, 2006a,b,c]. Thus, the impact of fly ash from plants co-firing coal and straw on concrete properties was concluded to be manageable and the amount of aerating agent the only issue requiring monitoring (entrainment of air in concrete plays a crucial role in preventing failure during freeze-thaw cycles and the amount of aerating agent appears to increase with herbaceous biomass content) [Wang and Baxter, 2006a,b,c].

Solid fuel combustion is a complex process involving several physical and chemical phenomena taking place simultaneously. Figure 3-10 illustrates the mechanism in pulverised fuel combustion. Having entered a furnace, the fuel particle heats up and undergoes drying. Moisture existing as free water within the particle pores and as water present in the fuel molecules evaporates, and is transported via the pores out of the particle [Heikkinen, 2005].

After drying, heat transfer from the surroundings further increases the particle temperature and initiates pyrolysis, during which volatile components are rapidly released as gaseous compounds (see Figure 3-10). Pyrolysis is typically completed in 10-200 ms for micron-range pulveried coal particles. As pyrolysis proceeds, the structure of the solid char residue changes continuously, it becomes more porous and may eventually break up (see Figure 3-10). The volatiles diffuse out of the particle and ignite homogeneously, as they meet an oxidising agent.

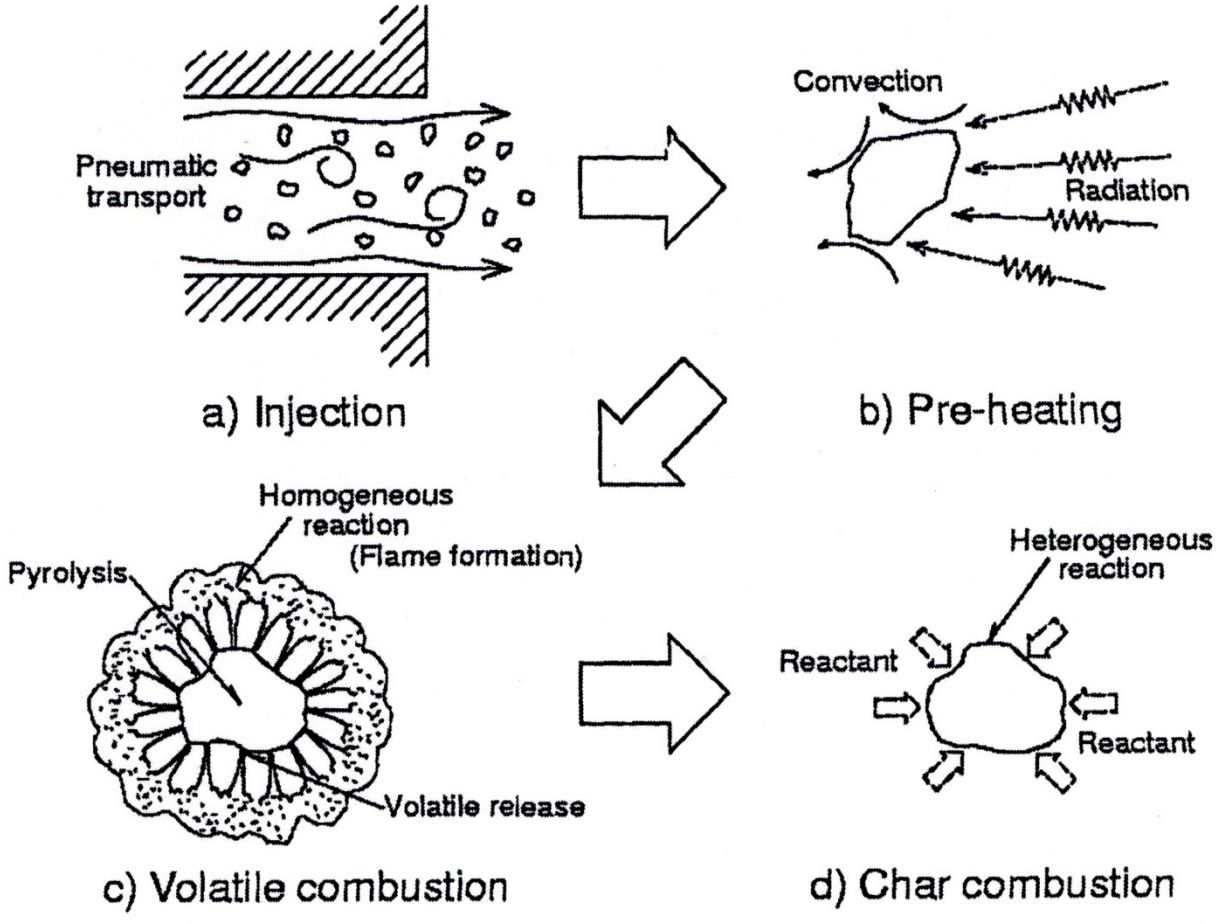

Figure 3-10: Course of events in PF-combustion. Source: [Heikkinen, 2005].

The final and slowest step in solid fuel combustion is the char burnout, where an oxidising agent from the surrounding bulk flow diffuses to the particle surface through a boundary layer. Subsequently, char oxidation takes place. If oxygen is present, char gasification rates by reactions with H_2O and CO_2 are negligible. The time required for the oxidation of PC char particles in utility scale applications is typically in the range 0.3-1 s, which is considerable longer than that required by devolatilisation. Therefore, in practice, the char combustion rate determines the residence time required to complete burnout [Heikkinen, 2005].

Co-firing of biomass and waste can be implemented using three concepts [NETBIOCOF, 2006; Heikkinen, 2005]:

- By direct co-firing where the secondary fuel is pre-treated together with coal in coal pulverisers or in separate mills, e.g. waste and biomass are mixed with the coal and fed through the coal burners into the boiler. Separate feeding lines and burners for secondary fuels can also be applied. This practice is cost-effective, since usually only small modifications in existing facilities are needed.
- In the indirect co-firing mode, secondary fuel is gasified in a separate unit, and the product gas is injected into a coal-fired furnace. The advantage of indirect co-combustion is that the secondary fuel and coal ashes are not mixed and a high fly ash quality can therefore be guaranteed at all times. A gasification unit for the secondary fuel, however, must be built. The capital investments for indirect co-firing are therefore higher than in the case of direct co-firing.
- The parallel combustion concept includes a complete separate combustion installation and steam cycle for the supplementary fuel. The steam produced from straw combustion could for example be upgraded to higher quality in a coal-fired boiler in order to reach a higher electrical efficiency. It is obvious that the investment costs of parallel combustion concept are high. It might, however, be the only feasible option for fuels with high alkali and chlorine contents that can cause severe slagging, fouling and corrosion problems in the furnace.

Of the co-firing concepts outlined briefly above, direct co-firing is currently the most popular option for co-firing coal and biomass (including straw) in Europe, due mostly to the relatively low investment cost of turning existing high-efficiency coal-fired power stations into co-firing plants [Baxter, 2004, 2005; Baxter and Koppejan, 2004]. Parallel co-firing units are also present, but mostly in the pulp and paper industry. Indirect co-firing options are currently considered to be too expensive for European markets, as proved by the co-firing experience in the UK [AEA Technology, 2000].

3.6. Development in Steam Quality and Plant Operation in Denmark

When the first generation of straw-fired CHP-boilers was build in the late 1980s, the level of data and understanding of emissions, deposit formation and corrosion in such plants were limited. Most of the knowhow at that time was derived from small-scale heat-production and distribution plants, as well as from coal-derived power plants. The first generation of plants for straw/wood chips firing constituted the Haslev, Slagelse, Rudkøbing and Måbjerg CHP plants. The experience from these plants, gained via massive measuring programmes in the first half of the 1990s, provided the basis for the development of a second generation of straw/wood chips fired plants, including the Masnedø, Maribo-Sakskøbing and Ensted CHP boilers.

As seen in Figure 3-11, there has been a significant progress on steam quality, mainly via an increase in the final superheater steam temperature from ~ 450 °C (first generation plants) to ~ [520 – 540 °C] (second generation plants). Furthermore, pressure has increased, as seen in Figure 3-11.

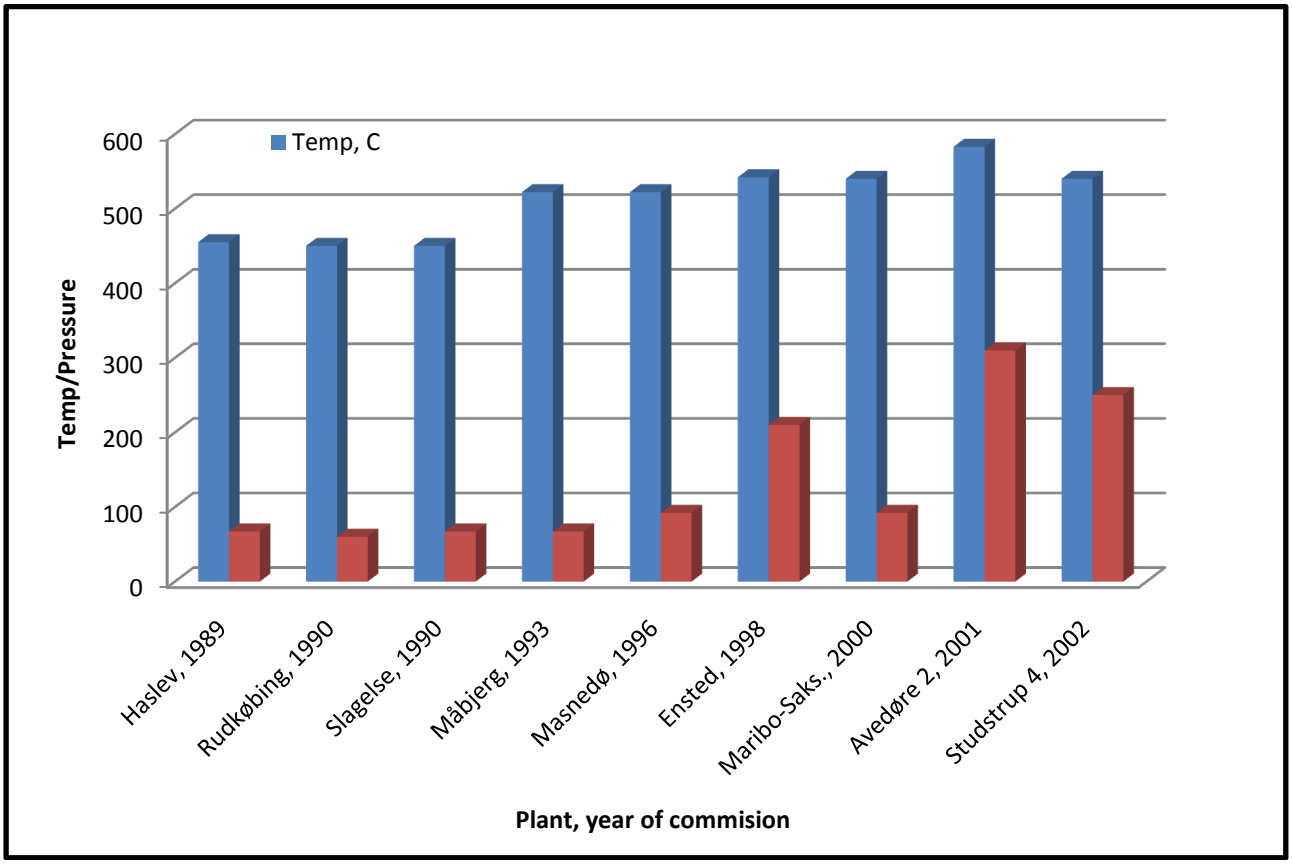

Figure 3-11: Development in steam quality parameters, i.e. steam temperature (blue bars) and pressure (red bars) vs. time, for plants fired or co-fired with straw. Source: [PSO-6523, 2006].

One of the main factors allowing this significant increase in the steam temperature is the application of slag tap superheaters, designed to collect the ash and make it work as a kind of protection against further harm to the superheater tube materials, compared to the classical superheaters applied in first generation straw-fired plants, which were designed to operate optimally without significant deposition.

The slag tap superheater proved to be efficient in systems fired with straw, having 3-7 % ash content and a high concentration of K, Ca and Si in the ash, while it may be difficult to generate the required amount of slag from other biomasses with a lower ash content, such as wood chips. Another aspect that must be taken into account, when designing a furnace equipped with slag tap superheaters for the combustion of straw is the size of the furnace, since a too small furnace may cause excessive heat (and temperature) loading in the furnace and thereby slag formation on the superheater tubes that may be difficult to control.

Concerning the co-firing of straw with coal, there is a very nice time and outline of the experiences when going from the initial attempts of co-firing at the Vestkraft Power Station, via the very comprehensive demo program at Midtkraft-Studstrup, Unit 1, to the current co-firing at Studstrup, Units 3 and 4, which represents state of the art approach to the direct co-firing of straw with coal in 2009. In addition to the data from these plants, valuable contributions on handling fuels and emissions, the use of additives, shedding of deposits, long-term corrosion and the performance of SCR catalysts have been gained from measuring campaigns at the Amager Power Station (firing of straw pellets), the Funen Power Station (co-firing of straw with natural gas), Ensted and Avedøre (separate firing of biomass in a dedicated boiler, followed by superheating to coal steam quality in a nearby coal-fired power station). Thus, in the case of co-firing most of developments have focused on how to handle fuels, how to burn fuels with very different characteristics (like coal and straw), and how to avoid short-term damaging effects on emission control equipment and long-term corrosive attack.

The next two chapters in this thesis deals with experiences of ash and deposit formation in plants dedicated to straw-firing (grate-fired units) or plants co-fired with coal and straw.

Chapter 4:

THERMAL CONVERSION OF STRAW IN DEDICATED CHP PLANTS

One option is to fire the straw in dedicated CHP plants, where the condensational heat from the steam is transferred to the recycling water from a district heat distribution net, thereby producing electrical power and heat, simultaneously. A CHP plant can therefore be located near any large town with a sufficient requirement for district heating, and access to a local distribution net. The energy released from the fuel fired in a CHP plant, is utilised by up to 85-90 %, while the electrical efficiency of a straw-fired plant is usually limited to 20-30 % [CBT, 1998].

The reason for this is that straw-fired CHP boilers generally have experienced operational problems with slagging, fouling, and corrosion (see Chapter 1), due to the high content of K and Cl in the straw (see Chapter 2). Thus, steam temperature has traditionally been kept as low as 450 °C, in order to limit corrosion damage. However, during the last 15-20 years, the final superheater steam temperature has increased from ~ 450 °C in the first generation of straw-fired CHP plants to ~ [520-540 °C] in the second generation.

This chapter contains an outline of the experiences on ash and deposit formation in dedicated straw -fired CHP plants in Denmark.

4.1. Danish CHP Plants with Experience on Straw-Firing

A number of Danish CHP plants have gained significant experience of separate straw-firing on a grate. The CHP-plants in Haslev, Slagelse and Rudkøbing were all started up in 1989/90, and was Denmarks first electrical power generating plants, fired exclusively with straw [CBT, 1998]. The plant at Masnedø, which was commissioned in 1996 is also exclusively straw-fired, but is designed for co-firing of up to 20 % wood chips on a thermal base. The nearby Maribo/Sakskøbing CHP plant, began operation in 2000 and is exclusively straw-fired. All the boilers at these plants are water tube boilers, equipped with a steam drums, and having natural circulation in the vaporiser system.

4.1.1. The Haslev and Slagelse CHP Plants

At the Haslev CHP plant, big bales of straw are fired directly, without any shredding, in four parallel cigar burner systems, where combustion takes place on the front surface of the bales. The injection of high-velocity secondary air into the furnace stabilises the combustion and ensures a high level of burnout. The straw input at full load is approximately 5.5 tonnes/h, corresponding to 23 MW_{th}. A convective evaporator is placed in the second pass, and a superheater placed in the third pass of the plant (see Figure 4-1). A bag filter is applied for the removal of fly ash particles.

The Slagelse CHP plant is a combination of a waste- and a straw-fired boiler, producing steam for the same turbine at 11.7 MW electrical power and 28 MJ/s heat, respectively. Approximately 65-70% of the output is based on straw bales [CBT, 1998], which are reamed and then fed by nine screw feeders onto a moving grate. The fuel input, at full load, is approximately 7.4 tonnes/h, corresponding to 31 MW_{th}. A superheater section is placed in the third pass (see Figure 4-1). An electrostatic precipitator is applied for removal of fly ash particles.

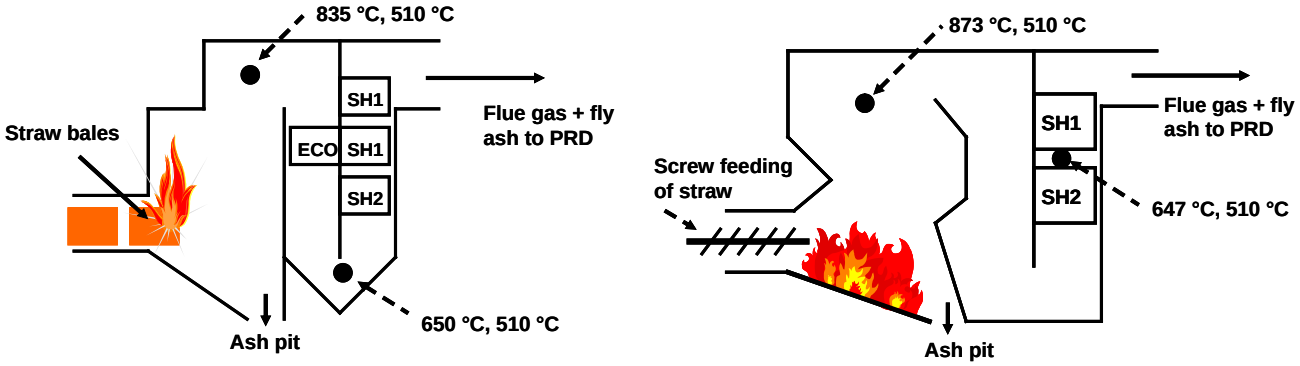

The Haslev CHP-plant

The Slagelse CHP-plant

Figure 4-1: Principal sketches of the CHP-plants in Haslev and Slagelse, respectively.

Both CHP plants - Haslev and Slagelse - have tried to minimise corrosion and deposition problems by limiting superheater temperature to a maximum of 450 °C. This has been done by placing the superheater sections so far back in the convective section, that the flue gas temperature is reduced to approximately 650-700 °C, before it is brought into contact with the primary superheater.

Technical data of the Haslev and Slagelse CHP plants are provided in Table 4-1.

Data:	Unit:	Haslev	Slagelse	Rudkøbing	Masnedø	Maribo-Sakskøbing
Started up	Year	1989	1990	1990	1996	2000
Firing system		Gigar burners	Shredded/ stoker	Shredded/ stoker	Shredded/ stoker	Shredded/ stoker
Filter type		Bag filter	Elec. filter	Bag filter	Elec. filter	Elec. Filter
Straw consumption	Tonnes/year	25.000	25.000	12.500	40.000	40.000
Water content in straw	%	10-25	10-25	10-25	Max 25	Max 25
Electrical power (net)	MW	5,0	11,7	2,3	8,3	9,3
Heat output	MJ/s	13	28	7,0	20,8	20,3
Full load electrical efficiency	%	23	27	21	26	29
Steam pressure	Bar	67	67	60	92	93
Steam temperature	°C	450	450	450	522	542
Max. steam flow	Tonnes/h	26	40,5	13,9	43,2	43,2

Table 4-1: Technical data on the straw-fired, decentralised CHP-plants, referred to in this thesis.
Source: Reproduced after [CBT, 1998].

4.1.2. The Rudkøbing CHP Plant

The Rudkøbing CHP plant is fired mainly with wheat straw, at a thermal output of 10.7 MW, i.e. 2.3 MWe + 7 MJ/s heat. After shredding, the straw falls down onto a stoker system, pushing the straw further on to the grate. The straw burns out on a vibrating grate, and the ash/slag falls into a water-cooled slag bath, from where it passes to a container. The firing capacity at full load is about 3 tonnes of straw/h.

The primary superheater at Rudkøbing is located in the third pass, and has an exit steam temperature of 435 °C. The secondary superheater is located in the second pass in the upper part of the furnace, where it reaches a final steam temperature of 450 °C, and creates 61 bars of pressure. Fly ash particles are removed in an electrostatic precipitator.

4.1.3. The Masnedø CHP Plant

At Masnedø, screw feeders place the straw on a stationary grate, where pyrolysis of the straw begins. The pyrolysis gases are then ignited by air, and the straw is moved further on to a (second) vibrating grate, where it burns out. An ash hopper is located at the end of the vibrating grate. At full load, the plant consumes 10 tonnes of straw/h, corresponding to a thermal output of 36.4 MW_{th}, distributed between 9 MW_{th} electricity and 23 MJ/s heat. As mentioned above, the plant has been designed to co-fire up to 20 % wood chips on a thermal base.

The final steam temperature at Masnedø is 522°C. The superheater in the top of the boiler is therefore constructed so that it is relatively easy to replace possible corroded superheater tubes.

4.1.4. The Maribo/Sakskøbing CHP Plant

The 34.3 MW_{th} Maribo/Sakskøbing CHP plant was designed for an electrical power output of 11.3 MW, and a heat production of 22,8 MJ/s. The annual consumption of straw is approx. 40000 tonnes at full load. Screw stokers push the straw through a feeding tunnel onto a grate system, consisting of an inclined movable grate, followed by a short horizontal push grate. After burning out, the ash/slag falls via a slag hopper, into a slag bath, filled with water from where a conveyor system transport the wet ash/slag to containers. The final steam temperature at Maribo-Sakskøbing is 542 °C.

4.2. Danish Experiences on Straw-Firing in Fixed-Bed Systems

Throughout the 1990s, the former electricity utility groups, ELSAM and ELKRAFT Power Company Ltd./Energy E2 (nowadays jointly, DONG Energy), conducted a wide range of measurements, in order to investigate the effects of firing large amounts of straw in CHP plants, including investigations of:

- Corrosion of and deposition on superheaters, at high metal temperatures;
- Resource mapping, and straw handling/storage/supply issues, and;
- Costs of operating of straw-firing on a grate

4.2.1. The Haslev and Slagelse Campaigns, 1994

In 1994, a total of 12 one-day measurements, were conducted at the straw-fired CHP plants in Haslev and Slagelse, at full boiler-load, in order to improve the understanding and characterisation of straw, for subsequent prediction of ash deposition propensities. [Stenholm et al., 1996; Jensen et al., 1997] provided a complete outline of this measuring campaign, and the main results gained.

The measuring period was approximately 8 hours for each experiment under relatively constant operational conditions, and the two boilers were fed by one type of straw with a reasonably uniform composition at a time. The actual measuring period followed a two-hour introductory period of firing with the same straw. The straw fired and its content of moisture, ash and K, Cl, and S for each experiment is provided in Table 4-2.

The measuring programme included, among several other aspects, air-cooled, cylindrical, deposition probes inserted near the superheaters, and in the furnace chamber. The surface temperature of the probes was kept as close as possible to 510 °C (see Figure 4-1 - which also provides an overview of the local gas temperatures).

The deposit removal system, normally applied at the two plants, including soot blowing, and iron ball cleaning, was stopped during the deposition measurements. After measurement, the probes were withdrawn from the boiler, and the deposit carefully removed.

SEM/EDX analyses showed that the composition of the superheater deposits resembled that of the fly ash, while the deposits formed in the furnace region were enriched particularly in Ca and Si, compared to the fly ash chemical composition (see Figure 4-2). There were also indications that the entrainment of the fly ash particles was higher from the cigar-burners applied in the Haslev CHP plant, compared to the screw-feeders applied in the Slagelse CHP plant [Jensen et al., 1997].

Reference:		Straw composition (%)				
Experiment Number	Straw type fired	Water Content	Dry straw			
			Ash[1]	K	Cl	S
Haslev, 1	Wheat	15.1	4.1	0.71	0.29	0.118
Haslev, 2	Wheat	13.5	4.9	1.29	0.52	0.104
Haslev, 3	Barley	12.0	5.0	2.05	0.56	0.102
Haslev, 4	Wheat	14.6	4.3	1.15	0.44	0.129
Slagelse, 1	Wheat	15.0	6.0	0.41	0.06	0.094
Slagelse, 2	Wheat	13.3	4.5	0.97	0.20	0.115
Slagelse, 3	Barley	11.6	4.5	1.83	0.32	0.068
Slagelse, 4	Barley	13.6	6.5	2.60	0.95	0.162
Slagelse, 5	Wheat	13.9	6.0	1.86	0.51	0.163
Slagelse, 6	Wheat	13.2	7.3	2.07	0.86	0.115
Slagelse, 7	Wheat	16.1	4.9	0.69	0.14	0.095
Slagelse, 8	Rape	14.0	8.3	1.69	0.33	0.395

Table 4-2: Main ash chemical composition and moisture content of the straws fired in the measuring campaigns at the Haslev and Slagelse CHP boiler, respectively. Source: [Jensen et al., 1997]. Note 1: 550 °C ash.

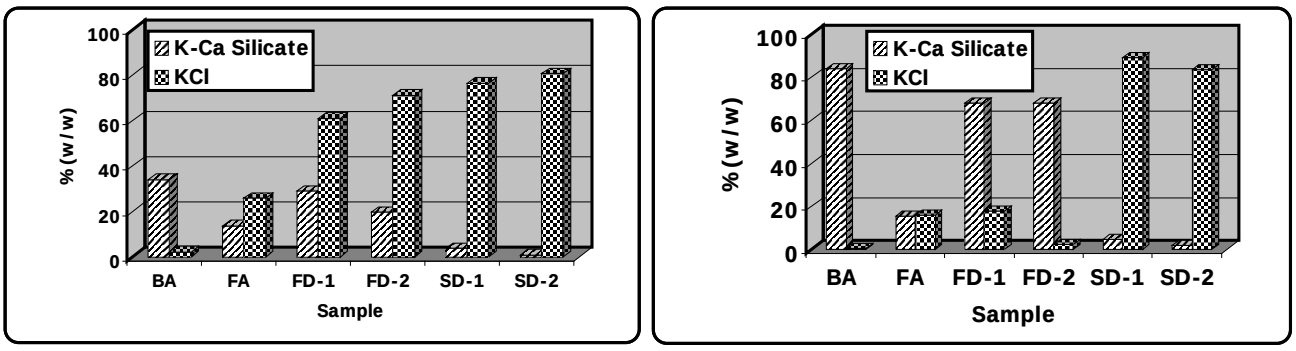

Figure 4-2: SEM/EDX analyses of bottom ash (BA), fly ash (FA), furnace deposits (FD) and superheater deposits (SD) form the Haslev respectively the Slagelse CHP plants. Source: [Frandsen et al., 1998].

Aerosol samples were collected just upstream of the particulate filter. The aerosol size distribution was studied, by use of a low-pressure cascade impactor, and a scanning mobility particle sizer, and reported in details by [Christensen and Livbjerg, 1996]. The aerosol measurements indicated a very high mass loading, up to ~ 2000 mg aerosols/Nm^3, for rape-straw, fired in the Slagelse CHP plant. The mean diameter of the aerosols was around 0.3 μm, and the

aerosols shown to consist almost solely of K, S and Cl, build-up as a core of K_2SO_4 covered by a layer of condensed KCl [Christensen and Livbjerg, 1996].

An almost linear correlation was found to exist between % K [on a dry base] in the straw fired, and the mass loading of aerosols [mg aerosol/Nm^3], in the flue gas (see Figure 4-3, left figure). Furthermore, another linear correlation was derived between the aerosol mass loading [mg aerosol/Nm^3] in the flue gas and the total deposition flux [g/m^2/h] on the probe inserted in the superheater section (see Figure 4-3, right figure). Thus, data from both Haslev and Slagelse indicate a relatively simple linear correlation between the amount of K being fed to a boiler, and the total amount of deposit formed in the superheater section of that boiler [Jensen et al., 1997].

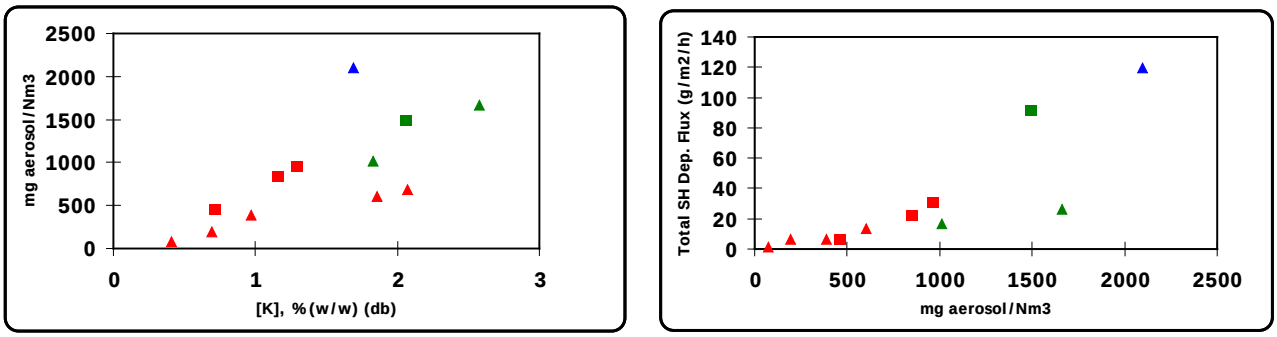

Figure 4-3: The aerosol mass loading [mg aerosol/Nm^3 flue gas] plotted against the [K] in the fuel, and the superheater deposition flux [g deposit/m^2/h], plotted against the aerosol mass loading in the flue gas. Δ: data from the Slagelse CHP plant, □: data from the Haslev CHP plant. Source: [Jensen et al., 1997].

4.2.2. The Rudkøbing Campaign, 1995

In order to quantify the effect of a final superheater (steam) temperature higher than 450 °C, corrosion measurements were conducted at the wheat straw-fired Rudkøbing CHP plant, in 1995. In addition to the corrosion measurements, a series of probe deposit measurements were carried out. The aim of the deposit measurements was to characterise the appearance, structure, and chemical composition of the deposits causing corrosion of the superheaters. For further details, please refer to [Michelsen et al., 1998].

An air-cooled, cylindrical probe was inserted in the upper part of the furnace, just in front of the secondary superheater. The gas temperature at this point was 725 – 750 °C (see Figure 4-4). Two probe surface temperatures were applied during the deposit measurements [Michelsen et al., 1998]:

- 460 °C, in order to simulate the metal temperature of the existing superheater tubes, and;
- 550 °C, in order to simulate an elevated steam temperature to be applied in future plants.

Exposure times of 2, 4, and 14-16 hours were applied in order to determine any changes in the chemical composition of the deposits as a function of time.

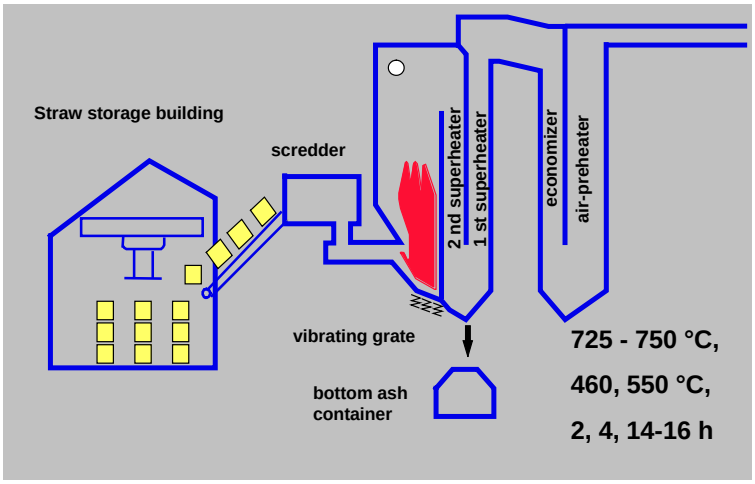

Figure 4-4: Sketch of the Rudkøbing CHP plant. Source: [Nielsen, 1998].

Samples of fly and bottom ash from the Rudkøbing CHP plant were collected and analysed. The fly ash had a relatively high content of unburned C (15-25 %(w/w)), indicating that the burnout of the straw was not optimal. K and Cl constituted in total, ~ 45-55 wt% of the fly ash (on a C-free basis).

CCSEM-analyses showed that most of the fly ash particles were in the 4-8 μm diameter size range, and consisted of either KCl, or of K, Si, Ca, and S covered by a layer of condensed KCl. Sulphur seemed to be associated mainly with Ca, and only to a lesser extent with K in the fly ash.

The probe deposits were rich in K and Cl, typically up to ~ 40-80 %(w/w), and to a lesser extent in Si, Ca, and S. No significant difference in the chemical composition of the deposits, was observed as a function of surface temperature, and only dilution effects were found in the content of K, Cl and S, in the deposits, as a function of exposure time (see Figure 4-5).

Detailed SEM-analyses of the deposits revealed that the upstream side of the probe consisted mainly of fly ash particles, and large quantities of condensed KCl [Michelsen et al., 1998]. A thin layer consisting entirely of condensed material was found close to the metal surface. This layer was about 20-30 μm thick on the 550 °C probes, but only 5-10 μm thick on the 460 °C

probes. Several outer layers rich in KCl, were identified in the upstream deposits (see Figure 4-5) [Michelsen et al., 1998].

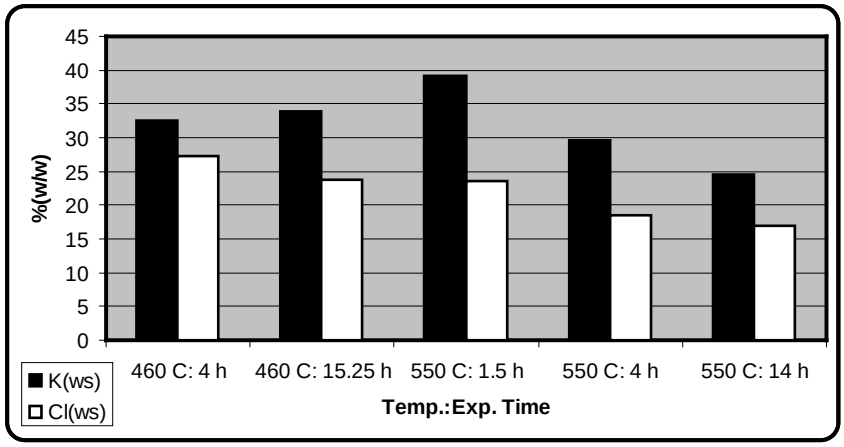

Figure 4-5: %(w/w) of water-soluble (ws) K and Cl vs. probe temperature and expo-sure time in the probe deposits from the Rud-køb ing CHP plant.
Source: [Nielsen, 1998]

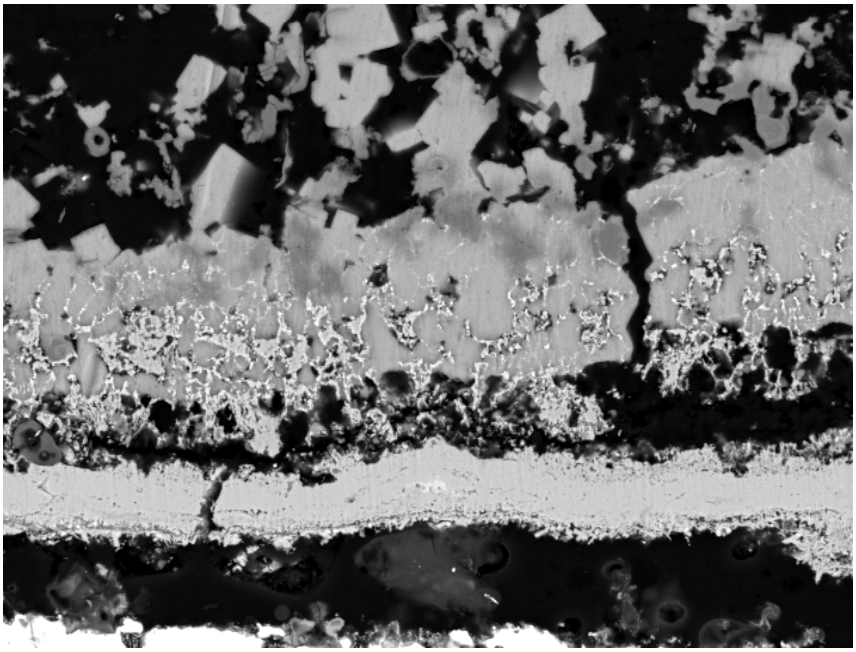

Figure 4-6: Close-up image of the inner layer of deposit D6, exposed for 14 hours with a surface temperature of 550 °C. 1 cm ≈ 186 μm. Source: [Michelsen et al., 1998].

The SEM analyses also revealed a major difference in the physical structure of the inner layers as a function of the probe temperature:

- On the 550 °C probes, the inner layers were very dense and consisted of almost pure KCl.
- The inner layers on the 460 °C probes, consisted of more angular particles and the layers were not nearly as dense as on the 550 °C probes (see Figure 4-6).

4.2.3. The Masnedø Campaigns, 1996-1997

The Masnedø CHP boiler was designed to burn straw and produce steam at maximum temperatures of 520 °C. Thus, based on the experience from the Rudkøbing CHP, the corrosion rates at the Masnedø CHP were expected to be quite high (due to the relatively high final superheater (steam) temperature applied). However, preliminary corrosion measurements at Masnedø showed relatively low corrosion rates [Montgomery and Karlsson, 1999]. Therefore, it was decided to investigate the deposits from the Masnedø CHP boiler further, and try to deduce an explanation for the relatively low corrosion rates observed.

Two types of deposits were analysed in the Masnedø campaigns: [1)] long-term 'mature' deposits, collected directly from in-boiler superheater tubes, during plant shut down and after a long exposure time (approximately one year), and [2)] short-term deposits collected on air-cooled, cylindrical probes, inserted into the boiler for much shorter exposure times (typically 1-8 hours) [Hansen et al., 2000].

Mature Deposits:

A total of ten mature deposit samples, were collected in the superheater area (OH2 and OH3) of the Masnedø CHP boiler (see Figure 4-7) and then analysed. Of these ten samples, four were still attached to the original boiler alloy. The remaining six deposit samples were removed carefully from the superheater tubes, by hand, which in a few cases caused a lack of innermost deposit layers/scales [Hansen et al., 2000]. The mature deposits were quite thick some up to 10 cm with a tendency of thicker deposits on the tertiary superheater (OH3), compared to the secondary superheater (OH2). Visually, the deposits had a layered structure, starting with a white, crystalline, very dense, inner layer, followed by another light coloured and dense, but almost transparent layer. On top of this, a porous and light grey layer of sintered fly ash particles appeared. For some of the deposits an additional outer layer with a rather high porosity was present [Hansen et al., 2000].

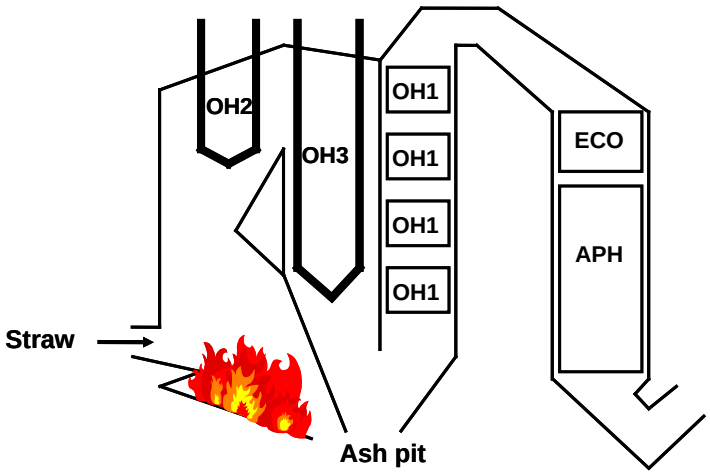

Figure 4-7: Principal sketch of the Masnedø CHP plant.

Figure 4-8: Complete structure of superheater deposit formed in the Masnedø CHP plant.
Source: [Hansen et al., 2000]

An example of an SEM-image is shown in Figure 4-8. This deposit was located on OH2, approximately 1.5 m from the top of the furnace, in cross flow to the main flue gas stream. A K_2SO_4-layer was identified on top of the oxide-scale in the bottom of the image. On top of this layer, several layers rich in KCl, some with a substantial amount of Ca-Si-rich fly ash particles embedded, can be seen on Figure 4-8. Although most of the mature deposits examined had a similar structure, the thickness of the individual layers varied both for the different deposit locations, and within the single deposit [Hansen et al., 2000].

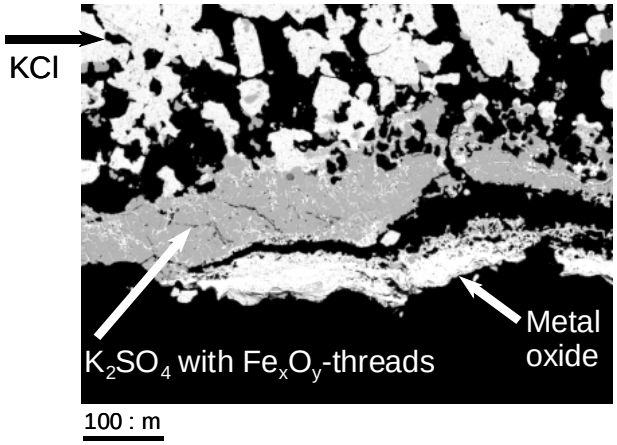

Figure 4-9: Close-up image of the inner deposit layer from the secondary superheater (OH2) at the Masnedø CHP plant. Source: [Hansen et al., 2000]

Figure 4-9 shows a close-up of the three innermost layers: [1)] the metal oxide scale (white) in the vey bottom, [2)] a K_2SO_4-layer in the middle (grey), and, [3)] a coarse, very porous layer of KCl in the upper part of the figure (light coloured) [Hansen et al., 2000]. A significant difference can be seen in the structure between the K_2SO_4-layer, and the KCl-layer in that the K_2SO_4-layer is dense, whereas the KCl-layer is very porous, indicating that the K_2SO_4-layer may have been molten [Hansen et al., 2000].

Another noticeable feature is the presence of (white) Fe_xO_y-threads in the K_2SO_4 layer. Magnifying the area showing the K_2SO_4 layer with Fe_xO_y-threads included, it was observed that these Fe_xO_y-threads reach exactly to the edge of the K_2SO_4 layer, indicating a close relation between the appearance of Fe_xO_y and K_2SO_4 [Hansen et al., 2000].

Further details on the structure and chemistry of oxide scales formed in dedicated straw-fired plants, are provided in Chapter 8 of the thesis.

Probe Deposits:

Deposits were also collected on probes, placed at two locations in the Masnedø CHP plant; [1)] in the top of the furnace, and [2)] in the top of the second pass of the boiler (see Figure 4-7). The probes were cylindrical, made of stainless steel, and cooled by water and/or compressed air [Hansen et al., 2000].

After six hours of exposure and at a metal temperature of 550 – 700 °C, the probe deposit sample collected near the top of the furnace showed an upstream deposit that was approximately 7 mm thick, and consisted mainly of a highly porous layer of sintered fly ash particles. A close-up investigation showed that the inner layer consisted of a mixture of Fe_XO_Y and KCl, where KCl was observed as small grains in the Fe_XO_Y-structure.

Another probe deposit sample was collected in the top of the convective pass (secondary pass) over six hours, at a metal temperature of 540 – 620 °C. A detailed SEM-investigation of this revealed an inner layer dominated chemically by Fe_XO_Y, with just minor KCl content and an outer layer of KCl, with Fe_xO_y-threads emerging out through it. Thus, the structure of this deposit layer is the same as the structure of the inner layer present in the mature, in-boiler deposits, except that in the probe deposit the Fe_xO_y-threads are winding out through a KCl-matrix, instead of through the K_2SO_4-matrix that was identified in the mature deposits.

4.2.4. The Ensted Campaign, 2002

The bio-boiler at Ensted, consists of a straw-fired boiler with a separate wood chips fired superheater, which is connected to the steam cycle at the nearby coal-fired Ensted Power Station, Unit 3 (EV3). Steam from the bio boiler and EV3 is directed to the steam turbine at EV3, producing a maximum effect of 633 MWth, of which 39 MW originates from the bio bioler.

In the original operation schedule, it was the intention that the straw-fired boiler would produce steam at 470 °C, which would be superheated to 542 °C in the wood chips fired superheater. The idea behind this was that wood chips usually contain less K and Cl than straw, thus, it was believed that a final steam temperature of (max.) 542 °C from the wood chips fired superheater would be reasonable. Nevertheless in 2000, it became clear that the wood chips fired superheater was heavily corroded and most of the internal surfaces were covered by Inconel, so the final steam temperature from it was lowered to 510 °C.

A thorough measuring campaign was conducted at the straw-fired CHP boiler in Ensted, in order to deduce the effect of:

- Boiler load;
- Air distribution;
- Moisture content in the fuel;
- Straw type, and;
- Use of additives

on the chemical environment in a straw-fired boiler [Montgomery et al., 2002]. The main objective of the campaign was to increase the understanding of the links between fuel fired, combustion conditions, deposit formation, flue gas temperatures and corrosion, in order to be able to;

- Evaluate the possibilities of adjusting the combustion conditions in order to reduce deposit formation and corrosion, and, to control the flue gas temperature;
- Evaluate the need for sootblowers along the walls of the furnace, and;
- Evaluate the possibilities of reducing deposit formation and/or corrosion by use of additives.

The additives tested were ammonium sulphate (S-additive) and ICA5000 and Bentonit (Al-Si-additives), and were introduced to the furnace with the fuel, in one dose (260 kg/h) for Bentonit and two doses (260 kg/h and 520 kg/h) for ICA5000 and ammonium sulphate.

Deposit samples were collected from probes in two positions along the panel walls in the furnace, at an average surface temperature of 335 °C and 385 °C respectively, as well as on a probe placed in the pendent superheater, at a surface temperature of ~ 600 °C.

The panel wall deposits were in all cases rich in K, Cl and Si. Use of additives did not affect the Cl-content in these deposits. A higher S content was found at 335 °C (lowest position for probe measurements in the furnace) deposit, when adding ammonium sulphate, while the Al-content in all deposits on the panel wall was higher when applying ICA5000 and Bentonit as additives [Montgomery et al., 2002].

The higher dose of ICA5000 caused high Si content in the panel wall deposits. In addition, more deposit was formed at 335 °C compared to 385 °C. Finally, it was found that oats straw caused a high K-content in the panel wall deposits than a mix of wheat and barley straw (the normal straw fired at Ensted).

Concerning the superheater deposits, it was found that deposits on the upstream side of the cylindrical probe placed within the pendent superheater were rich in K and Cl – the same phenomenon as reported for the Rudkøbing CHP plant. The highest K level at Ensted was found when firing oats, while the lowest S-level was found with moist straw or when adding a low dose of ammonium sulphate [Montgomery et al., 2002].

On the downstream side of the superheater probe, high levels of K and Cl were also found, although the Cl concentration fluctuated significantly as a function of the operational conditions. No clear effect of the use of additives on the Cl-concentration in the downstream deposits was found. Oat straw gave the lowest Cl-concentration in the downstream deposits, while the lowest S-level was found with moist straw or when adding the low dose of ammonium sulphate.

In summary, the extensive measuring campaign at the Ensted CHP plant showed that;

- By part-load, the temperature on the grate and within the furnace were lowered, which also caused a lower KCl-concentration in flue gas [Montgomery et al., 2002];
- Changes in air distribution were too small to cause any significant changes in the flue gas chemistry;
- Changes in moisture content in the fuel did not affect the KCl concentration in the flue gas;
- Oat straw produced higher concentrations of dust and aerosols, which caused a very low SO_2-emission;
- The additives applied caused only a minor decrease in KCl content in the flue gas, the most pronounced effect was observed for ammonium sulphate. The reduction in the KCl-concentration will, though, most likely not affect corrosion in the boiler, and;
- Lack of effect of the additives was most likely due to the way the additives were utilized in the furnace. Injection above the fuel-bed in the furnace may provide a much better effect for the additives, especially ammonium sulphate. This theory was later confirmed in a measuring campaign at the Avedøre CHP [Knudsen et al., 2005], see Chapter 10 of this thesis, for further details.

4.2.5. Mature Deposits: Masnedø vs. Ensted CHP, 2000 - 2002

In the Haslev and Slagelse campaigns, it was found that deposits formed in areas, with a relatively high flue gas temperature, contain relatively little Cl [Jensen et al., 1997]. Deposits formed on air-cooled probes at 510 °C, contained 8 – 13 %(w/w) Cl, at a flue gas temperature of 830 – 870 °C, but as much as 14 – 22 %(w/w) Cl, at a lower flue gas temperature of 650 °C.

Thus, an investigation of the effect of flue gas temperature, on the amount of Cl in a deposit, was conducted by comparing the chemical composition of deposit samples from the Masnedø and Ensted straw-fired CHP plants, the main characteristics of which are summarised in Table 4-3.

Different strategies were applied at the two plants, in order to minimise deposit formation and corrosion problems:

- At the Masnedø CHP, where the final superheater steam temperature is 520°C, a relatively large superheater area is applied, and soot blowing is not applied during operation.
- At the Ensted CHP, an external wood-fired superheater is applied in order to obtain a final steam temperature of 542°C, while the exit steam temperature in the straw-fired boiler is limited to 470°C.

Parameter:	**Masnedø CHP**	**Ensted CHP**
Fuel fired	Wheat straw	Wheat straw
Maximum fuel input	33 MW_{th}	100 MW_{th}
Max. superheater steam temp.	520 °C	470 °C
Normally applied air excess number (λ)	1.3	1.25
Flue gas temperature at SH2	960 – 1019 °C	< 900 °C
Superheater steam temperatures	387 – 521 °C	389 – 470 °C
Soot blowing	Not applied	1 time/8 hours
Samples collected at:	Test SH,SH2,SH3	SH1,SH3

Table 4-3: Main characteristics of the Masnedø and Ensted CHP plants. Source: [Jensen et al., 2004].

While the furnace walls in the Masnedø CHP plant were almost clean upon inspection, the superheater tubes were completely covered by a 2 to 15 cm thick layer of a dark brown deposit,

consisting of three distinct layers - a thin, dark brown, outer layer, a thick, porous, white intermediate layer and a thin, but structurally very complex inner layer [Jensen et al., 2004].

The outermost layer of the Masnedø superheater deposits was very porous and had an overall composition similar to that of the ash. It contained many Si- and Ca-rich particles glued together by KCl and some K_2SO_4, which had most likely been molten. The outer surface of the deposit was found to be dark brown, indicating a high level of unburnt carbon in the surface. But chemical analyses of the surface chemistry could not confirm this, since only very low levels of C was found, < 0.02 %(w/w). The intermediate layers from Masnedø contained some very large voids and open spaces, which indicated that the layer had at least been partly molten [Jensen et al., 2004]. Most of the intermediate layer was completely depleted for Cl, but was rich in Si, Ca and K. All the inner deposit samples studied, contained several sublayers, and were quite variable in composition and thickness, although they were always rich in K, S and Cl [Jensen et al., 2004].

The Ensted superheater deposit structure was completely different. It had a maximum thickness of only 2-4 cm, and a white outer surface. However, as with Masnedø three distinct layers were identified by SEM in the superheater deposit [Jensen et al., 2004]. It was found that the innermost layer contained Fe_XO_Y, covered by a sublayer of K_2SO_4, and then another porous sublayer of KCl rich flakelike structures. The intermediate layer contained many Si- and Ca-rich particles glued together by molten KCl. An inner layer, on top of the protective oxide-scale and rich in KCl was also reported in this study.

Since the straw-fired in the two boilers were similar [Jensen et al., 2004], the differences observed in the chemistry and structure of the intermediate deposit layers must be explained by the higher temperature of the Masnedø deposit.

One possible theory is that the intermediate layer at Masnedø may be depleted of Cl by a chemical reaction, initiated at a relatively high deposit temperature [Jensen et al., 2004]:

$$Ca\ Silicate + KCl + H_2O \rightarrow K - Ca\ Silicate + HCl \qquad (4\text{-}1)$$

Through this reaction Cl is released, and the chemical composition of the deposit approaches that of the bottom ash. An alternative explanation is that the intermediate deposit layer at Masnedø simply has been generated mainly by entrainment, and subsequent deposition by inertial impaction, of the bottom ash particles.

4.2.6. Maribo-Sakskøbing CHP Plant, 2001, 2004

The CHP plant in Maribo-Sakskøbing was commissioned in 2000. During the summer of 2001, after about one year in service, a significant number of mature, in-boiler deposits were taken for chemical analysis and physical investigation, in order to explore the chemistry of the inner deposit layers formed. The positions of the samples collected in 2001, are shown in Figure 4-10. Samples from approximately the same locations were intended in 2004, after three years in service.

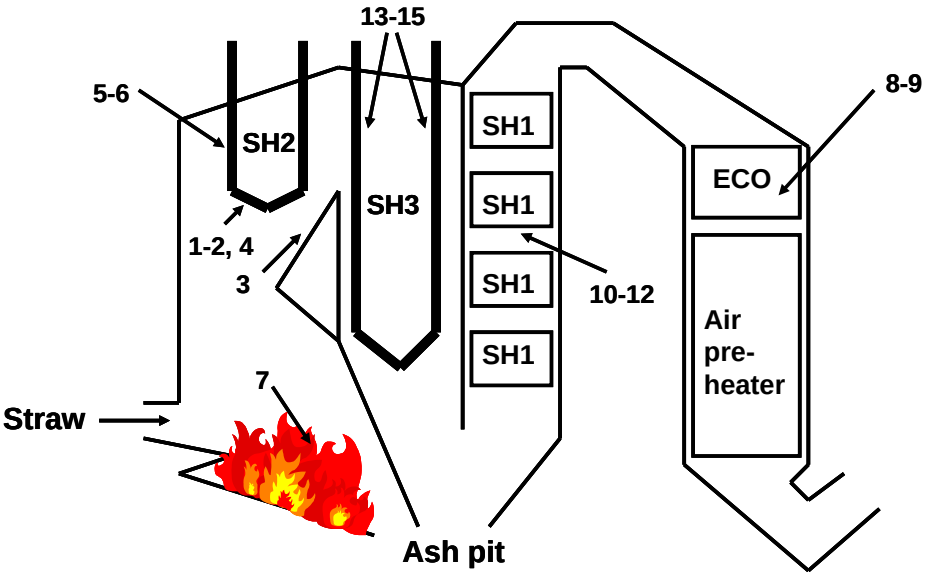

Figure 4-10: Mature, in-boiler deposits taken at the Maribo-Sakskøbing CHP plant in 2001. In 2004, a few samples were taken at SH2 and SH3.

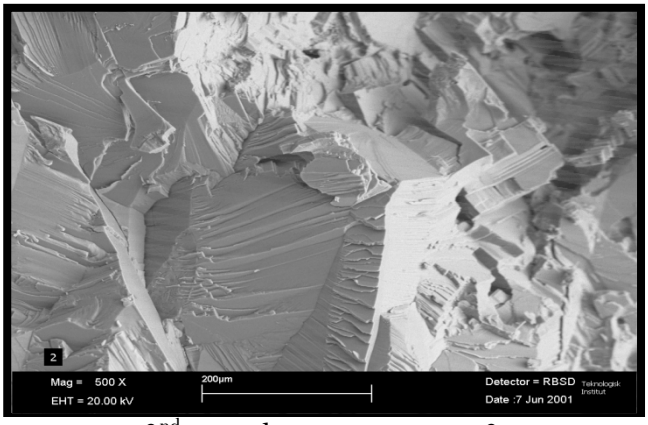

2nd superheater, position 2

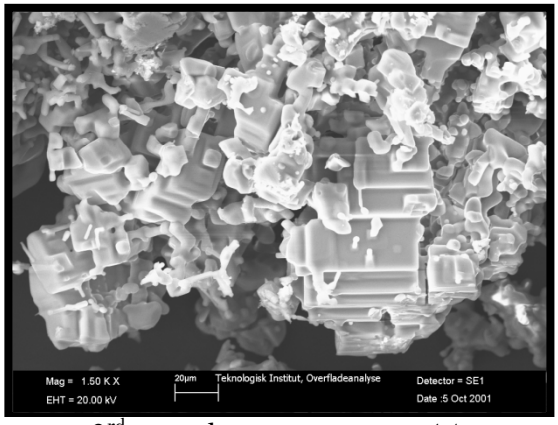

3rd superheater, position 14

Figure 4-11: Close-up images of the inner deposit layer found in position 2 at the secondary superheater, respectively position 14 at the 3rd superheater, in 2001.

In Figure 4-11, two close-up images of the inner deposit layer found in position 2 at the secondary superheater [SH2] and position 14 at the tertiary superheater [SH3], in 2001, are shown. Potassium chloride, KCl, no other elements – except K and Cl - was detected when investigating these inner layers by SEM-EDX.

Three years later that pattern had changed, since in 2004, deposit samples collected from the secondary superheater showed signs of an almost complete sulphation in the inner layer, while the inner layers formed on the tertiary superheater were only partially sulphated.

All of the middle and outer layers investigated in 2004 contained significant amounts of K and Cl, for both the secondary and the tertiary superheater. However, the inner layer from the secondary superheater was almost depleted of Cl. This supports the previous observations from Masnedø on the formation of a protective sulphate-rich inner layer in straw-fired utility boilers.

4.3. Summary

Several investigations of ash and deposit formation have been conducted at Danish straw-fired CHP boilers, including Haslev, Slagelse, Rudkøbing, Masnedø and Maribo-Sakskøbing. In all cases, very high concentrations of K and Cl, ~ 40-80 % of the total mass, have been measured in the fly ash, as well as in the inner layer of the deposits formed. The furnace ash reflects the chemistry of the bottom ash, and has a significant Ca and Si content, in addition to K and Cl. Furthermore, the aerosols formed in these plants have been shown to be very rich in K, S and Cl, and to be present in very high mass loadings, sometimes reaching ~ 800 – 2000 mg/Nm^3 (the latter probably being an extreme case for rape straw).

Due to the very high concentrations of K and Cl released from the straw, and the potential of corrosive attacks on heat transfer equipment, the metal temperature in the first generation straw-fired CHP plants had to be kept rather low at 450 °C, in order to avoid too fast corrosion. Therefore, the first generation plants had low electrical efficiencies. Nevertheless, for the second generation straw-fired CHP plants, the final superheater temperature has been increased to ~ [520 – 540 °C], creating higher electrical efficiency.

The means that can be applied to minimise these operational problems are:

- Resistant, but also much more expensive materials, which can better cope with the corrosive nature of alkali chloride salts at ~ 520-540 °C;
- To remove some of the corrosive species from the straw, before firing it on a grate. It has been demonstrated that grey straw, i.e. straw that has been washed out by nature (i.e. through rainfall on the field before collection and processing into bales) causes less corrosion and deposition than the normal yellow straw (with a normal level of K and Cl). Thus a pre-processing of the straw in order to remove the K and the Cl may be an option, although it is not clear, at present, whether this will be an economically attractive solution;

- To add an additive which will transform the highly flame-volatile Cl to a lesser corrosive form or prevent extensive sintering of deposits. This aspect will be addressed further in Chapter 9 of this thesis;
- Co-fire straw with another biomass, suitable for grate-firing and with lower ash, K, S and/or Cl content, e.g. wood, since this may cause a dilution of the system.
- Operate the plant with a reasonable soot-blower strategy. The effects and mechanisms of deposit shedding are addressed thoroughly in Chapter 10 of this thesis.

In addition to these immediate means of deposit and corrosion minimization, a certain modification of the boiler design may help minimise the corrosive problems, for example by introducing a division wall in the flue gas channel, thereby dividing the flue gas into a highly corrosive and a less corrosive fraction. There is also evidence from the Danish activities outlined in this chapter, that the contact pattern between hot flue gas and the heat transfer sections may affect corrosion in the actual boiler. The Masnedø and Maribo-Sakskøbing CHP boilers are examples of boilers designed to collect a rather thick depost/slag layer on the superheater tubes. Investigations at both plants revealed that the inner layer in this boiler was heavily sulphated after a certain operation time, and that the K_2SO_4-rich inner layer actually may help to protect heat transfer surfaces from further corrosive attack.

Chapter 5:

THERMAL CONVERSION OF STRAW IN SUSPENSION-FIRED UNITS

Co-firing of straw and coal in traditional coal-fired boilers, with a high electrical efficiency is the other major option for straw utilisation for heat and power production, employing the large investment and extensive infrastructure in existing fossil-fuel-based power systems [Baxter et al., 2000].

Danish coal-fired power plants, have electrical efficiencies in the range 43-48 % (higher heating value base), which is much higher than the electrical efficiency of 20-30 % in the smaller, conventional, dedicated straw-fired systems.

Straw co-firing causes a direct reduction of CO_2-emissions, in proportion to the straw co-firing share. When a proper choice of coal, boiler design and operation is made, the emission of traditional pollutants (SO_X, NO_X, etc.), and greenhouse gases (CO_2, CH_4, etc.) decreases [BioNorm, 2004]. Since straw has a lower content of inorganics than coals, a corresponding reduction in the quantities of solid residues from the plant is to be expected when co-firing [Baxter, 2004, 2005]. Thus, co-firing of coal and straw offers one of the most efficient and cheapest means of reducing greenhouse gas emissions from power generation, but is only applicable where coal firing plays a significant role in the electricity supply [Koppejan, 2004].

The major technical and non-technical challenges of biomass co-firing include [Sami et al., 2001; BioNorm, 2004; Koppejan, 2004; Maciejewska et al., 2006]:

1. Flame stability and unburned carbon issues;
2. Long term impacts of co-firing on the performance of SCR- and FGD- systems;
3. Effects on fly ash utilisation, e.g. reuse in cement or concrete production;
4. Effects on ash deposition and corrosion;
5. Pre-processing requirements for adequate conversion of the biomass share;
6. Effect of co-firing on the flows in boilers;

A recent survey of co-firing applications worldwide [Koppejan, 2004] indicated that more than 150 coal-fired power plants, have gained experience of co-firing coal with biomass or waste, at least on a trial basis. The majority of these are pulverised coal-fired boilers, but bubbling and circulating fluidised bed boilers, and grate-fired boilers have also been tested for co-firing capabilities. Co-firing activities have involved lignites, sub-bituminous coals, bituminous coals,

anthracites, petroleum coke, and oil. These fossil fuels have been co-fired with a very wide range of biofuels, including herbaceous and woody materials, wet and dry agricultural residues, and energy crops [Sami et al., 2001; Koppejan, 2004].

As already mentioned in Chapter 3 of this thesis, there are three basic options for co-firing for biomass materials in suspension-fired boilers [BioNorm, 2004; Maciejewska et al., 2006]:

- Direct co-firing is the least expensive, most straightforward and commonest approach. The biomass and coal are co-fired, using the same or separate mills and burners, depending mainly on the biomass fuel's characteristics.
- It is possible to apply a biomass gasifier to convert solid biomass into a fuel gas, which can subsequently be burned in a suspension-fired unit. This approach is known as indirect co-firing and offers a high degree of fuel flexibility.
- It is also possible to install a completely separate biomass-fired boiler and utilise the steam produced in this, in a nearby coal-fired power plant steam cycle. This approach has been applied in the Ensted and Avedøre, Unit 2, projects in Denmark.

Although more than 150 coal-fired power plants have experience of co-firing of a wide variety of biomass fuels, most plants have demonstrated operation for only a limited time period (typically a few weeks) or with a relatively low percentage of biomass being co-fired (on average 3% on an energy base) and for relatively clean types of (woody) biomass [Koppejan, 2004].

Below, is an outline of Danish experiences with coal-straw co-firing in PF-boilers.

In Table 5-1, major technical data for PF units that have been applied for coal-straw co-firing are provided.

5.1. Vestkraft Power Station, Unit 1, 1993-1994

From October 1993 to March 1994, a series of pioneering tests co-firing coal and wheat straw were conducted at the Vestkraft Power Station, Unit 1 (VKE1), in Esbjerg, Denmark. The boiler had a nominal input of 330 MW_{th}, and the final steam data measured 540 °C and 145 bar. It was wall-fired with 12 burners arranged in 3 rows. The two burners in the middle of the burner gallery were replaced by two cylindrical tubes for the introduction of straw during the tests. The straw was transported to the boiler pneumatically, via two separate straw cutters [EP94/0595].

In the original test plan, it was the intention to fire a highly volatile Colombian, coal with both 'grey' and 'yellow' wheat straw, and a Russian bituminous coal with 'yellow' wheat straw.

The terms 'grey' and 'yellow' refers to the amount of rain to which the straw has been exposed. Wheat straw washed through by rain on a field ('grey straw') is known to have a significantly lower content of K and Cl, than, for example wheat straw from a dry and sunny harvest ('yellow' straw). In practice, it proved impossible to control the straw quality during the tests, i.e. straw of almost equal quality was fired for the entire test period. A thermal input of 40 % straw was attempted, but it proved impossible, technically, to co-fire more than 25 % on a thermal base.

During the tests several operational stops were encountered in the straw cutting facility, and in some cases straw, introduced through the two central 'burners' (tubes) in the burner gallery, was blown directly across the furnace, ending up as a glowing phase of unburned carbonaceous materials, along the opposite wall. Here, it introduced a highly reducing local environment and caused pieces of straw, in particular the 'knees', to fall down to the bottom of the boiler, where it burned out in the ash hopper [Junker, 1997].

For the Colombian coal, a significant increase in the dust emission was observed during co-firing with straw (see Figure 5-1). For the Russian coal, although the dust emission was very high, no systematic dependence was found as a function of the straw fraction fired.

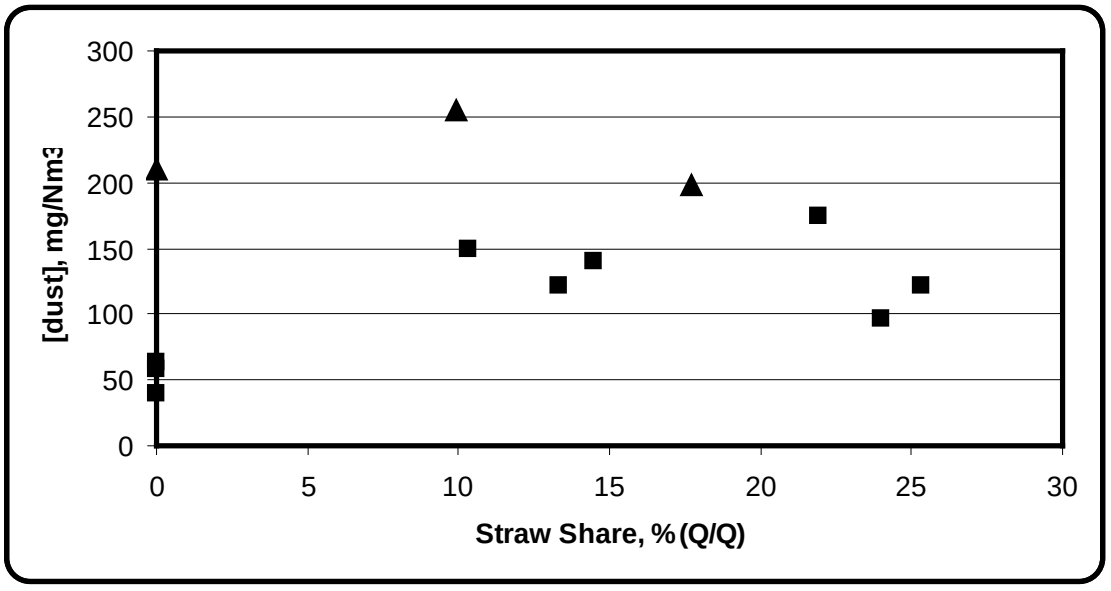

Figure 5-1: Dust emissions [mg/Nm^3, 6 % O_2, wet flue gas] vs. straw-fraction fired (on an energy base), as measured during the VKE1 coal-straw co-firing campaign. The triangles correspond to the Russian coal, while the squares represent the Colombian coal fired. Source: [EP94/0595].

Data:	Unit:	Vestkraft Unit 1	Amager Unit 3	Studstrup Unit 1	Studstrup Unit 4	Funen Unit 3	Ensted	Aved-øre
Started up	Year		1989	1968	1985	1974		
Firing system		Wall	Boxer	Wall	Boxer	Wall	Grate	Grate
Burner configuration		3 x 4	2 x 2 x 4	3 x 4	2 x 2 x 6			
Nominal efficiency	MWe	330 MWth	250	150	350	266		
Main fuel fired		Coal	Coal	Coal	Coal	Nat. gas	Straw	Straw
Straw share attempted	%(Q/Q)	25	20	20	20	3	100	100
Type of co-firing		Direct	Direct	Direct	Direct	Direct	Separate	Separate
Condition of biofuel		Straw	Pellets	Straw	Straw	Straw	Straw	Straw
Steam pressure	Bar	145	250		250	183		
Steam temperature	°C	540	545		540	540		
Steam production	kg/s							

Table 5-1: Technical data for the full-scale PF units referred to in this chapter.
Source: [CBT, 1998]

A thorough investigation of the fly ash was conducted, as a function of the straw-share fired. It was found that co-firing straw increased the content of total and available alkalies, whereas the content of water-soluble alkalies was almost constant in the fly ash. The content of SO_3 increased in the fly ash when (co-)firing the Colombian coal, while the Cl content increased for both coal types [EP94/0595] (see Figure 5-2).

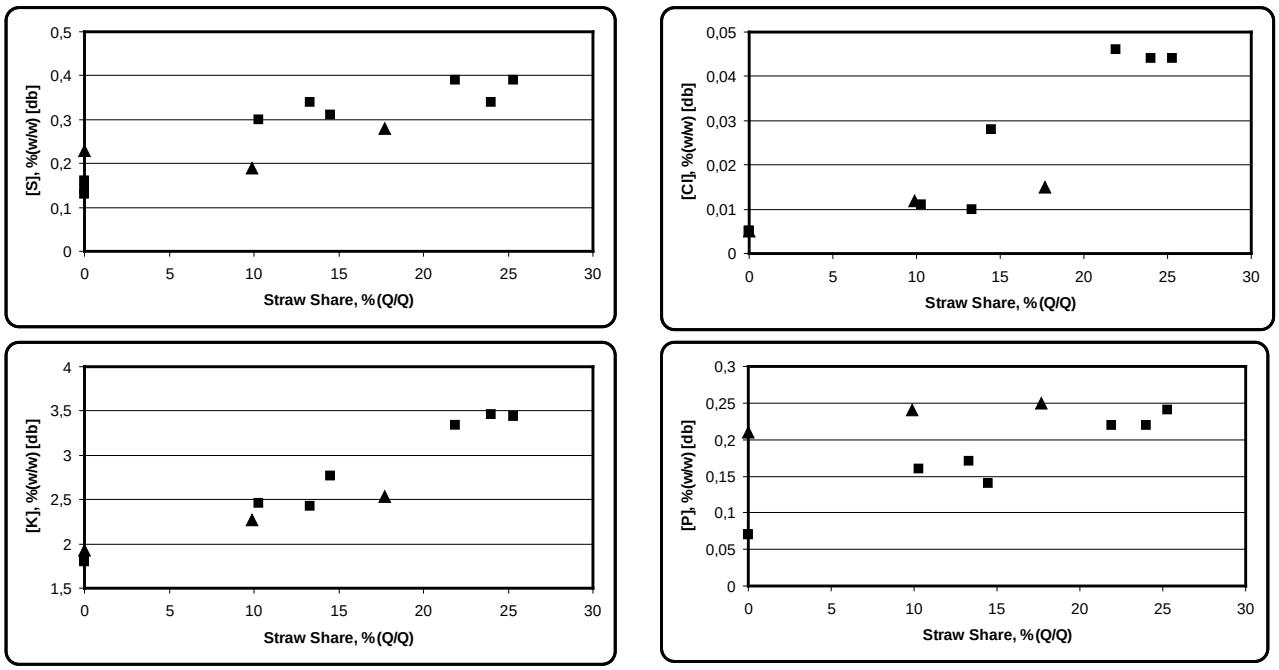

Figure 5-2: Concentration of S, Cl, K respectively P in the fly ash [%(w/w)] vs. straw-fraction fired (on an energy base), as measured during the VKE1 coal-straw co-firing campaign. The triangles correspond to the Russian coal, while the squares represent the Colombian coal fired. Source: [EP94/0595].

The capture of S in the fly ash proved to be rather low in all cases: 1-2 %(w/w) for firing of the Colombian coal alone and 5-6 %(w/w) when co-firing the Colombian coal and 25 % straw. For the Russian coal a 6-8 %(w/w) capture of S was observed independently of the feedstock fired. The Cl-capture was found to be up to 10 %(w/w) in the bottom ash, and up to 4 % in the fly ash [EP94/0595].

In 1994, the conclusion was that it would be almost impossible to keep the current limit for the total content of alkalies in fly ash if the straw share were higher than 10 % (on a thermal base) [EP94/0595].

5.2. Amager Power Station and the IFRF Semi-Industrial Furnace, 1994

In October 1994, experiments on co-firing wheat straw and coal were carried out at the Amager Power Station, Unit 3 (AMV3). The objectives were to investigate [1)] flame stability, [2)] flue gas emissions, [3)] performance of the electrostatic precipitator (ESP), [4)] short term effects on slagging and fouling in the furnace, and, [5)] potential effects of co-firing on the performance of the flue gas desulphurisation plant [Pedersen et al., 1996, 1997].

The main technical data for AMV3 are listed in Table 1. The boiler was a once-through type and designed for firing bituminous coal. It was fitted with 16 burners, in a staggered boxer arrangement, on the rear and front walls, respectively. The burners were air-staged, and had secondary and tertiary air inlets with swirl [Pedersen et al., 1996, 1997].

The experiments were divided into three series. Initially, one week of coal combustion was carried out in order to investigate the operation of the FGD plant with a high-S coal. In the second period, coal was blended with 10 % straw (on a thermal base) as pellets milled together with the coal, and, in the last period this share was increased to 20 %. During daytime, the power plant was operated at full load, whereas a reduced load occurred at night.

The coal fired was a Canadian high-S bituminous coal, with a lower heating value of 29.2 MJ/kg. The straw batches used were grown at two different locations in Denmark, but had a similar composition. In order to avoid difficulties with shredding the straw, it was delivered to the power station as compressed cylindrical pellets (~ 8 mm diameter, ~ 1000 kg/m^3 apparent density) which, although prepared without a binder, caused a small increase in the ash content, probably due to soil contamination.

The burners were operated with similar swirl and air inlets, irrespective of whether coal, or a coal-straw blend, was fired. Straw pellets and coal were mixed before entering the coal mills. Simultaneous grinding of coal and straw pellets in the roller mills caused no blockage [Pedersen et al., 1996, 1997].

During the co-firing of straw and coal, no severe operational problems were observed. Visual inspections of the flames were carried out during the test-firing, and no problems were discovered in sustaining a stable flame. However, when increasing the share of straw, the near-burner flame turned darker, indicating a lower temperature. On later inspection of the furnace, no flame impinging on the furnace walls was observed.

An increase in the straw share fired, increased S-retention, while the amount of excess air had no influence on this aspect. Increased S-retention in the ash may be explained by a higher content of K especially when co-firing an increased straw share, but Na and Ca may also play a

role. The potential for S-retention by Na, Ca and K increases from 4.3 % during coal-firing to 6.7 respectively 11.9 %, at 10 % and 20 % straw share, respectively on a thermal base.

Visual inspection before and after co-firing straw and coal showed that more deposit was formed on the pendent superheater during coal-firing as compared to co-firing. Only small amounts of deposits were formed on the tertiary superheater during co-firing (see Figure 5-3). In addition, minor slagging at the furnace walls, mainly around the burners, was observed both with and without co-firing.

Figure 5-3: Deposits formed on the pendent superheater in the top of the AMV3 furnace after one week of coal-firing (left image) and coal-straw co-firing (right image) during the AMV3 measuring campaign. Source: [Pedersen et al., 1996, 1997].

5.3. Midtkraft-Studstrup Power Station, Unit 1, 1996-1998

The Midtkraft-Studstrup Power Station, Unit 1 (MKS1), in Studstrup, Denmark, originally consisted of a 380 MW_{th} pc-boiler, and a 152 MW_e condensing turbine. The boiler was a two-pass wall-fired boiler, operated between 1968 and 1998. It was equipped with 12 conventional axial swirl burners, with four burners located at three levels. No flue gas cleaning was provided, except for an electrostatic precipitator for fly ash removal. During 1995, MKS1 was equipped to co-fire coal and straw, for demonstration purposes. The plant was taken permanently out of operation in 1998, due to excess capacity in the Elsam system. For further technical data, see Table 5-1.

The three medium-level burners in the MKS1 burner gallery were converted into combi-burners, meaning that the oil lance and flame watch were relocated, in order to clear the core of the burner for pneumatic straw-feeding (see Figure 5-4) [Wieck-Hansen et al., 2000]. In addition, the plant was equipped with a pilot plant after the ESP, for low-dust SCR catalyst testing. High-dust SCR catalyst tests were carried out directly in the flue gas, between the two economiser sections.

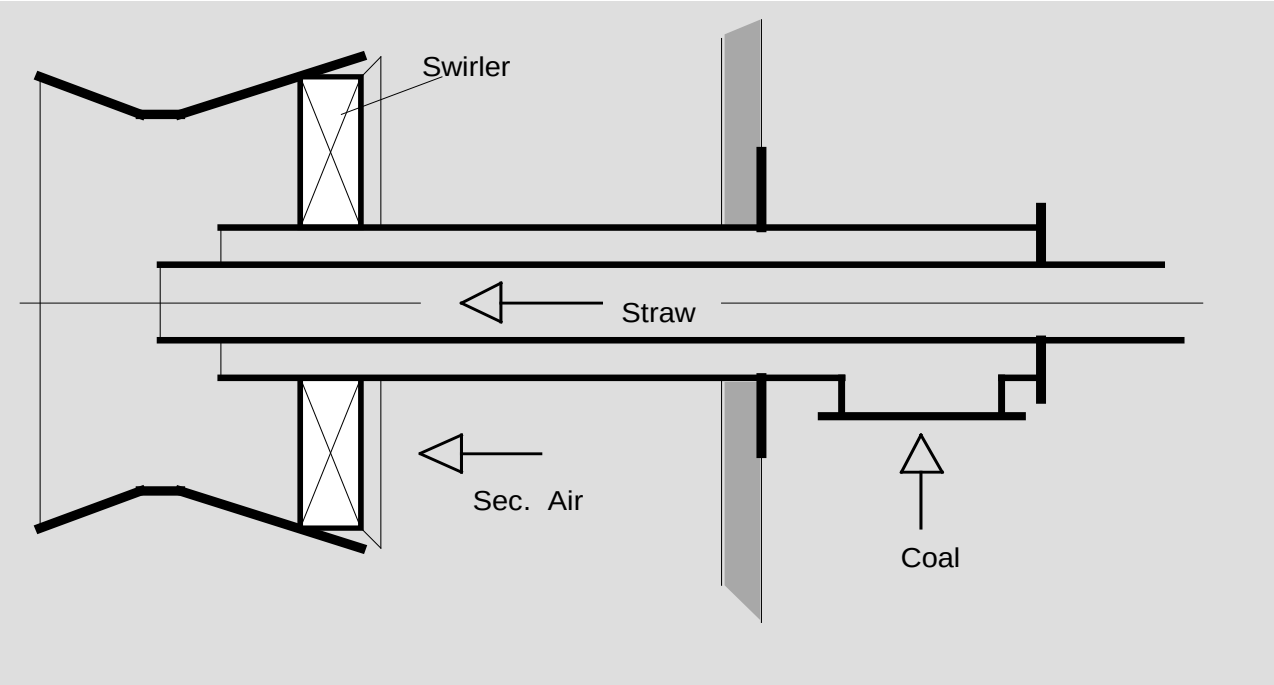

Figure 5-4: Coal-straw combi-burner for co-firing, as applied at MKS1. Source: [Andersen, 1998].

Several measurements were conducted in the MKS1 campaign (see Table 5-2) in order to test the following parameters:

- Straw share;
- Particle size of straw;
- Velocity in burners and pneumatic transport system;
- Boiler load
- Oxygen percentage

Load (%)	**Attempted straw fraction [energy base]:**		
	0 %	10 %	20 %
50 %	1		7
75 %	2		6
100 %	3,3B,E2,9,9B	4	5,E1,8,8B

Table 5-2: Experiment numbers vs. load variations and attempted straw shares in the MKS1 campaign. The maximum straw share reached was approximately 16 % on an energy base. Source: [Andersen, 1998].

In general, boiler performance was satisfactory. The unburned carbon in the bottom ash increased with increasing straw-share during co-firing. Burnout problems occurred most likely as a result of insufficient residence time for some of the straw particles, in the combustion zone [Wieck-Hansen et al., 2000].

The straw-handling equipment consisted of a storage facility, and a processing building. Storage was split into two sections, each having a capacity of 560 Heston bales. The bales were stacked in six layers and delivered to MKS1 by trucks. An overhead crane unloaded the trucks. During unloading, the bales were weighed, the moisture content measured by a microwave technique, and the data stored on a central logistics computer [Wieck-Hansen et al., 2000].

The processing plant consisted of four parallel lines each with the capacity to handle up to 5 tonnes of straw per hour. After being shredded, the flow of straw was made uniform, and the straw sucked through a stone trap, removing heavy tramp materials. From this point the straw was led into the hammer mill, where it was ground to pieces shorter than 30 - 50 mm, depending on the sieve applied.

Two types of cylindrical stainless steel probes with an outer diameter of 38 mm were used for deposit sampling at MKS-1. Water- and air-cooled probes were used in the hot positions 1-3, and air-cooled probes in the cooler positions 4 and 5 (see Figure 5-5). The set point metal temperatures used in the experiments were 400°C in probe positions 4 and 5, 540°C in probe positions 1-4, 580°C in probe positions 1-3, and 620°C in probe positions 1-3. At each metal temperature, deposit samples were collected after 15 minutes, 3 hours and 18 hours exposure in the boiler. In addition, a few deposits were collected after 72 hours exposure.

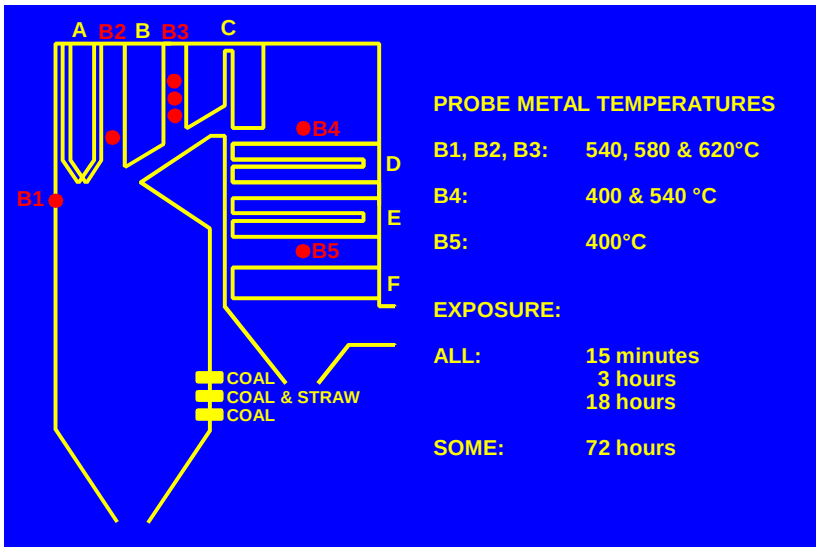

Figure 5-5: Sketch of the MKS1-boiler. Positions, metal temperatures and exposure times for the probe deposit measurements are shown. Source:[Andersen, 1998].

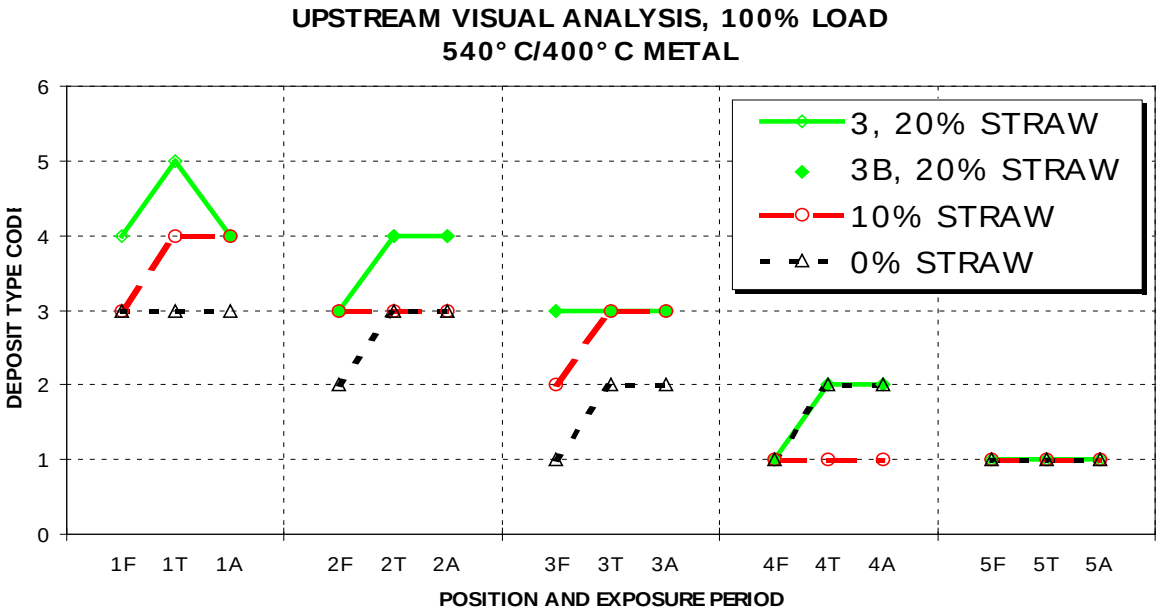

Figure 5-6: Deposit tenacity as a function of straw share, probe position and exposure time at 100 % load in the MKS1-boiler. Exposure times: F – 15 min, T – 3 hours, A – 18 hours. Source: [Andersen, 1998].

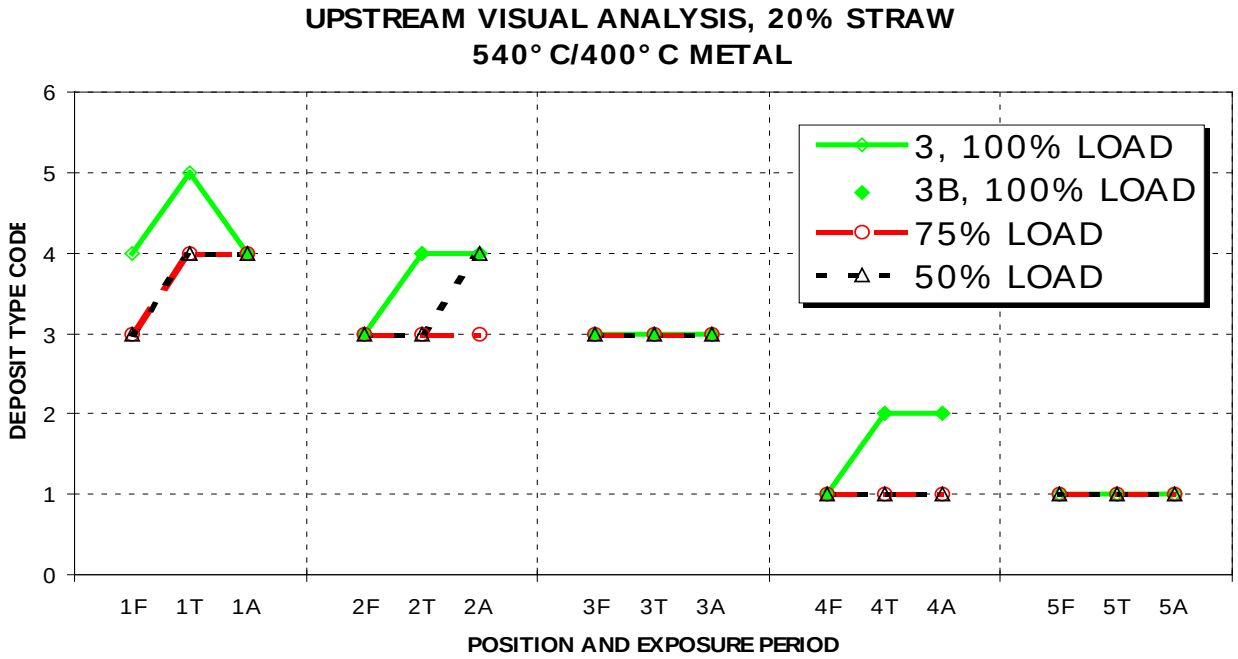

Figure 5-7: Deposit tenacity as a function of load, probe position and exposure time at 20 % straw share in the MKS1-boiler. Exposure times: F – 15 min, T – 3 hours, A – 18 hours. Source: [Andersen, 1998].

A total of more than 240 deposit samples were collected. It was therefore decided to develop a visual analysis technique based on the deposit physical appearance, in order to compare, for instance the deposit amount and tenacity of a huge number of deposits as a function of straw share, boiler load, exposure time etc. The visual analysis is based on a detailed SEM-investigation of the deposit samples [Andersen, 1998; Andersen et al., 2000] (see Figures 5-6 and 5-7).

It is evident from Figures 5-6 and 5-7, that the deposits formed in position 1 generally have a higher deposit index-value, than those formed further downstream in the flue gas channel (positions 2-5). Furthermore, increased straw share, load and exposure time causes increased tenacity of the deposits [Andersen, 1998; Andersen et al., 2000].

Based on the deposit measurements, the following conclusions were drawn from the demonstration programme [Wieck-Hansen et al., 2000]:

- The concentrations of Cl in the probe, and superheater deposits, were in all cases below 0,5 %(w/w). Thus, the main part of Cl is expected to leave the boiler, as gaseous HCl, and corrosion caused by Cl, are believed to be negligible.
- The main part of the K was captured by Al and Si, as K-Al silicates, while only a trace amount of K reacted with S, forming K_2SO_4. The formation of K_2SO_4 may cause sticky deposits, and [K] (the concentration of K) and [S] are observed to increase in upstream deposits, during co-firing.
- The coal-type almost fully controls the behaviour of K and Cl in the straw.
- Shedding was found to increase at 20 % straw share and full load, especially at high flue gas temperatures, for the upstream deposits.

Thus, to sum up the deposit investigations, fouling during co-firing may be handled well by soot-blowing, while slag formation in the furnace zone may cause problems.

Concerning Cl- and S-chemistry in flue gases, typical coals fired in Denmark are low in chlorine (< 0.1 %(w/w)), while the concentration in straw varies in the range: 0.2 – 0.6 %(w/w). With the low calorific value of straw compared to coal, the emission of HCl naturally increases, as a consequence of coal-straw co-firing. The mass balance studies at MKS1 showed that at 20 % straw share, the emission of HCl accounted for about 92 % of the total Cl-input [Hansen, 1997]. The S content is lower in straw than in coal. Thus, a reduction in the sulphur emission was expected during co-firing. In fact, it was found that the reduction was even higher than expected. From fly ash analyses, it was found that the S-capture increased from about 3 to 4 %, when co-firing straw with a typical coal, but when co-firing with a high-S coal, the capture was found to be as high as 7 %. The increased S-capture was most likely due to the formation of K_2SO_4 [Wieck-Hansen et al., 2000], as also found at AMV3.

A higher dust emission was expected, and verified, when co-firing straw with coal. Aerosol measurements did not show any increase in the amount of aerosols when co-firing, but their composition changed as a function of straw share [Nielsen, 1998].

5.4. RWE Test Facility, Reinhausen, Germany, 2000-2001

The experience from MKS1 indicated that coal quality has a pronounced effect on the formation of fly ash and deposits during the co-firing of coal and straw in PF units. Thus, as part of the EU-Deposit Prediction R&D-project, it was decided to investigate the effect of co-firing a typical Danish wheat straw, rich in K and Cl, with a Rheinish brown coal (lignite), rich in S, and in some cases also Na and Ca [EU-Deposit Prediction, 2001]

The experiments were carried out at the RWE Pulverized Fuel Combustion (PFC) test-rig in Reinhausen, Germany, firing three common Rheinish brown coals as reference, and co-firing these coals with pelletised straw (up to 30 % straw share on a thermal base).

The test-rig had a capacity of 1 MW_{th}. The total length of the furnace chamber ws 13.40 m, of which the radiant section constitute 7.50 m, with an inner diameter of 1.05 m (see Figure 5-8).

The furnace temperature was 1000 – 1500 °C, with a total residence time of 3-6 s. At full load, 100 – 190 kg/hr dry brown coal was fed to the test-rig.

A straw share of 15 and 30 % of the thermal input was intended, and the straw was added as pellets to the coal, before pre-drying/milling in a beater fan mill. The Rheinish brown coals fired, were from the open cast Hambach and Garzweiler mines, and showed comparable ash- and sulphur contents, but differences in the Na- and Ca-concentrations. The flue gas-temperature at the exit of the combustion chamber was kept at 1050, 1150 and 1250 °C respectively, and the air ratio (λ) near the burner varied between 0.8 and 1.1, and, was combined with air staging.

Deposit samples were collected on specially designed cylindrical, ceramic, un-cooled probes inserted into the test-rig, using doors at different positions for a given time. During each individual trial, samples of the fuel blends (near the burner), fly ashes (from the electrostatic precipitator), and deposit samples, were taken.

The results of the investigations are briefly summarised below.

The straw pellets fired, showed a good dosing behaviour, ensuring stable test conditions. It was possible to mill the straw pellets together with a raw, Rheinish brown coal, in a beater fan mill

with a classifier (up to 30 % straw on a thermal base). All the co-firing ratios investigated, experienced an adequate ignition and burning behaviour.

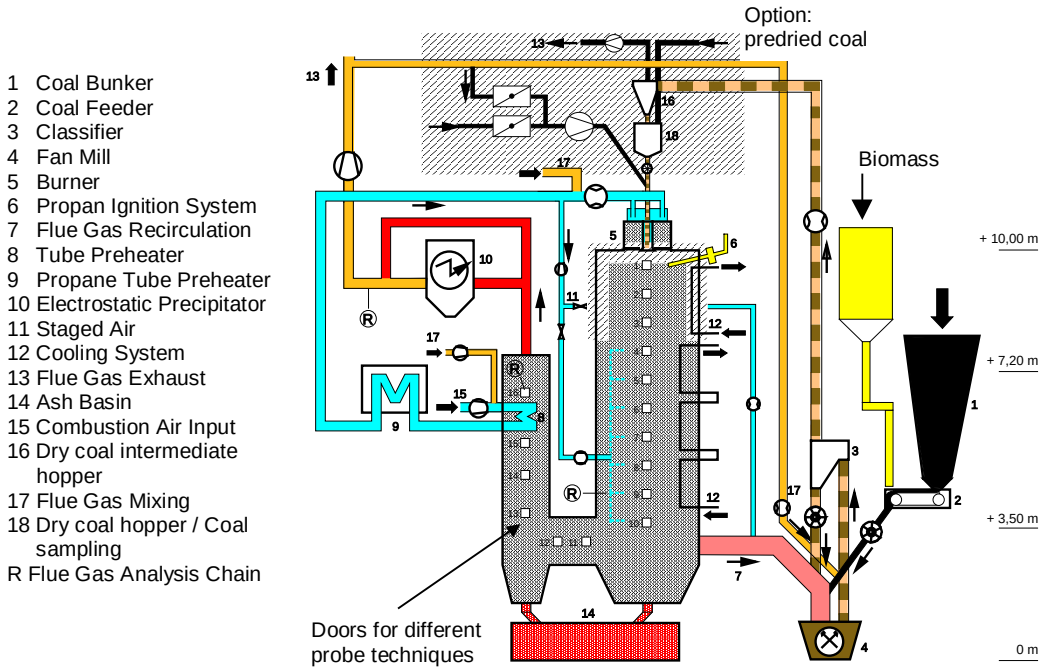

Figure 5-8: Flow scheme of the RWE PFC test rig (1MW).

The composition of the fly ash during co-firing is determined by the base coal fired. This effect is even more pronounced for the fly ash than for the deposits. There was no clear influence from the straw share on the fly ash particle size distribution. The main crystalline phases, detected by XRD-analysis on the co-firing fly ash, were: SiO_2, $CaSO_4$, Fe_2O_3, $Ca_2Fe_2O_5$, CaO, MgO. Potassium was highly enriched in the fly ash from co-firing straw and coal, compared to the fly ash from individual firing of the Rheinish brown coals.

The coal from the high-ash Garzweiler brown coal seam caused the formation of SO_4^{2-}-rich deposits, at temperatures up to 1150°C, and almost S-free, but Si-rich deposits with a soft consistency at 1250 °C. In comparison, the low-ash coal from Hambach produced SO_4^{2-}-rich deposits up to 1150 °C. Remarkably, the strength of the deposit at 1050 °C was harder than at 1150 °C. Co-firing with straw formed deposits with less S compared to individual firing of the Rheinish brown coals (see Figure 5-9).

Furthermore, deposits from co-firing had a higher content of K, than deposits formed when firing brown coal alone (see Figure 5-9). On a microscopic scale, the increased K content was found in the outer (glassy) layer of the deposits. No effect of P (from straw) was observed on the deposit properties.

Compact slags with low porosity were found only on probes near the flame-region - ports 1-2 in Figure 5-8. An increase in the hardness of deposits as a function of increased straw-share fired, was observed for all the investigated furnace exit gas temperatures (1050, 1150, 1250 °C).

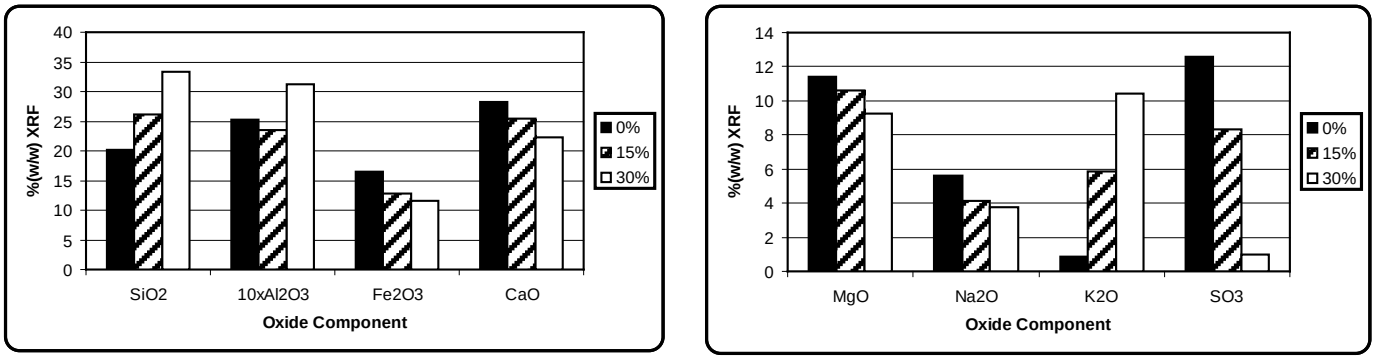

Figure 5-9: Chemical composition of deposit vs. straw share when co-firing straw with Hambach 42 brown coal. The deposits have been collected in port 10 of the RWE test rig with T_{gas} = 1050 °C. The chemical analysis is determined by use of X-Ray Flourescence analysis.

Thus, in order to sum up the RWE co-firing tests, the character of deposits formed during co-firing were determined mainly by the characteristics (ash content and composition) of the base coal fired. In fact, the influence of the increased amount of K added with increased straw share fired, as a fluxing agent, is very important for the formation of slags. The decreasing softening temperatures of the deposits from the co-combustion tests, indicate a potential danger of densification, pointing toward a higher frequency of cleaning devices like soot blowers in a full-scale boiler operation.

5.5. Midtkraft-Studstrup Power Station, Unit 4, 2002-2003

As mentioned above, in 1998, it was not possible to utilise fly ash from the co-firing of coal and straw for cement or concrete production, and commercial use of co-firing in PF furnaces was therefore not possible. This obstacle was partly removed some years later, when the requirements for fly ash for cement production were revised.

As a consequence, the 350 MW_e Studstrup Power Station, Unit 4 (SSV4), a coal-fired unit commissioned in 1985, was converted to coal-straw co-firing at the beginning of 2002 [Sander

and Wieck-Hansen, 2005]. The boiler is a once-through, single reheat type, fitted with 24 low-NOx burners on two levels arranged as an opposed wall firing set-up. The maximum straw-firing capacity of the boiler was around 20 tonnes/h, corresponding to a straw share of 10 % (energy base), at full boiler load. The steam temperature was 540 °C at 250 bar, see Table 5-1. The boiler was equipped with a semi-dry desulphurization plant. Four of the six upper level burners on the rear furnace wall were converted into combined coal/straw burners, modifications of which involved only a few minor changes. The oil lance and flame scanner were relocated, in order to clear the core of the burner for pneumatic straw feeding. Imported coals from South Africa and Colombia were fired. Most of the straw fired was wheat straw, but barley, oats, hay and rape straw were also received.

For each coal type, the planned combinations of boiler load and straw share are shown in Table 5-3.

Boiler load (%)	**100**	**100**	**100**	**75**	**75**	**50**	**50**	**30**	**30**	**30**
Straw share (%)	0	10	15	10	20	10	20	0	30	30

Table 5-3: Attempted boiler load and straw share (%(w/w)). Source: [Sander and Wieck-Hansen, 2005].

Alkali chemistry was studied by analysing the content of water-soluble elements (K, Na, Ca, Mg, Cl, P, and S) in fly ash from SSV4, as a function of straw share (0-20 % (weight base)), boiler load (30 – 100 %), and coal properties (three different coal types were selected in order to cover a range of ash contents: 6.5 – 15.0 %(w/w)) [Sander and Wieck-Hansen, 2005].

Fly ash samples were achieved by sampling from the flue gas duct, upstream of the ESP, by use of conventional flue gas sampling equipment. Selected samples of fly ash were analysed for their macro element content. Significant changes in fly ash composition were seen for K, Ca and P, and a mass balance calculation was set up for these elements.

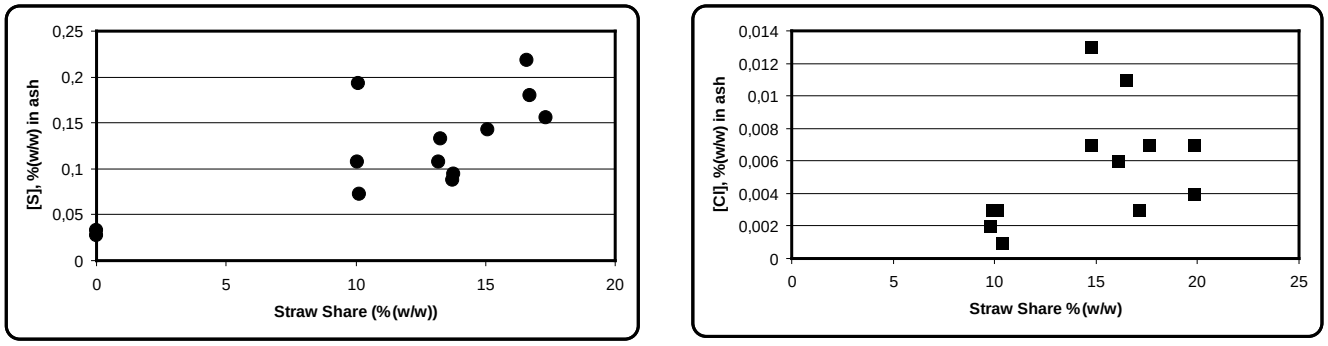

Figure 5-10: S- and Cl-content in fly ash samples from the coal-straw co-firing campaign at the Studstrup Power Station, Unit 4. Source: [Sander and Wieck-Hansen, 2005].

[S] was found to increase in the fly ash with an increase in the amount of straw share co-fired, in accordance with the findings from AMV3, although a certain scattering appeared in the data (see Figure 5-10). [Cl] in the fly ash was also increased by co-firing straw, but the level was very low, and showed significant scattering. In all combinations of coal type, load and straw share, [Cl] did not exceed 0.03 %. For all coal types, the content of water-soluble K in the fly ash increased when co-firing straw, but the level was different. The study of alkali chemistry indicated that an increased content of ash in coal improved the conversion of K from straw into insoluble K-Al silicates [Sander and Wieck-Hansen, 2005].

Based on the data from SSV4, it was concluded that by co-firing of up to 20 %(w/w) of straw in a coal-fired boiler [Sander and Wieck-Hansen, 2005]:

- Less than 5 % of the Cl in the fuels was captured by the fly ash, there is no risk of Cl corrosion, and; [Cl] in the ash is below the limits defined for utilisation in cement and concrete;
- The content of water-soluble K (mainly present as K_2SO_4) in the fly ash, increases when co-firing straw;
- The part of K from straw converted to K_2SO_4, depend on the content of ash and [S] in the coal; low conversion is obtained by high ash, and low [S];
- The risk of increased deactivation of high-dust SCR catalysts, is highest for coal with low ash or high S contents for high straw shares, and for straw with a high content of K;
- Fly ash from co-firing up to 20 %(w/w) of straw in coal-fired power stations can be applied for concrete production on equal basis as fly ash from coal-firing alone.

5.6. The Funen Power Station, 2001

In 2001, Elsam converted its natural gas-fired Funen Power Station, Unit 3 (FV3), in Odense, Denmark, to co-firing gas and straw. The conversion included establishing a straw pre-processing plant similar to the one at MKS1 with a capacity of 5 ton/hour. In addition, the burner system was modified [Overgaard et al., 2005].

FV3 consist of a 266 MW_e natural gas-fired unit, commissioned in 1974. The boiler was originally designed for oil-firing, but in 1979, it was converted into coal-firing, and in 1986, into natural gas-firing. The boiler a two-pass wall-fired single-reheat boiler fitted with 18 burners arranged on three levels. The final steam data were 535 °C, and 183 bar, see Table 5-1. No flue gas cleaning was provided, except for an electrostatic precipitator. Three burners were conver-ted to combi-burners capable of co-firing gas and straw, one fuel at a time.

The objective of the test programme at FV3 was to test whether co-firing natural gas and straw was a viable technology, for centralised natural gas-fired units, meaning that the concept from a technical point-of-view, is competitive compared to other straw utilisation concepts for electricity production [Overgaard et al., 2005].

During the test programme, natural gas, straw, meat and bone meal were used as fuels.

The introduction of straw through the modified burners was tried at all three burner levels, in order to find the most effective point/level, in terms of burnout and deposit formation. In addition, the introduction of straw through an observation door on the front wall of the boiler between burner levels 61 and 62 was tested. The test started on a burner in the top level, continued to a burner in the middle burner level, then the observation door between levels 61 and 62 was tested, and, finally, a burner in the lowest burner level was tested [Overgaard et al., 2005].

When co-firing straw and natural gas, a foreseen problem is sufficient cooling of the fly ash particles from the straw, before they approach the superheaters. If the fly ash particles from the straw have a temperature that is too high, they may soften and stick to the superheater tubes. The configuration of the furnace together with the opposed wall-firing gave a high upwards flow in the centre of the furnace [Overgaard et al., 2005]. This non-uniform flow distribution has a tendency to bring glowing straw particles high up in the furnace, and deep into the convective part of the boiler. During the tests it became clear that the further down in the furnace the straw was introduced, the less deposit formation was observed in the superheater section. In addition, fewer glowing particles could be observed through the observation doors in the superheater section. By introducing the straw in the lower part of the furnace, another problem occurred, since more unburned straw found its way to the bottom ash hopper. By introducing recirculation, the amount of unburned straw in the bottom ash was reduced to some extent.

The tests at FV3 showed that the 2S/Cl-ratio in the probe deposits formed close to SH2, SH3 and RH do not deviate significantly from the 2S/Cl measured in tests at 100 % straw-fired boilers. Flue gas measurements during the addition of S showed that SO_2 and HCl emissions increase indicating the transformation of KCl to K_2SO_4 (with the release of HCl). When S is added to the system, a considerable decrease in the concentration of Cl in the deposits was detected [Overgaard et al., 2005].

To sum up, co-firing of straw and natural gas does not seem to be the most efficient way to utilise straw in electricity production. When firing straw in suspension, a large part of the ash is carried upwards, in comparison to grate-fired boilers, causing extensive exposure to the superheaters, and the furnace gas temperature is typically higher in natural gas fired units,

which makes the straw ash more sticky. Co-firing of coal and straw is therefore a more efficient way to bring straw into electricity production [Overgaard et al., 2004, 2005].

5.7. Summary

As with dedicated, straw-fired CHP plants, several studies have been conducted in order to deduce the effect of coal-straw co-firing in suspension on ash and deposit formation and chemistry. The big advantage of these plants is that they possess a much higher electrical efficiency, 40 – 45 %, compared to 20-25 % for the dedicated straw-fired plants. Thus, by adding straw to PF firing in direct co-firing with coal, one can obtain a much more efficient CO_2-reduction than by generating the same amount of electricity in a dedicated straw-fired plant.

The baseline study of co-firing at the Midtkraft-Studstrup Power Station, Unit 1, MKS1, revealed that the storage and handling of straw for direct co-firing were indeed possible, and that the amount of deposits as well as the aerosol mass loading is not critical, provided that the coal co-fired is high in quality, i.e. an ash with a reasonably high content of Al-silicates.

The trick is to ensure that the K release from the straw is fixed in the Al silicate rich coal ash, thereby releasing Cl as the rather harmless HCl, instead of forming KCl, which may condense on heat transfer surfaces in the system, causing subsequent serious corrosion, as found in dedicated straw-fired systems.

Moreover, the test-firings conducted as part of the Deposit Prediction project at the RWE test facility in Germany, clearly high-lighted the consequences of applying low-quality coal. In these tests, a yellow (i.e. high-K) Danish straw was co-fired with German brown coal, a solution that cannot be recommended. Thus, the coal quality is a very important, controlling, parameter for the success of coal-straw co-firing.

Initially, the main concern was the quality of the ash produced during co-firing, would it be possible to sell and reuse the ash ? Nevertheless, now that the European fly ash quality standard has been changed politically, the main focus of co-firing is on the poisoning of SCR catalysts, a problem that remains to this day.

Some attempts have been made to co-fire straw with other fuels, e.g. straw at the Funen power station, but it turned out to be ineffective, due to the lack of Al silicate rich ash in natural gas, the sink that drains the flue gas for its content of K in coal-straw co-fired systems.

Chapter 6:

INVESTIGATION OF COAL-STRAW CO-FIRING IN PILOT-SCALE REACTORS

Carrying out full-scale experiments in order to test the performance of co-firing of coal and straw with respect to ash quality, deposition and/or corrosion is rather expensive and a huge logistical task. In addition, it is very difficult to control all relevant parameters in full-scale measuring campaigns. Thus, a number of investigations of deposit formation, and especially sulphation of ashes in co-fired systems, have been conducted at pilot-scale facilities. First and foremost, the Sandia National Laboratory Multi-Fuel Combustor (SNL-MFC) has been applied intensively [Junker, 1997; Robinson et al., 2002; Nielsen, 1998; Nielsen et al., 2000a], but experiments have also been conducted in the University of Toronto (UT) [Theis et al., 2006a-c] and the CHEC [Zheng et al., 2007] entrained flow reactors (EFRs). Below, is an outline of the major findings and results derived during these investigations.

6.1. [Junker, 1997] Deposition Studies at the SNL-MFC

The SNL-MFC is a pilot-scale (30 kW_{th}), down-fired, turbulent flow reactor simulating the gas temperature and composition profile experienced by particles in a real combustion system. The reactor is 4.2 metres high and has an inner ceramic tube, with an inner diameter of 15 cm (see Figure 6-1).

The SNL-MFC consists of a natural gas burner located at the top of the reactor, and seven electrically heated sections below that. Below these, is the test section of the combustor, which is an optically, and physically, accessible region, where probes and combustion diagnostics may be applied.

Further details on the SNL-MFC operation, and the characteristics of fuels typically fired in the reactor, are provided in detail in [Junker, 1997; Robinson et al., 2002].

In the test section of the SNL-MFC, ash deposition can be studied by means of two types of probes; one consisting of a tube, with an outer diameter of 16 mm (thereby matching the Stoke's number of particles in a commercial system), placed in cross flow with the gas; the other is constructed for the purpose of studying condensation.

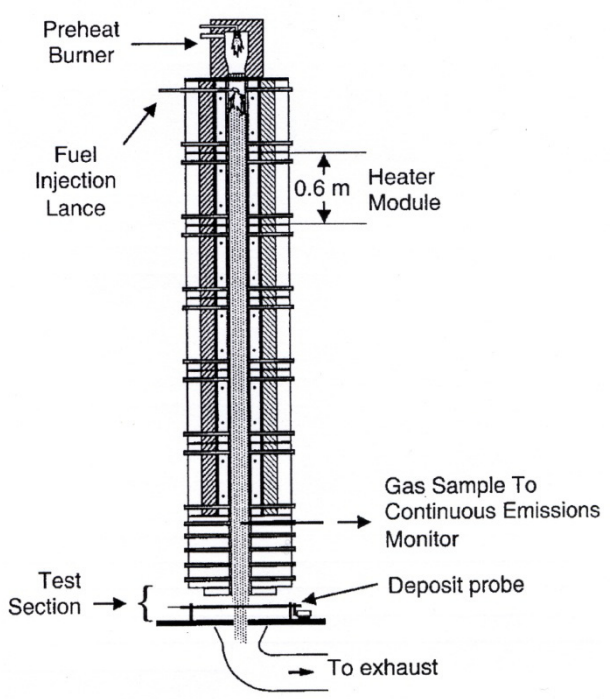

[Junker, 1997; Robinson et al., 2002] conducted a rather intensive study of co-firing of coal and straw in the SNL-MFC, examining deposit from the blends of four types of coal, namely Eastern Kentucky (EK), Pittsburgh No. 8 (P8), Black Thunder (BT), and a South American (SA) coal, with four different biomass fuels, Red Oak wood (RO), Imperical (American) wheat straw (IS), Danish wheat straw (DS), and Switchgrass (SG).

Figure 6-1: The SNL-MFC. Source: [Robinson et al., 2002].

For further details on fuel/blend characteristics, please refer to [Junker, 1997; Robinson et al., 2002].

The coal samples were fired in pulverised form, commercial grind, 70 % through 200 mesh. Samples of the biomass fuel were milled enough to pass through a 1-mm mesh.

Ash deposits from different blends of biomass and coal were collected using the 16 mm outer diameter, air-cooled probe, placed below the exit from the SNL-MFC, and designed to simulate a superheater coil as they appear in a commercial boiler. A constant probe surface temperature between 460 °C and 540 °C, was maintained during the experiments.

All combustion experiments were conducted with an excess O_2-concentration of 3 %(v/v), and a furnace exit gas temperature of 1000 °C. Deposit sampling was typically conducted over a 60 minute period, in order to ensure enough deposit on the probe for a wet chemical analysis to be conducted, but on the other hand this gave a short enough amount of time to minimise the risk of deposit shedding [Robinson et al., 2002]. A limited number of 4 hour tests were conducted in order to examine the influence of exposure time on the chemical composition of the deposits formed on the probe.

The results from the SNL-MFC measuring campaign are illustrated by use of three main parameters:

The ash deposition rate, DR, (grams of deposit per gram of fuel), is defined as:

$$DR = \frac{M_a}{0{,}13 \cdot M_f} \tag{6-1}$$

where M_a is the mass of ash deposit, M_f is the mass of the fuel fired, and 0.13 is the fraction of the cross sectional area of the MFC occupied by the probe [Robinson et al., 2002].

Particle collection efficiency β, is a more convenient parameter than the deposition rate comparing the ash deposition characteristics of different fuels, since it accounts for differences in fuel ash content. The particle collection efficiency is defined as:

$$\beta = \frac{DR}{X_a} \tag{6-2}$$

where X_a is the mass fraction of ash in the fuel on an as-received base.

The enrichment factor, EF_i, addressing enrichment of an element, i, in a deposit compared to the fuel ash, is defined as:

$$EF_i = \frac{X_{d,i}}{X_{a,i}} \tag{6-3}$$

where $X_{d,i}$ is the mass fraction of element i in the deposit on a carbon-free base, and $X_{a,i}$ is the mass fraction of element i in the fuel ash.

6.1.1. Results from the SNL-MFC Deposition Experiments

Over a one hour period, the EK-coal formed a relatively thin deposit, with a triangular shape on the leading edge (upstream side) of the probe, indicating that the fly ash particles from EK-coal are likely to bounce off upon impact. The deposits showed as a general powdery structure, and could easily be blown off the probe [Robinson et al., 2002].

When fired alone, the RO-wood formed almost no deposit. Closer examination by SEM revealed a fume-like deposit with only very few impacted particles on the upstream side of the probe. Shiny, bare metal was visible on the downstream side of the probe [Robinson et al., 2002].

The IS wheat straw formed significantly larger deposits, than the EK-coal and RO-wood. The IS-deposit had a ~1 cm thick layer of impacted particles with a columnar, boxy structure on the upstream side of the probe [Robinson et al., 2002]. The dark colour of the deposit was not due to unburned carbon, being as low as 0.6 % on a mass base. A thick white layer consisting of condensed alkali chlorides was observed along the sides, and on the down stream side of the probe.

Figure 6-2 shows the deposition rates (g deposit/kg fuel) measured while firing unblended fuels. The deposition rates for the coals are similar – 1.3; 2.0; 2.2; respectively 4.5 g of deposit per kg of fuel, for the BT, P8, EK and SA coals. However, a factor of almost 800 separated the ash deposition rates of the biomass fuels, with RO wood and IS wheat straw, as the two extremes within the experiment (see Figure 6-2) [Robinson et al., 2002]. The deposition rate of RO, 0.04 g deposit/kg of fuel, was found to be almost two orders of magnitude smaller than that of the entire suite of coals investigated. The deposition rate of switchgrass, 0.4 g deposit/kg of fuel, was also lower than that observed for the coals.

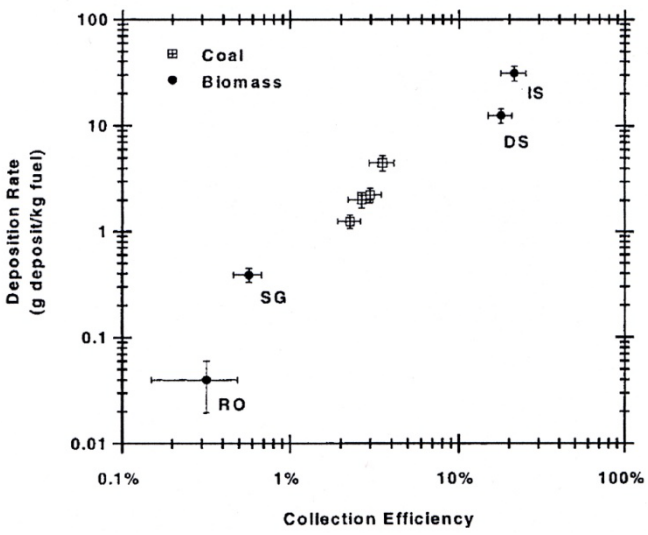

A factor of 65 separates the particle collection efficiencies of the different biomass samples, which reflects the significant differences in deposition characteristics of the biomass samples. [Robinson et al., 2002] attribute the factor of 65 to a combination of chemistry and particle size effects.

Figure 6-2: Deposition rate as a function of particle collection effici-ency. Source: [Robinson et al, 2002].

The high alkali-content (especially K) of the straw causes more sticky particles, and softer ash deposits, which increases the sticking probability of the fly ash particles. Furthermore, a typical straw fly ash particle is much larger than a wood fly ash particle from fuel particles of the same initial size, mainly because of the much higher ash content, and the presence of large silica grains in the straw. The larger particle size increases the impaction rates of IS-straw fly ash particles, compared to that of the RO-wood fly ash particles, since the inertial impaction efficiencies depend on the square of the particle diameter [Robinson et al., 2002].

The formation of alkali silicates may explain the enhancement in [Si] in the ash deposits formed while firing straw (see Figure 6-3a). Figure 6-3b shows significant changes in deposit alkali levels relative to fuel ash for the biomass fuels. The K-levels in both straw deposits are lower than those of the fuel ash. The same applies for S and Cl (see Figure 6-3c).

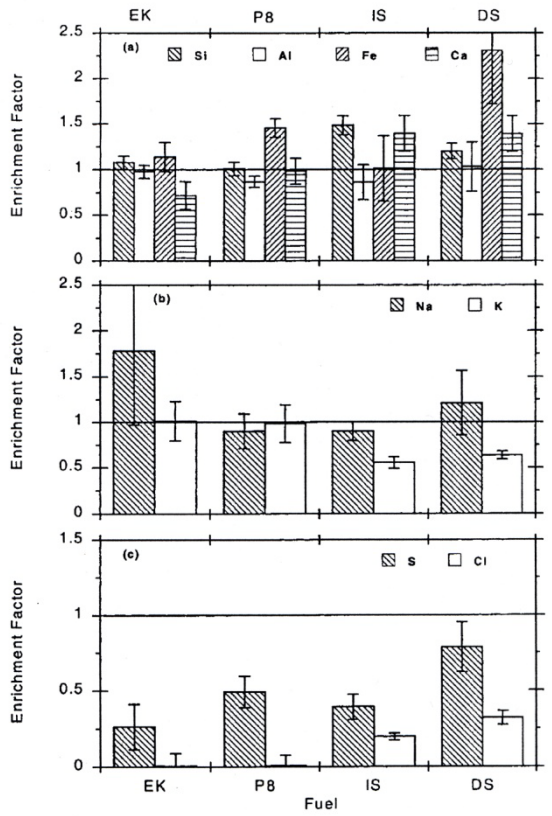

Figure 6-3c shows a substantial reduction of Cl and S concentration in the deposits formed while firing straw.

The depletion of alkali species in the straw deposits relatively to the fuel ash indicates that these species are released to the gas phase during the combustion process, which is consistent with the data reported by [Knudsen, 2004].

For short-duration tests such as these, gas-phase alkali primarily contributes to the deposit formation via condensation. In addition, alkali species can react with silicon in order to form alkali silicates.

Figure 6-3: Deposit composition reported as EFs. Source: [Robinson et al., 2002].

The data published by [Robinson et al., 2002] indicate that the particle collection efficiencies for all the co-fire blends, fall between the observed behaviours of the unblended fuels. Thus, blending straw with coal creates a fuel blend with lower collection efficiency than an unblended straw, but with higher collection efficiency than an unblended coal.

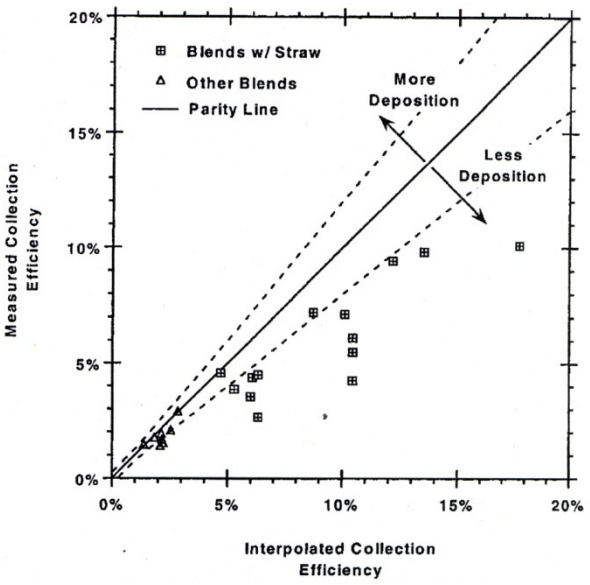

A parity diagram plots interpolated versus measured particle collection efficiencies for all of the co-fire blends [Robinson et al., 2002]. Such a diagram, combining all of the particle collection efficiency data for all of the co-fire blends, is shown in Figure 6-4. The dashed lines indicate an estimate of the experimental uncertainty (± 20 %). All of the blends fall on or below the parity line.

Figure 6-4: Particle collection efficiency measured while firing different fuel blends. Source: [Robinson et al., 2002].

Points below the line in Figure 6-4 indicate that the co-fire blends have a lower deposition rate than would be expected on the basis of the behaviour of the unblended fuels. This reduction seems to be particularly significant for coal-straw blends, the measured collection efficiencies for which are, on average 37 % lower than the interpolated values, a difference significantly larger than the expected experimental uncertainty [± 20 %] [Robinson et al., 2002].

Figure 6-5 shows parity plots of the effect of co-firing on the chemical composition of the deposits formed.

Figure 6-5a shows that, within experimental uncertainty, the Al-, Fe-, Ca-, and Si-levels of all the deposits fall on the parity line, indicating that the deposit composition of these non-volatile species is not significantly affected by co-firing [Robinson et al., 2002]. Figure 6-5b indicates that the deposit Na varies linearly with ash composition; while there is some enhancement in K-levels in some of the deposits [Robinson et al., 2002].

The Cl and S deposit data shown in Figure 6-5c reveal major changes in the deposit composition due to co-firing. On average, an enhancement factor of 7 was found in the S-level of co-fire deposit relative to expectations based on linear interpolation between the results from the tests of unblended fuel. There is a significant reduction in the Cl content for several of the deposits.

These results are in direct line with the data derived from AMV3, MKS1 and SSV4, and reported in Chapter 5 of this Thesis.

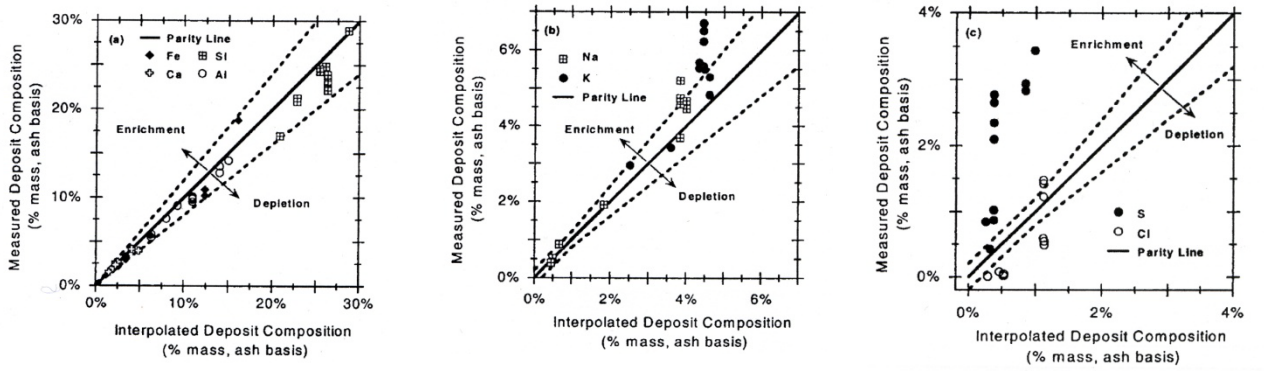

Figure 6-5: Deposit composition measured while co-firing different coal-straw blends. Source: [Robinson et al., 2002].

Figure 6-6 provides an experimental evaluation of KCl-K_2SO_4 chemistry in the deposits, created by plotting the deposit-[Cl] as a function of the ratio of twice the fuel-S to available fuel alkali for a variety of fuels. This scaling parameter was chosen because a value of unity is the stoichiometric ration of fuel-S to the alkali required, in order to convert all of the available

alkali to sulphate, and to release all of the Cl from a deposit to the gas phase as HCl. Values greater than unity indicate excess-S in the system, conditions under which equilibrium indicates that there should be negligible deposit-Cl [Robinson et al., 2002]. For values greater than 5, the Cl-content of an ash deposit is very low; between 1 and 5, some of the deposits have significant [Cl], whereas others have negligible Cl [Robinson et al., 2002].

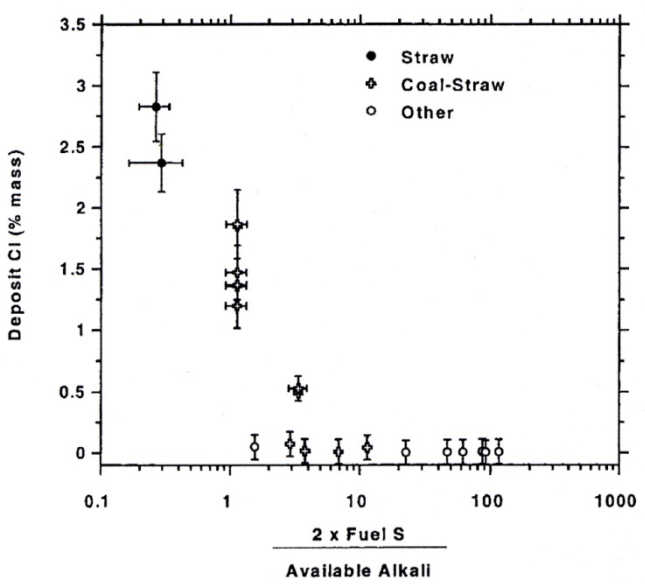

The presence of Cl in deposits formed from blends whose scaling parameter is greater than 1 indicates that kinetics or mass transfer limitations prevent the system from reaching equilibrium. Therefore, blending fuels just to exceed the stoichiometric ratio of fuel-S to available alkali will not ensure low Cl-levels in the deposit.

Figure 6-6: Measured [Cl] in deposits vs. 2S/alkali in the fuel feedstock, as found by [Junker, 1997; Robinson et al., 2002].

The data in Figure 6-6, indicate that the value of the proposed fuel-S-to-available alkali scaling parameter, must be at least 5 in order to avoid significant Cl deposit levels.

Thus, the main conclusions of the measurements in the SNL-MFC, can be summarised as [Junker, 1997; Robinson et al., 2002];

- The raw biomasses provided the highest measured deposition fluxes [g deposit/m^2h], while the coals provided the lowest deposition fluxes.
- No significant differences were found when comparing the deposition flux on the 460 °C to that of the 540 °C probe.
- No significant increase in deposition was observed at all, when co-firing red oak wood. In most cases, the ashes and deposits from wood chips-co-firing with coal were similar to the observations made from firing the actual coal alone.
- It is not possible to estimate precisely particle collection efficiency on a cylindrical probe, at least not by simple linear combination of the dry ash content or the available alkali in the respective raw fuels of the blend. Particularly when applying the dry ash content of the original fuels, an over prediction of about 37 % of the collection efficiency was found [Robinson et al., 2002].

6.2. [Nielsen, 1998] Deposition Studies at the SNL-MFC

Deposition studies in the SNL-MFC were also carried out by [Nielsen, 1998; Nielsen et al., 2000a], in order to better understand the behaviour of K, Cl and S, and the deposition characteristics, during straw-combustion. The effect of an increased S-level was investigated by the addition of either SO_2(g), or solid S, to the system, causing a target value of 500 ppmv SO_2(g) in the flue gas, compared to 30 - 60 ppmv during full-scale straw-firing [Nielsen, 1998; Nielsen et al., 2000a]. In addition, a few experiments were performed where straw was co-fired with a bituminous South American coal (the same as applied by [Junker, 1997; Robinson et al., 2002]). For more details about the experiments please refer to [Nielsen, 1998; and Nielsen et al. (2000a)].

Danish wheat straw, ground to a particle size below 200 μm, was applied in the experiments. The composition of the straw is provided by [Nielsen, 1998]. Two experimental conditions were applied; low and high temperature experiments. The low-temperature experiments were carried out without support-firing in the natural gas burner. The major data for the two experimental conditions are outlined in Table 6-1.

Combustion experiment:		Low temp.:	High temp.:
Combustion temperature	°C	900 - 1100	1200 – 1400
Gas residence time [1)]	S	~ 2.5	~ 1
Fuel flow	kg/h	3 - 4	3 – 4
O_2 [2)]	% (v/v)	6 - 8	6 – 8
T_{gas} at probe	°C	~ 700	~ 900
T_{metal} (probe)	°C	~ 500	~ 500

Table 6-1: Major experimental data for the combustion experiments conducted at the SNL-MFC by Nielsen and coworkers. [1)] Calculated assuming a constant temperature of 1000 °C, throughout the reactor. [2)] Measured in the last heating section before the test section. Source: [Nielsen, 1998].

6.2.1. Straw-Firing in the SNL-MFC

The deposits collected by Nielsen and coworkers consisted of two essentially different parts; [1)] an inner, uniform, smooth, white layer covering most of the surface area of the probe, and, [2)] the main part of the deposit, placed on the upstream side of the probe, and consisting of individual particles deposited by inertial impaction. In most of the experiments, the white layer covered the probe from clockwise position 7 to 5, but in some cases it covered the entire probe circumsphere. The layer consisted mainly of K, Cl and S and was up to several hundred

microns thick after 60 minutes of exposure. The layer physically consisted of small particles, having formed a characteristic dendritic structure emerging out from the tube surface (Figure 6-7), indicating diffusion as the main transport mechanism for these particles to the surface of the probe.

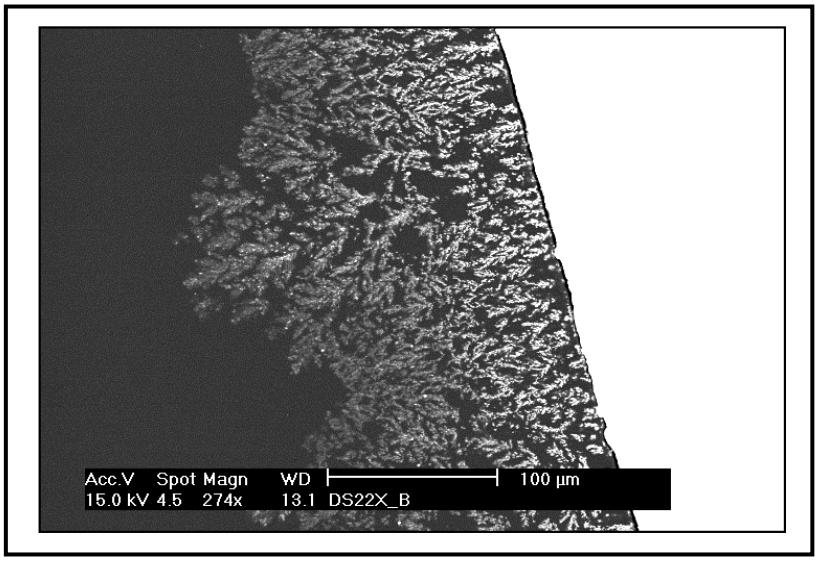

Figure 6-7: SEM micrograph of the side of deposit DS22 from the Sandia MFC experiments by [Nielsen, 1998]. The deposit was collected on the side of the deposit probe, in clock positions 7 – 9. It consisted of small particles forming a characteristic dendritic structure, emerging out from the surface. The layer is very porous and may act as an effective insulator against heat conduction through the deposit. Source: [Nielsen, 1998].

The outer deposits on the SNL-MFC probe were found to have a much more sintered and compact structure, and to be rich in Ca and Si, often present as K-Ca silicate ash particles, glued together by a K-rich salt-type 'glue'.

This deposit structure is in good agreement with the structure of deposits collected from full-scale boilers at Rudkøbing, Masnedø, Haslev/Slagelse and Maribo-Sakskøbing, and reported in Chapter 4 of this thesis. In both cases, a layered structure rich in K, S and Cl was found in the inner layers, while Ca and Si dominated in the outer layers (see Table 6-2 for an over all composition of the deposits) [Nielsen, 1998].

The experimental data gained by [Nielsen, 1998; Nielsen et al., 2000a] indicated that a certain fraction of K was released into the gas phase, while the majority of the Si and Ca remained in relatively large fly ash particles, in good agreement with the subsequent work of [Knudsen, 2004; van Lith, 2005; EU BioAsh, 2007]. This leads to K-depletion relative to the fuel ash

except in regions of the deposit where condensation or thermophoresis occurs, where enrichment in K is to be expected.

The [Cl] in the deposits was found to be quite constant in the range 3 - 5 %(w/w), see Table 6-2, but depleted compared to the Cl-level in the fuel. Chlorine is – just like K - enriched in regions of condensation or small-particle collection, but depleted in regions where inertial impaction dominates the deposit formation, i.e. the outer massive layer of the deposit [Nielsen, 1998; Nielsen et al., 2000a].

Exp. No.	Com. Tem.	Time h.min	Sulphur addition	Elemental ash analysis (% (w/w)):						
				Si	Al	Ca	K	P	Cl	S
DS[1)]				16.9	0.46	5.1	23.1	1.7	7.6	2.7
DS05	Low	.20	500 ppmv SO_2	24.6	0.57	8.6	15.9	2.1	3.4	0.79
DS06	Low	.20	500 ppmv SO_2	25.0	0.64	8.6	15.2	2.2	3.0	0.68
DS09	Low	1.		24.5	0.60	8.3	18.2	2.5	3.6	0.42
DS10	Low	.20		25.0	0.94	8.3	16.7	2.4	4.0	0.52
DS11	Low	.20		25.1	0.75	8.7	16.3	2.3	3.5	0.40
DS12	High	1.		22.5	0.63	7.9	19.5	2.7	3.8	0.78
DS14	High	1.		19.4	0.58	8.4	18.7	2.8	2.7	0.82
DS15	High	.20	500 ppmv SO_2	20.9	0.76	7.8	18.2	2.9	-	2.05
DS16	High	1.		21.4	0.47	8.1	17.3	2.7	3.9	1.3
DS17	High	1.	+ S [2)]	19.8	0.40	8.0	17.9	2.7	3.1	3.1
DS18	High	1.	+ S [2)]	18.3	0.36	8.1	20.1	3.0	3.8	3.4
DS19	Low	1.		24.6	0.43	8.0	16.1	2.0	5.2	0.88
DS21	Low	1.	+ S [2)]	24.1	0.42	8.0	15.1	2.0	4.0	1.6
DS22	High	1.	+ S [2)]	18.7	0.35	7.4	18.9	2.6	4.5	3.2
DS23	High	1.		19.2	0.33	7.7	20.2	2.7	6.7	1.7

Table 6-2: Elemental composition of the deposits from the MFC experiments (% (w/w)). [1)] DS represents the chemical composition of the straw ash, where all the Cl and S in the fuel are assumed to be present in the ash fraction. [2)] S was added to the fuel in order to obtain 500 ppmv SO_2 in the outlet gas. Source: [Nielsen, 1998].

For both combustion conditions tested low and high temperature the S content in the deposit when firing straw increased with an increased partial pressure of SO_2 (500 ppmv) in the system. During the low temperature experiments, the increase in [S] was minor, whereas during the high temperature experiments, the increase was much more significant. For the high-temperature experiments with S-addition, the deposit contained more S than the average fuel ash, indicating that the deposited ash absorbed some of the additional S. The increase in [S] was accompanied by a decrease in the [Cl] relative to [K]. This indicates that KCl is sulphated by reaction with SO_2 to K_2SO_4.

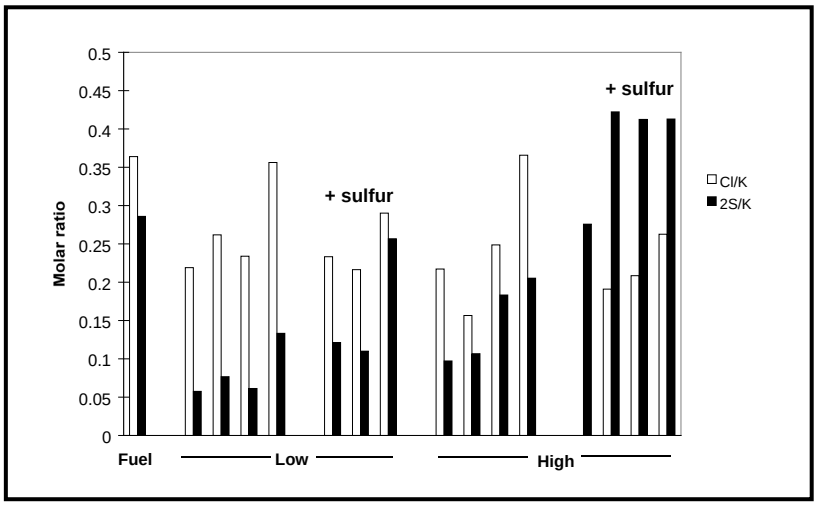

Figure 6-8: Molar ratios of Cl/K and 2S/K in deposits from straw combustion in the SNL-MFC. Source: [Nielsen, 1998].

Figure 6-8 shows the molar ratios of Cl/K and 2S/K in the deposits formed during straw-firing in the SNL-MFC. Assuming all Cl in the deposit to be present as KCl, and all S as K_2SO_4, the deposits contained more KCl than K_2SO_4 with the exception of the 'high temperature + S' experiments, where the deposits contained significantly more K_2SO_4 than KCl. Chlorine and S account for 26 – 67 % of the K in the deposits, which means that a part of K was not present as a salt in the deposit, but rather as K-silicates or K-Ca silicates (mainly in the outer deposits). This agrees with the results of the SEM analysis. However, part of the S may also be associated with Ca.

6.2.2. Formation of Deposits by Condensation in the SNL-MFC

Condensational phenomena in biomass-fired boilers were studied by means of a condensation probe placed just below the exit of the SNL-MFC. This probe consisted of two small (2 x 3 cm) vertical plates, placed approximately 2 cm apart. A larger horizontal plate (6 x 9 cm) completely covering the underlying plates, was placed 0.5 cm above the two vertical plates (see Figure 6-9).

With this design, the horizontal plate shields the vertical plates from the particles coming from above, thereby allowing only vapours and submicron particles to deposit on the vertical plates underneath. The sample plate was un-cooled, but remained at a temperature of around 300-400 °C, during all experiments [Nielsen,1998].

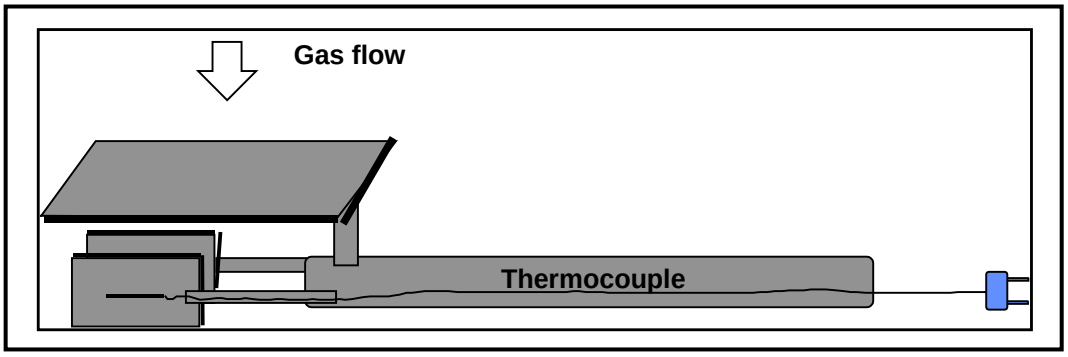

Figure 6-9: Schematic drawing of the condensation probe used in the Sandia MFC experiments. Source: [Nielsen, 1998].

The chemical composition of the condensed species was found by rinsing the stationary vertical plates with ultra pure water, and subsequently analysing the washing water for Cl^--, SO_4^{2-}-, K^+-, and Ca^{2+}-ions, by ion chromatography. Figure 6-10 shows the molar ratios of Cl/K and 2S/K respectively. The partial pressure of SO_2 in the combustor had a pronounced effect on the molar ratio for the high temperature experiments, but not for the low-temperature experiments.

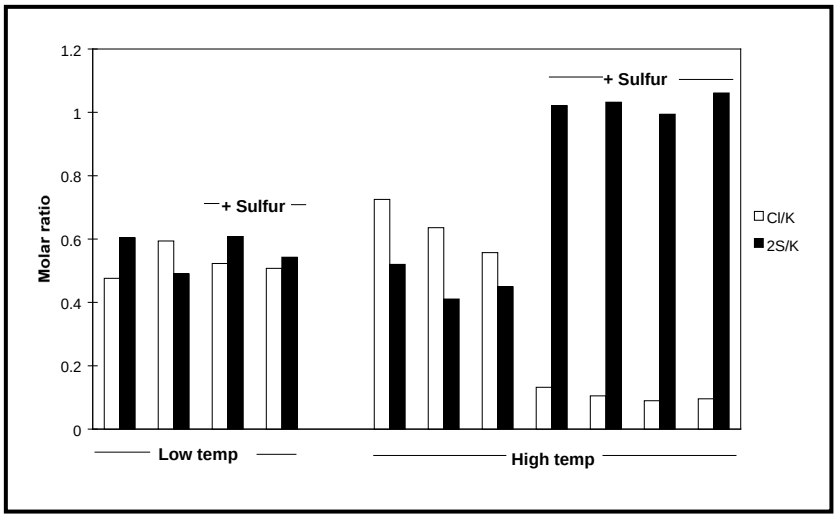

Figure 6-10: Molar ratios of Cl/K and 2S/K in wash water from the plates on the MFC condensation probe measurements. Source: [Nielsen, 1998].

One of the sample plates was placed directly in the vacuum chamber of an SEM, and analysed for morphology by SE-imaging (see Chapter 2 of this thesis). The deposit appeared to be a uniformly smooth layer, but a larger magnification revealed that the condensed layer was neither dense nor uniform (see Figure 6-11). The condensational deposits consisted of 1 - 2 µm angular particles of primarily KCl, and a sponge-like matrix consisting primarily of K_2SO_4, the

latter representing dendritic aggregates of aerosol particles. The condensed material consisted solely of K, Cl and S no other elements were present.

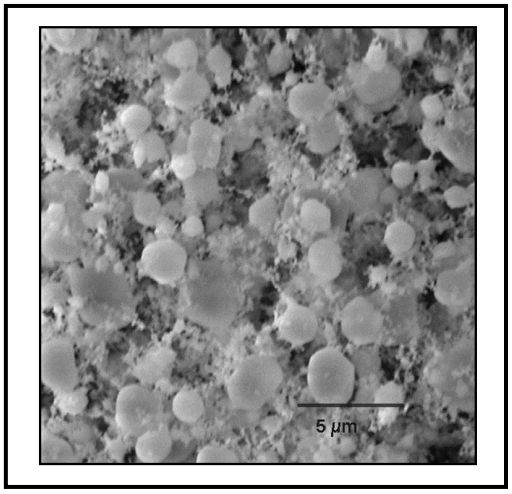

Figure 6-11: SEM micrograph of surface of plates from condensation probe experiments at the Sandia MFC. Source: [Nielsen, 1998].

6.2.3. Co-Firing of Straw and Coal in the SNL-MFC

Three experiments on co-firing Danish wheat straw and a bituminous South American coal, were conducted. The straw share co-fired was 30 %(w/w), which equals approximately 20 % straw on an energy base, i.e. comparable to the maximum straw share co-fired at MKS1 [Andersen, 1998], see Chapter 5 of this thesis. The SNL-MFC combustion tests were performed at the high combustion temperature, and with one hour exposure time.

The deposits formed when coal was burned alone, or in conjunction with 30 %(w/w) straw, were different from those formed during 'pure' straw firing. The deposits were thinner, brown in colour, and consisted of a characteristic Λ-shaped deposit on the top (i.e. the upstream side) of the probe. A homogeneous, beige layer of material was found along the sides of the probe (clock positions 1-2 and 10-11). SEM-analyses of the deposits revealed that the powdery layer on the side of the probe consisted of small spherical silicate- and aluminosilicate-particles. No sign of a dendritic structure was observed (see Figure 6-12). The morphology of the deposit along the sides of the probe may be explained by the adhesion of small non-sticky particles, which can rebound at impaction, and work their way towards the surface, causing a more random ordered deposit than is the case during straw firing which represents the 'stick on first contact' theory.

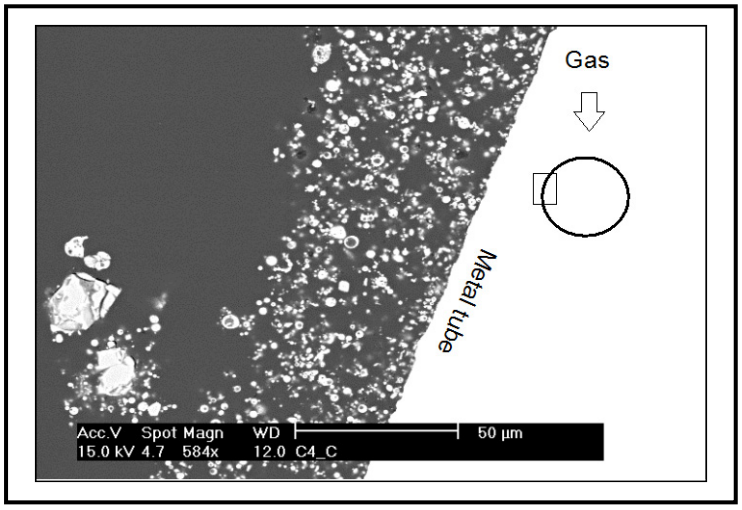

Figure 6-12: SEM micrograph of side of deposit from co-combustion experiments at the Sandia MFC. Source: [Nielsen, 1998].

In addition, for the co-firing feedstock, a number of experiments were conducted with the condensational probe, in order to investigate condensation in these systems. SEM-EDX analyses of the condensation plate revealed small individual particles, consisting mainly of Si and O, with minor amounts of K, S, and Al. Only trace amounts of Cl were detected. These findings agree with the composition of the wash water from the condensational probe, where only trace concentrations of Cl were detected [Nielsen, 1998].

The overall chemical compositions of the cylindrical probe deposits are shown in Table 6-3. The deposit from coal combustion has a high Si and Al contents. The deposit from experiment C1, where straw and coal are co-fired, contains more K and S than the 'pure' coal deposits, but less than the straw deposits, which is in good agreement with the data presented earlier in Chapters 4 and 5 of this thesis. The pattern for K is logical because straw contains significantly larger amounts of K than coal. Conversely, coal contains more S than straw, so the reason for the increased S in the deposits during co-firing compared to coal-firing, is that the increased quantity of K present in the system captures some of the S, as also seen at AMV3 [Pedersen et al., 1996].

Therefore, the S retention in the ash increases when a large amount of K is present in the ash ifself. The Cl content in the deposit is the same, regardless of whether coal is co-fired with straw or not, and is lower than in the deposits from 'pure' straw firing. This indicates that there is hardly any Cl present as KCl in the deposit, when straw is co-fired with coal, since K reacts with Si and Al in the coal ash, forming K-Al silicates simultaneously with an increased sulphation to K_2SO_4, caused by the higher level of sulphur. Chlorine is released as HCl(g).

Exp. #	Fuel	Elemental ash analysis (% (w/w)):						
		Si	Al	Ca	K	P	S	Cl
	Straw/S	16.86	0.46	5.04	23.03	1.35	2.72	7.55
	Coal/C	31.31	9.82	1.29	1.76	0.09	0.94	<0.01
DS14	S	19.43	0.58	8.43	18.67	2.75	0.82	2.65
DS16	S	21.4	0.47	8.10	17.30	2.70	1.30	3.90
DS23	S	19.2	0.33	7.70	20.20	2.70	1.70	6.70
C1	C + S	28.54	7.71	3.11	6.89	0.83	0.88	0.18
C2	C	30.43	10.29	1.14	1.97	0.27	0.30	0.18

Table 6-3: Chemical composition of deposits from the SNL-MFC experiments at high temperature combustion and one hour exposure time. S = straw, C = coal. [1)] The chemical composition of these fuel ashes is calculated assuming that all the Cl and S in the fuel are present in the ash fraction. Source: [Nielsen, 1998].

6.3. [Theis et al., 2006] Co-Firing Experiments in the TU EFR.

The main objective of the work by [Theis et al., 2006a-c] was to evaluate the deposition behaviour of biofuel mixtures with different fouling propensities, over the entire feedstock mixing range. Three biomass fuels were chosen for the experiments: [1)] eucalyptus bark, and, [2)] oat straw, as examples of highly fouling fuels, and, [3)] a Finnish peat as a clean fuel [Theis et al., 2006a].

The University of Toronto Entrained Flow Reactor (UT EFR) was chosen as the experimental facility, since it had proven highly reliable for recording deposition rates from black liquor firing, and had been proven flexible enough to operate under the conditions used for biofuel co-firing in power generation.

The UT-EFR consists of a combustion chamber, and an electrically heated tube furnace section (see Figure 6-13). The combustion chamber uses natural gas and air injected at an excess of 10 % O_2, in order to ensure complete burn out. The combustion temperature can be adjusted by the addition of diluted air. The electrically heated furnace consists of five mullite tubes that can be heated separately up to 1350 °C. Each unit measures 122 cm in height, and 18 cm in diameter [Theis et al., 2006b].

An air-cooled probe was horizontally inserted 10 cm below the exit of the lowest furnace section, i.e. the same principle applied in the SNL-MFC. The probe has an outer diameter of 25 mm, and a thermocouple suspended on the surface to measure the temperature. Before burning specified feedstock mixtures, all pure air-dried fuels samples were pre-cut in a coarse shredder, and milled to sizes smaller than 1 mm, in a blade mill [Theis et al., 2006a].

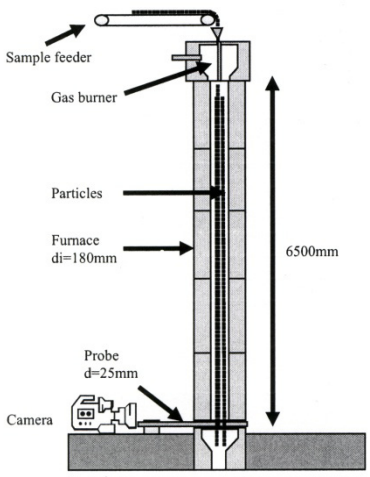

For each experiment, a mass of 500 g fuel mixture was fed continuously, for 40 min into the UT-EFR. Both the furnace and the flue gas temperature were set to 1000 °C, while the flue gas velocity was adjusted to 2 m/s, which corresponds to a residence time of 3 s in the UT-EFR. The probe surface temperature was set equal to 550 °C; typical conditions in the superheater region of conventional biomass-fired boilers.

Figure 6-13: The UT-EFR experimental setup. Source: [Theis et al., 2006a-c].

The probe has a removable ring in the centre to extract deposits for later analysis. After each experiment, the detachable ring was separated from the probe, and the central part of the upstream-side deposits was removed. The deposition rate was then measured by scratching off, and weighing the deposits, after the probe was removed from the UT-EFR [Theis et al., 2006b]. Some of the removed deposit was glued onto a metal plate, by a carbon tape, and was then coated with carbon, and analysed by SEM-EDX.

For fuel analyses, and further details on the UT-EFR, please refer to [Theis et al., 2006a-c].

As expected, peat exhibited the lowest fouling tendency, with a deposition rate of 20 g/m^{2}h, while straw proved to be a high-fouling fuel, with a deposition rate of 160 g/m^{2}h. The deposition rate of bark was in between, with a value of 80 g/m^{2}h [Theis et al., 2006b].

The data further indicates that the addition of just 30 %(w/w) peat to straw was sufficient to decrease the deposition rate for pure straw [Theis et al., 2006a]. Consequently, a mixture of peat and straw may contain up to 70 %(w/w) straw share, before causing increased deposition.

A distinctly non-linear deposition trend was observed for mixtures of peat and straw. The amount of deposits remained low up to about 60 %(w/w) straw, but then increased exponentially with a higher straw-fraction in the mixture. Below 60 %(w/w), the deposit composition changed only marginally [Theis et al., 2006c]. Potassium (K) indicates straw ash, while Al indicates peat ash. In deposits obtained from burning mixtures that contain less than 60 %(w/w) straw, it is observed that the amount of Al in the deposits decreases. At the same time, the deposition rate stays constant [Theis et al., 2006c], indicating that the deposit origin gradually shifts from peat ash characteristics to straw ash characteristics. In deposits obtained from mixtures that contain more than 70 %(w/w) straw, a strong exponential increase of K, Si and Ca was observed. At the same time, the deposition rate increased dramatically.

By adjusting the air flow, the probe surface temperature was set to 475, 500, 550, and 625 °C. When firing straw alone, additional deposition tests were conducted at 525 and 585 °C.

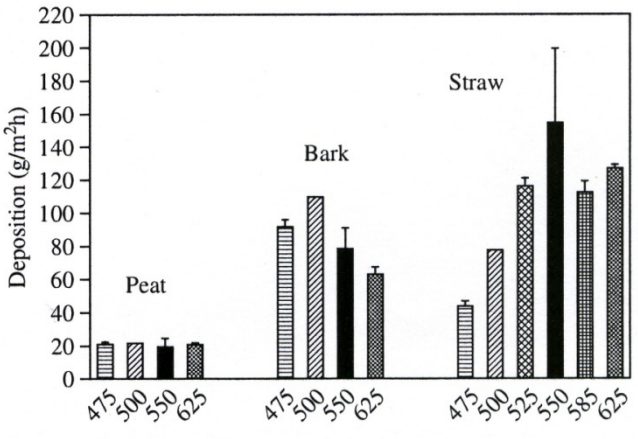

Figure 6-14 shows the averaged deposition rates [g/m²h] of peat, bark and straw at four to six different probe surface temperatures between 475 and 625 °C.

Figure 6-14: Average deposition rates of peat, bark and straw in the temperature range [475-625 °C]. Source: [Theis et al., 2006c].

When firing straw, the deposition rate increased with increasing probe surface temperature from 475 to 550 °C. At 585 and 625 °C, the deposition rate was the same as the one obtained at 525 °C. A large scatter for the deposition rate was observed at probe surface temperatures above 550 °C, when all together five deposition experiments lasting 40 minutes each were carried out over a time span of two years.

Figure 6-15 shows the average deposition rates obtained when burning mixtures of peat and straw as functions of mass fraction of straw in the mixture and probe temperature. It is evident that at straw shares > 70 % the deposition increases exponentially, particularly for the highest probe surface temperatures, i.e. 550 °C and 625 °C.

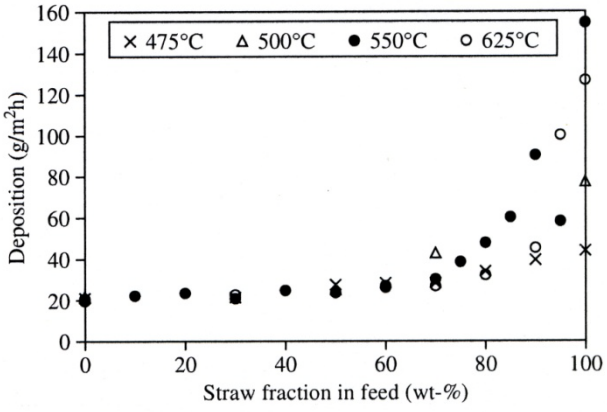

Figure 6-15: Average deposition rates as a function of the mass fraction of straw in the mixture and probe temperature. Source: [Theis et al., 2006c].

Figure 6-16 shows the average contents of the main ash forming element in the deposits obtained at three different probe surface temperatures, as a function of the straw fraction in the mixture. Si, Al, Ca, K, and S are expressed in terms of oxides, while Cl is expressed on an

elemental base. The dotted lines represent the calculated feed ash composition. All compositions in Figure 16, are calculated on a Fe-free base [Theis et al., 2006c].

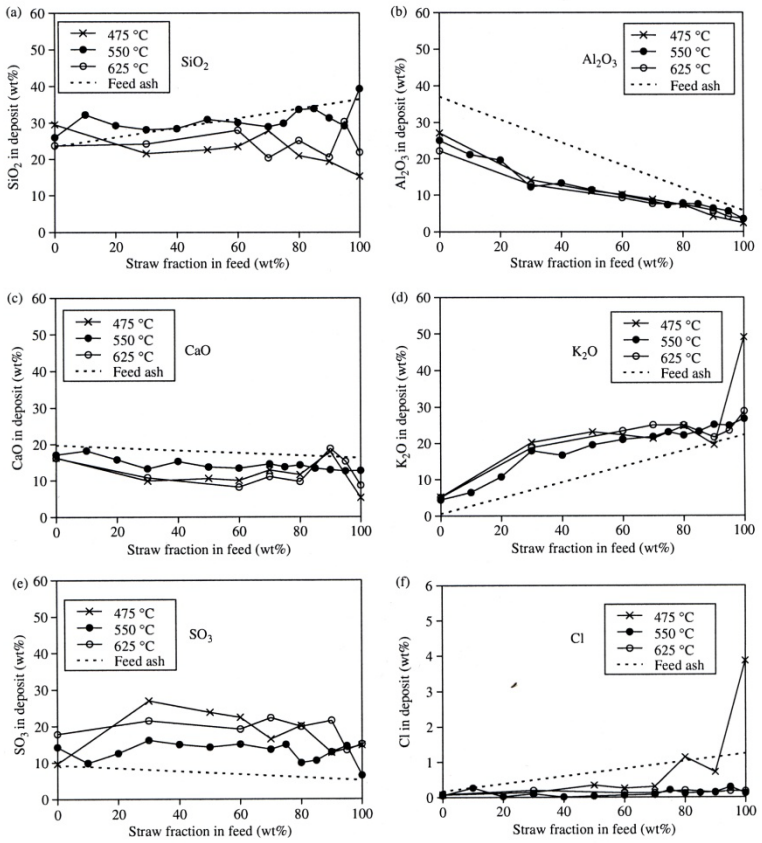

The content of Si remains almost constant regardless of the straw fraction in the mixture. The highest level occurs at a probe surface temperature of 550 °C, while there is only a minor difference between 475 °C and 625 °C [Theis et al., 2006c].

The content of Al in the deposits decreases with increasing straw fraction in the mixture.

Figure 6-16: Average content of main ash-forming elements in deposits vs. straw fraction and probe temperature Source: [Theis et al., 2006c].

Compared to the calculated feed ash composition, Al is significantly depleted in deposits obtained from mixtures with low straw content. The temperature of the probe surface does not have any effect [Theis et al., 2006c].

The content of Ca in the deposits decreases slightly with an increasing straw fraction in the mixtures. In most of the mixtures, the Ca-content was found to be highest in deposits formed at a probe temperature of 550 °C. The Ca-contents measured at 90 %(w/w) straw and 475 and 625 °C were observed to be exceptionally high. Compared to the calculated feed ash, Ca is slightly depleted in the deposits [Theis et al., 2006c].

The content of K in the deposits increased with increasing straw share in the feedstock (see Figure 6-16) which is in line with the full-scale observations made on this issue and outlined in Chapter 5 of this thesis. The K content was lowest in deposits obtained at a probe temperature of 550 °C. The deposits obtained at 100 %(w/w) straw, and 475 °C, were found to be exceptionally enriched in K, with a K content twice as high as that for 550 and 625 °C. Compared to the calculated feed ash composition, K was found to be always enriched in the

deposits [Theis et al., 2006c], which is again in line with the findings of [Junker, 1997; Robinson et al., 2002], see Section 6.1.

The [S] in the deposits did not change much with the increasing straw share in the feedstock. It was found to be lowest, in deposits obtained at 550 °C [Theis et al., 2006c]. No conclusive trend was found, concerning the probe surface temperatures of 475 and 625 °C. Compared to the calculated feed ash composition, S was always found to be enriched in the deposits.

In deposits formed at a surface temperature of 475 °C, [Cl] was found to rise significantly when the straw share exceeded 70 %(w/w). For probe surface temperatures of 550 and 625 °C, however, no such observation was made, probably due to evaporation of Cl-species at higher surface temperatures. Compared to the calculated feed ash composition, [Cl] was found in most cases to be depleted in the deposits, with the exception of the deposit formed at 475 °C, during pure straw firing [Theis et al., 2006c].

6.4. [Zheng et al., 2007] Co-Firing Experiments in the CHEC EFR.

The speciation of K when co-firing coal and biomass, determines to a large degree the important properties of fly ash and ash deposits. Potassium appears mainly in the following species [Zheng et al, 2007]:

1. KCl: A high [KCl] in a deposit may cause selective Cl-corrosion, during which chlorides extracts the Cr and Fe in the steel, leaving a Ni-rich skeleton. This will be further presented and discussed in Chapter 8 of this thesis. Accelerated deactivation of de-NO_x catalysts during coal and straw co-firing, may also take place if significant amounts of KCl, are present in the fly ash.
2. K_2SO_4: If K appears as K_2SO_4, less pronounced problems with boiler corrosion and ash utilisation are usually experienced, although sulfidation caused by K_2SO_4 in deposits in co-fired systems has been reported (see Chapter 8 of this thesis. Deactivation of the SCR catalyst may still take place.
3. K silicates: If K appears as silicates, deactivation of SCR catalysts will not take place due to the presence of K, but alkali silicates do have a relatively low melting temperature range, meaning that severe deposit formation in the furnace could be a problem.
4. K-aluminium-silicates: The melting temperature range of these species is higher than that of K silicates, and therefore less troublesome deposits (slags) are usually formed.

In all cases where the dominant K-species are not KCl, most Cl will escape the boiler as HCl in the flue gas, as found at MKS1 (see Chapter 5 of this thesis).

Thus, in order to investigate the interaction between inorganics from coal and straw, and in particular the effect of coal quality on fly ash and deposit properties, straw was co-fired with three kinds of coal in the CHEC solid fuel entrained flow reactor [Zheng et al, 2007].

The CHEC entrained flow reactor, is designed to simulate the environment of high temperature thermal reactors, such as suspension fired boilers. The complete facility includes equipment for data acquisition, gas supply, fuel feeding, gas preheating and the controlled extraction of gas and particles (see Figure 6-17). The reactor has an internal length of 2 m and an internal diameter of 8 cm, and can be electrically heated to a maximum wall temperature of 1500 °C.

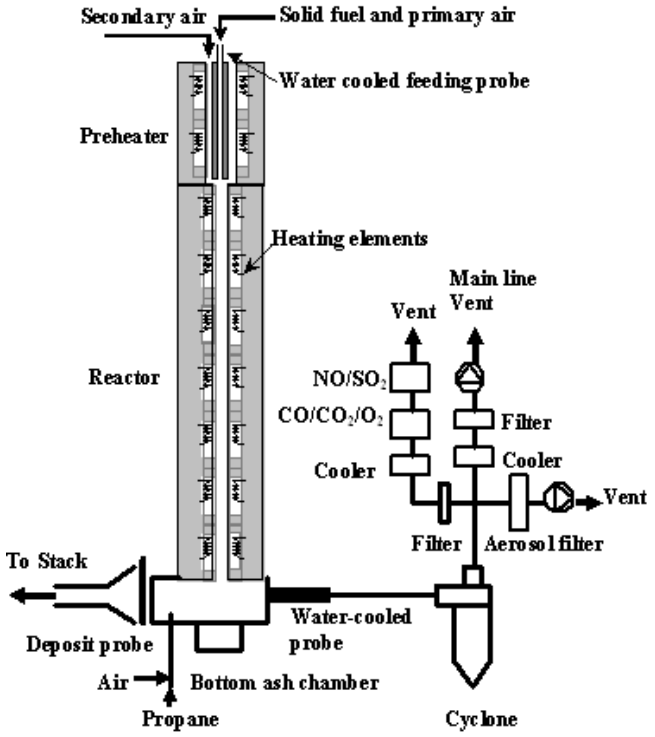

Figure 6-17: Sketch of the entrained flow reactor. Source: [Zheng et al., 2007].

The exit flue gas passes a water cooled flange when it flows from the reactor to the bottom chamber, and the temperature decreases significantly, to about 400-500 °C. A refractory-lined bottom chamber is mounted at the reactor tube exit, in order to turn the flue gas and direct it onto an air-cooled deposit probe used to simulate deposit formation on the superheater tubes. In order to obtain a reasonable gas temperature at the deposit probe, a small propane-fired burner is mounted in the exit flue gas channel, for support-firing.

During the deposit tests, and particle sampling, the flue gas temperature at the reactor outlet slit was set to 800 °C, and maintained at this level by adjusting the propane flow rate to the propane burner, while the temperature of the deposit probe surface, toward the flue gas, was set to 550 °C, and controlled by heating tape.

Figure 6-18 shows [SO_2] as function of the [S] in the feedstock. The [SO_2] clearly increases with increasing [S] in the feedstock. The SO_2 emissions are compared to stoichiometric calculations in which it is assumed that all sulphur in the fuel is released as SO_2. The difference between the maximum SO_2-emission and the measured SO_2-emission can be used to evaluate S retention in the ash.

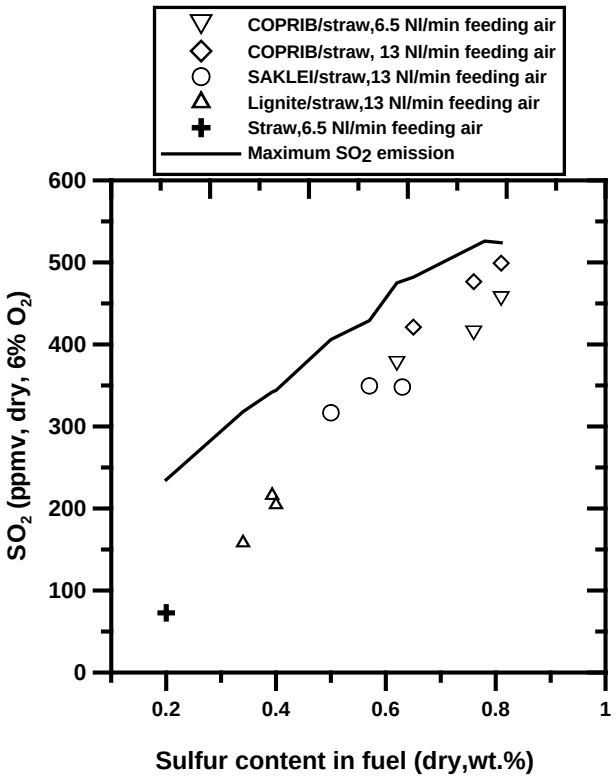

Figure 6-18: SO_2 emission as a function of sulphur content in the fuel. The maximum SO_2 emission is calculated by assuming all fuel sulphur is released as SO_2. Source: [Zheng et al., 2007].

Figure 6-18 also illustrates that S was retained in the ash, at an increasing fraction with increasing straw share, since the gap between $[SO_2]_{measure}$ and $[SO_2]_{theory}$ increases with increasing straw share, and that more S was retained in lignite ash than in ash from the high-rank and –quality coals SAKLEI and COPRIB ash [Zheng et al., 2007].

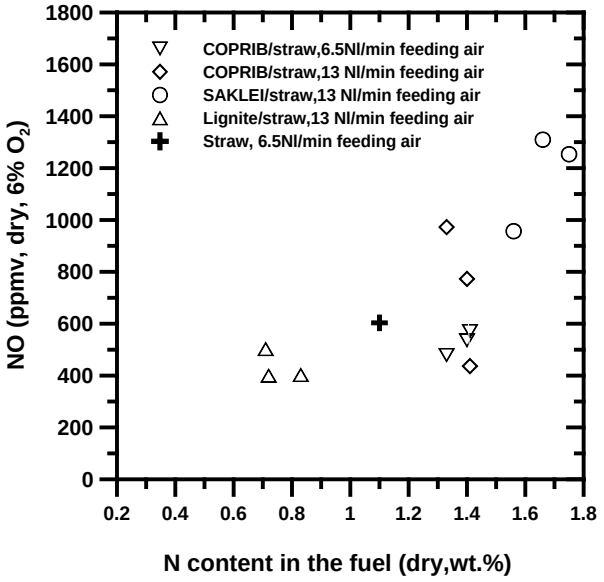

Figure 6-19: NO emission as function of nitrogen content in the fuel. Source: [Zheng et al., 2007].

The NO emission as a function of nitrogen content in the fuel mixture is illustrated in Figure 6-19. The general trend observed was, as expected, in that the NO emission increased with the N content in the fuel mixture. Although the total amount of combustion air kept constant, the NO emission increased when a higher amount of fuel feeding air was used.

Figure 6-20 illustrates the total [K] in fly ashes, as a function of the [K] in the fuel ash. A reasonable agreement is observed between the full-scale and pilot-scale data [Zheng et al., 2007]. The total [K] in fly ash is almost the same as that in fuel ash. Since most fuel ash ends up with fly ash in a suspension-fired system, it makes sense to predict the total K in fly ash, by use of the K-content in the fuel ash.

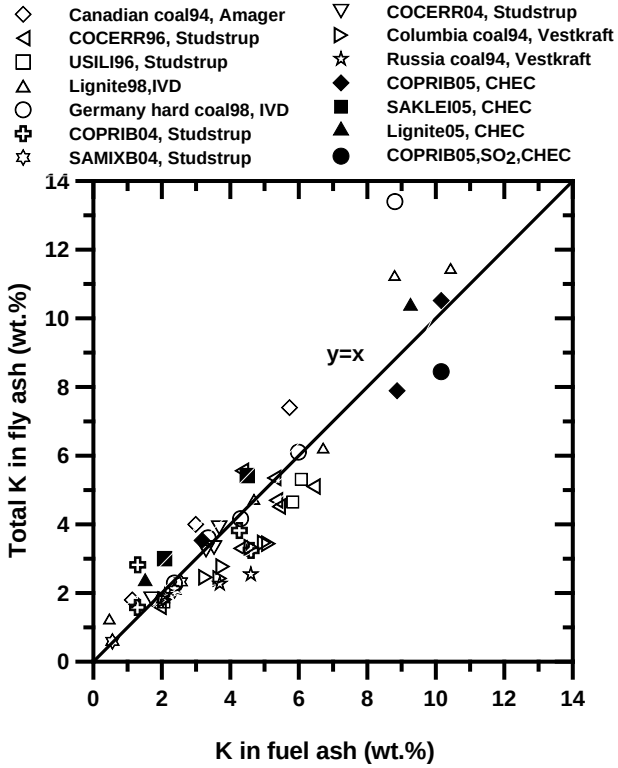

Figure 6-20: Total K in the fly ash as function of K in the fuel ash. Source: [Zheng et al., 2007].

The fraction of water-soluble K in the fly ash provides information on the fraction of K, appearing as salts (KCl and K_2SO_4) in the fly ash. Figure 6-21 illustrates the fraction of water soluble K in fly ash compared to total K as a function of the K/Si molar ratio in the fuel, for bituminous coal/straw and lignite/ straw co-firing, respectively. For bituminous coal/straw co-firing, similar trends were observed in full- and pilot-scale co-firing, i.e. the fraction of water-soluble K in fly ash generally increases with increasing K/Si molar ratio of the fuel.

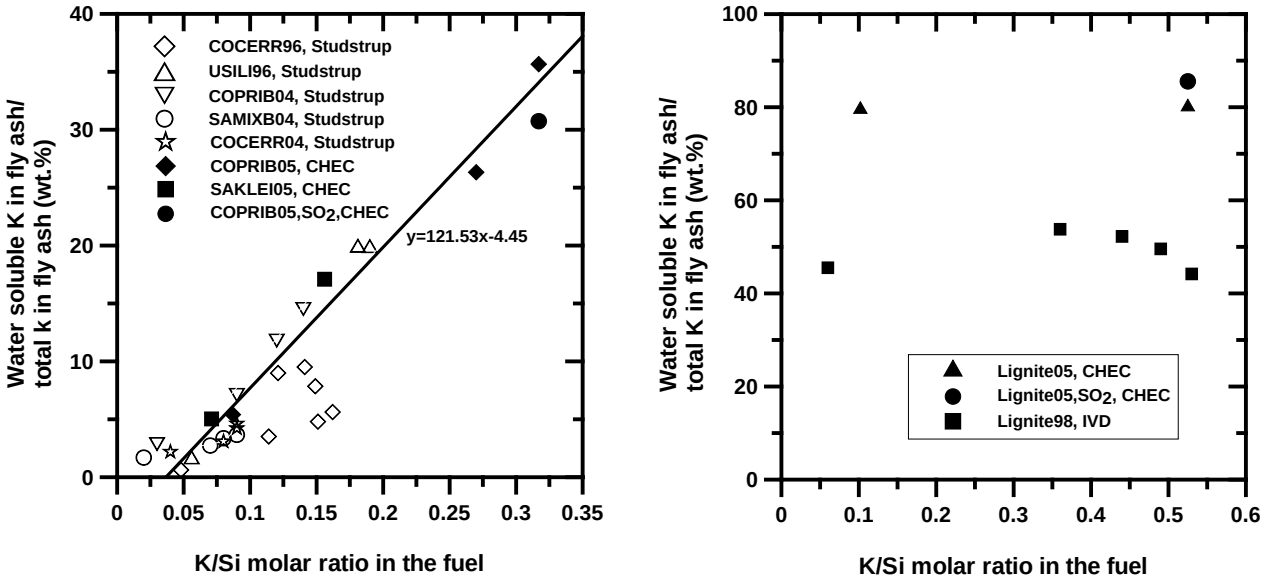

Figure 6-21: The ratio of water-soluble K in the fly ash to total K in the fly ash for co-firing bituminous coal and straw (left figure), and for co-firing lignite and straw (right figure), as a function of K/Si molar ratio in the fuel. Source: [Zheng et al., 2007].

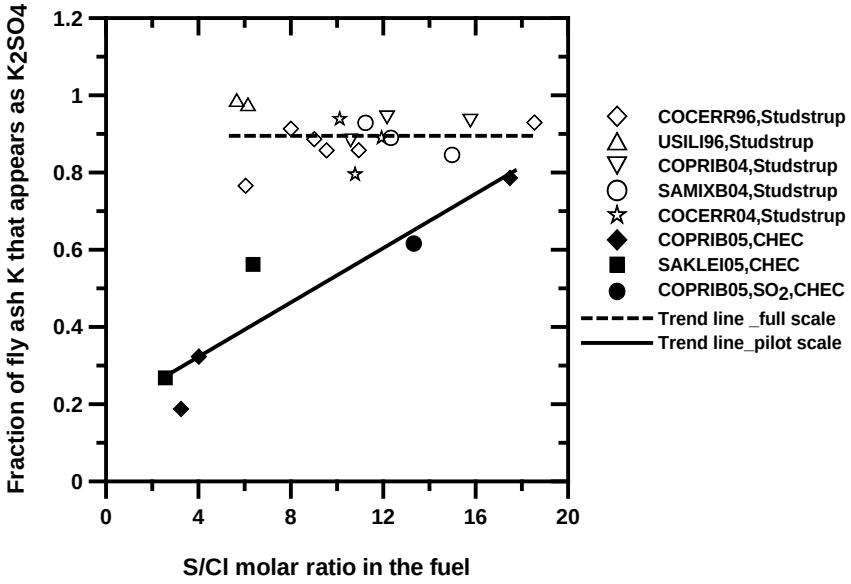

Figure 6-22: The fractions of K in fly ash that appears as K_2SO_4 as a function of the S/Cl molar ratio in the fuels when co-firing with bituminous coals. Source: [Zheng et al., 2007].

Figure 6-22 shows the fraction of the K in the fly ash, appearing as K_2SO_4 vs. the S/Cl-molar ratio in the fuel, for co-firing bituminous coal with straw.

The trend for the full-scale data is quite different from that of the pilot-scale data. The fraction of the water-soluble K, present as K_2SO_4 in the fly ash, in full-scale combustion seems to be independent of the S/Cl molar ratio in the fuel, and an average value of about 0.90. On the other hand the fraction of K that appears as K_2SO_4 increases almost linearly with the S/Cl molar ratio in the fuel for the pilot-scale data. There is less K in the form of K_2SO_4 in the fly ash from the entrained flow reactor compared to the full- scale data. This may be due to the shorter residence time in the entrained flow reactor (1 s) compared to the residence time in the full-scale pulverised fuel-fired boilers (3-5 s). The temperature profile in the entrained flow reactor and power plant boiler are also different. The flue gas in the entrained flow reactor is cooled from 1300°C to about 400-500°C by the water cooled flange in only about 0.1 s. The sulphation reaction can be influenced by both ash particle residence time and the gas temperature profile.

6.5. Summary

Two comprehensive studies of straw-, coal- and coal+straw co-firing have been conducted in the SNL-MFC. In both cases the data show that straw causes a much higher deposition rate than either coal or coal co-fired with straw. In addition to the higher depositional flux observed, the chemistry is also significantly affected, when changing from 'pure' straw-firing to co-firing of coal and straw.

The effect of an increased S level was investigated by the addition of either $SO_2(g)$, or solid S, to the system, causing a target value of 500 ppmv $SO_2(g)$ in the flue gas, compared to 30 - 60 ppmv during straw-firing in the full-scale [Nielsen, 1998; Nielsen et al., 2000a].

For both the combustion conditions tested - low and high - the S content in the deposit when firing straw increased with an increased partial pressure of SO_2 (500 ppmv) in the system. During the low temperature experiments, the increase in [S] was minor, whereas during the high temperature experiments, the increase was much more significant. For the high-temperature experiments with S addition, the deposit contained more S than the average fuel ash, indicating that the deposited ash absorbed some of the additional S. The increase in [S] was accompanied by a decrease in the [Cl] relatively to [K]. This indicates that KCl is sulphated by reaction with SO_2 to K_2SO_4. The temperature effect on sulfation of Cl-species in deposits was also seen, when firing waste wood in a 400 kW_{th} grate-fired test facility in Hard, Austria, as part of the former EU-BioAerosol project, 2000-2003 (see Figure 6-23).

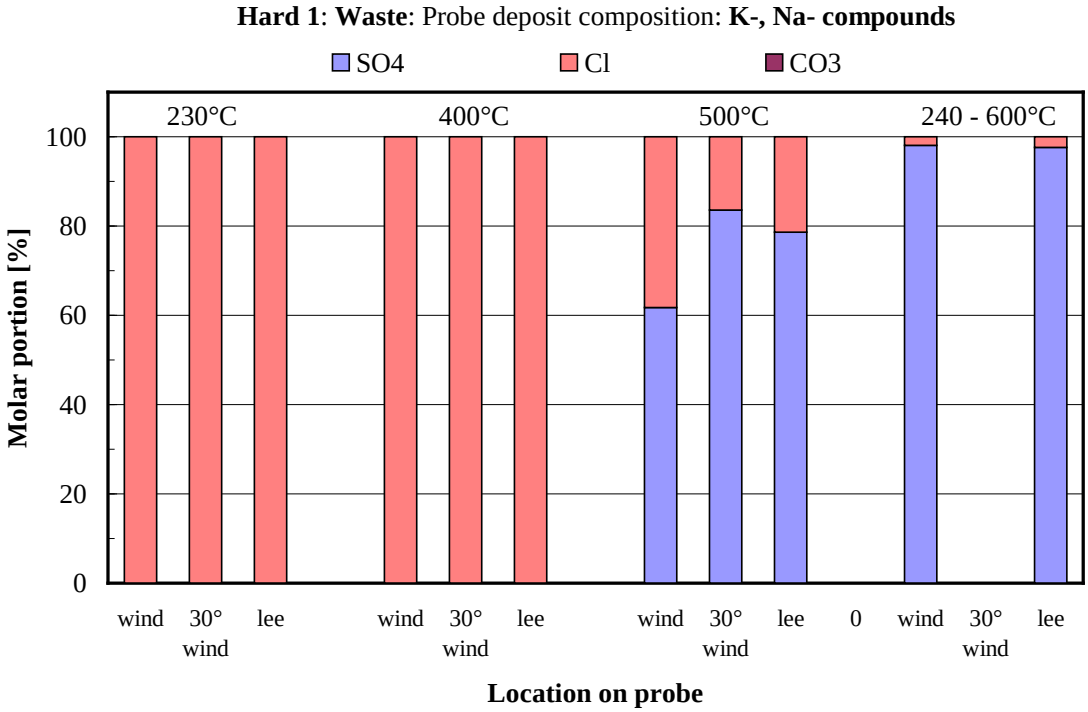

Figure 6-23: The presence of anions, i.e. sulphate, chloride and/or carbonate in deposits collected in a waste wood fired test facility in Hard, Austria. Source: [BioAerosols, 2003]

In Figure 6-23, it is seen that the deposits collected at 230 °C and 400 °C, are almost completely dominated by chlorides, while the probe, which was first exposed at 240 °C, and the increased to a surface temperature of 620 °C, contain almost only sulphate, only very little chloride is present. Thus, a higher temperature favours sulphates over chlorides.

Serious differences in the deposit physical structure are also reported by [Junker, 1997; Nielsen, 1998; Robinson et al., 2002]; while the straw deposits have a structure with a dendritic white

inner layer rich in KCl, and a more ash-like structure rich in K, Ca and Si on top of this, then the deposits from co-firing and from 'pure' coal-firing posses remarkable resemblances.

Thus, the main conclusions of the measurements in the SNL-MFC, can be summarised as [Junker, 1997; Robinson et al., 2002];

- The raw biomasses provided the highest measured deposition fluxes [g deposit/m^2h], while the coals provided the lowest deposition fluxes.
- No significant differences were found when comparing the deposition flux on the 460 °C to that of the 540 °C probe.
- No significant increase in deposition was observed at all, when co-firing red oak wood. In most cases, the ashes and deposits from wood chips-co-firing with coal were similar to the observations made from firing the actual coal alone.
- It is not possible to estimate precisely the particle collection efficiency on a cylindrical probe, at least not by simple linear combination of the dry ash content or the available alkali in the respective raw fuels of the blend. Particularly when applying the dry ash content of the original fuels, an over prediction of about 37 % of the collection efficiency was found [Robinson et al., 2002].

The study by Theis et al. revealed that straw can be co-fired with peat up to about 70 % straw share; above this limit the deposit formation accelerates seriously. A non-linear behaviour in the deposit amount as well as the deposit chemistry was observed when comparing data from co-firing experiments with linear combinations of basic fuel data for the 'pure' fuels.

Another interesting effect, revealed through the experiments by Theis et al., is the effect of surface temperature of the probe. In Figure 6-14, it is obvious that the deposition flux for straw increases when increasing the temperature from 475 °C to 550 °C, but at even higher temperatures, i.e. 585 and 625 °C, the deposition flux decreases, compared to 550 °C.

Data from the study by Zheng demonstrates that there are certain differences between full-scale data and data from the CHEC-EFR, especially for the fraction of fly ash K appearing as K_2SO_4 (see Figure 6-22). This difference is most likely due to the highly different cooling-profiles applied in full-scale and in the CHEC-EFR.

All-in-all, the lab-scale work has confirmed by far most of the observations made on the effects of coal-straw co-firing in full-scale suspension-fired units.

Chapter 7:

ON THE RELEASE OF CRITICAL ELEMENTS FROM SECONDARY FUELS

As outlined in the previous chapters of this thesis, the utilisation of straw for heat and power production is a significant technical challenge, particularly in grate-fired boilers, due mainly to the relatively high content of critical, flame-volatile elements like K, Cl, and S in straw. Formation of acidic pollutants, e.g. SO_2 and HCl, and high aerosol mass loading in parallel with deposition of potentially corrosive species like KCl on heat transfer surfaces are some of the problems encountered (see Figure 7-1).

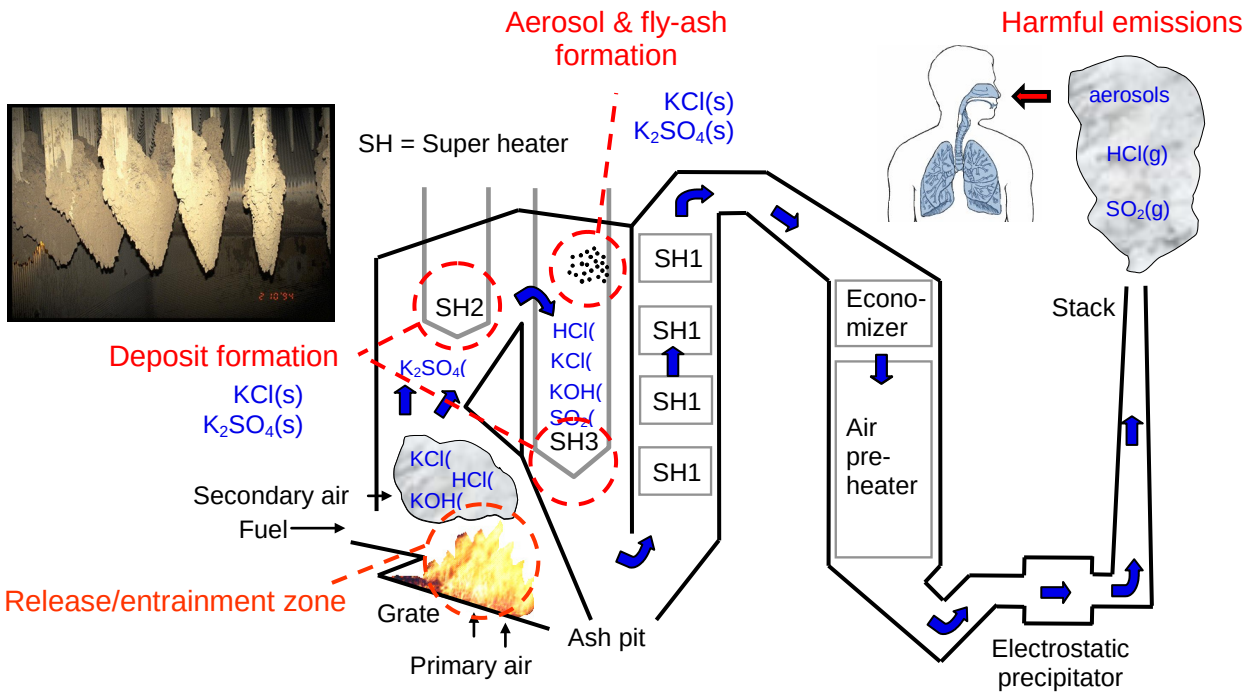

Figure 7-1: Overview of potential operational and emission problems related to K-S-Cl chemistry in a grate-fired furnace.

Therefore, the big question is: What is happening ?

Chlorine and part of S and K in straw, are released into the gas phase in the combustion zone, where S is present mainly as SO_2(g), K as KCl(g) and/or KOH(g), and Cl as KCl(g) and/or

HCl(g). The gaseous K-species interacts chemically or physically in the free board with fly ash particles or other species in the gas phase, forming e.g. K_2SO_4 (see Figure 7-1).

Following the release of critical elements, K, Cl and S, residual ash from char burnout of the straw can be divided into bottom and fly ash, in a ratio depending mainly on the furnace design, and the size distribution and density of the ash particles formed in the fuel-bed. The fly ash is entrained by the flue gas down through the convective sections of the boiler, where it may deposit on heat transfer surfaces, while the bottom ash leaves the system through the ash pit, at the end of the grate. The flue gas is cooled as it passes through the furnace and convective section. In case the cooling goes on too fast (i.e. with a too steep cooling-gradient, i.e. K/m-profile) or if there is insufficient surface area available in the system (provided by the entrained fly ash particles or by the heat transfer surfaces) there will be an excess of condensable gas molecules e.g. K_2SO_4, and the gas may become supersaturated locally by these gas molecules. This causes the gas molecules to form clusters. If the number of gas molecules in these clusters passes a certain critical number, a new macroscopic phase is formed, in the gas (homogeneous nucleation).

Alkali sulphate aerosols have been detected in the flue gas from straw combustion [Christensen et al., 1998; Christensen and Livbjerg, 1996, 2000] and in experiments using laboratory flow reactors [Jensen et al., 2000; Salmenoja et al., 1996], supporting the idea of a gas phase mechanism for aerosol formation.

Waste incineration on a grate is a well established thermal waste management technology in Denmark, as well as in many other countries in Western Europe and Japan, and it is gaining increasing importance these years due to increasing amounts of household waste being produced and more tight legislation on the content of combustibles in waste fractions being land-filled [DIRECTIVE 2000/76/EC]. The method is flexible with respect to operation, it reduces the volumes of solid waste significantly (typically by a factor of 8 – 10) thereby preserving landfill space. New and advanced flue gas cleaning technologies ensures very low gaseous and particulate emissions from modern incineration plants. Last but not least, it allows for recovery of energy, thereby also contributing to the reduction of greenhouse gas emissions as the waste fractions are largely of biogenic origin and therefore considered CO_2-neutral. The Danish strategy for waste management is still to increase recycling, and, at the same time, to reduce the volume of land-filled waste, in order to avoid loss of resources. Combined heat and electricity producing waste-to-energy (WtE) boilers are an integrated part of this strategy. In 2005, 24 % of the total reported Danish waste production – primarily municipal solid waste from households, the service sector, and the industry - was incinerated at 29 WtE plant located all over Denmark .

Anyhow, waste is a very inhomogeneous fuel, containing a significant fraction of incombustible material, which may be released from the grate during thermal conversion, forming inorganic

gas species and particulate matter (aerosols and fly ashes). The alkalis, several trace metals, S and Cl are among the volatile elements in waste [Bøjer et al., 2008], which besides the risk of harmful emissions to the environment, inorganic elements released from the fuel-bed (grate) may interfere severely upon ash softening, deposition and corrosion problems in the boiler, subsequently leading to decreased overall efficiency and costly, unscheduled shut-downs.

Quantification of the release of inorganic elements such as alkali metals, Cl, S, and heavy metals, to the free board (gas phase) in Waste-to-Energy (WtE) boilers is a challenge. The release of inorganic elements during combustion has previously been studied for annual biomass fuels by [Knudsen et al., 2004a,b], for woody biomass by [van Lith et al., 2006, 2008], and for a suite of selected biofuels by [Frandsen et al., 2007]. Through these studies, methods were developed to quantify the release of inorganic elements from the fuels in lab-scale reactors, simulating grate-firing (fixed-bed) conditions.

The objective of the work by [Steinsen, 2007] was to obtain quantitative data on the release of inorganic elements from dedicated, well-characterized waste fractions; in order to understand the release pattern and the link between the release and formation of fly ash and aerosols, in full-scale waste incinerators. The release of metals, S and Cl from dedicated waste fractions was quantified as a function of temperature in a lab-scale fixed-bed reactor. The waste fractions comprised Chromated Copper Arsenate (CCA) impregnated wood, shoes, automotive shredder waste and PVC (Poly-Vinyl-Chloride). The waste fractions was characterized by use of wet chemical analysis, and, based on the chemical composition of the initial fuel sample and the ash residue after the experiments; the release of inorganic elements was quantified. The lab-scale release results was subsequently compared to data from available full-scale partitioning studies (e.g. FORSKEL-5784), in which test runs with the addition of similar, dedicated waste fractions to a base-load waste had been performed in a grate-fired WtE boiler.

This chapter addresses specifically the release of K, S and Cl from waste fractions, wood types and a suite of annual biomasses.

7.1. The [Steinsen, 2007] Study

The specific fractions were all expected to contain high concentrations of one or more potentially harmful element, i.e., a heavy metal, alkali, Cl or S. The fuel samples were milled to a particle size < 4 mm prior to the release experiments. Samples of the milled fuels were further ground, homogenized, digested and chemically analyzed by DONG Energy A/S Laboratory at Ensted Power Station, Denmark. A chemical analysis of the fuels investigated is presented in Table 7-1. As seen, fuels were very different in ash content, as well as in organic, and inorganic, composition.

A lab-scale setup at the CHEC Research Centre, DTU Chemical Engineering, was applied to quantify the release. The method was similar to the one applied by [van Lith et al., 2006, 2008] on wood fuels. The setup, including: [1)] a gas mixing system, [2)] an electrically heated a horizontal tube reactor, [3)] a gas conditioning system, [4)] gas analyzers, [5)] a thermocouple, and, [6)] a data acquisition system, allowed for pyrolosis and combustion under well-controlled conditions. From online measurements of the sample temperature and the O_2, CO_2 and CO concentrations in the outlet gas, the conversion process was followed during an experiment. A sketch of the set-up is shown in Figure 7-2.

Batch experiments, with sample sizes of 2-10 g, were conducted at different temperatures in the range [500 – 1000 °C]. The fuel sample was placed in a Pt/Au crucible, and inserted in the preheated reactor, and a primary gas flow (5 N L/min) of pure N_2 was added to create a pyrolysis atmosphere. After 1 h of pyrolysis, 1 % (v/v) O_2 was introduced with the primary air, and the oxygen content was then increased stepwise to 20 % (v/v), in order to minimize the sample overshoot temperature during combustion.

Parameter	*Analyzing technique*	*Wood*	*Shoes*	*Shredder waste*	*PVC*
Moisture (wt .% db)	105 °C in nitrogen	10.44 ± 0.08	2.58 ± 0.21	2.05 ± 0.10	0.19 ± 0.01
Ash (wt.% db)	550 °C for 20h	1.81 ± 0.05	15.5 ± 0.03	72.8 ± 1.92	4.98 ± 0.0
Volatile content (wt.% db)	CEN/TS 15148 (900 °C, 7 min.)	84.0 ± 0.37	77.4 ± 0.59	32.1 ± 0.75	81.4 ± 0.07
Al (wt.% db)	Total digestion, ICP-OES	0.0355 ± 0.0038	0.276 ± 0.0007	**1.85 ±0.0778**	0.0440 ± 0.0020
Ca (wt.% db)	Total digestion, ICP-OES	0.129 ± 0.00	**2.84 ± 0.106**	**3.40 ± 0.10**	0.847 ± 0.023
Fe (wt.% db)	Total digestion, ICP-OES	0.0360 ± 0.0013	0.0634 ± 0.0013	**21.9 ± 0.99**	0.0230 ± 0.002
Si (wt.% db.)	Total digestion, ICP-OES	0.306 ± 0.021	**2.99 ± 0.007**	**11.6 ± 0.707**	0.0223 ± 0.0127
Ti (wt.% db.)	Total digestion, ICP-OES	0.0113 ± 0.0006	0.619 ± 0.023	0.150 ± 0.0007	**1.37 ± 0.058**
Cl (wt.% db.)	Calorimeter combustion, IC	<0.0100	3.20 ± 0.099	0.330 ±0.083	**48.7 ± 0.4**
S (mg/kg db)	Fuel: Calorimeter combustion, IC Ash: total digestion, ICP-OES	419 ± 1	**8610 ± 78**	**4890 ± 790**	525 ± 92
K (mg/kg db)	Total digestion, ICP-OES	157 ± 17	**533 ± 25**	**4630 ± 10**	70 ± 10
Mg (mg/kg db)	Total digestion, ICP-OES	118 ± 1	707 ± 48	**6060 ± 156**	57 ± 0.0
Na (mg/kg db)	Total digestion, ICP-OES	463 ± 11	**892 ± 54**	**11,900 ± 200**	267 ± 6
P (mg/kg db)	Total digestion, ICP-OES	144 ± 4	239 ± 11	975 ± 49	**1270 ± 58**
Pb (mg/kg db)	Total digestion, ICP-OES	26.9 ± 2.1	243 ± 8	**2810 ± 71**	**3530 ± 231**
Zn (mg/kg db)	Total digestion, ICP-OES	50.5 ± 0.1	**6840 ± 35**	**22,000 ± 4172**	140 ± 0
As (mg/kg db)	Total digestion, ICP-OES	**95 ± 10**	n.a.	n.a.	n.a.
Cd (mg/kg db)	Total digestion, GF-AAS	n.a.	n.a.	n.a.	0.120 ± 0.006
Cr (mg/kg db)	Total digestion, ICP-OES	317 ± 1.0	**2850 ± 28**	514 ± 136	n.a.
Cu (mg/kg db)	Total digestion, ICP-OES	215 ± 0.2	n.a.	**3230 ± 1421**	n.a.

Table 7-1: Chemical composition of the fuels investigated (mean ± stdev). Elements present in particular high concentrations in the different waste fractions are highlighted in bold.

After complete burnout (corresponding to a total residence time of app. 3 h), the sample was withdrawn from the reactor, and the residual ash was collected for chemical analysis. All runs were repeated to have 2 or 3 replicates (except for PVC at 1000°C which was not repeated), and ash from two of the experiments were selected for additional chemical analysis.

The release of single elements (g/g dry fuel) was quantified assuming that the released fraction of an element applied to the difference between the initial amount of an element in the fuel, and the residual amount retained in the ash.

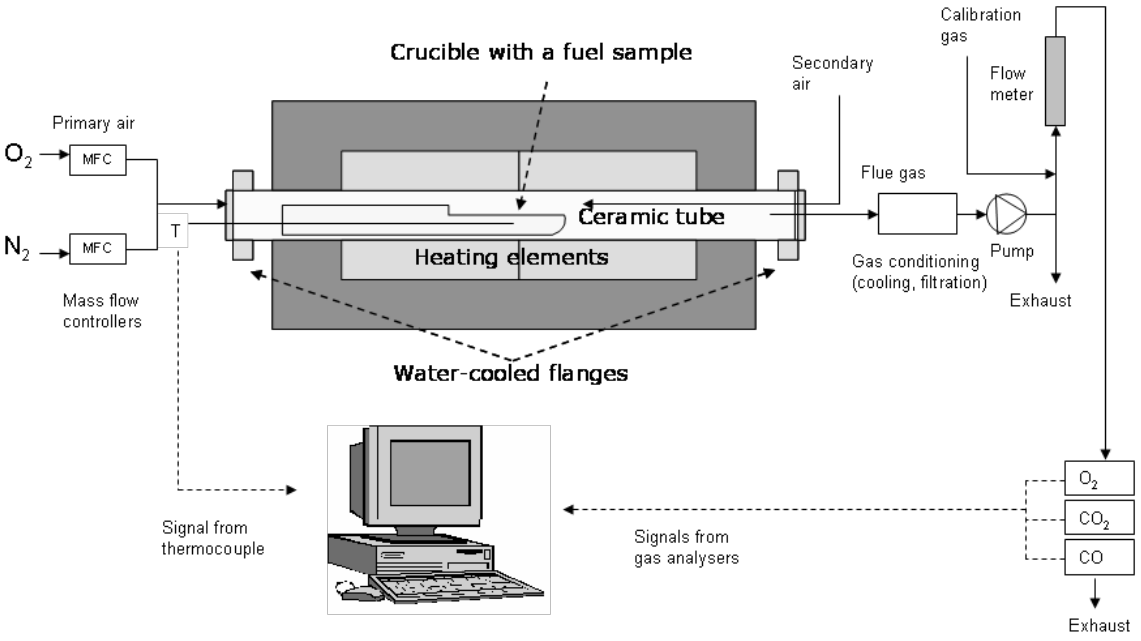

Figure 7-2: The laboratory set-up for release experiments

7.1.1. General Release Observations in the [Steinsen, 2007] Study

The lab-scale release experiments conducted by [Steinsen, 2007] revealed that, generally, the elements Al, Ca, Cr, Cu, Fe, Mg, Si and Ti were not released, or were only released in very small amounts. This behavior is in consistence with data from the literature [Belevi and Moench, 2000] and confirms the non-volatile nature of these elements. It also correlates well with the findings from the full-scale study at FASAN [Astrup et al., 2010; Pedersen et al., 2009], in which only a minor fraction [1 - 17 %] of these specific elements was released during the various experiments, with only minor variations between the different experiments. For Al, Cu, Fe and Si, the release was below 5 % in all the FASAN experiments, whereas for Ca and Cr it was around 15 %. Consistently, [Belevi and Moench, 2000] found in full-scale studies of waste incineration that around 90 % of Al, Ca, Cr, Mg, P and Ti was retained in the bottom ash during incineration, and in case of Cu, Fe and Si, it was even more than 95 %.

For the remaining elements, Pb, Zn, K, Na, Cl, S, and As, the lab-scale release was found to be both temperature dependent and to some extent also fuel specific, as illustrated for each element in Figures 7-3 to 7-9, and discussed below.

7.1.2. Lead (Pb) Release

The release of Pb was found to be strongly temperature dependent for all the waste fractions investigated, especially in the range [500 – 750 °C], see Figure 7-3: At 500°C, only minor amounts (< 20 %) of Pb were released, but the release increased sharply in the interval [500 – 750 °C], reaching 65 – 100 %. At 1000 °C, 85 – 100 % Pb was released from all four waste fractions.

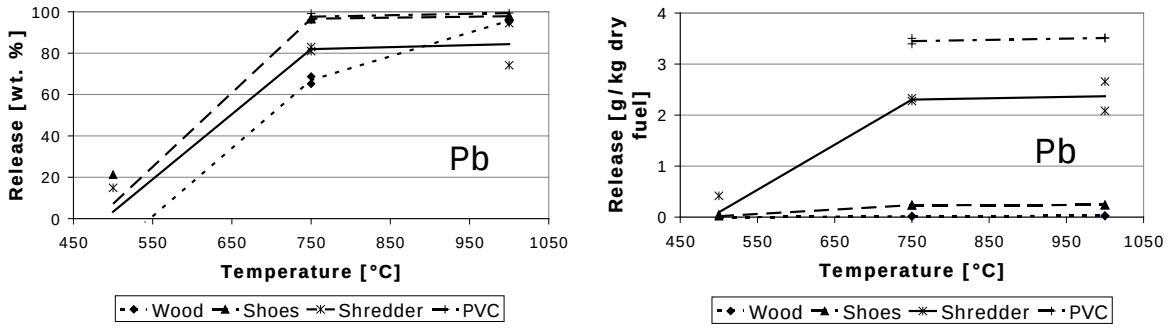

Figure 7-3: The relative and total release ([wt. %] and [g/kg dry fuel], respectively) of Pb, as a function of [T].

Whereas the release was almost complete already at 750 °C in the case of PVC and shoes, a further increase in the Pb-release was observed for CCA-impregnated wood and shredder waste in the temperature interval [750 – 1000 °C]. [Frandsen et al., 2007] reported a Pb release of about 40 % from waste wood at 700 °C, and almost complete release at 1000°C, using a similar lab-scale fixed-bed setup applied by [Steinsen, 2007]. The partial retention of Pb in this higher temperature interval may indicate either that a fraction of the Pb is associated with more stable compounds in these fuels (coatings, oxides), or it may be due to interactions of Pb with certain mineral phases in the fuel, forming more stable compounds such as Pb-aluminosilicates [van Lith et al., 2008] by secondary capture of Pb in a fixed bed. Literature suggest that mechanisms for Pb release include decomposition of Pb-carbonates to Pb-oxides and subsequent reduction of these compounds to volatile species such as PbO(g) or Pb(g) [van Lith et al., 2008].

In the FASAN campaign, the overall partitioning of Pb in the boiler revealed a high retention of Pb, as only about 20 % was released (recovered in the fly ash/aerosols), and averagely 80 % was retained in the bottom ash, when firing a base-load waste [Pedersen et al., 2009]. It was

not possible to link the overall Pb-partitioning in the full-scale study to any operating parameters, such as air distributions or monitored furnace temperatures (the temperature in the fuel layer on the bed was not known). On the other hand, the overall Pb-partitioning was found to vary with changes in feedstock composition, and the fraction present in the fly ash was significantly increased when adding e.g. PVC and shoes to the base-load waste, compared to CCA impregnated wood. Shredder waste did not change the Pb-release pattern notably as compared to the base-load waste conditions [Pedersen et al., 2009].

Thermodynamic equilibrium calculations predict that in an oxidative flue gas PbO(s) is stable at temperatures up to ~600 °C (at oxidizing conditions) when no Cl or S is present. Thermodynamic equilibrium analysis also suggest that the presence of Cl may enhance the volatility of several heavy metals by promoting formation of volatile heavy metal chlorides, while on the other hand, S may decrease the volatility due to formation of condensed sulphate-phases. These roles of Cl and S on heavy metal volatility (especially Pb) are renowned in literature and have also been shown experimentally in several studies [Hasselriis and Licata, 1996; Vassilev et al., 1999; Brunner and Mönch, 1986; Chiang et al., 1997; Tomoda et al., 2006; Mkilala et al., 2002; Tang et al., 2008; Wey et al., 2006], however, documentation of the effects based on full-scale studies is scarce. The data published by [Steinsen, 2007] however, revealed almost complete retention of Pb at 500 °C, even in the PVC experiment where huge amounts of Cl were available for formation of volatile Pb-chlorides. At 750 °C, the laboratory-scale release of Pb, correlates linearly with the S/(S+Cl) ratio in the fuels (R^2 = 0.92), indicating that at least at moderate temperatures (around 750 °C) Cl and S may be influencing the volatility of Pb.

According to the literature, the actual effect of Cl on the heavy metal volatility is strongly influenced by the source of chlorine added, and also of the affinity between chloride and the heavy metal ions and competing cations, respectively [Chiang et al., 1997; Tomoda et al., 2006; Tang et al., 2008; Wey et al., 2006]. The affinity between chloride and some relevant cat-ions (in decreasing order) is: H > Na/K > Pb > other trace metals [Chiang et al., 1997], meaning that the preferred combination is HCl, followed by the alkali-chlorides and then Pb-chlorides. [Tang et al., 2008] studied the effects of different Cl sources (PVC, $FeCl_3$, $CaCl_2$ and NaCl) on the volatilization of heavy metals (Pb, Zn, Cu and Cr) from tannery sludge during incineration (in lab.-scale), and found that the enhancing effect of the Cl-addition increased with increasing Cl/sludge ratio, increasing temperature, and increasing release capacity of chlorine radicals from the Cl sources. In other words, due to relatively low molecular bond energy, PVC releases more free Cl-radicals for the volatilization of heavy metals, at low temperatures, compared to the other Cl-sources. On the other hand, the releasing effect was smaller when NaCl was added as compared to $CaCl_3$, because the alkali metals have a greater affinity to chlorine than the earth-alkali metals. Literature data [Tomoda et al., 2006; Wey et al., 2006] suggest thermodynamically favorable mechanisms for formation of HCl(g) from

inorganic chlorides by reaction of NaCl with SO_2 or silicates, and subsequent chlorination of Pb (as illustrated in equation (7-1 to 7-3)):

$$2\,NaCl + SO_2 + H_2O + ½\,O_2 \rightarrow 2\,HCl + Na_2SO_4 \quad (7\text{-}1)$$

$$2\,NaCl + 6\,SiO_2 + Al_2O_3 + H_2O \rightarrow 2\,HCl + Na_2O.Al_2O_3.3SiO_2 \quad (7\text{-}2)$$

$$PbO + 2\,HCl \rightarrow PbCl_2 + H_2O \quad (7\text{-}3)$$

[Belevi and Langmeier, 2000] studied the evaporation behavior of metals in incinerator environments, by means of laboratory experiments on synthetic samples. Their Pb-source was a 50/50 mixture (on weight basis) of Pb-oxide and Pb-chloride, which was spiked, together with oxides and chlorides of Mn, Ni and Cd, on quarts. They found that the release of Pb was temperature dependent, and increased from almost zero release at 500 °C, through 53 % release at 700°C, to 73 % release at 900°C. They also found that addition of Cl increased the Pb-release slightly, especially at 700 and 900°C. They suggested that the mechanism for Pb-release included partly transformation of PbO to $PbCl_2$, and subsequent evaporation of $PbCl_2$ (g) (b.p. of $PbCl_2$ being 950°C).

7.1.3. Zinc (Zn) Release

The release of Zn was found by [Steinsen, 2007] to be both temperature dependent and fuel specific, see Figure 7-4. For PVC, the release was almost complete already at 500 °C, whereas a gradual increase with increasing temperature was observed for the other waste fractions. This indicates a different release mechanism for Zn in PVC as compared to the other waste fractions. Zn in PVC originates from stabilizers based on "metal soaps", i.e. Ca/Zn and Ba/Zn carboxylates [EU Green Paper on PVC, 2010], meaning that Zn in PVC is organically associated, and it may therefore be released during thermal degradation of the organic structure, at relatively low temperatures.

Carboxyl groups may start to decompose at temperatures < 300 °C The release pattern for Zn in the other three waste fractions investigated by [Steinsen, 2007] (increasing release with increasing temperature from [500 – 1000 °C]) is quite similar to what has previously been reported for wood fuels by [van Lith et al., 2008], and may be attributed to the reduction of ZnO(s) (and other Zn-compounds) to Zn(g) during pyrolysis.

In a laboratory evaporation study on synthetic ($ZnO/ZnCl_2$) samples, the release pattern for Zn was reported to be both temperature dependent, and sensitive to Cl- addition [Belevi and Langmeier, 2000], and it was suggested that the most important parameter for Zn release to

the gas phase below 900 °C was the availability of Cl. Thermodynamic considerations suggest a correlation to the content of Cl and S, but only at lower temperatures. $ZnCl_2(g)$ becomes stable at temperatures above app. 300 °C, while the availability of S may increase the vaporization temperature to app. 550 °C by formation of $Zn(SO_4)(s)$.

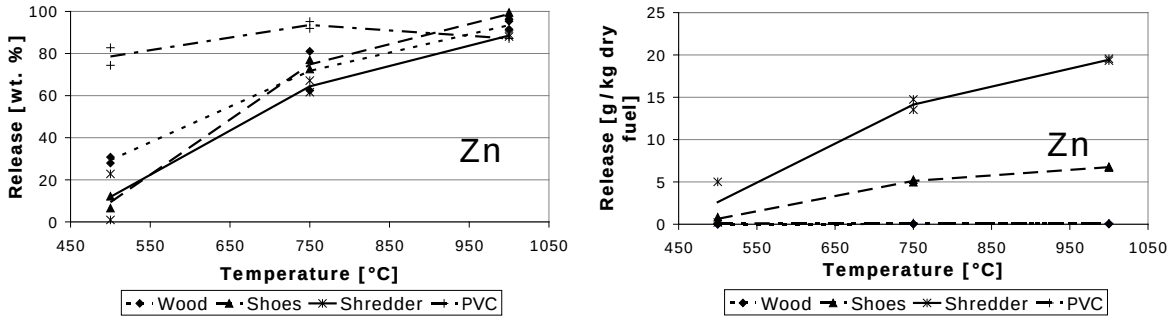

Figure 7-4: The relative and total release ([wt. %] and [g/kg dry fuel], respectively) of Zn, as a function of [T].

In the FASAN campaign, averagely 35 % of the Zn was released from the grate (recovered in the fly ash), and only minor variations were observed between the different experiments at FASAN, probably because the applied changes did not differ enough to cause significant changes in the overall partitioning Zn. Increased concentrations of Zn in the aerosols from the PVC and shoes experiments, however, indicated increased condensation of volatile Zn-species (such as Zn-chlorides) in these specific experiments [Pedersen et al., 2009].

7.1.4. Alkali Metal (K and Na) Release

For CCA-impregnated wood, the release of K and Na could not be determined, due to too low initial concentrations and inhomogeneity of the fuel (glass impurities etc.) [Steinsen, 2007]. For the other waste fractions, the release of alkalis (both K and Na) increased gradually with temperature, see Figures 7-5 and 7-6. The release pattern was similar for Na and K, but to some extent fuel specific. At 500 °C, between 5 % and 40 % Na and 10 - 30 % K was released; at 1000 °C, 50 – 90 % of both metals was released. In the case of shoes, the release increased sharply in the temperature range [750 – 1000°C] (from ~20 to ~90 % for both metals), whereas the increase was more gradual in the entire temperature range for PVC and shredder waste. For shredder waste only app. 50 % of Na and K was released even at 1000 °C, indicating a strong bonding of alkalis in this fuel. Nevertheless, due to the high initial concentration, the total release of alkalis from shredder waste was significant, ranging from 3-6 g Na/kg dry fuel and 1-2 g K/kg dry fuel.

The shoe sample investigated by [Steinsen, 2007] was rich in S (please refer to Table 1), hence the presence of alkali-sulphates may possible explain the sharp increase in alkali release in the temperature interval [750 – 1000 °C] for this fuel, as compared to PVC and shredder waste.

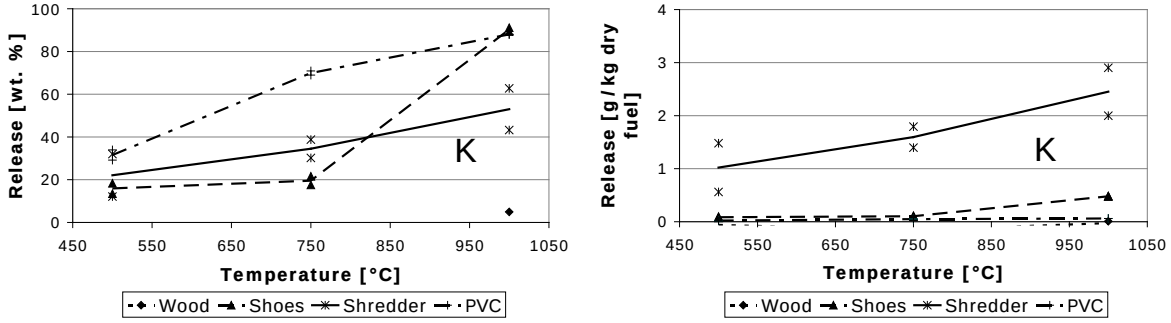

Figure 7-5: The relative and total release ([wt. %] and [g/kg dry fuel], respectively) of K, as a function of [T].

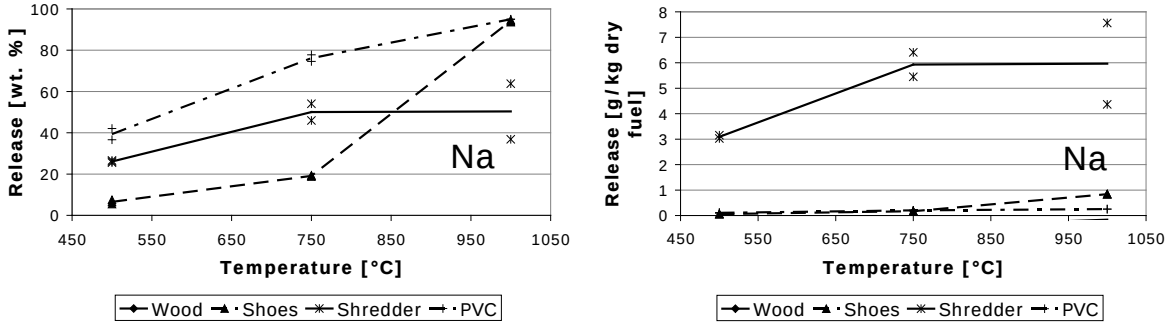

Figure 7-6: The relative and total release ([wt. %] and [g/kg dry fuel], respectively) of Na, as a function of [T].

In the FASAN campaign averagely 15 % Na and 35 % K, was released from the grate when firing base-load waste, and changes in the feedstock composition did not cause any significant changes in the partitioning of alkalis [Pedersen et al., 2009]. The high total release potential for alkali metals found for shredder waste in the lab-scale experiments, was not evident in the FASAN data either.

Addition of other waste fractions rich in alkali metals (road salt (NaCl) and household batteries (containing e.g. KOH), respectively) to the base-load waste, however, slightly increased the partitioning of one or both of the alkalis to the fly ash, and increased the mass load of aerosols; both effects may indicate increased vaporization of alkali metals (and subsequent increased nucleation/condensation) [Pedersen et al., 2009].

7.1.5. Chlorine (Cl) Release

PVC showed a very high release of Cl, at all temperatures, whereas for the other waste fractions, the Cl release increased gradually with temperature, see Figure 7-8. At 500°C, 60 % and 100 % Cl was released from shoes and PVC, respectively, whereas no Cl-release was observed in the case of shredder waste at this temperature. At 1000°C, the release from shoes reached 95 %, whereas only about 50 % was released from the shredder waste. (The Cl-content in the wood was too low to predict the actual release pattern for this fuel). It has been reported in the literature, that the thermal degradation of PVC occurs in two steps, and that the first stage is connected to the release of the Cl as HCl(g). The first step occurs in the temperature range 200 – 340°C resulting in a weight loss of app. 60 %, corresponding to the amount of HCl evolved. The second step occurs at 400-500°C producing a 28 % (w/w) loss [Sakata et al., 1996; Sørum et al., 2001].

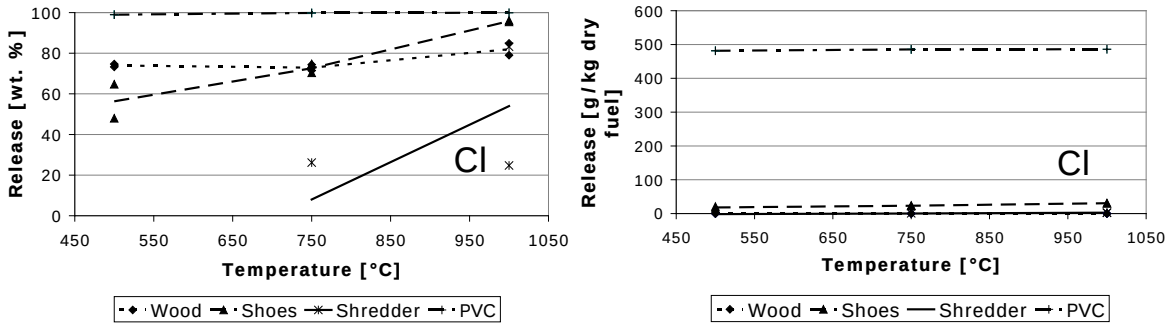

Figure 7-8: The relative and total release ([wt. %] and [g/kg dry fuel], respectively) of Cl, as a function of [T].

In the FASAN campaign, [72 - 89 %] of the Cl was released from the grate when firing base-load waste. The Cl released was distributed (in a ratio of app. 1:2) to the fly ash/aerosols, and to the gas phase, as HCl(g) [Pedersen et al., 2009]. It was found that when firing PVC, relatively more Cl was released to the gas phase, while less was recovered in the fly ash, in consistence with the thermal degradation mechanism for PVC suggested in the literature [Sakata et al., 1996; Sørum et al., 2001]. An opposite effect (relatively more Cl recovered in fly ash and relatively less in the gas phase) was seen when a source of inorganically bound Cl, i.e. NaCl salt, was added to the base-load waste during the FASAN campaign, an indication of the different release mechanism for metal-chlorides (vaporization of alkali-chlorides at temperatures > ~700 °C) suggested in the literature.

7.1.6. Sulfur (S) Release

The release of S from the waste fractions was found to be both temperature dependent and fuel specific [Steinsen, 2007]. For three of the fuels, i.e. CCA-impregnated wood, PVC, and shoes, a high release of S (60 – 95 %) were observed already at 500 °C, whereas in the case of shredder waste, only ~10 % was released at this temperature, see Figure 7-9.

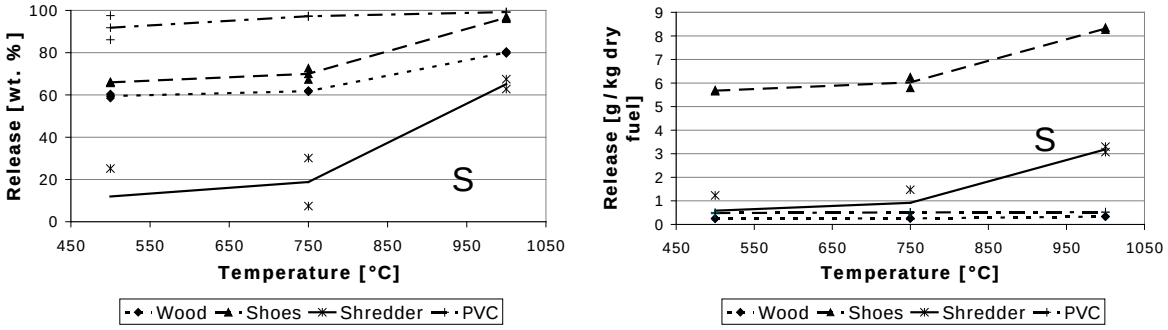

Figure 7-9: The relative and total release ([wt. %] and [g/kg dry fuel], respectively) of S, as a function of [T].

For PVC, the release was almost complete already at 500 °C, whereas a gradual increase with increasing temperature was observed for the other fuels. In the temperature range [500 – 750 °C], the S-release increased only slightly, whereas in the temperature range [750 – 1000 °C], the release increased from 60 – 80 % for CCA impregnated wood, from 70 – 100 % for shoes, and from 20 – 55 % for shredder waste. The partly retention of S, especially in the interval [500 – 750 °C] may be attributed the presence of metal-sulfates, that may remain stable even at quite high temperatures [van Lith et al., 2006, 2008]. In the shoes, as well as in CCA impregnated wood, some S has presumably been added as sulfate compounds in connection with the production of the materials. As an example in shoes, S is added as Cr-sulfate during leather tanning [Bahillo et al., 2004], and in CCA impregnated wood, S is added as Cu-sulfate during the impregnation process [Sipilä et al., 2007]. Hence, a significant amount of the S in these waste fractions may be present as sulphates. The release at lower temperatures is probably attributed to the release of organically bound S [van Lith et al., 2006, 2008].

In the FASAN campaign, on average 31 % S was retained in the bottom ash, while the rest was distributed between fly ash/aerosols, and the gas phase, respectively. The addition of CCA impregnated wood to the base-load waste, slightly changed the overall partitioning towards relatively less S, in the fly ash and relatively more in the gas phase, indicating that S was relatively more volatile when firing this waste fraction, as compared to the base-load waste. According to [Frandsen et al., 2005] analysis of a collection of fuels, aerosol, fly ash and emission data from boilers firing several different types of biomass, revealed that no clear correlation between the S-content and the SO_2-emission could be established, indicating that

the SO_2-emission is influenced by a number of different factors which are not yet fully understood. [Belevi and Moench, 2000] reported S retentions of 19 – 24 % in bottom ash when firing mixed waste and household waste, respectively, in a full-scale study.

7.2. The [van Lith, 2006, 2008] Studies

During wood combustion, inorganic elements such as alkali metals, sulfur, chlorine, and some heavy metals are partly released to the gas phase, which may cause problems in combustion facilities because of deposit formation and corrosion. Furthermore, it may cause harmful emissions of gases and particulate matter.

Three quantification methods, A-C, were developed by [van Lith et al., 2006]. In all three methods, the release of inorganic elements is quantified by a mass balance based on the weights and inorganic compositions of the fuel and the ash residues obtained by high-temperature (500–1150 °C) treatment in a laboratory-scale tube reactor. However, method A involved the pyrolysis and combustion of a small fuel sample (~30 g) in this reactor, whereas methods B and C involved initial pyrolysis and combustion, respectively, of a large fuel sample (~5 kg) in a bench-scale fixed-bed reactor at 500 °C. The methods were evaluated by comparing the data on the release of Cl, S, K, Na, Zn, and Pb from fiber board obtained by the three methods.

Large differences in the release trends (especially for S, Na, and Zn) were observed for the three methods because of the differences in sample size, oxidizing/reducing conditions, and the ash formation process.

[van Lith et al., 2006] obtained quantitative data on the release of inorganic elements during wood combustion by performing experiments under conditions that resemble grate-firing. The release was quantified by performing a mass balance, based on the weights and inorganic compositions of the fuel and residual ash samples. Three different experimental methods were developed and tested, the main difference between the methods being the size of the wood sample used. Because the ash content of some woody biomass fuels, such as wood chips, is relatively low (usually less than 1% (w/w) dry basis, db), it is desirable to obtain a higher quantity of residual ash as this will improve the accuracy of the chemical analysis of the ash and thereby the release data. Moreover, a larger fuel sample is expected to be more homogeneous in chemistry and to provide a better reproducibility of the results. On the other hand, there is a risk of secondary reactions between released species and the char when using a larger fuel sample [van Lith et al., 2006].

The release of inorganic elements during combustion of wood was quantified at various temperatures in the range of 500–1150 °C. To produce the high-temperature ash, three

different methods were used, involving two different experimental setups: [1)] a laboratory-scale tube reactor setup, and, [2)] a bench-scale fixed-bed reactor setup;

- Method A (wood combustion): this method involved pyrolysis, and subsequent combustion of a small wood sample, in the laboratory-scale tube reactor.
- Method B (char combustion): in this method, a large amount of wood was first pyrolyzed (at 500 °C) in the bench-scale fixed-bed reactor, and a small sample of the obtained char was then combusted in the laboratory-scale tube reactor.
- Method C (ash heating): in this method, a large amount of wood was completely combusted (at 500 °C) in the bench-scale fixed-bed reactor, after which a small sample of the obtained ash was heated in the laboratory-scale tube reactor.

7.2.1. Method A (Wood Combustion)

In order to study the release of inorganic elements during combustion of a small sample of woody biomass, a laboratory-scale tube reactor setup was designed and assembled. The setup included a gas mixing system, a reactor, a gas conditioning system, gas analyzers, a thermocouple, and a data acquisition system. The reactor consisted of a two-zone electrically heated oven, in which a cylindrical alumina tube was mounted horizontally, having water-cooled flanges at both ends. Inside the tube, a removable alumina tube was placed, in which a sample boat could be inserted [van Lith et al., 2006].

Two different types of sample boats were applied: [1)] a boat made out of an alumina tube with one end closed, and, 2) a smaller boat made of a platinum/gold alloy (95% Pt). In the case of experiments up to 850 °C, the fuel was inserted into the alumina boat, whereas in the case of experiments above 850 °C, the fuel was inserted into two Pt/Au boats, which were both placed into the alumina boat to facilitate the insertion and positioning of the sample [van Lith et al., 2006].

To prevent breakage of the alumina tubes as a result of thermal shock when a cold sample boat was inserted into the hot reactor, a layer of ceramic fiber insulation material was glued (using ceramic glue) inside the inner reactor tube, covering the bottom half. The front of the reactor could be sealed with a stainless steel plate, which contained openings for the primary gas inlet and a thermocouple that could be placed inside the fuel sample. Secondary air was added through a probe inserted at the back of the reactor. Measurements of the sample temperature and flue gas composition were acquired continuously and were monitored online during the experiments.

7.2.2. Methods B and C (Char Combustion and Ash Heating)

The bench-scale fixed-bed reactor setup (used in methods B and C) consisted of a gas supply system, a large oven, gas analyzers, two thermocouples, and a data acquisition system. The oven was electrically heated and contained a removable stainless steel container of 64 L in which the fuel sample was inserted. Inside this container, a stainless steel grid was placed, which served to distribute the gas evenly through the fuel sample. The gas was introduced through a tube below the grid, and a sample of the flue gas was directed to CO and CO_2 analyzers. The container with the fuel sample was shaken frequently to obtain a good mixing between the fuel and the air [van Lith et al., 2006].

The first part of the char combustion method (method B) consisted of the production of a large amount of char. This was done by inserting the container with a pre-weighed fuel sample (~5 kg) and a nitrogen flow of 3 NL/min into the bench-scale fixed-bed reactor. A small sample (15 g at temperatures up to 850 °C and 20 g at higher temperatures) of the char remains was then combusted in the laboratory-scale tube reactor setup. The conditions and procedure for this part of the method are the same as for the fuel combustion method described above.

The ash heating method (method C) involved the production of a large amount of low-temperature (500 °C) ash in the bench-scale fixed-bed reactor setup. This was also done in two stages.

- First, a large amount of fuel was pyrolyzed in exactly the same way as in the first part of the char combustion method (method B).
- During the second stage, the obtained char was subsequently combusted in the same setup, by changing the gas flow to 50 NL/min of nitrogen and 0.7 NL/min of oxygen (1.4% (v/v) O_2) but maintaining the temperature at 500 °C.

A small sample (0.5 g at temperatures up to 850 °C and 1 g at higher temperatures) of ash was then heated in the laboratory-scale tube reactor setup. The conditions and procedure for this part of the method are also the same as for the fuel combustion method described above.

The three methods were tested in a study firing a residue from the fiber board manufacturing industry. It consisted mainly of pieces of wood in various sizes (maximum ~1 cm), but it also contains some larger pieces of coating material. The chemical characteristics of the fiber board are presented in Table 7-2. The ash content (1.24% (w/w) db) and chemical composition of fiber board are comparable to spruce, except for the very high content of Ti (0.45% (w/w) db), originating from TiO_2 being present in the pigment of the coating. Furthermore, fiber board has a very high N content compared to spruce (about 25–30 times higher), which is due to the presence of N in the glue, binders, and coating. The higher Cl and heavy metal content in fiber board probably also originates from the glue, binders, and/or coating. In particular,

the concentration of Pb is very high in fiber board (about 35 times higher than in spruce). The relative standard deviation of the elemental analyses of the fuel is around ±5–10% [van Lith et al., 2006].

	fiber board	spruce
moisture (% (w/w))	6.8	6.6
ash (% (w/w) db)	1.24	0.95
Cl (% (w/w) db)	0.05	< 0.01
S (mg/g db)	0.3	0.1
K (mg/g db)	0.64	0.85
Na (mg/g db)	0.18	0.02
Ca (mg/g db)	1.5	1.9
Mg (mg/g db)	0.21	0.2
Ti (mg/g db)	4.5	<0.0021[a]
Si (mg/g db)	0.55	0.43
Al (mg/g db)	0.35	0.08
Zn (mg/kg db)	27	14
Pb (mg/kg db)	16	0.44
K/Cl	1.2	9.6
K/S	1.8	7.0
K/Si	0.84	1.4
K/Al	1.3	7.3
K/Ti	0.17	496

[a] Analyzed by a different laboratory.

Table 7-2: Characteristics of the fibre board fuel used in the experimental study, and wood chips from spruce for comparison (db = dry basis).

The results of the release experiments are presented in Figures 7-11 to 7-13. In general, it is observed that method A (wood combustion) yields the highest release values, and method C (ash heating) the lowest (except in the case of the release of K).

The release trends of the non-metals Cl and S are shown in Figure 7-10a and b, respectively. A very high release of Cl is observed for all three methods. In the case of method A (wood combustion), an almost complete release of Cl is observed already at 500 °C. In the case of methods B (char combustion) and C (ash heating), the release at 500 °C is ~85%, but increases to more than 95% at 700 °C. The quantity of S released to the gas phase is highly dependent on the experimental method used, especially in the low-temperature range (500–850 °C). Nevertheless, all three methods show a clear two-step release of S. In the first step (which starts below 500 °C), about 25–60% of S is released, depending on the experimental method used. In the second step, which starts around 850 °C, the release of S increases very rapidly with temperature to nearly 100% at 1150 °C in the case of all experimental methods [van Lith et al., 2006].

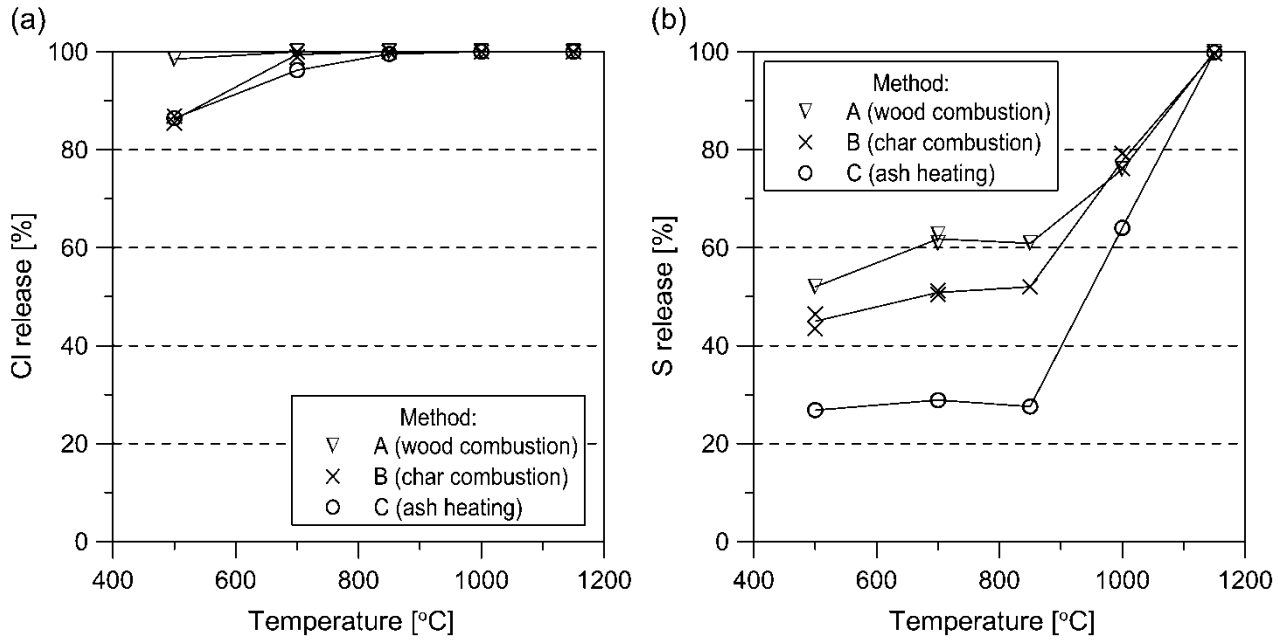

Figure 7-10: Release of the nonmetals Cl (a) and S (b) to the gas phase as a function of temperature during fiber board combustion by the three different methods. Source: [van Lith et al., 2006].

In Figure 7-11, the release data of the alkali metals K and Na are presented. In the case of all three methods, a relatively low release of K was observed in the entire temperature range of 500–1150 °C, with a maximum of around 30% obtained at the highest temperature in the case of method B (char combustion). However, the release trends of K obtained by methods A (wood combustion) and B (char combustion) do not show a progressive increase with temperature. The release data for Na obtained by methods A (wood combustion) and B (char combustion) were very similar (see Figure 7-9). A release of around 10–15% was observed at

low temperatures (500–700 °C), increasing to around 22% at 1000 °C. A relatively high Na release of around 60% in the case of method B (char combustion), and around 75% in the case of method A (wood combustion) was observed at 1150 °C. Slightly negative values for the release of Na were obtained at all investigated temperatures in the case of method C (ash heating), which is most likely due to an uncertainty in the experimental method [van Lith et al., 2006].

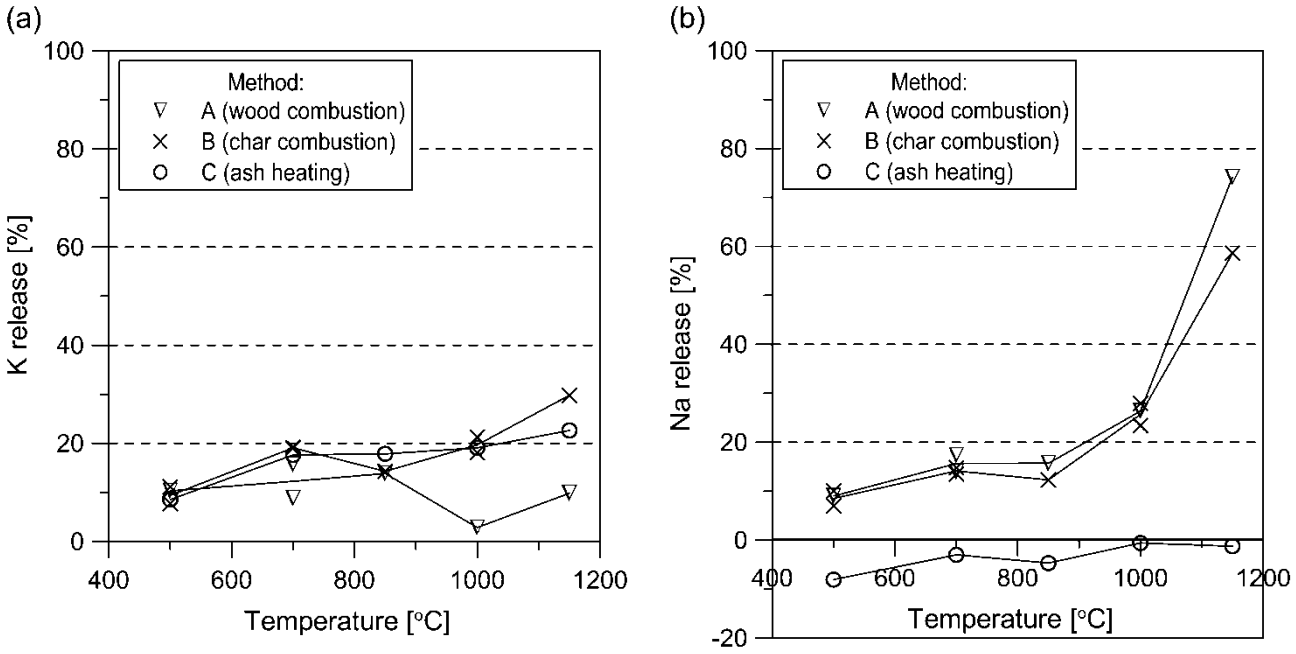

Figure 7-11: Release of the alkali metals K (a) and Na (b) to the gas phase as a function of temperature during fiber board combustion by the three different methods.

Figure 7-12 shows the release profile for the heavy metals Zn and Pb. Whereas only a minor release (below 10%) of Zn was observed, in the case of method C (ash heating), a significant release (up to around 90%) was found in the case of methods A (wood combustion) and B (char combustion). The fractions released for Zn at 700 and 850 °C are very different for methods A and B; in the case of method B, the release remains around 10% in this temperature interval, while the release increases to almost 40% in the case of method A. For the release of Pb, the data obtained by methods A and B are quite similar, except at 1000 °C. At this temperature, a nearly complete release is found in the case of method B, but a much lower release value is obtained when using method A. In the case of method C, a much lower release of Pb was obtained in the high temperature range (850–1150 °C) compared to the other two methods. In this case, the release increases more gradually to a maximum value of ~65% at 1150 °C [van Lith et al., 2006].

The results obtained for the release of inorganic elements during combustion of fiber board show that the experimental method and the temperature strongly affect the quantity of elemental release to the gas phase.

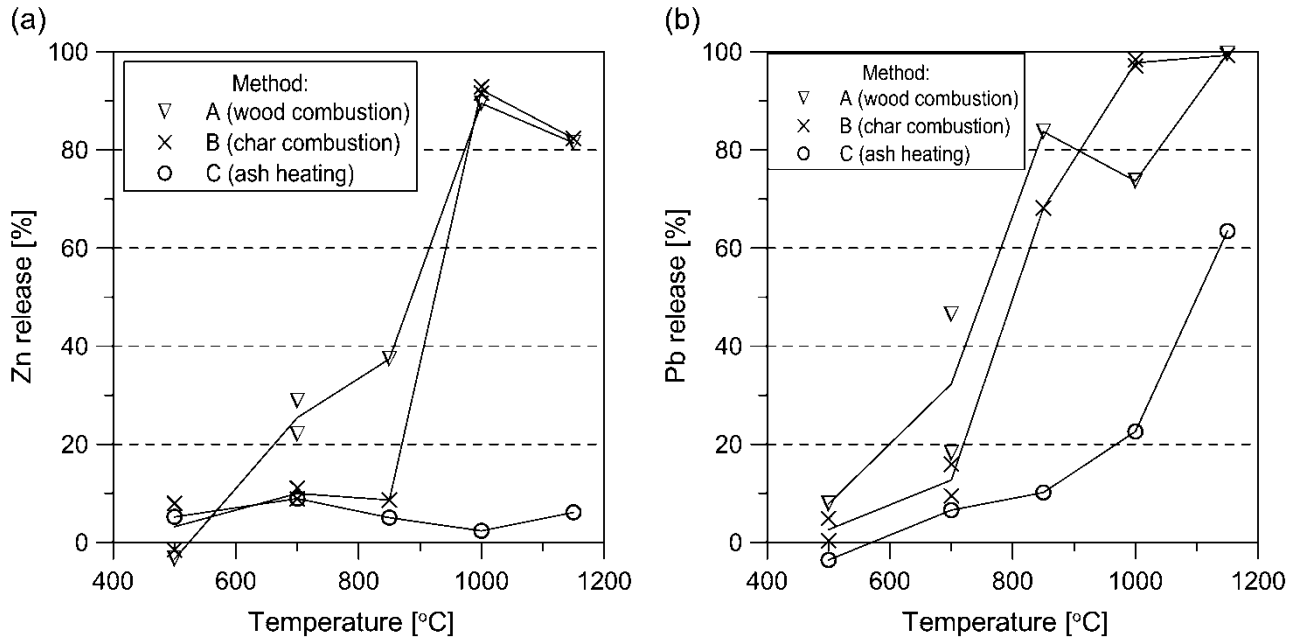

Figure 7-12: Release of the heavy metals Zn (a) and Pb (b) to the gas phase as a function of temperature during fiber board combustion by the three different methods.

7.2.3. Release of Chlorine from Fibre Board

A very high release (~85–100%) of Cl was obtained by all three methods, already at 500 °C (see Figure 7-10a). Some Cl release below 500 °C was also reported for various types of biomass by [Knudsen et al, 2004b; Jensen et al., 2000; Björkman et al., 1997; Zintl et al., 1998], who concluded that Cl was released as HCl(g), during devolatilization. However, the reaction mechanism by which HCl(g) is formed seems to be dependent on (1) the ash composition of the fuel, (2) the association of Cl in the fuel, and (3) the experimental conditions (surrounding atmosphere, heating rate, residence time, sample size) under which the fuel is converted [van Lith et al., 2006].

[Björkman and Strömberg, 1997] who studied the pyrolysis of various types of biomass fuels (sugarcane trash, switch grass, lucerne, and rape straw), found that 20–50% of the fuel Cl was released in a first step between 300 and 400 °C, and some more was released during a second step between 700 and 900 °C (except in the case of rape straw). Although the major fraction of Cl in these fuels was water-soluble and therefore most probably present as (alkali) salts, the

first step of the Cl-release could not have occurred by evaporation of KCl, because the vapor pressure of KCl is negligible at 400 °C. Thermodynamic considerations indicated that the Cl could be released in the form of HCl(g) at these temperatures, by reaction of KCl with steam formed from the biomass itself, in the presence of SiO_2 (see eq (7-4)), [Björkman and Strömberg, 1997].

$$2\,KCl(s) + n\,SiO_2 + H_2O(g) \rightarrow K_2O.(SiO_2)_n + 2\,HCl(g) \qquad (7\text{-}4)$$

However, no Cl release was observed from experiments with a sand–KCl mixture when simulated dry or wet flue gas was applied as the surrounding atmosphere, indicating that the Cl release is not influenced by a reaction with SiO_2. When KCl was added to wood with a very low Cl content (0.02% (w/w) db) to obtain a fuel with a Cl content of 1.82% (w/w) db, between 30 and 50% of the Cl was released already during pyrolysis at temperatures between 400 and 600 °C. From this finding, [Björkman and Strömberg, 1997] concluded that Cl could be released because of interaction with the organic material. This was further investigated by [Zintl et al., 1998] who studied the pyrolysis of mixtures of KCl and different biopolymers in the temperature range of 200–700 °C. On the basis of on their findings, they suggested that the initial low-temperature release of Cl may occur when KCl reacts in an ion-exchange reaction with chain-bonded carboxylic groups, yielding an alkaline carboxylate and HCl(g), according to eq (7-5) [van Lith et al., 2006].

$$R - COOH(s) + KCl(s) \rightarrow R - COOK(s) + HCl(g) \qquad (7\text{-}5)$$

This alkaline carboxylate is eventually degraded (at higher temperatures), according to eq (7-6).

$$R - COOK(s) \rightarrow R + CO_2(g) + K(g) \qquad (7\text{-}6)$$

[Jensen et al., 2000] also found a two-step release of Cl during pyrolysis of wheat straw; in the first step about 60% of Cl was released between 200 and 400 °C. They suggested that during pyrolysis of wheat straw the original straw matrix is destructed and the Cl is released from its solid-phase bonding sites and transferred to a liquid tar phase in the temperature range of 200–400 °C. From there, Cl may be released to the gas phase as HCl(g) or undergo secondary reactions with K to form KCl(s) or with basic functionalities on the char surface [van Lith et al., 2006].

[Knudsen et al., 2004b] investigated the release of Cl, S, and K during pyrolysis and combustion of annual biomass fuels. The fuels rich in Cl (~0.7–0.8% (w/w) db) showed a two-step release of Cl. Release of similar quantities of Cl (~20–60%, depending on fuel type) was observed during pyrolysis and combustion at 500 °C, indicating that the low-temperature

release of Cl takes place during devolatilization. However, the percentage of Cl released at 500 °C was much higher for the fuels with a lower (~0.05% (w/w) db) Cl content (up to 73% Cl was released in this case). This finding can be explained by the mechanism proposed by [Zintl et al., 1998] assuming that the number of proton-donating sites in the char is limited. In the case of a lower content of Cl in the fuel (e.g., present as KCl), a larger fraction of Cl has the opportunity to react with the proton-donating sites in the char, which may cause a higher percentage of Cl to be released as HCl(g) during devolatilization. [Knudsen et al., 2004b] also argued that the association of Cl in the biomass could have an influence on the Cl release during devolatilization. However, because both organically associated Cl and Cl present as salts may be released as HCl(g) (during devolatilization) or as gaseous salts (during char burnout) according to the above-mentioned mechanisms, it is difficult to determine the effect of the association of Cl in the fuel on the Cl release during devolatilization [van Lith et al., 2006].

The high Cl-release observed already at 500 °C during fiber board combustion was expected, since the Cl-content of the fuel is very low (0.05% (w/w) db), but a nearly complete release from biomass fuels at this temperature has not been reported previously in the literature [van Lith et al., 2006]. It is possible that most Cl is released as HCl(g) during devolatilization, as a result of the reaction of metal chlorides with the organic material according to eqn. (7-5) and because of the release of organically associated Cl. Chemical fractionation analysis of fiber board showed that the main part of the Cl was water-soluble [Pedersen, 2003]. We therefore believe that the main release mechanism of Cl from fiber board is the reaction of metal chlorides with the char during devolatilization. The metal chlorides in the fiber board fuel may originate from the wood fibers [Marchner, 2002] as well as from the glue, binders, and/or paint that were added during manufacturing. A small residual fraction (~10%) of Cl in fiber board was leachable in 1 M ammonium acetate [Pedersen, 2003] indicating that this fraction could be organically associated. The release of organically associated Cl is therefore thought to be of minor importance in the case of fiber board combustion [van Lith et al., 2006].

[Knudsen et al., 2005] showed that HCl(g) can be captured by biomass char (wheat straw, but also beech wood was investigated). Spectroscopic and chemical analyses of the char samples revealed that HCl(g) was mainly captured because of secondary reactions with the inherent metal species (mainly K) of the biomass. During combustion of Cl-laden char samples (obtained by HCl(g) addition under pyrolysis conditions), high retention values of Cl in the ash at temperatures up to 600 °C were observed. At higher combustion temperatures, Cl was gradually released to the gas phase due to evaporation of KCl.

Considering the fact, that a much larger fuel sample was used in methods B (char combustion) and C (ash heating), compared to that of method A (wood combustion), secondary reactions of HCl(g) with metal species in the char (e.g., K_2CO_3 and char-bound K) are likely to occur when the released HCl(g) from the lower part of the fuel bed diffuses through the char layer on top. This explains the lower release of Cl observed at 500 °C in the case of methods B and C. The

nearly complete release above 700 °C is most likely due to the evaporation of metal chlorides, formed by the secondary reactions.

7.2.4. Release of Sulfur from Fibre Board

A relatively high release was also observed for S during fiber board combustion at 500 °C, although the quantity released was found to be very dependent on the experimental method used (~55% release for method A, ~45% release for method B, and ~25% for method C) [van Lith et al., 2006]. In the case of all three methods, very little additional S was released in the temperature range of 500–850 °C, but a steep increase in the release of S with temperature above 850 °C and a complete release at 1150 °C was observed (see Figure 8b).

[Dayton et al., 1999] directly sampled the hot gases released during the devolatilization and combustion of small samples of various types of biomass fuels (including various types of wood) in a quartz-tube reactor, employing a molecular beam mass spectrometer (MBMS) system. They identified SO_2(g) during devolatilization of various types of biomass fuels (rice straw, wheat straw, switchgrass, wood, banagrass, and sugarcane bagasse) and suggested that this release of SO_2(g) was due to the oxidation of organic S in the plant matrix. Knudsen et al., 2004b] also found a relatively high release of S (~25–60%, depending on the fuel type) at 500 °C, when firing annual biomass. The fact that similar quantities (~25–40%) were released during pyrolysis of the same fuels at 500 °C suggests that the initial S release occurs during devolatilization. In earlier work, [Knudsen et al., 2004a] found that during pyrolysis of wheat straw, the fraction of sulfatic sulfur in the char remains constant up to 500–600 °C, whereas the total S content in the char is decreasing in this temperature range. This result confirms that the S release is due to the decomposition of organic S compounds rather than inorganic sulfates. Thus, the quantity of S released at 500 °C is highly related to the association of S in the fuel (i.e., to the ratio of organic versus inorganic S), rather than to the composition of the fuel. It seems therefore reasonable to conclude also in the case of fiber board, that the release of S below 500 °C occurred by decomposition of organic S during devolatilization. Chemical fractionation results for fiber board showed that ~40% of the S is water-soluble [Pedersen, 2003], which means that up to 60% of the S may be present as organic S compounds. This is in good agreement with the observed S release of ~52% at 500 °C in the case of method A (wood combustion) [van Lith et al., 2006].

The effect of the experimental method on the quantity of S released during combustion of fiber board at 500 °C is very pronounced, and can be explained by the occurrence of secondary reactions in larger fuel beds. During the first stage of methods B (char combustion) and C (ash heating), where a large sample of wood is pyrolyzed in the bench-scale fixed-bed reactor, the

SO_2(g) released as a result of the decomposition of organic S in the lower part of the sample could be captured by the overlying char by reaction with functional groups of the organic char matrix (resulting in char-bound S), or with inorganic species in the char (resulting in inorganic sulfates) during its way up with the gas flow [van Lith et al., 2006].

[Knudsen et al., 2005] found that substantial amounts of SO_2(g) relative to the inherent S content of wheat straw could be captured in the char at 400–950 °C. The fact that the S capture capacity of char from beech wood, which has a much lower ash content compared to wheat straw (0.36% versus 6–9%), was similar to that of wheat straw confirmed that SO_2(g) primarily reacts with functional groups in the char matrix (rather than with inorganic species in the char) [van Lith et al., 2006]. Furthermore, spectroscopic analysis of the char samples exposed to SO_2(g) indicated that S was predominantly found in nonionic form, such as organic compounds. Although the effect of secondary reactions in the larger-scale fixed-bed reactor experiments performed by [Knudsen et al., 2005] was not as pronounced as expected from their laboratory-scale investigation (in which up to 8 times the S content of the char added as SO_2(g) could be captured at 600 °C), secondary reactions seemed to play a significant role in the experiments in the bench-scale fixed-bed reactor (methods B and C). The 10–30% lower S release (at 500 °C) observed in the case of methods B and C compared to method A (where only the laboratory-scale tube reactor was used to pyrolyze and combust a small fuel sample) indicates that, during pyrolysis in the bench-scale fixed-bed reactor, SO_2(g) released from the lower parts of the bed was captured in the upper char layer. During char burnout, this char-bound S is most likely transformed into sulfates. Thermodynamic equilibrium calculations [Van Lith, 2005] of fiber board under combustion conditions, indicate that S is stable as a salt mixture of K_2SO_4 and Na_2SO_4 up to 950 °C, and as pure $CaSO_4$(s) up 800 °C. The presence of S as sulfates therefore explains why no or little additional S is released in the temperature range of 500–850 °C.

Because the release of S increases steeply above 850 °C, but no or little K is released above 1000 °C in the case of fiber board, another mechanism must be responsible for the S release observed in the range of 850–1150 °C. [Knudsen et al., 2004b] found an abrupt increase in the S release for Si-rich annual biomass fuels compared to Si lean annual biomass fuels above 700–800 °C, indicating that the S release at high temperature is influenced by the Si content of the fuel. This was in agreement with equilibrium calculations, which showed that K and Ca are preferably present as silicates (or as KCl(g)) above 800–900 °C during combustion of annual biomass fuels. If the K and Ca incorporated into silicates originally were present as sulfates, this would result in a release of S. Thermodynamic equilibrium calculations for fiber board indicate that K is preferably present as aluminosilicates above 950 °C [van Lith, 2005]. Furthermore, the calculations show that Ca is stable as $CaSO_4$(s) up to 750 °C, but seems to react with

$TiO_2(s)$ (which is present in very high concentrations in fiber board) at higher temperatures, resulting in the formation of $CaTiO_3(s)$ and the release of $SO_2(g)$, according to eq (7-7).

$$CaSO_4(s) + TiO_2(s) \rightarrow CaTiO_3(s) + SO_2(g) + ½O_2(g) \quad (7\text{-}7)$$

According to the calculations, Na_2SO_4 also reacts with $TiO_2(s)$ to form $(Na_2O)\cdot(TiO_2)_6(s)$, releasing $SO_2(g)$ around 950 °C [van Lith, 2005]. SEM-EDX analysis of ashes obtained by combustion of fiber board by methods B and C, at 1000 and 1150 °C, shows the presence of a melt phase mainly containing Ti, Ca, K, Si, and Al, in which $CaTiO_3$ crystals could be identified (see [van Lith, 2005]). This indicates that Ca and K react with titanates and alumino silicates at high temperature and supports the S release mechanism according to eq. (7-6) at high temperature. The ash obtained by method A at 1150 °C was not investigated by SEM-EDX, but a study of the ash obtained at 1000 °C showed that the ash consisted of Ti-rich flakes originating from the coating particles, which also contained Ca and K, and an ash structure mainly consisting of Ca, but also containing a significant amount of Ti. This also indicates that the TiO_2 originating from the coating particles reacts with metal species originating from the wood particles during combustion [van Lith et al., 2006].

The second release step of S observed during fiber board combustion in the range of 850–1150 °C is thus thought to be due to the release of SO_2 during the reaction of Ca-, K-, and Na sulfates with titanates and (alumino-) silicates. The fact that a complete release of S was found at 1150 °C in the case of all experimental methods indicates that the S captured by the char during devolatilization in the case of methods B (char combustion) and C (ash heating) is released as well during this second step [van Lith et al., 2006].

7.2.5. Release of Potassium from Fibre Board

The results obtained for K (see Figure 7-9a) indicate that no or little K (<20%) is released in the temperature range of 500–1150 °C during fiber board combustion. This release profile is different from those observed during combustion of woody biomass fuels [Misra et al., 1993] and annual biomass fuels [Knudsen et al., 2004b]. In the case of woody biomass fuels (various types of wood chips and bark), it was observed that the release of K started around 700–900 °C, depending on the wood type. At 1300 °C, a release of K of 63–97% was observed, depending on the wood type [Misra et al., 1993]. For annual biomass fuels, the release of K was found to increase from around 0% at 700 °C to around 50–90% at 1150 °C, the release profile in this temperature range being strongly dependent on the inorganic composition of the fuel [Knudsen et al., 2004b].

The only similarity between the release trend of fiber board, and those observed for other woody and annual biomass fuels is the small percentage (~10%) of K released below 500 °C. Qualitative release studies have shown that a small fraction of K is released during devolatilization below 500 °C in the case of birchwood [Davidsson et al., 2002a], wood waste [Davidsson et al., 2002b] and annual biomass fuels [Dayton et al., 1999; Davidsson et al., 2002b,c]. This is assumed to be due to the release of organically associated K during thermal degradation of the organic structure, probably in the form of KOH(g). Considering the high level of oxygen in biomass chars, it seems likely that part of K exists as metals ion-exchanged onto oxygen functionalities within the organic matrix. Chemical fractionation analysis of fiber board showed that a small part of K is organically associated [Pedersen, 2003] which may explain the 10% release of K observed during combustion of fiber board at 500 °C by all three methods. The larger fraction of K released during devolatilization (or combustion) at temperatures above 500–700 °C in the case of birchwood, wood waste, and annual biomass fuels are thought to be mainly due to vaporization of potassium salts. This is supported by the fact that water-leaching of biomass fuels greatly reduces the release of K during devolatilization at high temperature [van Lith et al., 2006].

The presence of Cl in the fuel has been found to enhance the release of K during pyrolysis and combustion of straw and other annual biomass fuels [Knudsen et al., 2004a,b]. In the case of (Cl-rich) annual biomass, the release of K in the form of KCl(g) occurs mainly between 700 and 800 °C, the fraction of K released being dependent on the K/Cl molar ratio of the fuel (20% release in the case of wheat straw, which has a K/Cl ratio of around 4, and 40–50% release in the cases of rice and barley, which have a K/Cl ratio of around 2) [Knudsen et al., 2004a,b]. Because in the case of fiber board combustion, almost all Cl is released already at 500 °C (most likely in the form of HCl(g) during devolatilization, as described above), the release of K by evaporation of KCl(g) at higher temperatures will be minimal [van Lith et al., 2006].

[Knudsen et al., 2004b] observed that, in the case of annual biomass fuels with a low Cl content (comparable to that of fiber board), a substantial release of K was observed between 700 and 800 °C. Moreover, the molar release of K from one of the fuels, carinata, investigated by [Knudsen et al., 2004b], above 800 °C is orders of magnitude higher than the combined Cl and S release, indicating that a major part of K is released as species other than KCl and K_2SO_4, in the entire range of 500–1150 °C. Furthermore, the release of KOH(g) has been observed in the case of combustion of biomass fuels with a high alkali metal and low Cl content (almond shells and almond hulls) at 1100 °C [Dayton and Milne, 1996] and in the case of combustion of switchgrass [Dayton et al., 1995] and poplar [Dayton and Milne, 1995] at 1100 °C in the presence of excess steam. As mentioned before, K may be released in the form of KOH(g) originating from K being ion-exchanged to oxygen functionalities in the char structure. The release of KOH(g) during combustion in the presence of water vapor may be due to the

dissociation of potassium carbonates (such as K_2CO_3 or a mixed calcium–potassium carbonate), as described by eq (7-8).

$$(Ca-)K-carbonate + H_2O \rightarrow 2KOH(g) + CO_2\ (+CaO(s)) \qquad (7\text{-}8)$$

[Knudsen et al., 2004b] experimentally determined and modeled the evaporation rate of K from K_2CO_3 in the absence respectively the presence of water, and found that the evaporation rate in the absence of water was more than 3 orders of magnitude lower than that in the presence of water (0.2% (v/v)) at 900 °C, and therefore this seems to be a reasonable explanation for the low release of K, even if K is present in the form of carbonates in the ash. Furthermore, it is possible that K_2CO_3 react with compounds such as (alumino-) silicates or titanates in the ash, forming stable K compounds and releasing CO_2(g).

[Knudsen et al., 2004b] found that the release of K during combustion at high temperature (900–1150 °C) is dependent on the Si-content of the fuel in the case of annual biomass. Fuels rich in Si (rice, barley, and wheat) showed a lower K release at 1150 °C (~50–80%), compared to fuels lean in Si (oat, carinata, and rape) (~80–90%). This was thought to be due to the incorporation of K into silicate structures in this temperature range, which was supported by SEM-EDX analyses of the ashes obtained by combustion of wheat straw at various temperatures [van Lith et al., 2006].

However, the low K/Ti ratio in fiber board compared to that in other biomass fuels, see [Knudsen et al., 2004b] (see Table 2) and the very low K release up to 1150 °C (<20%) indicate that K is probably also incorporated into titanates, which remain stable up to 1150 °C. A reaction of K with Ti was not predicted by the thermodynamic calculations, but the chemical compositions of the ashes obtained by the combustion experiments in the range of 500–1150 °C, indicate that $(K_2O)\cdot(TiO_2)_6$(s) may be formed during combustion in the entire temperature range of 500–1150 °C. The reason for the lower release of K observed at 1000 and 1150 °C in the case of method A (<10% release) compared to methods B and C (~20–30% release) remains unclear and indicates that the incorporation of K into silicate and titanate structures is a complex process [van Lith et al., 2006].

7.2.6. Release of Sodium from Fibre Board

Two different trends were observed for the release of Na from fiber board. In the case of methods A and B, the release of Na was low until 850 °C, but increased rapidly at higher temperatures to ~75% (method A) or ~60% (method B) at 1150 °C. In the case of method C, the Na release pattern is more similar to that of K: no release was observed in the entire range of 500–1150 °C [van Lith et al., 2006]. Compared to that of spruce, fiber board has a

significantly higher Na-content, probably originating from glue, binders, or coating added to the fuel during processing. According to chemical fractionation analysis of fiber board [Pedersen, 2003], the major fraction of Na (~75%) is water-soluble, indicating that Na is mainly present in the form of salts, such as nitrates and chlorides. A small fraction (~20%) of Na is leachable in ammonium acetate [Pedersen, 2003] indicating that this fraction may be organically associated. The observed release behavior of Na is very different from that of K in the case of methods A and B: the release of Na increases rapidly above 850 °C, whereas the release of K remains below 30% up to 1150 °C [van Lith et al., 2006].

Thermodynamic equilibrium calculations of fiber board showed that K may form silicates, already at low temperature (500 °C), but Na preferably forms sulfates [van Lith, 2005]. When $Na_2SO_4(s)$ starts to dissociate at higher temperature (above 800–900 °C), incorporation of Na into (alumino-) silicates is possible, but may be limited if the positions in the structure are already occupied by K. In that case, a larger fraction of Na will be released to the gas phase as NaOH(g). This may explain the Na-release above 850 °C, observed during combustion of fiber board according to methods A and B. In the case of method C, a low-temperature (500 °C) ash was produced, which was subsequently heated to higher temperatures. The fact that the inorganic elements are already present in ash-form at 500 °C may enhance the interaction between Na and other species in the ash, providing more possibilities of Na to be incorporated into ash structures [van Lith, 2005].

Because it was observed that all Cl was released at 700 °C, the release of Na by vaporization of NaCl is unlikely in the case of fiber board. The Na release above 850 °C in the case of methods A and B may also result from the dissociation of $Na_2CO_3(s)$, yielding NaOH(g). But the release of Na from Na_2CO_3 is probably dependent on the partial pressure of H_2O in the gas phase and may therefore be limited because the primary air used in the experiments did not contain $H_2O(g)$ [van Lith et al., 2006].

7.2.7. Release of Zinc from Fibre Board

The results for the release of Zn shown in Figure 10a, are very dependent on the experimental method for combusting the sample. In the case of methods A (wood combustion) and B (char combustion), the release is close to zero at 500 °C and around 80–90% above 1000 °C. However, in the case of method A, the release increases gradually with temperature, whereas in the case of method B, the release remains low until 850 °C and then increases rapidly with temperature. In the case of method C, a very low release (<10%) is observed in the entire range of 500–1150 °C [van Lith et al., 2006].

Extensive information is available about aerosol formation during wood combustion [Brunner et al., 2000, 2002; Hueglin et al., 1997; Lind, 1998; Obernberger et al., 2001; Johansson, 2002; Boman, 2003; Jöller et al., 2004] and transformations and emissions of metal elements during coal combustion [Sarofim et al., 1977; Flagan and Friedlander, 1978; Neville et al., 1980; Quann and Sarofim, 1982; Kaupinnen and Pakkanen, 1990; Hurley and Schobert, 1992, 1993]. The results of these studies indicate that Zn is released during wood combustion, probably similar to that described for coal combustion.

[Obernberger et al., 2001] used both wet chemical analysis methods and the SEM-EDX technique to chemically characterize aerosols formed during combustion of fiber board and other types of woody biomass fuels (wood chips, bark, and waste wood) in pilot- and full-scale grate-fired boilers. They found that Zn was present in all cases. Because aerosols are formed by the condensation of gas-phase species, this means that Zn is released to the gas phase during combustion of fiber board and other woody biomass fuels on a grate. In the case of waste wood and bark, it was found that the Zn concentration in the aerosols followed the particle size distribution, indicating that the Zn-containing aerosols could have been formed by agglomeration of ZnO nuclei. [Jöller et al., 2004] used transmission electron microscopy in combination with EDX analysis and found that Zn was present in the cores of the aerosols from bark combustion [van Lith et al., 2006].

Equilibrium calculations of Zn for fibre board were performed for both oxidizing and reducing conditions and showed a strong dependence of the excess air ratio (λ) on the stability of Zn(g) [van Lith, 2005] In the case of oxidizing conditions (λ = 1.5), it was observed that Zn preferably forms solid compounds with Al, Si, Fe, and Ti at temperatures up to 1000 °C, above which Zn mainly appears in the gas phase as Zn(g). In the case of reducing conditions, Zn(g) becomes stable at much lower temperatures (~600 °C in the case of λ = 0.5). This supports the theory that Zn is released as Zn(g) in the reducing atmosphere of the fuel particles and corresponds well to the observation that a fraction of Zn (~25%) is released already at 700 °C in the case of fiber board combustion by method A (wood combustion). In method B, the fuel sample was first pyrolyzed at 500 °C and then combusted at higher temperatures. Because no Zn is released at 500 °C, it will probably react with elements such as Al, Si, Fe, and Ti in the ash during the combustion phase. Under oxidizing conditions, Zn may then be released from these compounds at 1000 °C or higher.

Zn is an essential micronutrient in plants due to its catalytic and structural functions in enzymes and therefore naturally occurs in small amounts. Zn mainly occurs as low molecular weight complexes, storage metalloproteins, free Zn^{2+} ions, and insoluble forms associated with the cell walls [Welch, 1995; Brown et al., 1993]. Depending on the plant species, between 58 and 91% of the Zn in a plant can be in water-soluble form, which mainly includes the low molecular weight complexes. Zn present in proteins is usually tightly bound to the apoenzyme

and can only be removed with severe chemical treatment. The Zn occurring in membranes has a structural function, and is insoluble [Welch, 1995].

Chemical fractionation analysis of fiber board showed that small fractions of the Zn in fiber board are water-soluble (~10%) or acetate-leachable (~20%) [Pedersen, 2003]. This most likely comprises the Zn species naturally occurring in wood as low molecular weight complexes and free ions, as mentioned above. Zn^{2+} probably precipitates as salts, such as chlorides during drying of the wood. However, the major fraction of Zn was found in the HCl-leachable fraction [Pedersen, 2003], indicating that Zn is mainly present in less-soluble forms. These may include the metalloproteins naturally present in wood, but considering the higher Zn content of fiber board compared to that of chemically untreated wood chips (see Table 2), it probably also includes Zn compounds added to the fuel during production. ZnO is insoluble in water, but soluble in HCl, and is commonly used as a white pigment in paints. It is therefore likely that the major part of Zn in fiber board is present in the form of ZnO.

Organically associated Zn would probably be released during devolatilization or combustion at low temperatures, but because the release at 500 °C is very low or zero, this does not seem to be an important part of the total Zn release. The release of Zn by vaporization of $ZnCl_2$ seems to be unlikely as well, because it was observed that almost all Cl was released already at 500 °C, and the equilibrium calculations for fiber board do not predict that $ZnCl_2$ will be formed in the range of 400–1200 °C [van Lith, 2005].

Because Zn is expected to be mainly present as ZnO in fiber board, the principal mechanism of Zn release is most likely the release of Zn(g) during pyrolysis above 500 °C. This probably occurs according to the mechanism described for coal, in which ZnO(s) is reduced to Zn in the reducing environment of the char particles, which is volatilized from the char particles as Zn(g) at temperatures above 500 °C. This explains the increasing release of Zn with increasing temperature in the range of 500–1150 °C observed for method A. Because the pyrolysis temperature applied in the case of method B and C is 500 °C, no Zn is released by this mechanism. In the case of method B, ZnO will probably react with compounds containing elements such as Al, Si, and Fe in the ash during the combustion phase. The Zn release observed at 1000 and 1150 °C is most likely due to the vaporization of Zn from these compounds during char combustion (at locally reducing conditions). In the case of method C, melting of Ti-bearing phases were observed in the ashes obtained at 1000 and 1150 °C. This may have facilitated a reaction of Zn with Ti-bearing phases, which may have hindered the release of Zn, during heating to higher temperatures, so that even at 1150 °C the Zn release is minimal [van Lith et al., 2006].

7.2.8. Release of Lead from Fibre Board

The release of Pb from fiber board increased very rapidly with temperature from close to 0% at 500 °C to nearly 100% at 1150 °C in the case of methods A (wood combustion) and B (char combustion). The release of Pb observed by [Miller et al.' 2003] in their investigation of wood/bark combustion at 800 and 900 °C is very similar to the results obtained by methods A and B.

Equilibrium calculations were performed for fiber board combustion in both oxidizing and reducing conditions [van Lith, 2005]. In both cases, Pb was predicted to be stable as $(PbO)\cdot(Al_2O_3)_6(s)$ at low temperatures. In the case of oxidizing conditions ($\lambda = 1.5$), PbO(g) becomes stable above 650 °C, whereas in the case of reducing conditions ($\lambda = 0.5$), all Pb is predicted to be in the gas phase above 500 °C, in the forms of Pb(g), PbCl(g), and PbS(g).

The form in which Pb occurs in the fuel is unclear. Pb is not a mineral nutrient for plants, but may be present in small amounts due to the uptake of polluted air by the foliage or polluted groundwater by the roots and subsequent transport to other parts of the tree. Pb is also known to be used as white pigment in paints and might therefore be present in the coating of fiber board. The significantly higher Pb content of fiber board compared to that of spruce (see Table 2) suggests that this is the main source of Pb in fiber board. In this case, Pb would be present in the form of PbO_2 or $2PbCO_3\cdot Pb(OH)_2$.

During pyrolysis, lead carbonates will decompose to lead oxides, and PbO_2 will reduce to PbO. PbO may be reduced to the highly volatile Pb(g) in a reducing atmosphere or may vaporize as PbO(g) in an oxidizing atmosphere. The experimental results show that the release of Pb starts around 500 °C and indicate that the amount of Pb released is dependent on the oxidizing/reducing conditions. In the case of methods A and B, Pb is expected to be released mainly in the form of Pb(g) during pyrolysis. In the case of method C, no Pb is released during pyrolysis and combustion in the bench-scale fixed-bed reactor, because the temperature is too low (500 °C). Instead, the Pb compounds probably decompose to lead oxides during pyrolysis and interact with other ash particles during char burnout. Because of the high volatility of PbO above 500 °C, Pb will be released from the ash during heating to higher temperatures in the laboratory-scale tube reactor.

7. 3. Release of Critical Elements from Other Woody Fuels

Quantitative release data were obtained for a suite of wood fuels, by pyrolyzing and subsequently combusting small samples of wood (~30 g), at various temperatures in the range

of 500–1150 °C in a laboratory-scale tube reactor, and then performing mass balance calculations based on the weight measurements and chemical analyses of the wood fuels and the residual ash samples [van Lith et al., 2008].

Four types of wood fuels were selected for the release quantification experiments: spruce (wood chips), beech (wood chips), bark, and fiber board. All the fuel samples were received from wood combustion plant manufacturer MAWERA Holzfeuerungsanlagen GmbH, which is located in Hard, Austria [van Lith et al., 2008].

In order to be able to use the fuels in the laboratory release investigation, and to obtain a better physical and chemical homogeneity, the fuels were dried (at room temperature, until the water content of the fuels was in equilibrium with the moisture in the atmosphere), and subsequently milled using a 4-mm screen. The fiber board fuel was used as received, because it was relatively dry (6.8% (w/w) moisture), and contained relatively small particles (mainly pieces of wood with lengths up to ~1 cm, and some pieces of coating material of ~1 cm^2).

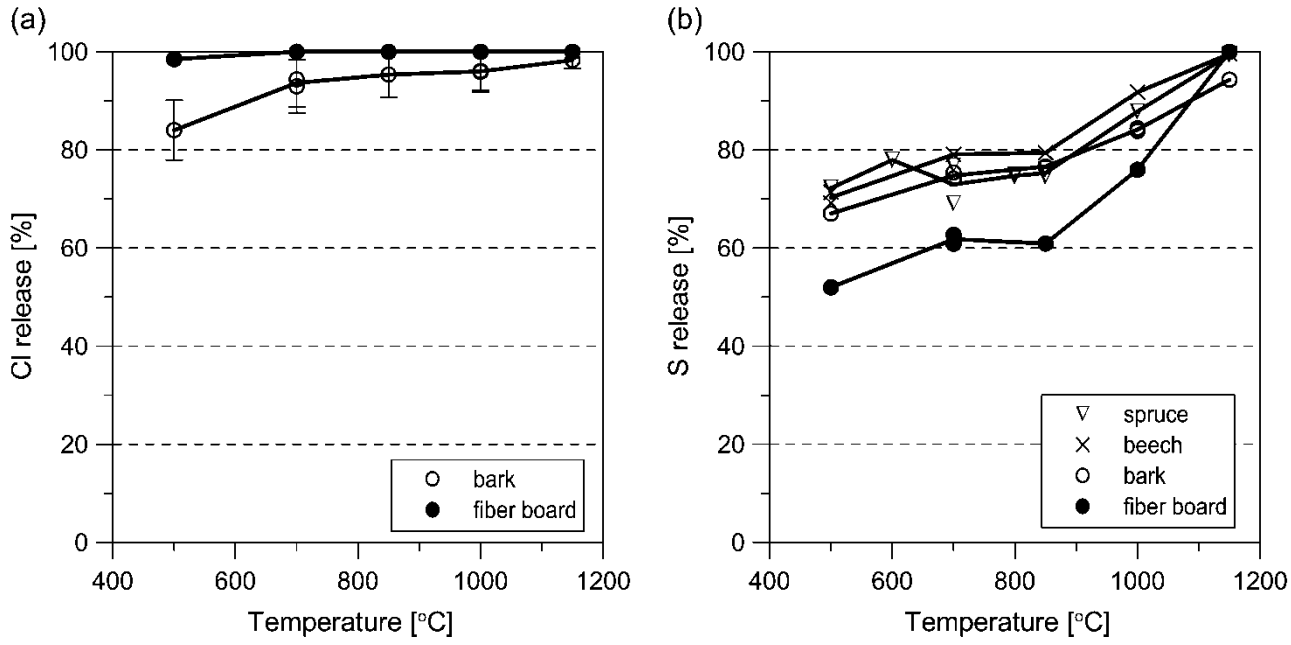

Figure 7-13: Release to the gas phase of the nonmetals Cl (a) and S (b) as a function of the combustion temperature, for different wood fuels. Note that the data points for the Cl release from bark in the range of 850–1150 °C represent the minimum release values. Source: [van Lith et al., 2008].

The fuels were found to be similar in organic composition, except that the fiber board has a high N content (3.6% (w/w) dry basis, db) compared to the other three fuels (0.13–0.47% (w/w) db). Spruce and beech have the lowest ash contents (<1% (w/w) db), and have similar

inorganic compositions. The only large difference between these fuels is the very low Si content of beech (0.03% (w/w) db) compared to spruce (0.43% (w/w) db). Of the four fuels, bark has the highest content of most of the main ash-forming elements, and thereby the highest ash content. The high Ti content of fiber board (0.45% (w/w) db) originates from the TiO_2 being present in pigment of the coating. Furthermore, fiber board has the highest Na-, Cl-, and Pb contents, probably because of the presence of glue, binders, and coating [van Lith et al., 2008].

For S, a two-step release is observed, but the quantity released is about 10–20% lower for fiber board compared to the other fuels up to 1000 °C. For spruce, beech, and bark, a relatively high S release of around 70% is observed at 500 °C. No or little additional S is released in the interval 500–850 °C, but at higher temperatures the release increases in a second step to ~95–100% at 1150 °C. For fiber board, an S release of ~50–60% was observed in the range of 500–850 °C, after which the release increases sharply to ~100% at 1150 °C.

The release data for the alkali metals K and Na are presented in Figure 7-14. For all the fuels, a relatively low release of K (<20%) was observed up to 800 °C.

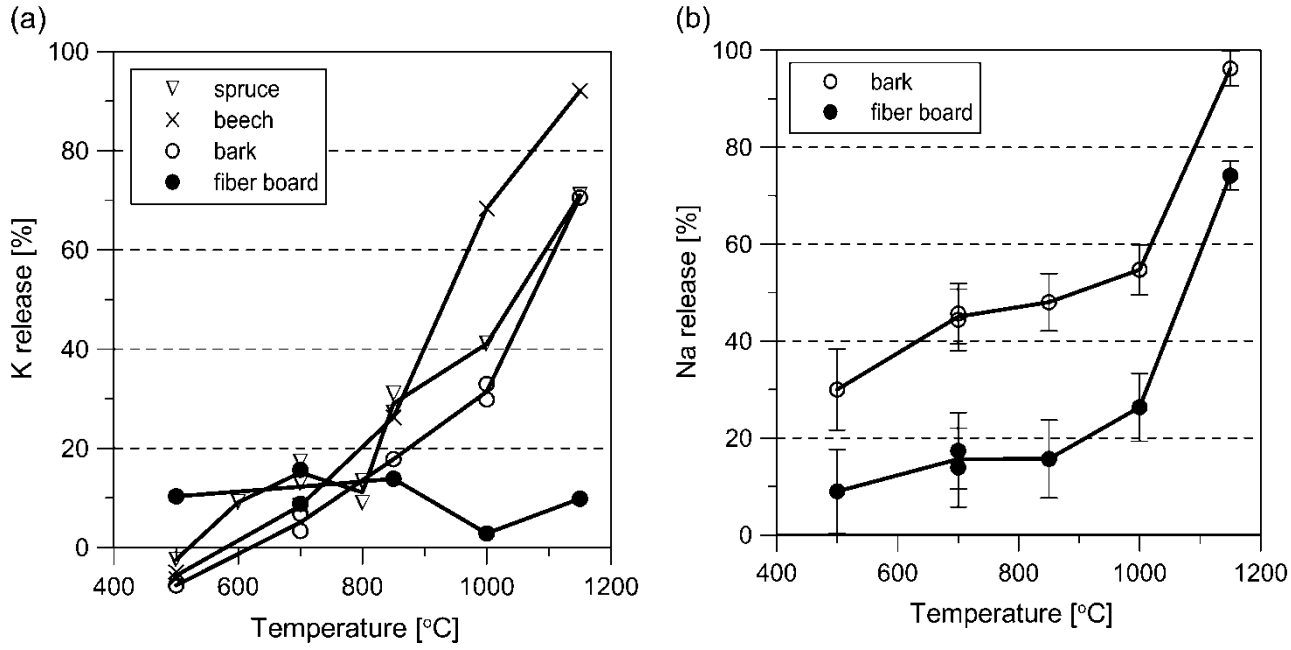

Figure 7-14: Release to the gas phase of the alkali metals K (a) and Na (b) as a function of the combustion temperature, for different wood fuels. Source: [van Lith et al., 2008].

The release of K in the temperature range 800–1150 °C was found to be strongly dependent on the fuel type. For beech, a sharp increase in the release was observed above 800 °C,

reaching ~90% at 1150 °C. Spruce and bark show a more or less similar release trend above 800 °C, where the release increased to ~70%, at 1150 °C. For fiber board, a very low release of K (~5–15%) is observed in the entire temperature range of 500–1150 °C [van Lith et al., 2008].

The Na release trends were similar for bark and fiber board: a gradual increase in the release in the interval 500–1000 °C, followed by a sharp increase to 1150 °C was observed. However, in the entire range of 500–1150 °C, the relative fraction of Na released from fiber board is about 20–30% lower than from bark. For bark, a nearly complete release of Na (96±4%) is observed at 1150 °C, whereas the release from fiber board is only 74±3% at this temperature [van Lith et al., 2008].

The release of Zn and Pb seems to start at (or slightly below) 500 °C for all the fuels. For spruce and bark, the release of Zn and Pb increases sharply to around 95–100% at 850 °C, see Figure 7-15.

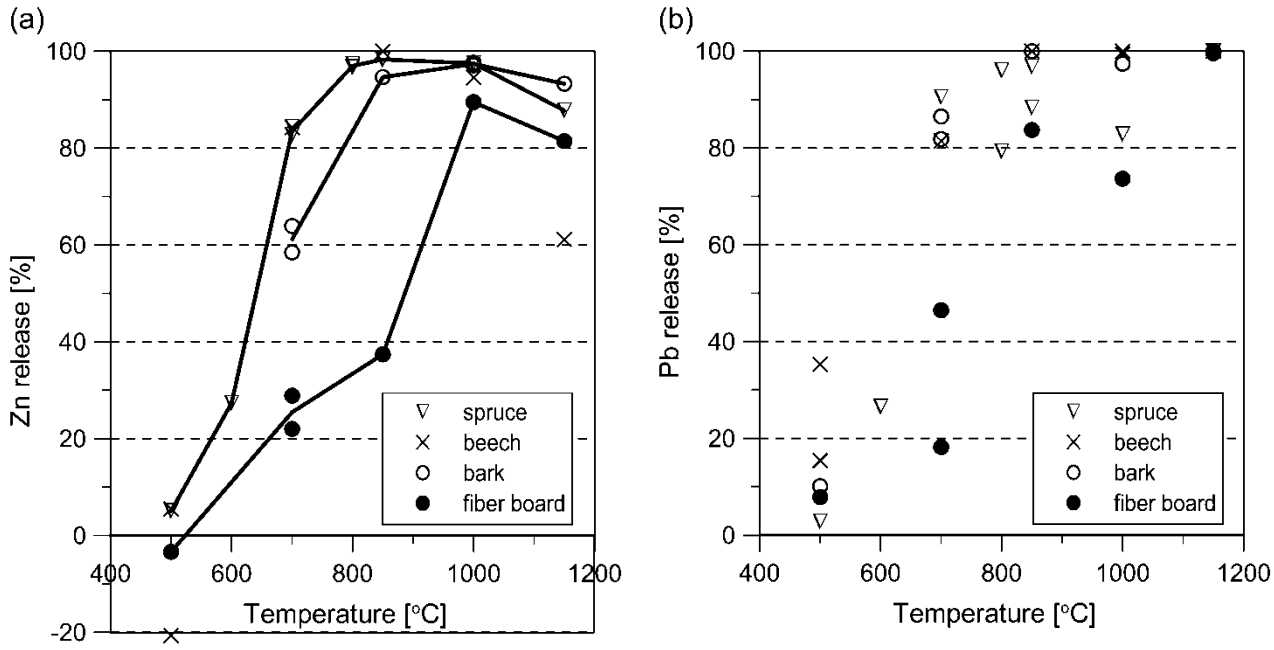

Figure 7-15: Release to the gas phase of the heavy metals Zn (a) and Pb (b) as a function of the combustion temperature, for different wood fuels.

It was concluded that in the case of fiber board, the principal mechanism for the (primary) release of Cl is the reaction of metal chlorides (e.g., KCl(s)) with carboxyl groups or other proton-donating sites in the char during pyrolysis, resulting in the formation of HCl(g), e.g., by eq (7-9).

$$Char - COOH + MCl(s) \rightarrow Char - COOM + HCl(g) \quad (7\text{-}9)$$

where Char represents the char matrix, and M represents either K or Na.

For all the fuels, a two-step release of S was observed: ~50–70% of the S was released below 500 °C, and the remaining S was gradually released in the interval 850–1150 °C (see Figure 7-13b). It is believed that, the release of S below 500 °C is due to the decomposition of organic sulfur compounds during the devolatilization stage, and therefore, that the quantity of S, released at 500 °C, is highly related to the association of S in the fuel, i.e., to the ratio of organic- versus inorganic S [van Lith et al., 2008].

Figure 7-13b shows that additional S is released above 850 °C, and that nearly all of the fuel-S was released at 1150 °C for all the fuels. Sulfur release above 800 °C is thought to be due to the decomposition or evaporation of alkali metal sulfates. Whereas decomposition appears to be the most common vaporization mechanism for Na_2SO_4 under combustion conditions [Ficalora et al., 1968; Cubiciotti and Kenesha, 1972] evaporation or sublimation seems to be most important for K_2SO_4 [Elieser and Howald, 1976]. According to [Knudsen et al., 2004a,b] the evaporation of K_2SO_4 becomes significant above 1000 °C. Because the release of S and K increases sharply above 1000 °C in the case of spruce, beech, and bark, the evaporation of K_2SO_4 may be an important S release mechanism in the interval 1000–1150 °C for those fuels. In the case of fiber board, however, no or only little K is released above 1000 °C, indicating that another mechanism must be responsible for the release of S during combustion of this fuel at high temperature. [van Lith et al., 2006] argued that this is most likely the release of SO_2 as a result of the reaction of Ca-, K-, and Na sulfates with titanates and (alumino-) silicates.

The release of K seems to start around 500–600 °C in the cases of spruce, beech, and bark, whereas for fiber board a small fraction of K (~10%) is released below 500 °C (see Figure 7-14a). The data indicate that the release of K is relatively low (<20%) up to 800 °C for all the fuels.

The release of K below 500 °C is due to the release of organically associated K, during thermal degradation of the organic structure in the devolatilization stage [Davidsson et al., 2002 a,b,c].

Potassium is an important mineral nutrient for plants. Because of its metabolic function, K is highly mobile within all levels of the plant – individual cells, tissues, and in long-distance transport via the xylem and phloem [Marshner, 2002] K is not structurally bound, but forms only weak complexes in which it is readily exchangeable [WynJones et al., 1979]. During drying of wood, the K originally present as free K^+ ions in the fluids is likely to precipitate in

the form of salts, such as KCl, K_2SO_4, KOH, and K_2CO_3. Some of the K in wood may be organically associated, i.e., ion-exchanged to the oxygen-containing functionalities of the organic material, in particular to the carboxyl groups, which are present in the hemicelluloses and pectins of wood [Bailey and Reeve, 1996].

It is well-documented that carboxyl groups start to decompose at a relatively low temperature (<300 °C) [Schafer, 1991]. This means that during pyrolysis, atomic K will be released by the following mechanism [van Lith et al., 2008]:

$$Char - COOK \rightarrow Char + CO_2(g) + K \quad (7\text{-}10)$$

However, at low temperature (<600 °C), phenol groups are still present in the char, so that the released atomic K may be bound to those groups in the char [van Lith et al., 2008]:

$$Char - C_6H_5 - OH + K \rightarrow Char - C_6H_5 - OK + H \quad (7\text{-}11)$$

Above 400 °C, also the phenol groups start to degrade, whereby a fraction of K may be released to the gas phase, probably in the form of K(g). During the combustion stage, the remaining char-bonded K is likely to be transformed into K_2CO_3(s), which is a stable compound at low temperature (<850 °C).

Therefore, it is believed that for wood fuels, the mechanism for the release of K in the range of 500–800 °C is the release of some of the char-bonded K, during pyrolysis. This can be explained by the decreasing number of oxygen-containing functional groups (e.g., phenol groups) in the char, with increasing temperature, causing a lower possibility of K to bind to the char matrix [van Lith et al., 2008].

Most likely, the decomposition of potassium carbonates, such as K_2CO_3, is the dominant mechanism of K release observed in the high temperature region (800–1150 °C) for spruce, beech, and bark. Thermodynamic equilibrium calculations indicate that the decomposition of K_2CO_3 starts above 800 °C. Thermo gravimetric analysis and differential thermal analysis of the wood ashes investigated by [Misra et al., 1993] indicated that the dissociation of Ca and K_2CO_3 takes place at 700–900 °C, depending on the wood type. The decomposition of K_2CO_3 may result in the formation of K(g), according to eqn (7-12);

$$K_2CO_3 \rightarrow 2K(g) + CO_2 + \tfrac{1}{2}O_2 \quad (7\text{-}12)$$

Upon vaporization, K(g) may react with other species present in the gas phase. When water is present in the gas phase, K(g) will convert to KOH(g). In the presence of HCl, the conversion

of K(g) to KCl(g) is more likely. According to [Knudsen et al., 2004a], the rate of decomposition of K_2CO_3 is strongly enhanced in the presence of water vapor.

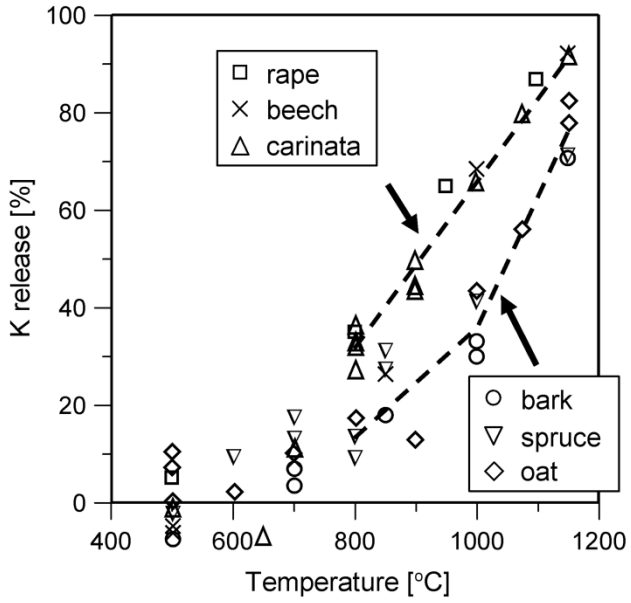

Figure 7-16: Comparison between the release of K from the wood fuels and the Cl lean annual biomass fuels studied by [Knudsen et al., 2004a].

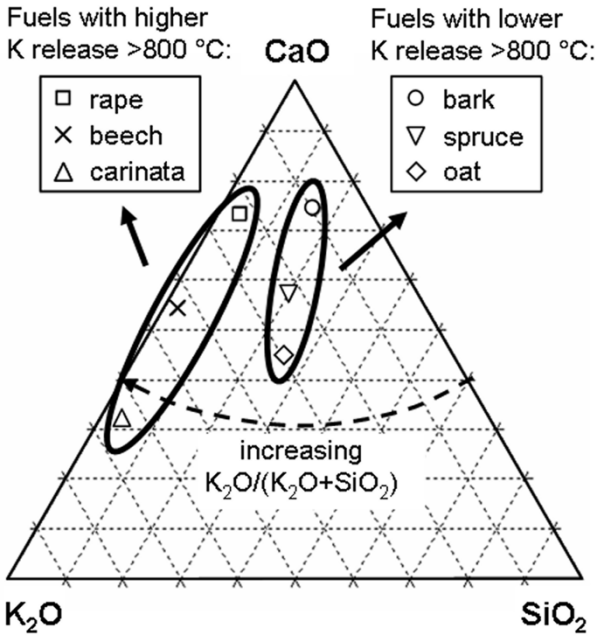

Figure 7-17: Comparison of the overall compositions (on a weight basis) of the wood fuels with the Cl lean annual biomass fuels studied by [Knudsen et al., 2004a].

Figure 7-16 shows, that the fuels (except fiber board), can be divided into two groups based on their K release behavior at high temperature (800–1150 °C):

- rape, beech, and carinata, for which the K release increases almost linearly from ~20–30% at 800 °C to ~90% at 1150 °C;

- bark, spruce and oat, for which the K release increases progressively from ~10–20% at 800 °C to ~70–80% at 1150 °C, and the K release is lower compared to the fuels in group 1 in the entire range of 800–1150 °C.

Figure 7-17 shows a clear distinction between the overall compositions of the fuels of group 1, compared to the fuels of group 2, but it also shows large variations in the overall composition between the fuels within the groups. Because the fuels within group 2 (i.e., rich in SiO_2) have significantly different CaO contents, whereas their K release profiles are very similar, it seems that the release of K is mainly influenced by the Si content of the fuel, or more precisely, by the $K_2O/(K_2O+SiO_2)$ ratio [van Lith, 2005].

The progressive release of K observed for the fuels in group 2, is most likely due to a higher quantity of K_2CO_3 being evaporated, at 1150 °C, during the pyrolysis stage, or due to the decomposition of K_2CO_3 during combustion before it reacts with the silicate, so that less K can be incorporated into silicates, during the combustion stage.

Although the K/Si ratio in fiber board is similar to that of bark, it is more likely that the release of K from fiber board is limited because of the interaction with Ti, which is present in high quantities in the fuel (0.45% (w/w) db), because of the white pigment in the coating. Possibly, K interacts with TiO_2, thereby forming $(K_2O)\cdot(TiO_2)_6(s)$ or amorphous Ti-containing phases, which remain stable up to 1150 °C [van Lith et al., 2008].

[Okuno et al., 2005] studied the release of alkali and alkaline earth metallic species during pyrolysis of pulverized pine wood in the temperature range of 400–900 °C in different reactors. It was observed that the release of K and Na started around 400 °C, and increased with increasing temperature during slow pyrolysis (i.e., heating at 1 °C/s in He) from a single layer of pine particles. However, during slow pyrolysis of a small bed of pine particles (~10 mg in total) in the absence of a forced flow, a complete retention of alkali metals in the char was observed in the entire range of 500–900 °C [Okuno et al., 2005]. These results indicate that, after being released to the gas phase, Na (similar to K) strongly interacts with the char surface within the fuel bed (even in a very small sample) after its initial release from the fuel particle, and that a carrier flow is needed to release Na from the fuel bed.

[Quyn et al., 2002a,b] found that the NaCl in Victorian brown coal was released as Cl and Na separately, which indicated that NaCl had reacted with the char, whereby Cl was released from the char as HCl(g), at low temperatures (~200 °C), and Na became bonded to the char and was (partly) released at higher temperatures. The work of [Quyn et al., 2002a,b] also showed that, even though Na is only present as NaCl and associated to the organic coal matrix, a high retention of Na is observed at low temperature during pyrolysis.

Considering the poor intercalating properties of Na on coal char, and activated carbon, the binding of Na to the char matrix by intercalation is not very likely in biomass chars [Wigmans et al., 1983].

According to this Na-release mechanism, the release at low temperature (<850 °C) is strongly dependent on the association of Na in the fuel: if a large fraction of Na in the fuel is associated with the organic matrix, and/or present as NaCl (instead of other salts or oxides), a higher release can be expected. However, the release of Na from the char matrix will depend on the char properties, such as the availability of oxygen-containing functional groups, which in turn depends on the organic structure of the fuel, and on how the organic structure decomposes during pyrolysis. It is therefore not surprising that the quantity of Na released at low temperature is different for bark and for fiber board [van Lith, 2005].

Above 850 °C, additional Na may be released because of the decomposition of carbonates, in a similar way as K (see eq (7-13));

$$K_2CO_3(g) \rightarrow 2K(g) + CO_2(g) + \tfrac{1}{2}O_2(g) \qquad (7\text{-}13)$$

The higher release of Na compared to K from fiber board at high temperature (>800 °C) is possibly because, according to equilibrium calculations [van Lith, 2005], K may form silicates, already at low temperature (500 °C), whereas Na preferably forms sulfates at low temperature. When Na_2SO_4(s) starts to dissociate at higher temperature (above 800–900 °C), incorporation of Na into (alumino-) silicates is possible, but may be limited if the positions in the structure are already occupied by K. This may result in the release of Na to the gas phase, while K is expected to remain in the (alumino-) silicate structures in the interval 850–1150 °C [van Lith, 2005].

[van Lith et al., 2006] argued that the release of Zn during fiber board combustion takes place by a mechanism similar to that proposed for coal combustion: ZnO(s) is reduced to Zn in the reducing environment of the char particles, which is volatilized as Zn(g) at temperatures above 500 °C.

Differences in the Zn release patterns, between the different fuels, may be due to differences in the association of Zn in the fuels, or due to differences in the inorganic compositions of the fuels. Zn is a micronutrient and is therefore naturally present in small quantities in plants. It has catalytic and structural functions in enzymes, by forming tetrahedral complexes with N-, O-, and particularly S ligands. Zn mainly occurs as (1) low molecular weight complexes, (2) storage metalloproteins, (3) free Zn^{2+} ions, and (4) associated with the cell walls [Welch, 1995; Brown et al., 1993]. According to chemical fractionation analysis of spruce, beech, and fiber board, most of the Zn in those fuels was not water-soluble, but could be leached by HCl

[Pedersen, 2003]. Because the low molecular weight complexes are water-soluble, and Zn occurring in membranes is insoluble [Welch, 1995]. Zn is probably mainly present in the form of metalloproteins in spruce and beech. This would mean that Zn is mainly associated with N, O, and S. Considering the higher Zn content of fiber board compared to spruce (see Table 2), it probably also includes Zn compounds added to the fuel during production. ZnO is insoluble in water, but soluble in HCl, and is commonly used as a white pigment in paints. It is therefore likely that the major part of Zn in fiber board is present in the form of ZnO.

The mechanism of the release of Zn, by the reduction of ZnO to Zn in the reducing environment of the char particles, explains the increasing release of Zn with increasing temperature in the range of 500–850 °C observed for all the fuels.

Above 850 °C, some Zn may interact with minerals in the ash. Because this process will be favored with increasing temperature (as the minerals start to melt) [Neville et al., 1981] a higher fraction of Zn may be retained in the ash at 1150 °C compared to 1000 °C.

If most of the Zn in the fiber board is indeed mainly present in the coating particles (as ZnO), it will be in close vicinity to TiO_2 and Al compounds, which may facilitate the interaction between them.

The release of Pb seems to start around 500 °C, followed by a sharp increase to 85–100% at 850 °C for all the fuels. Because Pb does not have a function in plants, it is most likely not associated with the organic structure of the wood. Chemical fractionation analysis of the fuels showed that the main fraction of Pb in spruce, beech, and fiber board was not soluble in water, but could be leached by HCl [Pedersen, 2003]. This indicates that Pb is probably not present in the form of chlorides or sulfates, but may be present as other salts, such as PbS, $PbCO_3$, or PbOH. The significantly higher Pb content of fiber board compared to spruce and beech (see Table 2) suggests that the major part of Pb in fiber board is present in the coating.

Equilibrium calculations were performed for the combustion of the wood fuels under both oxidizing and reducing conditions [van Lith, 2005]. Under oxidizing conditions ($\lambda = 1.5$), Pb was predicted to be stable as aluminates (e.g., $(PbO)\cdot(Al_2O_3)(s)$, or $(PbO)\cdot(Al_2O_3)_6(s)$) at low temperatures (up to ~600–800 °C), and as mainly as PbO(g) above ~500–650 °C (maximum 5–10% of the Pb was predicted to form $PbCl_2(g)$). Under reducing conditions ($\lambda = 0.5$), PbS(s) was found to be the preferred species at low temperature, and Pb(g) and PbS(g) become stable at a temperature as low as 400 °C.

However, considering that Pb is most likely present as carbonates, hydroxides, or oxides, a reducing atmosphere is needed to transform those species into volatile Pb species, such as

PbO(g) or Pb(g). The high Pb release observed at 700 °C (up to ~90%) therefore indicates that Pb is indeed released in a reducing environment, in a similar way as Zn.

Therefore, it seems likely that the partial retention of Pb in the range of 700–1000 °C is due to the interaction of Pb with TiO_2, Al_2O_3, SiO_2, or a combination of these oxides. The interaction of volatilized Pb and aluminosilicates (kaolinite) at 800 °C to form Pb-aluminosilicates was observed by [Scotto et al., 1994].

The experimental release data obtained in this study suggest that limiting the temperature inside the fuel bed to 800 °C could reduce the release of S, K, and Na from wood fuels, which would decrease the emission of SO_2 and the formation of alkali chlorides and sulfates by gas phase reactions. This in turn would limit the quantity of aerosols and the extent of deposit formation and corrosion inside the combustion unit. A lower temperature inside the fuel bed could probably be achieved by lowering the primary air flow rate through the fuel bed. However, because it may be difficult to reduce the temperature in the bed to below 800 °C, choosing the fuel or additive that would minimize the potential of ash deposition would probably be a more practical solution [van Lith et al., 2008].

An important thing to keep in mind, however, is that K-silicates have relatively low melting points and may cause slagging on the grate, which may lead to operational problems. Moreover, when entrained K-silicate particles impact on heat transfer surfaces, they may form solid deposits, which are hard to remove.

Because the decomposition of alkali carbonates is enhanced in the presence of water vapor, drying of the fuel before combustion would probably reduce the release of K.

For the utilization of ash, the concentration of heavy metals in the bottom ash should be kept as low as possible in order to stay below the limiting values for usage in forest or agricultural soils. From this perspective, a complete release of heavy metals would be desirable, provided that efficient particle filters are present to capture the heavy metal containing aerosols. However, when Zn- and Pb-containing aerosols condense earlier in the system, on superheater tubes, they may cause enhanced corrosion rates, as these elements generally decrease the melting point of ash deposits. Furthermore, when efficient particle filters are not present, such as in many small-scale combustion units, heavy metal containing aerosols are emitted to the atmosphere, causing potential health risks [van Lith et al., 2008].

7. 4. Release of Critical Elements from Annual Biomasses

As part of the EU-HiAl R&D-project, [Knudsen, 2004; Knudsen et al., 2004a], quantified the release and transformation of Cl, K, and S during combustion of a number of annual biomasses incl. straw under conditions resembling local conditions in the fuel-bed of a grate-fired boiler. Six different fuels were selected; rice, barley and wheat straw as Si-rich (SR) fuels, while oat, rape straw and a *carinata* variety [carinata is a thistle-species grown extensively in Southern Europe] were selected as Si-lean (SL) fuels [Knudsen, 2004] (see Table 7-3).

Property:	Rice	Barley	Wheat	Oat	Carinata	Rape
% H_2O	7.4	8.5	8.4	7.8	7.3	8.4
% Ash [dry]	7.6	6.9	4.8	3.8	4.9	2.7
K/Si [mole/mole]	0.63	2.0	1.1	1.5	20	8.1
Cl/K [mole/mole]	0.52	0.38	0.25	0.1	0.04	0.07

Table 7-3: Main compositional properties of the six fuels investigated by [Knudsen, 2004] for their release of K, S and Cl. Source: [Knudsen, 2004].

The work showed that combustion temperature as well as fuel composition greatly affected the quantity of Cl, K, and S released to the gas phase. The inherent content of Cl and Si had a large impact on the K-release from a specific fuel. Thus, two compositional parameters related to K release were defined: [1)] the K/Si molar ratio and [2)] Cl/K molar ratio in the fuel. The results of the release quantification are shown in Figures 7-18 to 7-20.

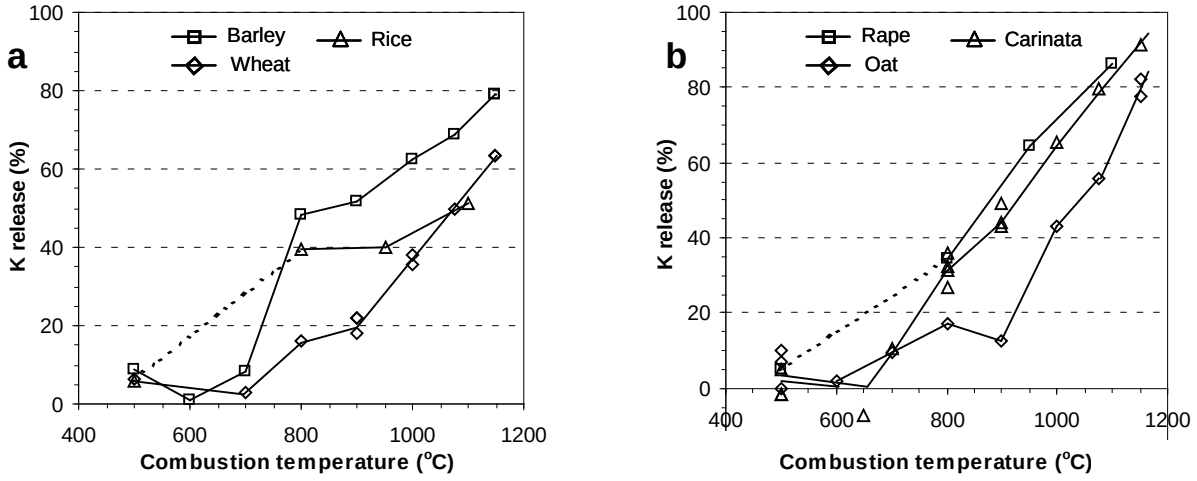

Figure 7-18: Percentage of fuel-K released to the gas phase as a function of combustion temperature. a) Si-rich fuels. b) Si-lean fuels. Source: [Knudsen, 2004].

For the Si-rich fuels K was found to be partly incorporated into Ca-K silicates above 600 °C, thereby limiting the K release at higher temperatures. Nevertheless, for Si-rich fuels with a high Cl/K ratio, i.e. rice and barley, a higher fraction of fuel-K was released as KCl between 700 and 900 °C, despite the inherent Si content compared to wheat straw, which has a somewhat lower Cl/K ratio. Thus, Cl and Si affect the K release in opposite directions. A low K/Si molar ratio limits the release of K, mainly due to formation of K silicates, while a high Cl/K molar ratio may increase the volatility of K, due to the relatively high vapor pressure of KCl, at combustion temperatures.

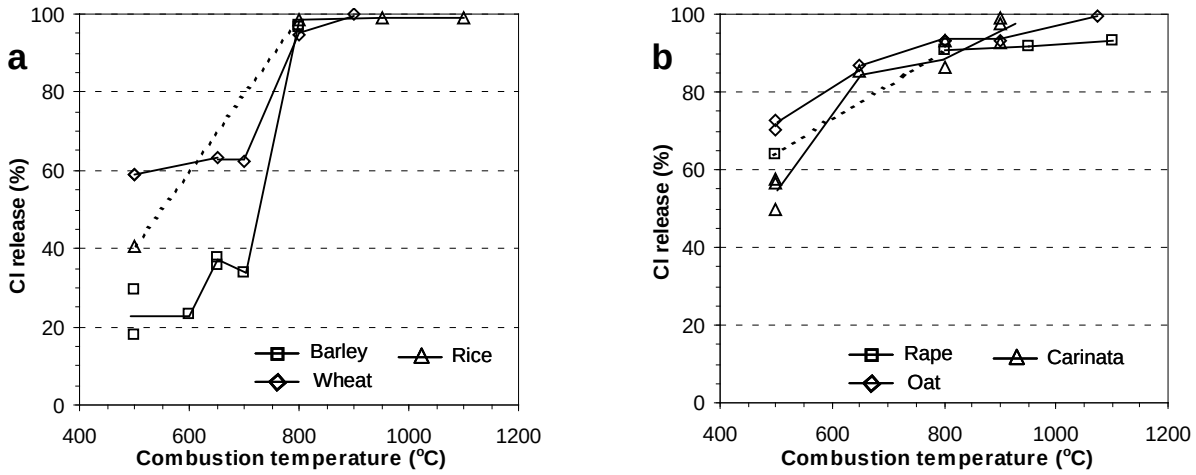

Figure 7-19: Percentage of fuel-Cl released to the gas phase as a function of combustion temperature, under fixed-bed conditions. a) Si-rich fuels. b) Si-lean fuels. Source: [Knudsen, 2004]

For the Si-lean biomass fuels K was gradually released mainly as KOH above 700-800 °C, due to decomposition of K_2CO_3 (see Figure 7-18).

Chlorine was released at temperatures as low as 500 °C, mainly due to evaporation of KCl. The Cl release was nearly complete at combustion at 800 °C, regardless of the ash composition, i.e. regardless of the K/Si and the Cl/K ratios of the fuels investigated (see Figure 7-19).

At 500 °C, around [30 – 60 %] of the fuel–S was released. The difference in the S-release at low temperature is most likely related to different associations of S in the fuel [Knudsen, 2004]. At temperatures above 700-800 °C, Si was found to enhance S release, since Ca and K were preferably incorporated into Ca-K silicates, instead of forming K_2SO_4. As a result, nearly all fuel-S was released from the Si-rich fuels at 1150 °C, whereas for the Si-lean fuels, 20-50% was retained in the ash (see Figure 7-20) [Knudsen, 2004].

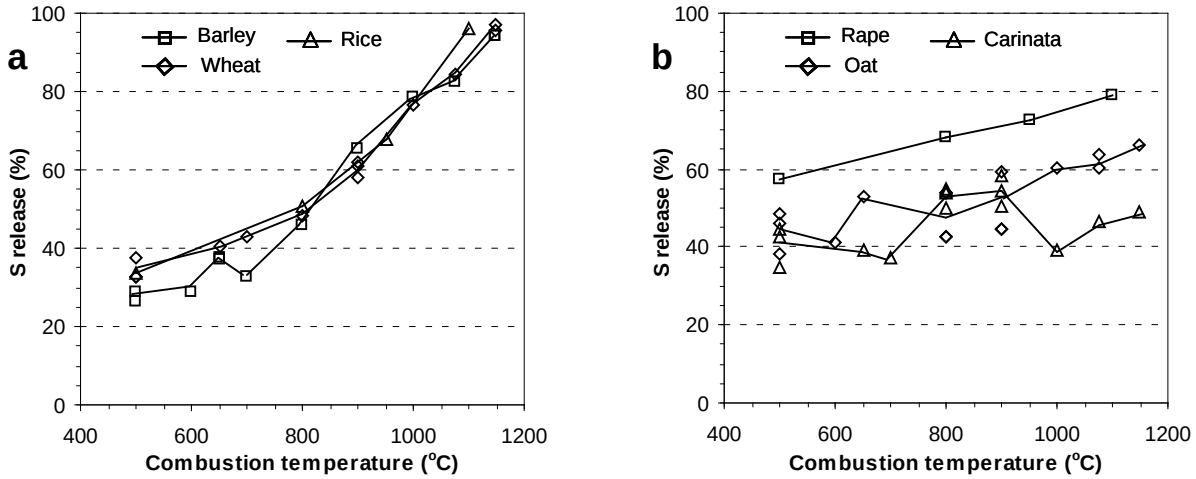

Figure 7-20: Percentage of fuel-S released to the gas phase as a function of combustion temperature under fixed-bed conditions. a) Si-rich fuels. b) Si-lean fuels. Source: [Knudsen, 2004].

Special emphasis was put on S chemistry, since [Knudsen, 2001, 2004] investigated the thermal conversion of two Danish wheat straws with different [S], during devolatilisation and subsequent char burn out. The work indicated that S is associated partly as an inorganic sulphate (40 - 50% of the total S), and partly as organic sulphur (40-60%) in wheat straw. Pyrolysis experiments indicated that a significant S release (35 - 50%) had already occurred during the initial devolatilisation stage, due to the decomposition of organically associated S [Knudsen, 2004] (see Figure 7-21). At pyrolysis temperatures above 500-600°C, the inorganic sulphate decomposed through interactions with the organic char matrix. During char burnout, at low temperatures (<500°C), no further S was released into the gas phase. Instead, S was completely transformed into sulphates in the ash. As the combustion temperature was increased, S was gradually released into the gas phase. Up to 55% of the total S was released at 950°C (see Figure 7-21). Pyrolysis experiments with the addition of SO_2 indicated that additional S may be fixed in the biomass char, and subsequently retained in the bottom ash during char burnout at 600-800°C. At higher temperatures, S retention in the char was low, and no additional S was bound in the bottom ash [Knudsen, 2004].

Equilibrium calculations indicated that lower S-retention at higher temperatures is caused by the incorporation of Ca and K into silicate structures. Thus, the maximum achievable S retention in straw ash is largely determined by the content of silicate relative to Ca and K in the fuel [Knudsen, 2004].

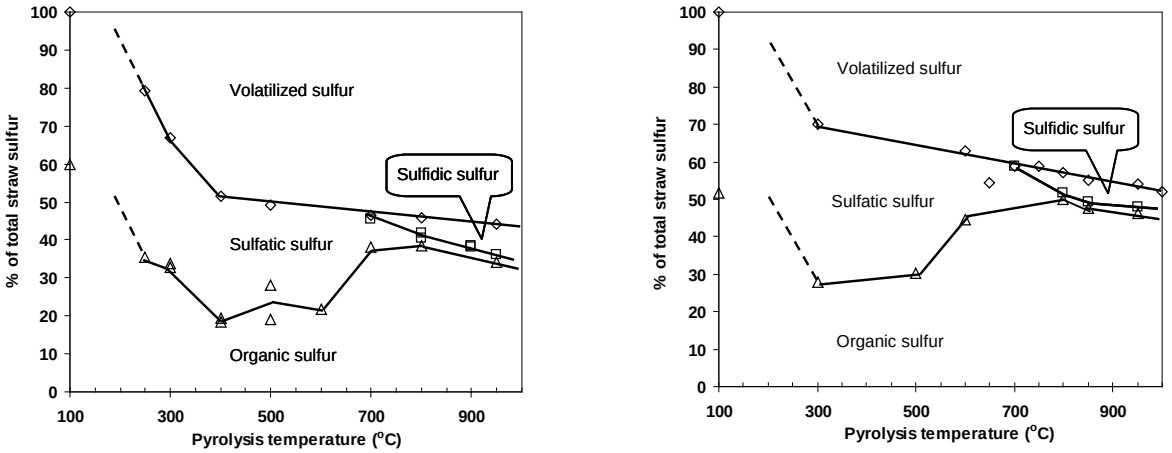

Figure 7-21: Distribution of sulfur forms in two Danish wheat chars. Source: [Knudsen, 2004].

7.4.1. Secondary Capture of Cl and S

As mentioned in Chapter 3 of this thesis, primary air is introduced below the grate, causing a net movement of gases upwards through the fuel bed. This raises the question of secondary capture of HCl and SO_2:

Will Cl and S released in the bottom of the fuel, bed be recaptured by the char, when moving upwards with the flue gas, through the char-loaded fuel-bed ?

[Knudsen, 2004] studied the secondary capture of HCl and SO_2 by straw char in the temperature range [400 - 950 °C]. Relatively high amounts of Cl and S was found to be retained in the char samples in the entire temperature range, compared to the inherent (original) content of Cl and S in biomass. Spectroscopic and chemical analyses revealed that HCl was captured by inherent metal species, whereas SO_2 was captured by the organic matrix [Knudsen, 2004]. It was concluded that the maximum Cl-retention was controlled by the content of inherent metal in the straw. Combustion of the Cl- and S-laden char samples resulted in high retention of Cl and S in the ash, at temperatures up to 600 respectively 800 °C. At even higher combustion temperatures, Cl and S were gradually released into the gas phase due to the evaporation of KCl, and dissociation of sulphates (K_2SO_4 and $CaSO_4$).

Combustion of wheat straw in a larger fixed-bed reactor indicated that the higher the fuel bed the more Cl and S could be retained in the bottom ash. This was caused mainly by the secondary capture of HCl and gaseous S-species in the thicker char layer of the higher reactor. Although the results from the somewhat smaller fixed-bed reactor indicated that secondary capture of Cl and S could be of importance during combustion of straw in larger beds, the

effect was found to be not as pronounced as expected from the laboratory work [Knudsen, 2004].

7.4.2. Effect of Ca, Si and P on Retention of K in Ashes

In addition to the secondary capture of S and Cl by char particles located further up along the vertical flow of the pyrolysis gases, there is another effect which may account for a substantial retainment of K in the bottom ash. The inherent content of Si and Ca may affect the K release during devolatilisation, pyrolysis and char burnout. Silicon may react with volatile K species, forming non-volatile K silicates. Calcium, on the other hand, will act in the opposite direction, i.e. not by direct reaction with K, but instead by reaction with some of the inherent Si, thereby preventing this from reacting with K. Thus, a high level of Ca, may increase the release of K, although the fuel also has a high content of Si.

[Novakovic, 2006] investigated the release of K from synthetic mixtures in the system K-Si-Ca. The experiments were conducted by exposing different synthetic mixtures placed into a Pt-Rh crucible either N_2 (solely) or N_2 saturated with water vapour.

Release of K from both KCl and K_2CO_3 in the systems K-Ca, K-Si and K-Si-Ca were investigated. As Ca sources, CaO and $Ca(OH)_2$ were applied, while quartz and celite were applied a Si sources. Quartz and celite both have the chemical formula SiO_2, but their physical structure, and thereby porosity, deviates substantially.

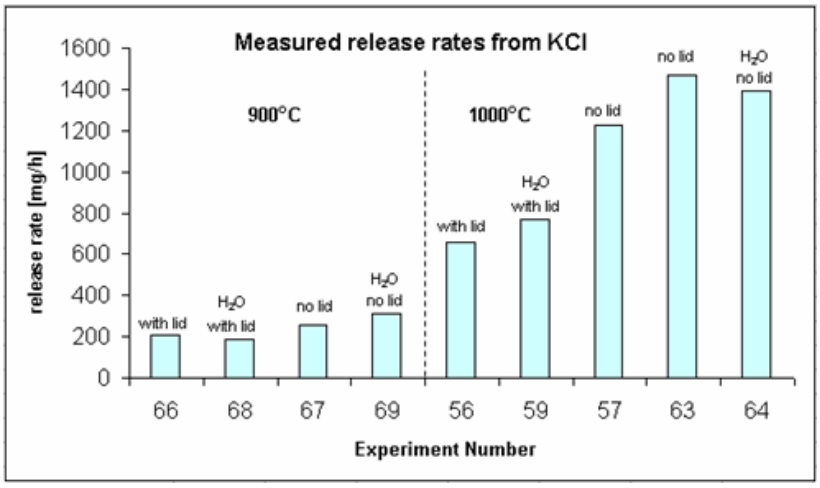

Increasing the temperature from 900 °C to 1000 °C increased the release rate of K from KCl significantly (see Figure 7-22).

Figure 7-22: Rate of K-release from KCl vs. temperature and atmosphere. Notice the strong T-effect. No effect of the $[H_2O]$, and use of a lid.
Source: [Novakovic, 2007]

In Figure 7-22, it can be seen that the presence of water does not have any significant effect on the rate of K release from KCl. Neither does the use of a lid on the crucible in the experiments, since almost equal results are obtained with and without a lid.But the temperature play a significant role for the K release.

For K_2CO_3, a similar temperature effect similar to the one seen in Figure 7-8, was observed, but in this case the effect of increasing the temperature was much stronger, in the presence of water vapour.

In Figure 7-23, the rate of K release from different mixtures of K_2CO_3 with Ca- and Si-sources, at 1000 °C is shown.

It is obvious in Figure 7-23, that the rate of K release is significantly lower from K-Si mixtures, compared to K_2CO_3 (alone). This strongly indicates a reaction between K_2CO_3 and the actual Si-source, thereby retaining K in the mixture as K silicate. Transferred to real life thermal straw conversion, this means that K may be retained by Si in the bottom ash of a grate-fired plant, which is in line with the findings in the release study by [Knudsen, 2004]. In Figure 7-9, it is also seen that the rate of K release is slightly higher when applying celite, instead of quartz as Si-source.

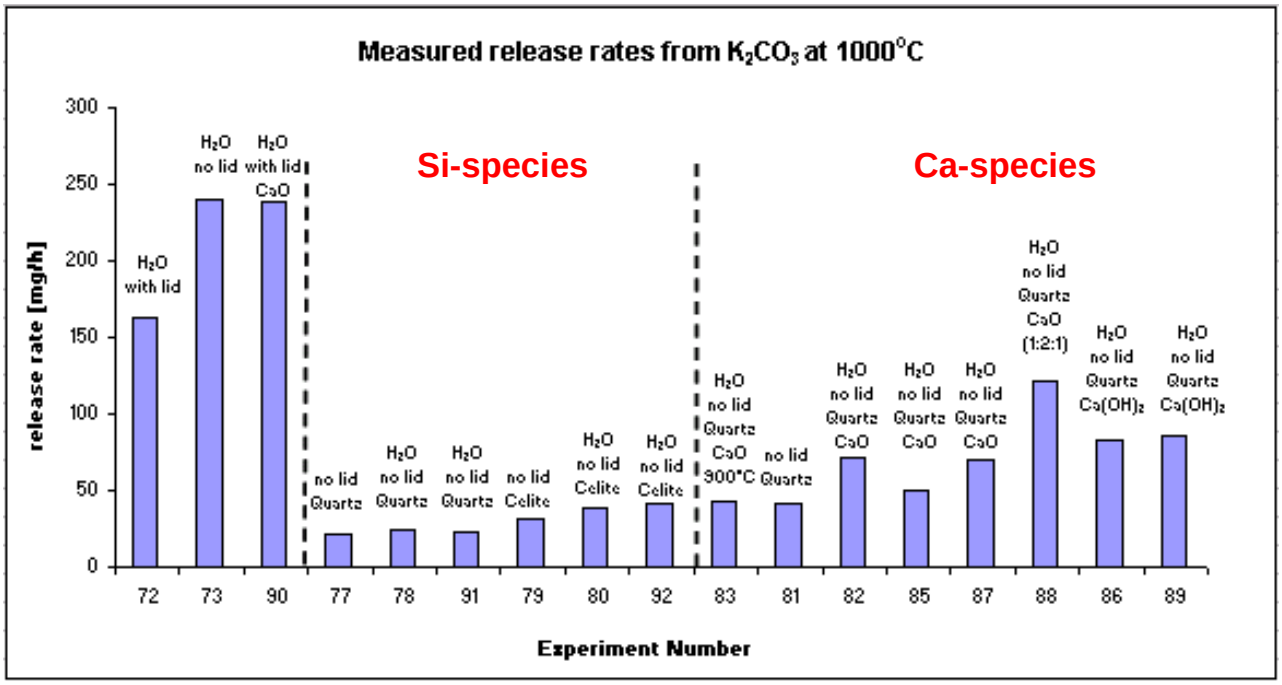

Figure 7-23: Rate of K release from different mixtures in the systems K-Si, K-Ca and K-Si-Ca. Base K-source K_2CO_3. All data corresponds to 1000 °C.
Source: [Novakovic, 2007a].

In Figure 7-23, it is also clearly apparent that addition of a Ca source to a K-Si mixture will increase the rate of K release. Thus, the experimental work of [Novakovic, 2006] indicates that

Ca may react with Si, thereby inhibiting Si from reacting with K, causing an increased rate of K release.

The effect of Ca in the K-Si-Ca system is particularly clear when comparing experiments 82/85/87 with experiment 88 in Figure 7-23. In experiment 88, a 1:2:1 mixture of K:Ca:Si was investigated, compared to the 1:1:1 molar blend applied in experiments 82, 85 and 87. It is that the increased amount of Ca causes a significant increase in the rate of K release [Novakovic, 2006].

In a subsequent study, the same technique was applied to mixtures in the system K-P-Ca, now using K_2CO_3 as a fixed source of K, and $Ca(PO_3)_2$ as a fixed source of P [Novakovic et al., 2009]. Different sources of Ca were applied (see Figure 7-24). It was observed that the Ca source did not affect the measured rate of K release, in contradiction to the P-content, which had a very pronounced effect on the K release rate. Thus, P acted in a way similar to Si.

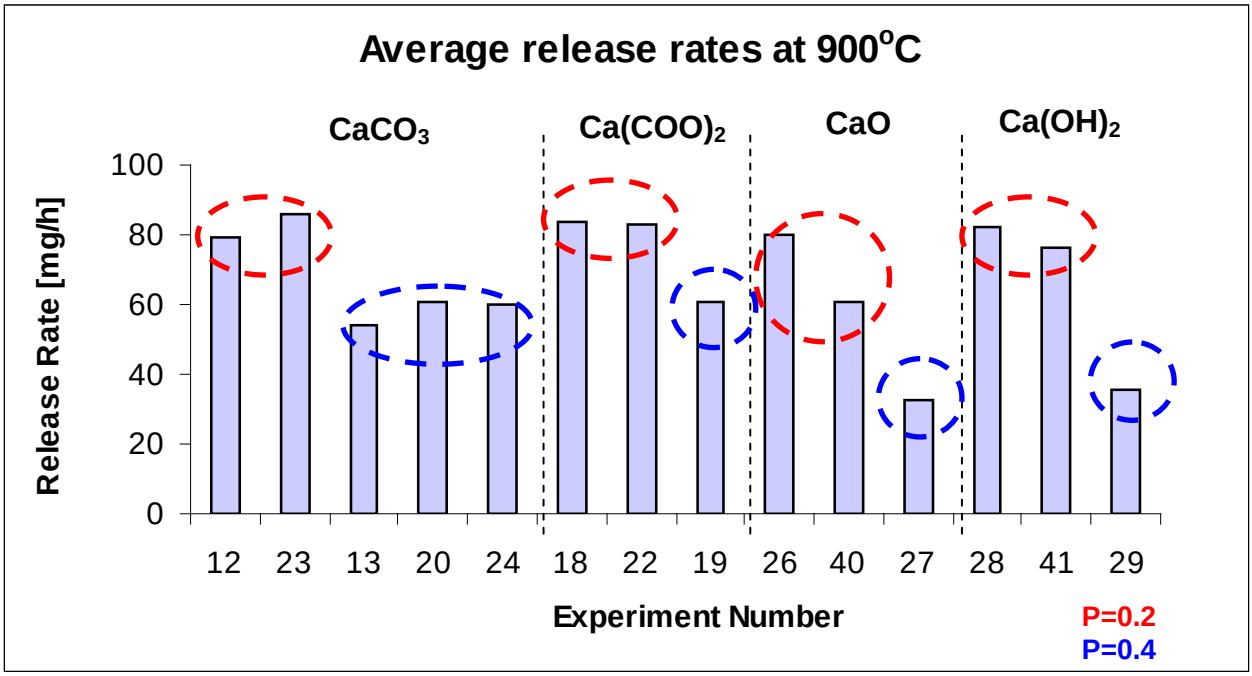

Figure 7-24: Rate of K-release from mixtures in the system K-P-Ca, as a function of different Ca-sources. Fixed K-source: K_2CO_3, and fixed P-source: $Ca(PO_3)_2$. All data correspond to 900 °C.
Source: [Novakovic, 2007].

The observations made by [Novakovic et al., 2009] not only related to the release of K from ashes derived from biofuels, but also raise certain interesting aspects in relation to the use of Ca-, Si- and P-bearing additives in furnaces. These aspects are outlined and discussed, in further detail in Chapter 10 of this thesis.

7. 5. Summary on the Release of Critical Elements

To sum up the brief outline of release studies provided above, a lot of high-quality data on the release of critical elements like K, Na, Cl, S, Pb and Zn, have been published, especially for firing of annual biofuels and wood fuels in fixed-beds. Recently, also a basic study on the release of critical elements from well-characterized waste fractions under fixed-bed conditions has been published.

In the release studies conducted so far, it has been shown that increasing temperature, reducing conditions and a high Cl/Me-ration usually facilitates release of metals (Me) like K, Na, Zn and Pb. On the other hand, a high S-level usually makes condensed sulfates thermodynamically stable, often at higher temperatures, than what is actual for condensed chlorides. The effect of Si (and Al) seems to be to fix a certain amount of especially the alkalis in condensed phases, thereby increasing the retention of these in the bottom ash fraction. Anyhow, Ca may seriously affect this chemical interaction by reacting with the (Al-) silicates, thereby preventing fixation of the alkalis. Secondary reactions between released (alkali) metals and char or ash inclusions in the fixed bed have been thoroughly investigated especially in systems fired with biofuels. For wood-type fuels, the role of P in the secondary interactions between gaseous alkali metal species and residual ash is still unclear.

Several chemical interactions between primarily released elements and char and ash species in the fuel bed have been revealed, some of which could constitute a base for controlled release, i.e. be used to keep volatile elements in the bed instead of being released to the freeboard. Fixation in the bed could decrease the amount of corrosive species condensed later on during cooling in the flue gas channel, and thereby help to increase the metal surface temperature on the final superheater, which may again cause a higher electrical efficiency.

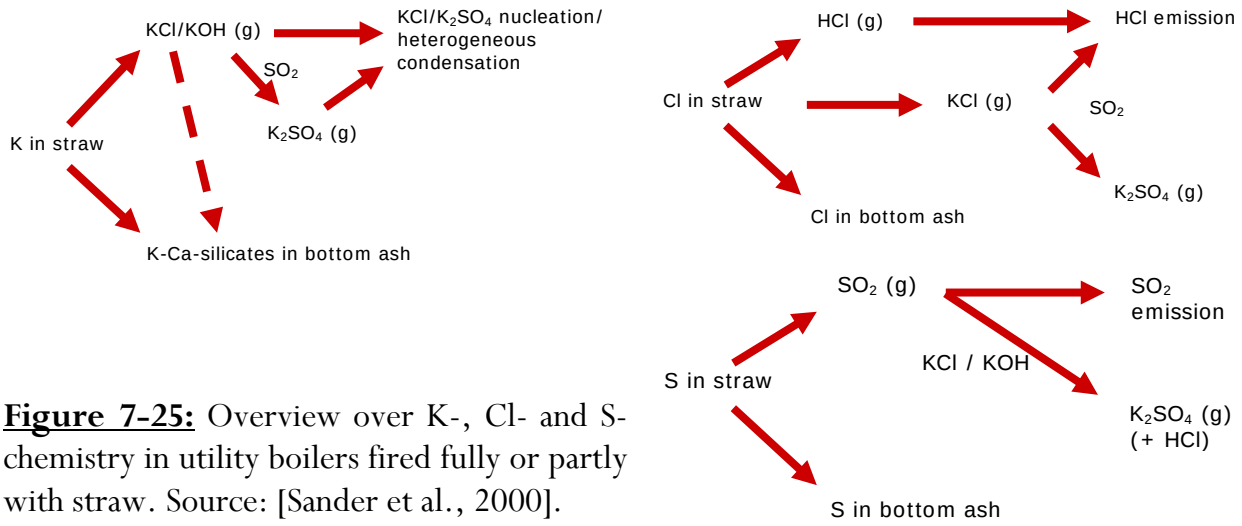

Figure 7-25: Overview over K-, Cl- and S-chemistry in utility boilers fired fully or partly with straw. Source: [Sander et al., 2000].

[Knudsen, 2004] showed that both the combustion temperature and the straw chemical composition, greatly affects the quantity of Cl, K, and S, being released to the gas phase during straw combustion. The [Cl] and [Si] showed to have a large impact on the K release and two compositional parameters are of particular importance to the K release; [1)] the K/Si molar ratio, and, [2)] Cl/K molar ratio in the fuel. Silicon will attempt to fix K as non-volatile K-silicates, while, Cl acts in the opposite direction by making K volatile, forming KCl.

But the release of K, S and Cl is not only controlled by primary interactions between K and S respectively Cl, there is also a secondary capture of K which may to a significant degree control the overall release. Potassium being released in the bottom of the fuel bed may interact with char particles located higher up in the fuel bed causing a secondary capture, a phenomenon investigated in details by [Knudsen, 2004]. In addition, there is a possibility of interactions between K and other ash forming species, like Si and Ca, which may affect the K release seriously. This was addressed thoroughly by [Novakovic et al., 2009].

An overview of the rather complex K-S-Cl chemistry and the interactions of these three elements with e.g. silica are shown in Figure 7-28 [Sander et al., 2000].

Thus, the fundamental data on release especially from biofuels fired in fixed-beds are available. The critical parameters, like temperature, fuel (ash) chemistry, local stoichiometry and sample preparation and size, controlling the release, have also been indentified and discussed thoroughly. Controlling chemical parameters like the (K+Na)/Si or the (K+Na)/Cl+2S ratios have at several occasions been proved to correlate well with the alkali release. Similar, controlling chemical parameters are not yet available for the heavy elements, like Zn and Pb.

In spite of the high-quality work and effort to quantify the release, there is still a gap in the theoretical quantification of the release, i.e. the ultimate goal, defining boundary conditions for free board chemical and physical processes for use e.g. in a CFD-frame, is still to be considered a future task. Much more development of single particle release models, as well as release from bed/ensembles of particles, and physical entrainment of particles e.g. from a fuel bed, is needed in the future.

Chapter 8:

FORMATION OF AEROSOLS IN FLUE GASES FROM STRAW

8.1. Gas Phase K-S-Cl Chemistry

As soon as they are released into the gas phase from the fuel bed, the critical elements K, S, and Cl may undergo a number of transformations in the freeboard of the boiler or the flue gas channel.

Sulphation of alkali chlorides is probably the most important transformation in relation to alkali chemistry and aerosol formation, deposition and corrosion and gaseous emissions. Alkali chlorides like KCl, may react with SO_2, forming sulphate according to the reaction:

$$2\,KCl + SO_2 + ½\,O_2 + H_2O \rightarrow K_2SO_4 + 2\,HCl \qquad (8\text{-}1)$$

This *sulphation*-reaction may take place either by means of O_2(g) and SO_2(g), as shown, or by direct reaction with SO_3(g). If water is present in the system, HCl(g) will be the gaseous product of the sulphation reaction, otherwise it will be Cl_2(g).

Several early studies on alkali sulphate formation were motivated mainly by operational problems related to deposition and corrosion in combustion systems [Christensen and Livbjerg, 1996; Christensen et al., 1998; Salmenoja et al., 1996; Michelsen et al., 1998; Glarborg, 2007; Livbjerg, 2001].

Sulphation may occur either in the gas phase or in the solid/condensed phase. Both homogeneous [Kohl et al., 1979; Fielder et al., 1984], and heterogeneous [Steinberg and Schofield, 1990, 1996, 2002; Durie et al., 1977] mechanisms have been proposed, and are still being discussed in the literature.

If the sulphation reaction (8-1) is broken into sub/elemental reactions, it has been indicated that the limiting reaction, is:

$$SO_2 + ½O_2 \rightarrow SO_3 \qquad (8\text{-}2)$$

Several studies have addressed the oxidation of SO_2 to SO_3, both homogeneously and heterogeneously. For a review of this reaction please refer to [Glarborg and Marshall, 2005].

In a real combustion system, the residence time in the gas phase is in the order of seconds, i.e. although the temperature near the flame zone may be high, > 1500 °C depending on the actual firing technology, there may not be time enough available to reach global equilibrium. Thus, in thermal fuel conversion systems, there may be several chemical kinetic limitations to encounter.

[Levy and Merryman, 1970] investigated the formation of SO_3 just outside the visible flame zone. They concluded that SO_3 was formed only by reaction of SO_2 with O-atoms, since the temperature and [SO_3] observed in the post flame probings were nearly constant, i.e not much reaction was happening in the post-flame zone. [Fenimore and Jones, 1965] proposed a mechanism, to test for the presence of steady-state ratios of SO_3 to SO_2 in lean flames:

$$SO_2 + O(+M) \Leftrightarrow SO_3(+M) \quad (8\text{-}3)$$

$$SO_3 + O(or\ H) \Leftrightarrow SO_2 + O_2(or\ OH) \quad (8\text{-}4)$$

It was proposed that the driving force in reaction (8-4) prevents equilibrium from being attained, and causes the observed non-equilibrium ratios. [Levy and Merryman, 1970] suggested that the depletion of SO_3 produced in the flame occurs mostly by O or H attack, rather than by thermal decomposition.

Recently, [Glarborg and Marshall, 2005] proposed a new mechanism for homogeneous sulphation involving the intermediates alkali oxysulphur (ASO_3Cl) and alkali hydrogen sulphate ($AHSO_4$). According to this mechanism, the oxidation of SO_2 to SO_3 is the first step in gaseous alkali sulphate formation. The subsequent step [Glarborg and Marshall, 2005] is an association reaction, involving alkali hydroxide (AOH), or alkali chloride (ACl), with SO_3:

$$AOH + SO_3(+M) \rightarrow AHSO_4(+M) \quad (8\text{-}5)$$

$$ACl + SO_3(+M) \rightarrow ASO_3Cl(+M) \quad (8\text{-}6)$$

If the alkali hydrogen sulphate and alkali oxysulphur chloride are sufficiently stable at high temperatures, they may participate in a series of shuffle reactions, leading to alkali sulphate formation:

$$ASO_3Cl + H_2O \rightarrow AHSO_4 + HCl \quad (8\text{-}7)$$

$$ASO_3Cl + AOH \rightarrow A_2SO_4 + HCl \quad (8\text{-}8)$$

$$AHSO_4 + AOH \rightarrow A_2SO_4 + H_2O \quad (8\text{-}9)$$

$$AHSO_4 + ACl \rightarrow A_2SO_4 + HCl \quad (8\text{-}10)$$

The proposed mechanism indicates a fast and efficient gas phase sulphation process, with oxidation of SO_2 being the rate limiting step, rather than alkali transformations.

Gaseous K_2SO_4 and Na_2SO_4 have been shown to be thermally stable, at moderate to high temperatures in vaporisation experiments. [Glarborg and Marshall, 2005] reported that some investigations have detected gaseous Na_2SO_4, by mass spectrometry in the post flame zone of a CH_4/O_2 flame, doped with NaCl and SO_2:

- [Steinberg & Schofield, 1990] studied the gas phase chemistry of Na and S in lean flames. Kinetic analysis of the data revealed that $NaSO_2$(g) was the only significant Na-S-species formed in fuel-lean flames. This is consistent with data from [Fenimore and Jones, 1965] who reported that the reaction NaOH(g) + SO_2(g) → $NaSO_2$(g) + OH contributed to the depletion of vapour phase Na. [Steinberg & Schofield, 1990] also gave estimates for Na_2SO_4(g)-formation rates under lean-flame conditions and found that it was kinetically limited, causing concentrations far from equilibrium. The authors conclude that there is insufficient time for Na_2SO_4(g)-formation in combustion systems.
- [Stearns et al., 1977, 1981] detected Na_2SO_4(g), when Na and S were added to a laminar flat flame burner. The molecule was formed in < 1 ms from the time when the reactants entered the flame.
- The data reported by [Steinberg & Schofield, 1990] and [Srinivasachar et al., 1990] suggest that Na_2SO_4(g) will not form under flame conditions.
- The data reported by [Schultz-Møller, 1997] also indicate a significant sulphation of KCl to K_2SO_4 in the gas phase.

It has been questioned [Steinberg and Schofield, 1990, 1996] whether sulphates like Na_2SO_4 and K_2SO_4 are actually formed in the gas phase, since measurements like these may be seriously affected by a deposit formed around the sampling orifice [Schofield and Steinberg, 1992].

Several studies on heterogeneous sulfation of alkali chlorides have been published;

- [Srinivasachar et al., 1990] suggested that at lower temperatures, below the dew point of NaOH, condensation of NaOH prior to reaction with gaseous SO_2(g) provides a plausible route for the formation of the solid Na_2SO_4, provided that the kinetics of the surface reactions are sufficiently fast.

- [Iisa et al., 1999] studied gaseous and liquid phase sulphation of KCl. KCl-particles were partially vaporised in a laminar entrained flow reactor, at 900-1100 °C, and allowed to react with SO_2 (g), O_2(g), and H_2O(g). Up to 100% conversion to K_2SO_4 was obtained in the gas phase during a residence time of 0.3-2.2 s. These data indicates that SO_3(g) was present in the gas phase, and that the sulphation process depend on the availability of SO_3(g).

According to gas phase kinetic considerations [Steinberg and Schofield, 1990, 2002] on the interactions of Na and S in flames, kinetic limitations rules out a homogeneous Na_2SO_4-formation mechanism in flames. The formation is claimed to be a surface phenomenon, and occur at a rate that is directly proportional to [Na] in the flame [Steinberg and Schofield, 1990]. Sodium is expected to condense as NaCl, which may then react with available S-containing gases, in the condensed phase.

8.2. Formation of Aerosols in Straw-Derived Flue Gases

The behaviour of aerosols is important to the environment, and in relation to the public health. Traffic, wood stoves, power plants (i.e. heat and power production), and natural sources (e.g. dust, sea salt, and volcanic dust) are major sources of airborne particles [Friedlander, 2000]. Recent studies have shown that fine particles, defined as those with $d_P < 2{,}5$ μm, possess a great impact on visibility, health, and water droplet formation in the atmosphere [Zeuthen, 2007]. Epidemiological evidence correlates the increase in particulate matter (PM) mass concentrations with cardiopulmonary disease and mortality. No specific particles property or component responsible for the toxicological effects has yet been identified. However, the importance of particle properties other than mass concentration, i.e. the chemical composition, particle size, and number concentration, have been emphasised as very important [Harrison and Yin, 2000; Lighty et al., 2000a,b].

Aerosol formation from coal combustion has been studied intensively over the years. Full-scale measurements [McCain et al., 1975; Kauppinen et al., 1990; Nielsen et al., 2002] as well as laboratory studies [Flagan and Taylor, 1981; Quann et al., 1990] have been carried out. Locally reducing conditions within a burning, porous, char particle will cause evaporation of e.g. SiO(g) from quartz inclusions in the coal at high temperature. When the SiO is re-oxidised just outside the burning char particle, it will condense directly by homogeneous nucleation and particles are formed in high number concentrations [Quann et al., 1990; Quann and Sarofim, 1982; Sarofim et al., 1977]. Similar reduction/volatilisation/reoxidation sequences may occur for other metal oxides [e.g. Ca, Mg].

Several laboratory studies of the particle formation in biomass-derived flue gases have been made [e.g. Jensen et al., 2000; Jimenez and Ballester, 2004, 2005a,b, 2006; Zeuthen, 2007],

as well as full-scale experiments [e.g. Christensen and Livbjerg, 1996; Valmari et al., 1998; Pagels et al., 2003; Nielsen, 2001; Wiinikka and Gebart, 2005; Johansson et al., 2003], and development of detailed computational models [e.g. Pyykönen and Jokiniemi, 2000; Jensen et al., 2000; Christensen and Livbjerg, 2000; Jöller et al., 2005; Glarborg and Marshall, 2005; Jokiniemi et al., 1994].

The fine particles generated in biomass combustion are chemically characterised, mainly, by the elements K, Na, Cl, and S and are formed by condensation of volatile vapours [e.g. Christensen and Livbjerg, 1996; Nielsen, 2001; Yamasoe et al., 2000; Skrifvars et al., 1998].

[Christensen et al., 1998] investigated aerosol formation during straw combustion. The aerosol particles sampled in full-scale consisted of KCl and K_2SO_4, with KCl being dominant, but K_2SO_4 being present in the core of the particles. A quenched equilibrium theory by which the KCl, K_2SO_4, HCl, and SO_2 is determined by the equilibrium sulphation of KCl at 812 ± 10 °C, was used to quantify the chemical composition of the aerosol particles, and [HCl] and [SO_2] in the flue gas. The authors suggested that aerosol formation is initiated by homogeneous nucleation of K_2SO_4, particles then grow by heterogeneous condensation of K_2SO_4 and KCl.

Observations on aerosols formation during cooling of synthetic flue gas containing $KCl/O_2/H_2O/N_2$ in a laboratory reactor [Jensen et al., 2000] support the theory of [Christensen et al., 1998].

As mentioned earlier some authors disagree that the extremely low vapour pressure of gaseous sulphate can account for sufficient presence of gaseous sulphate in the nucleation process [Steinberg and Schofield, 1996, 2002; Schofield, 2003]. Their main point of concern regarding the homogeneous formation of sulphate is that this reaction is kinetically very demanding. Instead they claims that the seeds for forming aerosols are already present in the flue gases when sulphate is formed at higher temperatures. Anyhow, several studies give reason to doubt this as the governing mechanism: the particle number concentrations found after the condensation of sulphate is order of magnitudes higher than the number concentrations observed in the hot flue gas [Jimenez and Ballester, 2004]. It was found by [Jensen et al, 2000] that the formation of particles by KCl in a laboratory furnace was easy to suppress. However, when SO_2 was added in addition to KCl, O_2 and H_2O, it was impossible to suppress the nucleation of new particles [Zeuthen, 2007]. In addition, [Jimenez and Ballester, 2004] and [Valmari, 2000] reported that particles sampled from flue gases at high temperatures are composed of almost pure K_2SO_4, with no traces of condensed KCl.

8.3. The Plug Flow Aerosol Condenser

The Plug Flow Aerosol Condenser (PFAC) is a mathematical model for simulation of the formation and evolution of a multicomponent aerosol during cooling of a flue gas with a certain content of condensible vapors. The model was originally developed in the ph.d.-thesis of [Christensen, 1995], and has been used by [Christensen and Livbjerg, 1996; Christensen et al. , 1998; Christensen and Livbjerg, 2000] for simulation of fine particle formation and change of gas composition during cooling of flue gases from the combustion of straw. The model equations include homogeneous nucleation of pure substances, growth by multi-component gas-to-particle conversion, and coagulation of spherical particles. The local gas phase composition is determined from a gas phase chemical equilibrium calculation combined with a finite reaction rate kinetics for slower reactions. In order to solve the model, the initial particle size distribution, the initial elemental molar fraction and the axial temperature profile have to be specified. For a more general introduction to modelling aspects of coagulation and condensational growth, see [Jacobson and Turco, 1995] and [Wu and Biswas, 1998].

The PFAC model use a general discret or sectional representation of the size distribution, ie. the size distribution is divided into a number of sections or size classes within which all particles are assumed to have the same properties [Gelbard et al., 1980]. Particle growth by heterogeneous condensation is handled by the moving sectional method [Gelbard, 1990]. The axial Runge-Kutta integration is interrupted in each time step, where the mean rates of homogeneous nucleation and coagulation is calculated. The model is a steady state plug flow model, axial diffusion is neglected and it is assumed that pressure is constant and that the gas phase is ideal.

8.3.1. PFAC Particle Size Distribution

Consider a multicomponent aerosol and characterize any aerosol particle by the mass content of each of n components $m = (m_1, m_2, \ldots, m_n)$. Assume that at a given position, all particles of the same size m have the same properties ie. temperature, charge, and morphology. The particle size distribution is approximated by a discontinous distribution consisting of N size classes, within each of which all particles have the same properties. The size and composition of particles in size class j is $m_j = (m_{j1}, m_{j2}, \ldots, m_{jn})$. The concentration of particles in size class j, Φ_j [particles/Nm^3], is defined as the number of particles in a unit volume of gas at the reference state, 1 atm. and 0 °C. As the equations of aerosol change are integrated axially, mj moves in m-space due to condensation or evaporation, referred to as the moving sectional method [Gelbard, 1990].

The change in number concentration, Φ_j, is a result of wall deposition or coagulation:

$$v_z \cdot \frac{d\Phi_j}{dz} = -\left(p_{wall,j} + p_{coag,j}\right) \tag{8-9}$$

where z is the axial coordinate, v_z is the gas velocity, and $p_{wall,j}$ and $p_{coag,j}$ are the rates of removal of particles by wall deposition respectively coagulation. The rate of wall deposition is given by [Christensen et al., 1998]:

$$p_{wall,j} = v_p\left(d_{pj}, T\right) \cdot \frac{A_w}{A} \cdot \Phi_j \tag{8-10}$$

where v_p is the steady state particle velocity towards the wall as a result of turbulent diffusion, impaction and/or thermoforesis, d_{pj} is the diameter of particles in size class j. The wall surface area per unit axial length, A_w, and the cross sectional area, A, may be expressed as functions of z.

8.3.2. PFAC Growth by Gas-to-Particle Conversion

The growth equation for particle size j are given by [Christensen et al., 1998]:

$$\frac{dm_{ji}}{dz} = \frac{A \cdot \rho_g}{W} \cdot I_i\left(y_i, m_j\right),\ j = 1,2,\ldots,N,\ i = 1,2,\ldots,n \tag{8-11}$$

where W is the gas mass flow and ρ_g is the gas density. The rate heterogeneous condensation, I_i, is calculated from:

$$I_i = \frac{dm_i}{dt} = \frac{2 \cdot \pi \cdot d_p \cdot D_i \cdot M_i}{R \cdot T}\left(p_i - p_{is}\right) \cdot F_{COR} \tag{8-12}$$

which is valid for small molar fractions of i, ie. $y_i = p_i/P << 1$. The particle temperature is approximated by the temperature of the gas. The correction factor F_{COR} for growth outside the continuum regime may be calculated either by use of the [Fuch and Sutugin, 1971] formula or by use of the interpolation formula by [Dahneke, 1983], in both cases as a function of the Knudsen number, Kn. Size dependent terms in eqn. (4-4) are calculated for the actual size of the corresponding size section at the given axial position. p_{iS} is the vapor pressure at the particle surface. It is a function of the temperature, size, composition, and structure of the particle, and can be written as:

$$p_{iS} = \zeta_i \cdot \gamma_i\left(d_p\right) \cdot p_i(T) \tag{8-13}$$

Here ζ_i is a function of structure and composition accounting for the reduction of vapor pressure due to the presence of other species, γ_i accounts for the Kelvin effect, and p_i is the vapor pressure over a flat surface of pure component i.

[Christensen, 1995] build in four different models for accounting for the surface microstructure of multicomponent particles:

- Segregated surface layer (condensation of a solid material on the surface of another solid material)
- Perfectly mixed particle (particles with perfectly mixed and ideal liquid or solid mixtures)
- Perfectly mixed surface layer (the same as the previous, but with slow mixing within the particle)
- Growth of pure crystals

8.3.3. PFAC Homogeneous Nucleation

In PFAC only homomolecular homogeneous nucleation is considered, ie. it is assumed that the seeds of new particles initially consist of a single species only. According to the classical nucleation theory [Hidy, 1984], molecular clusters grow by monomer addition alone, because the monomer concentration in the gas phase is assumed to be much larger than the concentration of dimers and trimers. This assumption is not valid for the nucleation of species such as the alkali chlorides, for which the dimers exist as stable species in chemical equilibrium with the monomers and in concentrations of comparable magnitude. Thus, in PFAC, the classical nucleation theory is modified to include both monomer and dimer additions to the molecular clusters with the monomer and dimer in chemical equilibrium. The nucleation rate (particles/m^3/s), J, is calculated as the product of three terms:

$$J = C_c \cdot Z \cdot N^e(q_c) \qquad (8\text{-}14)$$

where C_c is the rate by which molecules are incorporated in the critical cluster by collisions with monomer and dimer molecules [Christensen, 1995]:

$$C_c = \left(p_i + \sqrt{2} \cdot p_{i2}\right) \cdot \frac{\pi \cdot d_c}{k_B \cdot T} \cdot \sqrt{\frac{R \cdot T}{2 \cdot \pi \cdot M_i}} \qquad (8\text{-}15)$$

where p_i og p_{i2} are the monomer and dimer partial pressures respectively and d_c is the diameter of the critical cluster:

$$d_c = \frac{1}{K_3} \cdot \left(1 - 4 \cdot K_3 \cdot \delta_i + \sqrt{4 \cdot K_3 \cdot \delta_i + 1}\right) \qquad (8\text{-}16)$$

where δ_i is the Tolman length and:

$$K_3 = \frac{k_B \cdot T \cdot \ln(S_i)}{2 \cdot \sigma_{\infty i} \cdot v_{mi}} \tag{8-17}$$

where S_i is the saturation ratio of component i, $\sigma_{\infty i}$ is the macroscopic surface tension, and v_{mi} is the molecular volume.

The Zeldovich non-equilibrium factor, Z, is calculated from [Christensen et al., 1998]:

$$Z = \left[\frac{K_1 \cdot K_2}{9 \cdot \pi \cdot k_B \cdot T} \cdot \frac{K_1 \cdot q_c^{-1/3} + 4 \cdot \delta_i \cdot q_c^{-2/3}}{\left(K_1 \cdot q_c^{1/3} + 2 \cdot \delta_i\right)^3} \right]^{1/2} \tag{8-18}$$

where the parameters K_1 and K_2 are calculated from:

$$K_1 = \left(\frac{3 \cdot v_{mi}}{4 \cdot \pi} \right)^{1/3} \tag{8-19}$$

and:

$$K_2 = 3 \cdot \sigma_{\infty i} \cdot v_{mi} \tag{8-20}$$

The equilibrium concentration, $N^e(q_c)$ of clusters of the critical size is:

$$N^e(q_c) = \frac{p_i + p_{i2}}{k_B \cdot T} \cdot \exp\left(- \frac{\Delta G(q_c)}{k_B \cdot T} \right) \tag{8-21}$$

where $\Delta G(q_c)$ is given by:

$$\Delta G(q_c) = - q_c \cdot k_B \cdot T \cdot \ln(S_i) + \frac{K_2 \cdot q_c}{K_1 \cdot q_c^{1/3} + 2 \cdot \delta_i} \tag{8-22}$$

In the above equations, q_c is the number of molecules in the critically sized cluster, defined as:

$$q_c = \frac{\pi \cdot d_c^3 \cdot v_{mi}}{6} \tag{8-23}$$

As mentioned above, the commonly applied theory for prediction of the nucleation rate is the theory based on the central assumption of capillarity, which applies macroscopic properties like

bulk density and bulk surface tension of a planar interface to the microstructure [Becker and Döring, 1935]. Anyhow, the capillarity approximation fails for smaller clusters for which the geometries are not spherical and for which the atomic nature is important. The approximation is even worse for metallic aerosols, having much larger surface tensions, causing extremely high supersaturation ratios to lower the energy barrier for nucleation. Because of the extremely high supersaturation, the critical size for formation of a stable aerosol in a supersaturated vapor is very low, in the order of 1-10 atoms for mercury in the temperature range 260 – 400 K. Macroscopic properties such as surface tension are meaningless for clusters in this size range [Wu and Biswas, 1998].

In PFAC the curvature dependent surface tension, σ_i, is given by the Tolman equation [Vogelsberger, 1980]:

$$\sigma_i = \sigma_{\infty i} \cdot \left[1 + 4 \cdot \frac{\delta_i}{d_p} \right]^{-1} \qquad (8\text{-}24)$$

where $\sigma_{\infty i}$ is the macroscopic surface tension, δ_i is the Tolman length, and d_p is particle diameter. The macroscopic surface tension is treated as temperature dependent [Christensen and Livbjerg, 2000].

8.3.4. PFAC Coagulation

At the end of each Δz-step, new coagulation size classes are introduced. The number of collisions in [z, z+Δz] between particles from size classes i and j is calculated as a mean value in the interval [Christensen et al., 1998]:

$$\Phi_{ij} = \frac{A \cdot \rho_r \cdot \Delta z}{W} \cdot \beta(m_j, m_i) \cdot \Phi_j \cdot \Phi_i, \; j = 1, 2, \ldots, N, \; i = 1, 2, \ldots \qquad (8\text{-}25)$$

where β [m^3/s] is the collision frequency function. All collisions are assumed to lead to the formation of one new spherical particle. The mass of the new particle is $m_{ji} = m_j + m_i$. Particle collisions are due to Brownian motions, turbulent shear, and gravitational settling. The Brownian collision frequency function is calculated from the Fuchs interpolation formula for the entire particle range [Fuchs, 1964]. For submicron particles, Brownian coagulation is the dominant mechanism with a frequency function several orders of magnitude larger than those for gravitational settling and turbulent shear [Christensen, 1995].

For each new coagulation size class (m_c,Φ_c), the distance to the two closest existing size classes (#1 and #2) are found (λ_1,λ_2). In case only one of these lies within a distance of λ, the new size class is combined with that size class. In case both lie withinthe distance of λ, the new size class is split in two fractions: [1)] $\Phi_c \cdot \lambda_2/(\lambda_1 + \lambda_2)$ is combined with size class #1, and [2)] $\Phi_c \cdot \lambda_1/(\lambda_1 + \lambda_2)$ is combined with size class #2. Finally, in case no size class are closer than λ, a new size class is created. For $\lambda > \ln(2)$, a size class that coagulates with itself is combined with itself. This prevents rapidly growing particles in the lower end of the size spectrum from forming new sections and a smooth continuous distribution is easily derived. For $\lambda < \ln(2)$, many new size classes are formed between the original nucleation size classes. This is computationally, expensive and makes the calculation of a continuous distribution difficult.

8.3.5. PFAC Gas Phase Equations

The plug flow form of the continuity equation yields:

$$\frac{dy_i}{dz} = -\frac{\rho \cdot A \cdot R \cdot T}{W \cdot P} \cdot \left(r_{cond,i} + r_{g,i} + r_{w,i} \right) \qquad (8\text{-}26)$$

where y_i is the molar fraction. It is assumed that the total molar flow rate $c_t v_z A$ is constant. In eqn (8-17) r_i is the rate of removal of component i from the gas phase by heterogeneous condensation [cond], gas phase chemical reactions [g], and wall condensation [w]. The rate of heterogeneous aerosol condensation of component i is given by [Christensen et al., 1998]:

$$r_{cond,i} = \frac{\rho}{M_i \cdot \rho_r} \cdot \sum_{j=1}^{N} \Phi_j \cdot I_i(y_i, m_j), i = 1, 2, \ldots, N \qquad (8\text{-}27)$$

where I_i is given by eqn. (4-4).

The oxidation of SO_2, which precedes the formation of K_2SO_4, is assumed to take place in the gas phase. In PFAC, it is assumed that the oxidation of SO_2 is the rate limiting step for the formation of S(VI) compounds:

$$SO_2 + ½O_2 \Leftrightarrow SO_3 \Leftrightarrow H_2SO_4 \Leftrightarrow K_2SO_4 \qquad (8\text{-}28)$$

Consequently, SO_2 is the only non-equilibrium component, while all other species in the gas including the S(VI) compounds are assumed to be in mutual equilibrium.

The rate of reversible SO_2-oxidation is calculated from an empirical expression [Christensen et al., 1998]:

$$r_{SO2} = k_{SO2} \cdot ([SO_2] - [SO_2](eq)) \qquad (8\text{-}29)$$

where $[SO_2]$ is the molar concentration of SO_2 in the gas [moles/m^3] and $[SO_2](eq)$ is the corresponding equilibrium concentration, calculated for the hypothetical condition of SO_2 being in equilibrium with the other compounds.

The temperature dependence of the rate constant is assumed to be given by;

$$r_{SO2} = 1240\, s^{-1} \cdot \exp\left[\frac{-200\, kJ/mol}{R_g} \cdot \left(\frac{1}{T} - \frac{1}{1473\, K} \right) \right] \qquad (8\text{-}30)$$

For further introduction to the basic assumptions made and the numerical procedure applied in PFAC, please refer to [Christensen, 1995].

8.3.6. PFAC Numerical Solution

The equation system solved in PFAC, which consists of N·n growth equations (8-11), n equations for wall deposition (8-9), and n gas phase equations (8-26) can be formally written in the form:

$$\frac{dY}{dz} = f(Y) \qquad (8\text{-}31)$$

The equations are integrated axially by a third-order semi-implicit Runge-Kutta method well suited for integration of stiff differential equation systems [Villadsen and Michelsen, 1978]. The integration step-size is adjusted automatically to meet a specified accuracy for the dependent variables. The Runge-Kutta method requires knowledge of the partial derivatives of the right-hand sides f with respect to the variables Y. In PFAC, the Jacobian is evaluated by numerical pertubation of f(Y) [Villadsen and Michelsen, 1978].

Since particle mass and gas phase molar fractions cover many orders of magnitude, the logarithm of these variables are used internally in the code. Accordingly, the particle mass of component i cannot be 0, although this is predicted by the growth equations when the gas phase is unsaturated with component i. This numerical problem is handled by introducing a variable that informs about the existence of condensed component i in each particle size class. In case the condensed phase does not exist, the growth rate is set equal to 0.

In order to incorporate homogeneous nucleation, coagulation, and chemical equilibrium calculations, the Runge-Kutta integration is interrupted for each Δz.

At the end of each Δz interval, new size classes are introduced if homogeneous nucleation occurs. The number concentration of particles of pure component i formed in the interval [z,z+Δz], $\Phi_{hom,i}$ is found from:

$$\Phi_{\text{hom},i} = \int_z^{z+\Delta z} \frac{\rho_r \cdot A}{W} \cdot J_i \cdot dz, i = 1,2,\ldots,n. \quad (8\text{-}32)$$

where J_i is the nucleation rate for component i. The size of the new particles is set to the mean critical cluster size in the interval:

$$m_{\text{hom},i} = \rho_i \cdot \frac{\pi}{12} \cdot \left(d_{ci} \mid_z^3 - d_{ci} \mid_{z+\Delta z}^3 \right) \quad (8\text{-}33)$$

where d_{ci} is the critical cluster size for nucleation of component i. The gas phase mole fractions are updated accordingly:

$$\Delta y_i = -\frac{\rho}{\rho_r \cdot M_i \cdot c_t} \cdot m_{\text{hom},i} \cdot \Phi_{\text{hom},i}, i = 1,2,\ldots,n. \quad (8\text{-}34)$$

In order to keep the number of size classes (and thereby equations) low, the value of $\Phi_{hom,i}$ must exceed some lower limit before a new nucleation size class is created.

8.4. Parameters Controlling Aerosol Formation

A parametric study was conducted in the EU-BioAerosol project, simulating aerosol formation in a grate-boiler fired with wheat straw, mainly in order to investigate the effect of [1)] total surface area available for heterogeneous condensation, and; [2)] the feedstock composition, on the mass loading [mg/Nm^3] and the chemical composition (i.e. the ratio of KCl/K_2SO_4) of the aerosols formed.

- **Case 1:** Increased entrainment of ash from the fuel-bed into the freeboard, assuming constant number concentration of ash particles in the flue gas; This condition corresponds to a situation where a constant number of particles – with increasing diameters - per volume of flue gas are entrained from the fuel bed into the freeboard

and subsequently carried along with the flue gas. A fixed number concentration of 1000 particles/Ncm^3 was assumed. Particles with a diameter of 8 μm are considered as the standard case, where the entrainment is referred to 100 %. The other conditions investigated are 2, 12.5, 42, 195, and 1593 % entrainment of particles. An entrainment of 2 % corresponds to 1000 particles/Ncm^3 with a diameter of 2 μm, while an entrainment of 1563 % corresponds to 1000 20 μm particles/Ncm^3.

- **Case 2:** Instead of a constant number density, the mass of ash particles entrained could be constant; This is considered in the second case. A constant mass of particles with diameters between 6 and 14 μm was assumed, corresponding to number concentrations between 1185 particles/Ncm^3 (at 6 μm) and 95 particles/Ncm^3 (at 14 μm).
- Finally, **Case 3**, where the effect of feedstock composition was investigated by artificially changing the Cl:2S ratio in the range {10:90, 30:70, 50:50, 70:30, 90:10}, assuming constant SO_2 kinetics, ie. E_A = 200 kJ/mole and k_e = 1238 s^{-1}, and number concentration of 1000 particles/Ncm^3.

The same temperature profile and boiler geometry as used in [Christensen, 1995] for a grate-fired boiler utilising straw, was applied for this parametric study. The release of K, Cl and S in the parametric study was calculated based on the release work conducted by [Knudsen, 2004]. The composition and amount of flue gas produced during the combustion of the wheat straw was calculated as illustrated in [Frandsen, 1995] applying an appropriate average heating value for the fuel and assuming full load of the plant.

Gaseous species in equilibrium: KCl, K_2SO_4, $(KCl)_2$, K, K_2, KOH, $(KOH)_2$(g), KH, C, CO, CO_2, SO_3, H_2SO_4, Cl, HCl, H, H_2, O, O_2, OH, H_2O, N_2
Solid species in equilibrium: K_2CO_3, KOH, K_2O, K_2S, K_2SO_3, C, S
Gaseous species not in equilibrium: SO_2
Aerosol species: KCl, K_2SO_4

In the gas immediately after the flame zone, where the temperature may reach 1200 °C, a global equilibrium between the species listed in Table 8-1, was assumed in these simulations.

Table 8-1: Chemical species included in the present study.

8.4.1. Case 1: Constant Number Density of Coarse Particles

The first case deals with increased entrainment of ash from the fuel-bed, assuming constant number concentration of ash particles in the flue gas. This condition corresponds to a situation

where a constant number of particles – with increasing diameters - per volume flue gas are entrained from the fuel bed. A number concentration of 1000 particles/Ncm^3 was assumed, for particles with a diameter of 8 μm, where the entrainment is referred to 100 %.

The other conditions investigated correspond to 2, 12.5, 42, 195, respectively 1593 % entrainment of particles. An entrainment of 2 % corresponds to 1000 particles/Ncm^3 with a diameter of 2 μm, while an entrainment of 1593 % corresponds to 1000 20 μm particles/Ncm^3.

In Figure 8-1, the mass density of aerosols as predicted by PFAC for Case 1, is shown. It is seen that the mass loading of aerosol particles decreases with increasing mass of coarse ash particles entrained from the fuel bed. The same phenomenon was observed for the geometric mass mean diameters of the aerosols, which are also decreasing as a function of increased entrainment of ash particles.

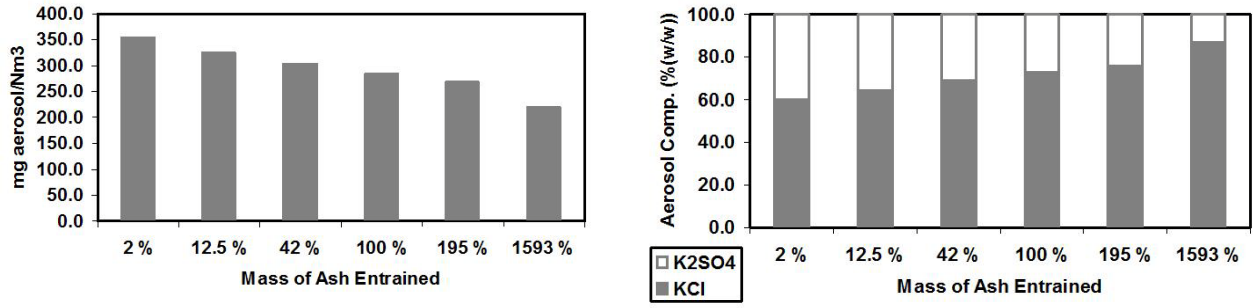

Figure 8-1: Aerosol mass density, mg aerosol/Nm^3, and chemical composition, %(w/w), predicted as a function of the mass of coarse mode fly ash particles entrained from the fuel bed.

These results may be explained by the increased surface area, provided by the increase in coarse ash entrainment, at constant number density. The more surface, the more heterogeneous condensation on this surface, and therefore as a consequence, less K_2SO_4 is available for formation of aerosols. Concerning the aerosol chemistry, it is seen in Figure 8-1, that the amount of KCl increases in the aerosols, while the amount of K_2SO_4 in the aerosols are decreasing significantly with increased amount of ash entrained at constant number density.

The data on Figure 8-1, shows that the increased mass of coarse ash particles – at constant number density - provide an increased surface area for condensation of K_2SO_4, whereby the amount of K_2SO_4 available for aerosol formation by nucleation decreases, leading to a simultaneous increase in the content of KCl in the aerosols.

The effect of increased surface area being provided by an increase in the mass of entrained ash particles at constant number density was also investigated. It was shown that the amount of particularly K_2SO_4, ending up in the aerosol fraction, in comparison to what condenses

heterogeneously on the coarse fly ash particles, decreases significantly with an increasing lift of mass of coarse ash particles from the fuel bed at constant number density.

8.4.2. Case 2: Constant Mass of Coarse Particles

The second case deals with a change in the number density, ie. the number of particles per unit volume of flue gas, at a constant mass of ash entrained. Thus, in reality this is a study of the effect of a change in particle size, and number density, on the aerosol physics, and, chemical composition.

In Figure 8-2, it is seen that the mass density of aerosols increases with increased particle size. An increase in particle size – at constant mass – is inextricably bound to a decrease in the number density and thereby in this case also in the surface area of the entrained ash particles.

Thus, the bigger the diameter of the entrained coarse fly ash particles, the smaller the surface area provided by these, and thereby the more K_2SO_4 available for homogeneous nucleation and subsequent increase in the aerosol mass loading.

This effect is also seen on Figure 8-2.

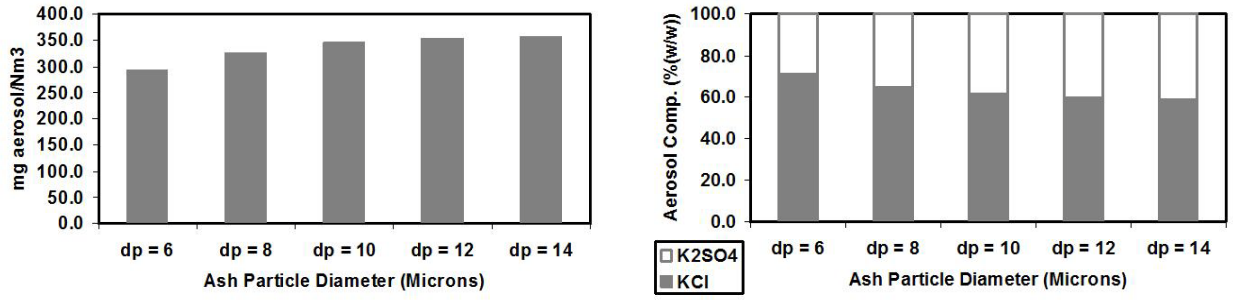

Figure 8-2: Aerosol mass density, mg aerosol/Nm^3 and chemical composition, %(w/w), predicted as a function of the diameter of the coarse mode fly ash particles entrained from the fuel bed (at constant mass entrainment).

8.4.3. Case 3: Effect of Cl:2S Ratio in Fuel Feedstock

In Case 3, the effect of fuel chemistry, and particularly the Cl:2S ratio in the fuel, was investigated. In Figure 8-3, it is seen that the aerosol mass loading increases when the major form of K is shifted from sulphate (at Cl:2S = 10%:90%) to chloride (at Cl:2S = 90%:10%).

In the sulphate dominated system app. 140 mg aerosol/Nm^3 is generated, while in the chloride dominated system app. 345 mg aerosol/Nm^3 is formed. The same tendency was observed for the geometric mass mean diameter, which is increasing with increasing Cl content up to about 50 % Cl and 50 % 2S, above which the geometric mass mean diameter remains almost constant around 0.1050 µm.

The chemistry of the aerosols are also significantly affected by the Cl:2S ratio, as seen in Figures 8-3. It is seen that in the sulphate dominated system (at Cl:2S = 10%:90%) 73 % of the aerosol consists of K_2SO_4, 27 % of KCl. In the chlorine dominated system the aerosol consists of 6 % K_2SO_4 and 94 % KCl. Although, it was shown that the fraction of K_2SO_4 being present in the aerosols compared to the total amount of K_2SO_4 condensed, increases when the chemistry shifts from S-rich to Cl-rich.

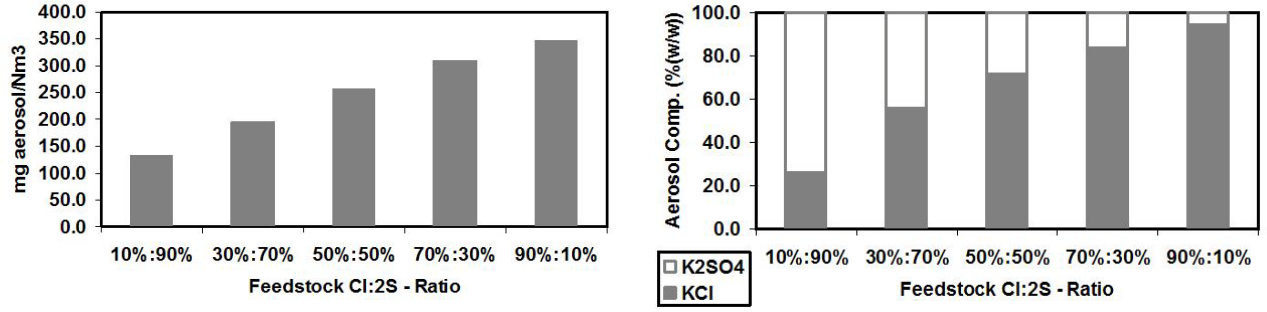

Figure 8-3: Aerosol mass density, mg aerosol/Nm^3 and chemical composition, %(w/w), predicted as a function of the Cl:2S ratio in washed wheat straw (at constant mass entrainment).

Thus, in order to sum up the parametric EU-BioAerosol study, the two key parameters controlling the aerosol composition and physics, in an existing plant, with a well defined boiler geometry and assuming a fixed gas phase sulphation kinetics, are: [1)] the surface are provided by coarse mode fly ash particles entrained from the fuel bed and carried along with the flue gases, and, [2)] the chemical composition of the fuel burned. In fact, it can be shown that by providing enough surface area for the K_2SO_4 and KCl in the gas phase to condense onto, nucleation and the subsequent coagulation may be suppressed completely, ie. no aerosol mode are formed during cooling of the gas [Christensen, 1995]. Another important feature of this parametric study is the role of the fuel chemical composition. In theory it may be possible to affect the chemical composition, size and mass formed of the aerosols by adding an appropriate amount of sulphur to fuel or the flue gas just above the fuel bed. This will introduce an additional amount of sulphur which may shift the potassium chemistry from a KCl to K_2SO_4, thereby affecting the aerosol formation and chemical composition. The latter is important when evaluating the corrosive potential of a biomass fuel.

8.5. Summary on K-Cl-S Chemistry and Aerosol Formation

A very important phenomenon in relation to K-S-Cl chemistry in straw-fired boilers, is the formation of aerosols. Sulphation plays a major role in this process. In case KCl(g) is sulphated to K_2SO_4(g), there is a risk of forming clusters of K_2SO_4 gas-molecules, due to either too fast cooling or lack of surface for heterogeneous condensation of K_2SO_4. If the clusters pass a certain critical size, the energy of forming a small droplet becomes smaller than the energy present in a cluster of gas molecules, and we say that a new phase is formed in the gas. This phenomenon is known as homogeneous nucleation, and is the initial step of aerosol formation. The pioneering work of Christensen and Livbjerg, clearly illustrated that aerosol mass loadings and chemistry can be explained by an aerosol formation mechanism based on homogeneous nucleation of K_2SO_4-nuclei, followed by coagulation and heterogeneous condensation of KCl on the surface of the coagulates.

Anyhow, there is still a scientific discussion going on whether the sulphation goes on in the gas phase or is promoted by catalytic activity of a solid material/surface. The Schofield-school, lead by Prof. K. Schofield from UC Davis, California, claims that a solid surface with catalytic activity is needed for the sulphation to go on. Nevertheless, [Glarborg and Marshall, 2005] proposed a promising new mechanism for the homogeneous sulphation process involving the intermediates alkali oxysulphur (ASO_3Cl), and alkali hydrogen sulphate ($AHSO_4$).

A parametric study was conducted by the use of PFAC [Christensen, 1995], in order to investigate the effect of feedstock chemistry vs. entrainment of ash particles from the fuel-bed. The two key parameters controlling the aerosol composition and physics in an existing plant with a well defined boiler geometry and assuming a fixed gas phase sulphation kinetics, was found to be: [1)] the surface provided by coarse mode fly ash particles entrained from the fuel bed and carried along with the flue gases, and, [2)] the chemical composition of the fuel burned. In fact, it can be shown that by providing enough surface for the K_2SO_4 and KCl in the gas phase to condense on, nucleation and the subsequent coagulation may be suppressed completely, ie. no aerosol mode will be formed during cooling of the gas [Christensen, 1995]. Another important feature of this parametric study is the role of the fuel chemical composition. In theory it may be possible to affect the chemical composition, size and mass formed of the aerosols by adding an appropriate amount of sulphur to the fuel or the flue gas just above the fuel bed. This will introduce an additional amount of sulphur which may shift the potassium chemistry from a KCl to K_2SO_4, thereby affecting the aerosol formation and chemical composition. The latter is important when evaluating the corrosive potential of a biomass fuel.

The aerosol formation mechanism suggested by Christensen and Livbjerg is uni-molecular, i.e. K_2SO_4 forms the initial nuclei for the subsequent coagulation and heterogeneous condensation.

This mechanism may be true in straw-fired systems, since K is the dominating ash-forming cation in these systems, but when firing other types of biomass, e.g. certain types og wood, there may be a significant amount of Na, which will affect the gas phase S/Cl-chemistry. Thus in these systems, a hetero molecular nucleation mechanism may take place. In Figure 8-4, the stability of a liquid solution in the system Na_2SO_4-K_2SO_4 is shown, as predicted by assuming global equilibrium in the system. It is seen that the liquid phase is stable in the temperature range [1026 – 1073 °C] if the system contains 5 % Na, and in the temperature range [860-1110 °C], in case the system contains 95 % Na. Thus, Na affects the presence of liquid phase and thereby the conditions at which the clustering of gas molecules goes on in these systems. In the BioAerosol EU-project, it was tried to predict the aerosol mass-loading and chemistry when firing different types of wood, by use of [Christensen, 1995]'s PFAC-algorithm, but failed to predict this precisely, most likely due to the presence and effect of Na in a real system firing e.g. fibre board. Much more research is needed in order to understand these mechanisms in details.

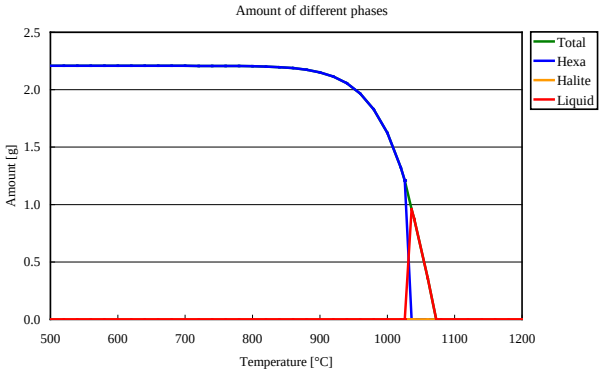

K = 0.1 %, Na/(K+Na) = 5 %,
Cl/(K+Na) = 0 %, S/(K_2+Na_2) = 100 %

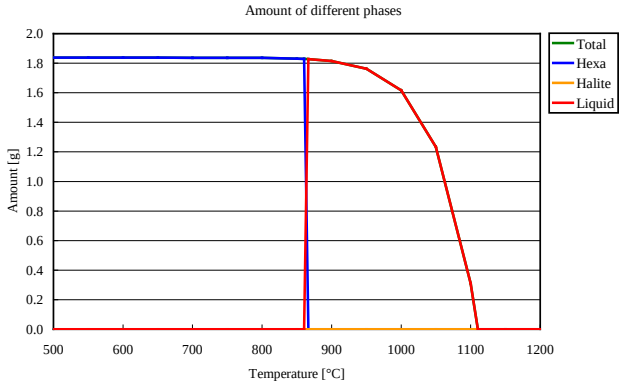

K = 0.1 %, Na/(K+Na) = 95 %,
Cl/(K+Na) = 0 %, S/(K_2+Na_2) = 100 %

Figure 8-4: Formation of solid and liquid phases of Na_2SO_4 and K_2SO_4, vs. temperature, in a system free of Cl, and with a low (5 %) content of Na, the left Figure, respectively a high (95 %) content of Na, the right Figure. Notice that the stability of the liquid solution in this system is highly affected by the concentration of Na. Source: [Dr. Rainer Backman, [BioAerosol, 2003]].

Chapter 9:

HIGH-TEMPERATURE CORROSION IN STRAW (CO)-FIRED BOILERS

The basic causes of a reduction in boiler tube lifetime in straw-fired boilers are the presence of Cl and K in and the release of these elements from straw, which combine to form low-melting, highly corrosive deposits on the tubes, as well as the heterogeneous chemical and physical nature of straw, making it difficult to handle and causes combustion conditions that are often very hard to control. The poor combustion characteristics of straw may cause regions of incomplete combustion, including localised reducing conditions (high CO levels), high heat flux from flame impingement and the presence of chemically aggressive species in inner layer deposits. Molten phases deposited on the heat transfer surfaces may remove protective oxide scale from the tube surfaces, thereby allowing rapid dissolution into the molten salts, and rapid oxidation [Nielsen, 1998].

Tube failures typically occur on the upstream side of the final stage superheater and near the locations of the soot blowers. Maximum tube thinning is located on the crown of the tube facing the gas flow [Wright and Krause, 1996]. The deposit layers in these zones consist typically of alkali and alkaline earth sulfates (very low [Cl]), a scale of iron oxide and an innermost, often laminated layer rich in KCl [Wright and Krause, 1996].

The sequence of events in the corrosion process involving such Cl-rich deposits are [Miller et al., 1972a,b]:

- Potassium (and other alkali and alkaline-earth), Cl, and SO_2 in the deposit, react with oxygen, producing K_2SO_4 and HCl or chlorine (Cl_2).
- The HCl/Cl_2 liberated reacts with the underlaying alloy to produce $FeCl_3$, which can further react with O_2 to form iron oxide and free chlorine, serving to perpetuate the corrosion process [Wright and Krause, 1996].

Straw contains significant amounts of K and Cl, which are present as KCl in parts of the combustion system. Significant levels of KCl have been detected in fly ash, particularly in inner layers of deposits formed in straw-fired plants. It has been suggested in several papers [Krause, 1989; Reid, 1971; Alexander, 1963] that corrosion of superheater tubes is driven by sulfation of alkali chloride to alkali sulfates, eg. KCl to K_2SO_4, causing a relatively high partial pressure of chlorine close to the metal (heat transfer) surface. Thus, the initiation reaction in the presence of KCl deposits may take the form of one of the reactions below, depending on the presence of SO_2:

$$2KCl + O_2 + SO_2 \rightarrow K_2SO_4 + Cl_2 \quad (9\text{-}1)$$

$$2KCl + SO_2 + H_2O \rightarrow K_2SO_4 + 2HCl \quad (9\text{-}2)$$

$$KCl + Fe_2O_3 + ½O_2 \rightarrow K_2Fe_2O_4 + Cl_2 \quad (9\text{-}3)$$

This role of SO_2 was demonstrated in laboratory experiments [Miller et al., 1972a,b] in which alloys were exposed to sulphate-chloride salt mixtures in a synthetic flue gas with and without SO_2. Introduction of 250 ppmv SO_2 in the gas phase caused large increases in corrosion rates. Increasing the SO_2 concentration to 2500 ppmv, caused a significant increase in the attack on carbon steel, but had only minor effect on T11. Type 321 stainless steel demonstrated slightly less corrosion at the higher [SO_2]-level. The rate of corrosion was also investigated while increasing the temperature from 427 to 538 °C, which caused a far higher increase in the corrosion rate, than an increase in [NaCl] in the deposit. These results indicate that only small amounts of alkali chloride in a superheater deposit may cause very serious corrosion [Krause, 1989].

Chlorine is known to be able to penetrate and destroy the oxide scale, probably through cracks and pores and at the metal/scale interface react with Cr and Fe, thereby forming volatile metal chlorides. A detailed study of disruption of the oxide scale on steel by HCl interaction from flue gas was reported by [Mayer et al., 1980]. Experiments were conducted at a metal temperature of 538 °C and a flue gas temperature of 1060 °C. Without HCl in the flue gas, a continuous non-porous scale consisting of FeO, Fe_2O_3, and Fe_3O_4 was formed. With 0.1 %(v/v) HCl present in the gas, the inner scale was continuous, but the outer Fe_2O_3-layer of the scale became blistered and cracked. This Fe_2O_3-layer in turn became porous and discontinuous when [HCl] in the gas was increased to 0.2 %(v/v). A further increase of [HCl] to 0.8 %(v/v) caused complete disintegration of the Fe_2O_3-layer, and the Fe_3O_4-layer became irregular and porous. The maximum [HCl] investigated was 2 %(v/v), a level which destroyed the continuity of both scale layers, thereby exposing the underlying metal to attack by O_2 and HCl. A mechanism of scale disruption proposed by [Crolet, 1993a,b], involves direct reaction, between the metal and the Cl, thereby producing a volatile oxychloride.

Both eqn (9-1) and eqn (9-3) above cause release of Cl_2-gas which may then migrate through the oxide scale, to react with the metal at metal-oxide scale interface according to eqn (9-4);

$$Cr + Cl_2 \rightarrow CrCl_2 \quad (9\text{-}4)$$

The $CrCl_2$ formed migrates out of the alloy due to its high volatility toward areas with a higher O_2 partial pressure, where it is converted to Cr_2O_3 and Cl_2 (eqn (9-5)):

$$2CrCl_2 + 1½O_2 \rightarrow Cr_2O_3 + 2Cl_2 \quad (9\text{-}5)$$

The precipitated Cr_2O_3 is non-protective and therefore susceptible to spallation. Chlorine then migrates into the corrosion front to form more metal chlorides. A similar reaction can occur for Fe, forming $FeCl_3$, if there is no Cr available for reaction at the metal-scale interface. Iron chloride, $FeCl_3$, will migrate more readily from the corrosion product, as it is more volatile than chromium chloride ($CrCl_2$) and is expected to form an oxide on top of the Cr_2O_3 at higher O_2 partial pressure. Thus, at lower temperatures which do not encourage evaporation of $CrCl_3$, $FeCl_3$ will still evaporate from the corrosion front [Montgomery et al., 2000a,b].

Several other corrosion mechanisms may be responsible for a corrosive attack of the nature observed in grate-fired units. [Spiegel and Grabke, 1991] suggests that chlorine may be liberated close to the metal surface, by NaCl reacting with the oxide scale, forming Na_2CrO_4 and $Na_2Fe_2O_4$. [Fujikawa and Maruyama, 1986] and [Hiramutsu et al., 1989] proposed that NaCl reacts with chromium carbide, preferably found at the grain boundaries, forming Na_2CrO_4 and Cl_2. Finally, [Shinata et al., 1986, 1987] studied the effect of NaCl on chromium, Cr-Ni alloys, and stainless steels. They suggested a mechanism where NaCl reacts with Cr_2O_3 to form Na_2CrO_4 in an initiation step, followed by the formation of a eutectic melt between NaCl and Na_2CrO_4. The oxidation reaction is going on in the melt, in which it is considered difficult to form a protective scale. The eutectic temperature in the system NaCl and Na_2CrO_4 is 577 °C.

Several field investigations of corrosion have been conducted at straw-fired CHP-boilers in Denmark over the past two decades [Larsen and Henriksen, 1996; Henriksen and Larsen, 1997; Montgomery and Karlsson, 1999; Montgomery et al., 2002a,b; Nielsen, 1998; Frandsen et al., 2006], providing basic data on corrosion rates of different materials at different temperatures and exposure times.

Below is an outline of Danish experiences with, and investigations on corrosion, in thermal fuel conversion systems fired solely or partly with straw.

9.1. Corrosion when Firing Straw on a Grate

A series of field campaigns have been carried out at the Rudkøbing, the Masnedø, and the Ensted CHP plants. These campaigns have typically consisted of: [a)] exposure of metal rings on water/air-cooled cylindrical probes, [b)] investigation of a number of materials built into a test superheater section and/or [c)] removal of sections of the actual superheater in a plant for specific deposit chemistry and corrosive potential analysis. Both austenitic steels and ferritic steels have been exposed, at steam temperatures typically in between 450 and 570 °C. The aim of the corrosion investigations has been to quantify corrosion rates and mechanisms accurately in existing superheaters as a function of material choice, exposure time or steam temperatures (i.e. increased efficiency).

9.1.1. The Rudkøbing CHP Plant

Only negligible corrosion was observed on existing superheater tubes, operated at a steam temperature of 450 °C ($T_{surface}$ ~ 480 °C) at the Rudkøbing CHP [Montgomery et al., 2000a]. Corrosion tests by an air-cooled cylindrical probe were conducted in which ferritic and high-alloyed austenitic steels were exposed to metal temperatures in the range [520-600 °C]. The corrosion probes were exposed for 450-3000 hours in a position in the top of the furnace where the gas temperature is ~ 725 °C. Both the metal loss and depth of the selective corrosion were quantified [Montgomery et al., 2000a].

The corrosion rate was found to be strongly dependent on metal temperature; below 480 °C, the corrosion rate was minimal, but from 520-550 °C increased corrosion rates were observed. At temperatures above 550°C, corrosion rates increased catastrophically [Montgomery et al., 2000a].

Selective corrosion was observed for the austenitic steels tested at Rudkøbing (AISI 347H and Sanicro 31 HT) at metal temperatures above 520 °C [Larsen and Henriksen, 1996]. Chromium, and to a lesser extent Fe, were removed from the alloy, leaving behind a degraded alloy phase enriched in Ni. The ferritic steel (X20) showed no signs of selective corrosion.

No signs of flue gas components other than Cl species were observed in the degraded metal zone. The corrosion rate at elevated temperature was found to be 2-20 times higher than what has been observed in PC and CFB boilers [Larsen and Henriksen, 1996].

The nature of the corrosive attacks observed at the Rudkøbing CHP-plant, indicated that corrosion was caused by either HCl or Cl_2 in the gas phase.

9.1.2. The Masnedø CHP Plant

At the Masnedø CHP, a corrosion investigation was performed using an air/water-cooled probe located in the boiler positions shown in Figure 9-1. In line with the Rudkøbing corrosion data, relatively high corrosion rates were observed at metal temperatures of 550°C, where no protective oxide scale was formed, while modest almost parabolic type corrosion (associated with formation of a more protective oxide scale), was observed at temperatures below 500°C [Montgomery et al., 2000a]. For austenitic steels, Cr was preferentially attacked at the grain boundaries, although selective corrosion of Cr within grains was also observed [Montgomery and Karlsson, 1999]. Based on corrosion rates from the test superheater, it was deduced that a Cr-content of 15-18 %(w/w) will give the lowest corrosion rates [Montgomery and Karlsson, 1999].

The observed, relatively low corrosion rates at the in-boiler superheater section of the Masnedø CHP plant may be explained by the presence of a K_2SO_4-layer acting as a protective layer (film) [Montgomery et al., 2000a; Hansen et al., 2000]. This is consistent with experimental studies [Alexander, 1963] showing that a layer of K_2SO_4 on top of a metal sample may slow down/inhibit selective Cl-corrosion, at temperatures below 700 °C, while a layer of KCl can significantly enhance corrosion at temperatures as low as 400 °C.

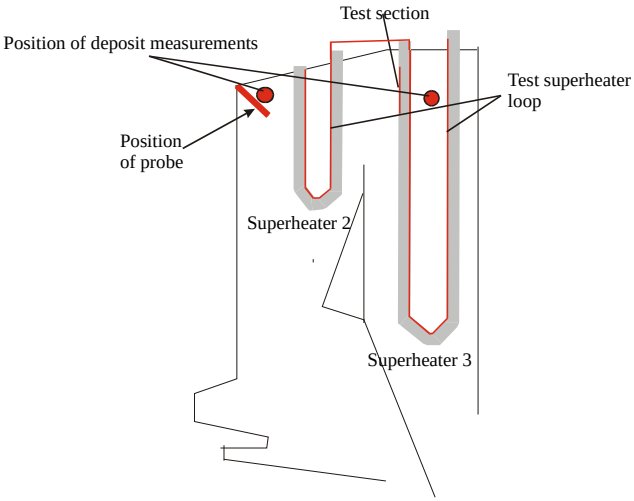

Figure 9-1: Schematic diagram of Masnedø CHP plant showing positions of corrosion and deposit investigations. Source: [Montgomery et al., 2000a]

9.1.3. The Maribo-Sakskøbing CHP Plant

Corrosion tests were also conducted at the Maribo Sakskøbing CHP plant by welding sections of different materials into superheater 2 and superheater 3. A detailed investigation of welds and tube sections after 1, 2 and 4 years of exposure was performed. The exposure time for each of the sections was defined as the time during which the exit steam temperature from superheater 3 had been > 500°C. This summed up to a total of more than 30000 hours of exposure for the period 2000-2006 [Montgomery et al., 2007].

Specimen rings were cut from the superheater tubes and were mounted in epoxy. Iron and Cr were found to oxidise forming an outer Fe-rich oxide and an inner Fe-Cr-rich oxide. The precipitated Cr oxide was non-protective and therefore spalled off with the deposit. Chlorine preferentially attacked Cr because it has a greater affinity for Cl than for Fe or Ni. The chromium chloride formed migrated out of the metal due to its high volatility to areas of a higher O_2 partial pressure and was oxidized to Cr_2O_3 and Cl_2, which then migrated to the corrosion front to form metal chlorides either by reaction with chromium carbides at grain boundaries or reaction with chromium within the grains [Montgomery et al., 2002a,b].

Temperature measurements were also performed at the Maribo-Sakskøbing CHP plant, showing that the temperature of the gas phase fluctuates greatly. The temperature measurements indicated that deposits with surface temperatures higher than 950°C ran off the superheater. This is in good agreement with the findings during the shedding measurements at the Avedøre CHP-plant.

In summary the test superheater sections at Maribo-Sakskøbing had a lower corrosion rate than the test superheater at Masnedø, and the probe data from Rudkøbing. Grained boundary corrosion attack was found to be the predominant factor for both superheater 2 and superheater 3. These results was extrapolated to give corrosion rates after longer exposure times, i.e. after 100000 hours superheater 3 will have a predicted metal loss of 3.9 mm and superheater 2 of 1.3 mm [Montgomery et al., 2002a,b].

9.2. Corrosion when Co-Firing Coal and Straw in PF Units

When co-firing coal and straw in suspension-fired units, KCl released from the straw reacts with mineral inclusions in coal char particles in the flame, forming K-Al silicates and K_2SO_4, while chlorine is, in the presence of water, released as HCl(g) according to the following reactions:

$$2KCl + Al_2O_3 + 6SiO_2 + H_2O \rightarrow K_2O.Al_2O_3.6SiO_2 + 2HCl \quad (9\text{-}6)$$

$$2KCl + SO_2 + H_2O \rightarrow K_2SO_4 + 2HCl \quad (9\text{-}2)$$

Due to this interaction, the corrosion rates observed during co-firing of coal and straw are much lower than those seen in straw-fired power plants, and are closer to those in coal-fired power plants.

9.2.1. Corrosion Tests at Midtkraft-Studstrup, Unit 1

Elsam carried out on-site corrosion investigations at the Midtkraft-Studstrup Power Station, Unit 1, MKS1 in order to test the corrosive potential of coal-straw co-firing [Andersen, 1998; Montgomery and Larsen, 2000b; Wieck-Hansen et al., 2000].

High-temperature corrosion was measured by; [a)] air/water-cooled corrosion probes located close to the superheater and [b)] test sections welded into the existing superheater [Larsen et al. 1996; Montgomery and Larsen, 2000b]. The positions of the test probes and sections in the platen and secondary superheater are shown in Figure 9-2. Corrosion investigations inside the platen superheater were undertaken in order to investigate how a high flue gas temperature (1100 °C)

and a relatively modest metal temperature (475 °C) influences the corrosion rate. An overview of the combination of experimental parameters is shown in Table 9-1.

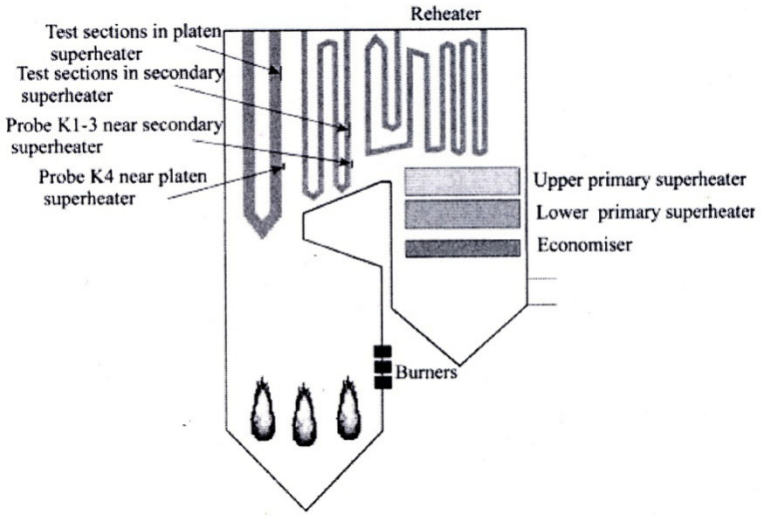

Figure 9-2: Schematic diagram of the Midtkraft- Studstrup Power Station, Unit 1, showing positioning of corrosion probes and test sections.
Source: [Montgomery and Larsen, 2000b]

Sample type:	Corrosion probes:				Test tube sections:	
Position:	2nd SH	2nd SH	2nd SH	Plat SH	2nd SH	Plat SH
Flue gas temp, °C	925	925	925	1100	925	1100
Steam temp, °C	520	550	580	500-530	540	475
Metal temp, °C (10 % straw)	556	580	612	550	565	525
Metal temp, °C (20 % straw)	541	563	586	588	565	525
Exp. Time, hr (10 % straw)	2540	2770	2770	2770	300	3000
Exp. Time, hr (20 % straw)	2980	3012	3012	3012	3012	3012

Table 9-1: Overview of the experimental parameters investigated during the MKS1 demo programme. Source: [Frandsen et al., 2006].

Material:	C:	Cr:	Ni:	Mo:	Si:	Mn:	Other:
13CrMo44	0.08 -0.18	0.70 – 1.10		0.40 – 0.60	0.10 – 0.35	0.40 – 1.00	
10CrMo910	0.07 – 0.15	2.0 – 2.5		0.9 – 1.1	0.20 – 0.50	0.40 – 0.70	Mn
X20CrMoV121	0.17 – 0.23	10.0 – 12.5	0.3 – 0.8	0.8 – 1.2	< 0.5	< 1	V
X8CrNiMoNb1616	0.04 – 0.10	15.5 – 17.5	15.5 – 17.5	1.6 – 2.0	0.30 – 0.60	< 1.50	Nb
TP321H	< 0.08	17.0 – 19.0	9.0 – 12.0		< 1.00	< 2.0	Ti
TP347H FG	0.04 – 0.10	17.0 – 20.0	9.0 – 13.0		< 1.00	< 2.00	Nb
Sanicro 31 HT	< 0.12	19.0 – 23.0	30.0 – 34.0		< 1.00	2.00	Al,Cu,Ti
HR3C	< 0.10	23.0 – 27.0	17.0 – 23.0		< 1.50	< 2.0	Nb,N
Castolin coating	?	30	Balance				B

Table 9-2: Specifications of the materials investigated in the MKS1 demo programme.
Source: [Montgomery and Larsen, 2002].

The set of temperatures chosen for the probes ranged from those actually used in the plant to 580 °C [Montgomery and Larsen, 2000b]. Test sections and probes were exposed to flue gas derived from combustion of coal+10% respectively 20% straw, for approximately 3000 hours. Detailed specifications of the materials investigated in the MKS1 demo programme are listed in Table 9-2.

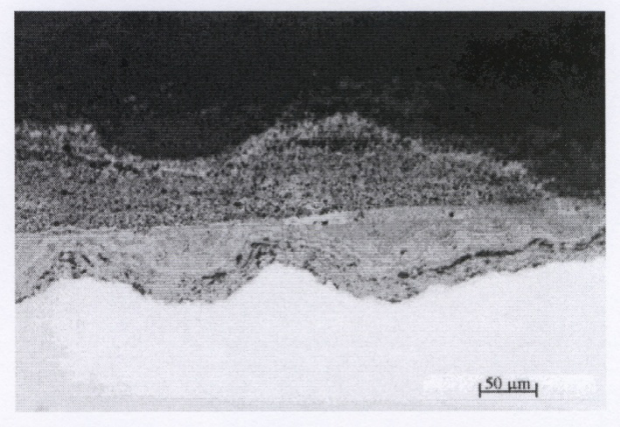

Figure 9-3: Two-layer oxide scale formed on top of X20CrMoV121 on corrosion probe 2 at a metal temperature of 563 °C, at 20 % straw co-fired. Source: [Montgomery and Larsen, 2000b].

At both 10 % and 20% straw share, a thick 2-layer oxide scale was found for 13CrMo44, 10CrMo910 as well as X20CrMoV121 (see e.g. Figure 9-3).

Some evidence of broad pits was also observed. The inner oxide scale was rich in Cr, while the outer scale was a Fe-oxide, with fly ash particles embedded along the outer rim. Sulfur was detected along the interface between the inner and outer oxide scale, and within the inner Cr-rich oxide scale in concentrations up to about 3 – 4 %(w/w), but sometimes as high as 13 %(w/w) [Montgomery and Larsen, 2000b].

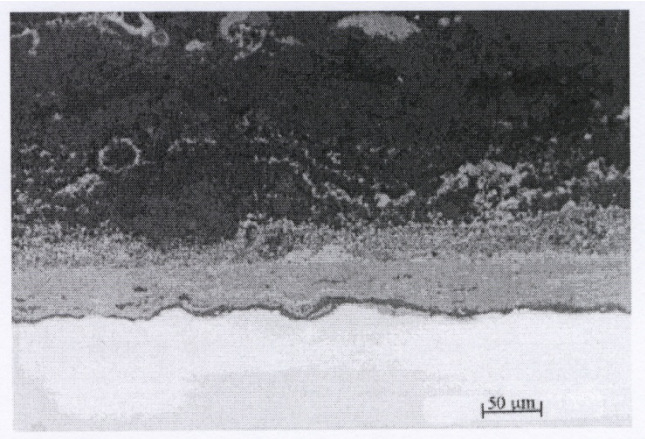

Figure 9-4: Oxide scale formed on top of X8CrNiMoNb1616 on corrosion probe 4 at a metal temperature of 588 °C, at 20 % straw co-firing. Source: [Montgomery and Larsen, 2000b].

For X8CrNiMoNb1616, an inner and outer oxide scale was also observed, in which the inner scale was rich in Cr, while the outer scale was an Fe-oxide, see Figure 9-4, i.e. a structure similar to that observed for X20CrMoV121 [Montgomery and Larsen, 2000b]. Sulfur was again present in the inner scale, and along the scale interface. Sulfur was also detected in grain boundaries along the corrosion front.

In summary, corrosion rates measured at 10 % straw share were similar to those reported for coal-firing. For both the secondary and the platen superheaters, the corrosion rate was highest for low-alloy ferritic steels like 13CrMo44 and 10CrMo910 and decreased with increasing alloying elements, giving HR3C and Sanicro 31 the lowest corrosion rates [Montgomery and Larsen, 2000b]. There were less corrosion products on the specimens when soot blowing was applied, indicating that soot blowing removed some of the oxide scale. It was also found that the corrosion rate was higher for the secondary superheater, i.e. a higher metal temperature had a more pronounced effect on the corrosion process than an increased gas temperature [Montgomery and Larsen, 2000b].

When co-firing 20 % straw, the corrosion rates were higher than at 10 % co-firing for all alloys tested in both the platen superheater and the secondary superheater. For ferritic steels, there was generally less corrosion products observed for the specimens with soot blowing than without. This trend was not seen for the austenitic steels [Montgomery and Larsen, 2000b].

9.2.2. Corrosion Tests at Midtkraft-Studstrup, Unit 4

Since 2002, the Studstrup Power Station, Unit 4 (SSV4), has been co-firing approximately 10 % straw (on an energy base) with coal. Corrosion was investigated by welding test sections into the superheaters 3 and 4 and the reheater loop. Test sections were removed after one year (7231 hours), 2 years (17719 hours), and, 3 years (22597 hours).

Position	3rd SH			4th SH			Reheater		
Flue gas temp, °C	1220	1220	1220	1020	1020	1020	940	940	940
Steam temp, °C	465	465	465	575	575	575	560	560	560
Metal temp, °C	485	485	485	595	595	595	580	580	580
Straw share, %	7.5	9.8	9.3	7.5	9.8	9.3	7.5	9.8	9.3
Exposure time, hr	7231	17719	22567	7231	17719	22597	7231	17719	22597

Table 9-3: Overview of the experimental parameters investigated at SSV-4. Source: [Frandsen et al., 2006].

An overview of experimental parameters investigated at SSV4 is provided in Table 9-3. Superheater 3 at SSV4 had an outlet steam temperature of 550°C. The tube investigated was midway between the inlet and outlet, and the actual steam temperature was estimated to be

465°C. The flue gas temperature before superheater 3 was 1220°C. Superheater 4 had an outlet steam temperature of 540°C. However, the actual outlet steam temperature of tube 18, where the test section was located was 575°C. The flue gas temperature, before superheater 4, was 1020°C. Finally, for the reheater tube investigated the outlet steam temperature 560°C. Since the test section was close to the outlet, it was assumed that it had a similar steam temperature. The flue gas temperature, before the reheater was 940°C [Frandsen et al., 2006; Montgomery et al., 2008].

The main elements detected in the deposits next to the corrosion products were Al, Si, Ca, S, K and Fe for all the samples investigated. In some cases, especially in the reheater section, the thickness and composition of the deposits were found to vary greatly with the flue gas direction, i.e. there were significant differences between the thickness and the chemical composition of up- and downstream deposits. High concentrations of K were associated with high concentrations of S, indicating the presence of K_2SO_4. Chlorine was only detected in the fly ash on a few occasions [Frandsen et al., 2006].

On the X20CrMoV121 samples in superheater 3, a two-layer oxide scale was formed. The inner oxide scale was rich in Cr, while the outer oxide scale was an almost pure Fe oxide, in which fly ash particles were embedded. At all exposure times, minor amounts of S were detected in the inner oxide scale, indicating the presence of sulphides or sulphates. Sulphur was also detected at the corrosion front, but there was no evidence of significant internal corrosion attack [Frandsen et al., 2006].

On the austenitic TP347H FG tubes in superheater 3, 2-layer oxide scales were also formed. The inner oxide scale was again rich in Cr, while the outer oxide scale was a pure Fe-oxide with fly ash particles incorporated. When compared to the X20CrMoV121 samples, both the inner and the outer oxide scale were much thinner when formed on TP347H FG. Sulphur was detected in the oxide scales, as well as along the corrosion front [Montgomery et al., 2008].

Only (the martensitic) X20CrMoV121 was exposed in superheater 4. All samples showed an inner and an outer oxide scale, where the inner oxide was rich in Cr, while the outer oxide scale was a Fe oxide. At all exposure times, S was detected in the oxide scales and along the corrosion front. Severe internal corrosion attack in the form of sulphidation was observed at grain boundaries, down to a depth of 40 µm, after only 7231 hours of exposure. The depth of the internal corrosion attack remained constant over time, while the Cr-rich inner oxide layer grew in thickness [Montgomery et al., 2008].

The reheater samples also showed a two-layer oxide scale structure, already after 7231 hours of exposure. On the upstream side, internal grain boundary attacks, rich in S and metallic alloying elements, i.e. sulphides, were observed to a depth of approximately 25 µm. After

17000+ hours of exposure, Cl appeared at the corrosion front, and the inner Cr-rich oxide scale was very thick in these areas [Montgomery et al., 2008].

9.3. EFP-96 Lab-Scale Study of Corrosion in Straw-Fired Boilers

Corrosion measurements were performed in lab-scale, in order to investigate the high-temperature corrosion of superheater tubes in straw-fired boilers under relatively well-defined and controlled experimental conditions [Nielsen, 1998; Nielsen et al., 1999]. Boat-shaped metal test elements covered with deposits were exposed to a synthetic flue gas in an electrically heated oven. The experiments were divided into two series according to their objectives:

1. To quantify the corrosion rate for metal test elements covered by a KCl-rich deposit
2. To test the influence of different deposit compositions on the metal test elements.

The experimental equipment applied consisted of a gas-mixing panel and two electrically heated ovens (see Figure 9-5). The deposits were placed on top of metal test elements which were placed on a specially designed quartz sledge (see Figure 9-6), and inserted into a quartz reactor in a horizontal oven. The metal test elements were approximately 20 mm long and 10 mm wide and boat-shaped with a thickness of 3 mm (see Figure 9-6). Two commercial superheater alloys were tested in the experiments, the ferritic X20CRMOV121 (X20) and the austenitic AISI 347HG (AISI 347). Test elements were not oxidized prior to exposure. The samples were exposed to a synthetic flue gas, simulating a straw-fired boiler [Nielsen, 1998]. The ovens were kept at a constant temperature of 550 °C.

An overview of the two test series is shown in Table 9-4.

Parameter:	Test of rate law:	Test of different deposits:
Deposit	KCl	KCl, K_2SO_4, eutectic mixture of KCl-K_2SO_4[1], real deposit from Rudkøbing CHP, no deposit
Exposure time	1 week, 1, 2, 3, 5 months	3 months
Temperature	550 °C	550 °C
Metals	X20, AISI 347	X20, AISI 347
Flue gas	Simulated straw combustion: 6 %(v/v) O_2, 12 %(v/v) CO_2, 400 pmmv HCl, 60 pmmv SO_2, N_2 saturated with water at room temperature to balance.	

Table 9-4: Experimental conditions for lab-scale corrosion experiments. Note: [1] – 47 %(mol/mol) KCl. Source: [Nielsen, 1998].

The corrosion attack observed in the lab-scale experiments was, in general, quite uniform. The corrosion products consisted mainly of oxides of Fe and Cr. The inner oxide scale contained both Fe and Cr oxides, whereas the outer part consisted primarily of Fe oxides. Thin layers of sulfide (chromium sulphide, Cr_2S_3) were observed on some of the elements immediately next to the base metal [Nielsen, 1998, Nielsen et al., 1999].

Internal corrosion attack was generally limited, but an internal attack of 10-50 µm depth was seen in some areas. The nature of the internal attack varied and occurred as cracks, voids, and internal attack through the grain boundaries. Figure 9-7 shows examples of internal corrosion.

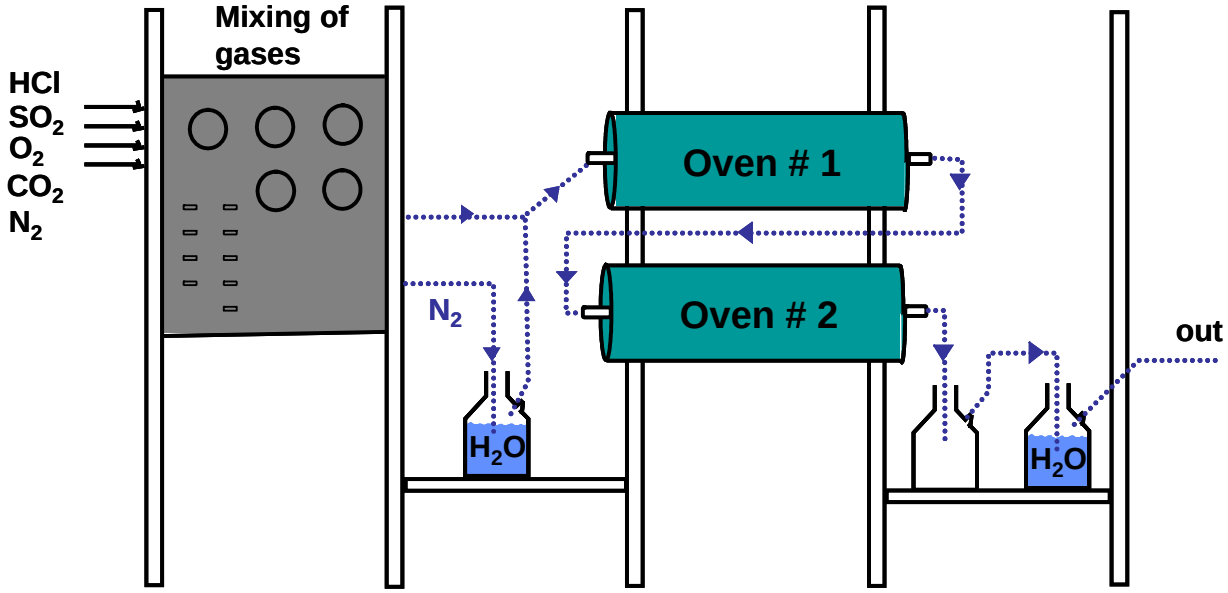

Figure 9-5: Experimental set-up for lab-scale corrosion experiments. Source: [Nielsen, 1998].

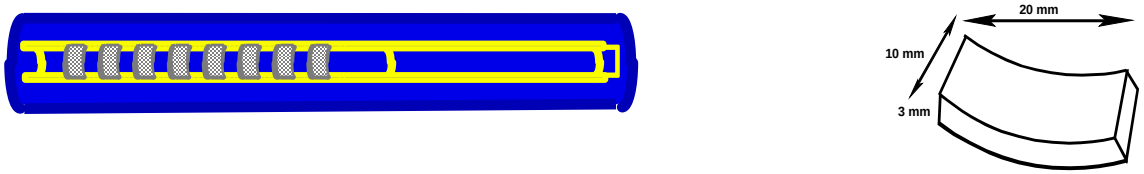

Figure 9-6: Reactor with quartz sledge for metal test elements. To the right, the dimensions of a test element. Source: [Nielsen, 1998, Nielsen et al., 1999].

The compositions of the two alloys are shown in Table 9-5.

Metal	Abr.	Fe	C	Cr	Ni	Mo	Si	Mn	Other
X20CRMOV121	X20	Bal	0.20	12	0.5	1.0	<0.5	<1.0	0.5V
AISI 347HG	AISI 347	Bal	0.07	18	12	-	<0.75	2.0	<1.2Nb+Ta

Table 9-5: Composition (%(w/w)) of iron-based alloys used in lab-scale corrosion experiments. Source: [Nielsen, 1998; Nielsen et al., 1999].

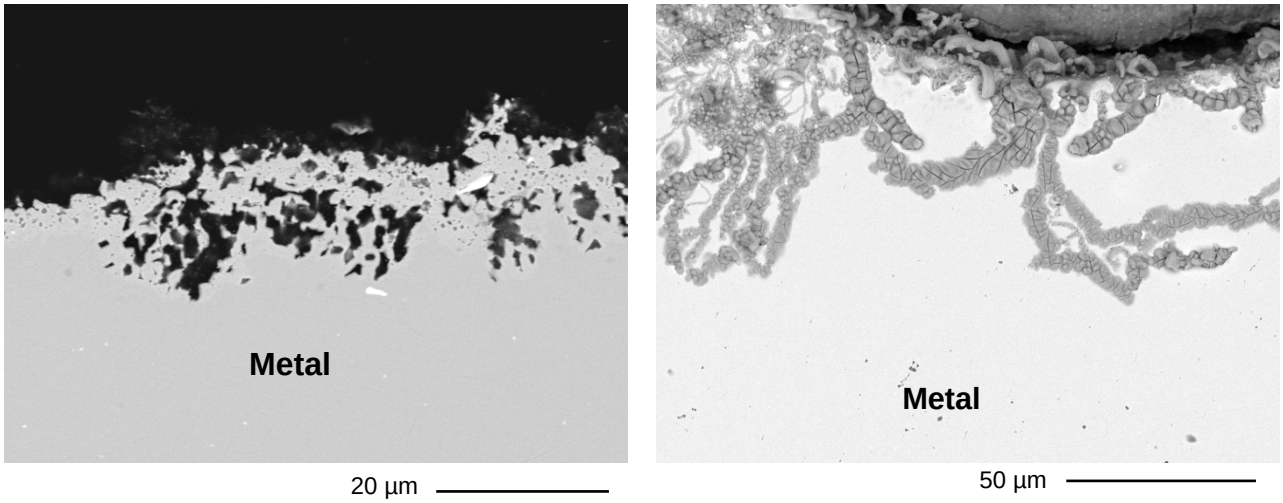

Figure 9-7: SEM micrographs showing examples of internal corrosion on test elements exposed to a synthetic flue gas in the laboratory. Source: [Nielsen, 1998].

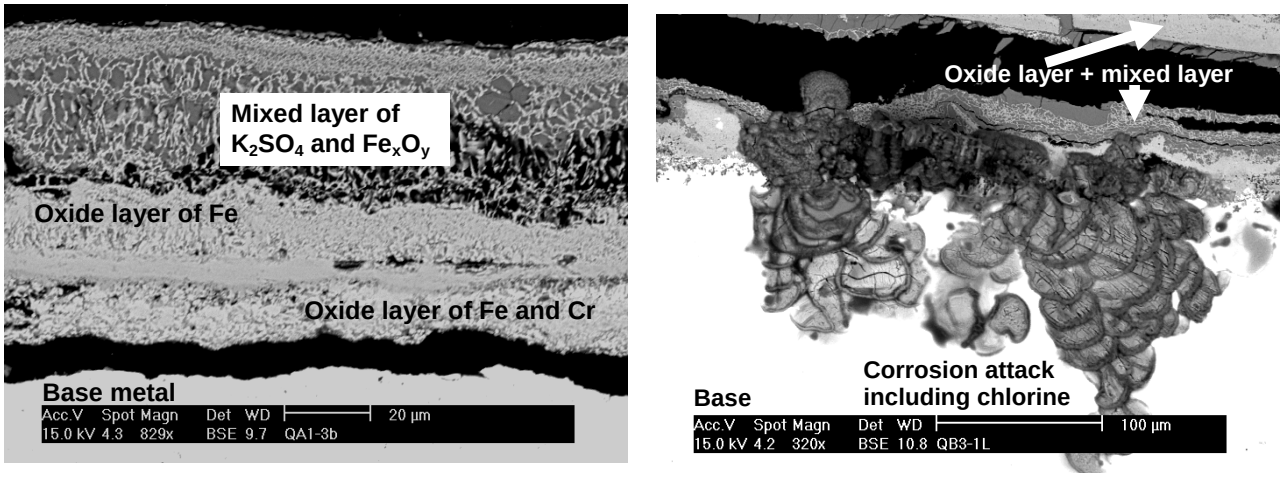

Figure 9-8: SEM micrographs, showing the scale structure on top of a corroded metal test element (left image), and internal attack of a test element covered by KCl-deposit. Source: [Nielsen, 1998].

Some test elements showed severe pits or areas of internal corrosion with depths up to 200 µm (Figure 9-8, right image). Chlorine was found in the pits, and the metal was depleted in Cr and Fe, but not in Ni. This indicates the partitioning of chlorine in the localised pitting attack.

On top of the oxide scales, a dense and very distinct 'mixed layer' of K_2SO_4 and Fe oxide (Fe_XO_Y) was present on all of the 20 samples analyzed (see Figures 9-8 and 9-9 left image). The structure of this layer was very characteristic, with threads of iron oxides (white) making up a framework in a matrix of K_2SO_4 (grey) (Figure 9-9). In the quite uniformly structured matrix, certain layers and areas of pure K_2SO_4 could be found (Figure 9-9).

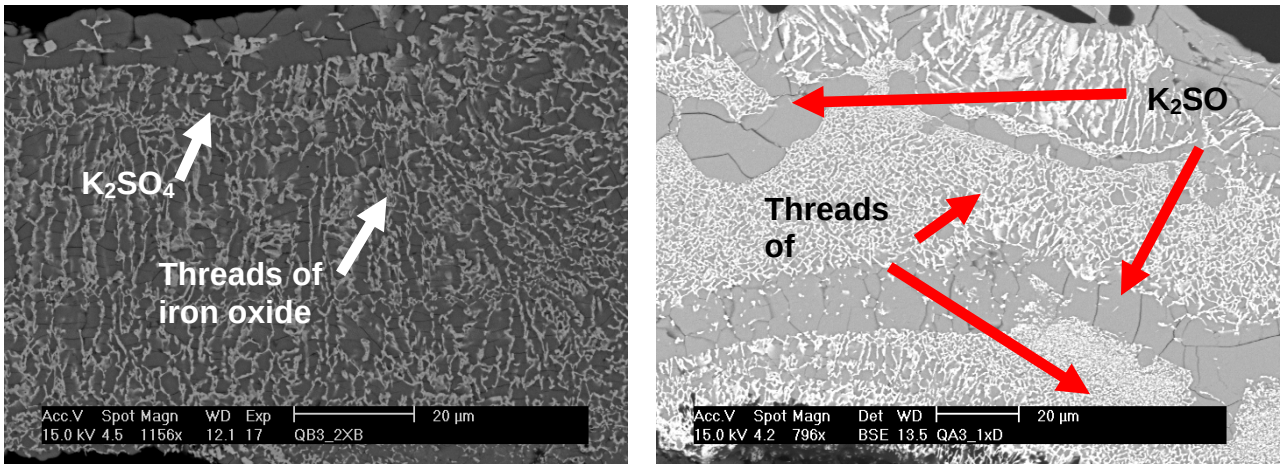

Figure 9-9: SEM micrograph of the inner layer of K_2SO_4 and iron oxide (left image), respectively of the inner layer of K_2SO_4 and iron oxide (right image). Source: [Nielsen, 1998].

After one week of exposure, the dense layer contained minor amounts of KCl in designated areas, see Figure 9-10, while in the samples exposed for one month or more, the mixed layer did not show any signs of Cl. The density and structure of the mixed layer indicate that it had been molten. In general, the threads of Fe_XO_Y were found only in combination with K_2SO_4 and did not enter zones rich in KCl. This is illustrated in Figure 9-11, where threads of Fe oxide in the K_2SO_4-layer are found between two KCl particles.

Individual particles consisting of KCl with a thin layer (0-10 µm) of K_2SO_4 at the surface were found on top of the mixed layer, indicating that the KCl particles reacted to some extent with the SO_2 in the gas.

The samples covered either by KCl-K_2SO_4 or real deposit from the Rudkøbing CHP plant, showed the same corrosion pattern as the ones covered by KCl. In contradiction, those covered with K_2SO_4 only showed a very thin layer of K_2SO_4 next to the metal oxide, but the characteristic structure in the mixed layer was not found [Nielsen, 1998; Nielsen et al., 1999].

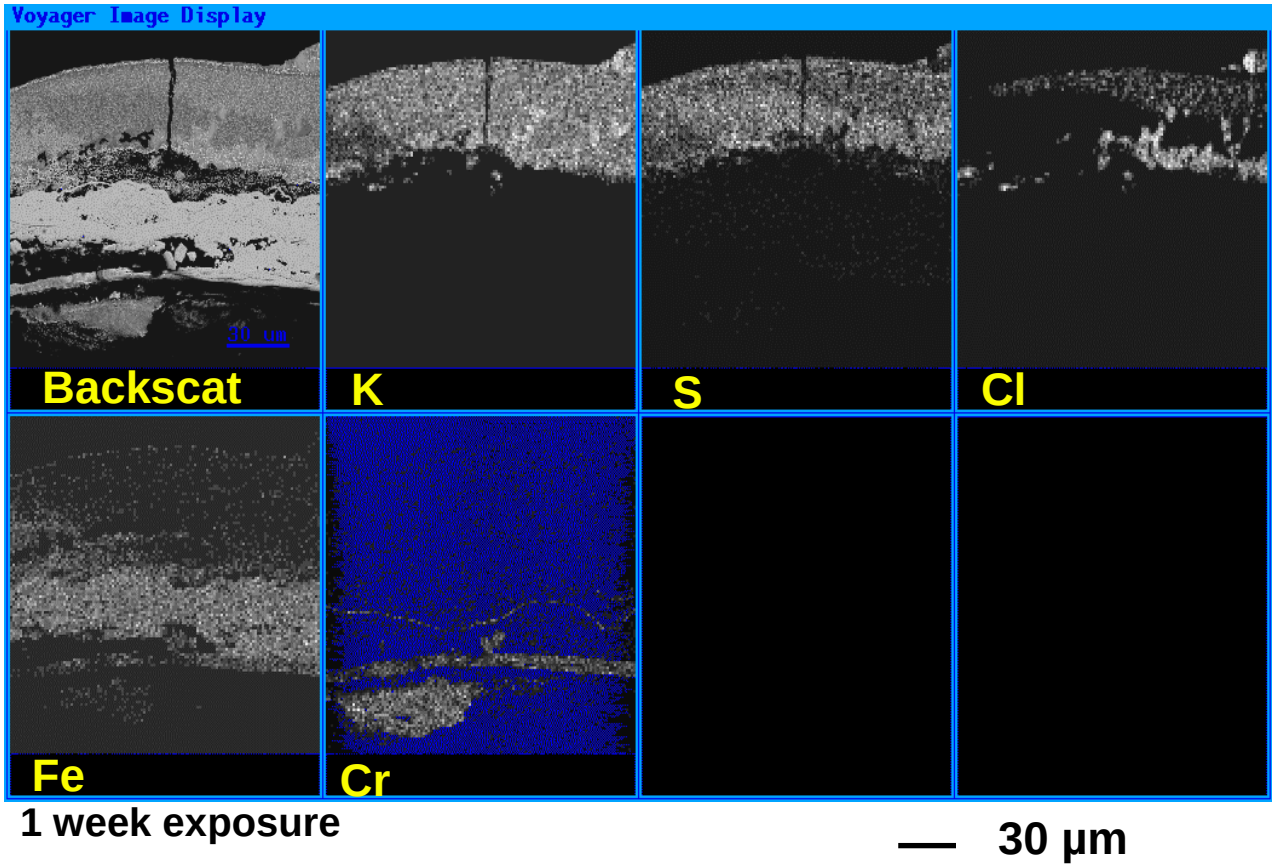

Figure 9-10: Elemental mapping of metal test elements covered by KCl, and exposed for one week in the CHEC corrosion test-rig. Source: [Nielsen, 1998].

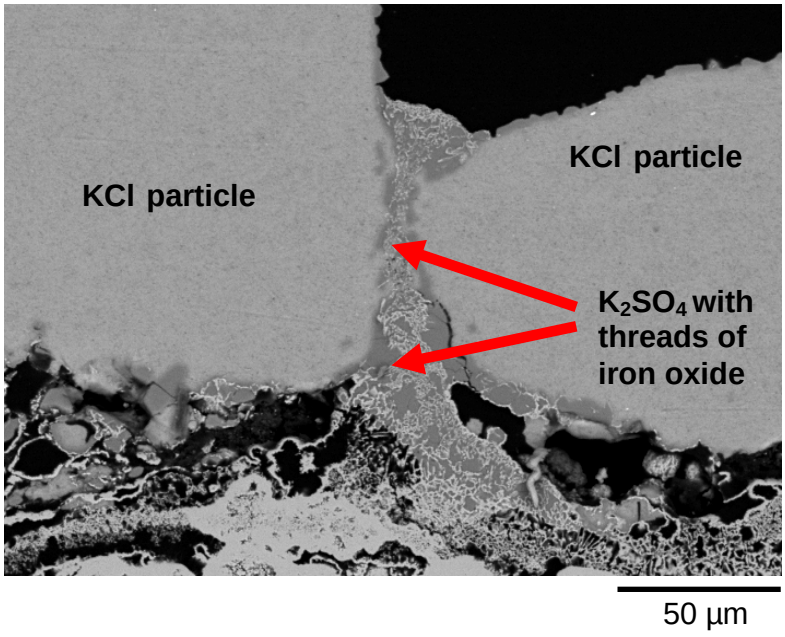

Figure 9-11: SEM micrograph of a mixed layer of K_2SO_4 and Fe oxide between two particles. Source: [Nielsen, 1998].

Figure 9-12 shows the thickness of the oxide scale as a function of exposure time for the X20 metal test elements covered by KCl. A similar result was obtained for AISI 347. The data points are shown as the mean value of the measured thickness of the oxide layers, and the error bars represent one standard deviation. The corrosion depth increased with time and the ferritic X20 was observed to suffer a greater corrosion attack than the austenitic AISI 347.

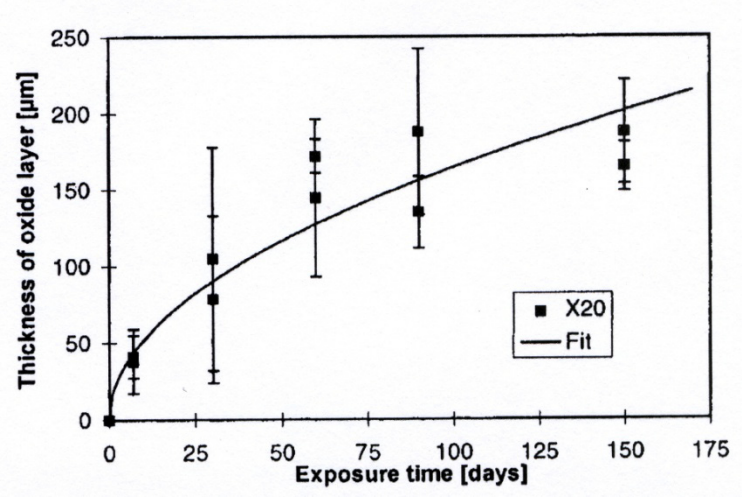

Figure 9-12: Thickness of oxide layer for X20 covered by KCl. Mean values. Error bars represent ± standard deviation. Source: [Nielsen, 1998].

The thickness of the oxide scale on test elements covered with different deposits is shown in Figure 9-13. It is clearly evident that deposits containing KCl (KCl, Rudkøbing, KCl-K_2SO_4) cause thicker oxide scales than the pure K_2SO_4 deposit as well as the absence of a deposit. Furthermore, X20 shows thicker oxide scales for all the deposits, compared to AISI 347. The picture becomes more profound when the thickness of the mixed layer is added to that of the oxide layer [Nielsen et al., 1999].

A mechanism for the Cl-induced corrosion including both the sulfation of KCl to K_2SO_4 and the essential presence of a molten phase was proposed by [Nielsen et al., 1999].

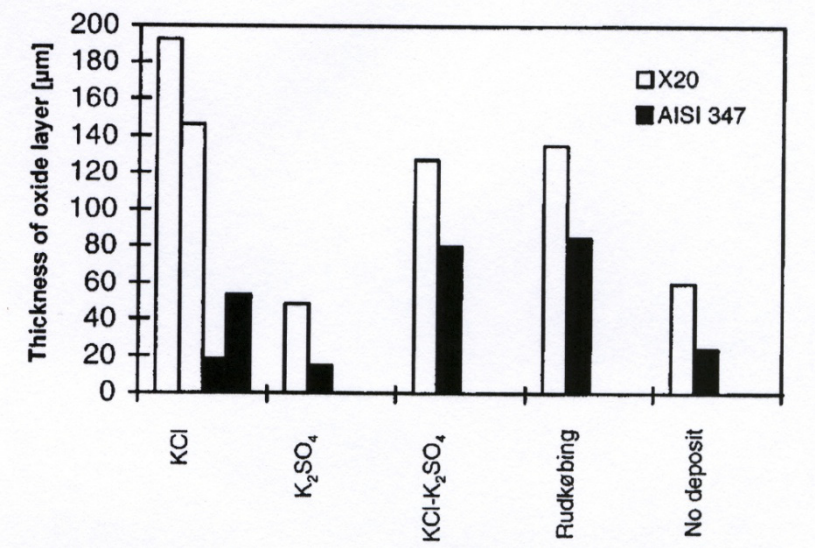

Figure 9-13: Thickness of oxide layer for metal test elements covered by different deposits.
Exposure time: 3 months.
Mean values shown.
Source: [Nielsen, 1998].

Potassium chloride, KCl, forms a melt with K_2SO_4, and different Fe-species (Fe_XO_Y, $FeCl_2$) adjacent to the oxide scale. Sulfation of KCl occurs rapidly in the melt, releasing HCl or Cl_2 close to the metal surface. Chlorine gas diffuses through the oxide scale, and reacts with Fe to form volatile iron chlorides ($FeCl_2$, $FeCl_3$), which are thermodynamically stable at the interface between the metal and the oxide scale where a very low O_2 partial pressure exists. They diffuse out through the scale, and oxidize as they reach areas with higher O_2 partial pressures. Thus, iron oxides will be formed either on top of the oxide scale or in the dense mixed layer on top of the oxide scale. This mechanism can explain the shift in corrosion behaviour with a temperature that has been observed in full-scale corrosion tests [Larsen & Henriksen, 1996]. At low metal temperatures, solid phase sulfation of KCl is slow and the corrosion governed by general oxidation. When the metal temperature exceeds the lowest melting temperature in the KCl/K_2SO_4/iron species system, the sulfation reaction becomes much more rapid, generating a high partial pressure of Cl_2/HCl. This may cause accelerated oxidation and selective corrosion of the metal [Nielsen et al., 1999].

9.4. FORSKEL-5820 Lab-Scale Study of Corrosion

Later, a lab-scale experimental set-up was applied for a detailed corrosion investigation consisting of the following components (see Figure 9-14) [van Lith et al., 2009]:

- A gas mixing panel, where gases such as N_2, O_2, CO_2, HCl, and SO_2 can be mixed.
- An electrically heated horizontal tube furnace, containing five horizontal quartz tube reactors.
- A gas cleaning system, consisting of a scrubber containing 1M NaOH and a drying column containing silica gel behind each reactor, in order to remove the acid gases (HCl and SO_2) and water from the exit gas.

This set-up was based on the experimental set-up used in the Ph.D. project of Hanne Philbert Nielsen at the CHEC Research Centre during 1996 [Nielsen, 1998]. The difference is that in the FORSKEL-5820 set-up, five quartz reactors were placed in parallel in a single horizontal tube furnace meaning that the exposure tests could be performed in a more efficient way.

Metal test elements were cut out of unexposed superheater tube material TP 347H FG (the composition of which is given in Table 9-6), resulting in arc-shaped specimens. The geometry of the specimens and the approximate dimensions are presented in Figure 9-15.

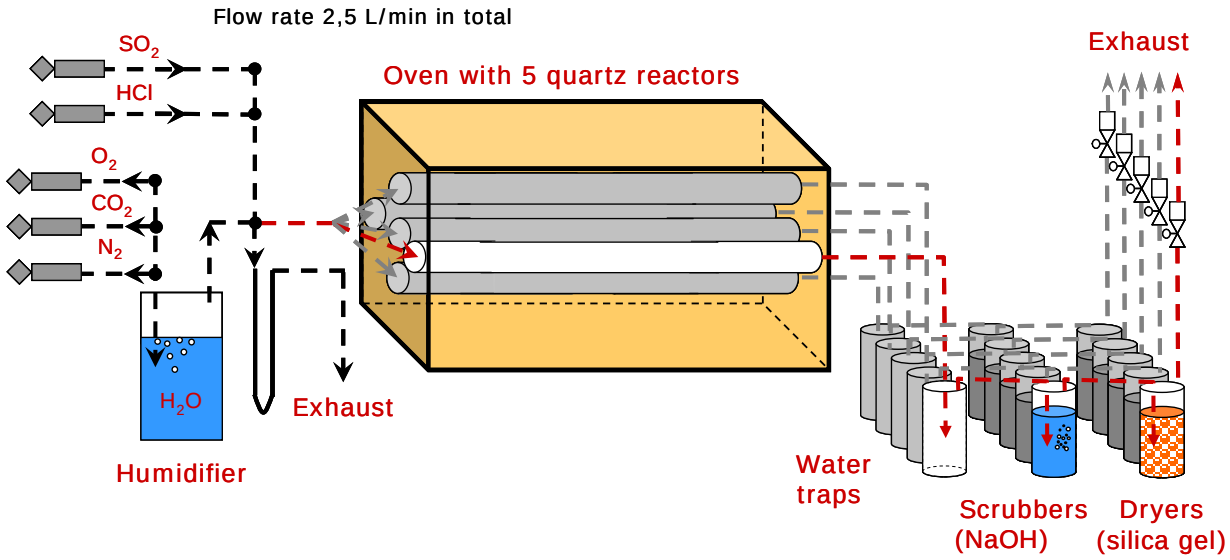

Figure 9-14: Experimental set-up to investigate the corrosion of superheater tubes under well-controlled conditions.

C	Si	Mn	P	S	Cr	Ni	Nb + Ta	Fe
0.06-0.10	<0.75	<2.00	<0.040	0.0030	17.0-20.0	9.00-13.00	0.481.0	bal.

Table 9-6: Composition of TP 347H FG (wt %)

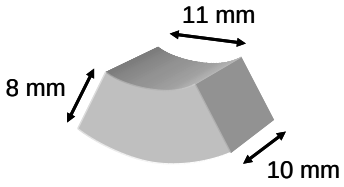

Figure 9-15: Approximate specimen geometry and dimensions.

Synthetic deposits were used, consisting of a simple salt (KCl) or a mixture of a simple salt (KCl) and simple oxides (SiO_2 or CaO) for dilution. The salt and oxides were mixed and blended in powder form. The initial KCl particle size was approximately 300 µm. In later experiments, a size fraction of 32-50 µm was used for KCl particles. SiO_2 was used in three different size ranges; 0.5-10 µm, 14-50 µm and 50-90 µm. CaO was crushed and sieved to a size range of 32-50 µm.

The synthetic deposits were placed (as uniform layers) on top of the metal test elements (on the inner arc) placed onto alumina sledges and inserted into the quartz reactors in the horizontal tube furnace. Some metal specimens without deposit were placed in the oven as well, as reference materials.

During the tests, the furnace was kept isothermal at 560 °C, which is the superheater metal temperature of the Maribo-Sakskøbing straw-fired boiler. The metal test elements were not oxidized prior to exposure. The samples were exposed to a synthetic flue gas, simulating the flue gas during straw-firing, or, co-firing of coal and straw.

Flue gas composition	Straw-firing					**Straw-firing no HCl**	**Cofiring**	**Cofiring low SO_2**
KCl particle size (μm)	~300			32-50	~300	~300		
Deposit oxide	SiO_2				CaO	SiO_2		
Deposit oxide particle size (μm)	14-50	0.5-10	50-90	14-50	32-50	14-50		
Experiment No.	1	2	3	4	5	6	7	8

Table 9-7: Experimental Conditions for the Corrosion Tests

Table 9-7 gives an overview of the three-day exposure tests performed at 560 °C. The experimental matrix was designed, in order to systematically investigate the effect of different parameters on sulfation and corrosion behavior.

The gases N_2, H_2O, O_2, CO_2, HCl, and SO_2 were mixed in the concentrations given in Table 9-8. 'Straw-firing' corresponds to the measured flue gas composition in a Danish grate-fired boiler firing 100% wheat straw [Nielsen et al., 1999] whereas 'co-firing' corresponds to the (in situ) measured flue gas composition in a Danish PF-fired boiler (Studstrup Power Station) co-firing coal and wheat straw (10% wheat straw on an energy basis) [Hansen, 1997; Hansen et al., 1998]. The effects of leaving out HCl from the flue gas in the straw-firing case and using a lower SO_2 concentration for the co-firing case were also investigated.

For the KCl-SiO_2 mixture, 25 wt % of KCl was chosen, since preliminary results had indicated that little or no Cl-induced corrosion could be observed when exposing specimens covered

with mixtures containing lower amounts of KCl (≤15 wt %) for one week to the straw-firing gas composition, at 560 °C [van Lith et al., 2009].

	O_2	CO_2	SO_2	HCl	N_2	H_2O
	% (v/v) dry	% (v/v) dry	ppmv dry	ppmv dry	% (v/v) dry	% (v/v)
straw-firing	6	12	60	400	82	2–3
straw-firing, no HCl	6	12	60	0	82	2–3
Cofiring	6	13	500	75	81	2–3
cofiring, low SO_2	6	13	200	75	81	2–3

Table 9-8: Gas Compositions

The effect of SiO_2 particle size on the sulfation behavior was studied by using three different particle size ranges; 14-50 μm, 0.5-10 μm, and 50-90 μm for SiO_2.

The effect of KCl particle size on sulfation behavior and corrosion attack was investigated by using a smaller size fraction (32-50 μm) in one of the experiments (for both the 100% KCl and the 25 wt % KCl deposits).

In one experiment, CaO was used instead of SiO_2 in order to investigate the effect of deposit oxide composition. CaO was chosen because Ca is also commonly found as a major element in deposits formed in boilers firing straw or other types of biomass.

9.4.1. Effect of KCl Concentration in the Deposits

In the first experiment, specimens covered with 100% KCl, a mixture of 25 wt % KCl - 75 wt % SiO_2 (particle size 14-50 μm), and specimens without deposit, were exposed to the straw-firing gas composition at 560 °C, for three days. SEM micrographs of selected areas of the 100% KCl and 25 wt % KCl samples, as well as a comparison of the results of the internal attack, oxide thickness and mixed layer thickness measurements for the 100% KCl sample and the 25 wt % KCl sample after exposure, are shown in Figure 8-17 [van Lith et al., 2009].

The sample covered with 100% KCl, showed a rather uniform corrosion attack: a band of selective corrosion of ~5 μm thickness, followed by a ~10 μm thick oxide scale and a ~30 μm thick mixed layer (see Figure 9-17a). The fact that small amounts of Cl (~1-4 wt %) were

detected at the corrosion front, and a Ni-rich skeleton was left behind, suggests that the Cr and Fe were removed by selective Cl corrosion.

The mixed layer on top of the oxide scale consisted of iron oxide threads in a layer of K_2SO_4, and had a molten appearance. Locally, some Cl was detected in the mixed layer. The corrosion morphology was similar to the findings of [Nielsen et al., 1999] for test elements covered with a KCl deposit, and exposed to a straw-derived gas composition, at 550 °C. Furthermore, the mixed layer was similar in morphology and chemistry to that observed on superheater tubes with a steam temperature of 520 °C, at the Masnedø straw-fired boiler, and on test tubes of various ferritic steels and TP 347H (metal temperatures of 490 °C) exposed at the Ensted straw-fired boiler [Montgomery et al., 2002b].

[Nielsen et al., 1999] argued that the mixed layer of iron oxide threads in K_2SO_4 observed in lab-scale exposure tests may be due to the formation of a melt containing KCl, K_2SO_4, Fe_xO_y, and possibly $FeCl_2$. When KCl is present in the molten phase, it readily sulfates to form more K_2SO_4, while simultaneously releasing gaseous chlorine. The composition of the melt thus changes continuously, until, at some point, solid K_2SO_4 and Fe_xO_y become the thermodynamic stable species and precipitate out, forming a solid phase with a pin-striped eutectic structure.

For the sample covered by 25 wt % KCl - 75 wt % SiO_2, a much thinner mixed layer (~9 μm on average) of iron threads in K_2SO_4 was found on top of the oxide scale. The reason for this could be the lower [Cl] in the sample (providing a lower amount of melt) and/or the presence of the SiO_2 particles (as will be discussed later). At some locations in the sample, a thin layer (<8 μm) of pure K_2SO_4 was present between the oxide and the mixed layer (see the SEM micrograph of Figure 9-16b). In general, a rather thin oxide scale (~8 μm on average) was formed, which is comparable to the sample with a 100% KCl deposit (see Figure 9-16). In contrast to the sample with a 100% KCl deposit, selective Cl corrosion occurred only locally, and the maximum depth was 5 μm. Only traces of Cl (<1 wt %) were found at the corrosion front [van Lith et al., 2009].

The reference sample (without deposit), showed a thin (<5 μm) and rather discontinuous oxide scale consisting of Fe and Cr oxides. At a few locations, minor internal attack was observed (<3 μm). Traces of S (<2 wt %), and Cl (<1 wt %) were found at the corrosion front.

SEM-EDX investigations showed partial sulfation of the KCl particles for both the test element initially covered with 100% KCl and that covered with 25 wt % KCl - 75 wt % SiO_2. In the case of the 100% KCl deposit, the sulfation product was mainly visible as rims of dense K_2SO_4 around the KCl particles in the outermost deposit layer and as small K_2SO_4 crystallite grains (<5 μm) around the KCl particles in the middle of the deposit. In the 25 wt % KCl case, the K_2SO_4 crystallite grains were attached to the surface of the SiO_2 particles. This result combined

with the thinner mixed layer observed, suggests that K_2SO_4 produced by the sulfation of KCl is present on the SiO_2 particles, so that less K_2SO_4 is formed on the oxide or mixed layer [van Lith et al., 2009].

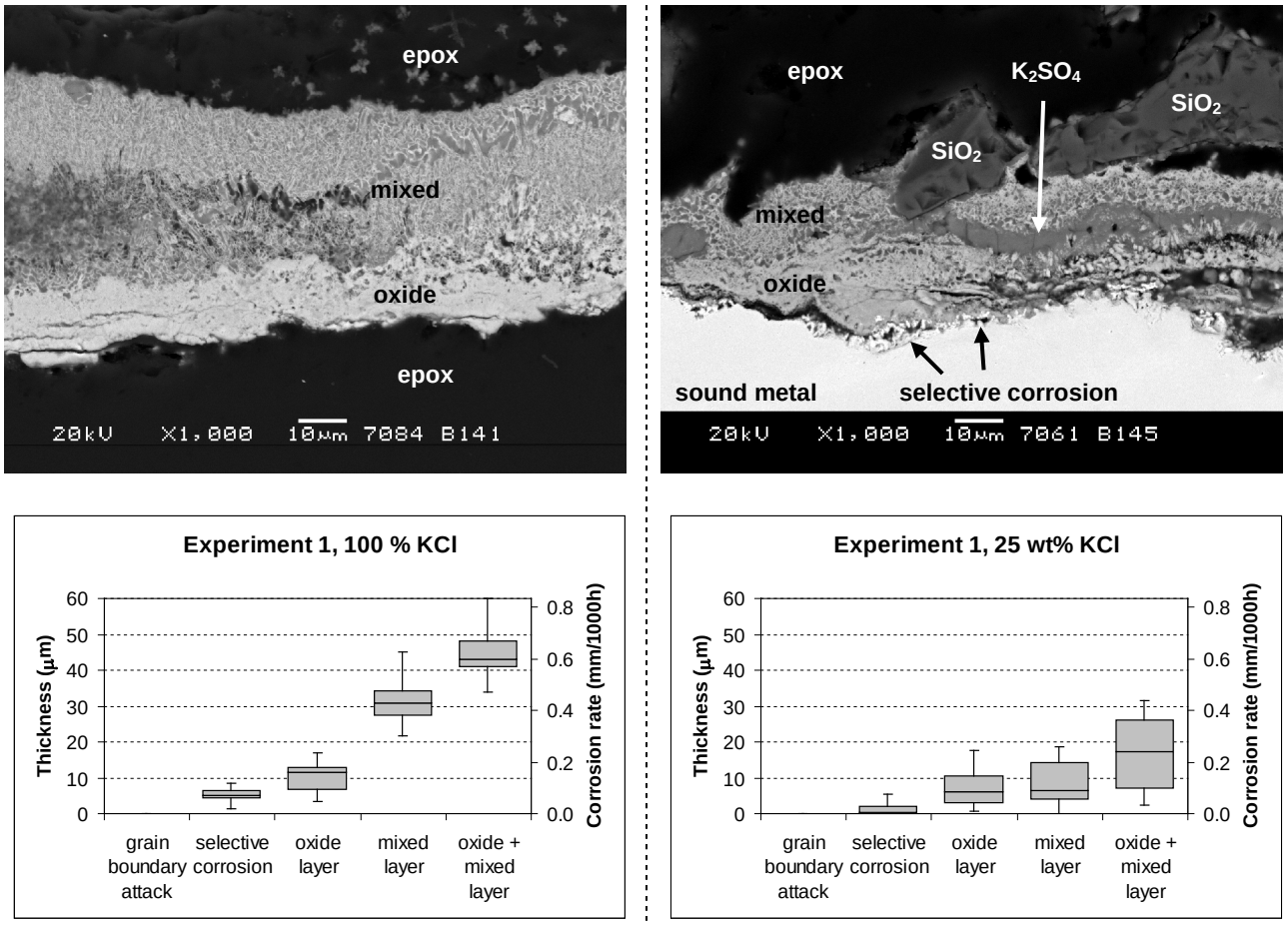

a) 100% KCl

b) 25 wt % KCl

Figure 9-16: Effect of percentage of KCl in the deposit on corrosion attack, for specimens initially covered with 100% KCl (a) and 25 wt % KCl - 75 wt % SiO_2 (b), exposed to a synthetic straw-firing gas composition at 560 °C, for three days. SEM micrograph to the left shows only the spalled oxide and mixed layer. In the graphs are the first and third quartile (the lower and upper lines of the grey boxes), the median value (the lines inside the grey boxes), and the minimum and maximum values (the ends of the vertical lines), based on 20-40 measurements are indicated. The corrosion rates were calculated assuming linear corrosion kinetics.

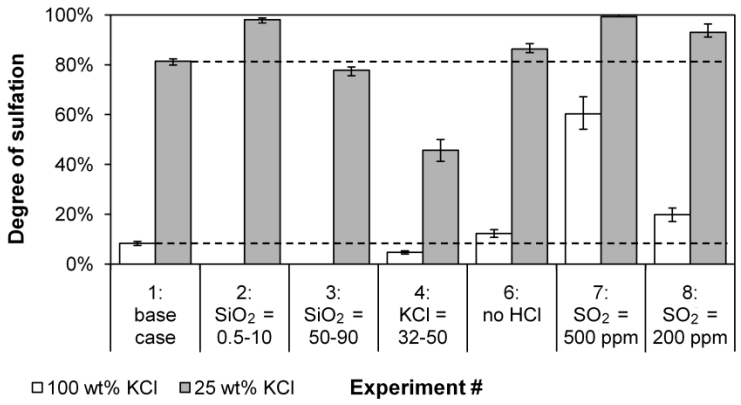

Figure 9-17: Degree of sulfation in the deposit after exposure, for the different experiments. White bars indicate experiments with an initially 100% KCl deposit, whereas grey bars indicate tests with an initially 25 wt % KCl - 75 wt % SiO_2 deposit. In experiment 1 (the "base case"), the samples were exposed to the straw-firing gas composition (60 ppm SO_2; 400 ppm HCl) at 560 °C, for three days, whereby the particle size of KCl was ~300 μm and that of SiO_2 14-50 μm.

ICP-OES analyses of the deposits showed that, the degree of sulfation was much higher (about ten times) in the 25 wt % KCl deposit compared to the 100% KCl deposit. The same trend was observed for all other experiments, as can be seen in Figure 9-17. A higher SO_2/KCl molar ratio in the 25 wt % KCl deposits could explain the higher degree of sulfation, but not by a factor 10. Other possibilities could be that the SO_2 is captured in between the SiO_2 particles, thereby increasing the possibility for reaction between KCl and SO_2, or that the presence of SiO_2 has a catalysing effect on the sulfation process.

[Jørgensen et al., 2007] studied the effects of quartz wool, crushed, nonporous alumina; and chips of steel (type 316) on the oxidation of SO_2 to SO_3 in a fixed-bed quartz reactor, in the temperature range of 750-1050 °C. They found no effect with quartz wool, a little catalytic effect with the alumina particles, but a strong catalytic effect with steel chips. The sulfation of solid KCl is known to be slow in the presence of SO_2, but orders of magnitudes faster in the presence of SO_3 [Halck, 2008; Gudzinska, 2007; Ozawa et al., 2003]. [Dennis and Hayhurst, 1988] investigated the effect of silica sand bed material (particles of 425-500 μm) on the oxidation of SO_2 in a fluidized bed reactor, made of 321 stainless steel, in the temperature range of 700-950 °C, and measured SO_2 oxidation rates approximately 100 times faster than expected for gas-phase oxidation. They concluded that SO_3 was produced mainly on the surface of the quartz sand, and therefore proposed a model in which O_2 and SO_2 competitively chemisorb on the sand, with the rate controlled by SO_2(g) reacting with adsorbed O atoms.

Knowing the initial amount of KCl in the deposits, and the degree of sulfation after exposure, the amount of HCl formed according to reaction (1) can be calculated for each sample. It was found that 36% more HCl was formed in the case of the 25 wt % KCl sample compared to the 100% KCl sample. The lower amount of selective corrosion, and thinner oxide and mixed layers, observed in the 25 wt % KCl deposit case indicates that less HCl reaches the metal surface, than in the case of the 100% KCl deposit. This could be explained by the fact that there are more KCl-particles present close to the metal surface in the case of the 100% KCl deposit, compared to the 25 wt % KCl deposit, causing a higher probability of HCl reaching the metal surface, instead of being removed with the flue gas.

9.4.2. Effect of SiO_2-Particle Size

In experiments 1-3, the effect of the size of the SiO_2-particle was investigated for deposits containing 25 wt % KCl. A comparison of the results concerning the oxide thickness and the mixed layer thickness measurements is shown in Figure 9-18. Minor internal attack (<5 μm) was observed in all three samples.

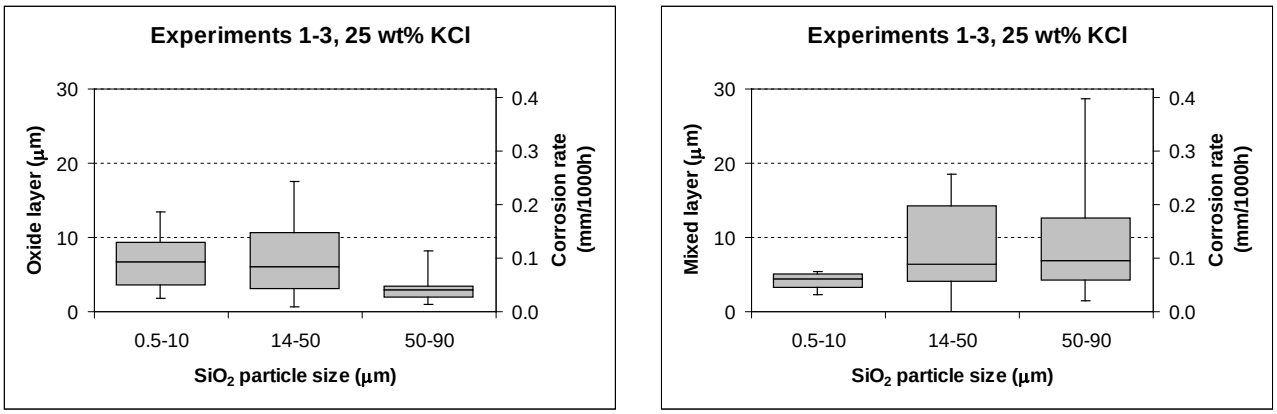

a) Oxide layer thickness b) Mixed layer thickness

Figure 9-18: Effect of SiO_2 particle size on the thickness of the corrosion products, for specimens covered with a 25 wt % KCl, and exposed to the straw-firing gas composition at 560 °C for three days.

The sample containing 0.5-10 μm SiO_2 particles showed a rather different sulfation and corrosion behavior compared to the sample containing 14-50 μm SiO_2 particles. SEM-EDX analysis showed that most of the K_2SO_4 in the sample was found on the surfaces of the SiO_2 particles closest to the original KCl particles, and only a small amount of K_2SO_4 seemed to have deposited on the oxide scale, as the mixed layer was relatively thin (~4 μm). The

thickness of the oxide scale (~7 μm), on the other hand, did not differ that much from the sample with the 14-50 μm SiO_2 particles.

For the sample with the 50-90 μm SiO_2 particles (experiment 3), a relatively small amount of K_2SO_4 was deposited on the SiO_2-particles. The mixed layer was somewhat thicker on average, compared to the 14-50 μm sample, and very thick (up to ~30 μm) at places close to KCl particles. The oxide scale was ~3 μm thick on average, which is considerably thinner than the oxide scale in the 14-50 μm sample (see Figure 9-18) [van Lith et al., 2009].

The ICP-OES analyses showed that the KCl in the deposit with the smallest SiO_2 particle size range (experiment 2) was almost completely sulfated, whereas the degree of sulfation in the deposits was around 80 % in the deposits with the other SiO_2 size fractions (experiments 1 and 3) (see Figure 9-17). This result supports the possible catalytic effect of the SiO_2 surface on SO_2 oxidation and thereby on the sulphation reaction.

9.4.3. Effect of KCl-Particle Size

An experiment similar to experiment 1 was performed by applying a smaller KCl particle size i.e. 32-50 μm instead of ~300 μm, in order to study the effect of KCl particle size on the sulphation and corrosion behavior [van Lith et al., 2009].

For the 100% KCl deposit, SEM analyses showed a relatively uniform corrosion attack (see Figure 9-19a), consisting of a more-or-less continuous band of selective corrosion (~2 to 5 μm thick), an oxide scale of ~15 μm, and a somewhat thinner mixed layer of iron oxide and K_2SO_4.

The effect of KCl particle size on the degree of sulfation in the deposit can be seen in Figure 9-17. For both 100% KCl and 25 wt % KCl deposit, it is seen that using a smaller KCl-particle size results in a lower degree of sulfation in the whole deposit. Now, since smaller KCl-particles have a larger specific surface area available for reaction with SO_2, a higher degree of sulfation would be expected. Other parameters, such as packing density or bed porosity, may therefore play a more important role in the sulfation of a KCl containing deposit. The deposits containing the smaller KCl particles may be more densely packed, resulting in lower bed porosity and a higher resistance to the gas flow, which could explain the lower degree of sulfation.

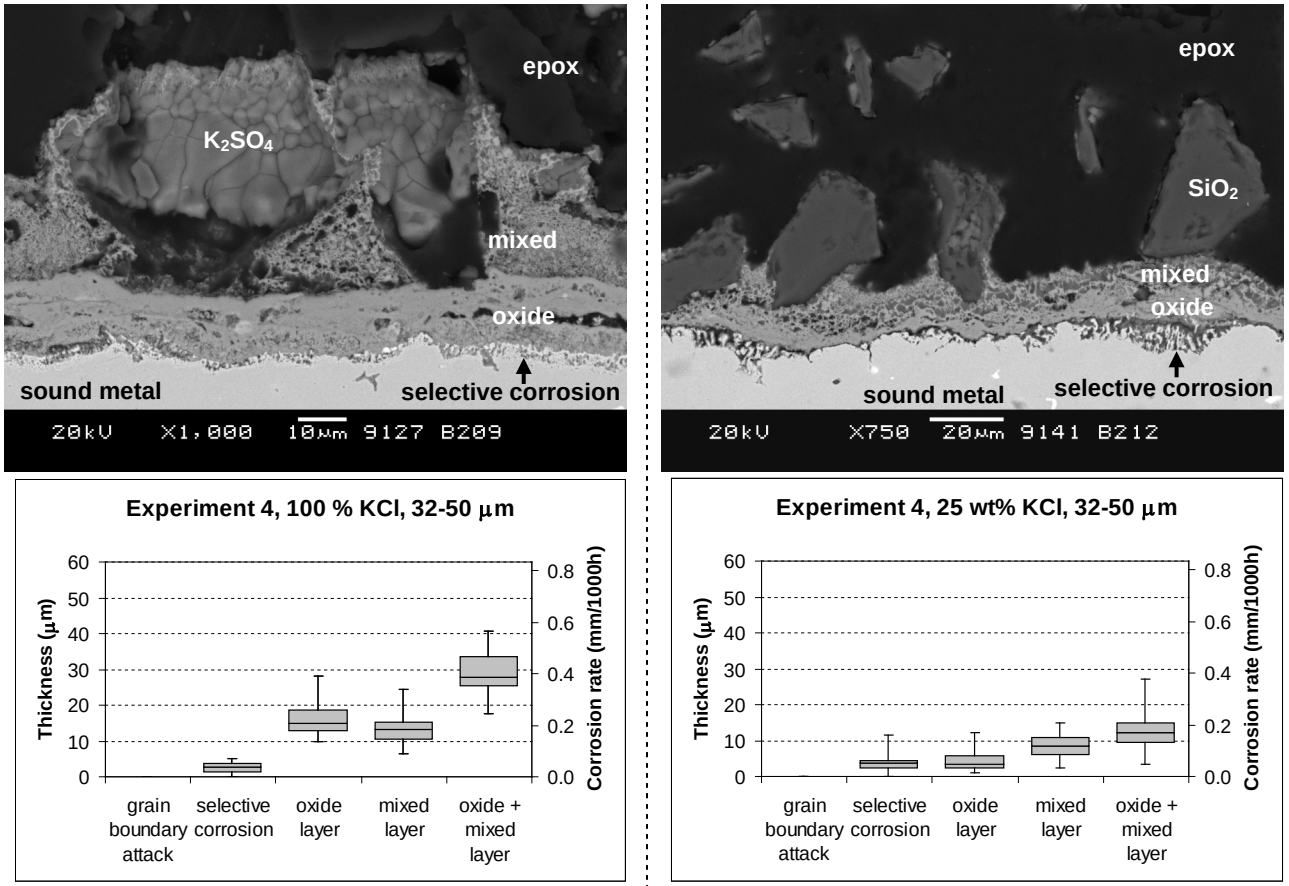

a) 100% KCl b) 25 wt % KCl

Figure 9-19: Corrosion attack for samples initially containing 100% KCl (a) and 25 wt % KCl - 75 wt % SiO_2 (b) exposed to the straw-firing gas composition at 560 °C, for 3 days, whereby the KCl particle size range was 32-50 µm.

9.4.4. Effect of Deposit Oxide Composition

In experiment 5, CaO-particles were used instead of SiO_2-particles, in the 25 wt % KCl deposit. The corrosion attack was found to be very different from that observed for the specimen covered by the KCl-SiO_2 deposit (experiment 1). Most apparent was the ~10 times thicker oxide layer formed in the KCl-CaO deposit (see Figure 9-20). The two SEM pictures in Figure 9-20 show the outer oxide layer and the inner oxide layer, which are separated by a large gap.

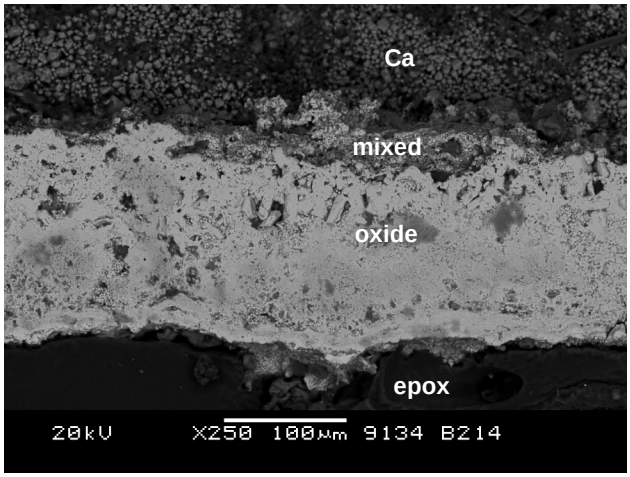

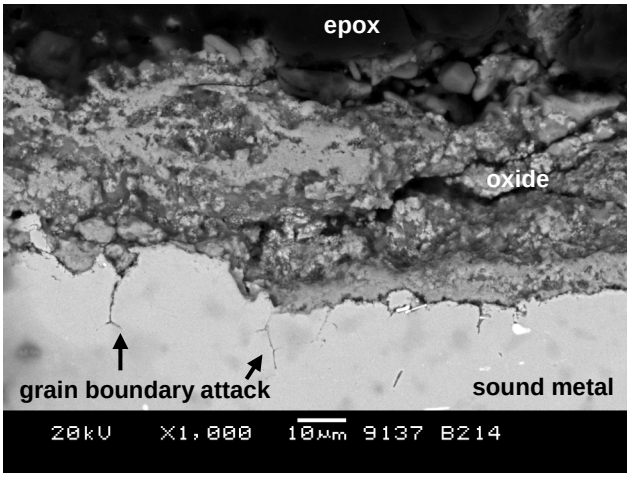

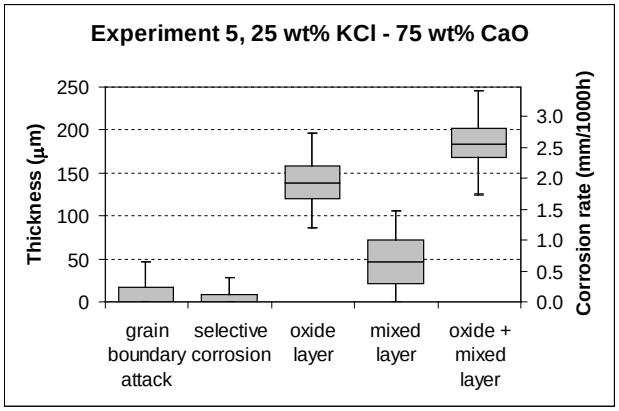

Figure 9-20: Corrosion attack for specimens initially covered with 25 wt % KCl - 75 wt % CaO, exposed to the straw-firing gas composition at 560 °C, for 3 days. Compare with Figure 20 (experiments performed under similar conditions, but using a SiO_2 instead of CaO) to see the effect of deposit oxide composition.

The outer oxide consisted of a Cr-rich layer in the bottom and a Fe-rich layer on top of this. The inner oxide layer was rich in Cr and Ni. Point and area analyses and X-ray mappings of the sample indicate that large quantities of Ca (up to 9 wt %) and Cl (up to 18 wt %) were present in both the inner and outer oxide layer. Smaller quantities of Cl (up to 6 wt %) were detected in the mixed layer. Furthermore, the mixed layer contained little or no K, but instead Ca was found together with S, probably as $CaSO_4$ [van Lith et al., 2009].

The fact that Ca is present close to the corrosion front means that it must have formed a melt together with other compounds, such as chlorides of Fe and Cr. To be able to form this melt at 560 °C, Ca has probably been present in the form of $CaCl_2$. This could be the result of a reaction of the CaO in the deposit, with the HCl from the flue gas. In fact, SEM-EDX analyses of the exposed sample indicate that $CaCl_2$ was present in the deposit as well as in large areas in the inner oxide layer close to the corrosion front. Thus, unlike SiO_2, CaO is not inert in the

deposit but plays a very important role in corrosive attack. It is noteworthy, that in the case of the CaO deposit, grain boundary attack is seen in addition to selective corrosion (see Figure 9-20).

9.4.5. Effect of the Presence of HCl in the Flue Gas

The effect of the presence of HCl was studied for samples exposed to the straw-firing gas composition (experiment 6). The results of the measurements of internal attack and oxide scale mixed layer thickness respectively are presented in Figure 9-21.

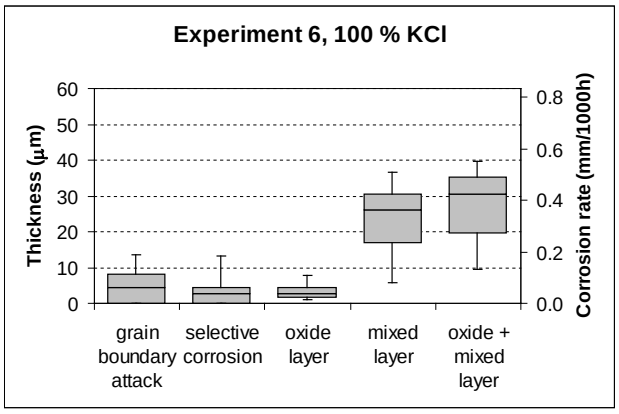

Figure 9-21: Corrosion attack for specimens covered with a 100% KCl deposit, exposed to the straw-firing gas composition without HCl, at 560 °C, for three days.

Grain boundary attack and local selective corrosion were observed, with small amounts of Cl (~1-2 wt %) present at the corrosion front. These observations indicate that HCl in the bulk gas phase is not essential for chlorine-induced corrosion to occur when a deposit containing KCl is present. Nevertheless, the average values of the thickness of the oxide scale and mixed layer were found to be lower than for the normal straw-firing case, suggesting that the presence of HCl in the flue gas enhances the corrosion rate [van Lith et al., 2009].

9.4.6. Effect of SO_2 Concentration in the Flue Gas

The effect of the SO_2 concentration in the flue gas was deduced by comparing the results of experiments 1 (straw-firing gas composition, containing 60 ppm SO_2), 7 (co-firing gas composition, 500 ppm), and 8 (co-firing gas composition with reduced SO_2 concentration, 200 ppm), emphasizing that the straw-firing gas composition contained a higher concentration of HCl (400 ppm) than the co-firing gas composition (75 ppm), see Figure 8-23.

For samples exposed to the co-firing gas composition, the degree of sulphation in the deposits was found to be considerably higher than that observed for the samples exposed to the straw-firing gas composition. For example, for specimens covered with a 25 wt % KCl deposit, the KCl-particles in the sample exposed to straw-firing gas composition were only partly sulphated, whereas the deposit was completely sulphated in the case of the sample exposed to the co-firing gas composition (see Figure 9-23 and Figure 9-17, experiment 7). The higher degree of sulphation can be explained by the higher concentration of SO_2 in the co-firing flue gas [van Lith et al., 2009].

The corrosion attack was found to be quite different for samples exposed to the straw-firing gas compared to the co-firing gas. Specimens covered with a 100% KCl deposit and exposed to the straw-firing gas showed an almost continuous layer of internal attack followed by a rather uniform oxide and mixed layer (see Figure 9-24a), whereas samples exposed to the co-firing gas composition showed a very irregular and localised internal attack and non-uniform thicknesses of the oxide scale and mixed layer (see Figure 9-24b). Furthermore, very little (≤1 wt %) or no Cl was detected at the corrosion front in the samples exposed to the co-firing gas composition, whereas ~1-4 wt % Cl was detected at the corrosion front in the samples exposed to the straw-firing gas composition [van Lith et al., 2009].

Samples exposed to the co-firing gas with reduced SO_2 concentration clearly showed a lower degree of sulfation of KCl in the deposit. For example, for the specimens covered with a 100% KCl deposit, it can be seen that the top particles of the deposit were completely sulphated when exposed to the cofiring gas (grey areas in Figure 9-25a), whereas only rims of the top particles were sulphated when exposed to the co-firing gas with a reduced SO_2 concentration (grey rims in Figure 9-25b), resulting in an overall degree of sulphation of around 20% according to the ICP-OES analysis (see Figure 9-17, experiment 8). For the samples with a 25 wt % KCl deposit, complete sulphation was observed when exposed to the cofiring gas, while some KCl was left in the deposits of the samples exposed to the cofiring gas with reduced SO_2 concentration (around 93% sulfation according to the ICP-OES analysis).

9.4.7. Effect of Temperature (560 °C vs. 600 °C vs. 640 °C)

Straw-firing conditions. The effect of temperature for straw-firing conditions was investigated by comparing the results of experiment 1, performed at 560 °C, and experiment 4, which was performed at 600 °C. An overview of the corrosion attack for each experiment is shown in Figure 9-26. The figure shows that increasing the temperature from 560 °C to 600 °C has a very pronounced effect on the corrosion attack, both for the sample containing a pure KCl deposit and for the sample containing a 25 wt% KCl –75 wt% SiO_2 deposit.

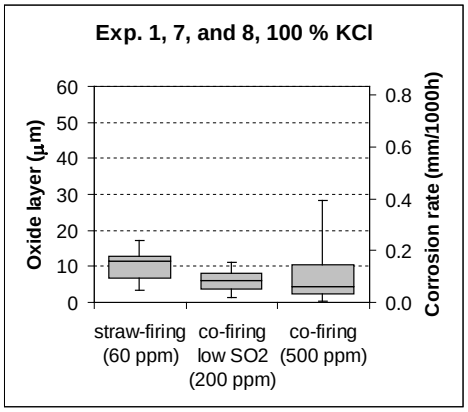

a) Oxide layer thickness

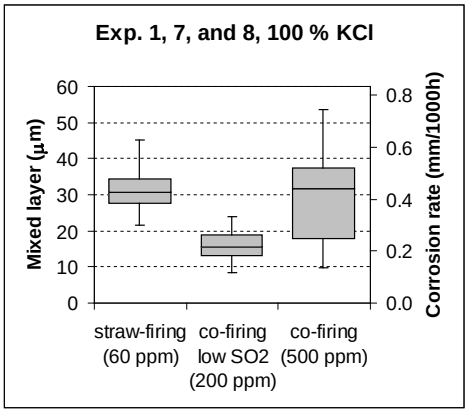

b) Mixed layer thickness

Figure 9-22: Effect of the SO_2 concentration in the gas flow (given in brackets) on the corrosion attack, for specimens covered with a 100% KCl deposit, exposed at 560 °C, for 3 days. See Figure 20 for graph explanation.

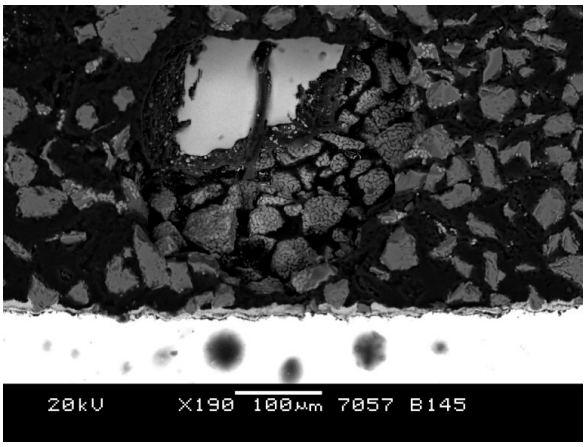

a) Gas composition: straw-firing

Large bright area: KCl; smaller grey particles: SiO_2; small light grey spots: K_2SO_4

b) Gas composition: cofiring

Small grey particles: SiO_2; Light grey areas / rims: K_2SO_4

Figure 9-23: SEM micrographs of cross-sections of the top of initially 100% KCl deposits, after exposure at 560 °C, for three days. The metal surface is visible in the bottom of the pictures.

As described above, for the specimen covered with a 100 % KCl deposit exposed at 560 °C, a rather uniform corrosion attack was observed, consisting of a band of selective corrosion of ~5 µm thick, followed by a ~10 µm thick oxide layer, and a ~30 µm thick mixed layer (see Figure 9-26a).

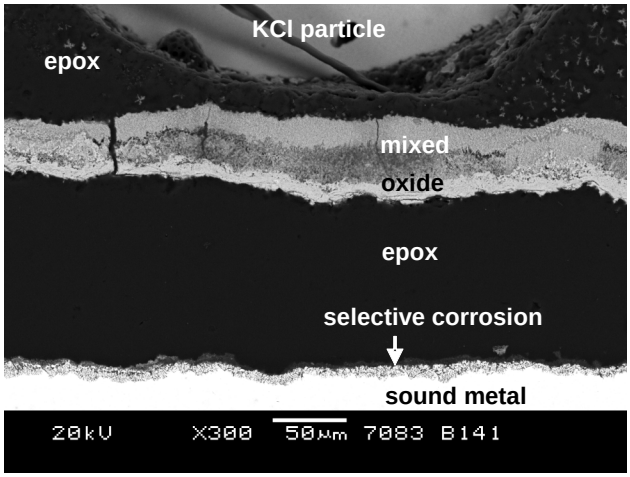

a) Gas composition: straw-firing

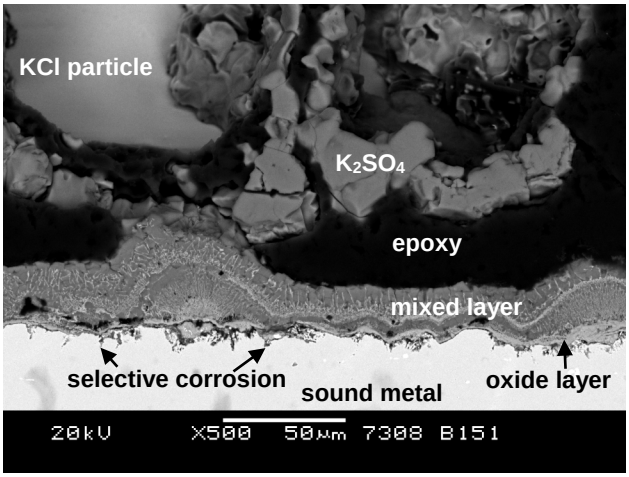

b) Gas composition: cofiring

Figure 9-24: SEM micrographs of cross sections of the corrosion products of specimens covered with a 100% KCl deposit, after exposure at 560 °C (1040 °F), for 3 days. Note: Pictures have different scales.

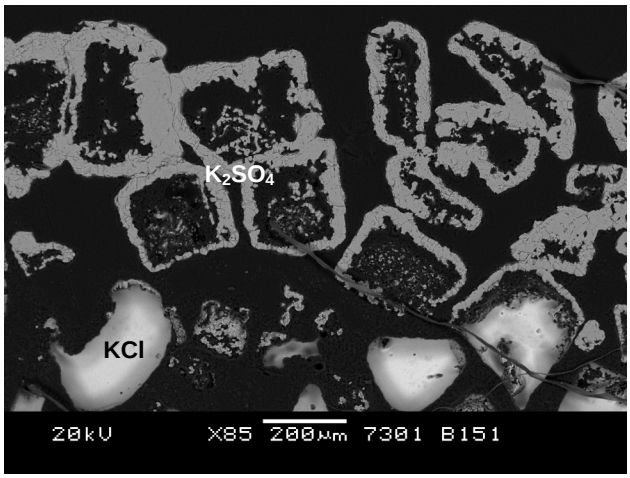

a) Gas composition: cofiring

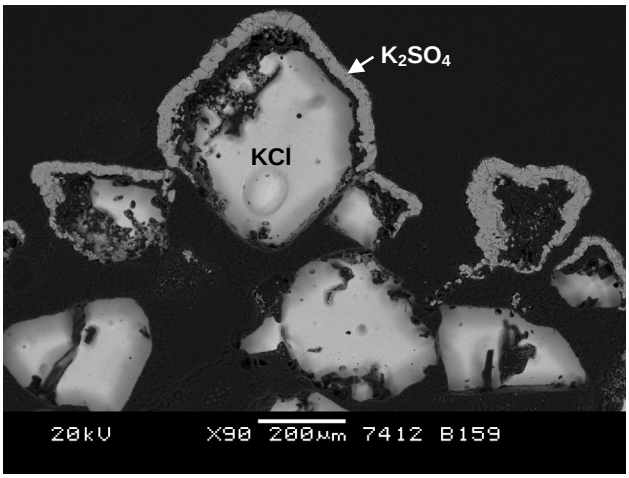

b) Gas composition: cofiring, low SO_2

Figure 9-25: SEM micrographs of cross sections of the top of initially 100% KCl deposits, after exposure at 560 °C, for 3 days.

SEM-EDX analysis of the specimen covered with a 100 % KCl deposit and exposed at 600 °C also showed a continuous band of selective chlorine corrosion (see Figure 9-27), but this was much thicker on average (~40 µm), and the thickness varied more within the cross-section of the sample. Mainly Cr was removed by this mechanism, leaving behind a skeleton rich in Fe and Ni. Small amounts of Cl (1–3 wt%) were detected within the band of selective corrosion. The SEM-investigation indicated that entire grains had been attacked, so the band of selective corrosion possibly also included grain boundary attack.

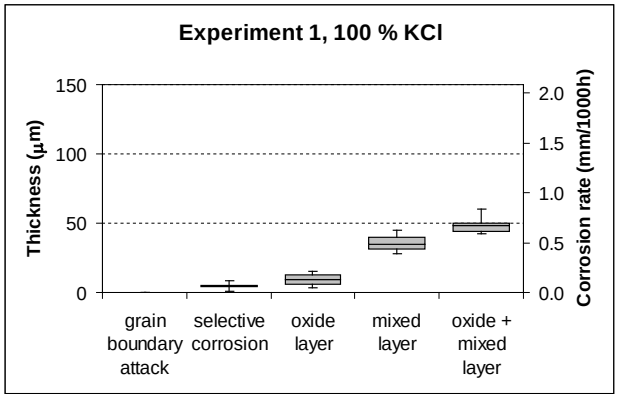

a) 100 % KCl, 560 °C

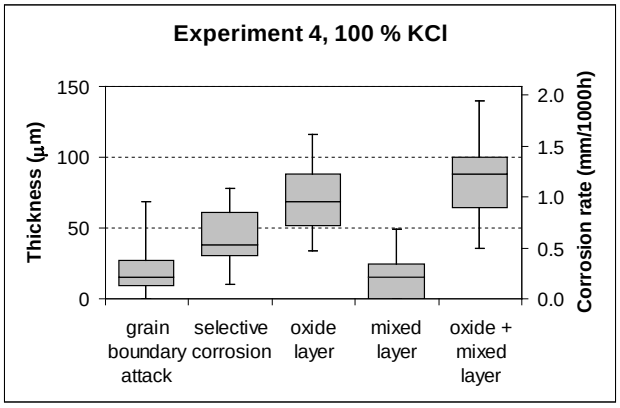

b) 100 % KCl, 600 °C

N.B.: Grain boundary attack was measured only in an area of ~350 µm wide, and underneath the selective corrosion

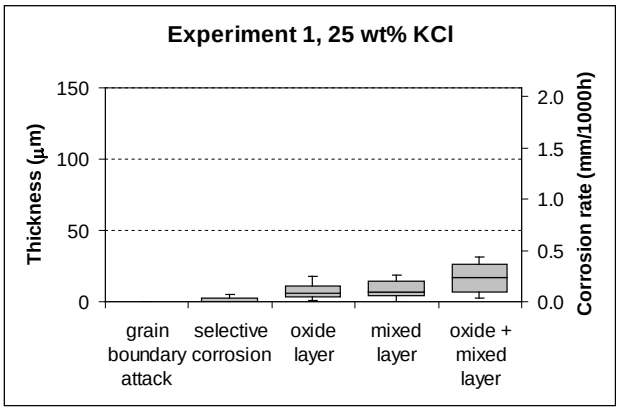

c) 25 wt% KCl , 560 °C

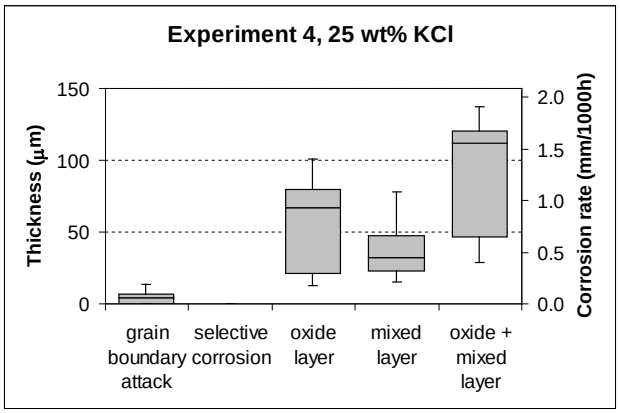

d) 25 wt% KCl, 600 °C

Figure 9-26: Effect of temperature on the corrosion attack, for specimens exposed to the straw-firing gas composition for three days.

Increasing corrosion attack with increasing temperature has also been observed in full-scale straw-fired boilers. [Montgomery et al., 2002b] reported that the corrosion rate of TP 347H FG approximately doubled at a metal temperature of 613 °C compared to at a metal temperature of 567 °C. At the higher metal temperature, selective removal of Cr and grain boundary attack was seen to a greater extent than at the lower temperature [Montgomery et al., 2002b].

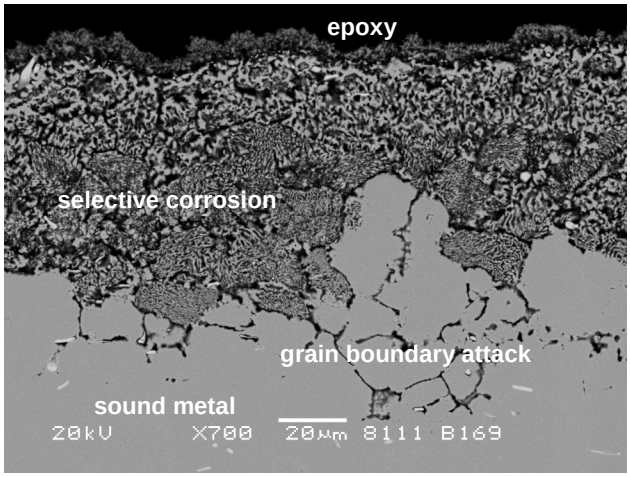

a) Internal corrosion attack

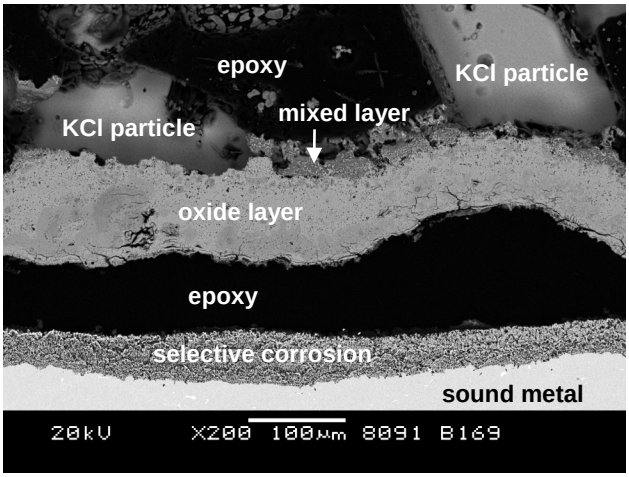

b) Corrosion products and part of deposit

Figure 9-27: SEM micrographs of a cross-section of a specimen covered with a 100 % KCl deposit after exposure to the straw-firing gas composition at 600 °C, for 3 days.

The effect of temperature on the degree of sulphation of KCl in the deposit is presented in Figure 9-28. The results show that the degree of sulphation is somewhat lower at 600 °C than at 560 °C, which corresponds to the lower equilibrium conversion of SO_2 to SO_3 at 600 °C compared to at 560 °C [Gudzinkas, 2007]. The fact that the corrosion attack is clearly enhanced at the higher temperature does not seem to correlate directly with the degree of sulfation in the deposit. Probably, a higher amount of molten phase formed and a faster diffusion of oxygen and chlorine at the higher temperature are more important for an enhanced corrosion attack [van Lith et al., 2009].

[Pedersen, 2009] conducted a series of measurements on test elements covered by 100 % KCl, 75 % KCl:25 % SiO_2, 100 % NaCl, and 80 % NaCl:20 % SiO_2 at 640 °C, concluding that test elements covered by a pure alkali chloride salt were significantly more corroded than those test elements covered by 75 % KCl and 80 % NaCl, respectively, i.e. diluted systems. Furthermore, [Pedersen, 2009] concluded that KCl causes more significant corrosion than NaCl, at 640 °C.

Co-firing conditions. The specimen covered with a pure KCl deposit and exposed to the co-firing gas at 600 °C showed very different corrosion morphologies within the sample, as well as compared to the sample exposed to 560 °C. In most areas of the sample, a rather uniform corrosion attack was seen, in the form of a ~5 µm thick band of grain boundary attack, with a ~25 µm thick oxide layer and a ~55 µm thick mixed layer, on top (see Figure 9-29b and Figure 9-30a). In contrast to the sample exposed to the straw-firing gas at 600 °C, the grain boundary attack was most likely the result of sulphidation, as some S (~2–8 wt%) but no Cl was detected at the grain boundaries. The oxide scale was divided into two parts (detached

from each other in most areas): the inner layer rich in Fe and Ni, whereas the outer layer was found to be rich in Cr but also contained some Ni. The mixed layer consisted not only mainly of Fe, K and S, but also contained some Cr.

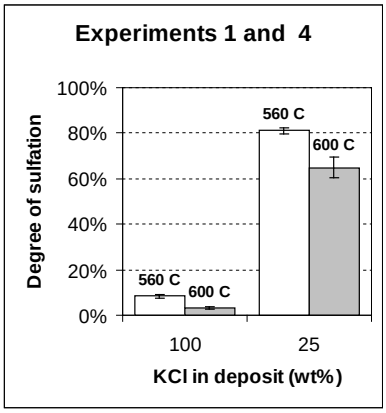

Figure 9-28: Effect of the temperature on the degree of sulfation of KCl in the deposit, for samples initially containing 100 % KCl and 25 wt% KCl – 75 wt% SiO_2 exposed to the straw-firing gas composition for 3 days. See Figure 21 for graph explanation.

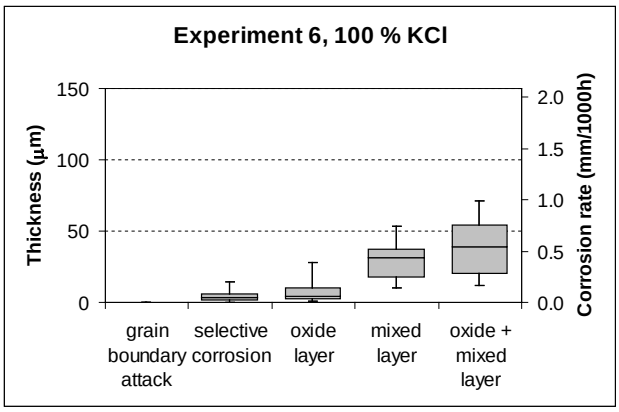

a) 100 % KCl, 560 °C

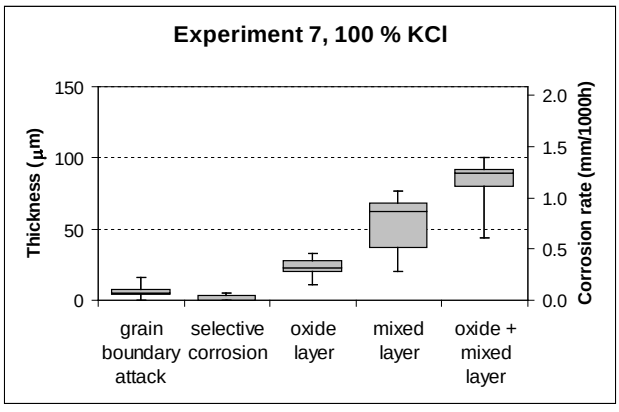

b) 100 % KCl, 600 °C

Figure 9-29: Effect of temperature on the corrosion attack for specimens exposed to the co-firing gas composition for 3 days.

Some areas in the mixed layer, close to the oxide layer were depleted in K and S, but contained some Cl (dark area in the middle of Figure 9-30a). At some of these locations, the mixed layers were detached from the oxide layer. The average oxide and mixed layer were thicker than observed for the sample exposed at 560 °C.

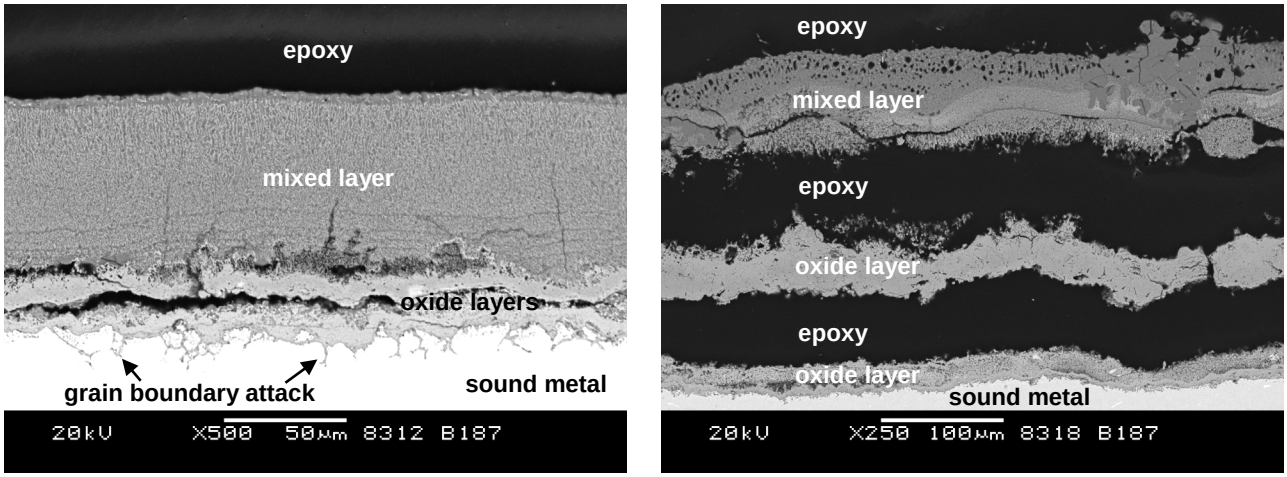

a) b)

Figure 9-30: SEM micrographs of a cross-section of a specimen covered with a 100 % KCl deposit after exposure to the co-firing gas composition at 600 °C, for 3 days.

At a few locations in the sample, selective corrosion of Fe was seen instead of the grain boundary attack. Some S (~1–6 wt%) and traces of Cl (<1 wt%) were detected in these areas.

9.4.8. Effect of Cat-Ion Mobility (KCl vs. NaCl, 600 °C)

Straw-firing conditions. Figure 9-31 shows the effects of salt composition (pure KCl vs. pure NaCl) on the corrosion attack for specimens exposed to straw-firing conditions at 600 °C. Large differences in both the internal attack and the thickness of the oxide and mixed layer can be seen.

First of all, the selective corrosion is more shallow and localised, for the specimen covered by NaCl. In the sample with NaCl, the areas of selective corrosion contained minor amounts of Cl and S (~1–3 wt%), whereas in the sample with KCl only Cl was detected. As for the sample with KCl, the sample with NaCl shows grain boundary attack, instead of selective corrosion in some areas of the sample, but the depth of attack was much less pronounced, and S was found at the grain boundaries [van Lith et al., 2009].

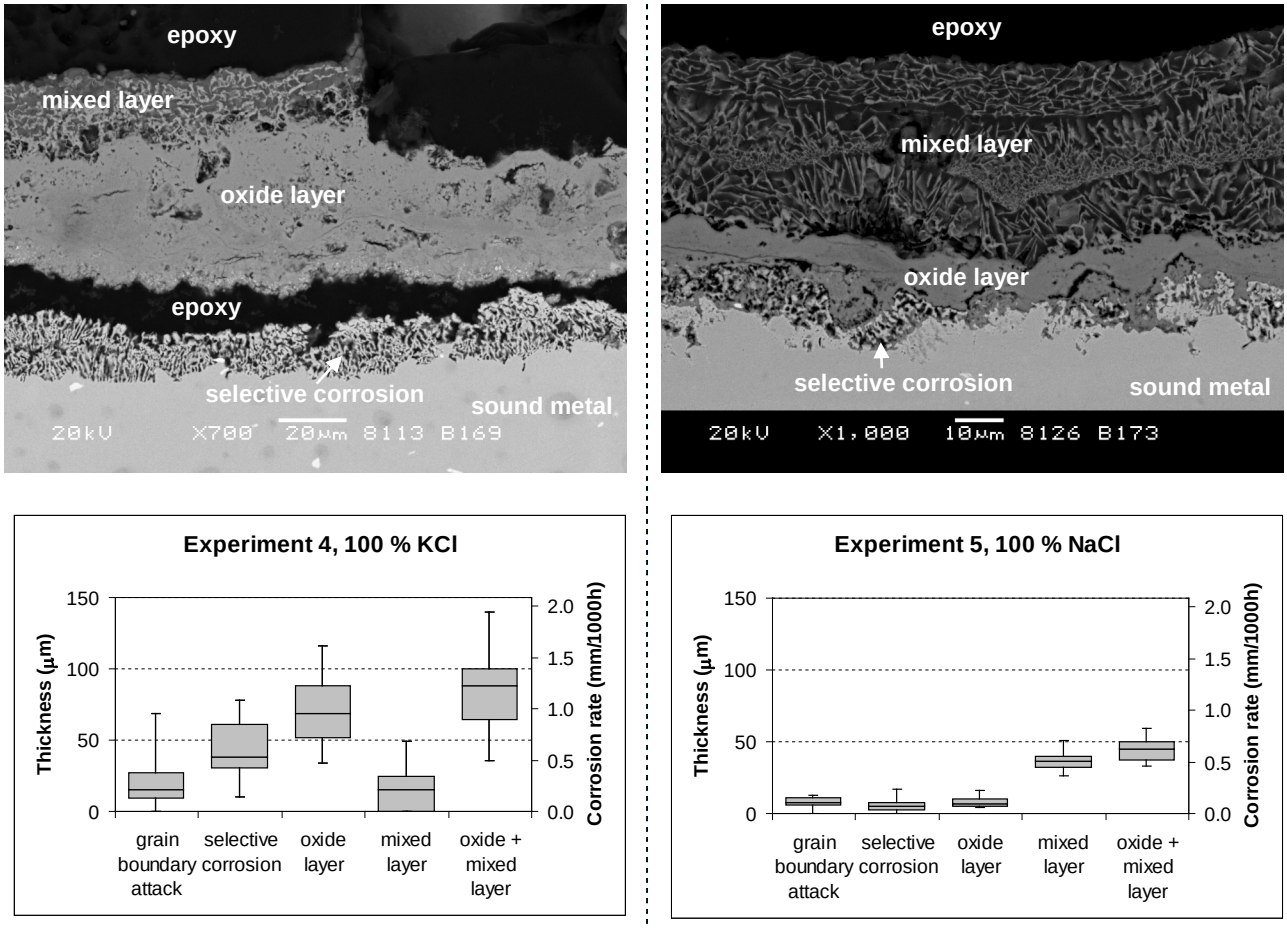

a) 100 % KCl

b) 100 % NaCl

Figure 9-31: Effect of salt composition on the corrosion attack, for specimens exposed to the straw-firing conditions at 600 °C for 3 days.

The oxide layer was much thinner, and showed less variation in thickness, for the sample with NaCl compared to the sample with KCl. Whereas the oxide layer of the sample with KCl was divided into a Cr-rich inner layer and a Fe-rich outer layer, both layers containing traces of Cl (<1 wt%) but no S, a divided oxide for the sample with NaCl did not appear, although high mounts of S (up to ~10 wt%) were locally present together with high amounts of Cr.

The mixed layer, on the other hand, was much thicker and of more uniform thickness for the sample covered with NaCl. The general morphology and chemistry of the mixed layer were found to be very similar for samples with KCl and NaCl: threads of mainly iron oxide in a matrix of potassium or sodium sulfate. However, in the case of NaCl, the iron oxide threads seemed straighter and better organised, and the mixed layer seemed to be composed of various layers on top of each other [van Lith et al., 2009].

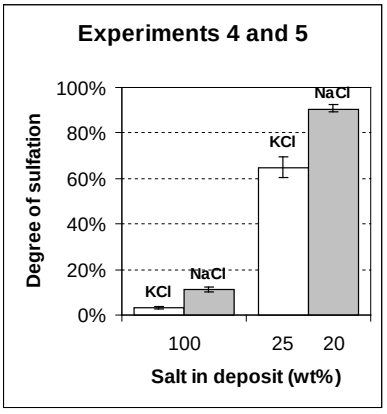

Figure 9-32: Effect of salt composition on the degree of sulfation of KCl in the deposit, for samples initially containing 100 % KCl / NaCl and 25 wt% KCl / 20 wt% NaCl (the remainder being SiO_2) exposed to the straw-firing gas composition at 600 °C for 3 days.

From Figure 9-32 it can be seen that the NaCl deposits were more sulfated than the KCl deposits exposed to the straw-firing gas at 600 °C. [Ozawa et al., 2003] also observed higher sulfation rates for solid NaCl than for solid KCl at both 450 °C and 650 °C, for particles with a mean diameter of 75–125 μm and a gas flow consisting of 0.9 % (v/v) SO_2, 5 % (v/v) H_2O, 10 % (v/v) O_2, and N_2 as balance. After two hours of exposure to this gas composition at 650 °C about 20 % of NaCl was sulphated, compared to about 10 % of KCl. The degree of sulphation was determined from the rate of HCl emission. Reasons for the much higher sulphation rates observed by [Ozawa et al., 2003] compared to this study are most likely the smaller particle size range and the higher concentration of SO_2 in the gas flow [van Lith et al., 2009].

Co-firing conditions. Large differences in corrosive behavior were also seen between the samples covered by KCl and samples covered by NaCl when exposed to the co-firing gas at 600 °C (see Figure 9-33). The sample with NaCl showed minor internal attack (maximum ~8 μm deep), but it was difficult to determine whether this was due to selective corrosion or grain boundary attack. Some S (~5 wt%) and traces of Cl (<1 wt%) were found at the corrosion front.

A very thin oxide layer (~3 μm) was observed for the sample with NaCl compared to the sample with KCl (~40 μm on average). This layer was rich in Fe, but in some locations an inner layer rich in Cr and S was also observed.

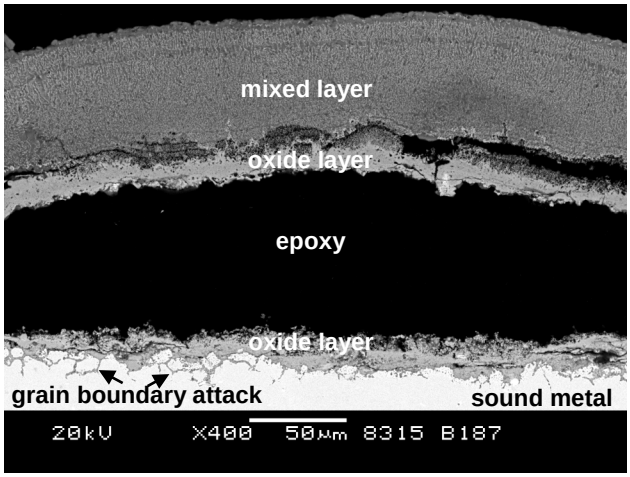

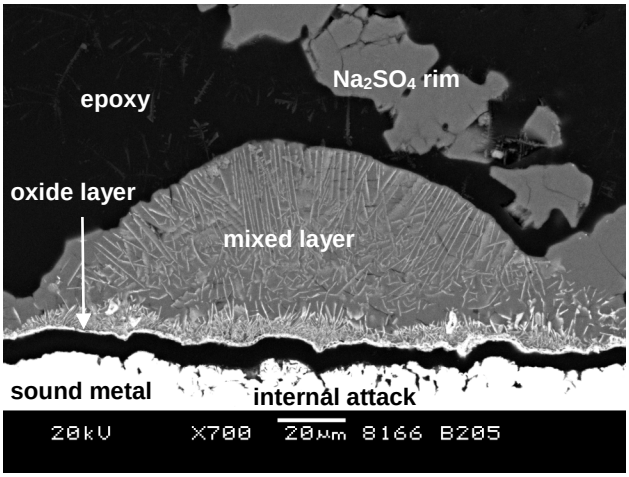

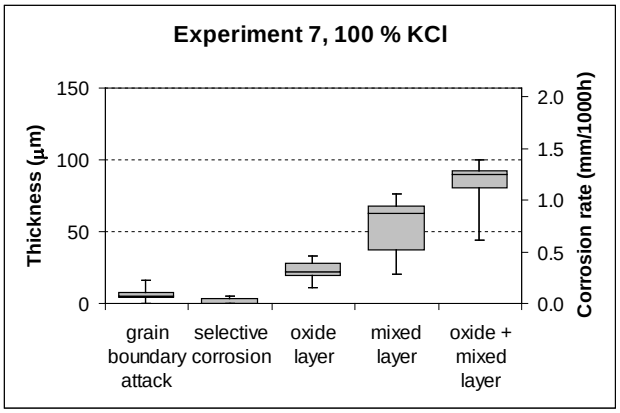

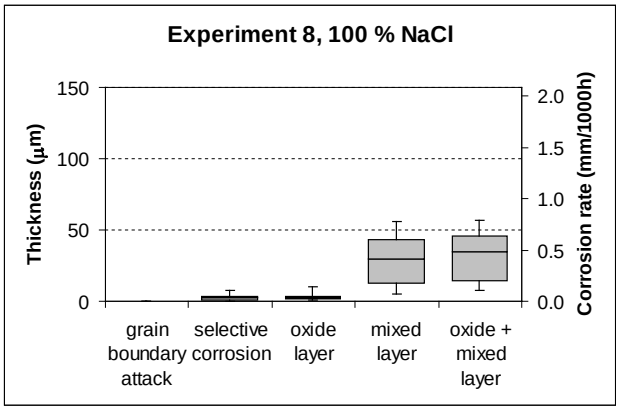

a) 100 % KCl

b) 100 % NaCl

Figure 9-33: Effect of salt composition on the corrosion attack, for specimens exposed to the co-firing gas composition at 600 °C for 3 days. See Figure 20 for graph explanation. N.B.: SEM micrographs have different scales.

Comparing Figure 9-34 with Figure 8-34, illustrates that the degree of sulfation of NaCl (similar to KCl) is higher when exposed to the co-firing gas compared to the straw-firing gas, most likely as a result of the higher SO_2 concentration. The degree of sulphation is higher for NaCl than for KCl in the co-firing case, as was also observed for the straw-firing case. SEM-EDX analysis of the deposits after exposure showed that NaCl (similar to KCl) is sulfated according to the "unreacted shrinking core model".

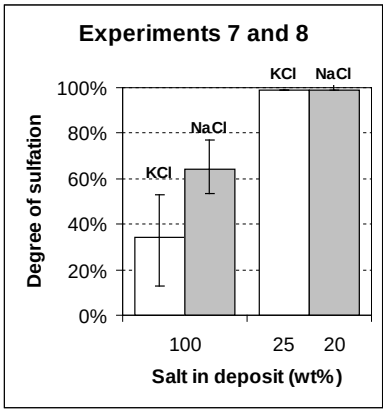

Figure 9-34: Effect of salt composition on the degree of sulphation of KCl in the deposit, for samples initially containing 100 % KCl / NaCl and 25 wt% KCl / 20 wt% NaCl (the remainder being SiO_2) exposed to the co-firing gas composition at 600 °C for three days.

The lab-scale corrosion tests reported in FORSKEL-5820 were performed under well-controlled conditions, simulating the conditions in straw-fired boilers and boilers co-firing coal and straw. The choice of metal composition, metal surface temperature, and gas compositions were based on knowledge and experience from full-scale biomass- and co-fired boilers in Denmark, defined in close dialogue with an industrial advisory group following the project. Other conditions such as the chemical and physical characteristics of the deposit, and the gas temperature and flow around the deposit are very complex and variable in full-scale boilers, and therefore had to be simplified in the lab-scale tests.

The following conclusions were drawn in FORSKEL-5820 [van Lith et al., 2009];

- It was found that an increase of the percentage of KCl in the deposit results in a more uniform and deeper internal attack on the specimen exposed.
- A characteristic mixed layer of iron oxide threads in the alkali sulphate matrix was formed under all conditions investigated. The thickness of this layer was strongly dependent on the experimental conditions. In the case of a 25 wt % KCl - 75 wt % SiO_2 deposit, a thinner mixed layer was formed compared to a pure KCl deposit, probably due to both the lower KCl content in the deposit and to the presence of SiO_2 particles providing surfaces for the K_2SO_4 grains (formed by the sulfation of KCl) to stick to.
- A deposit with small KCl particles sulfates to a lower degree than a deposit with large KCl particles, possibly because of a denser packing and lower bed porosity. Despite the significant influence on the degree of sulfation, the KCl particle size has minor effect on corrosion attack.
- Whereas SiO_2 particles are chemically inert, CaO particles react with HCl from the flue gas to form $CaCl_2$ affecting the corrosion mechanism. As a result, the corrosion rate was enhanced when CaO was present in the deposit compared to SiO_2.

- Samples exposed to a straw-firing, with and without HCl, showed that the presence of HCl in the flue gas is not essential for chlorine-induced corrosion to occur, particularly when a deposit containing KCl is present; rather, it enhances the corrosion rate.
- A higher concentration of SO_2 in the flue gas caused a higher degree of sulfation of KCl particles in the deposit. The sulfation of the KCl particles proceeds according to the "unreacted shrinking core model".
- Increasing the temperature from 560 °C to 600 °C results in local grain boundary attack for both straw-firing and co-firing conditions. In the case of co-firing conditions, the main mechanism for this type of attack is most likely sulphidation. In the case of straw-firing conditions, the selective corrosion is strongly enhanced at the higher temperature.
- NaCl had a considerably lower corrosion potential than KCl at all temperatures considered i.e. 560, 600 and 640 °C. For both straw-firing and co-firing conditions, the internal attack was much less severe and the oxide and mixed layers are much thinner in the presence of a NaCl deposit, as when compared to a KCl deposit.

9.5. Summary

A serious amount of work has been conducted in order to address problems in relation to corrosion in systems fired fully or partly (i.e. co-fired) with straw, both in the laboratory, under rather well-controlled conditions and in full-scale boilers, applying either cooled deposition/corrosion probes or cutting out sections of real tubes or test sections of superheaters.

The composition, structure and build-up over time of a deposit on a superheater tube in a full-scale boiler are dependent on many factors such as the boiler type and design, the temperature profile within the boiler and the composition of the fuel feedstock. Both short-term probe deposits and mature deposits on superheater tubes have been studied in grate-fired boilers utilizing 100% straw [Nielsen, 1998; Jensen et al., 2004]. The probe deposits from Rudkøbing CHP contained large amounts of K and Cl (the sum being 40-80 wt % of the deposit), and to a lesser extent, Si, Ca, and S. SEM-EDX analysis revealed that the deposits consisted of a layer of almost pure KCl close to the metal surface, followed by a very porous KCl-rich layer, and an outer layer consisting of fly ash particles rich in Si and Ca, and glued together by KCl [Nielsen, 1998]. The KCl-rich inner layer was found to be thicker and denser on the probe with a metal temperature of 550 °C, compared to the 460 °C probe. Mature deposits on corrosion probes (exposed for 450-3000 h) also consisted mainly of KCl and fly ash particles, but in some cases a layer of K_2SO_4 was also present, either next to the metal oxide on top of a KCl-Fe_xO_y layer or in between two KCl-Fe_xO_y layers. Studies at Masnedø CHP showed that deposits formed on probes at metal temperatures of 540-620 °C and exposed for six hours, consisted mainly of KCl with iron oxide threads (see [Nielsen, 1998]) whereas mature deposits consisted of various

layers, with the inner layer being rich in K_2SO_4 and iron oxide and the outer layers being rich in KCl.

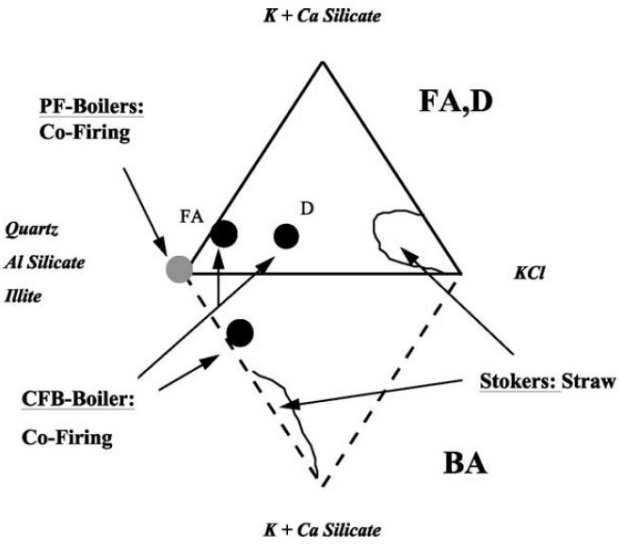

Figure 9-35: CCSEM compositional data for bottom and fly ashes, as well as probe deposits from wheat straw-fired grate boilers, a coal-straw co-fired CFB boiler, and a coal-straw cofired PF-boiler, illustrated in a triangular diagram consisting of: (1) quartz, Al-silicates, and illite; (2) K+Ca silicate; and (3) KCl. The top triangle provides the composition of fly ashes (FA) and probe deposits (D) and the bottom triangle contains the same information for the bottom ashes (BA). Source: [Frandsen et al., 1997].

Figure 9-35 shows a comparison of the compositions of probe deposits from straw-fired grate boilers, a coal-straw fired CFB-boiler, and a coal-straw cofired PF-boiler, based on computer controlled scanning electron microscopy (CCSEM) analysis [Frandsen et al, 1997]. The figure highlights that probe deposits from the coal-straw co-fired PF boiler are rich in aluminosilicates (often mixed with small amounts of Ca and K) and K_2SO_4.

No KCl was observed in the deposits, when co-firing coal and straw. This phenomenon was also observed in the Grenaa CFB-boiler, although in this case the probe deposits in the Grenaa boiler were enriched in Cl. The presence of KCl in a CFB boiler deposit may be due to the fact that combustion takes places at a lower temperature (~850 °C) compared to a PF-boiler (~1400-1700 °C). Mature deposits, on the other hand, contained very little KCl (<0.5 wt %), indicating a sulfation of the KCl in the deposit over time [Hansen et al., 1998]. The addition of limestone or lime to the bed in a CFB boiler (for sulfur capture) can result in an increased amount of Ca-particles in CFB deposits [Miles et al., 1996].

Thus, the compositions of superheater deposits are thus not only strongly dependent on boiler design and combustion conditions, but also change over time. Simplifying the deposit compositions in the lab-scale tests to pure KCl or mixtures of KCl-SiO_2 or KCl-CaO, and exposing these for only three days, will most likely result in higher corrosion rates compared to what will occur in full-scale boilers.

Another limitation of the lab-scale corrosion tests is that they are usually performed under isothermal conditions. In a full-scale boiler, the flue gas temperature is higher than the metal temperature of the superheater tube, meaning that a temperature gradient exists within the deposit. Lab-scale studies have been reported whereby a temperature gradient within the deposit was taken into account by exposing the specimens in a furnace in which the metal was air cooled [Kawahara et al., 2002]. These studies indicate that the presence of a temperature gradient results in a 2-10 times higher corrosion rate, depending on the environment.

9.5.1. Effect of Alloy Composition (Cr-Content)

In conventional coal-firing, alloys with high Cr-content causes lower corrosion rates however the opposite is the case for straw-firing plants. Results from three separate investigations at straw-fired plants [Henriksen et al., 1995; Larsen and Henriksen, 1996; Montgomery et al., 2000a] testing a variety of steels, revealed that, at high temperatures, high-Cr steels were rapidly attacked.

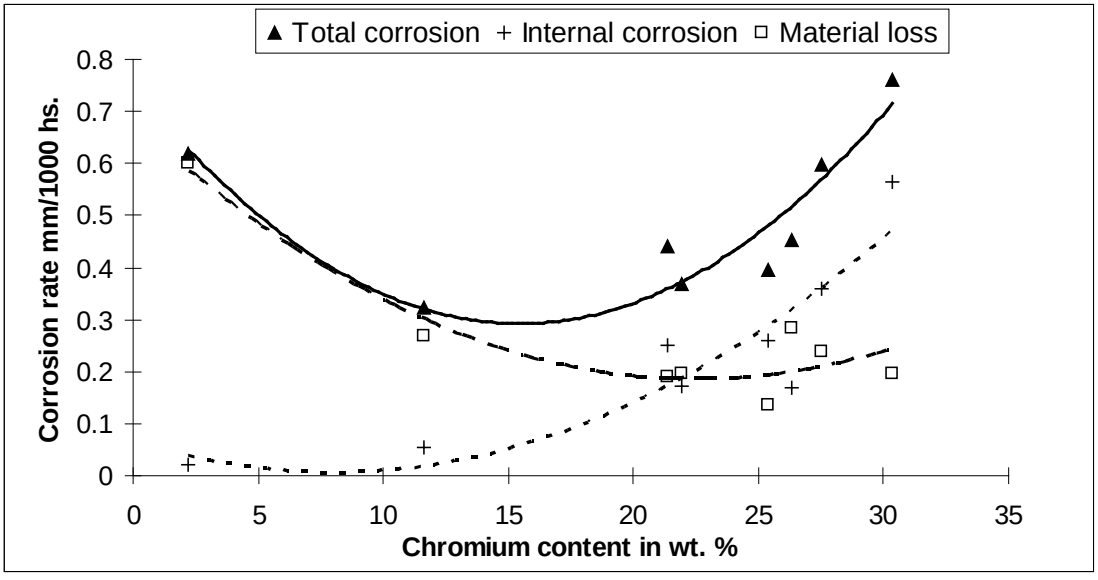

Figure 9-36: Corrosion rate with various chromium contents in the alloys at approx. 580°C. Source: [Montgomery et al., 2002a].

Figure 9-36 shows data on total corrosion rate, as a function of the Cr content in the metal for a range of alloys from a 2.5 % Cr to a 30% Cr steel [Montgomery et al., 2000a]. The low-Cr steels exhibit a high material loss, whereas the high-Cr steels are characterised by severe internal attack in the form of chromium depletion. These results indicate a minimum total corrosion rate of steels at an intermediate Cr content of 12-18% Cr [Montgomery and Karlsson, 1999].

9.5.2. Effect of Metal Surface Temperature

Selective removal of Cr and Fe from an alloy produces a porous structure and often also causes grain boundary attack. For austenitic steels, grain boundary corrosion is a precursor to corrosion within the grains. The corrosion products formed are Cr oxide and Fe oxides, which are present at the surface of the specimen. In many cases, Ni is also present in the outer corrosion product, as non-reacted nickel.

In Figure 9-37, the corrosion rate of 12-18% Cr steels is plotted against temperature [Montgomery et al., 2002a,b]. It is clearly seen that the rate of corrosion increases with the increasing temperature of the metal surface.

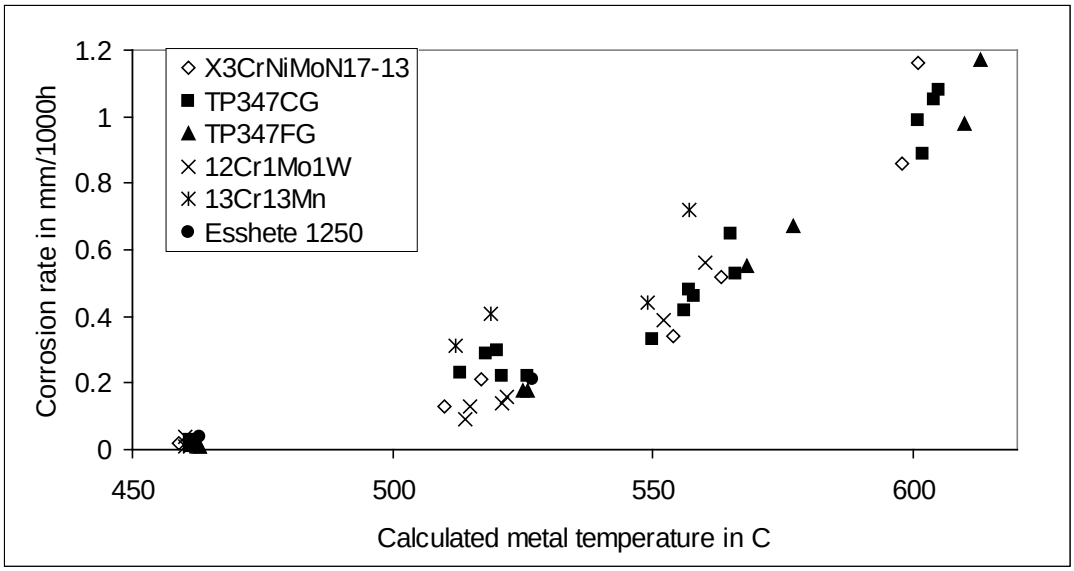

Figure 9-37: Corrosion rate of specimens in one investigation at the Masnedø straw-fired CHP-plant relating metal temperature to corrosion rate. Source: [Montgomery et al., 2002a,b].

For the austenitic alloys investigated, a gradual change in the corrosion morphology as a function of temperature was observed. Corrosion rates were modest at 460°C, where a protective Cr-rich Fe oxide scale was formed. With increasing temperatures of up to 525°C, the corrosion rates became more linear with respect to temperature. At around 500-520°C,

both grain boundary attack and protective oxide scales were observed for the same specimen. Above this temperature, Cr-depletion and grain boundary attack were always observed [Montgomery et al., 2002a,b].

9.5.3. Why Corrosion Rates are Lower in Co-Fired Systems

Co-firing of coal and straw in suspension at straw shares of 10-20 % on a thermal base removes the danger of catastrophic Cl-induced corrosion, as was observed at MKS1. The corrosion rates observed in co-firing systems are much lower than in straw-fired units, and are closer to the corrosion rates observed in coal-fired units. For comparative purposes, the corrosion rates for TP347H FG have been plotted in an Arrhenius-type plot (see Figure 9-38 assuming parabolic corrosion kinetics [Montgomery et al., 2002a,b]):

$$x^2 = 2 \cdot k_P \cdot t \qquad (9\text{-}7)$$

where x is the thickness of the corroded material and t is the time of exposure.

Parabolic kinetics were assumed for all three types of corrosion, although it was apparent from previous work that linear kinetics were more applicable for corrosion in 100 % straw-fired boilers at high temperatures [Montgomery and Karlsson, 1999]. It is clear from Figure 8-40 that the corrosion is significantly lower in co-fired plants compared to straw-firing on a grate.

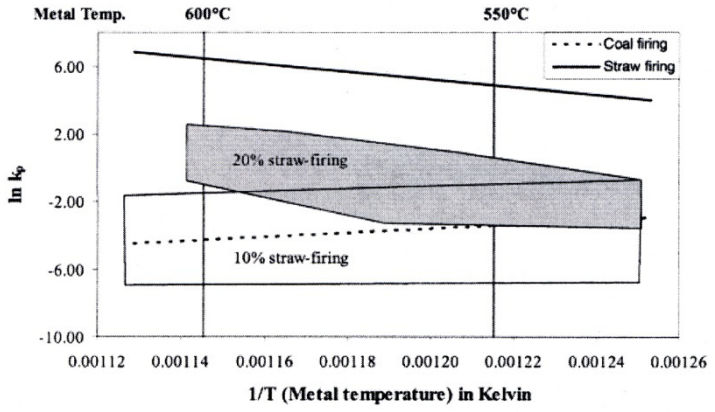

Figure 9-38: Arrhenius plot showing the corrosion of TP347H FG in co-firing compared to pure coal- and straw-firing, respectively. Source: [Montgomery et al., 2002a,b].

The most important outcome of the MKS1 corrosion investigation was that there was no sign of chlorine found in the deposits within the corrosion products or at the metal-oxide scale interface. This shows that KCl released from the straw, reacts with Al and Si in the coal ash, forming non-corrosive K-Al silicates and HCl in the gas phase [Andersen, 1998]:

$$2KCl + Al_2O_3 + 6SiO_2 + H_2O \rightarrow K_2O.Al_2O_3.6SiO_2 + 2HCl \qquad (9\text{-}6)$$

$$2KCl + SO_2 + H_2O \rightarrow K_2SO_4 + 2HCl \quad (9\text{-}2)$$

Formation of HCl(g) does not pose nearly as great a corrosive potential as the deposition of KCl followed by subsequent sulfation at the metal-oxide scale surface. An increase in the straw fraction fired caused a higher local concentration of KCl in the combustion chamber [Wieck-Hansen et al., 2000].

The corrosion may, though, be dependent on the coal type. Especially, coal types with a considerable content of water soluble alkali may provide a higher risk of increased corrosion rates than observed in the tests at MKS1.

9.5.4. Lab-Scale Corrosion Studies

[Nielsen et al., 1999] showed in a lab-scale study that metal samples covered by KCl particles, and then exposed isothermally at 550 °C to an SO_2-laden gas, after one month had a thin layer (5 – 20 μm) of K_2SO_4 with iron threads included on top of the oxide scale. This layer resembled the structure of the inner layer found in mature deposits from the Masnedø CHP-boiler. For samples exposed for only one week in the oven, the formation of the characteristic K_2SO_4-layer had barely started, and at this point small KCl inclusions were still present in the layer [Nielsen et al., 1999].

The following mechanism for the formation of a K_2SO_4-layer on top of the oxide scale was proposed by [Nielsen et al., 2000b]:

1. Initially, KCl deposits on the superheater surface for example by inverse sublimation of gaseous KCl, KCl(g) → KCl(s). The evidence of such a layer has been reported e.g. at the Maribo-Sakskøbing straw-fired CHP-boiler.
2. KCl reacts with Fe_xO_y, $FeCl_2$, or K_2SO_4, to form a molten phase. This reaction is likely to happen as KCl forms eutectic mixtures with $FeCl_2$ (at 355 °C), K_2SO_4 (at 690 °C) and possibly also Fe_xO_y, even though the latter has not been verified.
3. The molten KCl reacts with gaseous SO_3, and forms K_2SO_4. Gaseous SO_3 may be present, since Fe_xO_y is known to catalyse the oxidation of SO_2 to SO_3 [Harlow, 1944, 1949; Reid, 1971].

Potassium chloride, KCl, forms a melt with K_2SO_4 and different Fe components (Fe_XO_Y, $FeCl_2$) adjacent to the oxide scale. The sulfation reaction occurs rapidly in the melt, releasing HCl, or Cl_2, close to the metal surface. Chlorine gas has the ability to diffuse through the oxide scale and react with Fe to form volatile iron chlorides ($FeCl_2$, $FeCl_3$), which are thermodynamically stable at the interface between metal and the oxide scale, where a very low partial pressure of O_2 exists. They then diffuse out through the scale, and oxidize as they reach

areas with higher partial pressures of oxygen. Thus, iron oxides will be formed either on top of the metal oxide layer or in the dense mixed layer.

This mechanism can explain the shift in corrosion behaviour with temperature observed in full-scale corrosion tests [Larsen & Henriksen, 1996].

The corrosion studies presented in this chapter have produced some ideas and suggestions for further work on this issue [van Lith et al., 2009]:

1. The effects of oxide composition (e.g., using Al_2O_3 or CaO instead of SiO_2) on the sulfation and corrosion behavior need further attention. Tests with fly ashes from straw-fired and co-fired boilers instead of synthetic deposits should be carefully conducted.
2. The effect of temperature: both a dynamic change in the gas temperature in the reactor, differences between gas and metal temperatures and/or dynamic changes in the gas composition e.g. changes in [SO_2] or [HCl] vs. time as experienced in real plants are factors that need further attention via systematic lab-scale investigations.
3. The effect of different materials also requires further investigation. In FORSKEL-5820, a common superheater material was picked, based on experience from e.g. SSV4 and AVV2, but there may be other relevant materials or coatings to test.
4. It may also be worth studying the contact between the synthetic deposits and the test elements/specimens further. In EFP-96 and FORSKEL-5820, powdery deposit were applied, but deposits formed by evaporation of water from an aqueous solution of the relevant salts or a salt melt may provide an even tighter contact, and thereby probably a changed corrosion pattern.

9.5.5. Remedial Measures to Minimize Corrosion

Remedial measures involve reducing the temperature of the flue gas before the entry into the final superheater, and assuring turbulent conditions in the gas stream, in order to maximise the sulfation of the alkali chlorides in the gas stream, before contacting the hot tube surfaces. When these changes cannot be accomplished through modification operation of the boiler design changes are required, such as installing a sufficiently large evaporator section before the final superheater [Wright and Krause, 1996].

In case it is not possible to install screen tubes for the existing final superheater, it may be possible in some boilers to re-route the steam/water flow in the superheater section so that the coolest tubes comes into contact with the hottest gas. An example of this principle was the conversion of the original final superheater into an evaporator section, and to subdivid the original primary superheater to become the final superheater, as well as the primary superheater, in a German combustor [Schirmer, 1984]. This change resulted in a reduction in

flue gas temperature from 760 to 600 °C as it passed through the new evaporator. The tube wall temperature of the new evaporator was 270 to 275 °C, compared to 300 to 435 °C as the final superheater. Furthermore, the new final superheater had a wall temperature of 325 to 435 °C, while the flue gas temperature at this location was 450 to 600 °C [Wright and Krause, 1996].

Another approach is to install tubes of corrosion-resistant alloy in locations prone to attack. A number of boilers in the U.S. have several rows of superheater tubing made from Alloy 825. Corrosion in the convection zone may be aggravated by erosion from soot blowing, particularly when the cleaning medium is steam [Wright and Krause, 1996]. Sootblowing is thought to remove the existing scale/deposit, thus stripping the tube of a potential barrier to the corrosive reaction and exposing fresh metal to attack at a higher rate. Tubes adjacent to soot blower lanes are protected by shields, as in coal-fired utility boilers. Half shields, which cover only one face of the tube, have been used as well as full shields which completely encase the tubes. In many cases, these shields have been made from Type 309 stainless steel, but trials have been made with other alloys as well, including Alloy 625 and 825 [Wright and Krause, 1996].

In summary, the remedial measures credited with reducing corrosion of the superheater and other convection pass tubes in WtE boilers include those that [Wright and Krause, 1996];

- Minimize particle carry over from the combustion zone;
- Reduce the temperature of the flue gas entering the convection tube banks to a maximum of 760 °C. If this cannot be achieved because of furnace size limitations, the use of several rows of screen tubes (evaporator tubes) ahead of the superheater may be effective;
- Reduce the metal/steam temperature of the leading tubes in the first rows that contact the flue gas;
- Protect the first 2 – 4 rows of the final superheater, using devices such as metallic shields or ceramic protective tubes, although these require extensive maintenance to maintain attachment and alignment;
- Replace upstream rows of superheater tubes with a more resistant alloy, such as Alloy 825;
- Protect areas where directional changes in the flue gas flow occur, usually by shields or refractory coverings;
- Protect tubes adjacent to soot blower lanes predominately using shields;
- Replace soot blowers with mechanical rappers or sonic horns.

Chapter 10:

USE OF ADDITIVES TO MINIMIZE CORROSION AND AEROSOL FORMATION

An often applied option to minimize deposition and/or corrosion is injection of an additive. Basically, two types of additives are available: [a)] one which will affect the gas phase alkali-S-Cl and (thereby) the aerosol chemistry in the system, and [b)] another which deposit together with the coarse mode fly ash particles, but possess chemical and physical characteristics which will inhibit sintering of the deposit. The first type of additive may be useful in systems fired with biomass, where the initial deposit process is caused mainly by volatile alkali Cl- and S-species. Use of an additive may fix these volatile alkali species or affect the gas phase K-Cl-S chemistry and the aerosol formation, significantly.

This chapter provides a list of useable additives for the fixation of volatile alkali metal species or for influencing the gas phase K-Cl-S chemistry as well as a description of the chemical mechanism by which each of the additives work. In addition, Danish experiences of the influence of additives on aerosol mass loading and/or deposit chemistry profiles, are presented.

10.1. Potential Additives for Use in Straw-Fired Boilers

An alkali getter is defined as a fixed bed of granular, inorganic, solid additive material. The ideal additive material for a getter should possess the following characteristics:

- Rapid rates of adsorption;
- High load capacity;
- Chemical transformation of the alkali into a less corrosive form;
- Irreversible adsorption in order to prevent release of adsorbed alkali during process fluctuations;
- Cheap, and 'easy-to-get' in significant quantities, and;
- The solid product from the getter after exposure, should be easy to regenerate/reuse.

The working principle is that alkali compounds are removed from a gas stream by adsorption on to the surface of additive particles in the getter. Alkali gas molecules are transported across the boundary layer from the bulk flow to the solid surface, followed by attachment to a suitable

site on the surface of the additive. The rate of adsorption is limited by the slower of the two steps: [1)] molecular transport and [2)] attachment (adsorption) of gas molecules.

In order to understand the operational behavior/mechanism of an additive, one has to distinguish between two types of molecular attachment to a solid material: [a)] physical adsorption and [b)] chemisorption.

Physical adsorption (physisorption) is characterized by:

- Being dominated by Van der Waals or dispersion forces, ie. weak intermolecular interactions arising from dipole-dipole or induced dipole attractions;
- Approaches equilibrium fast;
- Is in general reversible, i.e. adsorbed alkali molecules may be released from the surface again;
- Hysteresis may occur, due to changes in the pore structure of the additive;
- The absorption energy, ΔH_{abs} ~ 4 - 40 kJ/mol is equal to the condensational energy (~ΔH_{cond}): i.e. physical adsorption is very quick, and;
- It may form several layers of adsorbed gas molecules on a solid surface, i.e. physisorption approaches condensation.

In contrast, chemical adsorption (chemisorption), is characterized by:

- A much stronger interaction than physical adsorption;
- Displays a chemical selectivity, particularly to solid and gas species in terms of chemical forces and orientation;
- Occur only as a monolayer;
- The chemisorption energy,$\Delta H_{chemsorp}$ ~ 40 - 600 kJ/mol is of the same order of magnitude as the reaction energy (~ ΔH_{reac}): i.e. chemisorption may be slow and may display the rate behavior characteristics of processes dependent on activation energy, and;
- Chemisorbed gases may be difficult to remove and may leave the solid surface altered.

At this point, it is worth noting that the main adsorption mechanism on Al-based additives is physisorption, while on Si-based additives it is chemisorption. Thus, in case a regenerative additive is needed, an Al-based material should be applied. On the other hand, if a strong

fixation of the gaseous alkali metal species is needed, e.g. in order to avoid leaching by water in a subsequent disposal of the additive, an Si-based material should be used.

There are in principal two practical ways of applying an additive:

- Passing the alkali-laden flue gas through a fixed bed of an appropriate additive (alkali getter) - this is the common technique applied to purify flue gases, in combined cycle power generation, or;

- Injecting the additive with the fuel or higher up in freeboard of the furnace for in-situ capturing of alkali species during combustion. This technique is frequently applied in pulverised coal combustion systems and grate-fired furnaces.

In the literature, by far most of the references deal with the first type of application, i.e. passing an alkali-laden gas through a fixed bed of additive. There is, though, a certain amount of data available on the application of additives under suspension-firing conditions i.e. conditions with a low mass loading of additive in the gas. Danish experiences on this will be outlined in the last part of this chapter.

10.2. Investigations of Alkali-Ash Reactions

[Steenari and Lindquist, 1998] investigated alkali-ash reactions by adding kaolinite (an Al-Si-based additive) or dolomite (a Ca-Mg-based additive) to samples of rape, wheat and barley ash under well-controlled lab-scale conditions. It was found that kaolinite reacted with K-salts from the straw ashes, forming high-melting K-Al silicates. Calcium from dolomite reacted with Si from wheat and barley ashes, not the rape ash. No interaction between dolomite and K species from the straw ashes was detected.

[Kyi and Chadwick, 1999] tested a number of additives for their efficiency in binding alkali metals released from lignite coals. They showed, by ashing coal samples in air and subsequent thermochemical analysis, that minerals with high Al and Si content were most effective in retaining NaCl, while minerals with only a high content of either Al or Si were often poor in their ability to retain NaCl.

Although interesting from a general ash formation point-of-view, the contact pattern between the ash/alkali species and the additive material in these investigations is far from being close to the conditions in for example a grate or a suspension-fired boiler. Thus, no further details will be provided on these investigations.

10.2.1 Investigations in Fixed Bed Systems

The fixed bed application of alkali getters have traditionally be divided into two types: [a)] **thermogravimetric methods** in which alkali capture by a single particle, or a small amount of particles, is monitored over the duration of time, and [b)] **packed bed methods** in which alkali capture is measured, by monitoring the alkali content of the gas exiting packed bed, and/or analyzing sorbent material at the completion of the test.

The thermogravimetric approach has mainly been used to study the effect of;

- Carrier gas flow rate (i.e. contact/residence time);
- Alkali concentration in the carrier gas;
- Carrier gas composition;
- Additive temperature;
- Additive particle size, and;
- To obtain data suitable for modeling of rate kinetics of single particle alkali sorption.

Packed bed methods have mostly been applied to investigate the effect of;

- Additive temperature;
- Superficial gas velocity;
- Carrier gas moisture content and composition;
- Partial pressure of SO_2 (g);
- Release of alkali species from as-received and regenerated getters, and;
- Displacement of alkali inherent in the getter material by alkali from the gas stream

The most common carrier gases applied, include: [1)] various simulated flue and producer (gasification) gases (sfgs), [2)] inert gases (most often Ar, N_2), [3)] methanol combustion products and [4)] air.

A list of materials tested as alkali additives in fixed bed reactor configurations, was provided by [Turn et al., 1998], who published a review on additives for fixed bed alkali getter systems, in biomass gasifier combined cycle power generation applications, see Table 10-1. The most often used Al-Si-based additives investigated are kaolinite, bauxite, diatomaceous earth and emathelite. The chemical composition of these is listed in Table 10-2.

Literature source:	Materials tested as alkali sorbents:
[Lee & Johnson, 1980]	Alundum, Diatomaceous Earth, Silica Gel, Burgess #10 Pigment, Attapulgus Clay, Activated Bauxite
[Punjak & Shadman, 1988], [Punjak, 1988], [Punjak et al., 1989]	Kaolinite, Bauxite, Emathelite
[Luthra & Leblanc, 1984]	Activated Bauxite, Activated Carbon
[Jain & Young, 1985]	Diatomaceous Earth, Activated Bauxite, Attapulgus Clay, Fullers Earth, Silica Gel, Dolomite, Calcined Dolomite, Alumina, Nortons Catalyst
[Mulik et al., 1981]	Kaolinite, ash from low-temperature coal char, ash from a high-temperature coal gasifier

Table 10-1: Materials tested as sorbents for alkali removal from flue gases. Source: [Turn et al., 1998].

Component:	Bauxite	Emathelite	Diatomaceous Earth	Kaolinite
SiO_2	7.0	73.4	92.0	52.1
Al_2O_3	88.3	13.9	5.0	44.9
Fe_2O_3	1.2	3.4	1.0	0.8
TiO_2	3.5	0.4		2.2
CaO		5.0	0.5	
MgO		2.6	0.5	
K	0.00	0.89	0.07	0.13
Na	0.01	0.14	0.93	0.02

Table 10-2: Composition of as-received sorbents, %(w/w). Source: [Turn et al., 1998].

10.2.1.1. Activated Bauxite

Activated Bauxite consists of app. 80 %(w/w) Al_2O_3 and 10 %(w/w) SiO_2 + impurities (see Table 10-2). The additive has the following characteristics [Punjak, 1988; Punjak et al., 1989]:

- The alkali adsorption on Bauxite is sensitive to the gas phase alkali concentration (increased adsorption with increased alkali level);
- KCl, NaCl, and K_2SO_4 are captured with equal efficiencies by Bauxite;
- Increased additive temperature decreases final additive alkali loading;

- The rate of adsorption is independent of superficial gas velocity above 25 cm/s;
- 99 % removal of gas phase alkali has been reported at gas-additive contact times of > 0.2 s using the fixed bed approach;
- At 850 °C and 10 bar, less than 2 %(w/w) alkali present in as-received Bauxite was found to be released to the gas phase, and;
- Bauxite is due to its high content of Al_2O_3 (i.e. main adsorption mechanism is physisorption), regenerative, when using boiling water (up to 10 % of the sorbent is lost as a result of the regeneration process).

The most likely chemical reaction to occur between Bauxite and alkali chloride, MCl, is, according to [Punjak, 1988]:

$$2MCl(g) + Al_2O_3 + H_2O(g) \rightarrow M_2O.Al_2O_3 + 2HCl(g) \quad (10\text{-}1)$$

10.2.1.2. Emathelite

Emathelite is a Si-based additive, containing approximately 70 %(w/w) SiO_2, 10 % Al_2O_3, ~ 1 % K_2O, ~0.1 % Na_2O + impurities (see Table 9-2). It has the following characteristics, as reported in the literature [Punjak, 1988; Turn et al., 1998]:

- Ca present in the additive is soluble in HCl, while all other elements, ie. Na, K, Si, Al, Mg, Fe and Ti, are HCl-insoluble;
- The loading capacity of emathelite is ~ [150 - 190 mg Na/g sorbent];
- Na is present as feldspar, albite, or a glassy Na-silicate after capture;
- More than 90 % of the K present in as-received emathelite is vapourized during exposure to a NaCl-laden gas stream;
- H_2O (g) is an essential reactant in the absorption mechanism of NaCl on emathelite;
- The adsorption process is temperature-independent in the range [700 - 900 °C], and;
- The adsorption process is initially (< 4h), dependent on the gas phase alkali concentration

For emathelite, [Turn et al., 1998] suggest the following chemical reaction with alkali chloride, MCl(g):

$$2MCl(g) + Al_2O_3.SiO_2 + 5SiO_2 + H_2O(g) \rightarrow M_2O.Al_2O_3.6SiO_2 + 2HCl(g) \quad (10\text{-}2)$$

In this reaction, please note that emathelite is a composed mineral with a certain content of eg. $Al_2O_3.SiO_2$(cr) and SiO_2(cr). So the reaction of these two species is very likely.

10.2.1.3. Diatomaceous Earth

Diatomaceous Earth is a mineral composed of 92 %(w/w) SiO_2 and 5 % Al_2O_3 + impurities (see Table 9-2). The characteristics reported in the literature [Punjak, 1988] are:

- NaCl, KCl, K_2SO_4 are equally well adsorbed by diatomaceous earth;
- The maximum alkali loading capacity of diatomaceous earth is reported to be: 18 mg Na/ g sorbent;
- The rate of alkali removal is independent of superficial velocities above 25 cm/s, and;
- 98 % alkali removal efficiency is reported for gas-sorbent contact times longer than 0.2 second

[Lee and Johnson, 1980] suggested the following chemical interaction occurs between diatomaceous earth and alkali chloride:

$$2MCl(g) + SiO_2 + H_2O(g) \rightarrow M_2O.SiO_2 + 2HCl(g) \qquad (10\text{-}3)$$

10.2.1.4. Kaolinite

Kaolinite is the most well-known, and characterized, additive tested for alkali removal from flue gases. It is composed of 45 %(w/w) Al_2O_3, 52 % SiO_2 and trace amounts of metals oxides including K (0.08 %) and Na (0.06 %).

When kaolinite particles are exposed to a hot environment (> 500 °C), the kaolinite ($Al_2O_3.2SiO_2.H2O$) is activated to form metakaolinite ($Al_2O_3.2SiO_2$), which is known to react with alkali hydroxides, MOH to form nephelite ($2Na_2O.Al_2O_3.2SiO_2$). Metakaolinite is deactivated above 950 °C and ultimately forms mullite ($3Al_2O_3.2SiO_2$) and silica (SiO_2), which may also react with NaOH to form water soluble silicates ($Na_2O.nSiO_2$) [Mwabe and Wendt, 1996].

Multi-phase, multi-component equilibrium calculations predict that in the absence of an additive, Cl or S, the primary gaseous Na-species at temperatures above 800 °C, is NaOH. At the dewpoint, the condensate of NaOH(g) will be Na_2CO_3(cr,l). In the presence of excess Cl, the dominant gaseous Na-species is NaCl, the dewpoint is lowered by approximately 200 °C and the condensate is NaCl(cr,l). Sulfur will increase the dewpoint for Na-species by about 250

°C, with the condensate being Na_2SO_4(cr,l). In the presence of kaolinite, Na-Al silicates like nephelite ($2Na_2O.Al_2O_3.2SiO_2$) are favoured at temperatures higher than 1000 °C, except at very high Cl-concentrations.

[Punjak and Shadman, 1988] found kaolinite to be a suitable sorbent for the removal of alkali from hot flue gases. The kinetics and mechanism of adsorption of NaCl vapor on kaolinite were studied at 800 °C under fixed bed conditions in both N_2 and simulated flue gas (sfg) atmospheres. Under nitrogen, both Cl and Na were retained by the sorbent; however, under simulated flue gas, only Na was retained. In both cases, the adsorption was found to be irreversible, i.e. of the chemisorption type. High-resolution scanning Auger spectroscopic analysis of kaolinite particles indicated the formation of a product layer during adsorption. Under a simulated flue gas atmosphere, the product layer appeared to be nephelite, a stable Na-Al silicate.

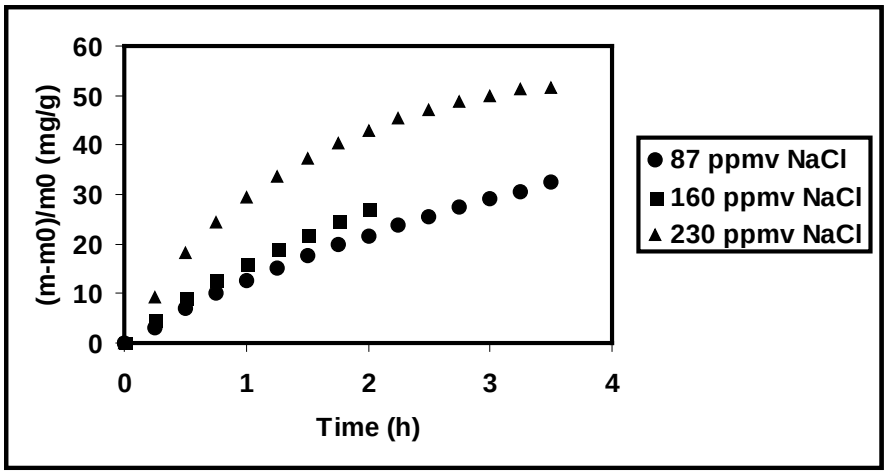

Figure 10-1: Temporal profile of NaCl adsorption on kaolinite under fixed bed conditions. Source: [Punjak and Shadman, 1988].

The rate of adsorption dropped with an increase in alkali loading (see Figure 10-1), and a maximum saturation limit was observed (see Figure 10-2). In the simulated flue gas atmosphere this saturation limit was found to be approximately five times higher than that under the ultra high purity (UHP) nitrogen atmosphere.

The additive features for kaolinite includes [Mwabe and Wendt, 1996; Punjak et al., 1989; Uberoi et al., 1990]:

- General alkali removal efficiency > 90 % (w/w);
- Adsorption occurs irreversibly, and at a rate dependent on the gas phase alkali concentration;

- A loading capacity of 266 mg Na/g sorbent has been reported in the literature. No similar data has been reported for K, and;
- H_2O (g) is necessary for the absorption process to occur.

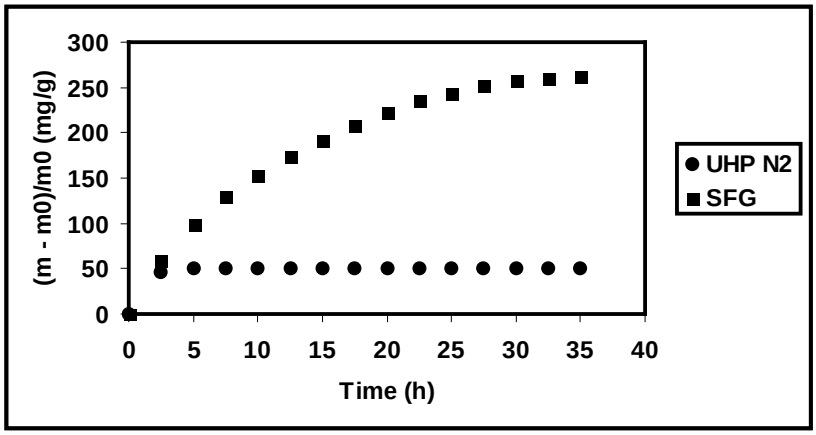

Figure 10-2: Maximum saturation limit for NaCl adsorption on kaolinite under ultra high purity (uhp) nitrogen respectively a simulated flue gas atmosphere. Notice that the saturation limit is about 5 times higher in the simulated flue gas (SFG) as compared with the ultra high purity (UHP) N_2. This is most likely due to the presence of water in the simulated flue gas. Source: [Punjak et al., 1989].

In a study of alkali adsorption on kaolinite in ultra-high purity (UHP) N_2(g), at 800 °C and 1 atm., [Punjak, 1988] additionally concluded that:

- An increase in the adsorption rate was observed with increased alkali concentration (independent of carrier gas);
- A decrease in the adsorption rate was observed with loading, and the presence of a saturation limit was evident;
- The saturation limit was strongly affected by the carrier gas composition: 5.2 % in N_2 vs. 26.6 % in a simulated flue gas, and;
- No desorption (release of adsorbed alkali material) of alkali is observed

[Turn et al., 1998] and [Uberoi et al., 1990] suggested the following mechanism for the reaction between alkali chloride and metakaolinite (dehydrated kaolinite):

$$2MCl(g) + Al_2O_3.2SiO_2 + H_2O(g) \rightarrow M_2O.Al_2O_3.2SiO_2 + 2HCl(g) \quad (10\text{-}4)$$

10.2.2. Investigations in Entrained-Flow Systems

[Schürmann et al., 2001] investigated alkali adsorption onto two different additive materials in a drop-tube furnace at the University of Stuttgart (IVD), Germany. A pulverized hard coal from Ensdorf/Saarland, Germany with an average particle size (d_{50}) of 61 µm, was used as reference fuel in the experiments. For the experiments, clay (d_{50} = 5 µm) and industrially produced, pure silica, SiO_2 (d_{50} = 16 nm, aerosil), were doped into the coal in a series of different proportions: 2 and 5 %(w/w) clay, and, 1, 1.5 and 2 %(w/w) aerosil. The clay consisted primarily of SiO_2 (58.9 %(w/w)) and Al_2O_3 (23.2 %(w/w)), while the rest was made up of moisture, Fe_2O_3 and K_2O. In all the experiments conducted, a total residence time of 10 s, and 3 % (v/v) O_2 in the flue gas were achieved by varying the mass flow of the fuel, and the combustion air. The temperature was varied from 1100 °C to 1400 °C.

The addition of aerosil caused a significant decrease in the measured gas phase alkali concentrations at the outlet of the reactor: For K, the gas phase concentration decreased from 4802 ppbv (raw coal) to 447 ppbv (2 % aerosil), at 1400 °C. When adding clay, the gas phase concentration of K decreased from 4802 ppbv (raw coal) to 1107 ppbv (5 %(w/w) clay) at 1400 °C. Similar results were obtained for Na.

The authors suggested the following possible mechanisms for interaction between alkali chloride, MCl, M ∈ {Na, K}, and silica:

$$2MCl(g) + SiO_2 + \tfrac{1}{2}O_2 \rightarrow M_2O.SiO_2 + Cl_2(g) \quad (10\text{-}5)$$

$$2MCl(g) + H_2O + 2SiO_2 \rightarrow M_2O.2SiO_2 + 2HCl(g) \quad (10\text{-}6)$$

Notice in these reactions the interaction of O_2 or H_2O, which are important for ensuring a significant alkali chloride-sorbent interaction.

Concerning the reaction between alkali chlorides, MCl, M ∈ {Na, K}, and the clay sorbent, [Schürmann et al., 2001] suggests the following reactions:

$$2MCl(g) + Al_2O_3.2SiO_2 + H_2O(g) \rightarrow M_2O.Al_2O_3.2SiO_2 + 2HCl(g) \quad (10\text{-}4)$$

$$2MCl(g) + Al_2O_3.2SiO_2 + \tfrac{1}{2}O_2(g) \rightarrow M_2O.Al_2O_3.2SiO_2 + Cl_2(g) \quad (10\text{-}7)$$

SEM investigations of ashes from these experiments indicate the presence of a liquid phase on the surface of the additive particles at 1400 °C, which may be necessary in order to increase alkali capture significantly (compared to the capture at 1100 °C).

[Gudenau et al., 1998] developed a new process for gas cleaning at temperatures above 1300 °C, which offers simultaneous removal of particulates and alkali vapors from hot flue gases. The concept is based on the principle of a conventional wet scrubber and application of a venturi scrubber, using molten slag as scrubber fluid, which is injected into the hot gas flow and spreads there in the form of a sticky network which will agglomerate the particulate matter and bind/adsorb the alkali vapor in the flue gas. A total of 10 slags in the CaO-MgO-SiO_2-Al_2O_3 system with viscosities in the range 1-4 Pa·s under operating conditions, were tested. The authors conclude that it is possible to capture alkali vapors by molten slag droplets, as the dispersion of slag in the gas stream increases its surface area in the reaction zone, thereby making the reaction more effective:

$$2MCl(g) + Al_2O_3.nSiO_2 + H_2O(g) \rightarrow M_2O.Al_2O_3.nSiO_2 + 2HCl(g) \quad (10\text{-}8)$$

10.3. Full-Scale Investigation of Additive Effect

If an additive is applied in a straw-fired boiler and fixes a certain amount of the alkali metals, less alkali is available for aerosol formation in that boiler. In order to investigate this effect, a series of aerosol measurements were carried out at the Avedøre Power Station, Unit 2 (AVV2) in Denmark, in November-December, 2004, while applying different additives in the boiler [Zeuthen, 2007].

AVV2 is a modern multi-fuel plant with two boilers of which the biomass boiler has a capacity of 100 MW_{th}. The plant combines power from a biomass steam cycle and a fossil fuel ultra-supercritical steam cycle, along with heat recovery steam generators (total capacity; 570 MW). The steam cycle of the biomass boiler operates with steam at 300 bar and is superheated to 580 °C. Approximately 25 tons/h of wheat straw is utilised at full load. The plant is equipped with baghouse filters. Straw is fed to the boiler on a vibrating grate, where primary air is supplied through the grate, and secondary air is in jected in the freeboard.

Aerosol measurements were carried out upstream from the bag house filter, in order to investigate the effect of additives on the aerosol mass loading and chemistry. The temperature at the location was 170 °C. Sulphur dioxide and HCl concentrations in the boiler were measured continuously. Figure 10-3, shows schematically the bio-boiler and the sampling locations of the aerosol measurements. For further details, please refer to [Zeuthen, 2007].

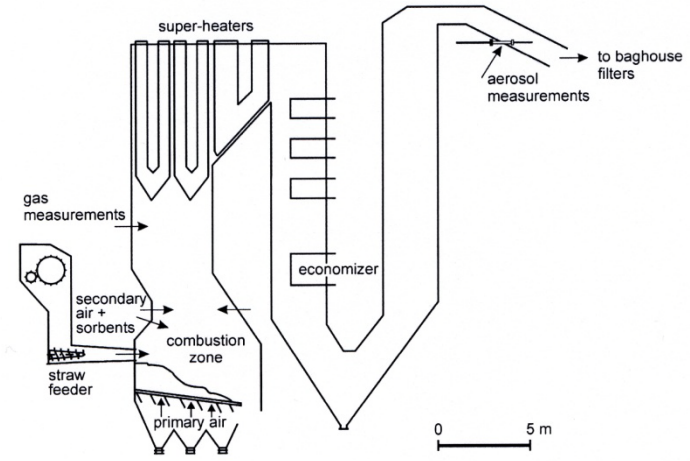

Figure 10-3: Principal sketch of the AVV-2 bio-boiler in Denmark. The locations of the combustion zone, air and sorbent injection, gas measurements, and aerosol measurements are shown in the figure. Source: [Zeuthen, 2007].

Six additives were tested during the measurements: ammonium sulphate, monocalcium phosphate, Bentonite, ICA5000, clay and chalk. The choice of sorbents was based on the following assumptions [Zeuthen, 2007]:

- Bentonite and clay will absorb alkali, while monocalcium phosphate would bind alkali in phosphates;
- Ammonium sulphate is expected to bind K as sulphate, and realsing Cl as HCl, while simultaneously providing ammonia for the reduction of NO_X, by selective non-catalytic reduction (SNCR);
- ICA5000 is a commercial sorbent for waste incineration, developed for the reduction of deposit formation in these systems, and;
- Chalk is often added to some small scale household combustors, in order to reduce the amount of slag from the combustion process. This full-scale test provided a chance to test chalk in a much larger scale.

The chemical composition and mean diameter of Bentonite, ICA5000, and clay are provided in Table 10-3. Chalk ($CaCO_3$), monocalcium phosphate, and ammonium sulphate were of technical quality, with > 95 % purity. The powder diameter given by the manufacturer was approximately 5 μm for chalk, and approximately 500 μm for monocalcium phosphate. Ammonium sulphate vaporizes and decomposes completely shortly after injection into the boiler therefore no particle size is provided for this sorbent.

The additives were injected continuously into the boiler together with the secondary air, above the vibrating grate (see Figure 10-3). Table 10-4 shows operational data for all runs at the AVV-2 boiler. The fuel analyses obtained by ISO standard methods are provided by [Zeuthen, 2007].

Sorbent:	**Bentonite**	**ICA5000**	**Clay**
Total moisture (%)	8.9	7.2	1.4
C (%)	-	0.2	1.3
Cl (%)	-	< 0.1	< 0.1
Al (%)	10.1	7.9	10.0
Ca (%)	0.87	0.75	1.7
Fe (%)	6.6	2.0	4.9
K (%)	2.3	1.4	2.3
Mg (%)	1.7	0.78	0.32
Na (%)	0.99	0.17	0.26
P (%)	-	0.020	0.080
S (%)	-	0.071	0.050
Si (%)	24	30	25
Mean diameter [µm]	20.7	43.7	47.9

Table 10-3: Chemical composition of Bentonite, ICA5000, and clay. All elements, except C is determined by ICP-OES. Carbon is measured by a carbon analyser. Data for Bentonite is provided by the manufacturer. All elements, except water, are provided as %(w/w), on a dry base. Source: [Zeuthen, 2007].

Run	Date; time	# of LPI measure-ments	Feed rate of sorbent (kg/h)	Relevant element ratio (mol/mol)
Reference	11-23;9-12 am	3	0	Si:K = 2.3, S:K = 0.23
Chalk	11-24;9-12 am	3	216	Ca:K = 0.5, Ca:S = 4.5
Increased primary air	11-24;3-5 pm	2	0	Si:K = 2.3
ICA5000	11-25;9-12 am	3	582	Al:K = 0.49, Si:K = 3.6
Monocalcium phosphate	11-26;9-12 am	2	351	P:K = 0.71
Bentonite, low	12-01;9-12 am	3	450	Al:K = 0.37, Si:K = 5.6
Bentonite, high, reduced load	12-01; 1-4 pm	2	900	Al:K = 0.98, Si:K = 6.1
Bentonite, high	12-07;9-11 am	2	900	Al:K = 0.60, Si:K = 2.1
Clay	12-02;9-12 am	2	654	Al:K = 0.67, Si:K = 5.3
Seed grass	12-02;1-4 pm	3	0	Si:K = 1.6
Ammonium phosphate, high	12-06;9-12 am	2	360	S:K = 0.83
Ammonium phosphate, low	12-06; 1-4 pm	3	180	S:K = 0.44

Table 10-4: List of runs during the campaign, number of LPI measurements and the feeding rate of sorbents. Some selected stoichiometric ratios are given for the individual runs. They are calculated with the assumption that all S in the fuel and 50 % of all K is released to the gas phase from the grate combustion zone. The element ratios include measured element content in the sorbent and the fuel ash. Source: [Zeuthen, 2007].

Aerosols were collected on aluminium foils in a 10-stage berner low-pressure cascade impactor (LPI), with an aerodynamic diameter range of 0.03 – 12.7 µm.

Figure 10-4 shows the mass-based size distribution for all twelve runs of the field measurements. Each distribution curve is the mean of 2 to 3 measurements. The particle size distributions in Figure 10-4 clearly show that the addition of ammonium sulphate, monocalcium phosphate, clay, ICA5000 and Bentonite causes a large reduction in the mass loading of particles, whereas the addition of chalk *increases* the mass concentration of fine particles by more than 30 %.

For ammonium sulphate, monocalcium phosphate, Bentonite, ICA5000 and clay, the addition of sorbents reduces the $PM_{2.5}$ by 50 % or more. For Bentonite and ammonium sulphate it is worth noting that doubling the rate of sorbent feeding only leads to a 5-10 % reduction in the $PM_{2.5}$ mass loading of the flue gas. The chemical composition of the fine particles as a function of particle size is shown in Figure 10-5.

10.3.1. Ammonium Sulphate

Ammonium sulphate, $(NH_4)_2SO_4$, is added to increase the sulfation of alkali chloride in order to minimize the Cl-content of the deposits. The sorbent dissociates, and react with KCl, to form sulphate:

$$(NH_4)_2SO_4 \rightarrow 2NH_3 + SO_3 + H_2O \quad (10\text{-}10)$$

$$2KCl + H_2O + SO_3 \rightarrow K_2SO_4 + 2HCl \quad (10\text{-}11)$$

Ammonium sulphate caused a reduction of the mass concentration of $PM_{2.5}$ to 42 % of the reference level at the lowest feeding rate and 31 % at the highest feeding rate of ammonium sulphate. [Jimenez and Ballester, 2005b] observed an increased SO_4/Cl-ratio in fine particles, when increasing the concentration of SO_2 in the flue gas, but this effect was not observed in the measurements at AVV2 when adding ammonium sulphate.

Ammonium sulphate has been recognized as a good additive for the reduction of corrosion and aerosol formation, although its beneficial effects are obtained at the expense of an increased SO_2 emission [Zeuthen, 2007].

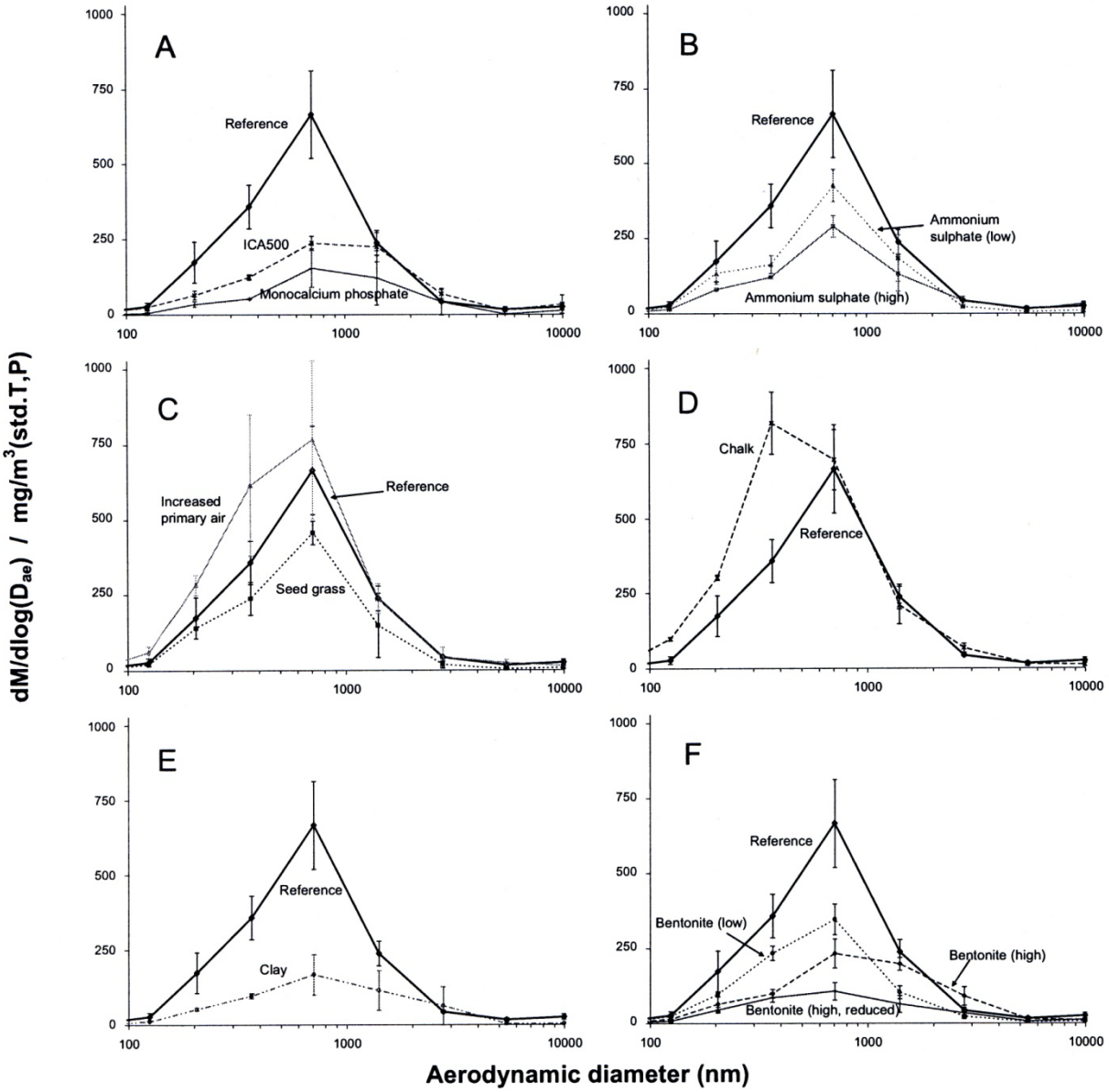

Figure 10-4: Mass-based size distributions from measurements by cascade impactor. The reference run is shown together with: A) ICA5000 and mono-calcium phosphate, B) ammonium sulphate at high and low feeding, C) combustion of grass and test of the effect of increased air flow, D) chalk, E) clay, and, F) Bentonite at high and low feeding rate, and with reduced load on the boilers. All flue gas concentrations are converted to a reference state of dry gas at atmospheric pressure, at 0 °C, and 6 % O_2. Source: [Zeuthen, 2007].

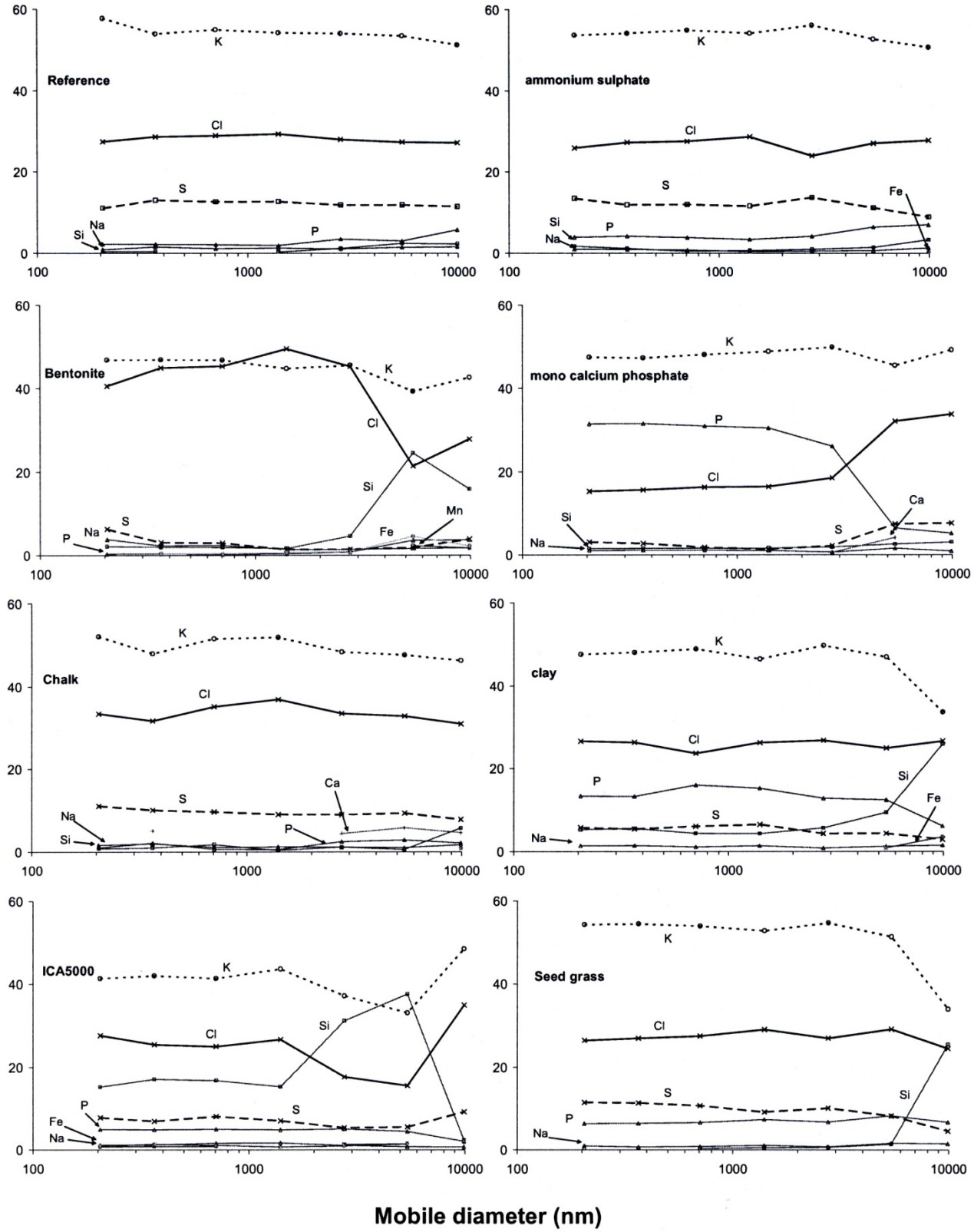

Figure 10-5: Chemical composition of fine particles as determined by EDX. Source: [Zeuthen, 2007].

10.3.2. Monocalcium Phosphate

Monocalcium phosphate, $Ca(H_2PO_4)_2$, is used as an additive in order to capture alkali metals (i.e. K in straw-fired systems) as phosphates, releasing Cl as HCl and, thereby reducing the content of Cl in the deposits. The AVV2 measurements support this effect, since the $PM_{2.5}$ was reduced to 28 % of the reference value, when adding monocalcium phosphate. However, the additive releases volatile P species, which are transferred to the fine particles, some of which may contain more than 30 % P [Zeuthen, 2007].

10.3.3. Bentonite

Bentonite (consisting mainly of montmorillonite) is applied as an additive in order to capture alkali, as aluminiumsilicates. The observed reduction of the aerosol mass loading, was found to be considerable. With the lowest sorbent feeding rate, a reduction to 54 % is obtained, while a 49 % reduction was found at the highest sorbent feeding rate.

The S concentration in the fine particles was found to be very low when adding Bentonite. The particles were composed of almost pure KCl [Zeuthen, 2007].

Laboratory measurements showed a reduction in the aerosol mass loading of 45 %, while the number concentration increases by a factor of 8. Thus, reduced mass loading is caused by alkali capture from the gas phase, which in turn causes homogeneous nucleation to occur at a lower temperature. This provides less time for coagulation to occur in the system, and may be the reason for the higher particle mass number concentration, and the smaller particle diameters observed when applying this sorbent [Zeuthen, 2007].

10.3.4. ICA5000

This sorbent (composed of oxides of Si, Al and Fe) was applied in order to capture alkali metals in species with high melting points. The $PM_{2.5}$ concentration was reduced to 52 % when applying ICA5000. The chemical composition of the fine particles shows a small reduction in the S-content, while the presence of 15-30 % Si indicates that some fine sorbent particles may be present in this size range. The content of Si in the fine particles must originate from the sorbent. Laboratory measurements [Zeuthen, 2007] show a reduction in the aerosol mass loading (to 80 %), and a small increase in the number concentration [16 %]. Thus, the effect of ICA5000 was weaker than for Bentonite and clay, which could very well be due to the larger particle size of the additive providing a smaller contact area for adsorption of alkali [Zeuthen, 2007].

10.3.5. Clay

As ICA5000, clay (consisting mainly of oxides of Al, Si and Fe) was applied in order to capture alkali metals in chemical species with high melting points. $PM_{2.5}$ was reduced to 34 % of that of the reference case and the amount of S in the fine particles was lowered, while more than 10 % P was observed. Laboratory tests showed a reduction to 60 % of the fine particles mass loading, and a 48 % increase in the number concentration, compared to the reference case. The effect on particle diameter was less pronounced than for Bentonite [Zeuthen, 2007].

10.3.6. Chalk

Chalk, or limestone, $CaCO_3$, is generally applied as an additive in order to reduce emissions of SO_2. In the AVV2 campaign, the additive was entrained with the flue gas flow since no considerable increase in Ca was seen in the slag during the test [from 7.2 to 8.2 %(w/w) Ca in the slag] [Zeuthen, 2007]. $PM_{2.5}$ was *increased* by more than 30 %, [S] in the fine particles was slightly reduced compared to the reference run. The increase in $PM_{2.5}$ can not be explained by sampling an additional amount of fine additive materials. A small amount of Ca was observed only in particles larger than 2 μm. The concentration of SO_2 in the flue gas was reduced from 39 ppm to 26 ppm. The increase in $PM_{2.5}$ could be explained either by the capture of Si by Ca in $Ca_3Si_2O_7$ or by the fact that limestone is known to have a grain-micrograin structure, which upon rapid heat-up could cause explosion (break-up) of limestone particles, thereby forming a fume of tiny CaO-rich particles.

The mass loading of $PM_{2.5}$ in the laboratory investigation was increased by almost a factor three, while the number concentration increased by 20 times and the average particle diameter was reduced considerably. The smaller particle diameter suggests that limestone as an additive changed the nucleation mechanism. In that case chalk can not be recommended as a sorbent when considering the effects observed on aerosol formation.

10.4. Investigation of Additive Effects on Deposit Chemistry

In addition to minimizing aerosol mass loading in boilers, application of an additive may influence chemistry and degree of sintering of deposits. This effect of different additives has been extensively studied in the CHEC solid fuel entrain flow reactor. An introduction to and outline of the results are provided below.

The CHEC solid fuel entrained flow reactor was originally designed to simulate the environment of high temperature thermal reactors such as suspension-fired boilers, entrained

flow gasifiers or the freeboard of grate-fired boilers. It is specially well-suited to study heterogeneous reactions at high temperature and short residence times.

Deposit samples were collected on the deposit probe placed just outside the reactor. The outer metal tube of the probe can be removed so the deposit can be weighed and stored intact for later analysis. The probe was cooled by preheated air to obtain a surface temperature of 550 °C, which is of relevance to superheater coils, while the flue gas temperature was kept at around 800 °C near the deposit probe. The deposit probe was exposed to the ash-loaded flue gas from 1½ to 6 hours.

The diagnostics of the experiments included:

- Measurement of the total mass of deposit for later analysis;
- Images taken of the deposit;
- Measurement of the total amount of large fly ash particles (cyclone ash, > 2.5 μm), aerosols (< 2.5 μm), and bottom ash;
- Determination of the water soluble K, Cl and S content of the deposit, aerosols and fly ash, and;
- On-line gas concentration measurements of SO_2, O_2, CO and CO_2.

The Cl-content of the deposit ash is a good indicator of the corrosiveness of the deposit. Thus, the evaluation of the efficiency of the tested additives was primarily based on their capability to reduce the Cl-content in the deposit, beyond the reduction caused by simple dilution (the amount of total ash increases when using an additive).

The diagnostics of the CHEC-EFR contained measurements of deposition flux, water-soluble K, Cl and S in the deposit, aerosols, fly ash and bottom ash. In addition, gas concentrations of SO_2, O_2, CO, CO_2 and NO where measured. In most of the experiments, the gas temperature was kept between 690 and 800 °C, just upstream of the deposition probe. The surface temperature of the deposition probe was kept at 470 °C.

10.4.1. Ca- and P-Rich Additives

Experiments at the Ensted CHP boiler have shown that it is possible to reduce the [Cl] in deposits significantly by adding P and Ca. Phosphor may react with KCl according to the following global reaction, whereby Cl is released to the gas phase as HCl:

$$2aKCl(g) + ½aH_2O + P_2O_5 \rightarrow (K_2O)_a.P_2O_5 + aHCl(g) \quad (10\text{-}12)$$

Thus, the objective of the work by [Jensen et al., 2005] was to test the capability of Ca- and P-rich additives to minimize problems with deposit formation and corrosion when firing biomass in suspension in the CHEC-EFR.

An additive that can minimize corrosion and deposition problems will ideally fix all K, in species with relatively high melting temperatures (in order to minimize the formation of strongly sintered deposits that are difficult to remove) and release the Cl to the gas phase as HCl (in order to minimize corrosion). Thus, if the addition of Ca and P to a biomass is to be beneficial several processes have to take place:

- The P should react with the alkali metals and release Cl as HCl(g)
- The Ca should not react with P and thereby inhibit its reaction with the alkali metals
- The alkali phosphates or alkali Ca phosphates formed should have high melting temperatures in order to prevent the formation of strongly sintered deposits.

In order to test the capability of different additives, six reference experiments with coal, bark, pine wood, beech wood and wheat straw, as well as seven experiments with mixtures of additives and different biomass fuels were performed in the CHEC-EFR. The most used additive was $CAP_{0.36}$ which is a liquid P- and Ca-containing additive with a molar ratio of Ca to P of 0.36. Besides the $CAP_{0.36}$, aluminium sulphate ($Al_2(SO_4)_3$) and a coal ash rich in Al and Si, were tested as additives.

It was observed when firing biomass in the CHEC-EFR, that fuels with high K-content have high capability to bind fuel-Cl in the deposit. In experiments where a high molar ratio of P/(Na+K) i.e. in the range [1.94 - 3.19] and a molar ratio of P/Ca in the range [0.78 - 0.88] were obtained in the fuel ash (including the additives), a high reduction efficiency of Cl in the deposit ash was obtained. If a relatively high amount of Ca is available more Ca-phosphate is generated, preventing the phosphate to react with the alkali chlorides.

Therefore, it is important to be very careful concerning the molar ratio of P/Ca in the resultant fuel additive mixture. If the molar ratio of P/Ca is around 0.5, a large surplus of Ca is present and will be available for reaction with P, whereby more Ca-phosphate is generated and, as a consequence, less P is available for the reaction with KCl. On the other hand, if an additive with a large surplus of P compared to Ca (but not compared to K and Na) is applied, mixtures of NaCl, KCl and KPO_3 and P_2O_5, with melting temperatures below the melting temperature of KCl, may be formed, and may most likely cause increased deposit formation. Thus, both the P/Ca and the P/(Na+K) ratio must be addressed when evaluating a Ca-P rich additive [Jensen et al., 2005].

10.4.2. The Effect of Other Additives on Deposit Chemistry

In order to apply the data gained from the full-scale measurements of additive behaviour at AVV-2, a series of experiments were conductedin the CHEC-EFR [PSO-3149, 2004];

- Coal-straw co-firing, without an additive. The effect of the particle size of the straw, and the probe surface temperature were investigated, as well as the reproducibility of the experiments.
- Experiments with addition of S. Sulphur dioxide, SO_2, and ammonium sulphate were added (independently of each other) in order to check their influence on the K-S-Cl chemistry of the flue gas.
- Experiments with the addition of kaolin. The effect of the amount of kaolinite added was investigated. In addition, a series of experiments were conducted in order to investigate, fundamentally, the reaction between KCl(g), and single particles of kaolinite under a fixed-bed, gas-solid contact pattern.
- Effect of different additives like fly ash from pulverized coal firing, diatomite (also known as cellite, a very porous Si-mineral) quartz, aluminium hydroxide, calcium carbonate, TASP (a dry solid, FGD-residue), and monocalcium phosphate.

It was found that the deposition flux, during straw-firing (the reference experiment) was around 240 g/m^2/h. Typically, around 40 % of the ash formed during straw-firing was removed through the bottom ash chamber, meaning that 60 % of the ash was entrained with the flue gas to the deposition probe at the flue gas exit [PSO-3149, 2004].

The deposits were in most cases very fragile, and easy to remove from the probe. The lack of strongly sintered deposits is most likely due to the relatively low flue gas temperature and the relatively short total exposure time, usually around ~ 1½ hour.

An increase of the probe temperature from 470 °C to 650 °C, caused a decrease in [Cl] in the deposit from 11.4 %(w/w) to about 7.2 %(w/w), and an increase in the deposition flux from 240 to 400 g/m^2/h. [K] was observed to be constant when increasing the temperature, while there was an increase in [S].

Below, is a brief outline of the effect of the different additives tested.

10.4.2.1. Addition of Sulphur

Experiments were conducted with the addition of SO_2 to the combustion air, in order to cause a reaction between SO_2 and KCl, thereby forming K_2SO_4 and HCl. Based on these experiments it was concluded that, during suspension firing of straw, a huge amount of SO_2 (compared to

the stoichiometric necessary amount of S) is needed in order to decrease [Cl] in the deposit significantly. Even when adding three times the necessary amount of SO_2, the deposit still contained 6 %(w/w) Cl, and a flue gas level of ~ 2000 ppm SO_2 was measured. A detailed investigation of the deposits formed, indicated that part of the S added was fixed as $CaSO_4$. A relatively lower increment of [S] in the filter and cyclone ash was measured and then compared to the increment in the deposit, indicating that part of the sulfation takes place directly in the deposit. The deposition flux was not affected to a significant degree by the addition of SO_2 [PSO-3149, 2004].

An experiment with addition of ammonium sulphate [$(NH_4)_2SO_4$] was conducted. When ammonium sulphate decomposes at high temperature, it releases SO_3, which may react rapidly with KCl. Thus, allowing direct access to SO_3 without a pre-step of oxidation was believed to cause a more efficient sulfation of KCl. Regardless, the experiment gave the same overall result as the experiments with addition of SO_2, most likely because the addition of ammonium sulphate was done in the high-temperature zone together with the fuel, whereby the SO_3 released decomposed to SO_2. The addition of ammonium sulphate at a lower temperature is expected to cause a better effect for this additive.

10.4.2.2. Addition of Kaolinite

The addition of kaolinite caused a significant reduction of [Cl] in the deposits. Injection of the stoichiometric amount of kaolinite, reduced [Cl] in the deposit from 15 %(w/w) to ~ 4 %(w/w). Only around half of this reduction was due to dilution of the ash, caused by the an additional amount of ash (kaolinite). Application of kaolinite also caused a decrease of [K] in the deposits, while [SO_2] in the flue gas went up from 50 ppmv to about 100 ppmv. This indicates that kaolinite reacts with both KCl and K_2SO_4, since the additional amount of SO_2 in the flue gas most likely originated from K_2SO_4, having already reacted with kaolinite [PSO-3149, 2004].

The effect of the kaolinite to straw-K - ratio was also investigated. Adding kaolinite, a kaolin to straw K – ratio equal to 2.15 caused a reduction of water-soluble K in the deposits to around 2.2 %(w/w), whereas a simple dilution only caused the reduction of [K] in the deposits to 7.3 %(w/w). For Cl, a kaolinite to straw-K – ratio equal to 2.15 reduced [Cl] to 0,5 %(w/w) while a simple dilution alone caused a [Cl] level of 4,7 %(w/w).

10.4.2.3. Other Additives

The general outcome of applying other additives (rather than sulphur and kaolin) was that the deposition flux increased proportionally to the ash (additive) amount added [PSO-3149, 2004]:

- The fly ash had a positive effect on the [Cl] in the deposits, but turned out to be less efficient than kaolinite or the Si-based additives [quartz and diatomite]. The chemical composition of the fly ash was comparable to that of kaolinite, but the mean particle size of the fly ash was bigger. Since the fly ash particles had already been molten once (in the furnace where they where originally formed), it is possible that this ash is less efficient as additive. Experiments with Bentonite addition gave almost no effect, except for the dilution.
- Si-based additives like quartz and diatomite had a positive effect on [Cl] in deposits. Diatomite particles were bigger than the quartz particles, but then in addition they were more porous.
- Additives based on either Ca or Al, such as calcium carbonate ($CaCO_3$) and aluminium hydroxide ($Al(OH)_3$) did not show any significant effects on [Cl] in the deposit.
- The addition of TASP (a dry residue from FGD plants), consisting mostly of 70 %(w/w) $CaSO_3$, the rest being $CaSO_4$ and $CaCO_3$, gave no significant reduction in [Cl].
- Finally, monocalcium hydroxide ($Ca(H_2PO_4)_2$) gave a high reduction of [Cl] in the deposits. Nevertheless, only a single experiment was conducted with this additive, so care must be taken when interpreting this result. Equilibrium calculations indicate that the addition of P may have a positive effect when K is fixed as K_2HPO_4, but also indicates that P_2O_5 is present in the gas phase at temperatures above 1100 °C. Thus, it is possible that gaseous K and P react and are subsequently present in the aerosol fraction.

10.5 Summary

The co-firing of coal and straw at the Midtkraft-Studstrup Power Station clearly indicated that a significant proportion of the volatile K released from straw, will react with coal-derived fly ash particles rich in Al and Si [Andersen, 1998; Andersen et al., 2000]. At Midtkraft-Studstrup only limited problems related to deposition and corrosion were observed, since K was fixed in fly ash particles as K-Al silicates or was transformed to K_2SO_4 and deposited in the convective pass of the boiler, and thereby most of the Cl was emitted as HCl(g).

Based on the outline of alkali sorbents provided in this chapter and in the open literature, the following conclusions may be drawn:

- Most fixed bed alkali getter tests reported in the literature have been performed in the T/P range: [750 - 950 °C] / 1 -10 bars. Those studies performed on entrained flow systems at a higher temperature ([1000 – 1400 °C]) have proven succesful.
- The dependence of additive activity on carrier gas type (composition) has been reported several times. Water is most likely needed to ensure a reasonable rate of adsorption.

- Another important factor is the temperature, since several investigators report the necessity of a liquid phase on the sorbent in order to ensure a reasonable rate of adsorption.
- Sorbent materials composed primarily of SiO_2 have the advantage of irreversibly chemisorbing alkali in their solid matrix (causing a direct release of Cl and HCl)
- Al_2O_3-based sorbents sequester alkali predominantly through physical adsorption, thus exhibiting higher rates of alkali loading with decreasing temperatures. These sorbents are amenable to material regeneration and alkali recovery using boiling water
- Alumina, kaolinite and activated bauxite capture in general the largest percentage of NaCl and KCl.
- Silica, graphite and limestone capture only a small percentage of the alkali delivered (unless applied with very small particle sizes)
- Limestone is not an appropriate sorbent for alkali capture

An additive used when co-firing straw and natural gas at high temperature must be an additive based on an Al-Si-rich material (the presence of Al will cause an easy opening of the Si backbone structure of the additive, thereby ensuring a more rapid reaction between the volatile alkali and the additive). A relatively small particle size is suggested in order to ensure that the additive particles after reaction with the volatile alkali do follow the gas stream lines and that they have a high temperature, which may ensure formation of a melt on the surface of the additive particles, and again cause easy adsorption. Gas conditioning, eg. by injecting or adding S may also be a solution, but one has to be aware that an increased level of S will increase the dew point for the alkali metals (alkali sulfates) and thereby potentially shorten the time of reaction between the alkali metal(s) and the additive.

Six additives were tested in the full-scale biomass-fired AVV-2 plant: ammonium sulphate, monocalcium phosphate, Bentonite, ICA5000, clay and chalk. The choice of sorbents was based on the following assumptions [Zeuthen, 2007].

The addition of ammonium sulphate, monocalcium phosphate, clay, ICA5000, and Bentonite causes a large reduction in the mass loading of particles, whereas the addition of chalk *increases* the mass concentration of fine particles by more than 30 %.

For ammonium sulphate, monocalcium phosphate, Bentonite, ICA5000 and clay, the addition of sorbents reduces the $PM_{2.5}$ by 50 % or more. For Bentonite and ammonium sulphate, it is worth noting that doubling the rate of additive feeding only leads to a 5-10 % reduction in the $PM_{2.5}$ mass loading of the flue gas.

Thus, all the additives, showed positive effects, except for chalk, meaning that it is possible to affect K-S-Cl chemistry and thereby aerosol formation and subsequently deposition in boilers fired with biomass.

Further analyses of additive effects were conducted on $CAP_{0.36}$, aluminium sulphate ($Al_2(SO_4)_3$), a coal ash, sulphur dioxide (SO_2), and ammonium sulphate, kaolinite, quartz and diatomite, calcium carbonate ($CaCO_3$), aluminium hydroxide ($Al(OH)_3$), and TASP.

For sulphur, it was concluded based on the experiments conducted in the CHEC-EFR, that during suspension firing of straw a very huge amount of SO_2 (compared to the necessary stoichiometric amount of S) is needed in order to decrease [Cl] in the deposit significantly. Even when adding three times the necessary amount of SO_2, the deposit still contained 6 %(w/w) Cl, and a flue gas level of ~ 2000 ppm SO_2 was measured [PSO-3149, 2004].

The addition of kaolinite caused a significant reduction of [Cl] in the deposits. Injection of the stoichiometric amount of kaolinite, reduced [Cl] in the deposit from 15 %(w/w) to ~ 4 %(w/w). Only around half of the reduction is due to the natural dilution of the ash, caused by adding of an additional amount of ash (kaolinite). Application of kaolinite also caused a decrease of [K] in the deposits, while [SO_2] in the flue gas went up from 50 ppmv to about 100 ppmv [PSO-3149, 2004].

In summary, some effects can be attributed to the additives, but whether the application of additives is the best solution to ash and deposit formation in systems fired with straw, is still doubtful. Additives may be applied in short time periods in order to affect the flue gas chemistry of the boiler, but this approach is probably neither the most optimal nor permanent solution.

Chapter 11:

SHEDDING OF ASH DEPOSITS

Ash deposited on heat transfer surfaces act as a resistance and may thereby inhibit heat transfer to the steam cycle. If not removed, deposits may reduce boiler thermal performance and, in severe cases, completely plug flue gas channels and subsequently cause unscheduled boiler shutdowns. Deposits may also cause severe corrosion of heat transfer surfaces. Thus, effective deposit removal is very important, in order to ensure a maximum boiler thermal efficiency and availability [Frandsen, 2005].

Deposit shedding can be defined as the process of deposit removal from heat transfer surfaces.

Mechanisms of natural shedding include [Zbogar et al., 2009]: [1)] erosion, [2)] gravity shedding and [3)] thermal shock. Erosion is the process of removing a sintered deposit by impacting SiO_2-rich fly ash particles. Gravity shedding occurs when the gravity force on a deposit is big enough to cause [1)] a break inside the deposit or [2)] flow of molten phases inside or along the surface of a deposit. Thermal shock-induced shedding is caused by temperature changes due to the difference in the thermal expansion coefficients of tubes and deposits. A sudden temperature gradient (e.g. due to fluctuations of the flue gas- or steam temperature), may cause an uneven expansion of [1)] deposit and tube or [2)] distinct, adjacent, deposit layers, leading to deposit fractures [Zbogar et al., 2009].

On the other hand, mechanical devices for deposit removal can be implemented into the boiler, often referred to as artificial shedding. Soot-blowing is one such process, in which a pressurized fluid is used to induce a mechanical and/or thermal shock that will cause a crack or fissure in the deposit. On the other hand, shedding may also be caused without any operational or mechanical influence e.g. by erosion, gravity shedding, or simply by a thermal shock caused by a load change of the actual boiler.

Deposit formation processes have been studied thoroughly over several decades [Frandsen, 2009], as documented in the previous chapters of this thesis, while knowledge about deposit shedding is relatively limited. Most of the studies available in the open literature deal with their removal in the kraft recovery boilers [Tran et al., 1988; Piroozmand et al., 1998; Kaliazine et al., 1999], with compositions somewhat different compared to biomass deposits, as discussed by [Zbogar et al., 2009].

Below is an introduction to deposit shedding, including an outline of recent data derived from measuring campaigns with focus on shedding at Danish power stations.

11.1. Sintering of Ash Deposits

During deposit consolidation and maturation, a process known as sintering occurs. Sintering is the process of particle-to-particle attachment, which causes increased contact between the ash particles in a deposit during heating. The driving force for sintering is lowering of the surface energy of the involved particles, i.e. densification by sintering leads to a decrease in the surface area between the condensed phase and the gas, and thereby a lower surface energy, as solid-vapor interphases are replaced by solid-solid (or liquid) interphases with lower energy [Skrifvars, 1994].

Sintering may occur through several different mechanisms, see Figure 11-1 [Skrifvars, 1994; Hansen, 1998];

- Liquid state sintering causes densification through the appearance and mobility of a melt. The amount of melt present controls the rate of neck formation between the particles. Liquid state sintering may involve a viscous liquid (e.g. melted silicates), and is typically referred to as viscous flow sintering [Raask, 1985].
- Chemical reaction sintering occurs when a reaction between particles leads to the formation of a third component, which forms a neck between the particles. Sulfation of low-temperature fouling deposits is a classical example of this [Hurley et al., 1994]
- Solid state sintering, where densification is achieved through changes in particle shape, may occur through several mechanisms. Material may be transported to the neck area by: [1)] diffusion along the particle surface, [2)] diffusion through the interior of particles, or [3)] diffusion through the surrounding gas phase by vaporization, and, subsequent condensation [Zbogar et al., 2009].

The main consequence of sintering is densification of deposits occuring through filling of a large fraction of the deposit pores with liquid [Nowok, 1996].

11.2. Brittle Break-up and Debonding of Deposits

A soot-blower jet impact can cause high internal stress in a deposit. For a weak brittle deposit this may lead to a break-up of the deposit as shown in Figure 11-2. Brittle failure originates from the deposit surface, which is directly affected by the impact of the jet pressure. The jet penetrates into the cracks and fissures along the deposit surface and opens them, which causes the deposit to break.

One analysis [Ebrahimi-Sabet, 2001; Kiliazine et al., 1997] showed that, for a broad range of deposit geometries, deposit break-up depends only on the peak impact pressure, PIP (i.e. the local stagnation pressure in a soot-blower jet [Zbogar et al., 2009]), and the deposit's tensile strength, which varies from location to location within a boiler due to variations in deposit composition, formation mechanism and flue gas temperature.

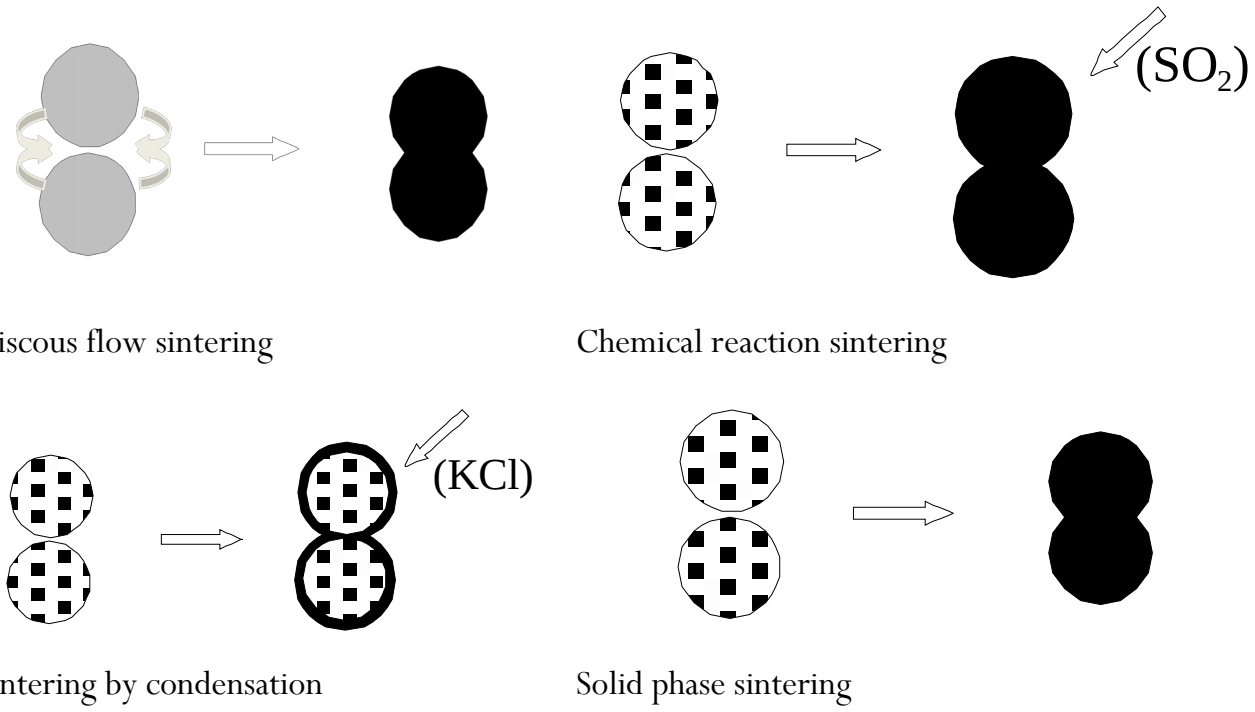

Figure 11-1: Different mechanisms of sintering. Source: [Skrifvars, 1994; Hansen, 1998].

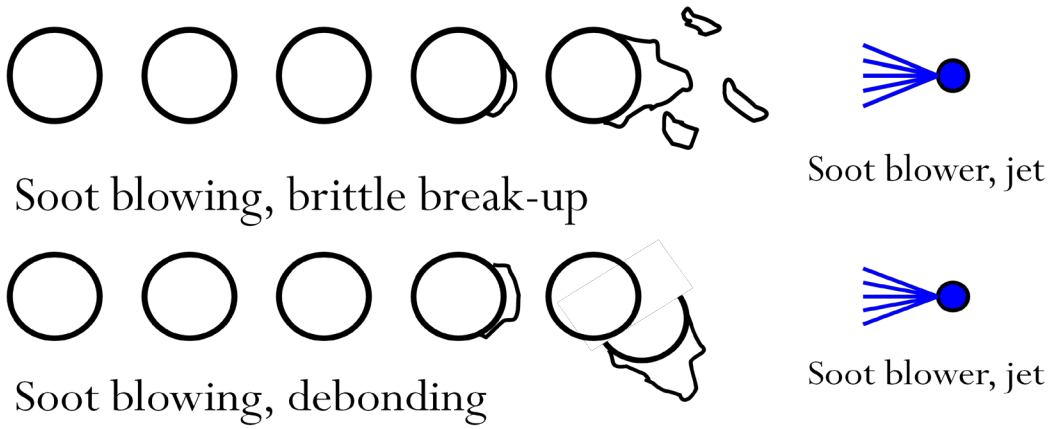

Figure 11-2: Two mechanisms of deposit removal: a) Brittle break-up, and b) Debonding. Source: [Kamiya et al., 2001].

Dense, hard deposits on the other hand, can be removed by debonding from the tube surface, as shown in Figure 10-4. This happens when the generated stress (e.g. by sootblowing) exceeds the adhesion strength at the tube-deposit interface. If a strong deposit is attached weakly to a tube surface, it might be removed by debonding, even by a weak jet.

Deposit debonding is influenced by adhesion strength at the deposit-tube interface [Kaliazine et al., 1999]. The adhesive bonding between the deposit and the tube surface is decreased when the deposit layer closest to the tube is a very porous layer. The chemical composition and the thermal characteristics of the oxide scale formed on the boiler tubes also influence the strength of the adhesive bond. Apart from thermal shock, caused by differences in thermal expansion between the oxide scale and the deposit, vibrations can also promote debonding by decreasing the tube-deposit adhesive bond.

Several types of deposit sootblower jet interactions may cause debonding, e.g. [Kaliazine et al., 1999; Ebrahimi-Sabet, 2001]; [1)] when the jet impact direction induces a shear stress on the deposit-tube interface, [2)] when a jet impact induces high frequency vibration in the deposit-tube system, and/or [3)] when tube banding and flexure, caused by impingement of the high velocity jet, induce strains in brittle deposits. Sootblower jets and the flow of the flue gases may cause vibrations of boiler tubes and deposits. While excessive vibrations may lead to metal fatigue and ultimately to tube failure, moderate vibrations may break the bond between a tube and a deposit, thus being useful in deposit removal [Zbogar et al., 2009].

11.3. Mechanisms of Deposit Shedding

Shedding mechanisms can be classified in two ways:

- Based on the part of the deposit where shedding takes place, as given in Table 11-1 or;
- Based on the deposit type, as given in Table 11-2 (modified from [Oka et al., 1997])

Table 11-1 lists the position of deposit removal for a number of shedding mechanisms. Erosion and melting cause the removal of deposit mass from the deposit surface, while gravity force, mechanically and thermally induce stress, which causes removal of the deposit mass from the deposit-tube surface or inside the deposit itself.

Table 11-2 shows how different shedding mechanisms influence different deposit types. While erosion and gravity force can cause shedding of powdery deposits, they do not influence heavily sintered deposits or running slags. Running slags are removed from the heat transfer surfaces by melting. Heavily sintered deposits are shedded mainly due to thermal stress and, to a lesser extent mechanical stresses [Stitt et al., 2002].

Removal mechanism		Position of deposit removal		
		Tube-deposit interface	Within the deposit	Deposit surface
A	Erosion			+
B	Gravity shedding	+	+	
C	Melting (i.e. flow of liquid slag)			+
D	Thermally induced tensions: a) by combustion fluctuations b) by load changes c) by soot blowing	+	+	
E	Mechanically induced tensions: a) by mechanical fluctuations b) by soot blowing	+	+	

Table 11-1: Position of the deposit mass removal, depending on the shedding mechanism, modified from [Oka et al., 1997].

Mechanism	Deposit type			
	Powdery	Lightly sintered	Heavily sintered	Liquid slag
Erosion	++	+	-	-
Gravity shedding	++	+	-	-
Melting (i.e. flow of liquid slag)	-	-	-	++
Thermal shock	-	+	++	-
Mechanical shock	++	++	+	-

Table 11-2: Occurrence of the deposit removal mechanism, depending on the deposit type, modified from [Oka et al., 1997].

11.3.1. Erosion of Deposits

Deposits may be eroded when sharp-edged fly ash particles (mainly unreacted quartz) collide with non-molten (hard) areas on a deposit surface, as shown in Figure 11-3. Erosion damage may be described as a gradual removal of material caused by repeated deformation (resulting from the normal component of the incoming particle impact velocity) or cutting actions (related to the tangential component of impact velocity) [Raask, 1988]. Deformation wear is

more prominent for brittle materials, whereas ductile materials are eroded mainly by the cutting mechanism.

Sootblowing can also cause erosion of the deposit, especially when saturated steam is used as the sootblowing medium, since water may condense out of saturated stream, creating small water droplets in the sootblowing jet. These droplets can impact on the deposit, and erode it.

The study by [Latella et al., 1999], which deals with the erosive wear of porous and highly dense liquid-phase sintered alumina ceramics, showed that sample porosity affects both the mechanical properties, and the erosion performance. In a low-porosity sample (2.5 %), erosion mainly caused intergranular cracking and chipping. Mass removal due to erosion was more extensive when the sample had a higher porosity (17.8 %) at all the impact angles tested. This is caused by a relatively low material hardness of the highly porous structure (17.8 %), which is likely to contribute to a significant enhancement in inelastic deformability. This will contribute to extensive material loss. The maximum erosion rate of ductile materials (e.g. metals and alloys) has been found to be at the intermediate impact angles (e.g. 15°, 30°), while the maximum erosion rate of brittle materials (e.g. glass) is usually observed at the normal impact angle (90°) ([Oka et al., 1997]).

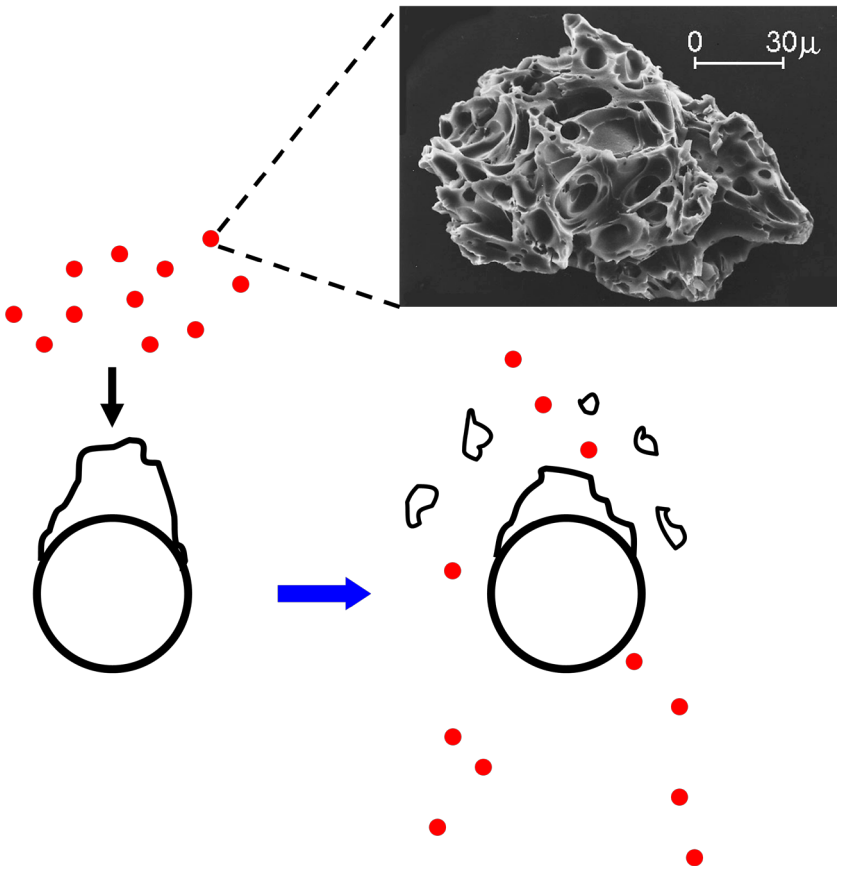

Figure 11-3: Deposit removal by erosion. Non-sticky, hard fly ash particles with lots of sharp edges (very common for quartz), collide with a non-sticky deposit surface, causing;

- Deformation (Ductile deposits)
- Cutting action (Brittle deposits)

Controlling parameters in erosion of deposits;

- Concentration of Quartz in fly ash ensamble
- Velocity upon impact
- Angle of impaction

According to [Oka and Yoshida, 2005a,b] it is generally considered, that material hardness is one of the main mechanical properties associated with erosion damage. Brittleness seems to be useful in characterizing erosion of ceramic materials. An erosion wear-resistant material has a hardness value higher than that of the impacting particle material. Results presented by [Raask, 1988] indicate that a wear-resistant material should have a hardness value about 500 kg/mm^2 higher than the impacting particle. The hardest mineral species in coal and biomass fly ash is un-reacted quartz [Raask, 1988], with a hardness value of about 1100 kg/mm^2. Thus, the usual indication for tube erosion is high silicate content and a high ratio of silicate to alumina [Latella and O'Connor, 1999].

11.3.2. Gravity Shedding and Flow of Liquid Slag

Gravity shedding is caused by gravity acting on a deposit and eventually breaking it down. A force balance is established between the gravitational force and the forces that keep the deposit on the (tube) surface, i.e.: [1)] the adhesion strength (between the deposit and the tube), and/or [2)] the deposit tensile strength (between/inside the deposit layers). When gravity is greater than the strength of the deposit (break-up of weak deposits) or the force between the deposit and the tube (detachment of deposit pieces), the deposit falls off, as shown in Figure 11-4. Gravity shedding of ash deposits depends on the gas temperature profile in the boiler and within the deposit, the deposit composition and the degree of deposit sintering [Zbogar et al., 2008].

Another form of gravity shedding is deposit removal by liquid flow. If the temperature is enough for development of low-viscosity slags, molten phases may run down the boiler walls. The temperature gradient through such a deposit will cause the slag layers close to the wall surface to be solid, while the outer deposit layer may be molten. With a relatively constant flue gas temperature, an equilibrium deposit thickness will be reached, where the mass flow of running slag balances the mass flow of depositing particles. An experimental investigation of deposit shedding [Zbogar et al., 2006] showed that melting is an important deposit shedding mechanism when firing straw.

11.3.3. Shedding Induced by Thermal Shock

Thermal stress occurs due to differences in the thermal expansion coefficient between the deposit and the tube metal/oxide scale or for that matter between different deposit layers. The thermal expansion coefficient α [m/mK], is defined as the increase in the length of a sample per unit increase in temperature, and can be used to determine if the materials are thermally compatible. Experience from the fabrication of glass/metal seals and manufacturing of enamel-coated products [Holland, 1964; Raask, 1985] shows that, for strong seals or adhering coatings, it is necessary to have compatible coefficients of the thermal expansion for metal, α_m and

coating material, α_g. For an enamel coating on steel [Raask, 1985] it is appropriate to have $\alpha_g \cong 0{,}9\ \alpha_m$.

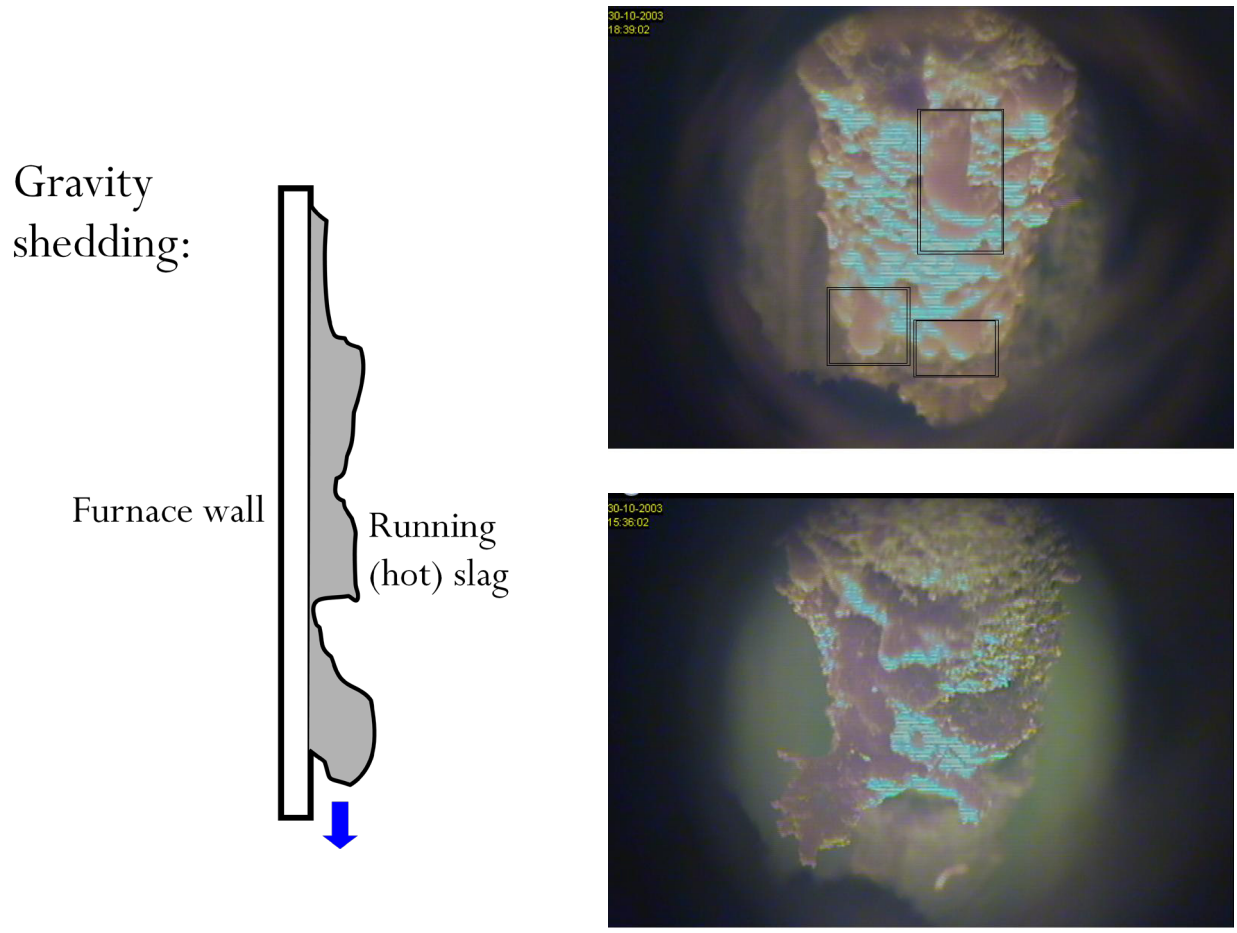

Figure 11-4: Gravity shedding of ash deposits.

Thermal expansion coefficients of steels and deposit constituents are provided in Table 11-3. In the case of mild steel, there are no big differences in the thermal expansion characteristics (11-12·10^{-6} K^{-1} for mild steel, and 5-9·10^{-6} K^{-1} for deposit constituents). Thus, when a strongly bonded ash deposit is once formed on a tube, it is not easily removed by thermal cycling. The thermal expansion of austenitic steel (16-18·10^{-6} K^{-1}) is significantly higher than that of oxides and deposit materials. In the absence of a boiler deposit, oxide scale (8-10·10^{-6} K^{-1}) is able to absorb thermal stresses, and the adhesive film remains intact upon cooling. However, it appears that oxide scale is unable to absorb thermal stresses in a similar manner when contaminated and constrained by bonded ash deposits. It is therefore common that ash deposits peel off austenitic tubes upon cooling, whereas the deposit formed on ferritic steels under the same conditions, remain firmly attached to the tubes [Raask, 1985].

Material	Thermal expansion coefficient, α [10^{-6}/K]
Steels	
Mild and ferritic steels	11-12
Austenitic steels	16-18
Oxides	
Tube metal oxides (Fe_3O_4, Cr_2O_3, NiO)	8-10
Deposit constituents	
Glassy material	6-9
Quartz (crystalline)	5-8
Silicates in fired brick	7-8

Table 11-3: Thermal expansion coefficients of steels and deposit constituents.

11.4. Soot-Blowing in Industrial Furnaces

The frequency of naturally caused shedding may be increased by different techniques built into the boiler like soot-blowing, cleaning by ultrasound, detonation waves, shot cleaning, and/or rapping gears. The asymptotic growth of an ash deposit can be changed to a periodic process by use of these active methods for deposit removal. Heat transfer between the flue gas and the working fluid is a dynamic process, affected by the thickness and porosity of deposit layers and by the intensity and the frequency of cleaning heat transfer surfaces.

Cleaning heat transfer surfaces, which is implemented in a boiler's operational schedule, is practical as long as the ash deposits are not highly sintered or strongly attached to the surface. Some deposits are removed almost immediately by sootblowing, leaving an almost clean tube surface. In other cases, deposits are difficult to remove and may leave a thin coverage of deposits on which subsequent deposition takes place [Wain et al., 1991].

Different soot-blowing mediums are used for removing different deposits. Water is the most effective medium for removing heavily sintered or slagged deposits. The use of water creates a pressure wave due to quick expansion of the liquid water to steam [Kailazine et al., 1997;

Ebrahimi-Sabet, 2001]. The major drawback of this cleaning method is that it causes abrasion and erosion of the boiler tubes, and consumes large amounts of high-pressure steam [Jameel et al., 1994; Kaliazine et al., 1997].

11.5. Shedding Measurements at the Avedøre 2 CHP Plant

An experimental study shedding of deposits has been conducted at the Avedøre 2 CHP-plant (AVV2) [Zbogar et al., 2005]. A scheme of the boiler showing the actual probe positions within the boiler is shown in Figure 11-5.

An advanced deposit probe was mounted in the secondary superheater region of AVV2, in order to investigate deposit shedding. The goal was to determine the governing shedding mechanisms under conditions similar to those prevailing in the actual furnace chamber.

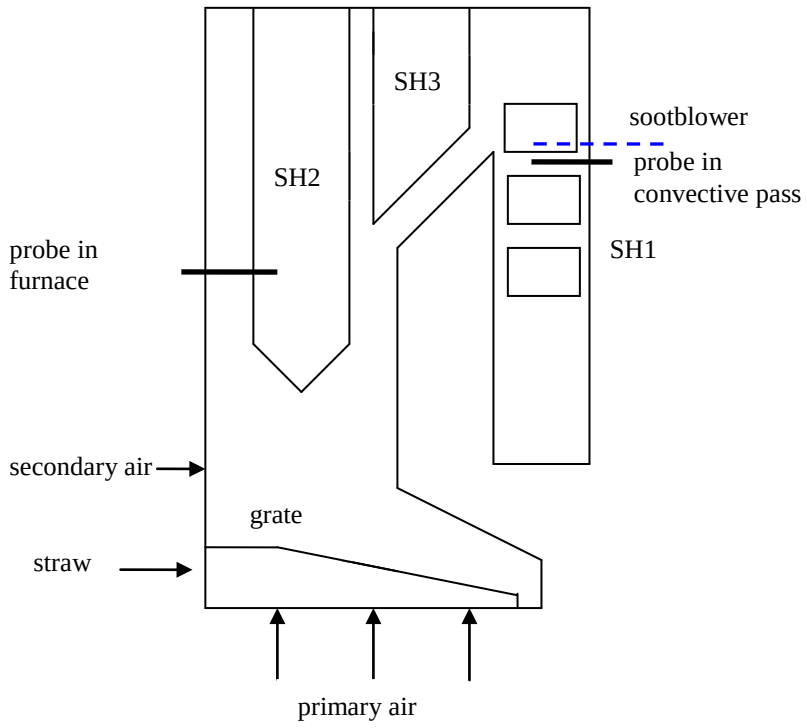

Figure 11-5: Schematic diagram of the grate fired boiler at the Avedøre power plant. Source: [Zhou et al., 2007].

Quantitative insight into the shedding process was obtained by measuring the heat uptake and the mass gain caused by deposit formation on and shedding from the probe. The shedding

probe [Zbogar et al., 2005] was kept inside the boiler for a total of 18 days in order to get a flair of the boiler dynamics and the effect of this on shedding. During this period, the boiler was shut down twice; after day 13, and again after day 17 [Zbogar et al., 2005].

The shedding probe was designed especially to conduct measurements relevant for deposit shedding, i.e. [1)] the temperatures and the flows of the cooling media (which was applied to quantify heat uptake by the probe) and [2)] deposit mass changes on the probe during operation. A scheme of the experimental set-up of the probe is shown in Figure 11-6.

The probe was a double annular probe, made of stainless steel and cooled by the counter-current flows of water and compressed air. The probe surface temperature was set to 500 °C, in order to simulate the superheater tubes in a biomass-fired boiler.

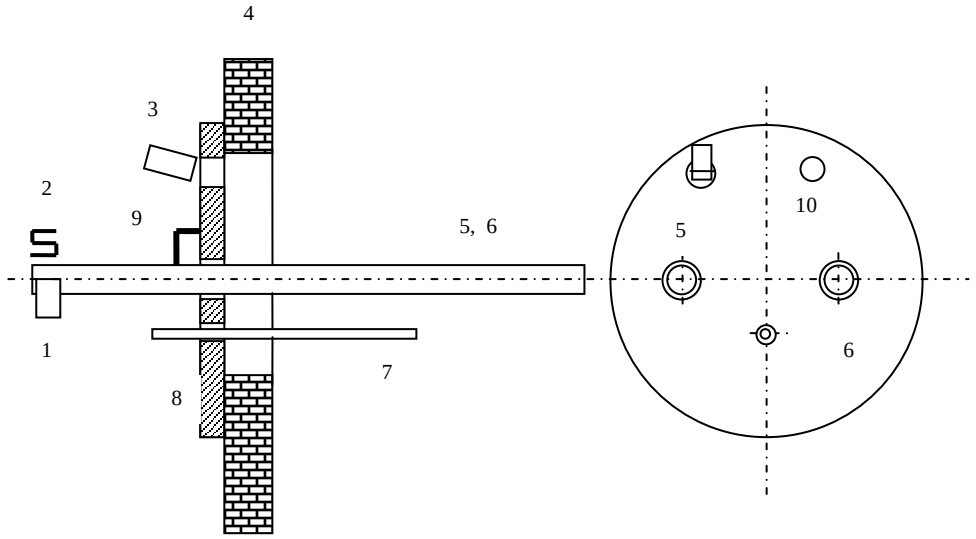

Figure 11-6: The shedding probe set-up applied in the AVV-2 straw-fired boiler. Notes: 1: balance weight, 2: load cell, 3: CCD camera, 4: boiler wall, 5: artificial sootblower probe, 6: deposit probe, 7: TC for flue gas temperature measurement, 8: flange, 9: probe hinge mounting, 10: incandescent light. Source: [Zhou et al., 2007].

The mass change due to deposition was measured using a load cell, which detects changes in mass due to deposition by detecting the force needed to keep the probe in a horizontal position. The total deposit mass was estimated by a momentum balance calculation, taking into account the forces that act on the probe. In the calculations it was assumed that the part of the probe inside the boiler would be covered by an uniform layer of ash deposit. The experiments showed that this mass measurement technique works very well, despite the strong fluctuations produced by flue gas flow [Zbogar et al., 2006].

The probe was continuously monitored by video using a high resolution CCD camera placed below the probe in front of a glass window on the furnace wall. Due to constant fouling of the glass window, it was periodically cleaned by pressurized air.

The measurements showed that, the flue gas temperature in the boiler fluctuated strongly in the range between 800 and 1100 °C and with an average temperature around 1000 °C. The main shedding mechanism, under these conditions, was melting of the outer surface of the ash deposit, and subsequently detached the ash droplets.

Observations of the shedding probe by the video camera showed that deposit build-up consisted of a number of stages. The time duration of these stages, most probably depended on the flue gas temperature, fly ash composition, and ash flux [Zbogar et al., 2005]:

- The initial stage of deposition, i.e. the formation of the inner white layer, could not be observed directly on the video recordings, but its existence was clearly visible when the probe was taken out of the boiler.
- The second stage of deposit formation can be described as the 'straw-web formation phase', where unburned (or partially burned) straw and fly ash particles form a 'web-like' deposit on the probe. On the video recordings, it looks as if some of the attaching particles did burn, prior to, or just after the attachment to the tube, although this may be difficult to distinguish clearly due to a very bright environment inside the boiler. The formation of a straw-web started rather early after the probe was inserted into the boiler (it was noticed approximately 25 minutes after the probe was fully inserted), indicating that condensation and inertial impaction, at these high flue gas temperatures occur in parallel. The absence of melt in the inner deposit layer indicates that the incoming particles, i.e. fly ash, unburned and partly burned straw, were partly molten in order to be able to stick to the surface. Figure 11-7 (left hand side) shows the shedding probe approximately 100 minutes after it was fully inserted into the boiler. The flue gas temperature was around 900 °C, and the solid network made of unburned and partly burned straw pieces and fly ash is clearly visible. This solid deposit sheds off the probe by gravimetric shedding of solid material.
- As time passed by and the deposit grew, the formation of drops between the deposit solid net became noticeable, which can be noted as the third stage of deposit formation. Figure 11-9 (right hand side) shows the shedding probe after 21 hrs in the boiler, when the flue gas temperature was around 1050 °C. At this high temperature, the outer layer of the deposit was already molten, and it flowed down the probe in the form of a running slag.

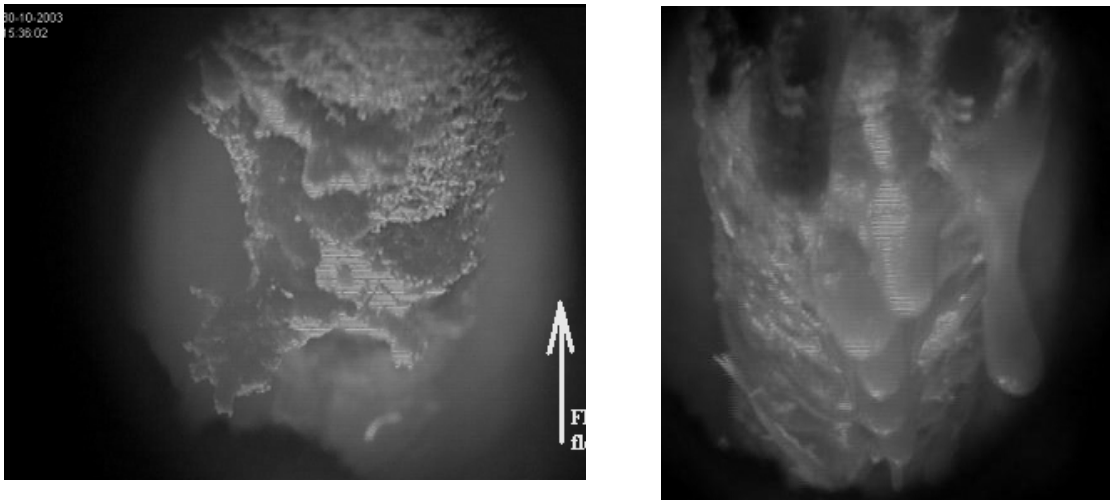

Figure 11-7: Images of the shedding probe after approximately 100 min. (left hand image) respectively 21 hours (right hand image) of exposure in the straw-fired AVV-2 boiler. Source: [Zbogar et al., 2006].

After the probe was taken out of the boiler, it was noticed that the deposit consists of two major, although weakly attached layers [Zbogar et al., 2005]:

- An inner white layer, formed mainly by condensation, and being app. 3 mm thick. It was porous and powdery in structure, containing small white and transparent crystals, but quite hard to remove from the probe. The existence of melt in this layer was not noticed.
- The outer deposit layer was brown, and 5-8 cm thick. It looked like it solidified from the melt, since the deposit was fused and highly porous. Gas voids inside the solid continuous phase were big, around 0.5 cm in maximum size.

Figure 11-10 shows the shedding probe after it was taken out of the boiler, and the outermost slagged layer removed. A white powdery layer was seen on the probe. The figure also shows the cross-sectional structure of the outer deposit layer that was attached to the probe (tube circumsphere is still visible in the bottom of the image). It was noticed that the outer, solidified layer was easy to remove from the inner, powdery layer, while the inner layer itself was hard to remove from the tube surface. Thus, it was concluded that 'the weak point' of the deposit-tube system was the attachment between the inner powdery layer and the outer slagged layer [Zbogar et al., 2005].

Video observation of the boiler superheaters and furnace walls confirmed that the slag flowed down the boiler walls in the same manner as it flowed down the probe.

Deposit build-up can be directly observed on the video and through the measurements of the probe mass gain. It is also possible to follow the deposit formation indirectly by observing heat uptake by the probe. The heat uptake and the weight measurements for the eighteen days in which the probe was exposed averaged over 10.000 seconds together with the flue gas temperature in Figures 11-8 and 11-9 [Zbogar et al., 2005]. Between day 5 and 7, the flue gas temperature was not measured, while at day 6, the data acquisition system was not started. On day 13, the boiler was shut down for the first time, then on day 15 restarted again, and finally on day 17 it was shut down for the second time.

Since the deposit acts as a thermal resistance, the heat uptake by the probe is expected to decrease after the deposit was formed. This is noticed in Figure 11-8, as a decrease of the measured heat uptake over time, between days 2 and 10, while the flue gas temperature does not vary as much. Figure 11-8 also shows that, during the initial deposit build-up phase (0-6 days), the probe heat-uptake decreased from approximately 13 kW to 7 kW. In the relatively stable period from day 7 to day 13, a heat uptake above 7 kW was only observed when the flue gas temperature was above 1050 °C. It was concluded that the flue gas temperature increases the heat uptake on a short time scale, since the trends of these two properties are simultaneous.

Two regions can be distinguished in Figure 11-9, namely the initial steep mass increase (days 1-6) and a later, somewhat slower, mass increase. The mass gain did not reach a completely steady state, i.e. it did not become constant, most probably due to the fact that the ash deposit behavior changed drastically in the temperature range 800 – 1100 °C, because the deposit was either semi-molten (lower temperatures, slow flow of melt, which contained solid particles) or completely molten (high temperatures - running slag).

After the boiler was restarted, prior to the first shut down, the initial heat uptake was increased due to the partial detachment of deposits from the tube (see Figure 11-8). An increase in the deposit mass was again noticed when the boiler was restarted, between day 15 and 17 (see Figure 11-9). This mass flux was much higher compared to the initial mass flux, possibly due to the existence of the initial layer on the probe, or because the fuel used on day 15 to 17 had a higher ash content.

In a later study of shedding, a series of well controlled soot-blowing experiments were performed at AVV2 using the shedding probe and a probe sootblower [Zhou et al., 2007]. The probe system was placed in the top of the second draught near the primary superheater where the flue gas temperature was approximately 750°C. Deposit was allowed to accumulate on the probe and a separate sootblower probe was used to expose the deposit to jets of pressurized air with known PIP. The influence of residence time and surface temperature of the shedding probe on the required PIP values was quantified. Besides information on the removability of the deposits it was also possible to obtain information on deposit chemistry, deposit formation rate and heat transfer to the probe.

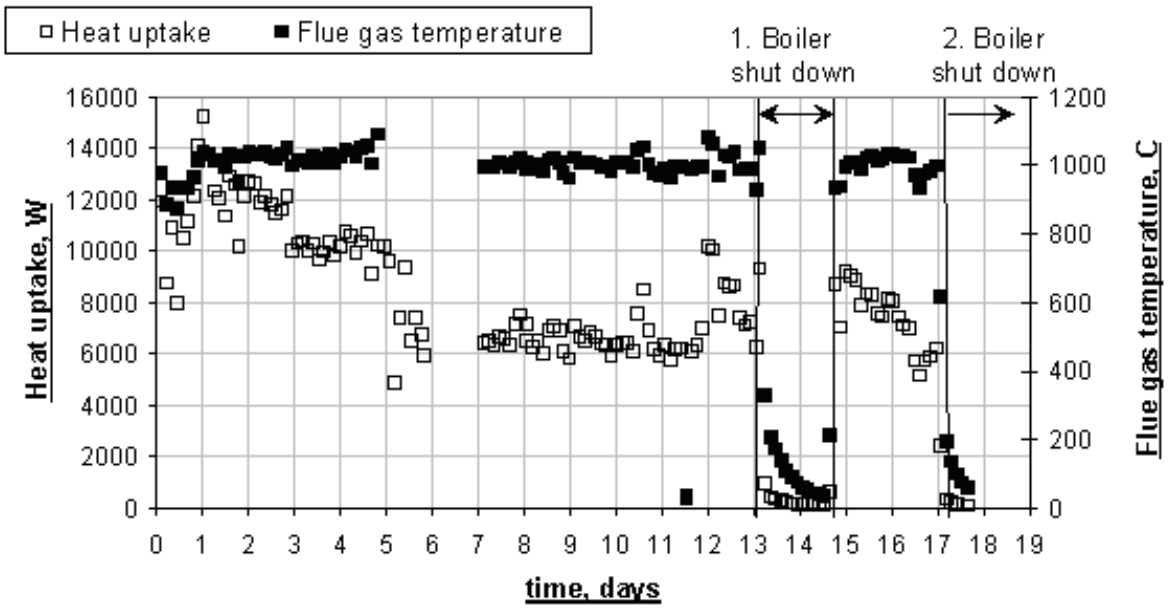

Figure 11-8: The heat uptake by the shedding probe, and the flue gas temperature, both averaged over 10.000 seconds. Source: [Zbogar et al., 2005].

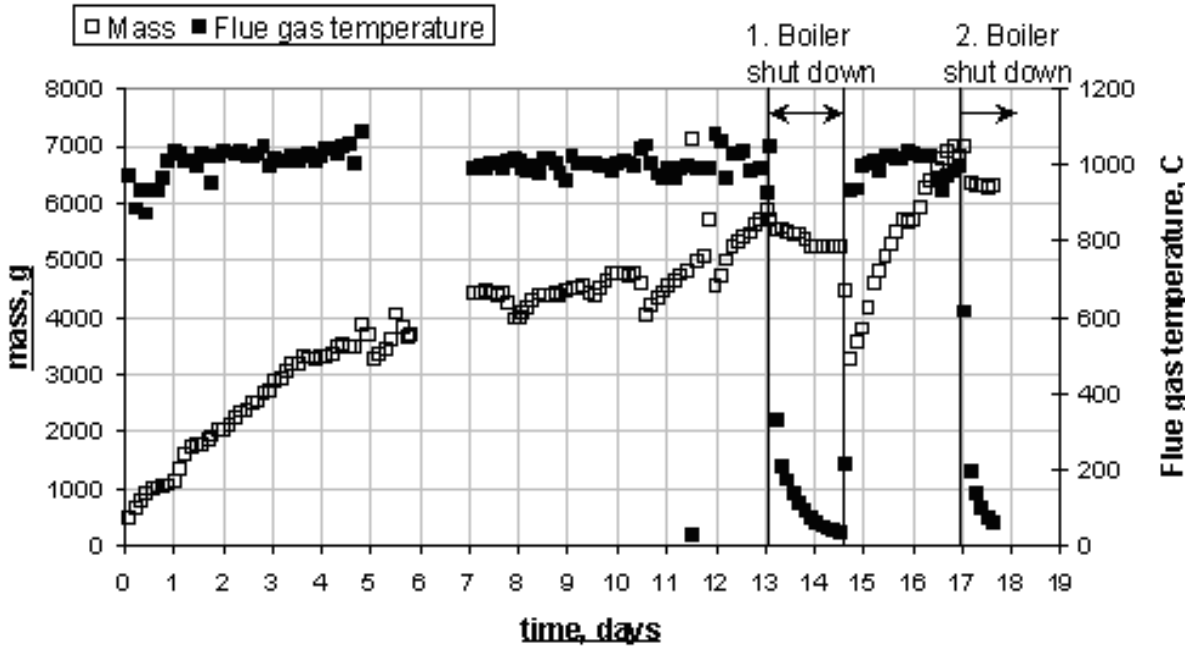

Figure 11-9: The mass build-up by the probe and the flue gas temperature, both averaged over 10.000 seconds. Source: [Zbogar et al., 2005].

Probe temperatures from 400 to 550°C were applied, and the total exposure time of the shedding probe in the boiler was more than 2100 hours.

It was observed that increased residence time or probe temperature meant that less of the upstream outer layer deposit was removed. At a probe temperature of 400°C nearly all deposit was removed even at moderate PIP-values. At 450°C and 500°C the required PIP increased with time, and at 550°C even with the maximum available PIP of 190 kPa, no deposit was removed.

Besides the quantification of the PIP needed to remove the shedding probe deposits, several conclusions were drawn [Zhou et al., 2007]:

- By use of the probe weight measurements, the deposit formation rate between sootblowing events could be determined. The mean deposition rate seemed to be reasonably independent of the probe temperature and was measured to be in the range [30 - 45 g/m^2h].
- The influence of sootblowing on heat uptake depends on the surface temperature of the probe. At probe temperatures of 500 °C and 550 °C the heat uptake initially decrease, but levelled off 4-6 days after the probe was placed in the boiler, while the heat uptake was kept constant at a probe temperature of 400 °C.
- The probe temperature also affects the deposit porosity significantly, i.e. the porosity was rather high at 400°C, but significantly lower at higher temperatures.
- Compared with the concentrations of elements in the fly ash, the upstream deposits were rich in the non-volatile elements Ca and Si. A tendency for less Cl in the high temperature probe deposits was observed.

11.6. Summary

In June 2000 DTU hosted a Topic Orientated Technical Meeting (TOTEM) within the frame of the International Flame Research Foundation (IFRF) on recent and future development of ash and corrosion research activities. One of the conclusions at that meeting was that there – at that time – was a fundamental lack of understanding and means of quantification of shedding of deposits. The above outline will prove that we took that challenge seriously and have gained a significant step forward in the description and understanding of shedding mechanisms.

Experimentally, the advantage of the shedding probe developed and applied by [Zbogar et al., 2005] is that it can give steady and stable measurements of heat uptake and mass accumulation. Among the important achievements at AVV-2 is that we were able to detect mass changes on the probe, despite strong fluctuation of the flue gas velocity inside the boiler. The video

recording of the probe showed to be a simple and very useful technique for providing qualitative knowledge of the shedding process.

The video recordings showed that for flue gas temperatures in the range [800 – 1100 °C] the deposit develops in distinct phases in the beginning, a solid network of unburned and partly burned straw pieces, and fly ash is formed, which sheds mainly due to gravitational force. As the thickness of the deposit increases, the surface temperature of the deposit increases and formation of molten phases begins at the surface.

In full-scale shedding measurements with the shedding probe it was expected that, for a long exposure time, the deposit mass would reach a constant value due to an established equilibrium between ash deposition and shedding, or 'forces' building up and removing deposit, but as shown in this chapter, this steady state was never reached and it is questionable whether it is at all possible to reach a steady-state in deposit build-up vs shedding/rmoval.

In the later soot-blowing study, it was observed that increased residence time or probe temperature meant that less outer layer (upstrteam) probe deposit could be removed. At a probe temperature of 400°C, all deposit could be removed even at moderate PIP values. At 450°C and 500°C, the required PIP increased with time, and at 550°C, even with the maximum available peak impact pressure of 190 kPa, no deposit could be removed.

A number of minor projects have been defined as part of the shedding activities, including a detailed study of sintering of deposits. The strength increase in deposits can be related to melt formation although some strength increase seems to appear before the initial melting of the sample begins. The strength decrease at higher temperatures was found to be caused by volatilization of some ash components. A characteristic sintering temperature T_{sint} can be defined as the temperature where the compression strength increases above 2 N/mm^2. The sintering and strength development of an ash is influenced by chemical composition, ash particle size, sintering time and probably also flue gas composition. The measured sintering temperatures (T_{sint}) of the ashes investigated as part of our sintering studies, lead to the following conclusions:

- For very alkali-rich ashes dominated by K, Na, S and Cl, with only a low content of Si and Ca, T_{sint}-values in the range [370 - 470°C] were observed.
- Straw- and grass-derived ashes, with a high content of Si and K, had T_{sint} values in the range [610 - 710°C].
- For wood ashes, rich in both Si, K and Ca T_{sint}-values > 780°C were observed.
- Ashes from coal (bituminous) and coal straw co-firing (maximum 20% straw share on an energy basis), had T_{sint}-values in the range [920 - 1010°C].

Chapter 12:

ACCUMULATING AND COMMUNICATING THE MATERIAL

In 1994, I had the pleasure of following an ash and trace element course provided by the Energy and Environmental Research Centre, at University of North Dakota, Grand Forks, North Dakota. The EERC course focused fully on coal-fired systems, but I adapted the idea and decided to develop a similar course with the focus on biomass-fired systems.

Thus, an intensive course has been defined, based on several years of cooperation on ash and trace element chemistry in thermal fuel conversion systems, between the Technical University of Denmark (DTU) and the Åbo Akademy University, Finland (AAU). The basic idea behind the course is to accumulate recent data on fuel characterization, slagging, fouling, corrosion and trace element transformations in a course that can be provided for industry people. This ensures understanding and application of the research, and provides the industry with a forum for discussion of the latest research results on these issues in biomass-fired systems, as well as feed back from the industry to the research institutions on important new research subjects.

The first version of the course was provided at AAU in March 1996. Since then, several versions have been provided all over Scandinavia at a rate of one to two courses per year, always with several industry people participating and taking an active part in the course. The course serves not only as an educational tool for new people in the energy producing industry, but also as a way of updating know-how to the latest stage (state-of-the-art) (see [Frandsen et al., 2006])

The course covers all relevant aspects on ash and deposit formation and corrosion in modern thermal fuel conversion systems including fuel and ash characterization, formation and transport of different ash fractions, deposit formation and corrosion, boiler aspects and case studies.

12.1. Introduction to the Course

Ash deposition on heat transfer surfaces has been an extensive research area over several years. Today, a good qualitative understanding of many of the phenomena exists [Benson et al., 1993, Bryers, 1996].

Most of the earlier works concentrated on coal [Benson et al., 1993, Bryers, 1996], but in the last decade biomass and waste-fractions have become more and more relevant as fuels, due to their CO_2-neutrality (for biomass, the CO_2 uptake during growth equals CO_2 release during combustion).

Biomass resources include wood residues, agricultural residues (such as straw and food processing residues) and dedicated energy crops. The combustion of biomass fuels and waste fractions, in particular annual crops and herbaceous materials, often leads to the formation of unmanageable deposits, as well as increased corrosion of heat transfer surfaces at high steam temperatures [Frandsen, 2005].

A Nordic Ash and Trace Element Chemistry short course was provided for the first time in March 1996, consisting of a series of presentations outlining recent research activities. After the first course, it was decided to develop it to contain also fundamental, text-book material on ash and deposit formation, corrosion and trace element chemistry, in order to provide a consistent, full package course for industry as well as academia.

The basic idea of the course is to provide the industry with quick, easy-to-access, up-to-date information on the latest research and development within ash and trace element chemistry.

12. 2. The Form of the Course

The course consists of a number of oral presentations running on fully PowerPoint-based slides, covering the following main subjects:

- Fuel characterization including basic fuel data achieved with both conventional methods (proximate, ultimate analyses, ash fusion tests) and advanced methods (SEM/EDX, CCSEM, chemical fractionation)
- Ash characterization methods (TGA/DSC analyses, SEM/EDX, CCSEM, SEMPC, viscosity measurements)
- Boiler aspects with respect to ash behaviour
- Formation of ash species (release of ash-forming elements, formation of aerosols and residual ash, gas phase chemistry, entrainment of ash particles)
- Transport of ash species (diffusion, thermophoresis, inertial impaction)
- Adhesion of ash particles to a surface (amount of liquid phase, viscosity of slag)
- Consolidation and shedding of deposits (mechanisms of sintering and shedding, heat transfer in deposits)
- Corrosion (low- and high-temperature corrosion mechanisms, deposit-alloy interactions)

- Case studies (types of measurements, design and operation of probes, specific cases at plants)
- Trace element transformations

Thus, the course is a combination of information on methods of characterisation fuels and ashes, boiler design and, finally, a formal outline of formation of a troublesome deposit through a number of consecutive steps:

- Release of ash-forming elements during pyrolysis, and subsequent char burnout
- Formation of aerosols from flame-volatile, ash-forming species or elements, heterogeneous condensation of ash forming species, and formation and entrainment of residual ash during char burnout
- Transport of different ash forming species from bulk gas to the heat transfer surfaces of the system
- Adhesion and consolidation of ash forming species to the heat transfer surfaces
- Build-up, sintering, shedding, and heat transfer in deposits

The presentations are usually supported by a number of exercises, where the participants are allowed to address simple calculation problems as part of the course.

The total length of the course may be from 3-4 hours up to five full days, depending on the request for exercises, experiments, lab- or full-scale visits during the course.

12.3. Fuel Characterization

This part of the course provides an outline of fundamental fuel characterization procedures like the ultimate, proximate and bulk ash chemistry analyses (see Figure 12-1).

The fuels considered are mainly coal and biofuels, such as different types of wood and annual biomasses, but also waste-fractions are also included. Different liquid fuels like oil/oil-derivates and orimulsion are also being introduced.

The standard methods for characterizing a fuel, are the proximate and ultimate analyses. In the proximate analysis, the total moisture, air-dried moisture (=inherent), volatile matter, ash and fixed carbon of the fuel are given. In the ultimate analysis, the elemental composition of the organic matrix of the fuel is given, which includes the carbon, hydrogen, nitrogen, sulphur and oxygen (by difference) content of the fuel.

Recently, more advanced methods have become available. These include chemical fractionation analysis (CFA) and scanning electron microscopy (SEM) combined with energy dispersive X-ray analysis (EDX). These new and advanced methods provide more information about the abundance, size and association of inorganic components in the fuel. For low-rank, subbituminous and lignitic coals, wood and biomass, the quantification, abundance and type of inorganic elements can be characterized by chemical fractionation. In this method, inorganic constituents are selectively extracted from the fuel by successive leaching steps with different materials [Benson and Holm, 1985; Blomqvist, 1998; Zevenhoven, 2001]. The method may be applied as an input for addressing deposition propensities for fuels and fuel mixtures [Zevenhoven et al., 2003; Yrjas et al., 2004].

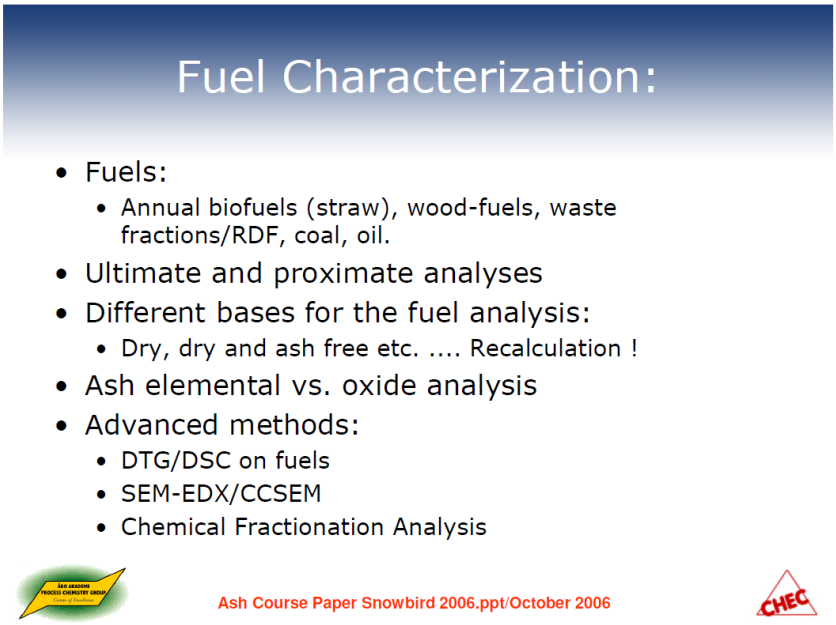

Figure 12-1: Fuel characterization issues addressed in the course.

12.4. Ash Characterization

Several methods exist for the characterization of ashes, i.e. their chemical composition, melting and/or rheological properties (see Figure 12-2). The main focus is on:

- Thermal Gravimetric Analysis (TGA)/Differential Scanning Calorimetry (DSC) analyses,
- Scanning Electron Microscopy Energy Dispersive X-ray analysis,
- Computer Controlled Scanning Electron Microscopic (CCSEM) analyses,
- Scanning Electron Microscopy Point Count (SEMPC) analyses, and,

- Viscosity measurements

Thermal Gravimetric Analysis (TGA)/Differential Scanning Calorimetry (DSC) analyses are used to quantify the release of volatile species from low temperature (~ 550 °C) biomass-derived ashes, but may also be applied to identify ash transformations incl. melting in ash samples and the temperature ranges of ash fusion [Hansen, 1997; Hansen et al., 1999a,b].

In Scanning Electron Microscopy (SEM), a sample is examined using an electron beam. Two signal types are commonly used for producing images of the sample: Secondary Electrons (SE) and Back Scattered Electrons (BSE). The image produced by secondary electrons is a light/shadow image that reflects the surface of the sample. On a backscatter electron (BSE) image, the intensity of the backscattered electrons is a function of the atomic number; the higher number, the brighter it appears. It is possible to distinguish the mineral particles in the BSE image, as they appear brighter than the organic fuel matrix and the mounting media. Energy Dispersive X-ray (EDX) detection is generally used for semi-quantitative chemical analysis.

Computer Controlled SEM (CCSEM) makes it possible to quantify the size, shape (deviation from circularity), quantity and semi-quantitative composition of mineral grains in a fuel or a fly ash sample based on backscatter electron imaging and energy dispersive x-ray analysis. Limitations in the technique as well as comparisons between CCSEM-analyses and bulk chemical analyses are provided in the course.

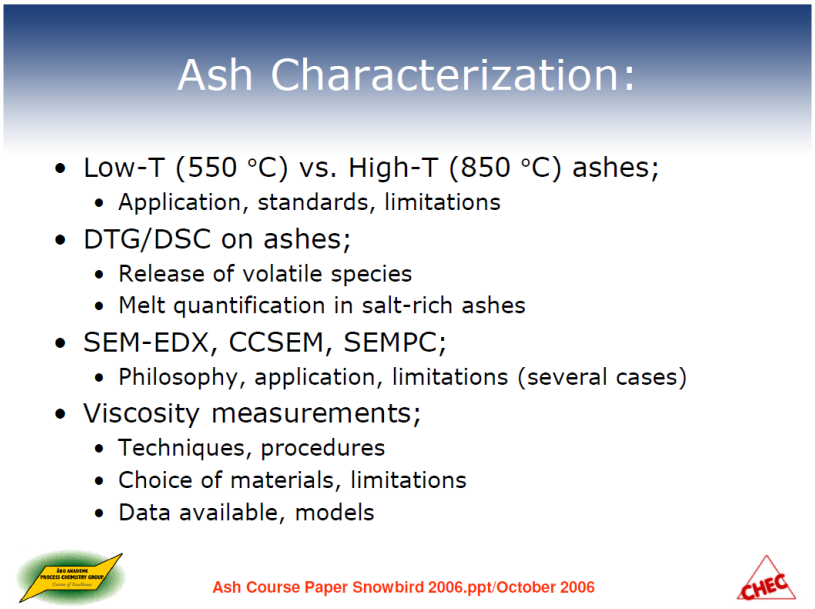

Figure 11-2: Ash characterization issues addressed in the course.

A Scanning Electron Microscopy Point Count (SEMPC) is a technique similar to CCSEM, but does not provide any size distributional data, since it is developed for studying sintered ash

samples in deposits (where it may be impossible to identify individual ash particles). Examples of comparisons between SEMPC analyses and bulk ash chemical compositions are shown in the course.

The rheology (flow properties) of ashes is introduced, together with an outline of how to measure ash viscosities and how to estimate the viscosity of an ash sample with a known chemistry at a given temperature.

12.5. Boiler Aspects

The boiler technology aspect is important, since it not only affects the actual physical ash-split in the furnace, but also the temperature profile throughout the furnace and in the flue gas channel. This may strongly affect residual ash formation, and the super saturation of flue gas with flame-volatile ash-forming species, leading to subsequent aerosol formation in the system. The course provides an introduction to fundamental boiler technology, i.e. the principle of operation of different types of boilers, and the basic ideas behind a steam power plant. The types of combustion technologies considered are; grate firing (mainly of biofuels and waste fractions), suspension firing (of coal and co-combustion of coal and various biomasses) and fluid-bed combustion (coal, waste, biomass and mixtures thereof). The main focus is on the ash chemistry aspects of different boiler technologies (see Figure 12-3).

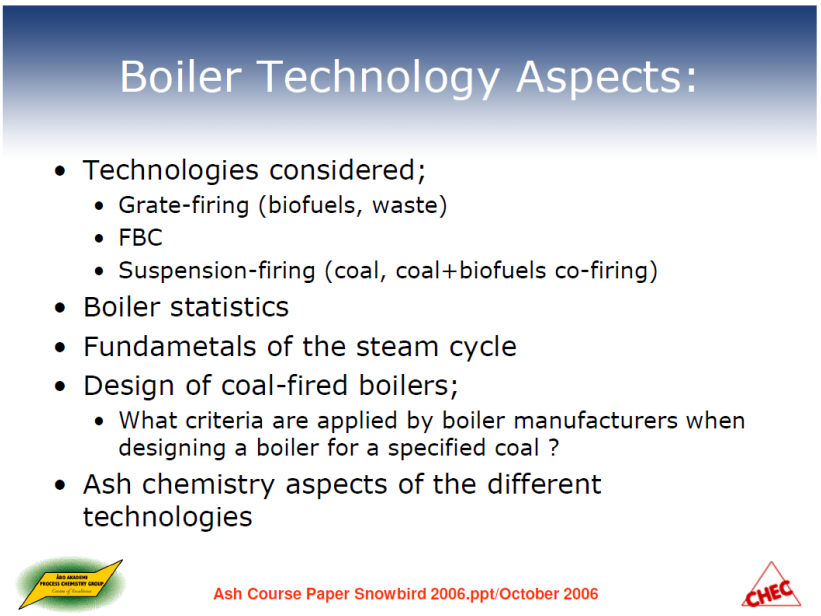

Figure 12-3: Boiler aspect issues covered in the course.

12.6. Formation of Ash Species

Formation of ash species is the main topic in the course. Formation and chemical composition of submicron particles, and coarse fly ash particles is addressed (see Figure 11-4).

The basic idea is to follow the ash-forming elements from their association in the fuel, through either release to the gas phase or remaining in the char, to different fly ash size fractions (either aerosols or residual ash particles).

First, the release of elements is outlined. Good data for the release of K, Na, S, Cl, Zn and Pb from annual biomasses (energy crops, straw, miscanthus, etc.) and wood-type fuels (like beech, spruce, waste wood, bark and fibre board) can be found in the literature [Knudsen, 2004; van Lith, 2005] and are subsequently outlined.

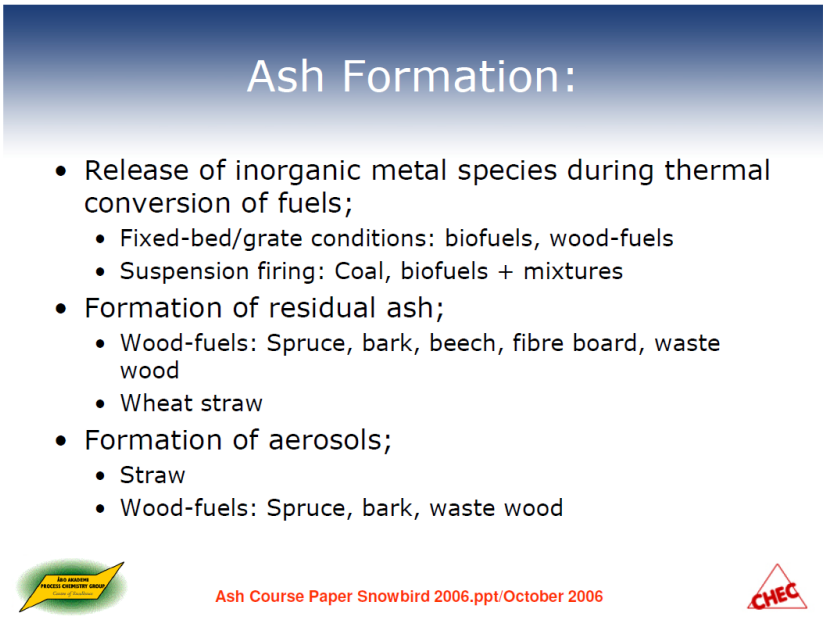

Figure 12-4: Aspects of ash formation treated in the course.

Secondly, we look at how these elements may form fly ash. This happens via at least two major mechanisms, which causes a bimodal size distribution. A major peak located from 3-50 μm [Flagan and Friedlander, 1978], comprises the so-called residual ash, with a mean particle size of about 10 μm. Another, minor, peak comprises the submicron ash particles, which have a mean particle size of about 0.1 μm [Flagan and Friedlander, 1978].

For coal combustion in a PC-fired unit, the residual ash constitutes approximately 98-99 wt% of the total fly ash. The submicron ash particles constitute approximately 1-2 wt% of the total fly ash and are often named as an inorganic "fume" [Flagan and Friedlander, 1978].

Submicron ash particles are formed either by flame-volatilised metal species, or due to thermal or chemical decomposition (inorganic reaction) of the inorganic constituents. In the near vicinity of a char particle surface, or as a consequence of too little surface being present or too rapid cooling of the flue gas, super saturation of flame-volatilised metal species may occur, thereby leading to nucleation and formation of very small nuclei. These can then grow by coagulation and homogeneous condensation. The nuclei may agglomerate and afterwards coalesce into spherical particles, thereby leading to a narrow peak in the size distribution of the particles [Flagan and Friedlander, 1978].

12.7. Transport of Ash Species

This section of the course deals with the transport of ash species in a boiler, i.e. inertial impaction, thermophoresis and diffusion (see Table 12-5).

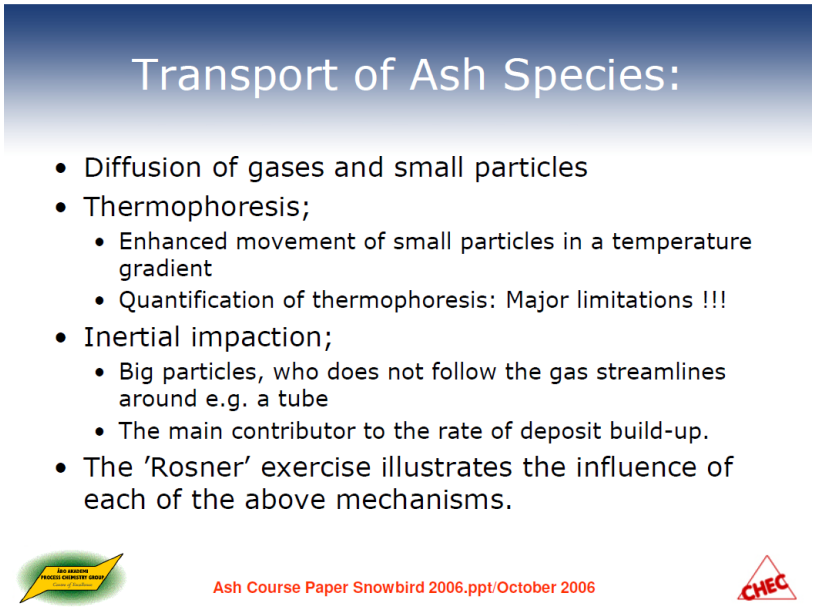

Table 12-5: Aspects of ash formation introduced in the course.

Transport to and the capture of ash species on heat transfer surfaces is a function of the size, the chemical and physical properties of the transported species and the combustion system's

geometry and conditions such as the gas flow pattern, the velocity profile, the local temperature, etc. [Bryers, 1996]. Sub-micron particles and vapour phase species are transported by small particle or vapour phase diffusion [Flagan and Friedlander, 1978] or by thermophoretic forces: whereas coarse particles (d_P > 10 μm) are deposited mainly by inertial impaction [Samms and Watt, 1966].

Particles entrained in a gas flow in a space where a temperature gradient acts upon them are subject to a thermophoretic force, leading to movement towards lower temperature areas. This phenomenon is known as thermophoresis. A temperature gradient within the particle itself can also lead to diffusion through thermophoresis [Flagan and Friedlander, 1978].

Condensation is not a transport mechanism, but it may enhance diffusion by removing condensing gaseous species from the immediate proximity above a deposit, through at least one of two different mechanisms:

- Vapors diffuse through the boundary layer and condense heterogeneously on a heat transfer surface, on the surface of an already formed deposit or within a porous deposit, or,
- Vapors may nucleate homogeneously in the boundary layer, and then be transported by either small particle diffusion or thermophoresis.

Inertial impaction takes place when large particles (usually d_p > 10 μm in PC-fired boilers) have too large an inertial momentum to follow the gas streamlines around the heat transfer surface (usually a tube), and instead impact on the surface [Samms and Watt, 1966] accounts for the bulk of deposit growth.

The principle of each of these mechanisms, as well as calculational tools for their quantification is outlined in the course. An exercise in the course provides an example of how quickly each of the main transport mechanisms works.

12.8. Adhesion of Particles to Surfaces

This part of the course deals with the stickiness/adhesion of ash particles to heat transfer surfaces. The importance of different types of liquid phases on particle adhesion is presented. In addition, other types of adhesion mechanisms are reviewed (see Figure 12-6).

When arriving at a heat transfer surface, an ash particle may either stick to the surface or rebounced from it and be carried away from the point of impact by the flue gas. The sticking and adhesion of an ash particle depends upon several factors.

Sticking mechanisms where a liquid phase is present, either in the particle arriving at a surface or on the surface, is usually dominating. This liquid phase may be either viscous or non-viscous.

Other adhesion mechanisms such as chemical reactions between particles and surface, as well as between particles and an existing deposit, may also be active.

Capture efficiency is a measure of the propensity of a material to stick to a surface when impacted. For PC- fired systems this measure has been shown to depend upon the viscosity of the incoming Si-rich particles and/or a molten deposit surface, as well as the morphology of the deposit [Benson et al., 1993]. The capture efficiency has been described through a sticking coefficient that is a function of the viscosity of the ash particle and the heat transfer surface.

The molten phase acting as a sticking agent can also be non-viscous. This has been found in biomass firing where ionic salt-type alkali sulfates and chlorides are present [Hupa and Backman, 1983; Backman et al., 1987, 1999; Skrifvars et al., 1999]. In this case, the amount of molten phase plays the major role for stickiness.

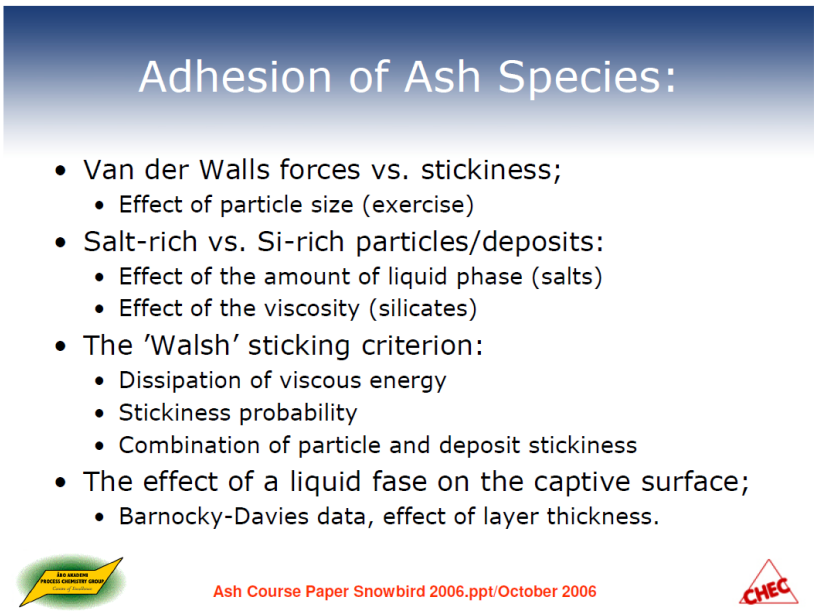

Table 12-6: Aspects of adhesion of ash species introduced in the course.

12.9. Consolidation and Shedding of Deposits

Ash deposition may constitute a serious operational problem in utility boilers, particularly when the amount of deposited ash is large. The operational considerations include the ease of removal of ash from the heat transfer surface (the bonding efficiency on the heat transfer surface and the deposit strength), deposit viscosity/flow properties, and heat transfer to the water/steam cycle. Among the factors, that determines these characteristics are the chemical composition, temperature, porosity, and deposit morphology.

Mechanisms of sintering and shedding, as well as heat transfer in deposits are the major issues in this part of the course (see Figure 12-7). Several years of research on sintering at the Åbo Akademi [Skrifvars, 1994], as well as in shedding of deposits at DTU [Zbogar et al., 2005], is implemented in the course material, which also includes several calculational exercises on the adhesion of particles to surfaces.

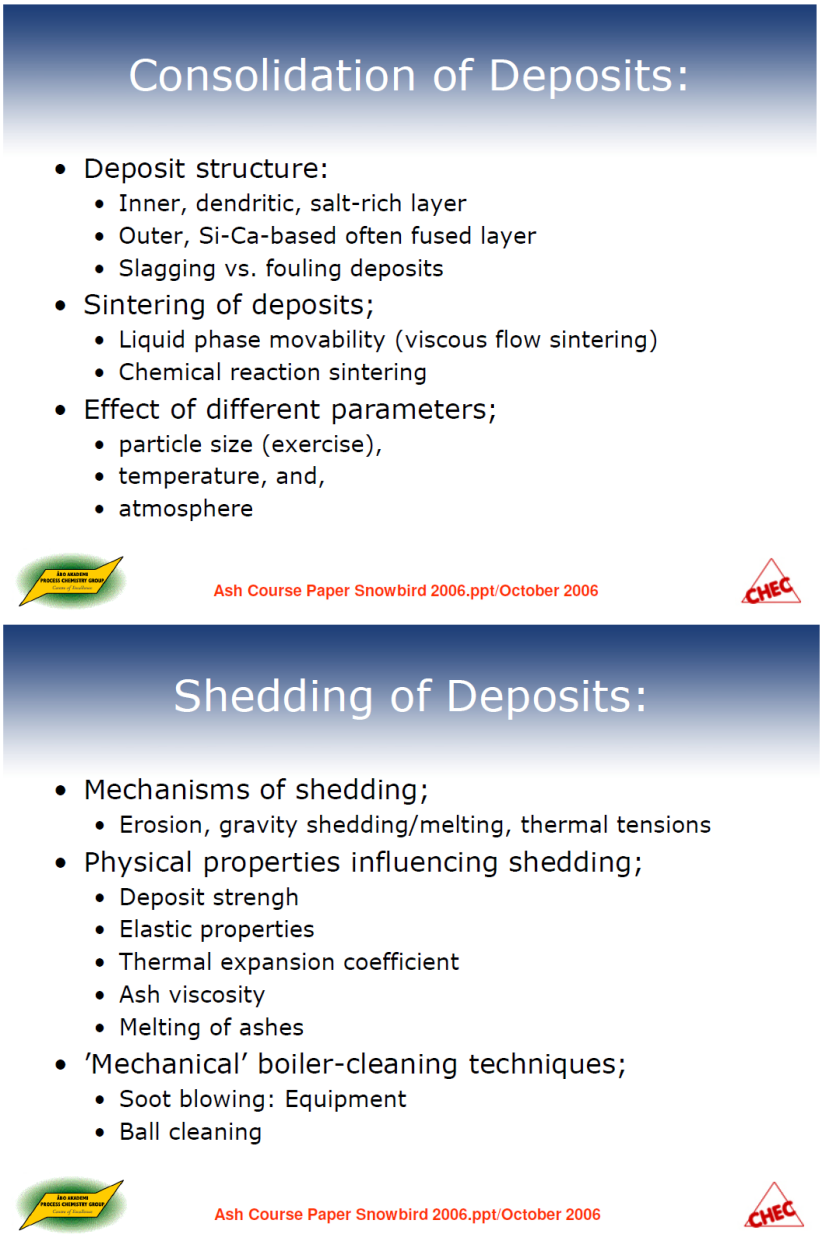

Figure 12-7: Aspects of consolidation and shedding of deposits as introduced in the course.

12.10. Cl-Induced Corrosion in Combustion Systems

In this part of the course the main focus is on Cl-induced corrosion caused by accumulative sulfation of metal chlorides deposited in the inner layer of deposits (see Figure 12-8), as this has proved to be a major corrosion mechanism in biomass- and waste-fired boilers.

The inner layer of a deposit in a biomass- or waste-fired utility often consists of a thin layer rich in metal chlorides, e.g. KCl, NaCl, $ZnCl_2$ or $PbCl_2$ [Nielsen et al., 2000a]. These chlorides are extremely chemically aggressive at temperatures above 500 °C, and may cause serious corrosion by reaction with Fe and Cr in the alloys forming the heat transfer equipment.

Experience from several years of corrosion studies at Danish Power Stations is provided, side by side with lab-scale studies [Nielsen et al., 1999, 2000a; Nielsen, 1998] designed to outline corrosion rate-laws for materials covered by different types of corrosive salt blends.

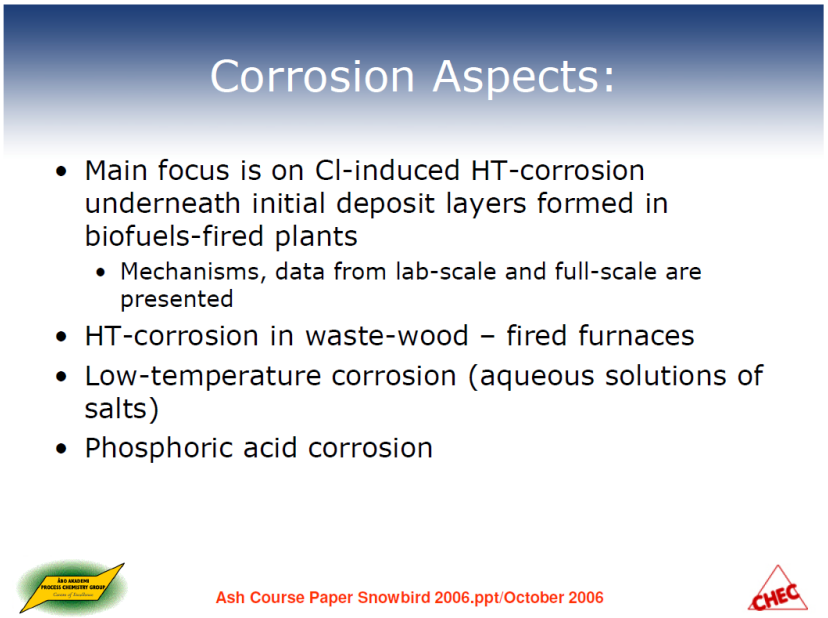

Figure 12-8: Aspects of corrosion treated in the course.

12.11. Case Studies

As with all other teaching, the easiest way to make an illustrative point is by a practical example. The course does contain several case studies, mainly from Danish Power Stations, which are sub-divided into two categories (see Figure 12-9):

- Grate-firing cases
- Suspension-firing cases

Figure 12-9: Case studies introduced in the course.

The grate-firing cases cover a classical full-scale study of ash and deposit formation and corrosion at the Rudkøbing CHP Plant [Nielsen, 1998], a study of short-time probe deposits [Frandsen et al., 2003], mature in-boiler deposits [Hansen et al., 2000], low-temperature corrosion [Frandsen et al., 2002] at the Masnedø CHP Plant, and, finally, a study of mature in-boiler deposits in one of the most recent stand-alone straw-fired boilers, the Maribo-Sakskøbing CHP Plant, in Denmark.

Suspension-fired cases cover the main study of the influence of coal-straw co-firing on ash formation and deposition at the Midtkraft-Studstrup Power Station [Hansen et al., 1999a,b, Andersen, 1998; Andersen et al., 2000], straw/oil-firing at the Kyndby Power Station [Nielsen, 1998] and, finally, an outline of a fundamental Danish study of ash and deposit formation in PC fired furnaces in the early 1990s [Laursen, 1997; Laursen et al., 1998].

12.12. Ash and Deposit Formation in WtE Plants

The recent focus on increasing the thermal conversion of waste and waste fractions has brought special attention to the characterization of waste-derived ashes, ash chemistry in waste-to-

energy (WtE) plants, corrosion and deposition and operation of different types of waste incineration plants [Frandsen et al., 2004; Frandsen, 2005; Arvelakis and Frandsen, 2005]. In this part of the course, the main focus is on the physical and chemical characterization of different types of waste, as well as ashes derived from waste incineration. Special problems connected to ash deposition and particularly corrosion, as well as ash quality aspects in WtE plants, is thoroughly addressed (see Table 12-10).

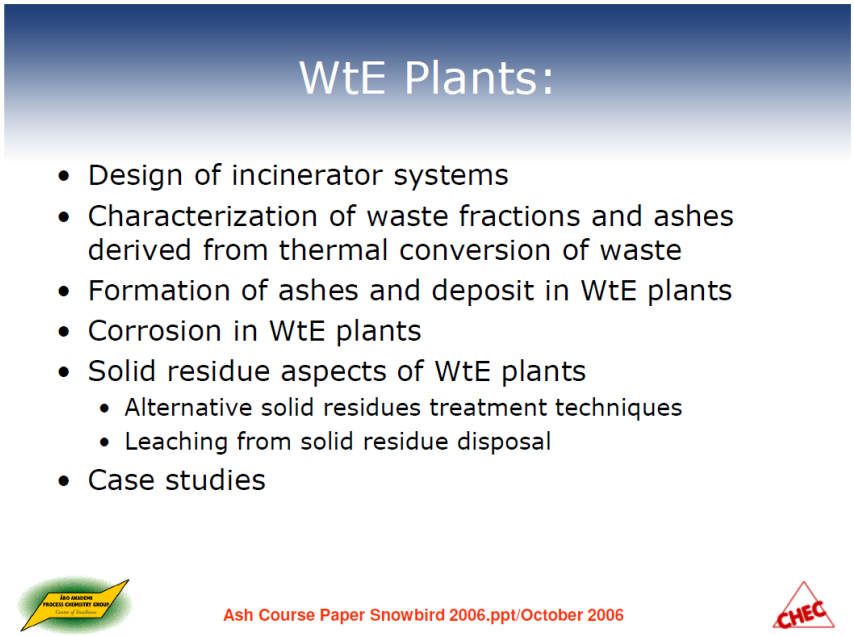

Figure 12-10: Aspects of deposit consolidation, heat transfer and shedding covered in the course.

12.13. Modeling of Ash Transformations and Deposition

Early in the course's history decided to add a session on modelling of ash deposition in furnaces. Two main concepts are considered:

- Multi-phase, multi-component Global Equilibrium Analysis (GEA), and,
- Mechanistic modelling and empirical prediction of ash deposition

An outline of the necessary assumptions and limitations within multi-phase, multi-component GEA is provided. Several examples of how GEA may provide valuable chemical and physical information about different processes in a thermal fuel conversion system are provided.

Another way of trying to predict ash deposition propensities is by empirical ash chemistry and plant indices. The base for, and limitations of, these predictions are explained in the course.

Even more complex is mechanistic modelling of ash deposition. The course provides a fundamental outline of the necessary sub-models for this purpose, including:

- Defining the frame and boundary conditions of the model
- Formation of ash species (release, gas phase transformations, formation of aerosols and residual ash)
- Transport of ash species (diffusion, thermophoresis, inertial impaction)
- Adhesion of ash species
- Build-up and consolidation of deposits
- Heat transfer in and shedding of deposits

Not every aspects of firing all types of solid fuels is covered, but the modelling reflects several years of research at Åbo Akademy University and DTU, and therefore has a strong focus on biomass-fired systems as well as heat recovery boilers.

Finally, a number of exercises have been developed over the years and are provided as a fully integrable part of the course, see Figure 12-11.

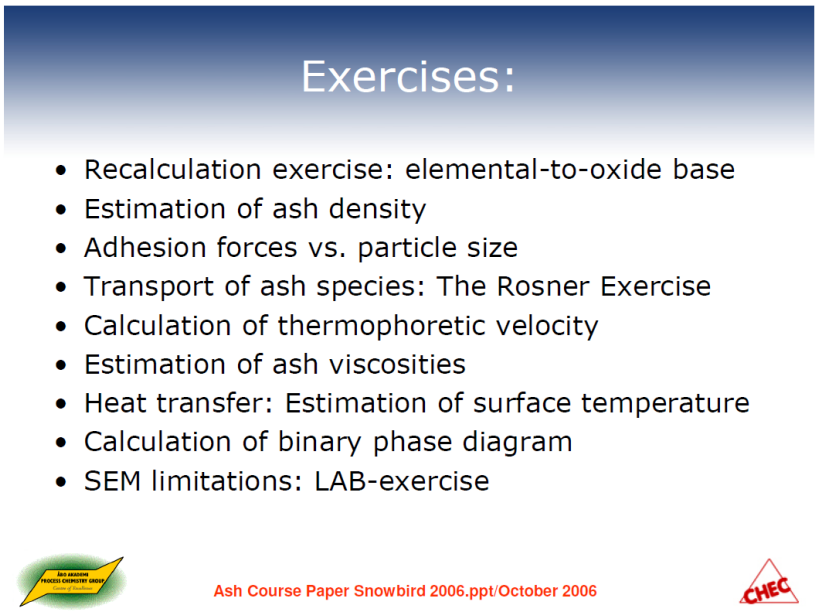

Figure 12-11: Exercises implemented in the course.

12.14. Summary and Conclusions

A short course on ash and trace element chemistry in heat and power boilers has been developed within the framework of the Nordic Energy Research, through several years of close

cooperation between the Åbo Akademi University and the Technical University of Denmark (DTU). The course has proven to be a great success, for a number of reasons:

- It allows the industry to train their employees in ash and trace element chemistry and, to keep updated with the newest data and information on this research area. There has been a significant change of employees within Danish power utilities over the years, thus creating a continuous need to teach and educate new people in this area;
- It allows the universities to accumulate research and thereby helps to build a continuous history frame within research on ash, deposition and corrosion, and;
- It has kept tight contact between the Åbo Akademi University and DTU over the years.

The course still needs to be developed, aiming at a fully web-based teaching module in the near future (see Figure 12-12).

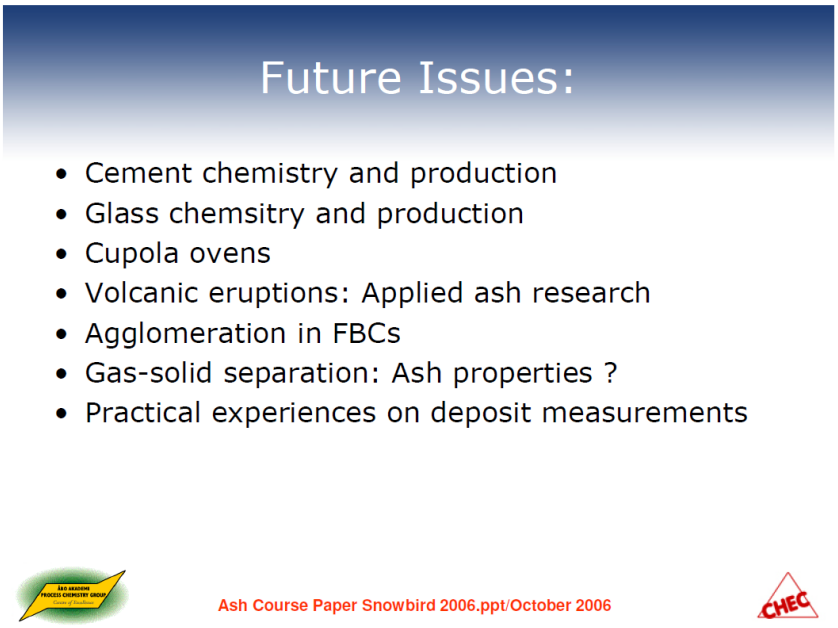

Figure 12-12: Future issues to be implemented in the course.

Chapter 13:

SUMMARY AND CONCLUSIONS

This thesis contains an outline of Danish experiences of ash and deposit formation and corrosion, when utilizing straw for heat and power production, seen mainly in relation to research activities within the CHEC Research Centre at the Department of Chemical and Biochemical Engineering at the Technical University of Denmark during 1991 to 2009.

Major findings on ash deposition and corrosion in grate-fired units during co-firing in PF-fired suspension-boilers and in pilot-scale facilities have been outlined. The main conclusion is that, in the grate-fired units, utilization of straw will cause problems if the steam temperature is kept too high, i.e. > ~ 540 °C. On the other hand, straw may be co-fired with coal, which is fully manageable from a deposition and corrosion point of view, provided that the coal is of high quality, i.e. has a certain amount of Al-silicates in the ash, which will react with K and release Cl and HCl. These species are not nearly as harmful at high temperatures as KCl(s) deposited directly on the heat transfer surfaces. A change in the regulation of the quality of the fly ash allowed for cement and concrete production moved the main obstacle for coal-straw co-firing as a means of utilizing straw for energy production in suspension-fired boilers with a high electrical efficiency. Now, only the potential problem of poisoning of SCR-catalysts by K-species from the straw remains to be solved.

Several investigations into ash and deposit formation have been conducted at Danish straw-fired CHP-boilers including Haslev, Slagelse, Rudkøbing, Masnedø and Maribo-Sakskøbing. In all cases, very high concentrations of K and Cl, ~ 40-80 % of the total mass, have been measured in the fly ash, as well as in the inner layer of the deposits formed. The furnace ash reflects the chemistry of the bottom ash and has a significant content of Ca and Si, in addition to K and Cl. Further, the aerosols formed in these plants have been shown to be very rich in K, S and Cl, and to be present in very high mass loadings, sometimes reaching ~ 800 – 2000 mg/Nm^3 (the latter probably being and extreme case for rape straw).

Due to the very high concentrations of K and Cl released from the straw, and the potential of corrosive attacks on heat transfer equipment, metal temperature in the first generation straw-fired CHP-plants had to be kept rather low at ~ 450 °C, in order to avoid overly fast corrosion. Therefore, first generation plants had low electrical efficiencies. For the second generation straw-fired CHP plants though, the final superheater temperature was increased to ~ [520 – 540 °C], causing higher electrical efficiency.

The means that can be applied to minimize these operational problems are:

- Resistant, but also much more expensive materials, which can better cope with the corrosive nature of alkali chloride salts at ~ 520-540 °C;
- Remove some of the corrosive species from the straw, before firing it on a grate. It has been demonstrated that grey straw, i.e. straw that has been washed out by nature (through rainfall on the field before collection and processing into bales) causes less corrosion and deposition than normal yellow straw (with a normal level of K and Cl). Thus, pre-processing of the straw in order to remove K and Cl may be an option, although it is not clear, at present, whether this will be an economically attractive solution;
- Add an additive which will transform the highly flame-volatile Cl to a lesser corrosive form or will prevent extensive sintering of deposits. This aspect was addressed in Chapter 9 of this thesis;
- Co-fire straw with another biomass, suitable for grate-firing and with lower content of ash, K, S and/or Cl, e.g. wood, since this may cause a dilution of the system.
- Operate the plant with a reasonable soot-blower strategy. Effects and mechanisms of shedding of ash are addressed thoroughly in Chapter 10 of this thesis.

In addition to these immediate means of deposit and corrosion minimization, a certain modification of the boiler design may help minimize corrosive problems, e.g. by introducing a division wall in the flue gas channel, thereby dividing the flue gas into a highly corrosive and less corrosive fractions. There is also evidence that the contact pattern between the hot flue gas and the heat transfer sections may affect corrosion in the actual boiler. The Masnedø and Maribo-Sakskøbing CHP-boilers are examples of boilers designed to collect a rather thick depost/slag layer on the superheater tubes. Investigations at both plants reveal that the inner layer in these boilers was heavily sulphated after a certain operation time, and that the K_2SO_4-rich inner layer actually may help to protect heat transfer surfaces from further corrosive attack.

As with dedicated, straw-fired CHP-plants, several studies have been conducted in order to deduce the effect of coal-straw co-firing in suspension on ash and deposit formation and chemistry. The big advantage of these plants is that they possess a much higher electrical efficiency, 40 – 45 %, compared to 20-25 % for the dedicated straw-fired plants. Thus, by adding straw to PF-fired in direct co-firing with coal, one can obtain a much more efficient CO_2-reduction than by generating the same amount of electricity in a dedicated straw-fired plant.

The baseline study of co-firing at the Midtkraft-Studstrup Power Station, Unit 1, MKS1, revealed that storage and handling of straw for direct co-firing was indeed possible, and that the amount of deposits as well as the aerosol mass loading is not critical, provided that the coal

co-fired is of high quality, i.e. an ash with a reasonably high content of Al-silicates. The trick is to ensure that K release from the straw is fixed in the Al silicate-rich coal ash, thereby releasing Cl as the rather harmless HCl, instead of forming KCl, which may condense on heat transfer surfaces in the system, causing subsequent serious corrosion, as in the dedicated straw-fired systems.

The test-firings conducted as part of the Deposit Prediction Project at the RWE test facility in Germany clearly indicated the consequences of applying low-quality coal. In these tests, a yellow (i.e. high-K) Danish straw was co-fired with German brown coal, a solution that cannot be recommended. Thus, the coal quality is a very important, controlling, parameter for the success of coal-straw co-firing.

There have also been several activities in lab-scale concerning the ash deposition propensities of utilizing straw for heat and power production.

Two comprehensive studies of straw-, coal- and coal+straw co-firing have been conducted in the SNL-MFC. In both cases, the data show that straw causes a much higher deposition rate than either coal or coal co-fired with straw. In addition to the higher depositional flux observed, the chemistry is also significantly affected, when changing from 'pure' straw-firing to co-firing of coal and straw. The effect of an increased S-level was investigated by the addition of either SO_2(g) or solid S to the system, causing a target value of 500 ppmv SO_2(g) in the flue gas, compared to 30 - 60 ppmv during straw-firing in full-scale [Nielsen, 1998; Nielsen et al., 2000a].

The temperature effect on the sulphation of Cl-species in deposits was also seen when firing waste wood in a 400 kW_{th} grate-fired test facility in Hard, Austria, as part of the former EU-BioAerosol project in 2000-2003 (see Figure 6-23).

In Figure 6-23, it is evident that the deposits collected at 230 °C and 400 °C are almost completely dominated by chlorides, while the probe which was first exposed at 240 °C and the increased to a surface temperature of 620 °C, contain almost only sulphate with very little chloride is present. Thus, a higher temperature favours sulfates over chlorides.

The study by Theis et al. revealed that straw can be co-fired with peat up to about 70 % straw share. Above this limit, deposit formation accelerates seriously. A non-linear behaviour in the deposit amount and deposit chemistry was observed when comparing data from co-firing experiments with linear combinations of basic fuel data for the 'pure' fuels.

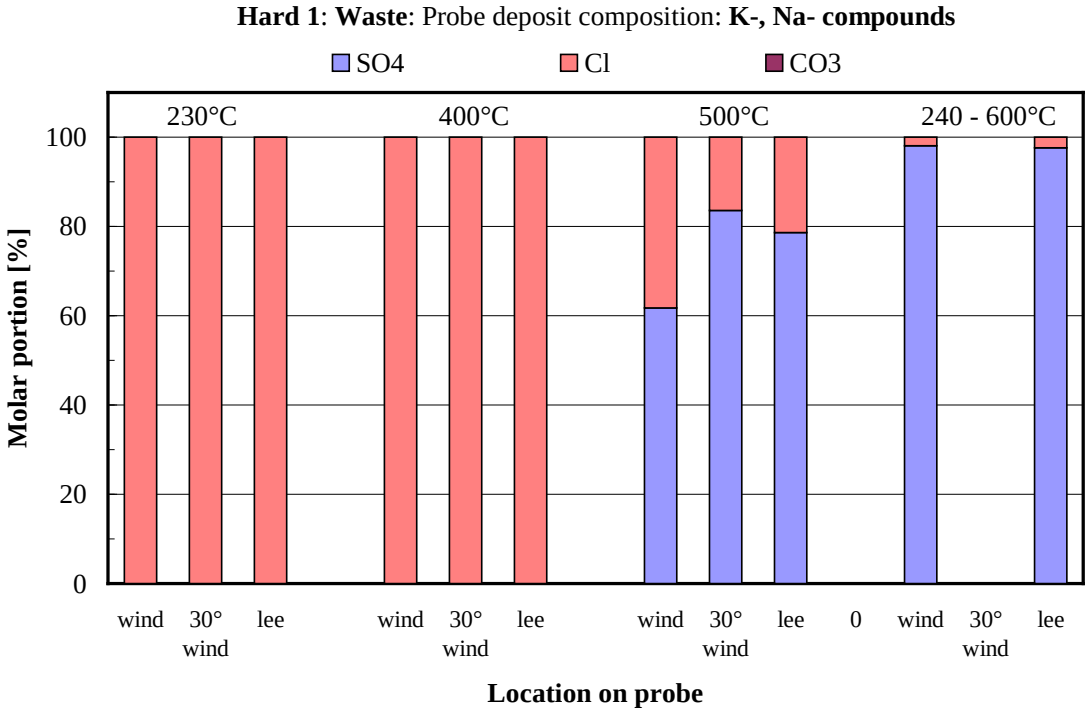

Figure 6-23: The presence of anions, i.e. sulphate, chloride and/or carbonate in deposits collected in a waste wood-fired test facility in Hard, Austria. Source: [BioAerosols, 2003]

An attempt has been made to connect the release of K, S, and Cl via gas phase chemical kinetics and physical transformations to aerosol formation. In this context, Si/K and Cl/K ratios play a major role for the release, although working in opposite directions. A high Si/K-ratio indicates the chance of forming non-volatile K-silicates, while a high Cl/K-ration pulls in the opposite direction indicating increased volatilization of K through interactions with Cl. For the deposits, the Cl/S-ratio in the fuel is very important, a high Cl/S in the fuel will cause a high Cl-level in the deposits, while an excess of S will cause the deposit chemistry to shift toward the less harmless K-sulfate. Moreover, the secondary capture of K by either char or active Ca-Si-rich ashes in the char structure has been addressed.

Concerning corrosion and material aspects in plants (co-)fired with straw, the data generated in Denmark during the last two decades are in line with deposition investigations, indicating potential severe corrosion in the dedicated straw-fired plants (grates), but somewhat lower corrosion when co-firing straw with coal in suspension boilers.

The co-firing of coal and straw at the Midtkraft-Studstrup Power Station clearly indicated that a significant proportion of the volatile K released from the straw will react with residual fly ash particles rich in Al and Si formed from the coal (Andersen (1998), Andersen et al. (2000)). At Midtkraft-Studstrup only limited problems related to deposition and corrosion were observed,

since K was fixed in fly ash particles as K-Al silicates or was transformed to K_2SO_4 and deposited in the convective pass of the boiler. Consequently most of the chlorine was emitted as HCl(g), without having attacked heat transfer surfaces in the boiler.

The application of additives for minimizing aerosol formation and/or deposition in straw-fired boilers was outlined in Chapter 10. A clear effect of additives on aerosol mass loading and chemistry was shown at the AVV-2, while test-firing in the CHEC-EFR (entrained flow reactor) indicated that the deposit chemistry may also be affected seriously by the proper choice of an additive. Six additives were tested in the full-scale biomass-fired AVV-2 plant: ammonium sulphate, monocalcium phosphate, Bentonite, ICA5000, clay and chalk. Based on the work reported in Chapter 9, a good suggestion for an additive to be used when co-firing straw and natural gas at a high temperature will be an Al-Si based material (the presence of Al will cause an easy opening of the Si backbone structure of the additive, thereby ensuring a quicker reaction between volatile alkali and the additive). A relatively small particle size is suggested in order to ensure that the additive particles after reaction with the volatile alkali actually follow the gas stream lines and that they have a high temperature. This will ensure formation of a melt on the surface of the additive particles, which will again cause easier adsorption. Gas conditioning, eg. by injecting or adding S may also be a solution, but one has to be aware that an increased level of S will increase the dew point for the alkali metals (alkali sulfates) and possibly shorten the time for reaction between the alkali metal(s) and the additive.

Finally, shedding of ash deposits was described. We were able to quantify the mass gain of deposit as well as the heat-uptake in the probe via an intelligent new shedding probe design. The data from the shedding probe were applied to take the modelling of deposit build-up and shedding to a whole new level of understanding and quantification.

In addition to the outline of the different ash/deposit formation and corrosion studies considered in this thesis, a significant contribution to the analytical investigation of fuels, ashes and deposits has been made especially two points: the development of a melt quantification method based on STA for salt rich ashes (i.e. ashes with an ionic structure), and, the adaption of SEM analyses on straw derived ashes.

The STA melt quantification method proved to be a lot more precise than the standard ash fusion cone tests, which are often very subjective, i.e. depending on 'the eyes that looks at the sample'. The STA based method is precise but difficult to apply, and a lot of further work is needed to transfer it from an expert tool to a common lab procedure.

We also took an active part in developing CCSEM and SEMPC from a technique applied only to coal and coal-derived ashes, to a technique that can be applied on biomass and (nowadays) even waste-derived ashes. At the Banff 2008 Ash Conference, I provided an overview of

development within ash research during the last 20 years, as it can be seen via the former United Engineering Foundations ash conference series [Frandsen, 2009].

All the activities described in this thesis document the importance of the CHEC Research Centre. We have been able to maintain continuity in research and development in this important field since 2001, when we had a change in the political system in Denmark, causing serious down-grading of the former Energy Research Program, which was partly dedicated to promoting sustainable energy solutions, e.g. utilization of straw for heat and power production. Nevertheless, via the strong bond between our research activities and the Danish power industry, we have been able to retain and build upon our knowhow, and create from this the ash and trace element short course outlined in this thesis.

Having read this thesis, a natural question arising is, are there any gaps. If there are, where are these gaps in our understanding of the ash and deposit formation process ?

First and foremost, concerning the characterization of straw, it is still doubtful whether an ash produced during controlled combustion at a maximum of 550 °C in the laboratory will resemble ash produced in full-scale. As indicated in Chapter 2 of this thesis, standard bulk ash chemical analysis is a tradition in the analysis of fuels, although there are a number of major drawbacks in this way of generating an ash. As illustrated in Chapter 1 elements may be associated either as mineral, organically or as simple salts in a fuel. By applying the standard ashifying technique all original elemental associations in the fuel was destroyed, i.e. all original associations of the inorganic elements are transformed into oxide form. This means that Na originally present as organically associated Na or as a simple salt will now appear as Na_2O. Thus, very important information on the behavior of the different associations of Na in that fuel is lost. It may be convenient to express the content of Na in ash for a fuel on either an elemental base or as an oxide, but is does not provide any details on the original speciation of the elements, and thereby the fate and behavior of the original association of Na in that fuel. This problem is significant for fuels with a high content of organically associated elements or elements present as simple salts, like low-rank coals or biomasses (including straw). For coals of a higher rank, most of the inorganics are actually present as mineral inclusions, with chemical appearance not far away from the oxide basis as the result of bulk ash chemical analysis. Nevertheless, even for coal, it could turn out to be problematic to base predictions of ash behavior on bulk ash analysis, which is principally a rough mean/average chemistry of the coal ash.

In addition to the violence on the original fuel chemistry, there are huge differences between the conditions of lab equipment and full-scale conditions, e.g. concerning heat-up rate and residence time, not to mention particle-to-particle contact pattern.

Thus, there is still a need to develop a method to produce 'real' fly ash in the laboratory, and extreme care must be taken if basing predictions of ash behavior solely on bulk ash chemistry. Other, more advanced, analytical techniques or – even better - real combustions tests in a set-up with a temperature-time history equal to thermal conversion of the straw in full-scale, should supply the bulk ash chemistry.

The SEM technique originally adapted for analyses of coal and coal ash products has been developed significantly for use nowadays on straw. This technique provides a unique chance to understand the physical nature and structure of biofuels and ashes derived from these. Nonetheless, one has to be very careful when documenting these analyses, since the quality of the images and thereby the entire outcome link strongly to system parameters applied when performing the SEM analysis. This technique is still to be considered as an expert tool.

In addition to the problems of producing a reliable ash from a fuel in the laboratory, there are also problem of analyzing this ash and getting reasonable results from the analysis. One good example is ash fusion tests, where a characteristic geometric shape such as a conus or a cubus is heated at a low rate in a controlled atmosphere, and the temperature corresponding to certain characteristic shapes, like initial deformation, hemispherical shape and fluid/molten state are determined. This technique was developed for coal ash almost a Centery ago, but, as shown in Chapter 2, studies of ash fusion by other techniques indicate that the first melting in a straw-derived ash sample may appear at a temperature up to 300 °C lower than measured by the standard conus ash fusion test. Thus, analytical ash techniques developed for Si-rich coal ashes should be used with extreme care on straw (biomass)-derived ashes.

Another point where our current understanding is weak is on formation of fly ash from straw. Far more research is required on this in order to be able to understand and quantify fly ash chemistry and size distribution. Formation of fly ash is the key missing link between straw as a fuel, and deposits formed in straw-fired systems, as well as in the understanding and quantification of fixation of K via secondary interactions with ash inclusions. Release of K, S and Cl, the formation of residual ash during char burnout, secondary reactions between K, S and/or Cl alredy released and char particles or ash inclusions on the surface of ash particles (secondary reactions), development of fly ash structure and chemistry, as well as entrainment of fly ash particles from the fuel-bed will need a significant boost in research, in order to improve for example the prediction of ash deposition in straw-fired systems.

In close connection with residual ash formation and the release of K, S and Cl from straw is aerosol formation in the gas phase. As indicated in Chapter 7, the basic mechanisms suggested by Christensen, by which K_2SO_4 nucleates homogeneously may explain aerosol formation in straw-fired systems. However, in real life there is often a shift in fuel (quality) or straw is co-fired with e.g. wood chips, and there is always a risk that other mechanisms or elements may

play a major role in aerosol formation. The effect of Na on supersaturation in the system K_2SO_4/Na_2SO_4, therefore needs further attention.

Modeling of ash and deposit formation has not been addressed specifically in this thesis there is a significant amount of high-quality data available from a number of EU and national research projects that cover the period 1991 to 2009. Through these years, the Commission has insisted on funding the generation of a serious amount of new experimental data, while attempts to model these data have seldom been granted.

Concerning modeling, two points should be made here. First, a proper understanding and quantification of ash and deposit formation will require elements of **both** chemistry and physics. The idea of performing predictions based on fuel compositional data, as attempted over the years for coals via for example the acid-to-base ratio, will most likely not cause a precise quantification of aerosol, ash and deposit formation. There are several physical processes involved, all of which have to be addressed. Secondly, trying to predict ash or deposit formation by Computational Fluid Dynamics (CFD) is also dangerous. The output from such codes looks nice to the eye, and CFD may indeed provide the flow and some simple gas phase chemistry, but the essence of a deposition model – like the adhesive properties of ash particles - will have to be adapted from the literature and programmed for CFD and user-defined functions.

Referencer:

AEA Technology; "European Co-Combustion of Coal, Biomass and Waste", **Final Report EU-Project Contract No. DIS-0506-95-UK, 2000.**

G.D. Agarwal, A.K. Agarwal; "Environmental Implications of Using Biomass as an Alternative Source of Energy: A Critical Assessment", **TERI Information Monitor on Environmental Science, 4(2), pp. 79-86, 1999.**

P.A. Alexander; *Laboratory Studies of the Effects of Sulphates and Chlorides on the Oxidation of Superheater Alloys*; **The Mechanism of Corrosion by Fuel Impurities, Eds. R. Johnson and D. J. Littler, Butterworths, 1963, pp 571-582.**

K.H. Andersen; *Deposit Formation during Coal-Straw Co-Combustion in a Utility PF-Boiler*; **Ph.D.-Thesis, Department of Chemical Engineering, Technical University of Denmark, ISBN-87-90142-43-8, 1998.**

K.H. Andersen, F.J. Frandsen, P.F.B. Hansen, K. Wieck-Hansen, I. Rasmussen, P. Overgaard, K. Dam-Johansen; *Deposit Formation in a 150 MW_e Utility PF-Boiler during Co-combustion of Coal and Straw*; **Energy & Fuels, 14(4), pp 765-780, 2000.**

H.R. Anderson, A. Ponce de Leon, J.M. Bland, J.S. Blower, D.P. Strachan; *Air Pollution Daily Mortality in London, 1987-92*; **British Medical Journal (Clinical Research Edition), 312, 665 – 669, 1996.**

S. Arvelakis, F.J. Frandsen; *Study on Analysis and Characterization Methods for Ash Material from Incineration Plants*; **Fuel; 84; 1725 – 1738, 2005.**

T. Astrup, C. Riber, A.J. Pedersen; *Effects of waste input composition and furnace operation on MSW incinerator emissions and residues*; **Journal of Hazardous Materials, submitted 2010.**

R. Backman, M. Hupa, E. Uppstu; *Fouling and corrosion mechanisms in the recovery boiler superheater area*; **TAPPI Journal; 70; 6, 1987.**

R. Backman, M. Hupa, B.-J. Skrifvars; *Predicting the melting behaviour superheater deposits in boilers during biomass combustion, in Impact of mineral impurities in solid fuel combustion*; **(Eds. Gupta, R., Wall, T., Baxter, L), Kluwer Academic/Plenum Publisher, New York, 1999.**

J.H.E. Bailey, D.W. Reeve; *Determination of the Spatial Distribution of Trace Elements in Jack Pine, Pinus banksiana Lamb., by Imaging Microprobe Secondary Ions Mass Spectrometry*; **J. Pulp Paper Sci., 22, 274–278, 1996.**

L.L. Baxter, D.R. Hardesty; "The Fate of Mineral Matter During Pulverized Coal Combustion", **In: Coal Combustion Science, Sandia Quarterly Progress Report, April-June, 1992, SAND92-8227, 1992.**

L.L. Baxter, B.M. Jenkins, T.R. Miles, T.R. Miles Jr., T. Milne, D.C. Dayton, R.W. Bryers, L.L. Oden; *Inorganic material deposition in biomass boilers*; **In Chartier, P., Ferrero, G.L., Henius, U.M., Hultberg, S., Sachau, J., Wiinblad, M. (Eds.),** ***Biomass for Energy and the Environment. Proc. of 9th European Bioenergy Conference*****, June 24-27 1996, Copenhagen, Denmark, Pergamon, Published by Elsevier Science, ISBN 0-08-0428-495, pp. 1114-1122, 1996.**

L.L. Baxter, R. DeSollar; *Applications of Advanced Technology to Ash-Related Problems*, **Proc. Eng. Found. Conf., Waterville Valley, NH, July 16-21, 1995, ISBN-0-306-45376-2, 1996.**

L.L. Baxter, M. Rumminger, T. Lind, D. Tillman, E. Hughes; *Co-firing Biomass in Coal Boilers: Pilot- and Utility-scale Experiences*; **Proc. Biomass for Energy and Industry: 1st World Conference and Technology Exhibition, Seville, Spain, 2000.**

L.L. Baxter; *Biomass Co-firing Overview*; **Proc. 2nd World Conference on Biomass for Energy, Industry, and World Climate Protection, May 10-14, Rome, Italy, 2004.**

L.L. Baxter, J. Koppejan; *Co-combustion of biomass and coal*; **Euroheat and Power, (1), 34-39, 2004.**

L.L. Baxter; *Biomass-coal co-combustion: opportunity for affordable renewable energy*; **Fuel 84, 1295-1302, 2005.**

R. Becker and W. Döring; **Ann. Phys, 1935, 24, 719 – 735.**

H. Belevi, H. Moench; *Factors determing the element behavior in municipal solid waste incinerators. 1. Field studies*; **Environ. Sci. Technol., 34, 2501-2506, 2000.**

S.A. Benson, P.L. Holm; *Comparison of Inorganic Constituents in Three Low-Rank Coals*; **Ind. Chem. Prod. Res. Dev., 24, 145-150, 1985.**

S.A. Benson, M.L. Jones, J.N. Harb; *Ash formation and deposition*; **In: L.D. Smoot (Ed),** ***Fundamentals of Coal Combustion - for Clean and Efficient Use*****, Coal Science and Technology 20, Elsevier Science Publishers, Amsterdam, ISBN 0-444-89643-0, Chapter 4, 299-373, 1993.**

BioNorm; Pre-Normative Work on Sampling and Testing of Solid Biofuels for the Development of Quality Assurance Systems", **Final Report EU-Project Contract No. ENK6-CT-2001-00556, Eds. M. Kaltschmitt, M. Hein, F. Müller-Langer, 2004.**

E. Björkman, B. Strömberg; *Release of Chlorine from Biomass at Pyrolysis and Gasification Conditions*; **Energy & Fuels, *11*, 1026-1032, 1997.**

J.-P. Blomqvist; *Predicting the ash formation and properties when firing biomass ín a fluidized bed boiler*; **MSc Thesis (in Swedish), Åbo Akademi, 1998.**

C. Boman; *Particulate Matter and Products of Incomplete Combustion from Residential Biomass Pellet Appliances - Emissions and Potential for Future Technology*; **Ph.D. Thesis, Umeå University, Umeå, Sweden, 2003.**

L. Boonsongsup, K. Iisa, W. J. Frederick; *Kinetics of the Sulfation of NaCl at Combustion Conditions*; **Ind. Eng. Chem. Res.; 36; pp 4212-4216, 1997.**

L. Boonsongsup, K. Iisa, W. J. Frederick; *Sulfation of Potassium Chloride at Combustion Conditions*; **Energy & Fuels; 13; pp 1184-1190, 1999.**

Brigham Young University: http://www.byu.edu/webapp/home/index.jsp

G.L. Borman, K.W. Ragland; *Combustion Engineering*; **WCB McGraw-Hill, 1998.**

P.H. Brown, I. Cakmak, Q. Zhang; *Form and Function of Zinc in Plants. In Zinc in Soils and Plants*; **Robson, A. D., Ed.; Kluwer Academic Publishers: Dordrecht, The Netherlands; pp 90-106, 1993.**

P.H. Brunner, H. Mönch; *The flux of metals through municipal solid waste incinerators*; **Waste Management & Research, 4, 105-119, 1986.**

T. Brunner, J. Dahl, I. Obernberger, P. Pölt; *Chemical and Structural Analyses of Aerosol and Fly-Ash Particles from Fixed-Bed Biomass Combustion Plants by Electron Microscopy*; **In Proceedings of the 1st World Conference on Biomass for Energy and Industry; Sevilla, Spain, June 5-9, 2000; ETA: Florence, Italy; pp 1991-1995, 2000.**

T. Brunner, M. Joeller, I. Obernberger, F.J. Frandsen; *Aerosol and Fly Ash Formation in Fixed Bed Biomass Combustion Systems using Woody Biofuels*; **In: Proceedings of the 12th European Conference and Technology Exhibition on Biomass for Energy, Industry and Climate Protection; Amsterdam, The Netherlands, June 17-21, 2002; ETA: Florence, Italy; pp 685-689, 2002.**

R.W. Bryers; *Fireside Slagging, Fouling, and High-Temperature Corrosion of Heat-Transfer Surface due to Impurities in Steam-Raising Fuels*; **Progress in Energy and Combustion Science, 22(1), pp 29-120; 1996.**

M. Bøjer, P.A. Jensen, F.J. Frandsen, K. Dam-Johansen,O.H. Madsen, K. Lundtorp; *Alkali/Chloride release during refuse incineration on a grate: Full-scale experimental findings*; **Fuel Processing Technology 89, 528-539, 2008.**

CBT, Centre for Biomass Technology; *Straw for Energy Production – Technology – Environment – Economy*; **Report Ed. L. Nikolaisen, ISBN-87-90074-20-3, 1998.**

K.-Y. Chiang, K.-S. Wang, F.-L. Lin, W.-T. Chu; *Chloride effects on the speciation and partitioning of heavy metal during the municipal solid waste incineration process*; **The Science of the Total Environment, 203, 129-140, 1997.**

K.A. Christensen; *The Formation of Submicron Particles from the Combustion of Straw*; **Ph.D.-Thesis, Department of Chemical Engineering, Technical University of Denmark, ISBN-87-90142-04-7, 1995.**

K.A. Christensen and H. Livbjerg; *A Field Study of Submicron Particles from the Combustion of Straw*; **Aerosol Sci. Techn., 25, 185 – 199, 1996.**

K.A. Christensen, M. Stenholm, H. Livbjerg; *The Formation of Submicron Aerosol Particles HCl and SO_2 in Straw-Fired Boilers*; **J. Aerosol Sci.; 29 (4); pp 421-444, 1998.**

K.A. Christensen and H. Livbjerg; *A Plug Flow Model for Chemical Reactions and Aerosol Nucleation and Growth in an Alkali-Containing Flue Gas.* **Aerosol Sci. Technol., 33, 470 – 489, 2000.**

R.E. Conn, L.G. Austin; *Studies of the Sintering of Coal Ash Relevant to Pulverized Coal Utility Boilers. 1 Examination of the Raask Shrinkage-Electrical Resistance Method*; **Fuel; 63(12); pp 1664-1670, 1984.**

J.L. Crolet; *The eltrochemistry of corrosion beneath corrosion deposits*; **J. Mat. Sci., 28, pp. 2577-2588, 1993a**.

J.L. Crolet; *Mechanisms of uniform corrosion under corrosion deposits*; **J. Mat. Sci., 28, pp. 2589-2606, 1993b**.

D. Cubiciotti, F.J. Keneshea; *Thermodynamics of Vaporization of Sodium Sulfate*; **High. Temp. Sci., *4*, 32–40, 1972.**

I.W. Cumming, A. Sanyal; *An Electrical Conductance Method for Predicting the Onset of Fusion in Coal Ash*; **Proc. Eng. Found. Conf., Henniker, NH, July 12-17, 1981.**

I.W. Cumming, W.I. Joyce, J.H. Kyle; *Advanced Techniques for the Assessment of Slagging and Fouling Propensity in Pulverized Coal Fired Boiler Plant*; **J. Inst. Energy, pp 169-175, 1985.**

B. Dahneke; *Simple Kinetic Theory of Brownian Diffusion in Vapors and Aerosols*; **In: 'Theory of Dispersed Multiphase Flow', R. E. Meyer (Ed.), Academic Press, N. Y., 97 – 138, 1983.**

K.O. Davidsson, B.J. Stojkova, J.B.C. Pettersson; *Alkali Emission from Birchwood Particles during Rapid Pyrolysis*; **Energy & Fuels, 16, 1033-1039, 2002a.**

K.O. Davidsson, J.G. Korsgren, J.B.C. Pettersson, U. Jäglid; *The Effects of Fuel Washing Techniques on Alkali Release from Biomass*; **Fuel, 81, 137-142, 2002b.**

K.O. Davidsson, J.B.C. Pettersson, R. Nilsson; *Fertiliser Influence on Alkali Release during Straw Pyrolysis*; **Fuel, 81, 259-262, 2002c.**

D.C. Dayton, T.A. Milne; *Mechanisms of Alkali Metal Release During Biomass Combustion*; ***ACS, Div. of Fuel Chemistry, 40*** **(3), 758-762, 1995.**

D.C. Dayton, R.J. French, T.A. Milne; *Direct Observation of Alkali Vapor Release during Biomass Combustion and Gasification. 1. Application of Molecular Beam/Mass Spectrometry to Switchgrass Combustion*; **Energy & Fuels, 9, 855-865, 1995.**

D.C. Dayton, B.M. Jenkins, S.Q. Turn, R.R. Bakker, R.B. Williams, D. Belle-Qudry, L.M. Hill; *Release of Inorganic Constituents from Leached Biomass during Thermal Conversion*; **Energy & Fuels; 13; pp 860-870; 1999.**

D.C. Dayton, T.A. Milne; *Laboratory Measurements of Alkali Metal Containing Vapors Released during Biomass Combustion*; **In Applications of Advanced Technology to Ash-Related Problems in Boilers; Baxter, L., DeSollar, R., Eds.; Plenum Press: New York, 1999.**

R.J. Delfino, C. Sioutas, S. Malik; *Potential Role of Ultrafine Particles in Associations between Airborne Particle Mass and Cardiovascular Health*; **Environmental Health Perspectives 113, 924 – 946, 2005.**

J.S. Dennis, A.N. Hayhurst; *The formation of SO_3 in a fluidized bed*; **Combust. Flame 1988, 72, 241–258.**

DIRECTIVE 2000/76/EC OF THE EUROPEAN PARLIAMENT AND OF THE COUNCIL of 4 December 2000 on the incineration of waste (OJ L332, P91 - 111).

R.A. Durie, J.W. Milne, M.Y. Smith; *The Deposition of Salts from Hydrocarbon Flames Containing Sodium and Sulfur Species*; **Comb. and Flame 30, 221-230, 1977.**

S.A. Ebrahimi-Sabet; *A Laboratory study of deposit removal by debonding and its application to fireside deposits in kraft recovery boiler*; **Ph.D.Thesis. University of Toronto, 2001.**

EERE: Energy Efficiency and Renewable Energy, U.S. Department of Enery, **http://www1.eere.energy.gov/ba/pba, document 'direct_fire_bio.pdf', 2008.**

J. Eliezer, R.A. Howald; *Thermodynamics of the Vaporization Process for Potassium Sulfate*; **J. Chem. Phys., *65*, 3053–3062, 1976.**

ENS, *Den Danske Energistyrelses Hjemmeside*, **www.ens.dk, 2006.**

EP94/0595; *Halmtilsatsfyringsforsøg på VESTKRAFT, blok 1. Målekampagner vedrørende restprodukter og emissionsforhold*; **ElsamProject Note, 1994.**

EU Deposit Prediction; *Prediction of Ash and Deposit Formation for Biomass Co-Combustion*; **EEC-DGXII Contract No. JOR-398-0198, 1998-2001, Final Report, June 2001.**

EU BioAerosols, **Final Report, EU DGXII Contract No. ERK6-CT1999-00003, 2003.**

EU BioAsh, **Final Report, EU DGXII Contract No. SES-CT2003-502679, 2007.**

EU Green Paper on PVC (2010): GREEN PAPER on Environmental issues of PVC. European Council of Vinyl Manufactures (ECVM): http://www.pvc.org/The-PVC-Industry/ECVM. Retrieved January 2010.

A. Faaij; "Modern Biomass Conversion Technologies", **Mitigation and Adaption Strategies for Global Change, 11, pp. 343-375, 2006.**

C.P. Fenimore, G.W. Jones; J. Phys. Chem. 69, 3593, 1965.

P.J. Ficalora, O.M. Oy, D.W. Muenow, J.L. Margrave; *Mass Spectrometric Studies at High Temperatures. XXIX. Thermal Decomposition and Sublimation of Alkali Metal Sulfates*; **J. Am. Ceram. Soc. 51(10), 574 – 577, 1968.**

W.L. Fielder, C. A. Stearns, F. J. Kohl; *Reactions of NaCl with Gaswous SO_3, SO_2, and O_2*; **J. Electrochem. Soc., Solid-State Science and Technology; pp 2414-2417; 1984.**
R.C. Flagan, S.K. Friedlander; *Particle Formation in Pulverized Coal Combustion - A Review*; **In Recent DeVelopments in Aerosol Science; Shaw, D. T., Ed.; Wiley: New York; pp 25-59, 1978.**

R.C. Flagan, D.D. Taylor; *Laboratory Studies of Submicron Particles from Coal Combustion*; **Proc. Int. Comb. Symp. 18, 1227 – 1237, 1981.**

F. J. Frandsen; *Trace Elements from Coal Combustion.* **Ph.D.-Thesis, Dept. of Chem. Eng., Technical University of Denmark, ISBN 87-90142-03-9, 1995.**

F.J. Frandsen, H.P. Nielsen, P.A. Jensen, L.A. Hansen, H. Livbjerg, K. Dam-Johansen, P.F.B. Hansen, K.H. Andersen, H.S. Sørensen, O.H. Larsen, B. Sander, N. Henriksen, P. Simonsen; *Deposition and Corrosion in Straw- and Coal-Straw Co-Fired Utility Boilers, Danish Experiences*; **Proc. United Eng. Found. Conf. on Impact of Mineral Impurities in Solid Fuel Combustion, Kona, Hawaii, November 2-7, pp 271-283, 1997.**

F.J. Frandsen, H.P. Nielsen, L.A. Hansen, P.F.B. Hansen, K.H. Andersen, H.S. Sørensen; *Ash Chemistry Aspects of Straw and Coal-Straw Co-Firing in Utility Boilers*; **Proc. 15th Annual International Pittsburgh Coal Conference, GreenTree Marriott Hotel, Pittsburgh, PA, USA, September 14-18, 1998.**

F.J. Frandsen, L.A. Hansen, H.S. Sørensen, K. Hjuler; *Characterization of Ashes from Biofuels*. **Final Report for EFP-95 J. No. 1323/95-0007, ISBN-87-7782-000-2, 1998.**

F.J. Frandsen, J. Hansen, P.A. Jensen, K. Dam-Johansen, M. Montgomery, L.D. Fenger, J.N. Jensen, A. Karlsson, N. Henriksen, J.P. Jensen; *Deposit Formation and Corrosion in the Air Pre-Heater of a Straw-Fired Combined Heat and Power Production Boilers*. **IFRF Combustion Journal, Paper No. 200204, 2002.**

F.J. Frandsen, J. Hansen, P.A. Jensen, K. Dam-Johansen, S. Hørlyck, A. Karlsson; *Ash and Deposit Formation in the Biomass Co-Fired Masnedø Combined Heat and Power Production Plant*; **IFRF Combustion Journal, Paper No. 200304, 2003**.

F.J. Frandsen, K. Laursen, O.H. Larsen; *Advanced Inorganic Characterization and Comparison of the Chemistry of Ashes from Waste Incinerators*; **Proc. 23rd Annual Int. Conf. on Incineration and Thermal Treatment Technologies, Sheraton Wild Horse Pass, Phoenix, Arizona, May 10-14, 2004.**

F.J. Frandsen; *Utilizing biomass and waste for power production—a decade of contributing to the understanding, interpretation and analysis of deposits and corrosion products*; **Fuel, 84, 1277–1294, 2005.**

F.J. Frandsen, B.-J. Skrifvars, R. Backman; *Effective Communication of Research to the Industry – A Nordic Ash and Trace Element Chemistry Short Course*; **In: N.S. Harding, T.F. Wall, F. Wigley, F.J. Frandsen, M. Hupa, D.A. Tillman, Proc. Int. Conf. 'Impact of Fuel Quality on Power Production', Snowbird, October 29 – November 3, 2006.**

F.J. Frandsen, S.C. van Lith, R. Korbee, P. Yrjas, R. Backman, I. Obernberger, T. Brunner, M. Jöller; *Quantification of the release of inorganic elements from biofuels*; **Fuel Processing Technology, 88, 1118-1128, 2007.**

F.J. Frandsen; *Ash Research from Palm Coast, Florida to Banff, Canada: Enter of the Biomass in Modern Power Boilers*; **Energy & Fuels, 23, 3347 – 3378, 2009.**

R.B. Frandsen, M. Montgomery, O.H. Larsen; *Field test corrosion experiences when co-firing straw and coal: Ten years status within Elsam*; **4th International Workshop "Materials Issues Governing the Performance of Advanced 21st Century Energy Systems" held in Wellington, New Zealand, February 2006.**

S.K. Friedlander; *Smoke, Dust and Haze*; **Oxford University Press, 2000.**

R.E. Fryxell, C.A. Trythall, R.J. Perkins; *Vapor Pressure of Liquid Sodium Sulfate from 954 to 1204 °C*; **Corrosion 29(11), 423 – 428, 1973.**

N.A. Fuchs; *Mechanics of Aerosols*; **Pergamon, New York, 1964.**

N.A. Fuchs and A. G. Sutugin; **Int. Rev. Aerosol Phys. Chem., 1971, 1 – 60.**

H. Fujikawa, N. Maruyama; *Corrosion Behavior of Austenitic Stainless Steels in High Chloride-Containing Environment*; **Materials Science and Engineering; A120; pp 201-306; 1986.**

K. Galbreath, C.J. Zygarlicke, G. Cassuccio, T. Moore, P. Gottlieb, N. Agron-Olshima, G. Huffman, A. Shah, N. Yang, J. Vleeskens, G. Hamburg; *Collaborative Study of Quantitative Coal Mineral Analysis Using Computer-Controlled Scanning Electron Microscopy*; **Proc. Eng. Found. Conf., Waterville Valley, NH, July 16-22, 1995. Eds. L.L. Baxter and R. DeSollar, Application of Advanced Technology to Ash-Related Problems in Boilers, ISBN 0-306-45376-2, 1995.**

F. Gelbard, Y. Tambour, J. H. Seinfeld; *Sectional Representation for Simulating Aerosol Dynamics.* **J. Colloid Interface Sci., 76(2), 541 – 556, 1980.**

F. Gelbard; *Modeling Multicomponent Aerosl Particle Growth by Vapor Condensation.* **Aerosol Sci. Technol., 12, 399 – 412, 1990.**
J.R. Gibson, W.R. Livingston; *The Sintering and Fusion of Bituminous Coal Ashes*; **In: S. A. Benson, 'Inorganic Transformations and Ash Deposition during Combustion', United Engineering Foundation International Conf., Palm Coast, FA, March 10-15, 1991; 1992, ISBN-0-7918-0657-X.**

J.S. Gittinger, W.J. Arvan; "Considerations for the Design of RDF-Fried Refuse Boilers", **Proc. Power-Gen Europe '98, Document BR-1657, Milan, Italy, June 9-11, 1998.**

P. Glarborg, P. Marshall; *Mechanism and Modeling of the Formation of Gaseous Alkali Sulfates*; **Combustion and Flame 141, 22 – 39, 2005.**

P. Glarborg; Hidden *Interactions – Trace Species Governing Combustion and Emissions*; **Proc. Int. Comb. Symp. 31, 77 – 98, 2007.**

K. Gotthjælp, P. Brøndsted, P. Jansen, J. Markussen, M. Montgomery, E. Maahn; *High Temperature Corrosion in Biomass Incineration Plants*; **EFP95 Project No. 1323/95-0008. ISBN 87-550-2305-3, 1997.**

H.J. Grabke, E. Reese, M. Spiegel; *The effects of chlorides, hydrogen chloride, and sulfur dioxide in the oxidation of steels below deposits.* **Corros. Sci. 1995, *37* (7), 1023–1043.**

M. Grønli; *Theoretical and Experimental Study of the Thermal Degradation of Biomass*; **Ph.D.-Thesis, Norwegian University of Science and Technology, NTNU, 1996.**

H.W. Gudenau, H. Hoberg, A.R. Pande, M. Weinberg, J.-E. Becker; *High-temperature fuel gas cleaning and removal of alkalis using molten slag.* **Proc. Inst. Mech. Eng., 212, A, 151 – 158, 1998.**

A. Gudzinkas; *Sulphation of Solid KCl (Report 07-02)*; **M.Sc. Thesis, Åbo Akademi: Åbo, Finland, 2007.**

K. Görner; *Technische Verbrennungssysteme – Grundlagen, Modellbildung, Simulation*; **Springer Verlag, Berlin, ISBN – 3-540-53947-6, 1991.**

C.S. Halck; *Solid Phase Sulphation of Potassium Chloride to Potassium Sulphate*; **M.Sc. Thesis, Technical University of Denmark: Lyngby, Denmark, 2008.**

J.C. Halle, K.H. Stern; The Effect of Silica on the Thermal Decomposition of Sodium Sulfate; Corrosion Sci. 20(10), 1139 – 1142, 1980.

L.A. Hansen; *Melting and Sintering of Ashes*; **Ph.D.-Thesis, Department of Chemical Engineering, Technical University of Denmark, ISBN-87-90142-31-4, 1998.**
L.A. Hansen, F.J. Frandsen, K. Dam-Johansen, H.S. Sørensen; *Quantification of fusion in ashes from solid fuel combustion*, **Thermochimica Acta; 326; pp 105-117; 1999a.**

L.A. Hansen, F.J. Frandsen, K. Dam-Johansen, H.S. Sørensen, B.-J. Skrifvars; *Characterization af Ashes and Deposits from High-Temperature Coal-Straw Co-Firing*; **Energy and Fuels; 13(4); pp 803-816; 1999b.**

L.A. Hansen, H.P. Nielsen, F.J. Frandsen, K. Dam-Johansen, S. Hørlyck, A. Karlsson; *Influence of deposit formation on corrosion at a straw-fired boiler*; **Fuel Processing Technology; 64; pp 189-209; 2000.**

P.F.B. Hansen; *MKS1 Demonstration Programme. Mass balances and flue gas emissions*; **Confidential Internal Report, I/S MIDTKRAFT and ELSAM, July 1997.**

P.F.B. Hansen, K.H. Andersen, K. Wieck-Hansen, P. Overgaard, I. Rasmussen, F.J. Frandsen, L.A. Hansen, K. Dam-Johansen; *Co-firing straw and coal in a 150-MW_e utility boiler: in situ measurements*; **Fuel Processing Technology; 54; pp 207-225; 1998.**

W.F. Harlow; *Causes of High Dewpoint Temperatures in Boiler Flue Gases*. **Proc. Inst. Mech. Engrs., 151: 293, 1944.**

W.F. Harlow; *Causes of Flue Gas Deposits and Corrosion in Modern Power Plants*; **Proc. Inst. Mech. Engrs., 160: 359, 1949.**

R.M. Harrison, J. Yin; *Particulate Matter in the Atmosphere: Which Properties are Important for its Effects on Health ?*; **The Sci. of the Total Env. 249(1-3), 85-101, 2000.**

F. Hasselriis, A. Licata; *Analysis of heavy metal emission data from municipal waste combustion*; **Journal of Hazardous Materials, 47, 77-102, 1996.**

B.S. Haynes, M. Neville, R.J. Quann; A.F. Sarofim; *Factors Governing the Surface Enrichment of Fly Ash in Volatile Trace Species*; **J. Colloid and Interface Sci., 87(1), 266 – 278, 1982.**

J.M. Heikkinen; *Characterization of Supplementary Fuels for Co-Combustion with Pulverized Coal*; **M.Sc.-Thesis, Environmental and Energy Engineering, Tampere University of Technology, ISBN-952-91-9224-X, 2005.**

K.R.G. Hein; *Sustainable Energy Supply and Envionment Protection – Strategies, Resources and Technologies*;**In: R. Gupta, T. Wall, M. Hupa, F. Wigley, D. Tillman, F.J. Frandsen,**

Proc. Int. Conf. 'IMPACT OF FUEL QUALITY ON POWER PRODUCTION AND THE ENVIRONMENT', Banff Conference Centre, Banff, Alberta, Canada, Sept. 29 - Oct. 4, 2008.

N. Henriksen, O.H. Larsen, R. Blum, S. Inselman; *High-temperature Corrosion when Co-Firing Coal and Straw in Pulverized Coal Boilers and Circulating Fluidized Bed Boilers; VGB Conference*; **Corrosion and Corrosion Protection in Power Plants, Essen, November 29 and 30, pp 6.1-6.23, 1995.**

N. Henriksen and O.H. Larsen; *Corrosion in ultra supercritical boilers for straw combustion*; **Materials at High Temperatures, 14 (3) pp. 227-236, 1997.**

N. Henriksen, M. Montgomery, O.H. Larsen; *Korrosion in energieerzeugenden Anlagen VDI-Berichte 1680*; **VDI Verlag GmbH Düsseldorf, pp. 111-133, 2002.**

N. Henriksen, O. Busse, J.B. Johnsen; *Forebyggelse af korrosion og belægningsdannelse i flisfyrede kedler.* **PSO-projekt nr. 3142. notat nr. 02-0346d, 2003.**

G. M. Hidy; *AEROSOLS – An Industrial and Enviromental Science*; **Academic Press Inc., N. Y., 1984.**

N. Hiramutsu, Y. Uematsu, T. Tanaka, M. Kinugasa; *Effect of Alloying Elements on NaCl-Induced Hot Corrosion of Stainless Steels*; **Materials Science and Engineering, A120, 319-330, 1989.**

L. Holland; *The properties of glass surfaces*; **Chapman and Hall, London, 1964.**

C.H. Hueglin, C.H. Gaegauf, S. Künzel, H. Burtscher; *Characterization of Wood Combustion Particles: Morphology, Mobility, and Photoelectric Activity*; **Environ. Sci. Technol., *31*, 3439-3447, 1997.**

M. Hupa, R. Backman, R.; **In: Slagging and fouling during combined burning of bark with oil, coal, gas or peat. In: Fouling of heat exchanger surfaces (Ed. R. W. Bryers), United Engineering Trustees, New York, N.Y., USA, 419-432, 1983.**

J.P. Hurley, H.H. Schobert; *Ash Formation during Pulverized Subbituminous Coal Combustion. 1. Characterization of Coals, and Inorganic Transformations during Early Stages of Burnout*; **Energy Fuels, 6, 47-58, 1992.**

J.P. Hurley, H.H. Schobert; *Ash Formation during Pulverized Subbituminous Coal Combustion. 2. Inorganic Transformations during Middle and Late Stages of Burnout*; **Energy & Fuels, 7, 542-553, 1993.**

J.P. Hurley, S.A. Benson, A.K. Metha; *Ash Deposition at Low Temperatures in Boilers Burning High-Calcium Coals*; **In: J. Williamson and F. Wigley, 'The Impact of Ash Deposition on Coal-Fired Power Plants', United Engineering Foundation International Conf., Solihull, Birmingham, UK, June 20-25, 1993; 1994, ISBN-1-56032-293-4.**

K. Iisa, Y. Lu, K. Salmenoja; *Sulfation of Potassium Chloride at Combustion Conditions*; **Energy & Fuels 13(6), 1184 - 1190, 1999.**

M.Z. Jacobson and R.P. Turco; *Simulating Condensational Growth, Evaporation and Coagulation of Aerosols Using a Combined Moving and Stationary Grid*; **Aerosol Sci. Technol., 22, 73 – 92, 1995.**

R.C. Jain, S.C. Young; *Laboratory/Bench Scale Testing and Evaluation of A.P.T. Dry Plate Scrubber.* **Report No. DOE/ET/15492-2030, Air Pollution Technology Inc., San Diego, CA, 1985.**

J.R. Jensen, L.B. Nielsen, S. Schultz-Møller, S. Wedel, H. Livbjerg; *The Nucleation of Aerosols in Flue Gases with a High Content of Alkali – A Laboratory Study*; **Aerosol Sci. and Techn. 33, 490 – 509, 2000.**

P.A. Jensen, M. Stenholm, P. Hald; *Deposition Investigation in Straw Fired Boilers*; **Energy and Fuels, 11: 1048-1055, 1997.**

P.A. Jensen, F.J. Frandsen, K. Dam-Johansen, B. Sander; *Experimental Investigation of the Transformation and Release to Gas Phase of Potassium and Chlorine during Straw Pyrolysis*; **Energy & Fuels; 14(6); pp 1280-1285; 2000.**

P.A. Jensen, B. Sander, K. Dam-Johansen; *Pretreatment of straw for power production by pyrolysis and char wash*; **Biomass & Energy; Vol. 20; pp 431 – 446, 2001a.**

P.A. Jensen, B. Sander, K. Dam-Johansen; *Removal of K and Cl by leaching of straw char*; **Biomass & Energy; 20; pp 447 – 457; 2001b.**

P.A. Jensen, F.J. Frandsen, J. Hansen, K. Dam-Johansen, N. Henriksen, S. Hörlyck; *SEM Investigation of Superheater Deposits from Biomass-Fired Boilers*; **Energy & Fuels; 18, pp 378-384, 2004.**

P.A. Jensen, H. Zhou, A. Zbogar, J. Hansen, F.J. Frandsen, P. Glarborg, B. Madsen, H. Stang; *Final Report – Ash Deposit Formation and Removal in Biomass-Fired Boilers. Fundamental Data Provided with Deposit Probes*; **Final Report Energinet.dk PSO-Project 4106, 2005.**

S. Jimenez, J. Ballester; *Formation and Emission of Submicron Particles in Pulverized Olive Residue (Orujillo) Combustion*; **Aerosol Sci. and Techn. 38, 707 – 723, 2004.**

S. Jimenez, J. Ballester; *Influence of Operating Conditions and the Role of Sulfur in the Formation of Aerosols from Biomass Combustion*; **Combustion and Flame 140, 346 – 358, 2005a.**
S. Jimenez, J. Ballester; *Effect of Co-Firing on the Properties of Submicron Aerosols from Biomass Combustion*; **Proc. Int. Comb. Symp. 30, 2965 – 2972, 2005b.**

S. Jimenez, J. Ballester; *Particulate Matter Formation and Emission in the Combustion of Different Pulverized Fuels*; **Combustion Sci. and Techn. 178, 655 – 683, 2006.**

L.S. Johansson; *Characterisation of Particle Emissions from Small-Scale Biomass Combustion*; **Ph.D. Thesis, Chalmers University of Technology, Göteborg, Sweden, 2002.**

L.S. Johansson, C. Tullin, B. Leckner, P. Sjövall; *Particle Emissions from Biomass Combustion in Small Combustors*; **Biomass and Bioenergy 25, 435 – 446, 2003.**

J.K. Jokiniemi, M. Lazaridis, K.E.J. Lehtinen, E.I. Kauppinen; *Numerical-Simulation of Vapor Aerosol Dynamics in Combustion Processes*; **J. Aerosol Sci. 25, 429 – 446, 1994.**

H. Junker; *Co-firing Biomass and Coal. Plant Comparisons and Experimental Investigation of Deposit Formation*; **Ph.D. Thesis, Elsamprojekt A/S, September 1997.**

H. Junker, L.L. Baxter, A.L. Robinson, and K.E. Widell; *Mechanisms of Deposit Formation when Co-Firing Coals and Biofuels*; **Proc. Eng. Found. Conf. "*The Impact of Mineral Impurities in Solid Fuel Combustion*", November 2-7, 1997, Kona, Hawaii, USA, 1997.**

M. Jöller, T. Brunner, I. Obernberger, I. Letofsky-Papst; *Investigation of Formation Pathways of Aerosol Particles Formed during Fixed Bed Combustion of Woody Biomass Fuels*; **In Proceedings of the 227th ACS National Meeting (Fuel Chemistry DiVision), Anaheim, CA, March 28- April 1, 2004; American Chemical Society: Washington, DC, 2004.**

M. Jöller, T. Brunner, I. Obernberger; *Modeling of Aerosol Formation during Biomass Combustion in Grate Furnaces and Comparison with Measurements*; **Energy & Fuels 19, 311 – 323, 2005.**

T.L. Jørgensen, H. Livbjerg, P. Glarborg; *Homogeneous and heterogeneously catalyzed oxidation of SO_2*; **Chem. Eng. Sci., 62, 4496 – 4499, 2007.**

A. Kaliazine, D.E. Cormack, F. Piroozmand, H.N. Tran; *Sootblower optimisation II: Deposit and sootblower interaction*; **Tappi Journal 80(11), 1997.**

A. Kaliazine, H.N. Tran, D.E. Cormack; *The Mechanisms of Deposit Removal in Kraft Recovery Boilers*; **Journal of Pulp and Paper Science 25, 1999.**

H. Kamiya, Y. Sekiya, M. Horio; *Thermal stress fracture of rigid ceramic filter due to char combustion in collected dust layer on filter surface*; **Powder Technology 115, 139-145, 2001.**

E.I. Kauppinen, T.A. Pakkanen; *Coal Combustion Aerosols: A Field Study*; **Environ. Sci. Technol., 24, 1811-1818, 1990.**

Y. Kawahara; *High Temperature Corrosion Mechanisms and Effect of Alloying Elements for Materials Used in Waste Incineration Environment*; **Corrosion Science, 44, 223–245, 2002.**

J.N. Knudsen; *Volatilization of Inorganic Matter during Combustion of Annual Biomass*; **Ph.D.-Thesis, Department of Chemical Engineering, Technical University of Denmark, ISBN-87-91435-11-0, 2004.**

J.N. Knudsen, P.A. Jensen, W. Lin, F.J. Frandsen, K. Dam-Johansen; *Sulfur Transformations during Thermal Conversion of Herbaceous Biomass*; **Energy Fuels, 18, 810-819, 2004a.**

J.N. Knudsen, P.A. Jensen, K. Dam-Johansen; *Transformation and Release to the Gas Phase of Cl, K, and S during Combustion of Annual Biomass*; **Energy Fuels, 18, 1385-1399, 2004b.**

J.N. Knudsen, P.A. Jensen, W. Lin, K. Dam-Johansen, K; *Secondary Capture of Chlorine and Sulfur during Thermal Conversion of Biomass*; **Energy Fuels, 19, 606-617, 2005.**

J.N. Knudsen, O.H. Larsen, M. Montgomery, O. Biede, J.P. Jensen; *Belægningsdannelse og Korrosion I hlamfyrede kedler. Fyringsforsøg på AVV2s Biokedel*; **Report, PSO-Project FU-1202, 2005 (in Danish).**

P. Kofstad; *High Temperature Corrosion*; **Elsevier Applied Science, New York, 1988**.

R. Korbee, J.H.A. Kiel, M. Zevenhoven, B.-J. Skrifvars, P.A. Jensen, F.J. Frandsen; *Investigation of Biomass Inorgnaic Matter by Advanced Fuel Analysis and Conversion Experiments*, **In: N. S. Harding, L. L. Baxter, F. Wigley and F. J. Frandsen, 'Power Production in the 21th Century: Impact of Fuel Quality and Operations', Proc. United Engineering Foundation International Conf., Snowbird, Utah, USA, October 28 – November 2, 2001; 2001.**

F.J. Kohl, G.J. Santoro, C.A. Stearns, D.E. Rosner; **J. Electrochem. Soc. 126, 1054-1061, 1979.**

J. Koppejan; *Overview of experiences with cofiring biomass in coal power plants*; **IEA Bioenergy Task 32: Biomass Combustion and Cofiring, 2004.**

H.H. Krause; *Corrosion by Chlorine in Waste-Fuelled Boilers*; **In: R.W. Bryers (Ed.), Incinerating Municipal and Industrial Waste, Hemisphere Publishing Corporation, 1989.**

S. Kyi, B.L. Chadwick; *Screening of potential mineral additives for use as fouling preservatives in Victorian brown coal combustion.* **FUEL, 78, 845 – 855, 1999.**

O.H. Larsen and N. Henriksen; *Ash Deposition and High Temperature Corrosion at Combustion of Aggressive Fuels*; **Proc. Power Plant Technology, Kolding 4-6 Sept. pp 7.1-7.18., 1996.**

O.H. Larsen, N. Henriksen, S. Inselmann, R. Blum; *The Influence of Boiler Design and Process Conditions on Fouling and Corrosion in Straw and Coal/Straw-Fired Ultra Supercritical Power Plants*; **Proc. 9th European Bioenergy Conference: Copenhagen, Denmark, 1996.**

O.H. Larsen; *Superheater corrosion in PC-boilers, MKS1 Demoprogramme, Corrosion tests at 10 and 20% straw share*; **Internal Report, Fælles-kemikerne, FK-rapport 98-4.09, 1998.**

B.A. Latella, B.H. O'Connor; *Effect of porosity on the erosive wear of liquid-phase-sintered alumina ceramics*; **J.Am.Soc 82(8), 2145-2149, 1999.**

K. Laursen; *Characterisation of Minerals in Coal and Interpretations of Ash Formation and Deposition in Pulverized Coal Fired Boilers*; **Ph.D. Thesis, Geological Survey of Greenland and Denmark, ISBN 87-7871-022-7, 1997.**

K. Laursen, F.J. Frandsen, O.H. Larsen; *Ash Deposition Trials at Three Power Stations in Denmark*; **Energy & Fuels; 12(2); 429 – 442, 1998.**

B. Leckner; "Co-Combustion – A Summary of Technology", **Thermal Science, 11(4), pp. 5-40, 2007.**

S.H.D. Lee, I. Johnson; *Removal of Gaseous Alkali Metal Compounds from Hot Flue Gas by Particulate Sorbents.* **J. Eng. Power, Trans. ASME, 102, 397 – 402, 1980.**

Al. Levy, E.L. Merryman, W.T. Reid; **Env. Sci. and Technol. 4, 653-662, 1970.**

J.S. Lighty, J.M. Veranth, A.F. Sarofim; *Introduction to the Air & Waste Management Association's 30th Annual Critical Review*; **J. Air & Waste Management Association 50, 1562 – 1564, 2000a.**

J.S. Lighty, J.M. Veranth, A.F. Sarofim; *Combustion Aerosols: Factors Governing their Size and Composition and Implications to Human Health*; **J. Air & Waste Management Association 50, 1565 – 1618, 2000b.**

T. Lind, T. Valmari, E. Kauppinen, W. Maenhaut, F. Huggins; *Ash formation and heavy metal transformations during fluidized bed combustion of biomass*; **In: Ashes and Particulate Emissions from Biomass Combustion, Series Thermal Biomass Utilization, 3th Ed. BIOS, Graz, Austria, ISBN-3-7041-0254-7, 1998.**

H. Livbjerg; **Int. IEA Seminar, Bioenergy Task 32: Biomass Combustion and Cofiring, 2001.**

W.R. Livingston; *Straw ash characteristics*; **Babcock Energy Ltd., Babcock Report Number 34/91/08, Contractor Report, Department of Energy, ETSU B 1242, 1991.**

M.J.F. Llorente, J.E.C. García; *Concentration of elements in woody and herbaceous biomass as a function of the dry ashing temperature*; **Fuel, 85, pp 1273-1279, 2006.**

S. Van Loo, J. Koppejan; *Handbook of biomass. Combustion and Co-firing*; **Twente University Press. ISBN 9036517737, 2003.**

K.L. Luthra, O.H. Jr. LeBlanc; *Adsorption of NaCl and KCl on Al2O3 at 800 – 900 °C.* **J. Phys. Chem., 88, 9, 391 – 397, 1984.**

A. Maciejewska, H. Veringa, J. Sanders, S.D. Peteves; "Co-Firing of Biomass with Coal: Constraints and Role of Biomass Pre-Treatment", **DG JRC, Institute for Energy, ISBN 92-79-02989-4, 2006.**

Y. Mamane, R. Willis, T. Conner; *Evaluation of Computer-Controlled Scanning Electron Microscopy Applied to an Ambient Urban Aerosol Sample*; **Aerosol Sci. and Techn., 34, pp 97-107, 2001.**

H. Marschner; *Mineral Nutrition of Higher Plants*; **2nd ed., Academic Press, London, ISBN-0-12-473543-6, 2002.**

P. Mayer, H.J. Westwood, A.V. Manolescu; *Corrosion Related Problems in Fossil Fired Boilers*; **J. Materials for Energy Systems, 2, pp. 55-64, 1980**.

H.P. Michelsen, F.J. Frandsen, K. Dam-Johansen, O.H. Larsen; *Deposition and high temperature corrosion in a 10 MW straw fired boiler*; **Fuel Processing Technology; 54; pp 95-108, 1998.**

T.R. Miles, T.R. Miles Jr., L.L. Baxter, R.W. Bryers, B.M. Jenkins, L.L. Oden; *Alkali Deposits Found in Biomass Power Plants. A Preliminary Investigation of Their Extent and Nature*; **National Renewable Energy Laboratory, 1617 Cole Boulevard, Golden, Colorado, 1994.**

T.R. Miles, T.R. Miles Jr.; L.L. Baxter, R.W. Bryers, B.M. Jenkins, L.L. Oden; *Boiler Deposits from Firing Biomass Fuels*; **Biomass and Bioenergy, 10, 2-3, 125-138, 1996.**

P.D. Miller, H.H. Krause, J. Zupan, Walter K. Boyd; *Corrosive Effects of Various Salt Mixtures Under Combustion Gas Atmospheres*; **Corrosion-NACE, 28(6), pp. 222-225, 1972**.

P.D. Miller, H.H. Krause, D.A. Vaughan, W.K. Boyd; *The Mechanism in High Temperature Corrosion in Municipal Incinerators*; **Corrosion-NACE, 28(7), pp. 274-281, 1972**.

B. Miller, D.R. Dugwell, R. Kandiyoti; *The Influence of Injected HCl and SO2 on the Behavior of Trace Elements during Wood-Bark Combustion*; **Energy Fuels, 17, 1382-1391, 2003.**

M.K. Misra, K.W. Ragland, A.J. Baker; *Wood Ash Composition as a Function of Furnace Temperature*; **Biomass Bioenergy, 4, 103- 116, 1993.**

Montana State University; www.montana.edu, 2006.

M. Montgomery, A. Karlsson; *Corrosion Investigations at Masnedø Combined Heat and Power Plant - Part II*; **Internal Report, ELKRAFT Power Company, Denmark, November 1997.**

M. Montgomery, A. Karlsson; *In situ Corrosion Investigation at Masnedø CHP Plant*; **Materials and Corrosion, 50 579-584, 1999.**

M. Montgomery, F.J. Frandsen, A. Karlson, O.H. Larsen; *Corrosion Investigation in Straw-fired Power Plants in Denmark*; **Proc. United Eng. Found. Conf. on Effects of Coal Quality on Power Plant Performance: Ash Problems, Management and Solutions, Park City, UT, USA, May 9-13, 2000a.**

M. Montgomery, F.J. Frandsen, O.H. Larsen; *The Effect of Co-Firing with Straw and Coal on High Temperature Corrosion.* **Proc. United Eng. Found. Int. Conf. on 'Effects of Coal Quality on Power Plant Management: Ash Problems, Management and Solutions', Park City, Utah, May 8-11, 2000b.**

M. Montgomery, A. Karlsson, O.H. Larsen; *Field test corrosion experiments in Denmark with biomass fuels Part I: Straw firing*; **Materials and Corrosion 53 pp. 121-131, 2002a.**

M. Montgomery, O. Biede and O.H. Larsen; *High Temperature Corrosion in straw fired power plants: Influence of steam/metal temperature on corrosion rates for TP347H*; **Materials for Advanced Power Engineering 2002 Part II pp 957-966, 2002b.**

M. Montgomery, O. Biede, O.H. Larsen; *Corrosion Investigations at Masnedø Combined Heat and Power Plant, Part VII*; **Energy E2 Interim Report, 2002c.**

M. Montgomery, T. Vilhelmsen, S.A. Jensen; *Potential High Temperature Corrosion Problems due to Co-Firing of Biomass and Fossil Fuels*; **Materials and Corrosion, 59(10), 783 – 793, 2008.**

P.R. Mulik, D.F. Ciliberti, M.A. Alvin, M.M. Ahmed, D.M. Bachovchin, D.L. Kearns; *Simultaneous high-temperature removal of alkali and particulates in a pressurized gasification system.* **Report No. DOE/ET/11026-T1. Westinghouse Electric Corporation, Research and Development Center, 1981.**

P.O. Mwabe, J.O.L. Wendt; *Mechanisms governing trace sodium capture by kaolinite in a downflow combustor.* **Proc. 26th Symp. (Int.) on Comb., The Combustion Institute, 1996.**

NETBIOCOF; "New and Advanced Concepts in Renewable Energy Technology for Biomass", Final Report for **Integrated European Network for Biomass Co-Firing, Priority 6 – Sustainable Energy Systems, Project No. SES6-CT-020007, 2006.**

M. Neville, R.J. Quann, B.S. Haynes, A.F. Sarofim; *Vaporization and Condensation of Mineral Matter during Pulverized Coal Combustion*; **In Eighteenth Symposium (International) on Combustion, Waterloo, Canada, August 17-22, 1980; The Combustion Institute: Pittsburgh, PA, 1981.**

H.P. Nielsen; *Deposition and High-Temperature Corrosion in Biomass-Fired Boilers*; **Ph.D.-Thesis, Department of Chemical Engineering, Technical University of Denmark, ISBN-87-90142-47-0, 1998.**

H.P. Nielsen, F.J. Frandsen, K. Dam-Johansen; *Lab-Scale Investigations of High-Temperature Corrosion Phenomena in Straw-Fired Boilers*; **Energy & Fuels; 13(6), pp 1114-1121, 1999.**

H.P. Nielsen, L.L. Baxter, G. Sclippa, C. Morey, F.J. Frandsen, K. Dam-Johansen; *Deposition of Potassium Salts on Heat Transfer Surfaces in Straw-Fired Boilers: A Pilot-Scale Study*; **Fuel; 79; pp 131-139; 2000a.**

H.P. Nielsen, F.J. Frandsen, K. Dam-Johansen, L.L. Baxter; *The Implications of Chlorine-Associated Corrosion on the Operation of Biomass-Fired Boilers*; **Progress in Energy and Combustion Science; 26; pp 283-298; 2000b.**

L.B. Nielsen; *Combustion Aerosols from Potassium-Containing Fuels*; **Ph.D.-Thesis, Department of Chemical Engineering, Technical University of Denmark, 1998.**

M.T. Nielsen; *Field Study of Combustion Aerosols*; **Ph.D. Dissertation, Department of Chemical Engineering, Technical University of Denmark, 2001.**

M.T. Nielsen, H. Livbjerg, C.L. Fogh, J.N. Jensen, P. Simonsen, C. Lund, K. Poulsen, B. Sander; *Formation and Emission of Fine Particles from Two Coal-Fired Power Plants*; **Comb. Sci. and Techn. 174, 79 – 113, 2002.**

Al. Novaković; *Release Studies in the System K-Ca-Si,* **B.Sc. Thesis, Department of Chemical Engineering, Technical University of Denmark, Kgs. Lyngby, Denmark, 2006.**

Al. Novakovic; A. *Release Studies in the System K-Ca-P(-Mg) – The Effect of the Ca/P-Ratio*, **M.Sc. Thesis, Department of Chemical Engineering, Technical University of Denmark, Kgs. Lyngby, Denmark, 2007.**

Al. Novakovic, S.C. van Lith, F.J. Frandsen, P.A. Jensen, L.B. Holgersen; *Release of Potassium from the Systems K-Ca-Si and K-Ca-P*; **Energy & Fuels, 23, 3423 – 3428, 2009.**

J.W. Nowok; *Densification, shrinkage and strength development in selected coal ashes*; **Journal of the Institute of Energy 69, 9-11, 1996.**

In. Obernberger, J. Dahl, T. Brunner; *Formation, Composition and Particles Size Distribution of Fly-Ashes from Biomass Combustion Plants*; **Proc. 4th Biomass Conf. of the Americas, Sept. 1999, Oakland, CA, USA, pp. 1377 – 1385, ISBN-0-08-043019-8, 1999.**

In. Obernberger, T. Brunner, M. Jöller; *Characterization and Formation of Aerosols and Fly-Ashes from Fixed-Bed Biomass Combustion*; **In Proceedings of the International IEA Seminar 'Aerosols from Biomass Combustion'; Zurich, Switzerland, June 27, 2001; Verenum: Zurich, Switzerland; pp 69-74, 2001.**

Y.I. Oka, H. Ohnogy, T. Hosokawa, M. Matsumura; *The impact angle dependence of erosion damage caused by solid particle impact*; **Wear 203-204, 573-579, 1997.**

Y.I. Oka, T. Yoshida; *Practical estimation of erosion damage caused by solid particle impact. Part 1: Effects of impact parameters on a predictive equation*; **Wear 259, 95–101, 2005a.**

Y.I. Oka, T. Yoshida; *Practical estimation of erosion damage caused by solid particle impact. Part 2: Mechanical properties of materials directly associated with erosion damage*; **Wear 259, 102–109, 2005b.**

T. Okuno, N. Sonoyama, J. Hayashi, C.-Z., C. Sathe, T. Chiba; *Primary Release of Alkali and Alkaline Earth Metallic Species during the Pyrolysis of Pulverized biomass*; **Energy Fuels, 19, 2164–2171, 2005.**

N. Otsuka, T. Kudo; *High-Temperature Corrosion of Advanced Materials and Coatings*; **In: Y. Saito, N. Onay, T. Maruyama (Eds.), Elsevier Science Publishers, B.V. 1992.**

P. Overgaard, B. Sander, H. Junker; *Two years operational experience and further development of full-scale co-firing of straw*; **Proc. of 2nd World Biomass Conference, May 10-14, Rome, Italy, 1261-1264, 2004.**

P. Overgaard, E. Larsen, K. Friborg, T. Hille, P.A. Jensen, S. Knudsen; *Full-Scale Tests on Co-Firing of Straw in a Natural Gas-Fired Boiler*; **Proc. 14th European Biomass Conf. and Exhibition, Paris, France, October 17-21, 2005.**

S. Ozawa, K. Naruse, K. Ito, Y. Kojima, H. Matsuda, S. Mishima, M. Endo, T. Yanase; *Evolution of HCl from KCl, $CaCl_2$ and NaCl in an SO_2-O_2-H_2O atmosphere under a simulated condition of municipal waste incineration*; **J. Chem. Eng. Japan, 2003, *36* (7), 867-873.**

J. Pagels, M. Strand, J. Rissler, A Szpila, A. Gudmundsson, M. Bohgard, L. Lillieblad, M. Sanati, E. Swietlicki; *Characteristics of Aerosol Particles Formed during Grate Combustion of Moist Forrest Residue*; **J. Aerosol Sci. 34, 1043 – 1059, 2003.**

A.J. Pedersen, F.J. Frandsen, C. Riber, T. Astrup, S.N. Thomsen, K. Lundtorp, L.F. Mortensen; *A Full-Scale Study on the Partitioning of Trace Elements in Municipal Solid Waste Incineration – Effects of Firing Different Waste Types*; **Energy and Fuels, 23, 3475 – 3489, 2009.**

J.S. Pedersen; Belægningsinitieret korrosion i biomassefyrede kedler, B.Sc.-projekt, DTU Kemiteknik, Januar 2009.

L.S. Pedersen, H.P. Nielsen, S. Kiil, L.A. Hansen, K. Dam-Johansen, F. Kildsig, J. Christensen, P. Jespersen; *Full-scale co-firing of straw and coal*; **Fuel; 75(13), pp 1584-1590, 1996.**

L.S. Pedersen, D.J. Morgan, W.L. van de Kamp, J. Christensen, P. Jespersen, K. Dam-Johansen; *Effects on SO_x and NO_x Emissions by Co-Firing Straw and Pulverized Coal*; **Energy & Fuels; 11; pp 439-446; 1997.**

R.S. Pedersen; *Residual Ash Formation during Combustion of Woody Biomass*; **M. Sc. Thesis, Technical University of Denmark, Lyngby, Denmark, 2003.**

F. Piroozmand, H.N. Tran, A. Kaliazine, D.E. Cormack; *Strength of recovery boiler fireside deposits at high temperatures*; **Tappi Proceedings 1, 169-179, 1998.**

PSO-3149; *Halmtilsatsfyring i naturgasfyret kraftværkskedel*; **Slutrapport, PSO-Eltra Projektnummer 3149, August 2004 (in Danish).**

W.A. Punjak; *High Temperature Interactions of Alkali Vapors with Solids during Coal Combustion and Gasification.* **Ph.D.-Dissertation, Department of Chemical Engineering, University of Arizona, Tucson, AZ, 1988.**

W.A. Punjak, F. Shadman; *Aluminosilicate Sorbents for Control of Alkali Vapors during Coal Combustion and Gasification.* **Energy and Fuels, 2, 5, 702 – 708, 1988.**

W.A. Punjak, M. Uberoi, F. Shadman; *High-Temperature Adsorption of Alkali on Solid Sorbents.* **AIChE J., 35, 7, 1186 – 1194, 1989.**

J. Pyykönen, J. Jokiniemi; *Computational Fluid Dynamics Based Sectional Aerosol Modeling Schemes*; **J. Aerosol Sci. 31, 531 – 550, 2000.**

R. Quann, A.F. Sarofim; *Vaporization of Refractory Oxides during Pulverized Coal Combustion*; **In: Nineteenth Symposium (International) on Combustion; Haifa, Israel, August 8-13, 1982; The Combustion Institute: Pittsburgh, PA; pp 1429-1440, 1982.**

R.J. Quann, M. Neville, A.F. Sarofim; *A Laboratory Study of the Effect of Coal Selection on the Amount and Composition Generated Submicron Particles*; **Comb, Sci. and Techn. 74, 245 – 265, 1990.**

D.M. Quyn, H. Wu, H., C.-Z.; *Volatilization and Catalytic Effects of Alkali and Alkaline Earth Metallic Species during the Pyrolysis and Gasification of Victorian Brown Coal. Part I. Volatilization of Na and Cl from a Set of NaCl-Loaded Samples*; **Fuel, 81, 143–149, 2002a.**

D.M. Quyn, H. Wu, S.P. Bhattacharya, C.-Z.; *Volatilization and Catalytic Effects of Alkali and Alkaline Earth Metallic Species during the Pyrolysis and Gasification of Victorian Brown Coal. Part II. Effects of Chemical Form and Valence*; **Fuel, 81, 151–158, 2002b.**

E. Raask; *Sintering Characteristics of Coal Ashes by Simultaneous Dilatometry-Electrical Conductance Measurements*; **J. Thermal Anal., 16, pp 91-98, 1979.**

E. Raask; *Mineral impurities in coal combustion*; **Hemisphere Publishing Corporation, Washington, 1985.**

E. Raask; *Erosion wear in coal utilization*; **Hemisphere Publishing Corporation, 1988.**

R.A. Rapp; *Chemistry and Electrochemistry of the Hot Corrosion of Metals*; **Corrosion, 42, pp 568-577, 1986**.

W.T. Reid; *External Corrosion and Deposits - Boilers and Gas Turbines*; **American Elsevier, New York, 1971.**

A.L. Robinson, H. Junker, S.G. Buckley, G. Sclippa, L.L. Baxter; *Interactions between Coal and Biomass when Co-firing*. **Proc. 27th Symposium (International) on Combustion, Boulder, CO, Combustion Institute, 1998.**

A.L. Robinson, H. Junker, L. L. Baxter; *Pilot-scale investigation of the influence of coal-biomass co-firing on ash deposition*; **Energy & Fuels, 16(2), 343 – 355, 2002.**

Y. Sakata, M.A. Uddin, K. Koizumi, K. Murata; *Thermal degradation of polyethylene mixed with poly(vinyl chloride) and poly(ethyleneterephthalate)*; **Polymer Degradation and Stability, 53 111-117, 1996.**

K. Salmenoja, K. Mäkela, M. Hupa, R. Backman; *Superheater Corrosion in Environments Containing Potassium and Chlorine*; **Journal of the Institute of Energy, 69, pp 155-162, 1996.**

M. Sami, K. Annamalai, M. Wooldridge; *Co-firing of coal and biomass fuel blends*; **Prog. Energy Combust. Science 27, 171–214; 2001.**

J. Samms, J. Watt; **British Coal Utilization Research Association Bulletin, Vol. 30, p. 225, 1966.**

B. Sander; *Properties of Danish Biofuels and the Requirements for Power Production*; **Biomass and Bioenergy, 12, 3, 177-183, 1997.**

B. Sander, N. Henriksen, O. H. Larsen, A. Skriver, C. Ramsgaard-Nielsen, J. N. Jensen, K. Stærkind, H. Livbjerg, M. Thellefsen, K. Dam-Johansen, F. J. Frandsen, R. van der Lans, J. Hansen; *Emissions, Corrosion and Alkali Chemistry in Straw-Fired Combined Heat and Power Plants*; **Proc. 1st World Conference on Biomass for Energy and Industry, Sevilla, June, 5-9, 2000.**

B. Sander, K. Wieck-Hansen; *Full-Scale Investigations on Alkali Chemistry and Ash Utilization by Co-firing of Straw*; **Proc. 14th European Biomass Conf. and Exhibition, Paris, France, October 17-21, 2005.**

A. Sanyal, A.K. Metha; *Development of an Electrical Resistance Based Ash Fusion Test*; **In: J. Williamson and F. Wigley, 'The Impact of Ash Deposition on Coal-Fired Power Plants', Proc. United Engineering Foundation International Conf., Solihull, Birmingham, UK, June 20-25, 1993; 1994, ISBN-1-56032-293-4.**

A.F. Sarofim, J.B. Howard, A.S. Padia; *The Physical Transformation of the Mineral Matter in Pulverized Coal under Simulated Combustion Conditions*; **Combust. Sci. Technol., 16, 187-204, 1977.**

H.N.S. Schafer; **In: The Science of Victorian Brown Coal: Structure, Properties, and Consequences for Utilization; Durie R. A., Ed.; Butterworth-Heinemann: Oxford, Chapter 7, 1991.**

K. Schofield; *A New Method for the Direct Flame Calibration of Nebulized Additive Concentrations*; **Comb. And Flame 133, 147 – 156, 2003.**

H. Schürmann, S. Unterberger, K.R.G. Hein, P.G. Monkhouse, U. Gottwald; *The influence of fuel additives on the behaviour of gaseous alkali-metal compounds during pulverized coal combustion.* **Faraday Discuss., 119, 433 – 444, 2001.**

M.V. Scotto, M. Uberoi, T.W. Peterson, F. Shadman,J.O.L. Wendt; *Metal Capture by Sorbents in Combustion Processes*; **Fuel Proc. Technol., 39, 357–372, 1994.**

Y. Shinata, Y. Nishi; *NaCl-Induced Accelerated Oxidation of Chromium*; **Oxidation of Metals, 26, pp 201-212, 1986.**

Y. Shinata, F. Takahashi, K. Hashiura; *NaCl-Induced Hot Corrosion of Stainless Steels*; **Materials Science and Engineering; 87; pp 399-405; 1987.**

Y. Shinata; *Accelerated Oxidation Rate of Chromium Induced by Sodium Chloride*; **Oxidation of Metals, 27, pp 315-330, 1987.**

H.T. Shirley; *Effects of Sulphate-Chloride Mixtures in Fuel-Ash Corrosion of Steels and High-Nickel Alloys*; **Journal of Iron and Steel Institute; pp 144-153; 1956.**

J.P. Singer; *Combustion. Fossil Combustion. A Reference Book on Fuel Burning and Steam Generation*; **Combustion Engineering , Inc., ISBN-0-9605974-0-9, 1991.**

J. Sipilä, M. Zevenhoven, R. Zevenhoven; *Combined thermal treatment of CCA-wood waste and municipal sewage sludge for arsenic emissions control*; **Report 2007-1, Åbo Akademi University, Faculty of Technology, Heat Engineering Laboratory, 2007.**

N.M. Skorupska; "Coal Specifications – Impact on Power Station Performance", IEA Coal Research Report IEACR/52, ISBN-92-9029-210-5, 1993.

B.-J. Skrifvars; *Sintering Tendency of Different Fuel Ashes in Combustion and Gasification Conditions*; **Academic Dissertation, Report 94-6, Department of Chemical Engineering, Combustion Chemistry Research Group, Åbo Akademi, ISBN 951-650-357-8, 1994.**

B.J. Skrifvars, R. Backman, M. Hupa, G. Sfiris, T. Abyhammer, A. Lyngfelt; *Ash Behavior in a CFB Boiler During Combustion of Coal, Peat or Wood*; **Fuel 77, 65 – 70, 1998.**

B.-J. Skrifvars, T. Laurén, R. Backman, M. Hupa, P. Binderup-Hansen; *The role of alkali sulfates and chlorides in post cyclone deposits from circulating fluidized bed boilers firing biomass and coal*; **In: Impact of mineral impurities in solid fuel combustion. (Eds. Gupta, R., Wall, T., Baxter, L), Kluwer Academic/Plenum Publisher, New York, 1999.**

M. Spiegel, H.J. Grabke; *High Temperature Corrosion of Low and High Alloy Steels in Simulated Waste Incineration Atmospheres*; In: '*Incinerating Municipal and Industrial Waste. Fireside Problems and Prospects for Improvement'* **edited by R. W. Bryers, Hemisphere Publishing Corporation, pp 758-764, 1991.**

S. Srinivasachar, J.J. Helble, A.A. Boni, N. Shah, G.P. Huffman, F.E. Huggins; *Mineral behavior during coal combustion. 2. Illite transformations*; **Prog. Energy Comb. Sci., 16, 293 – 302, 1990.**

E.N. Steadman, C.J. Zygarlicke, S.A. Benson, M.L. Jones; *A Microanalytical Approach to the Characterization of Coal, Ash and Deposits*; **Proc. ASME Seminar on Fireside Fouling Problems, Provo, UT, 1991.**

B.M. Steenari, O. Lindquist; *High-Temperature Reactions of Straw Ash and the Anti-Sintering Additives Kaolin and Dolomite.* **Biomass and Bioenergy, 14(1), 67 – 76, 1998.**

M. Steinberg, K. Schofield; *Flame deposition Chemistry of Sodium Sulfate*; **Handbook of Chemistry and Physics, 68th ed., Chemical Rubber Company Inc., Boca Raton Florida, 1987.**

M. Steinberg, K. Schofield; *The Chemistry of Sodium with Sulfur in Flames*; **Progress in Energy and Comb. Sci. 16, 311 – 317, 1990.**

M. Steinberg, K. Schofield; *Controlling Chemistry in Flame Generated Surface Deposition of Na_2SO_4 and the Effects of Chlorine*; **Proc. Int. Comb. Symp. 26, 1835 – 1843, 1996.**

M. Steinberg, K. Schofield; *The Controlling Chemistry of Surface Deposition from Sodium and Potassium Seeded Flames Free of Sulfur or Chlorine Impurities*; **Comb. And Falme 129, 453 – 470, 2002.**

S.D. Steinsen; *Release of Inorganic Metals, S and Cl from Waste Fractions*; **Master Thesis, Department of Chemical Engineering, Technical University of Denmark, Lyngby, April 2007.**

M. Stenholm, P.A. Jensen, and P. Hald; *Fuel and Firing Characteristics of Biomass - Combustion Trials*; **Final Report from EFP-93 Project (in Danish), Journal No. 1323/93-0015, The Danish Energy Research Programme, 1996.**

M. Stenseng; *Pyrolysis and Combustion of Biomass*; **Ph.D.-Thesis, Department of Chemical Engineering, Technical University of Denmark, ISBN-87-90142-65-9, 2001.**

M. Stenseng, A. Zolin, R. Cenni, F.J. Frandsen, A. Jensen, K. Dam-Johansen; *Thermal Analysis in Combustion Research, Journal of Thermal Analysis and Calorimetry*; **Ed. T. Bridgwater; Blackwell Science; 64; pp 1325 – 1334, 2001.**

S. Stitt, H. Junker, L.L. Baxter; *Optimisation of Deposit Removal in Biofueled Boilers: Review of Control Systems, Technologies and Mechanisms*; **Project No. Eltra 3144; TW 13317.00, 2002.**

J. Szomolanyiova, T. Vorisek, J. Zeman, N. Lambergar, D. Bohunicka, M. Jaloviar, L. Zidek, M. Zarkadoula, L. Gavriil, N. Djouras, B. Meuleman, M. Tijmensen, H. Gaj, A. Hunnik, A. Karner; "Pilot Projects Support . ForBiom Project – Phase 3", **Final Report SAVE Programme, Contract No. 4.1031/Z/02-067/2002, 2005.**

H.S. Sørensen; *Computer Controlled Scanning Electron Microscopy (CCSEM) Analysis of Straw Ash*, **In: R. P. Gupta, T. F. Wall and L. L. Baxter, 'Impact of Mineral Impurities in Solid Fuel Combustion', Proc. Eng. Found. Conf., Kona, Hawaii, USA, November 2 - 7, 1997; ISBN-978-0306461262, 1997.**

H.S. Sørensen, P. Rosenberg, H.I. Petersen, L.H. Sørensen; *Char porosity characterization by scanning electron microscopy and image analysis*; **Fuel, 79, 1379 – 1388, 2000.**

L. Sørum, M.G. Grønli, J.E. Hustad; *Pyrolysis characteristics and kinetics of municipal solid wastes*; **Fuel, 80, 1217-1227, 2001.**

P. Tang, Y.C. Zhao, F.Y. Xia; *Volatility of heavy metals during incineration of tannery sludge in the presence of chlorides and phosphoric acid*; **Waste Management & Research, 26, 369 – 376, 2008.**

M. Theis, B.-J. Skrifvars, M. Hupa, H. Tran; *Fouling tendency of ash resulting from burning mixtures of biofuels. Part 1: Deposition rates*; **Fuel, 85, pp. 1125-1130, 2006a.**

M. Theis, B.-J. Skrifvars, M. Zevenhoven, M. Hupa, H. Tran; *Fouling tendency of ash resulting from burning mixtures of biofuels. Part 2: Deposit chemistry*; **Fuel, 85, pp. 1992-2001, 2006b.**

M. Theis, B.-J. Skrifvars, M. Zevenhoven, M. Hupa, H. Tran; *Fouling tendency of ash resulting from burning mixtures of biofuels. Part 3: Influence of probe surface temperature*; **Fuel, 85, pp. 2002-2011, 2006c.**

K. Tomoda, M. Matsuno, T. Nakamura, T. Takasu; *Chlorination-volatilization behavior of Pb in fly ash treatment by roasting method*; **High Temperature Materials and Processes, 25, 5-6, 275-284, 2006.**

H.N. Tran, D. Barham, D.W. Reeve; *Sintering of fireside deposits and its impact on plugging in kraft recovery boilers*; **Tappi journal, 109-113, 1988.**

S.Q. Turn, C.M. Kinoshita, D.M. Ishimura, J. Zhou, T.T. Hiraki, S.M. Masutani; *A review of sorbent materials for fixed bed alkali getter systems in biomass gasifier combined cycle power generation applications.* **J. Inst. Energy, 71, 163 – 177, 1998.**

M. Uberoi, W.A. Punjak, F. Shadman; *The Kinetics and Mechanism of Alkali Removal from Flue Gases by Solid Sorbents.* **Prog. Energy Combust. Sci., 16, 205 – 211, 1990.**

T. Valmari, E.I. Kauppinen, J. Kurkela, J.K. Jokiniemi, G. Sfiris, H, Revitzer; *Fly Ash Formation and Deposition during Fluidized Bed Combustion of Willow*; **J. Aerosol Sci. 29, 445 – 459, 1998.**

T. Valmari; *Potassium Behavior during Combustion of Wood in Circulating Fluidized Bed Power Plants*; **Ph.D. Dissertation, VTT Technical Research Centre of Finland, 2000.**

S.C. van Lith; *Release of Inorganic Elements during Wood-Firing on a Grate*; **Ph.D.-Thesis, Department of Chemical Engineering, Technical University of Denmark, ISBN-87-91435-29-3, 2005.**

S.C. Van Lith, V. Alonso-Ramirez, P.A. Jensen, F.J. Frandsen, P. Glarborg; *Release to the Gas Phase of Inorganic Element during Wood Combustion. Part 1: Development and Evaluation of Quantification Methods*; **Energy & Fuels, 20, 964 – 978, 2006.**

S.C. van Lith, F.J. Frandsen, M. Montgomery, T. Vilhelmsen, S.A. Jensen; *Lab-Scale Investigation of Deposit-Induced Chlorine Corrosion of Superheater Materials under Simulated Biomass-Firing Conditions*; **Proc. Int. Conf. *Impacts of Fuel Quality on Power Production and the Environment*, Banff, Alberta, Canada, September 29 – October 3, 2008.**

S.C. van Lith, F.J. Frandsen, M. Montgomery, T. Vilhelmsen, S.A. Jensen; *Lab-Scale Investigation of Deposit Induced Chlorine Corrosion of Superheater Materials under Simulated Biomass-Firing Conditions*; **Proc. Int. Conf. *EUROCORR 2008*, Edinburgh, UK, September 7-11, 2008**

S.C. van Lith, P.A. Jensen, F.J. Frandsen, P. Glarborg; *Release to the Gas Phase of Inorganic Element during Wood Combustion. Part 2: Influence of Fuel Composition*; **Energy & Fuels, 22, 1598 – 1609, 2008.**

S.C. van Lith, F.J. Frandsen, M. Montgomery, T- Wilhelmsen, S.A. Jensen; *Lab-Scale Investigation of Deposit-Induced Chlorine Corrosion of Superherater Materials under Simulated Biomass-Firing Conditions. Part 1; Exposure at 560 °C*; **Energy and Fuels, 23, 3457-3468, 2009**

S.V. Vassilev, C. Braekman-Danheux, P. Laurent, T. Thieman, A. Fontana; *Behaviour, capture and inertization of some trace elements during combustion of refuse-derived char from municipal solid waste*; **Fuel, 78, 1131 – 1145, 1999.**

S. Vargas; *Straw and Coal Ash Rheology*; **Ph.D.-Thesis, Department of Chemical Engineering, Technical University of Denmark, ISBN-87-90142-64-0, 2001.**

S. Vargas, F. J. Frandsen, K. Dam-Johansen; *Rheological properties of high-temperature melts of coal ashes and other silicates*; **Progress in Energy and Combustion Science; 27; pp 237 – 429; 2001.**

D.A. Vaughan, H.H. Krause, W.K. Boyd; **Batelle Interim Report to US EPA, June 1974.**

J. Villadsen and M. L. Michelsen; *Solution of Differential Equations by Polynomial Approximation*; **Prentice-Hall, New Jersey, 1978.**

S.E. Wain, W.R. Livingston, A. Sanyal, J. Williamson; *Thermal and Mechanical Properties of Boiler Slags of Relevance to Sootblowing*; **In: S. A. Benson, 'Inorganic Transformations and Ash Deposition during Combustion', United Engineering Foundation International Conf., Palm Coast, FA, March 10-15, 1991; 1992, ISBN-0-7918-0657-X.**

S. Wang, L.L. Baxter; *Biomass Fly Ash in Concrete: Strength, Durability and Kinetics*; **Proc. Conf. Impacts of Fuel Quality on Power Production, Snowbird, UT, 2006a.**

S. Wang, L.L. Baxter; *Fly ash and concrete*; **Concrete Producer 24(8): 48-49, 2006b.**

S. Wang, L.L. Baxter; *Ash Utilization and Coal Pre-Treatment Issues*; **TOTeM 28 - Topic Oriented Technical Meeting: Mercury, Trace Metals, and Fine Particulates - Issues and Solutions, Salt Lake City, Utah, 2006c.**

R.M. Welch; *Micronutrient Nutrition of Plants*; **Crit. Rev. Plant Sci., 14, 49-82, 1995.**

M.-Y. Wey, J.-C. Chen, H.-Y. Wu, W.-J. Yu, T.-H. Tsai; *Formations and controls of HCl and PAHs by different additives during waste incineration*; **Fuel, 85, 755-763, 2006.**

K. Wieck-Hansen, P. Overgaard, O.H. Larsen; *Co-firing coal and straw in a 150 MWe power boiler experiences*; **Biomass & Bioenergy, 19, 395-409, 2000.**

T. Wigmans, H. Haringa, J.A. Moulijn; *Nature, Activity and Stability of Active Sites during Alkali Metal Carbonate-Catalysed Gasification Reactions of Coal Char*; **Fuel, *62*, 185–189, 1983.**

H. Wiinikka, R. Gebart; *The Influence of Fuel Type on Particle Emissions in Combustion of Biomass Pellets*; **Comb. Sci. and Techn. 177, 741 – 763, 2005.**

J. Williamson, F. Wigley; *The Impact of Ash Deposition on Coal Fired Plants*, **Proc. Eng. Found. Conf., Solihull, UK, June 20-25, 1993, ISBN-1-56032-293-4, 1994.**

I Wright, H.H. Krause; *Assessment of Factors Affecting Boiler Tube Lifetime in Waste-Fired Steam Generators: New Opportunities for Research and Technology Development*; **National Renewable Energy Laboratory, Golden, Colorado, Rep. No. NREL/TP-430-21480, 1996.**

C.-Y. Wu and P. Biswas; *Study of Numerical Diffusion in a Discrete-Sectional Model and Its Application to Aerosol Dynamics Simulation*; **Aerosol Science and Technology, 29, 359 – 378, 1998.**

R.G. WynJones, C.J. Brady, J. Speirs; *Ionic and Osmotic Relations in Plant Cells*; **In Recent Advances in the Biochemistry of Cereals; Laidman, D. L., Wyn Jones, R. G., Eds.; Academic Press: London, pp 63–103, 1979.**

M.A. Yamasoe, P. Artaxo, A.H. Miguel, A.G. Allen; *Chemical Composition of Aerosol Particles from Direct Emissions of Vegetation Fires in the Amazon Basin: Water-Soluble Species and Trace Elements*; **Atm. Environment 34, 1641 – 1653, 2000.**

N.Y.C. Yang, L.L. Baxter; *Instrument and Sample Preparation Considerations for Computer-Controlled Scanning Electron Microscopy (CCSEM) Analyses*; **In: S. A. Benson, 'Inorganic Transformations and Ash Deposition during Combustion', United Engineering Foundation International Conf., Palm Coast, FA, March 10-15, 1991; 1992, ISBN-0-7918-0657-X.**

P. Yrjas, B.-J. Skrifvars, T. Laurén, M. Hupa, J. Roppo, M. Nylund, P. Vainikka; *Deposit measurements at Alholmens Kraft during co-firing - a case study of the world's largest biofuelled CFB. Proceedings*; **Proc. 21st International Pittsburgh Coal Conference, September 14-16, 2004, Osaka, Japan, CD-ROM, 2004.**

A. Žbogar, P. A. Jensen, F. J. Frandsen, J. Hansen, P. Glarborg; *Experimental Investigation of Ash Deposit Shedding in a Straw-Fired Boiler*; **Energy & Fuels; pp 512-519; 2006.**

A. Žbogar, F.J. Frandsen, P.A. Jensen, P. Glarborg; *Shedding of Ash Deposits*; **Progress in Energy and Combustion Science, , 35, pp 31 - 56; 2009.**

J.H. Zeuthen; the Formation of Aerosols Particles during Combustion of Biomass and Waste, **Ph.D.-Thesis, Department of Chemical Engineering, Technical University of Denmark, ISBN-87-91435-54-4, 2007.**

M. Zevenhoven; *Ash-Forming Matter in Biomass Fuels*; **Ph.D.-Thesis, Åbo Academy University, Finland, ISBN-952-12-0813-9, 2001.**

M. Zevenhoven, B.-J. Skrifvars, P. Yrjas, R. Backman, C. Mueller, M. Hupa; *Co-firing in FBC - A challenge for fuel characterisation and modelling*; **Proc. 17th International Conference on Fluidised Bed Combustion, Paper 86, May 2003, Jacsonville, Florida USA, 2003.**

Y. Zheng, P.A. Jensen, A.D. Jensen, B. Sander, H. Junker; *Ash Transformation during Co-Firing Coal and Straw*; **Fuel, 86, pp. 1008-1020, 2007.**

F. Zintl, B. Strömberg, E. Björkman; *Release of Chlorine from Biomass at Gasification Conditions*; **Biomass for Energy and Industry; pp 1608-1611; 1998.**

F. Zintl, B. Strömberg, E. Björkman; *Release of Chlorine from Biomass at Gasification Conditions*; **In: 10th European Conference and Technology Exhibition Biomass for Energy and Industry Proceedings of the International Conference, Wurzburg, Germany, June 8-11, 1998; CARMEN: Rimpar, Germany, 1998.**

H. Zhou, P.A. Jensen, F.J. Frandsen; *Dynamic Mechanistic Model of Superheater Deposit Growth and Shedding in a Biomass-Fired Grate Boiler*; **Fuel 86, 1519-1533, 2007.**